# JAAVSO

Volume 45
Number 1
2017

## The Journal of the American Association of Variable Star Observers

# Photometric Analysis of HD 213616: a Multi-modal δ Scuti Variable Star

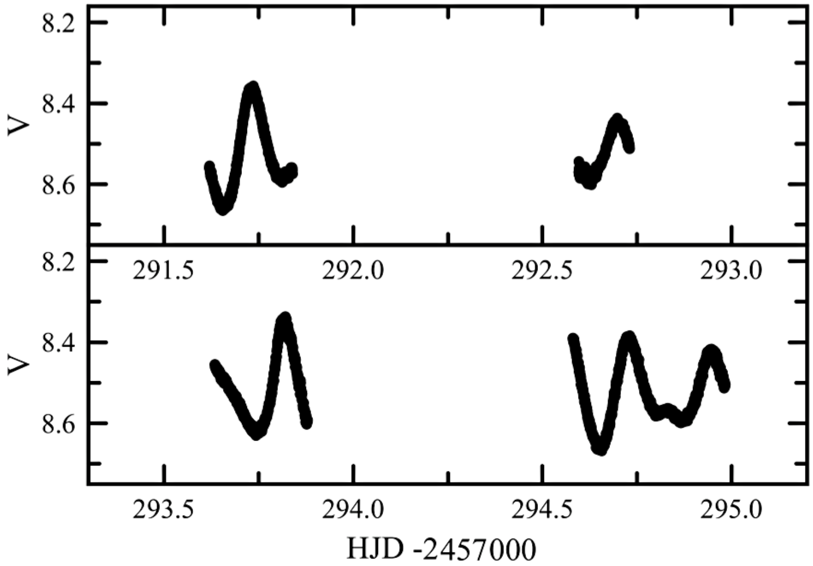

Light curve of HD 213616 from the first four nights of observation.

## *Also in this issue...*

- Photometric Analysis of Three ROTSE Contact Binary Systems
- The VESPA Survey: 100 New Variable Stars Discovered in Two Years
- Studies of the Long Secondary Periods in Pulsating Red Giants. II. Lower-Luminosity Stars
- Southern Clusters for Standardizing CCD Photometry

*Complete table of contents inside...*

The American Association of Variable Star Observers
49 Bay State Road, Cambridge, MA 02138, USA

# The Journal of the American Association of Variable Star Observers

**Editor**
**John R. Percy**
Dunlap Institute of Astronomy
and Astrophysics
and University of Toronto
Toronto, Ontario, Canada

**Associate Editor**
**Elizabeth O. Waagen**

**Production Editor**
**Michael Saladyga**

**Editorial Board**
**Geoffrey C. Clayton**
Louisiana State University
Baton Rouge, Louisiana

**Zhibin Dai**
Yunnan Observatories
Kunming City, Yunnan, China

**Kosmas Gazeas**
University of Athens
Athens, Greece

**Edward F. Guinan**
Villanova University
Villanova, Pennsylvania

**John B. Hearnshaw**
University of Canterbury
Christchurch, New Zealand

**Laszlo L. Kiss**
Konkoly Observatory
Budapest, Hungary

**Katrien Kolenberg**
Universities of Antwerp
and of Leuven, Belgium
and Harvard-Smithsonian Center
for Astrophysics
Cambridge, Massachusetts

**Ulisse Munari**
INAF/Astronomical Observatory
of Padua
Asiago, Italy

**Nikolaus Vogt**
Universidad de Valparaiso
Valparaiso, Chile

**Douglas L. Welch**
McMaster University
Hamilton, Ontario, Canada

**David B. Williams**
Whitestown, Indiana

**Thomas R. Williams**
Houston, Texas

**Lee Anne M. Willson**
Iowa State University
Ames, Iowa

## The Council of the American Association of Variable Star Observers 2016–2017

| | |
|---|---|
| Director | Stella Kafka |
| President | Kristine Larsen |
| Past President | Jennifer L. Sokoloski |
| 1st Vice President | Roger S. Kolman |
| 2nd Vice President | Kevin B. Marvel |
| Secretary | Gary Walker |
| Treasurer | Bill Goff |

Councilors

Richard Berry
Tom Calderwood
Joyce A. Guzik
Michael Joner
Katrien Kolenberg
Richard S. Post
Gregory R. Sivakoff
William Stein

**ISSN 0271-9053 (print)**
**ISSN 2380-3606 (online)**

# JAAVSO

## The Journal of
## The American Association
## of Variable Star Observers

Volume 45
Number 1
2017

AAVSO
49 Bay State Road
Cambridge, MA 02138
USA

ISSN 0271-9053 (print)
ISSN 2380-3606 (online)

## Publication Schedule

*The Journal of the American Association of Variable Star Observers* is published twice a year, June 15 (Number 1 of the volume) and December 15 (Number 2 of the volume). The submission window for inclusion in the next issue of JAAVSO closes six weeks before the publication date. A manuscript will be added to the table of contents for an issue when it has been fully accepted for publication upon successful completion of the referee process; these articles will be available online prior to the publication date. An author may not specify in which issue of JAAVSO a manuscript is to be published; accepted manuscripts will be published in the next available issue, except under extraordinary circumstances.

## Page Charges

Page charges are waived for Members of the AAVSO. Publication of unsolicited manuscripts in JAAVSO requires a page charge of US $100/page for the final printed manuscript. Page charge waivers may be provided under certain circumstances.

## Publication in *JAAVSO*

With the exception of abstracts of papers presented at AAVSO meetings, papers submitted to JAAVSO are peer-reviewed by individuals knowledgable about the topic being discussed. We cannot guarantee that all submissions to JAAVSO will be published, but we encourage authors of all experience levels and in all fields related to variable star astronomy and the AAVSO to submit manuscripts. We especially encourage students and other mentees of researchers affiliated with the AAVSO to submit results of their completed research.

## Subscriptions

Institutions and Libraries may subscribe to JAAVSO as part of the Complete Publications Package or as an individual subscription. Individuals may purchase printed copies of recent JAAVSO issues via Createspace. Paper copies of JAAVSO issues prior to volume 36 are available in limited quantities directly from AAVSO Headquarters; please contact the AAVSO for available issues.

## Instructions for Submissions

The *Journal of the AAVSO* welcomes papers from all persons concerned with the study of variable stars and topics specifically related to variability. All manuscripts should be written in a style designed to provide clear expositions of the topic. Contributors are encouraged to submit digitized text in MS WORD, LATEX+POSTSCRIPT, or plain-text format. Manuscripts may be mailed electronically to journal@aavso.org or submitted by postal mail to JAAVSO, 49 Bay State Road, Cambridge, MA 02138, USA.

Manuscripts must be submitted according to the following guidelines, or they will be returned to the author for correction:

Manuscripts must be:
1) original, unpublished material;
2) written in English;
3) accompanied by an abstract of no more than 100 words.
4) not more than 2,500–3,000 words in length (10–12 pages double-spaced).

Figures for publication must:
1) be camera-ready or in a high-contrast, high-resolution, standard digitized image format;
2) have all coordinates labeled with division marks on all four sides;
3) be accompanied by a caption that clearly explains all symbols and significance, so that the reader can understand the figure without reference to the text.

Maximum published figure space is 4.5″ by 7″. When submitting original figures, be sure to allow for reduction in size by making all symbols, letters, and division marks sufficiently large.

Photographs and halftone images will be considered for publication if they directly illustrate the text.

Tables should be:
1) provided separate from the main body of the text;
2) numbered sequentially and referred to by Arabic number in the text, e.g., Table 1.

References:
1) References should relate directly to the text.
2) References should be keyed into the text with the author's last name and the year of publication, e.g., (Smith 1974; Jones 1974) or Smith (1974) and Jones (1974).
3) In the case of three or more joint authors, the text reference should be written as follows: (Smith et al. 1976).
4) All references must be listed at the end of the text in alphabetical order by the author's last name and the year of publication, according to the following format: Brown, J., and Green, E. B. 1974, *Astrophys. J.*, **200**, 765.
   Thomas, K. 1982, *Phys. Rep.*, **33**, 96.
5) Abbreviations used in references should be based on recent issues of JAAVSO or the listing provided at the beginning of *Astronomy and Astrophysics Abstracts* (Springer-Verlag).

Miscellaneous:
1) Equations should be written on a separate line and given a sequential Arabic number in parentheses near the right-hand margin. Equations should be referred to in the text as, e.g., equation (1).
2) Magnitude will be assumed to be visual unless otherwise specified.
3) Manuscripts may be submitted to referees for review without obligation of publication.

## Online Access

Articles published in JAAVSO, and information for authors and referees may be found online at: https://www.aavso.org/apps/jaavso/

# The Journal of the American Association of Variable Star Observers
# Volume 45, Number 1, 2017

## *Editorial*

## *Variable Star Research*

## *Instruments, Methods, and Techniques*

*Table of Contents continued on following pages*

## *Variable Star Data*

## *Abstracts of Papers and Posters Presented at the 105th Annual Meeting of the AAVSO, Held in Burlington, Massachusetts, November 10–12, 2016*

*Table of Contents continued on next page*

# Editorial

## Education and Public Outreach: Why and How

**John R. Percy**
Editor-in-Chief, *Journal of the AAVSO*

*Department of Astronomy and Astrophysics, and Dunlap Institute for Astronomy and Astrophysics, University of Toronto,*
*50 St. George Street, Toronto, ON M5S 3H4, Canada; john.percy@utoronto.ca*

*Received May 18, 2017*

I've written a lot about education and public outreach (EPO), e.g. Percy (2002, 2012, 2014). These papers are freely available on the website of the *Journal of the Royal Astronomical Society of Canada*. Why write again? Because I get the sense that, in some countries, science is under threat. Science is essential to our well-being—not just our economy, but our health, environment, and culture. Among the hallmarks of science, it promotes rational thinking and critical thinking, and evidence-based decision-making—all of which are essential, but often in short supply.

I am also motivated by having recently served on a panel on "Science Culture in Canada" at the 2017 conference of the Canadian Association of Science Centres. This panel arose from a comprehensive report on this topic (Council of Canadian Academies 2014). This report is freely available on-line; see the References section for the URL. If you don't have time to read the whole report, at least read the twelve-page Executive Summary. Among other things, it notes that Canada ranks very highly, internationally, on science engagement, highly on science knowledge and attitude to science, but less highly on the production of university graduates with science-related degrees.

An interesting recent development, discussed at a pre-conference meeting, is the creation of STEM "ecosystems" (STEM is an acronym for science, technology, engineering, and mathematics). A STEM ecosystem is a local partnership of organizations which provide formal or informal learning opportunities, especially for young people. In the last two years, over forty such partnerships have been created in the U.S. Vancouver has applied to be the first such ecosystem outside the U.S. There is much to be gained from partnership in public outreach (Percy 2012). For more information, see STEMEcosystems.org. Check it out! It has lessons for science culture everywhere.

Here in Canada, we are cautiously optimistic about the future of science in our country. A major report, "the Naylor report," was recently released by the federal goverment (Advisory Panel 2017); see References for the URL. David Naylor, who chaired the report panel, is an eminent medical scientist and former president of my university. Canada actually has a Minister of Science who is a scientist, and a Minister of Health who is a doctor (and a Minister of Transport who was an astronaut, and a Cabinet which is half women!).

Professional and amateur scientists can support and enhance science, and science culture, through EPO. Professional scientists have an *obligation* to do so—to communicate the nature, importance, and excitement of their work to the public—because, for most of us, our salaries and research costs are paid by the taxpayer. For amateur scientists such as AAVSO observers, the motivation can be to support science, or simply to convey their passion to the public.

EPO comes in many forms: illustrated presentations, hands-on demonstrations, star parties, sidewalk astronomy, Boy Scout and Girl Scout badge workshops, school visits, observatory tours, and so forth.

If you have the opportunity to choose your EPO audience, don't just "preach to the converted." Seek out new audiences, large audiences, and especially underserved audiences. I'm currently doing a lot of school visits, but presentations to teachers are even higher-impact. I give presentations to later-life learners, to residents of retirement homes and even nursing homes—a growing demographic of taxpayers/voters who are interested in and supportive of astronomy, and of science in general. I give presentations in public libraries, because that gets me and astronomy out into the many communities across Toronto. I give presentations to school and university science and astronomy clubs—the scientists of the future. At the same time, I and my colleagues are investigating and joining partnerships that will connect us to underserved populations, such as inner-city youth, immigrants, and Aboriginal communities.

How to do it? Details are in the three papers referred to above; they are all available on ADS or on my outreach webpage http://www.astro.utoronto.ca/~percy/EPOindex.htm I have also summarized them on one page which you can find at:

http://www.astro.utoronto.ca/~percy/STEMoutreach.pdf

In short: you must decide whether your objective is to educate, inform, entertain, engage, inspire, recruit, fundraise, or just "sell your subject." Always consider the nature and needs of your audience. If your objective is to change the views of people with deep-seated misconceptions (such as the cause of the seasons), or deep-seated beliefs (such as young-Earth creationism), then special strategies are needed.

Then you have to decide what content, visuals, and demonstrations to include. Don't try to give a full course of astronomy in one hour. Just select highlights. Remember that you have to *engage* the audience, and leave a good impression of astronomy and astronomers.

Audience engagement will depend also on your delivery skills. Plan, organize, and rehearse. Be clear, concise, jargon-free, and enthusiastic. Be audible, and make your visuals visible. Leave lots of time for questions and answers.

Afterwards, reflect on your experience, and how it could be improved. In some outreach settings, a short, simple feedback questionnaire can be useful. If you have had success, make it known to your colleagues, and encourage them to do likewise.

*JAAVSO* welcomes papers on various aspects of EPO: examples which are unusually novel, efficient, or effective, especially if they are suited to new or underserved audiences. Papers which report on formal research on EPO are also welcome. For examples, go to the *JAAVSO* search site https://www.aavso.org/apps/jaavso/search/ and choose the category "education and outreach" box to search. You will find 78 results!

## References

Advisory Panel for the Review of Federal Support for Fundamental Science. 2017, *Investing in Canada's Future: Strengthening the Foundations of Canadian Research* (www.sciencereview.ca).

Council of Canadian Academies. 2014, *Science Culture: Where Canada Stands* (www.scienceadvice.ca/en/assessments/completed/science-culture.aspx).

Percy, J. R. 2002, *J. Roy. Astron. Soc. Canada*, **96**, 196.

Percy, J. R. 2012, *J. Roy. Astron. Soc. Canada*, **106**, 240.

Percy, J. R. 2014, *J. Roy. Astron. Soc. Canada*, **108**, 132.

# Photometric Analysis of the Solar Type, Totally Eclipsing, Southern, Near Critical Contact Binary, CW Sculptoris

**Ronald G. Samec**
**Cody L. Norris**
*Astronomy Group, Department of Natural Science, Emmanuel College, 181 Springs Street, P.O. Box 129, Franklin Springs, GA 30639; ronaldsamec@gmail.com; s.cln@ec.edu*

**Bob L. Hill**
*Astronomy Program, Department of Chemistry and Physics, Bob Jones University, 1700 Wade Hampton Boulevard, Greenville, SC 29614*

**Walter Van Hamme**
*Physics Department, Florida International University, 11200 SW 8th Street, Miami, FL 33199*

**Danny R. Faulkner**
*Johnson Observatory, 1414 Bur Oak Court, Hebron, KY 41048*

*Received October 31, 2016; revised December 5, 2016; accepted March 8, 2017*

**Abstract** CW Sculptoris is a solar type ($T_1 \sim 5750$ K) eclipsing binary. It was observed in October and November 2014 at Cerro Tololo InterAmerican Observatory in remote mode with the 0.6-m SARA South reflector. Three times of minimum light were calculated from our present observations, one secondary and two primary eclipses. In addition, six observations at minima were determined from archived All Sky Automated Survey Data. An increasing period was determined from all available times of minimum light with a $1.14 \pm 0.16 \times 10^{-10} \times E^2$ quadratic term. A $BVR_cI_c$ simultaneous Wilson-Devinney Program solution reveals that the system has a mass ratio of ~0.44, and a component temperature difference of ~200 K. The Roche Lobe fill-out is only 3%. This may indicate that the system has recently come into contact. The inclination is ~84°. An eclipse duration of 19.5 minutes was determined for the primary eclipse.

## 1. Introduction

This paper represents the first precision and multicolor photometric study of CW Sculptoris, an interesting EW Southern, solar-type eclipsing binary.

## 2. History and observations

The variable, GSC 7517 0234, was observed by the All Sky Automated Survey (ASAS 232801-3359.8.; Pojmański 2002). In "Reports on New Discoveries" (Otero *et al.* 2004; http://www.astrouw.edu.pl/~gp/asas), it was designated as an EW binary, with magnitude range 12.13–12.87 (V) with the following ephemeris:

$$JD = 2452940.676 + 0.385588\,d \qquad (1)$$

The ASAS data are plotted in Figure 1, phased with the period above. Six "times of low light" were determined from the ASAS plots by taking points of low light near the primary and secondary minima:

HJD Min I = 2452177.603, 2452466.793, 2454404.752,
HJD Min II = 2453647.652, 2454669.843, 2455101.701.

The variable was included in the "Automated Variable Star Classification" using *The Northern Sky Variability Survey* and classified as an EW type (Hoffman *et al.* 2009).

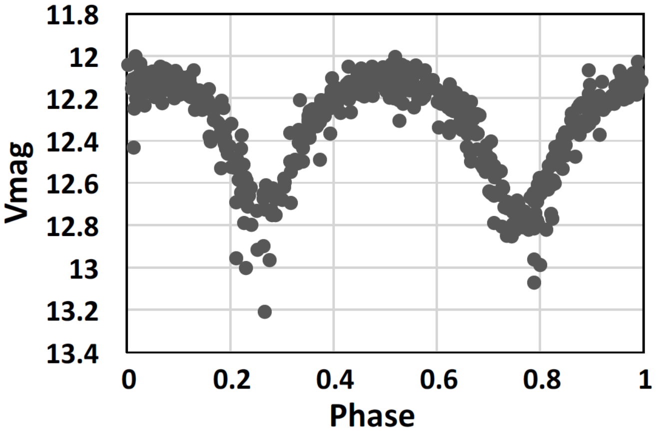

Figure 1. CW Scl phase plot from ASAS data (Pojmański 2002).

CW Scl was included in the "80th Name List of Variable Stars" (Kazarovets *et al.* 2013).

This system was observed as a part of our student/professional collaborative studies of interacting binaries from data taken from SARA observations. The observations were taken by Samec, Faulkner, Hill, and Van Hamme. Reduction and analyses were mostly done by Samec and Norris. The Observations were taken with the Southeastern Association for Research in Astronomy (SARA South) telescope at Cerro Tololo InterAmerican Observatory (CTIO) in remote mode. The 0.6-meter F/11 reflector was used on four nights, 9, 10, 19 October, and 15 November 2014 with the ARC Camera

Table 1. Information on the stars used in this study.

| *Star* | *Name* | *R.A. (2000)*<br>*h m s* | *Dec. (2000)*<br>*° ′ ″* | *V* | *J–K* |
|---|---|---|---|---|---|
| V | SW Scl<br>3UC113-502395<br>GSC 07517-00234 | 23 28 01.095 | –33 59 51.75[1,2] | 12.28 | 0.40 |
| C | GSC 7517 0304<br>3UC112-498808 | 23 27 47.540 | –34 05 51.67[1] | 13.26 | 0.46 |
| K (Check) | GSC 7517 0049<br>3UC112-498812 | 23 27 56.625 | –34 02 19.52[1] | 13.24 | 0.32 |

*[1] UCAC3 (USNO 2012). [2] USNO CCD Astrograph Catalog (Zacharias et al. 2012).*

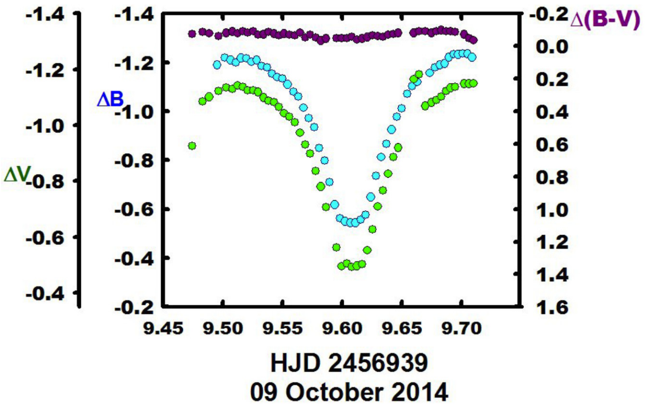

Figure 2a. CW Scl. B,V delta magnitudes and color curves taken on 9 October 2014.

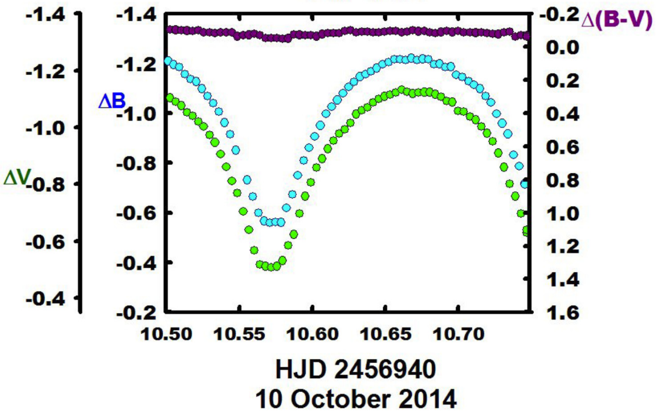

Figure 2b. CW Scl. B,V delta magnitudes and color curves taken on 10 October 2014.

cooled to –110 C using $BVR_cI_c$ Johnson/Cousins standard filters. Figures 2a and 2b give sample nightly curves in B, V delta magnitude and color magnitudes as a function of phase plots in the sense of V–C from 2014, October 9 and 10, respectively.

## 3. Positions and finding chart

The finding chart, given here for future observers, is shown as Figure 3. The coordinates and magnitudes of the variable star, comparison star, and check star are given in Table 1. The C–K values stayed constant throughout the observing run with a nightly precision of V = 6–7 mmag. Exposure times varied from 100–120s in B, 50–75s in V, and 40–60s in $R_c$ and $I_c$.

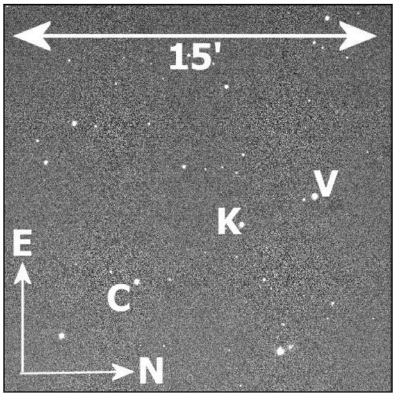

Figure 3. CW Scl finding chart. Variable (V), Comparison (C), and Check (K).

## 4. Period study

Three times of minimum light were calculated from our present observations, one secondary, and two primary eclipses:

$$\text{HJD Min I} = 2456939.60799 \pm 0.0002,$$
$$2456976.62450 \pm 0.0002$$
$$\text{HJD Min II} = 2456940.57227 \pm 0.0006.$$

In addition, six observations at minima were determined from archived All Sky Automated Survey data:

HJD Min I = 2452177.603, 2452466.793, 2454404.752,
HJD Min II = 2453647.652, 2454669.843, 2455101.701.

The following linear and quadratic ephemerides were determined from all available times of minimum light:

$$\text{JD Hel Min I} = 2456976.6241 \pm 0.0005\text{ d} + 0.38558774 \pm 0.00000008 \times E \quad (2)$$

$$\text{JD Hel Min I} = 2456976.6246 \pm 0.0003\text{ d} + 0.38558897 \pm 0.0002 \times E + 0.000000000114 \pm 0.000000000016 \times E2. \quad (3)$$

The O–C curve shown in Figure 4 is a smoothly increasing quadratic over the course of 13.3 years and nearly 13,000 orbits. The table of O–C residuals, both linear and quadratic calculations, are given in Table 2. In a conservative scenario, the period is increasing so the mass ratio is becoming more disparate, where the more massive component is the gainer. According to the light curve solution the more massive component is presently 2.6 times that of the less massive one. The ephemeris yields a $\dot{P} = 3.03 \times 10^{-8}$ d / yr or a mass exchange rate of

$$\frac{dM}{dt} = \frac{\dot{P} M_1 M_2}{3P (M_1 - M_2)} = \frac{1.75 \times 10^{-8} M_\odot}{d.} \qquad (4)$$

It is commonly thought that the more massive component steadily absorbs the secondary during normal evolution. However, this short interval of increasing period in a solar type binary may be overcome by a secular period decrease due to magnetic braking. Alternatively, the curve seen in the O-C diagram may be a part of a sinusoidal oscillation due to a third body. More timings over a decade or more are needed to determine the actual nature of the current period change.

## 5. Light curves and temperature determination

The light curves were phased using Equation 2. These are given as Figures 5a and 5b. A table of light curve characteristics averaged at quadratures is given in Table 3. Photometry from the 2MASS All-Sky Catalog of Point Sources (2MASS; Skrutskie *et al.* 2006) gives J–K = 0.40. This is G5V, T ~ 5750 K (Cox 2000).

We used this value for the primary component in our light curve solution. The curve is of 0.8% to 1.0% precision in $BVR_cI_c$. The amplitudes of the light curves are 0.6–0.7 in magnitude from $I_c$ to B. The O'Connell effect (magnitude difference in the maxima), classically thought of as an indicator of spot activity, is only 0.005–0.020 magnitude in all filters, and the Wilson-Devinney program (WD; Wilson and Devinney 1971) needed no spots to solve the light curves. But night-to-night variations are occurring as seen in the light curves. The difference between the primary and secondary minima is only 0.03–0.04 magnitude, indicating a high degree of physical and thermal contact. The WD solution indicates that the system is of W-type (the more massive star is cooler), but night-to-night variations show that the minima may be essentially equal. We believe that rapidly varying spots are inducing this complication. The indications are that this is an active contact binary.

## 6. Synthetic light curve solution

The B,V,$R_c$, and $I_c$ curves were carefully pre-modeled with BINARY MAKER 3.0 (Bradstreet and Steelman 2002) fits in all filter bands. The parameters were then averaged and input into a four-color simultaneous light curve calculation using the Wilson code (Wilson and Devinney 1971; Wilson 1990, 1994, 2001, 2004; Van Hamme and Wilson 1998; Van Hamme and Wilson 2003). These fits were all contact binaries, so the solution was computed in Mode 3 (the contact mode). Circular and gravitationally locked orbits are assumed. Convective parameters, g = 0.32, (Lucy 1967), A = 0.5 (Ruciński 1969), were used. Since the eclipses were total, no q-search was needed to have fair results (Terrell and Wilson 2005). However, the referee wisely noted since there had been no previous determinations or observations that one should be conducted. Because of the total eclipse we ran a limited q-search from 0.2 to 1.0. It is shown in Figure 6. The mass ratio minimized at q ~ 0.44. Opening up the q-value along with all the other parameters, we determined a final solution. Third light was also tested, but only yielded both low order, positive and negative values, so it was abandoned. A geometrical representation of the system is given in Figures 7a, b, c, and d at quadratures so that the reader may visualize the configuration and relative size of the stars as compared to the orbit. The synthetic light curve solution is given in Table 4. The normalized curves overlaid by our light curve solutions are shown as Figures 8a and 8b.

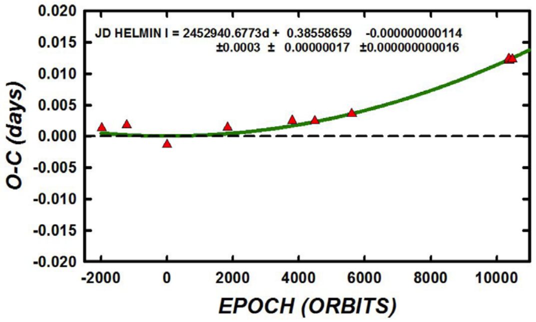

Figure 4. CW Scl. Quadratic O–C residuals from the period study.

## 7. Conclusion

CW Scl is a moderate period, P = 0. 38558897 (8) d W UMa eclipsing binary. The thirteen-year orbital study reveals an increasing quadratic ephemeris, which indicates that the binary's mass ratio is steadily becoming more extreme. 2MASS photometry gives a temperature for the primary component of ~5750 K for this G5V type variable. The Wilson-Devinney Program solution gives a mass ratio of ~0.4, and a component temperature difference of ~200 K. The system is probably magnetically active and the curve's night-to-night variation is on the order of V ~ 0.05 magnitude, as easily seen in the eclipse curve. The Roche Lobe fill-out is only 3% for this near critical contact binary. The inclination is 84° so that it is totally eclipsing, with an eclipse duration of ~19.5 minutes. The W UMa binary is of W-type (the less massive component is slightly hotter). This is the usual case for shallow contact binaries. It is thought to be due to the prevalence of spots on the larger component.

Further eclipse timings are need to affirm the orbital evolution found here. We finally note that radial velocity curves are needed to obtain absolute (not relative) system parameters.

## 8. Acknowledgements

We wish to thank the Southeastern Association for Research in Astronomy for allocation of observing time, and the Department of Natural Science, Emmanuel College for encouraging us to continue this undergraduate research.

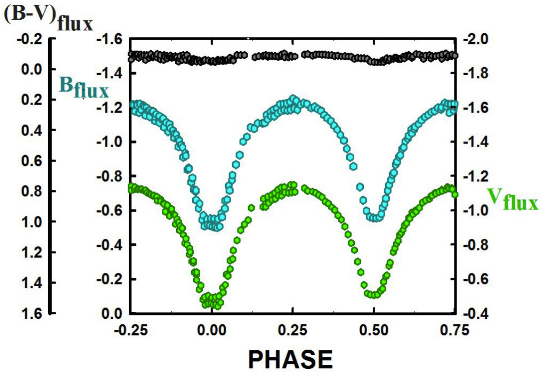

Figure 5a. CW Scl. B,V delta magnitude and color magnitudes vs. phase plots in the sense of V–C.

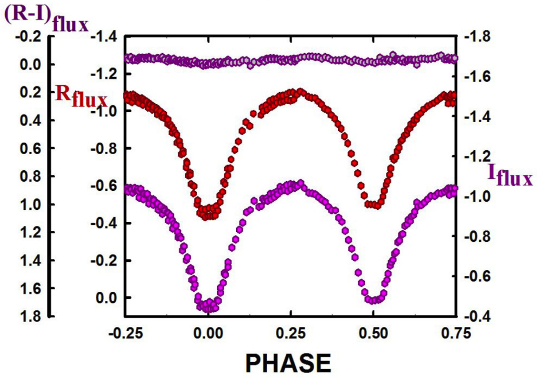

Figure 5b. CW Scl. $R_c$,Ic delta magnitude and color magnitudes vs. phase plots in the sense of V–C.

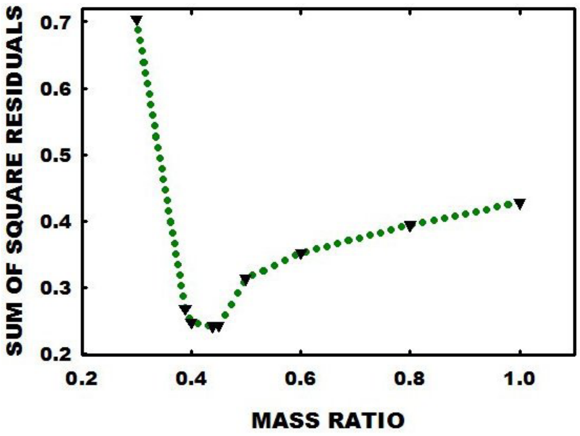

Figure 6. Q-search for CW Scl. The search minimizes at q ~ 0.44.

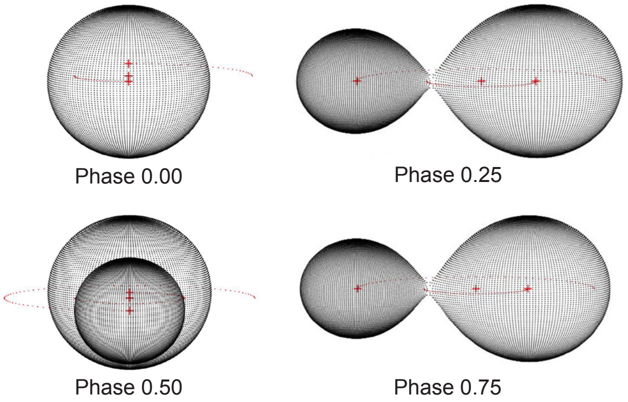

Figure 7. a: Roche Lobe surfaces from our BVRI solution, phase 0.00 (the primary eclipse). b: Roche Lobe surfaces from our BVRI solution, phase 0.25. c: Roche Lobe surfaces from our BVRI solution, phase 0.50. d: Roche Lobe surfaces from our BVRI solution, phase 0.75.

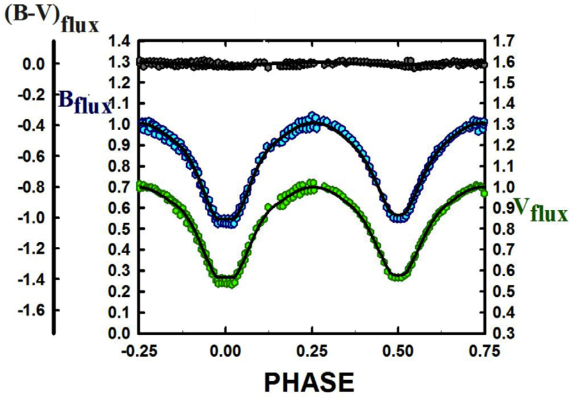

Figure 8a. B,V synthetic light curve solutions overlaying the normalized flux curves.

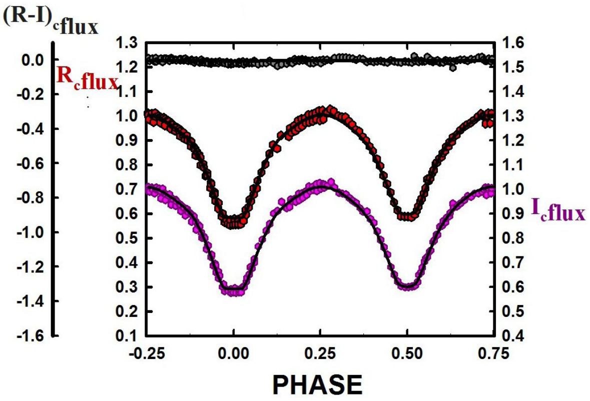

Figure 8b. Rc,Ic synthetic light curve solutions overlaying the normalized flux curves.

## References

Bradstreet, D. H., and Steelman, D. P. 2002, *Bull. Amer. Astron. Soc.*, **34**, 1224.

Cox, A. N., ed. 2000, *Allen's Astrophysical Quantities*, 4th ed., Springer, New York.

Hoffman, D. I., Harrison, T. E., and McNamara, B. J. A. 2009, *Astron. J.*, **138**, 466.

Kazarovets, E. V., Samus, N. N., Durlevich, O. V., Kireeva, N. N., and Pastukhova, E. N., 2013, *Inf. Bull. Var. Stars*, No. 6052, 1.

Lucy, L. B. 1967, *Z. Astrophys.*, **65**, 89.

Otero, S. A., Greaves, J., Wils, P., and Pojmański, G. 2004, *Inf. Bull. Var. Stars*, No. 5600, 4.

Pojmański, G. 2002, *Acta Astron.*, **52**, 397.

Ruciński, S. M. 1969, *Acta Astron.*, **19**, 245.

Skrutskie, M. F., *et al.* 2006, *Astron. J.*, **131**, 1163.

Terrell, D., and Wilson, R. E. 2005, *Astrophys. Space Sci.*, **296**, 221.

U.S. Naval Observatory. 2012, UCAC-3 (http://www.usno.navy.mil/USNO/astrometry/optical-IR-prod/ucac). [VizieR On-line Data Catalog: I/315]

Van Hamme, W. V., and Wilson, R. E. 1998, *Bull. Amer. Astron. Soc.*, **30**, 1402.

Van Hamme, W., and Wilson, R. E. 2003, in *GAIA Spectroscopy, Science and Technology*, ed. U. Munari, ASP Conf. Ser. 298, Astronomical Society of the Pacific, San Francisco, 323.

Wilson, R. E. 1990, *Astrophys. J.*, **356**, 613.

Wilson, R. E. 1994, *Publ. Astron. Soc. Pacific*, **106**, 921.

Wilson, R. E. 2001, *Inf. Bull. Var. Stars*, No. 5076, 1.

Wilson, R. E. 2004, *New Astron. Rev.*, **48**, 695.

Wilson, R. E., and Devinney, E. J. 1971, *Astrophys. J.*, **166**, 605.

Zacharias, N., Finch, C. T., Girard, T. M., Henden, A., Bartlett, J. L., Monet, D. G., and Zacharias, M. I. 2012, *The Fourth U.S. Naval Observatory CCD Astrograph Catalog* (UCAC4), VizieR On-line Data Catalog (http://cdsarc.u-strasbg.fr/viz-bin/Cat?I/322).

Table 2. CW Scl observations ΔB, ΔV, ΔR, and ΔI, variable minus comparison star (Epoch 2400000+).

| *ΔB* | *HJD* *2456930+* | *ΔB* | *HJD* *2456930+* | *ΔB* | *HJD* *2456930+* | *ΔB* | *HJD* *2456930+* | *ΔB* | *HJD* *2456930+* |
|---|---|---|---|---|---|---|---|---|---|
| –1.187 | 9.4950 | –1.001 | 9.6455 | –1.138 | 10.5169 | –1.201 | 10.6523 | –1.059 | 46.5727 |
| –1.205 | 9.5014 | –1.029 | 9.6498 | –1.121 | 10.5208 | –1.226 | 10.6562 | –1.023 | 46.5797 |
| –1.217 | 9.5065 | –1.084 | 9.6542 | –1.095 | 10.5246 | –1.221 | 10.6601 | –0.971 | 46.5848 |
| –1.206 | 9.5108 | –1.076 | 9.6585 | –1.071 | 10.5285 | –1.219 | 10.6639 | –0.910 | 46.5908 |
| –1.215 | 9.5152 | –1.108 | 9.6628 | –1.040 | 10.5323 | –1.220 | 10.6678 | –0.837 | 46.5959 |
| –1.213 | 9.5195 | –1.156 | 9.6732 | –1.007 | 10.5362 | –1.218 | 10.6717 | –0.765 | 46.6002 |
| –1.188 | 9.5239 | –1.173 | 9.6775 | –0.959 | 10.5400 | –1.219 | 10.6756 | –0.721 | 46.6031 |
| –1.204 | 9.5282 | –1.187 | 9.6817 | –0.910 | 10.5439 | –1.221 | 10.6794 | –0.661 | 46.6060 |
| –1.181 | 9.5325 | –1.196 | 9.6856 | –0.856 | 10.5477 | –1.212 | 10.6833 | –0.612 | 46.6089 |
| –1.174 | 9.5368 | –1.218 | 9.6894 | –0.737 | 10.5555 | –1.199 | 10.6871 | –0.545 | 46.6130 |
| –1.143 | 9.5412 | –1.221 | 9.6933 | –0.659 | 10.5593 | –1.184 | 10.6910 | –0.508 | 46.6159 |
| –1.143 | 9.5455 | –1.223 | 9.6971 | –0.598 | 10.5632 | –1.178 | 10.6949 | –0.518 | 46.6196 |
| –1.128 | 9.5498 | –1.232 | 9.7010 | –0.563 | 10.5670 | –1.161 | 10.6987 | –0.512 | 46.6224 |
| –1.112 | 9.5541 | –1.251 | 9.7048 | –0.556 | 10.5709 | –1.150 | 10.7026 | –0.507 | 46.6254 |
| –1.079 | 9.5589 | –1.239 | 9.7087 | –0.555 | 10.5748 | –1.135 | 10.7070 | –0.504 | 46.6283 |
| –1.046 | 9.5632 | –0.580 | 9.8098 | –0.560 | 10.5787 | –1.114 | 10.7108 | –0.500 | 46.6312 |
| –1.017 | 9.5675 | –0.637 | 9.8137 | –0.617 | 10.5825 | –1.103 | 10.7147 | –0.507 | 46.6340 |
| –0.982 | 9.5718 | –0.715 | 9.8175 | –0.670 | 10.5864 | –1.066 | 10.7186 | –0.562 | 46.6370 |
| –0.934 | 9.5764 | –0.778 | 9.8214 | –0.748 | 10.5902 | –1.043 | 10.7224 | –0.611 | 46.6399 |
| –0.848 | 9.5807 | –0.820 | 9.8245 | –0.808 | 10.5941 | –1.006 | 10.7263 | –0.663 | 46.6428 |
| –0.790 | 9.5850 | –0.884 | 9.8284 | –0.867 | 10.5979 | –0.968 | 10.7301 | –0.717 | 46.6457 |
| –0.717 | 9.5893 | –0.922 | 9.8322 | –0.913 | 10.6018 | –0.918 | 10.7340 | –0.776 | 46.6486 |
| –0.640 | 9.5937 | –0.967 | 9.8361 | –0.958 | 10.6056 | –0.843 | 10.7378 | –1.108 | 46.6846 |
| –0.571 | 9.5980 | –1.018 | 9.8413 | –1.003 | 10.6095 | –0.787 | 10.7417 | –1.110 | 46.6875 |
| –0.549 | 9.6023 | –1.070 | 9.8451 | –1.034 | 10.6134 | –0.712 | 10.7456 | –1.130 | 46.6910 |
| –0.553 | 9.6067 | –1.072 | 9.8490 | –1.050 | 10.6172 | –1.169 | 46.5215 | –1.148 | 46.6949 |
| –0.552 | 9.6110 | –1.216 | 10.4847 | –1.087 | 10.6211 | –1.182 | 46.5266 | –1.148 | 46.6989 |
| –0.550 | 9.6153 | –1.226 | 10.4886 | –1.103 | 10.6250 | –1.178 | 46.5330 | –1.165 | 46.7028 |
| –0.583 | 9.6196 | –1.220 | 10.4924 | –1.126 | 10.6288 | –1.169 | 46.5381 | –1.178 | 46.7067 |
| –0.656 | 9.6239 | –1.196 | 10.4976 | –1.143 | 10.6327 | –1.154 | 46.5456 | –1.185 | 46.7106 |
| –0.743 | 9.6282 | –1.203 | 10.5015 | –1.157 | 10.6366 | –1.146 | 46.5507 | –1.182 | 46.7146 |
| –0.806 | 9.6326 | –1.191 | 10.5053 | –1.172 | 10.6404 | –1.122 | 46.5568 | –1.186 | 46.7185 |
| –0.867 | 9.6369 | –1.180 | 10.5092 | –1.180 | 10.6443 | –1.111 | 46.5620 | –1.194 | 46.7224 |
| –0.923 | 9.6412 | –1.156 | 10.5130 | –1.197 | 10.6482 | –1.085 | 46.5676 | –1.186 | 46.7263 |

*Table continued on following pages*

Table 2. CW Scl observations ΔB, ΔV, ΔR, and ΔI, variable minus comparison star (Epoch 2400000+), cont.

| *ΔV* | *HJD* 2456930+ | *ΔV* | *HJD* 2456930+ | *ΔV* | *HJD* 2456930+ | *ΔV* | *HJD* 2456930+ | *ΔV* | *HJD* 2456930+ |
|---|---|---|---|---|---|---|---|---|---|
| –1.084 | 9.4830 | –0.766 | 9.6339 | –1.040 | 10.5181 | –1.087 | 10.6416 | –0.921 | 46.5813 |
| –1.101 | 9.4884 | –0.826 | 9.6383 | –1.020 | 10.5220 | –1.100 | 10.6455 | –0.885 | 46.5864 |
| –1.121 | 9.4962 | –0.886 | 9.6426 | –1.002 | 10.5258 | –1.108 | 10.6494 | –0.809 | 46.5923 |
| –1.135 | 9.5028 | –0.919 | 9.6469 | –0.973 | 10.5297 | –1.114 | 10.6535 | –0.744 | 46.5974 |
| –1.130 | 9.5079 | –0.944 | 9.6512 | –0.946 | 10.5335 | –1.122 | 10.6574 | –0.704 | 46.6010 |
| –1.141 | 9.5122 | –1.014 | 9.6555 | –0.906 | 10.5374 | –1.131 | 10.6613 | –0.639 | 46.6039 |
| –1.136 | 9.5166 | –1.068 | 9.6694 | –0.860 | 10.5412 | –1.124 | 10.6651 | –0.595 | 46.6068 |
| –1.125 | 9.5209 | –1.081 | 9.6746 | –0.810 | 10.5451 | –1.118 | 10.6690 | –0.541 | 46.6097 |
| –1.125 | 9.5252 | –1.090 | 9.6789 | –0.769 | 10.5489 | –1.122 | 10.6729 | –0.481 | 46.6139 |
| –1.118 | 9.5296 | –1.102 | 9.6829 | –0.703 | 10.5528 | –1.123 | 10.6768 | –0.450 | 46.6167 |
| –1.098 | 9.5339 | –1.121 | 9.6868 | –0.640 | 10.5567 | –1.123 | 10.6806 | –0.458 | 46.6204 |
| –1.087 | 9.5382 | –1.133 | 9.6906 | –0.567 | 10.5605 | –1.116 | 10.6845 | –0.459 | 46.6233 |
| –1.082 | 9.5426 | –1.137 | 9.6945 | –0.518 | 10.5644 | –1.106 | 10.6883 | –0.451 | 46.6262 |
| –1.064 | 9.5469 | –1.148 | 9.7022 | –0.511 | 10.5682 | –1.092 | 10.6922 | –0.451 | 46.6291 |
| –1.043 | 9.5512 | –1.148 | 9.7060 | –0.508 | 10.5721 | –1.088 | 10.6961 | –0.442 | 46.6320 |
| –1.030 | 9.5555 | –0.543 | 9.8110 | –0.511 | 10.5760 | –1.057 | 10.6999 | –0.464 | 46.6349 |
| –1.009 | 9.5602 | –0.615 | 9.8149 | –0.531 | 10.5799 | –1.054 | 10.7038 | –0.522 | 46.6379 |
| –0.973 | 9.5645 | –0.678 | 9.8187 | –0.585 | 10.5837 | –1.037 | 10.7082 | –0.567 | 46.6408 |
| –0.931 | 9.5689 | –0.779 | 9.8257 | –0.623 | 10.5876 | –1.026 | 10.7121 | –0.618 | 46.6436 |
| –0.897 | 9.5732 | –0.824 | 9.8296 | –0.697 | 10.5914 | –1.003 | 10.7159 | –0.660 | 46.6465 |
| –0.835 | 9.5777 | –0.869 | 9.8334 | –0.757 | 10.5953 | –0.979 | 10.7198 | –0.718 | 46.6494 |
| –0.780 | 9.5821 | –0.913 | 9.8373 | –0.806 | 10.5991 | –0.951 | 10.7236 | –1.022 | 46.6855 |
| –0.707 | 9.5864 | –0.958 | 9.8425 | –0.858 | 10.6030 | –0.909 | 10.7275 | –1.021 | 46.6884 |
| –0.562 | 9.5951 | –0.986 | 9.8463 | –0.889 | 10.6068 | –0.859 | 10.7313 | –1.044 | 46.6921 |
| –0.495 | 9.5994 | –1.001 | 9.8502 | –0.924 | 10.6107 | –0.801 | 10.7352 | –1.062 | 46.6961 |
| –0.504 | 9.6037 | –1.129 | 10.4898 | –0.952 | 10.6146 | –0.757 | 10.7390 | –1.068 | 46.7000 |
| –0.493 | 9.6080 | –1.115 | 10.4936 | –0.978 | 10.6184 | –0.697 | 10.7429 | –1.087 | 46.7039 |
| –0.496 | 9.6123 | –1.110 | 10.4988 | –0.993 | 10.6223 | –0.629 | 10.7468 | –1.085 | 46.7078 |
| –0.502 | 9.6167 | –1.103 | 10.5027 | –1.014 | 10.6262 | –0.640 | 10.7468 | –1.104 | 46.7117 |
| –0.552 | 9.6210 | –1.090 | 10.5065 | –1.046 | 10.6301 | –1.092 | 46.5282 | –1.103 | 46.7157 |
| –0.627 | 9.6253 | –1.076 | 10.5104 | –1.059 | 10.6339 | –0.994 | 46.5692 | –1.105 | 46.7196 |
| –0.708 | 9.6296 | –1.053 | 10.5142 | –1.069 | 10.6378 | –0.969 | 46.5743 | –1.108 | 46.7236 |

| *ΔR* | *HJD* 2456930+ | *ΔR* | *HJD* 2456930+ | *ΔR* | *HJD* 2456930+ | *ΔR* | *HJD* 2456930+ | *ΔR* | *HJD* 2456930+ |
|---|---|---|---|---|---|---|---|---|---|
| –1.075 | 9.4996 | –0.692 | 9.6306 | –1.088 | 10.4829 | –0.785 | 10.6000 | –0.959 | 10.7168 |
| –1.077 | 9.5045 | –0.741 | 9.6349 | –1.105 | 10.4868 | –0.839 | 10.6039 | –0.929 | 10.7206 |
| –1.085 | 9.5089 | –0.791 | 9.6392 | –1.096 | 10.4907 | –0.867 | 10.6077 | –0.902 | 10.7245 |
| –1.080 | 9.5132 | –0.837 | 9.6435 | –1.076 | 10.4958 | –0.896 | 10.6116 | –0.873 | 10.7283 |
| –1.086 | 9.5175 | –0.893 | 9.6479 | –1.072 | 10.4997 | –0.929 | 10.6154 | –0.817 | 10.7322 |
| –1.072 | 9.5219 | –0.940 | 9.6522 | –1.070 | 10.5035 | –0.952 | 10.6193 | –0.773 | 10.7360 |
| –1.069 | 9.5262 | –0.919 | 9.6565 | –1.052 | 10.5074 | –0.976 | 10.6232 | –0.721 | 10.7399 |
| –1.068 | 9.5305 | –0.986 | 9.6608 | –1.036 | 10.5113 | –0.988 | 10.6271 | –0.670 | 10.7438 |
| –1.056 | 9.5348 | –1.019 | 9.6712 | –1.013 | 10.5151 | –1.009 | 10.6309 | –0.599 | 10.7477 |
| –1.042 | 9.5392 | –1.031 | 9.6755 | –1.005 | 10.5190 | –1.024 | 10.6348 | –1.040 | 46.5191 |
| –1.027 | 9.5435 | –1.055 | 9.6798 | –0.979 | 10.5228 | –1.035 | 10.6386 | –1.042 | 46.5242 |
| –1.015 | 9.5478 | –1.063 | 9.6838 | –0.961 | 10.5267 | –1.044 | 10.6425 | –1.060 | 46.5305 |
| –0.988 | 9.5522 | –1.065 | 9.6876 | –0.931 | 10.5305 | –1.056 | 10.6464 | –1.047 | 46.5357 |
| –0.963 | 9.5569 | –1.081 | 9.6915 | –0.906 | 10.5344 | –1.071 | 10.6506 | –1.045 | 46.5432 |
| –0.954 | 9.5612 | –1.083 | 9.6953 | –0.865 | 10.5383 | –1.085 | 10.6544 | –1.032 | 46.5483 |
| –0.917 | 9.5655 | –1.089 | 9.6992 | –0.827 | 10.5421 | –1.074 | 10.6583 | –1.019 | 46.5544 |
| –0.886 | 9.5698 | –1.099 | 9.7031 | –0.771 | 10.5460 | –1.088 | 10.6621 | –1.006 | 46.5595 |
| –0.838 | 9.5744 | –1.100 | 9.7069 | –0.721 | 10.5498 | –1.086 | 10.6660 | –0.982 | 46.5652 |
| –0.787 | 9.5787 | –1.090 | 9.7108 | –0.667 | 10.5537 | –1.088 | 10.6699 | –0.969 | 46.5703 |
| –0.729 | 9.5830 | –0.543 | 9.8119 | –0.601 | 10.5575 | –1.083 | 10.6738 | –0.932 | 46.5773 |
| –0.657 | 9.5874 | –0.607 | 9.8157 | –0.547 | 10.5614 | –1.089 | 10.6777 | –0.885 | 46.5824 |
| –0.598 | 9.5917 | –0.660 | 9.8196 | –0.501 | 10.5652 | –1.076 | 10.6815 | –0.831 | 46.5883 |
| –0.522 | 9.5960 | –0.750 | 9.8233 | –0.500 | 10.5691 | –1.067 | 10.6854 | –0.769 | 46.5935 |
| –0.476 | 9.6003 | –0.755 | 9.8266 | –0.498 | 10.5730 | –1.062 | 10.6892 | –0.698 | 46.5988 |
| –0.473 | 9.6047 | –0.803 | 9.8304 | –0.493 | 10.5769 | –1.051 | 10.6931 | –0.655 | 46.6017 |
| –0.482 | 9.6090 | –0.846 | 9.8343 | –0.514 | 10.5807 | –1.035 | 10.6969 | –0.610 | 46.6046 |
| –0.478 | 9.6133 | –0.877 | 9.8395 | –0.573 | 10.5846 | –1.022 | 10.7008 | –0.558 | 46.6075 |
| –0.491 | 9.6176 | –0.908 | 9.8433 | –0.625 | 10.5884 | –1.005 | 10.7052 | –0.500 | 46.6116 |
| –0.549 | 9.6219 | –0.932 | 9.8472 | –0.694 | 10.5923 | –0.999 | 10.7091 | –0.455 | 46.6145 |
| –0.620 | 9.6263 | –0.954 | 9.8510 | –0.739 | 10.5962 | –0.985 | 10.7129 | –0.445 | 46.6182 |

*Table continued on next page*

Table 2. CW Scl observations ΔB, ΔV, ΔR, and ΔI, variable minus comparison star (Epoch 2400000+), cont.

| Δ*R* | *HJD* *2456930+* | Δ*R* | *HJD* *2456930+* | Δ*R* | *HJD* *2456930+* | Δ*R* | *HJD* *2456930+* | Δ*R* | *HJD* *2456930+* |
|---|---|---|---|---|---|---|---|---|---|
| –0.430 | 46.6211 | –0.466 | 46.6357 | –0.694 | 46.6503 | –1.029 | 46.7009 | –1.055 | 46.7206 |
| –0.436 | 46.6240 | –0.513 | 46.6386 | –0.979 | 46.6861 | –1.044 | 46.7048 | –1.061 | 46.7245 |
| –0.438 | 46.6269 | –0.567 | 46.6414 | –0.999 | 46.6891 | –1.046 | 46.7087 | | |
| –0.438 | 46.6298 | –0.609 | 46.6443 | –1.007 | 46.6931 | –1.052 | 46.7127 | | |
| –0.441 | 46.6327 | –0.655 | 46.6472 | –1.020 | 46.6970 | –1.059 | 46.7166 | | |

| Δ*I* | *HJD* *2456930+* | Δ*I* | *HJD* *2456930+* | Δ*I* | *HJD* *2456930+* | Δ*I* | *HJD* *2456930+* | Δ*I* | *HJD* *2456930+* |
|---|---|---|---|---|---|---|---|---|---|
| –1.033 | 9.5003 | –0.921 | 9.6529 | –0.949 | 10.5197 | –1.023 | 10.6551 | –0.879 | 46.5783 |
| –1.041 | 9.5053 | –0.933 | 9.6573 | –0.931 | 10.5235 | –1.041 | 10.6590 | –0.839 | 46.5834 |
| –1.040 | 9.5096 | –0.978 | 9.6616 | –0.930 | 10.5274 | –1.039 | 10.6628 | –0.795 | 46.5893 |
| –1.030 | 9.5139 | –0.989 | 9.6720 | –0.894 | 10.5313 | –1.041 | 10.6667 | –0.730 | 46.5945 |
| –1.034 | 9.5183 | –0.991 | 9.6763 | –0.873 | 10.5351 | –1.044 | 10.6706 | –0.681 | 46.5994 |
| –1.042 | 9.5226 | –1.014 | 9.6806 | –0.829 | 10.5390 | –1.042 | 10.6745 | –0.629 | 46.6023 |
| –1.027 | 9.5270 | –1.017 | 9.6845 | –0.783 | 10.5428 | –1.035 | 10.6784 | –0.583 | 46.6052 |
| –1.017 | 9.5313 | –1.025 | 9.6883 | –0.739 | 10.5467 | –1.037 | 10.6822 | –0.542 | 46.6081 |
| –1.007 | 9.5356 | –1.048 | 9.6922 | –0.696 | 10.5505 | –1.038 | 10.6861 | –0.481 | 46.6122 |
| –0.990 | 9.5400 | –1.044 | 9.6960 | –0.619 | 10.5544 | –1.012 | 10.6899 | –0.447 | 46.6151 |
| –0.986 | 9.5443 | –1.056 | 9.6999 | –0.568 | 10.5582 | –1.013 | 10.6938 | –0.451 | 46.6188 |
| –0.966 | 9.5486 | –1.062 | 9.7038 | –0.522 | 10.5621 | –0.990 | 10.6976 | –0.437 | 46.6216 |
| –0.946 | 9.5529 | –1.058 | 9.7076 | –0.486 | 10.5659 | –0.980 | 10.7015 | –0.438 | 46.6246 |
| –0.928 | 9.5576 | –0.485 | 9.8087 | –0.477 | 10.5698 | –0.965 | 10.7059 | –0.437 | 46.6275 |
| –0.915 | 9.5620 | –0.516 | 9.8126 | –0.480 | 10.5737 | –0.951 | 10.7098 | –0.441 | 46.6304 |
| –0.879 | 9.5663 | –0.583 | 9.8164 | –0.484 | 10.5776 | –0.941 | 10.7136 | –0.442 | 46.6332 |
| –0.856 | 9.5706 | –0.654 | 9.8203 | –0.493 | 10.5814 | –0.920 | 10.7175 | –0.479 | 46.6362 |
| –0.801 | 9.5751 | –0.683 | 9.8234 | –0.566 | 10.5853 | –0.905 | 10.7213 | –0.518 | 46.6391 |
| –0.750 | 9.5795 | –0.722 | 9.8273 | –0.615 | 10.5892 | –0.865 | 10.7252 | –0.568 | 46.6420 |
| –0.694 | 9.5838 | –0.780 | 9.8311 | –0.671 | 10.5930 | –0.823 | 10.7290 | –0.608 | 46.6449 |
| –0.628 | 9.5881 | –0.811 | 9.8350 | –0.714 | 10.5969 | –0.792 | 10.7329 | –0.646 | 46.6478 |
| –0.559 | 9.5925 | –0.860 | 9.8402 | –0.771 | 10.6007 | –0.751 | 10.7367 | –0.947 | 46.6838 |
| –0.500 | 9.5968 | –0.876 | 9.8440 | –0.810 | 10.6046 | –0.696 | 10.7406 | –0.952 | 46.6867 |
| –0.460 | 9.6011 | –0.908 | 9.8479 | –0.852 | 10.6084 | –0.641 | 10.7445 | –0.981 | 46.6899 |
| –0.462 | 9.6054 | –0.969 | 9.8517 | –0.883 | 10.6123 | –0.587 | 10.7484 | –0.977 | 46.6939 |
| –0.472 | 9.6098 | –1.055 | 10.4811 | –0.900 | 10.6161 | –1.008 | 46.5201 | –0.986 | 46.6978 |
| –0.460 | 9.6141 | –1.051 | 10.4837 | –0.924 | 10.6201 | –1.015 | 46.5252 | –0.996 | 46.7017 |
| –0.480 | 9.6184 | –1.067 | 10.4875 | –0.949 | 10.6239 | –1.024 | 46.5315 | –1.009 | 46.7056 |
| –0.544 | 9.6227 | –1.041 | 10.4914 | –0.956 | 10.6278 | –1.017 | 46.5367 | –1.026 | 46.7096 |
| –0.617 | 9.6270 | –1.019 | 10.4965 | –0.970 | 10.6316 | –0.993 | 46.5442 | –1.032 | 46.7135 |
| –0.670 | 9.6313 | –1.015 | 10.5004 | –0.985 | 10.6355 | –0.986 | 46.5493 | –1.027 | 46.7174 |
| –0.745 | 9.6357 | –1.011 | 10.5043 | –1.003 | 10.6393 | –0.964 | 46.5554 | –1.037 | 46.7214 |
| –0.784 | 9.6400 | –0.996 | 10.5081 | –1.002 | 10.6432 | –0.959 | 46.5605 | –1.043 | 46.7253 |
| –0.833 | 9.6443 | –0.982 | 10.5120 | –1.015 | 10.6471 | –0.934 | 46.5662 | | |
| –0.869 | 9.6486 | –0.972 | 10.5158 | –1.016 | 10.6513 | –0.912 | 46.5713 | | |

Table 3. Period Study Results, CW Scl.

| *No.* | *HJD 2400000+* | *Cycle* | *Linear Residual* | *Quadratic Residual* | *Weight* | *References* |
|---|---|---|---|---|---|---|
| 1 | 52177.6 | –12446.0 | 0.0037 | 0.0009 | 0.3 | ASAS 23801–3359.8 (ASAS 3) |
| 2 | 52466.79 | –11696.0 | 0.0034 | 0.0016 | 0.3 | ASAS 23801–3359.8 (ASAS 3) |
| 3 | 53647.65 | –8633.5 | –0.0005 | 0.0011 | 0.3 | ASAS 23801–3359.8 (ASAS 3) |
| 4 | 54404.75 | –6670.0 | –0.0017 | 0.0009 | 0.3 | ASAS 23801–3359.8 (ASAS 3) |
| 5 | 54669.84 | –5982.5 | –0.0025 | 0.0002 | 0.3 | ASAS 23801–3359.8 (ASAS 3) |
| 6 | 55101.7 | –4862.5 | –0.0027 | 0.0000 | 0.3 | ASAS 23801–3359.8 (ASAS 3) |
| 7 | 52940.68 | –10467.0 | –0.0012 | –0.0013 | 1 | Otero *et al.* 2004 |
| 8 | 56939.61 | –96.0 | 0.0003 | –0.0001 | 1 | Present Observations |
| 9 | 56940.57 | –93.5 | 0.0006 | 0.0002 | 1 | Present Observations |
| 10 | 56976.62 | 0.0 | 0.0004 | –0.0001 | 1 | Present Observations |

Table 4. Light curve characteristics.

| *Filter* | *Phase* | *Magnitude Min. I* | *Phase* | *Magnitude Max. II* |
|---|---|---|---|---|
| | 0.0 | | 0.25 | |
| B | | –0.526 ± 0.023 | | –1.204 ± 0.024 |
| V | | –0.466 ± 0.024 | | –1.123 ± 0.022 |
| R | | –0.458 ± 0.008 | | –1.076 ± 0.019 |
| I | | –0.451 ± 0.013 | | –1.034 ± 0.010 |

| *Filter* | *Phase* | *Magnitude Min. II* | *Phase* | *Magnitude Max. I* |
|---|---|---|---|---|
| | 0.50 | | 0.75 | |
| B | | –0.557 ± 0.002 | | –1.216 ± 0.019 |
| V | | –0.511 ± 0.002 | | –1.127 ± 0.015 |
| R | | –0.498 ± 0.003 | | –1.085 ± 0.018 |
| I | | –0.482 ± 0.018 | | –1.053 ± 0.010 |

| *Filter* | *Min. I – Max. I* | *Min. I – Min. II* |
|---|---|---|
| B | 0.69 ± 0.048 | 0.031 ± 0.026 |
| V | 0.66 ± 0.046 | 0.045 ± 0.025 |
| R | 0.63 ± 0.027 | 0.040 ± 0.011 |
| I | 0.60 ± 0.023 | 0.030 ± 0.031 |

| *Filter* | *Max. II – Max. I* |
|---|---|
| B | 0.012 ± 0.044 |
| V | 0.004 ± 0.037 |
| R | 0.009 ± 0.037 |
| I | 0.019 ± 0.020 |

Table 5. CW Scl Light curve solution.

| *Parameters* | *Values* |
|---|---|
| λB, λV, λR, λI (nm) | 440, 550, 640, 790 |
| xbol1,2 , ybol1,2 | 0.647 0.647 0.176 0.176 |
| $x_{1I,2I}$ , $y_{1I,2I}$ | 0.590 0.590 0.260 0.260 |
| $x_{1R,2R}$ , $y_{1R,2R}$ | 0.674 0.674 0.269 0.269 |
| $x_{1V,2V}$ , $y_{1V,2V}$ | 0.745 0.745 0.256 0.256 |
| $x_{1B,2B}$ , $y_{1B,2B}$ | 0.829 0.829 0.185 0.185 |
| $g_1$ , $g_2$ | 0.32, 0.32 |
| $A_1$ , $A_2$ | 0.5, 0.5 |
| Inclination (°) | 84.2 ± 0.3 |
| $T_1$, $T_2$ (K) | 5750, 5968 ± 9 |
| $\Omega_1$, $\Omega_2$ | 2.749 ± 0.005 |
| Pshift | 0.5 |
| q ($m_2$ / $m_1$) | 0.439 ± 0.004 |
| Fill-out (%) | 3 ± 1 |
| $L_1 / (L_1 + L_2)_I$ | 0.655 ± 0.002 |
| $L_1 / (L_1 + L_2)_R$ | 0.651 ± 0.002 |
| $L_1 / (L_1 + L_2)_V$ | 0.645 ± 0.002 |
| $L_1 / (L_1 + L_2)_B$ | 0.631 ± 0.002 |
| $HJD_o$ (days) | 2456976.6241 ± 0.00015 |
| Period (days) | 0.385578 ± 0.000002 |
| $r_1$, $r_2$ (pole) | 0.426 ± 0.001, 0.291 ± 0.002 |
| $r_1$, $r_2$ (side) | 0.454 ± 0.002, 0.304 ± 0.002 |
| $r_1$, $r_2$ (back) | 0.482 ± 0.002, 0.337 ± 0.004 |

*Errors are from WD full set standard deviations (formal errors). The temperature, $T_1$ is fixed from the 2MASS determination and may carry a 200–250 K error.*

# Photometric Analysis of Three ROTSE Contact Binary Systems

**Surjit S. Wadhwa**
*Astronomical Society of NSW, Sydney, NSW, Australia; surjitwadhwa@gmail.com*

*Received September 18, 2016; revised December 19, 2016; accepted December 21, 2016*

**Abstract** Ground-based photometry of three ROTSE contact binary systems was analyzed using the Wilson-Devinney method. One system with a very low mass ratio below q = 0.06 and one with high mass ratio with a complete eclipse and edge-on inclination were found and represent candidates for further study.

## 1. Introduction

The W Ursae Majoris (W UMa) group of short-period contact eclipsing binaries are important test beds for theories of stellar evolution. Numerous new contact systems have been discovered recently through the automated sky survey programs and dedicated amateur observing efforts. Quite a large percentage of the new discoveries remain largely un-analyzed even though data are of sufficient quality to yield at least basic physical information. In a previous paper published in this journal I have demonstrated how analysis of amateur observations of a contact binary star for which little other information is available can yield a satisfactory photometric solution (Wadhwa 2004). In this first paper I present photometric solution for three binary systems discovered by the The Robotic Optical Transient Search Experiment (ROTSE) that have had follow up ground-based observations published.

GSC 963-246 (R.A. $16^h\ 27^m\ 44.9^s$, Dec.+11° 03' 38" (2000)) was discovered by the ROTSE mission and catalogued as a contact system by Gettel *et al.* (2006). Ground-based dual-band (R and V) photometry was reported in 2007 (Blättler and Diethelm 2007). Preliminary analysis confirmed the contact binary nature of the system with the following basic elements: JD (min I, hel) = 2453898.3997 + 0.337043 × E; magnitude (R) variation of 0.41 mag. for the primary eclipse and 0.36 mag. for the secondary eclipse. The photometry data are available publically (http://ibvs.konkoly.hu/pub/ibvs/5701/5799-t4.txt). The R band data were analyzed to determine mass ratio and other parameters in the present study.

Ground-based observations of GSC 3034-299 (R.A. $14^h\ 05^m\ 08.985^s$, Dec. +38° 54' 18.74" (2000)) were reported in Blättler and Diethelm (2006). Preliminary analysis confirmed the contact binary nature of the system with the following basic elements: JD(min I, hel) = 2453382.6919 + 0.395010 × E; unfiltered (near R) yielded a magnitude range of 11.46–12.20 mag. (primary eclipse) and 11.46–12.13 mag. (secondary eclipse). The photometry data are available publically (http://ibvs.konkoly.hu/pub/ibvs/5601/5699-t10.txt). The data although unfiltered are reported to be near-red bandpass and were analyzed as R band data.

GSC 2587-1888 (R.A. $16^h\ 29^m\ 19.89^s$, Dec. +35° 40' 02.90" (2000)) is another ROTSE variable with ground-based photometry in both the R and V bands reported in 2007 (Blättler and Diethelm 2007). Preliminary analysis confirmed the contact binary nature of the system with the following basic elements: JD(min I, hel) = 2453877.4694 + 0.310726 × E; primary and secondary eclipses have a magnitude variation of 0.17 in the R band. The photometry data are available publically (http://ibvs.konkoly.hu/pub/ibvs/5701/5799-t2.txt). The R band data were analyzed in this study.

## 2. Light curve analysis

The mass ratio of a contact binary system is usually determined by radial velocity studies. The mass ratio is then used to determine other features of the system such as the inclination, degree of contact, and temperature variations. However, where radial velocity data are not available, under certain circumstances, such as when the system exhibits at least one total eclipse, a systematic search of the parameter space for various values of the mass ratio can be employed to determine the correct mass ratio for the system (Terrell and Wilson 2005). This is sometimes referred to as the grid search method and has previously been employed on many data sources, including data obtained through automated sky patrols (Wadhwa 2004, 2005).

As radial velocity data were not available for any of the systems analyzed in this paper, the grid search method as described in the above-referenced articles was employed. In addition, very few basic data are available for the systems and certain assumptions with respect to the temperature of the primary were required as outlined below. In each case the available data indicated a probable convective envelope, therefore gravity brightening was set at 0.32 and bolometric albedos were set at 0.5. Black body approximation was used for the stars' emergent flux and simple reflection treatment was applied. The maximum magnitude of the stars is not well known, therefore the photometric data were normalised to the mean magnitude between phases 0.24 and 0.26 in each case. This methodology has previously been applied to the analysis of All Sky Automated Survey and ground-based amateur observations (Wadhwa 2004, 2005).

## 3. Individual systems

### 3.1. GSC 963-246 = ROTSE1 J162744.97+110336.5, V1179 Her

The SIMBAD database gives a B–V value of 0.54 for the system leading to a calibrated temperature of 6100 K. The mass ratio search grid (Figure 1) demonstrated a nice clear minimum with the mass ratio at 0.14. Based on this, other parameters of the photometric solution are summarized in Table 1. As can be seen, the temperature of the secondary is similar to that of the primary, indicating good thermal equilibrium, however, it

Table 1. Photometric Solution for GSC 963-246.

| *Parameter* | *Value* |
|---|---|
| Mass Ratio (q) | 0.14 + 0.004 |
| T2 | 6122 K + 49 K |
| Potential | 2.021 + 0.01 |
| Inclination (i) | 78.15 + 1.4 |
| Fillout | 60.3% |

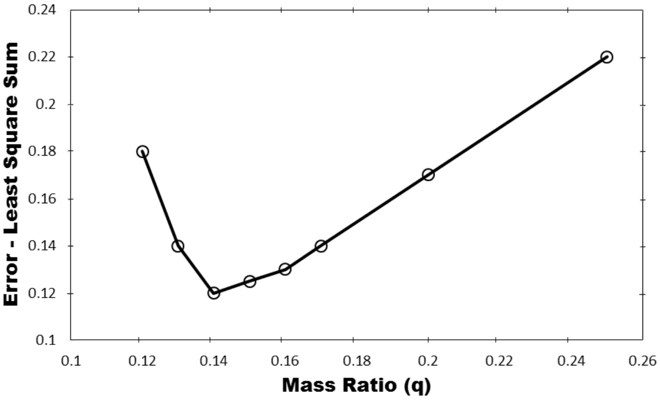

Figure 1. Mass ratio search grid for GSC 963-246. The best fit as indicated by the least sum of squares occurs at q = 0.14.

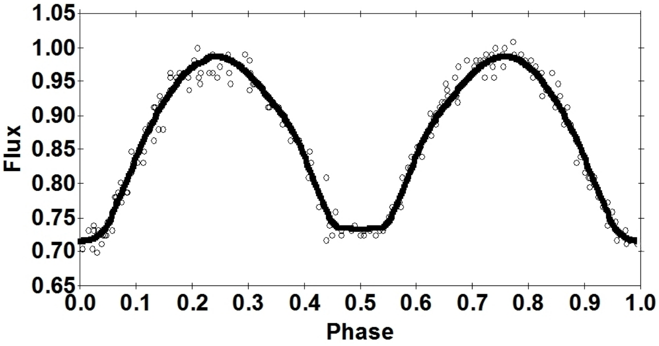

Figure 2. GSC 963-246 light curves. Solid line = fitted curve; Open circles = observed curve.

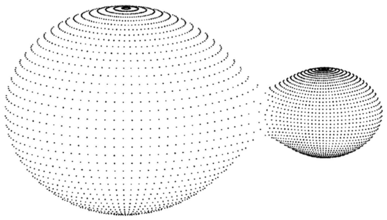

Figure 3. Three dimensional model of GSC 963-246.

Table 2. Basic photometric elements for GSC 3034-299.

| *Parameter* | *Value* |
|---|---|
| Mass Ratio (q) | 0.50 + 0.01 |
| T2 | 5664K + 25K |
| Potential | 2.813 + 0.02 |
| Inclination(i) | 90.00 |
| Fillout | 21.0% |

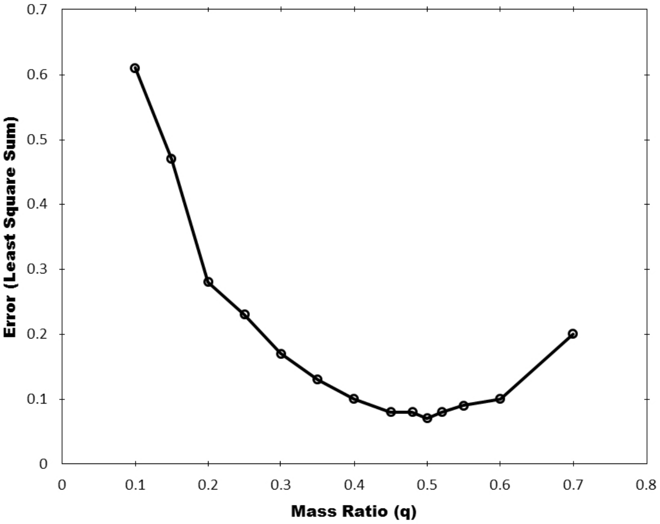

Figure 4. Mass ratio search grid for GSC 3034-299. There is a clear minimum at q = 0.5.

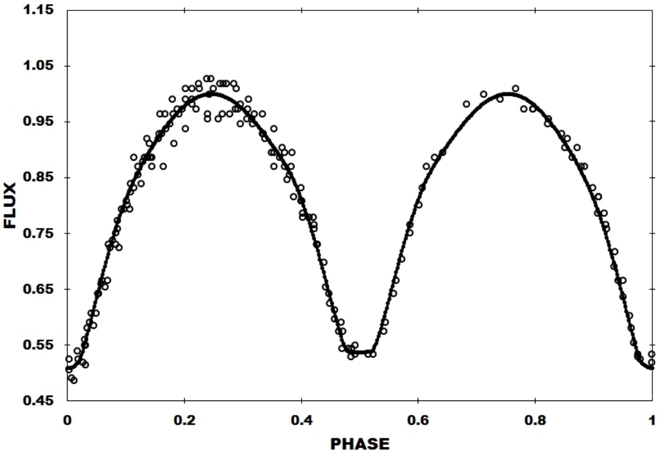

Figure 5. Fitted (solid line) and observed (open circles) light curves for GSC 3034-299.

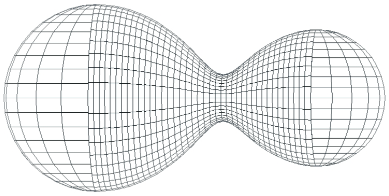

Figure 6: 3D representation of GSC 3034-299.

is somewhat difficult to classify the system as either A or W type. Based purely on the values of the photometric solution the system would be of W-Type. The fitted light curves are shown in Figure 2, while a three-dimensional representation (Bradstreet 1993) is shown in Figure 3.

### 3.2. GSC 3034-299 = ROTSE1 J140509.23+385417.9, GN CVn

This system has an effective temperature of 5660 K based on a B–V of 0.63 as per the SIMBAD database. The light curve has relatively deep minima, suggesting a higher mass ratio than usual for contact binary systems. The presence of a complete eclipse would suggest a high almost edge-on inclination. As with the previous example the grid search method was applied to search for the mass ratio of best fit. As illustrated in Figure 4 the system has a clearly defined minimum error at q = 0.5. The remainder of the photometric solution is summarized in Table 2, confirming an edge-on inclination and good thermal contact with no difference in the temperatures between the stars. Observed and fitted light curves are shown in Figure 5 while the three-dimensional representation (Bradstreet 1993) is shown in Figure 6.

Since the initial analysis of this system the author has become aware that the system had been analyzed previously by Samec *et al.* (2012). The 2012 analysis reached a very similar solution with a mass ratio of 0.48 with good thermal contact, high inclination of 89.6 degrees, and 24% fillout. The closeness of the two solutions adds further confidence that analysis of amateur observations can yield high quality and useful scientifically valid analysis.

### 3.3. GSC 2587-1888 = NSVS 7913634, TYC 2587-1888-1

GSC 2587-1888 is another ROTSE variable and is largely unstudied. The SIMBAD database yields a B–V of 0.48 corresponding to an effective temperature of 6393 K. Visual inspection of the light curve (Figure 7) clearly indicates a total eclipse. Prior to starting the mass ratio search grid manual light curve fitting was used to get an approximate starting point. During this process it became clear that the system most likely had a very low mass ratio, as all attempts to manually fit the light curves with q > 0.1 yielded non-physical systems. The automated differential corrections would also only lead to either very poorly fitting or non-physical systems when the mass ratio was greater than 0.1. Similarly very low mass ratios (q < 0.05) also yielded poorly fitting solutions, which is not surprising given that as calculated by Ruciński (1993) the maximum amplitude for systems with mid-range contact and mass ratios less than 0.05 would be less than 0.14 magnitude. Our system exhibits amplitude well in excess at 0.17 magnitude, which suggests a mass ratio above 0.05 but below 0.09.

A reasonable manual fit was made at the high end of this range at q = 0.09 and the other parameters adjusted to yield the best solution for this mass ratio. The mass ratio was then allowed to be an adjustable parameter and differential corrections iterations performed again. The mass ratio quickly drifted down with marked improvement in the fitting profile. The best fit (Figure 7, Table 3) was achieved with a possible record low mass ratio for a contact system of q = 0.059 with the secondary star considerably hotter than the primary. A three-dimensional representation (Bradstreet 1993) is shown in Figure 8.

Table 3. Basic photometric elements for GSC 2587-1888.

| *Parameters* | *Value* |
|---|---|
| T2 | 6727 K + 73 K |
| Inclination (i) | 66.23 + 1.13 |
| Potential | 1.815 + .01 |
| Mass Ratio (q) | 0.059 + .02 |
| Fillout | 19.15% |

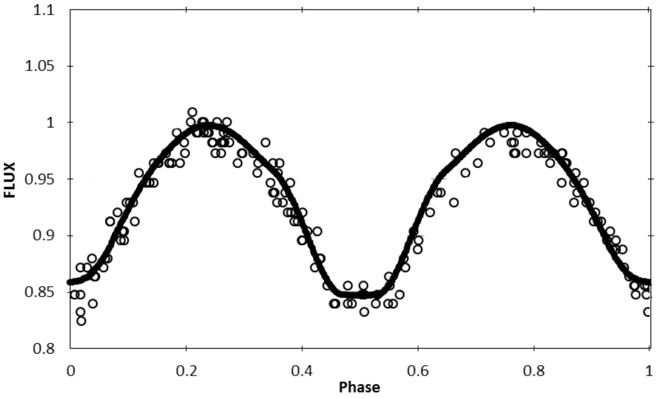

Figure 7. The best fit (solid line) and the observed (open circles) light curves for GSC 2587-1888.

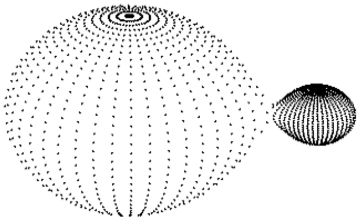

Figure 8. Three-dimensional representation of GSC 2587-1888 showing the extremely small secondary in shallow contact with its much larger primary.

The mass ratio of 0.059 is significantly smaller than the theoretical lower limit of 0.07 (Li and Zhang 2006). The theoretical limit, however, is valid for stars in good thermal equilibrium and with high degree of contact (> 70%). Our system is somewhat different, with a very shallow contact of 19% and poor thermal equilibrium. Although a very rare event it is possible that GSC 2587-1888 is a newly formed low mass contact system having only recently moved from the semi-detached to the contact phase. Unfortunately the confidence in the low mass ratio must be tempered as the analysis was performed on a small photometric sample with moderate error. However, the system clearly deserves a more thorough study.

## 4. Conclusion

An analysis of the ground-based photometry of three ROTSE variables has identified GSC 2587-1888 as a possible very low mass ration system which is in the early phase contact. The study again highlights the importance of analysis of all data regardless of whether they are professional or amateur in deepening our understanding of contact binary astronomy.

## 5. Acknowledgements

This research made use of the SIMBAD database, operated by the CDS at Strasbourg, France.

## References

Blättler, E., and Diethelm, R. 2006, *Inf. Bull. Var. Stars*, No. 5699, 1 (Report 13, Table 10).

Blättler, E., and Diethelm, R. 2007, *Inf. Bull. Var. Stars*, No. 5799, 1 (Report 1, Table 4; Report 4, Table 10).

Bradstreet, D. H. 1993, BINARY MAKER 2.0 light curve synthesis program, Contact Software, Norristown, PA.

Gettel, S. J., Geske, M. T., and McKay, T. A. 2006, *Astron. J.*, **131**, 621.

Li, L., and Zhang, F. 2006, *Mon. Not. Roy. Astron. Soc*, **369**, 2001.

Ruciński, S. M. 1993, *Publ. Astron. Soc. Pacific*, **105**, 1433.

Samec, R., Jaso, A., White, J., Faulkner, D. R., Blum, N., and Van Hamme, W. 2012, *ISRN Astron. Astrophys.*, 2012, article 972572.

Terrell, D., and Wilson, R. 2005, *Astrophys. Space Sci.*, **296**, 221.

Wadhwa, S. S. 2004, *J. Amer. Assoc. Var. Star Obs.*, **32**, 95.

Wadhwa, S. S. 2005, *Astrophys. Space Sci.*, **300**, 289.

# The VESPA Survey: 100 New Variable Stars Discovered in Two Years

**Ulisse Quadri**
*IAU station 565, Bassano Bresciano Astronomical Observatory; AAVSO; Unione Astrofili Italiani (UAI); Italian Supernovae Search Project (ISSP); Via S. Michele,4, Bassano Bresciano, Italy; info@ulisse.bs.it*

**Luca Strabla**
*IAU station 565, Bassano Bresciano Astronomical Observatory; Italian Supernovae Search Project (ISSP); Via Paolo VI, Palazzolo Sull'Oglio, Italy; lucapietro.strabla@fastwebnet.it*

**Roberto Girelli**
*IAU station 565, Bassano Bresciano Astronomical Observatory; Italian Supernovae Search Project (ISSP); Via G. Migliorati, Bassano Bresciano, Italy; ro.girelli@tiscali.it*

*Received September 27, 2016; revised November 18, 2016; accepted December 29, 2016*

**Abstract** We describe the VESPA project made at IAU station 565, Astronomical Observatory in Bassano Bresciano (BS), Italy. It is one photometric survey of the northern hemisphere which has the aim of discovering and investigating new variable stars. In the first two years of activity we have discovered 100 new variable stars in the course of observations carried out from August 2014 to September 2016. The newly discovered stars comprise 80 eclipsing binary stars (66 of them classified as W Ursae Majoris, 11 as β Lyrae, and 3 β Persei), one rotating (ROT), one ellipsoidal variable (ELL), and 18 pulsating variables (5 of them classified as RRAB, 7 RRC, 3 HADS, 2 δ Scuti and one Cepheid). Variability classification is based on the properties of the optical light curves that we obtained using our 255 mm F/4.7 Newton robotic telescope.

## 1. Introduction

The VESPA project (Variable Star Search Project for Automated Telescope) is made at IAU station 565, Bassano Bresciano Observatory, Brescia, Italy (www.osservatoriobassano.org). It is a CCD photometric survey of the northern hemisphere, which has the aim of discovering and investigating new variable stars in the magnitude range 13.5 < V < 16.5.

In the course of observations carried out from August 2014 to September 2016, we obtained 50,865 images with 120-second exposure on 253 nights (Table 1), and we have discovered 100 new variable stars (Tables 2 and 3; Figure 4). We have determined the type (Table 4), the period, the epoch, and the amplitude for all the discovered stars. A key to the sources of observations shown in Figure 4 is given in Table 5.

## 2. Instrumentation and methodology

Observations were obtained using our homemade 255-mm F/4.7 Newton telescope (Figure 1), equipped with Starlight Xpress Trius-SX9 CCD camera, with a sensor area of 1392 × 1040 pixels (Pixel size: 6.45 x 6.45 μm). This configuration results in a FOV (field of view) of 25.8' × 19.2'. We configured the camera in a 2 × 2 binning mode with angular resolution of 2.22 × 2.22 arcsec/pixel. The camera is equipped with a Sony ICX285A CCD and dual stage cooler. The observations were obtained with the CCD operating at the temperature of –10° C (in hot seasons) and –15° C (in cold seasons). Observations were made using a Johnson V filter or were unfiltered and reduced to a V zeropoint (CV).

Table 1. Summary of the observations.

| *Date* | *Nights* | *Images* | *Hours/Month* |
|---|---|---|---|
| 2014 Aug | 15 | 2319 | 77 |
| 2014 Sep | 15 | 2863 | 96 |
| 2014 Oct | 17 | 2671 | 89 |
| 2014 Nov | 8 | 1207 | 40 |
| 2014 Dec | 6 | 1553 | 52 |
| 2015 Jan | 15 | 3219 | 107 |
| 2015 Feb | 8 | 1340 | 45 |
| 2015 Mar | 1 | 254 | 9 |
| 2015 Apr | 10 | 1689 | 56 |
| 2015 May | 5 | 582 | 19 |
| 2015 Jun | 5 | 678 | 23 |
| 2015 Jul | 18 | 2468 | 82 |
| 2015 Aug | 15 | 3044 | 102 |
| 2015 Sep | 9 | 1750 | 58 |
| 2015 Oct | 11 | 1814 | 61 |
| 2015 Nov | 15 | 3383 | 113 |
| 2015 Dec | 5 | 761 | 25 |
| 2016 Jan | 10 | 2219 | 74 |
| 2016 Feb | 4 | 845 | 28 |
| 2016 Mar | 10 | 2827 | 94 |
| 2016 Apr | 2 | 522 | 17 |
| 2016 May | 5 | 1083 | 36 |
| 2016 Jun | 2 | 241 | 8 |
| 2016 Jul | 16 | 2733 | 91 |
| 2016 Aug | 16 | 5225 | 174 |
| 2016 Sep | 10 | 3575 | 119 |
| Total 26 | 253 | 50865 | 1695 |

The telescope is located near the Bassano Bresciano Astronomical Observatory, at the coordinates 45° 19' 32" N, 10° 07' 49" E (WGS84) in a home-made dome that slides on rails and closes automatically at the end of the session or in bad weather.

Table 2. Main characteristics of discovered stars.

| *Name* | *R.A. (J2000)* | | | *Dec. (J2000)* | | | *Type* | *Maximum Magnitude* | *Minimum Magnitude* | *Filter* | *Period (days)* | *Epoch (HJD)* |
|---|---|---|---|---|---|---|---|---|---|---|---|---|
| | *h* | *m* | *s* | ° | ' | " | | | | | | |
| VESPA_V1 | 22 | 02 | 42.26 | +27 | 56 | 11.9 | EW | 15.68 | 15.83 | V | 0.231335 | 2456884.49382 |
| VESPA_V2 | 20 | 29 | 59.18 | +16 | 13 | 24.8 | EW | 14.13 | 14.74 | CV | 0.410520 | 2456887.53907 |
| VESPA_V3 | 20 | 30 | 57.66 | +16 | 20 | 18.2 | RRC | 13.82 | 14.19 | CV | 0.269646 | 2456897.46106 |
| VESPA_V4 | 20 | 33 | 27.57 | +16 | 33 | 49.3 | EW | 14.20 | 14.49 | CV | 0.367287 | 2456900.41422 |
| VESPA_V5 | 20 | 33 | 52.03 | +16 | 37 | 16.2 | EW | 14.12 | 14.29 | CV | 0.251410 | 2456900.44974 |
| VESPA_V6 | 20 | 33 | 31.01 | +16 | 45 | 30.7 | EW | 15.30 | 15.57 | CV | 0.435868 | 2456902.43919 |
| VESPA_V7 | 20 | 28 | 10.70 | +15 | 57 | 48.4 | EB | 14.50 | 15.04 | CV | 0.515464 | 2456914.48392 |
| VESPA_V8 | 20 | 29 | 04.95 | +16 | 20 | 54.9 | EW | 12.68 | 13.20 | V | 0.689388 | 2454656.74000 |
| VESPA_V9 | 22 | 14 | 34.94 | +41 | 10 | 29.2 | RRAB | 15.20 | 16.14 | CV | 0.470367 | 2456923.47856 |
| VESPA_V10 | 22 | 15 | 01.38 | +40 | 55 | 41.6 | EW | 14.99 | 15.40 | CV | 0.301903 | 2456923.33854 |
| VESPA_V11 | 22 | 15 | 32.47 | +42 | 02 | 21.4 | EW | 14.56 | 15.35 | CV | 0.324274 | 2456929.59510 |
| VESPA_V12 | 22 | 00 | 50.64 | +43 | 28 | 05.5 | EW | 14.82 | 15.65 | CV | 0.308914 | 2456953.27595 |
| VESPA_V13 | 22 | 16 | 11.34 | +41 | 44 | 34.4 | EB | 13.17 | 13.78 | CV | 1.065884 | 2456956.26090 |
| VESPA_V14 | 21 | 59 | 34.23 | +43 | 44 | 20.1 | EW | 14.62 | 15.05 | CV | 0.307018 | 2456954.34605 |
| VESPA_V15 | 22 | 01 | 56.59 | +43 | 38 | 14.4 | EW | 14.36 | 14.91 | CV | 0.368932 | 2456953.31305 |
| VESPA_V16 | 22 | 01 | 01.40 | +43 | 07 | 47.5 | HADS | 14.61 | 14.80 | CV | 0.074446 | 2456958.42234 |
| VESPA_V17 | 22 | 00 | 22.75 | +42 | 47 | 16.3 | EB | 13.58 | 13.85 | CV | 0.612290 | 2456981.34566 |
| VESPA_V18 | 21 | 59 | 21.72 | +42 | 55 | 59.6 | EW | 13.42 | 13.83 | V | 0.707333 | 2456961.37362 |
| VESPA_V19 | 01 | 21 | 57.75 | +47 | 49 | 33.3 | EW | 11.66 | 11.92 | CV | 0.401534 | 2456963.48117 |
| VESPA_V20 | 21 | 57 | 47.66 | +43 | 12 | 52.1 | RRAB | 15.54 | 16.65 | CV | 0.500800 | 2456980.70800 |
| VESPA_V21 | 01 | 55 | 59.74 | +51 | 43 | 06.8 | EW | 12.74 | 12.87 | CV | 0.398786 | 2457021.33460 |
| VESPA_V22 | 01 | 54 | 36.50 | +51 | 40 | 25.7 | EW | 12.47 | 12.75 | CV | 0.331038 | 2457021.31500 |
| VESPA_V23 | 01 | 56 | 15.56 | +52 | 26 | 54.9 | HADS | 11.84 | 12.22 | CV | 0.097959 | 2457032.28910 |
| VESPA_V24 | 01 | 56 | 01.71 | +52 | 20 | 26.7 | RRC | 16.26 | 16.89 | CV | 0.255661 | 2457031.31195 |
| VESPA_V25 | 05 | 29 | 11.37 | +36 | 18 | 53.1 | EW | 12.88 | 13.02 | CV | 0.244124 | 2457046.42710 |
| VESPA_V26 | 05 | 29 | 07.71 | +37 | 07 | 19.0 | EW | 15.04 | 15.48 | CV | 0.350117 | 2457061.36990 |
| VESPA_V27 | 15 | 03 | 17.13 | +40 | 01 | 24.3 | EW | 14.10 | 14.22 | CV | 0.335815 | 2457094.54690 |
| VESPA_V28 | 14 | 56 | 16.91 | +42 | 20 | 08.7 | RRC | 14.83 | 15.20 | CV | 0.405029 | 2457128.47030 |
| VESPA_V29 | 14 | 23 | 33.18 | +40 | 28 | 42.5 | DSCT | 14.10 | 14.16 | CV | 0.244056 | 2457154.48110 |
| VESPA_V30 | 20 | 28 | 04.41 | +17 | 05 | 58.7 | RRC | 13.88 | 14.31 | CV | 0.297016 | 2457214.43030 |
| VESPA_V31 | 20 | 28 | 22.41 | +17 | 02 | 29.0 | RRC | 15.38 | 15.64 | CV | 0.226653 | 2457215.44521 |
| VESPA_V32 | 20 | 28 | 35.95 | +16 | 29 | 50.7 | EB | 12.80 | 13.01 | V | 0.324731 | 2457220.47750 |
| VESPA_V33 | 20 | 28 | 10.72 | +16 | 58 | 28.5 | EW | 13.55 | 13.70 | CV | 0.628050 | 2457218.42190 |
| VESPA_V34 | 20 | 28 | 22.92 | +17 | 25 | 25.9 | RRC | 15.68 | 16.06 | CV | 0.182098 | 2457221.50940 |
| VESPA_V35 | 20 | 26 | 52.66 | +16 | 07 | 38.5 | HADS | 14.23 | 14.53 | CV | 0.092075 | 2457226.48610 |
| VESPA_V36 | 20 | 28 | 47.63 | +17 | 27 | 52.1 | EW | 15.19 | 15.48 | CV | 0.426604 | 2457221.44360 |
| VESPA_V37 | 20 | 25 | 52.43 | +15 | 59 | 09.5 | EW | 15.47 | 15.85 | CV | 0.378992 | 2457226.41856 |
| VESPA_V38 | 20 | 25 | 55.45 | +15 | 55 | 03.5 | EW | 14.92 | 15.19 | CV | 0.539153 | 2457229.52320 |
| VESPA_V39 | 20 | 26 | 26.08 | +16 | 13 | 29.5 | EW | 13.64 | 14.31 | V | 0.531559 | 2457240.43710 |
| VESPA_V40 | 20 | 25 | 29.70 | +15 | 55 | 35.5 | EB | 13.97 | 14.52 | CV | 0.627498 | 2457242.46690 |
| VESPA_V41 | 20 | 26 | 01.99 | +17 | 16 | 05.5 | EW | 14.67 | 15.19 | CV | 0.415141 | 2457248.45400 |
| VESPA_V42 | 20 | 25 | 55.36 | +17 | 12 | 00.5 | EW | 16.00 | 16.55 | CV | 0.314593 | 2457255.36630 |
| VESPA_V43 | 20 | 25 | 58.88 | +16 | 04 | 59.7 | EW | 16.79 | 17.48 | CV | 0.337285 | 2457238.43280 |
| VESPA_V44 | 20 | 25 | 45.96 | +15 | 56 | 50.7 | EW | 17.30 | 18.20 | CV | 0.385902 | 2457238.46340 |
| VESPA_V45 | 20 | 24 | 56.29 | +16 | 34 | 20.8 | EW | 15.75 | 16.10 | CV | 0.354840 | 2457267.43020 |
| VESPA_V46 | 20 | 25 | 26.75 | +16 | 48 | 43.6 | EW | 16.13 | 16.90 | CV | 0.335819 | 2457260.39690 |
| VESPA_V47 | 20 | 24 | 44.51 | +16 | 48 | 59.5 | EW | 13.98 | 14.08 | CV | 0.287455 | 2457266.51978 |
| VESPA_V48 | 21 | 57 | 23.21 | +43 | 43 | 44.6 | EW | 12.98 | 13.22 | V | 0.382097 | 2457271.40468 |
| VESPA_V49 | 21 | 55 | 09.40 | +43 | 12 | 00.1 | RRAB | 15.64 | 16.85 | CV | 0.457989 | 2457271.40140 |
| VESPA_V50 | 21 | 56 | 17.50 | +43 | 06 | 30.1 | ELL | 14.40 | 14.51 | CV | 0.42497 | 2457272.51000 |
| VESPA_V51 | 21 | 55 | 18.52 | +43 | 43 | 50.4 | EW | 14.32 | 14.60 | CV | 0.429272 | 2457272.43140 |
| VESPA_V52 | 21 | 55 | 33.79 | +43 | 13 | 40.2 | EW | 15.63 | 16.15 | CV | 0.326901 | 2457272.46870 |
| VESPA_V53 | 21 | 55 | 16.50 | +43 | 38 | 24.7 | EW | 16.84 | 17.59 | CV | 0.352131 | 2457272.43590 |
| VESPA_V54 | 21 | 55 | 59.08 | +43 | 52 | 47.3 | EW | 14.63 | 15.15 | CV | 0.447872 | 2457287.55890 |
| VESPA_V55 | 21 | 58 | 51.40 | +44 | 03 | 14.4 | EB | 16.54 | 17.03 | CV | 0.378575 | 2457285.26930 |
| VESPA_V56 | 21 | 58 | 28.30 | +44 | 02 | 39.9 | CEP: | 16.70 | 17.60 | CV | 0.488907 | 2457286.33280 |
| VESPA_V57 | 21 | 56 | 20.52 | +44 | 00 | 50.6 | EB | 15.25 | 16.00 | CV | 0.49385 | 2457304.38380 |
| VESPA_V58 | 23 | 06 | 00.72 | +52 | 48 | 28.7 | DSCT | 14.09 | 14.26 | CV | 0.101393 | 2457317.27760 |
| VESPA_V59 | 23 | 07 | 47.22 | +53 | 08 | 32.6 | EW | 15.63 | 16.01 | CV | 0.346930 | 2457317.49470 |
| VESPA_V60 | 23 | 07 | 05.97 | +53 | 15 | 07.3 | EW: | 15.11 | 15.33 | CV | 0.258547 | 2457317.46000 |
| VESPA_V61 | 23 | 06 | 54.85 | +53 | 01 | 13.6 | EB | 14.40 | 14.88 | V | 0.521825 | 2457318.40000 |
| VESPA_V62 | 21 | 57 | 32.58 | +44 | 11 | 53.2 | EW | 15.76 | 16.42 | V | 0.437156 | 2457336.47790 |
| VESPA_V63 | 22 | 15 | 36.03 | +49 | 57 | 26.2 | EA | 14.75 | 15.57 | CV | 0.397447 | 2457328.36290 |
| VESPA_V64 | 06 | 20 | 02.96 | +24 | 31 | 00.5 | EW | 14.30 | 15.10 | CV | 0.483931 | 2457358.53500 |
| VESPA_V65 | 05 | 26 | 25.66 | +37 | 18 | 59.1 | EW | 14.75 | 15.25 | CV | 0.276202 | 2457334.64860 |
| VESPA_V66 | 21 | 57 | 58.06 | +44 | 14 | 25.4 | EW | 16.14 | 16.42 | CV | 0.377845 | 2457336.46710 |
| VESPA_V67 | 04 | 42 | 39.24 | +20 | 20 | 36.0 | EW | 13.75 | 13.89 | CV | 0.404445 | 2457404.3349 |

*Table continued on next page*

Table 2. Main characteristics of discovered stars, cont.

| *Name* | *R.A. (J2000)* | | | *Dec. (J2000)* | | | *Type* | *Maximum Magnitude* | *Minimum Magnitude* | *Filter* | *Period (days)* | *Epoch (HJD)* |
|---|---|---|---|---|---|---|---|---|---|---|---|---|
| | *h* | *m* | *s* | ° | ' | " | | | | | | |
| VESPA_V68 | 04 | 40 | 47.61 | +20 | 38 | 58.9 | EB | 12.49 | 12.81 | CV | 1.867115 | 2457405.45456 |
| VESPA_V69 | 05 | 55 | 32.35 | +10 | 13 | 39.8 | EB | 15.03 | 15.60 | V | 0.406012 | 2457424.43617 |
| VESPA_V70 | 05 | 56 | 09.59 | +10 | 19 | 44.5 | EW | 15.86 | 16.51 | CV | 0.448186 | 2457424.4737 |
| VESPA_V71 | 05 | 55 | 55.69 | +10 | 25 | 40.1 | EW | 16.05 | 16.95 | CV | 0.282211 | 2457424.3464 |
| VESPA_V72 | 05 | 55 | 35.92 | +10 | 10 | 41.0 | EW | 17.20 | 17.90 | CV | 0.405469 | 2457424.4409 |
| VESPA_V73 | 07 | 09 | 29.07 | +24 | 02 | 15.3 | EW | 15.02 | 15.41 | CV | 0.425751 | 2457429.45313 |
| VESPA_V74 | 07 | 09 | 46.41 | +24 | 12 | 00.3 | EW | 17.34 | 17.76 | CV | 0.341853 | 2457429.48899 |
| VESPA_V75 | 07 | 09 | 40.11 | +24 | 13 | 03.1 | EA | 14.40 | 14.86 | CV | 1.105988 | 2457429.4171 |
| VESPA_V76 | 15 | 01 | 27.29 | +19 | 02 | 42.7 | ROT | 15.05 | 15.32 | CV | 0.446332 | 2457466.5402 |
| VESPA_V77 | 19 | 29 | 55.23 | +43 | 59 | 32.9 | EW | 17.36 | 18.14 | CV | 0.266673 | 2457577.4281 |
| VESPA_V78 | 20 | 24 | 00.72 | +16 | 05 | 13.6 | EW | 16.90 | 17.70 | CV | 0.429332 | 2457580.5226 |
| VESPA_V79 | 20 | 22 | 19.15 | +16 | 09 | 09.5 | EW | 14.90 | 15.23 | CV | 0.458647 | 2457587.543 |
| VESPA_V80 | 20 | 22 | 26.51 | +16 | 30 | 57.8 | EW | 17.10 | 17.95 | CV | 0.438596 | 2457596.3932 |
| VESPA_V81 | 20 | 22 | 26.40 | +16 | 36 | 00.6 | RRC | 14.37 | 14.76 | CV | 0.266504 | 2457600.5385 |
| VESPA_V82 | 20 | 23 | 09.48 | +16 | 43 | 21.4 | EW | 16.87 | 17.47 | CV | 0.304543 | 2457600.4959 |
| VESPA_V83 | 20 | 22 | 58.03 | +16 | 38 | 38.5 | EW | 16.70 | 17.50 | CV | 0.356628 | 2457596.4292 |
| VESPA_V84 | 20 | 22 | 34.41 | +16 | 30 | 39.4 | EW | 16.45 | 16.95 | CV | 0.370557 | 2457596.44 |
| VESPA_V85 | 20 | 23 | 00.81 | +17 | 17 | 18.4 | RRAB | 15.58 | 16.53 | CV | 0.590231 | 2457602.4502 |
| VESPA_V86 | 20 | 22 | 28.61 | +16 | 57 | 21.0 | RRAB | 15.65 | 16.52 | CV | 0.584052 | 2457602.4394 |
| VESPA_V87 | 20 | 22 | 00.51 | +17 | 00 | 59.1 | EW | 15.54 | 16.46 | CV | 0.390820 | 2457604.5495 |
| VESPA_V88 | 20 | 21 | 59.18 | +17 | 10 | 36.5 | EW | 15.07 | 15.51 | CV | 0.224842 | 2457602.559 |
| VESPA_V89 | 20 | 24 | 51.91 | +17 | 24 | 40.9 | EW | 16.26 | 16.98 | CV | 0.349912 | 2457608.3857 |
| VESPA_V90 | 20 | 23 | 58.29 | +17 | 44 | 30.4 | EA/RS | 15.05 | 15.75 | CV | 0.404912 | 2457613.4108 |
| VESPA_V91 | 20 | 23 | 29.90 | +17 | 34 | 56.5 | EW | 14.32 | 14.65 | CV | 0.320912 | 2457614.5985 |
| VESPA_V92 | 20 | 23 | 16.71 | +17 | 35 | 26.6 | EW | 15.13 | 15.53 | CV | 0.344223 | 2457614.5725 |
| VESPA_V93 | 20 | 24 | 11.14 | +17 | 36 | 57.9 | EB | 14.42 | 14.70 | CV | 0.819545 | 2457614.5751 |
| VESPA_V94 | 20 | 19 | 57.74 | +16 | 58 | 50.6 | EW | 14.72 | 15.12 | CV | 0.346042 | 2457632.3915 |
| VESPA_V95 | 20 | 20 | 27.48 | +16 | 48 | 48.2 | EW | 14.07 | 14.40 | CV | 0.36193 | 2457638.3591 |
| VESPA_V96 | 20 | 20 | 32.03 | +17 | 35 | 57.6 | EW | 16.40 | 17.10 | CV | 0.33209 | 2457623.3103 |
| VESPA_V97 | 20 | 22 | 04.07 | +16 | 40 | 44.2 | EW | 15.90 | 16.26 | CV | 0.302188 | 2457639.2871 |
| VESPA_V98 | 20 | 21 | 42.04 | +17 | 14 | 44.5 | EW | 16.01 | 16.48 | CV | 0.417834 | 2457624.2079 |
| VESPA_V99 | 20 | 21 | 18.65 | +17 | 41 | 37.2 | EW | 14.86 | 15.18 | CV | 0.403108 | 2457637.5187 |
| VESPA_V100 | 20 | 20 | 26.39 | +17 | 19 | 26.8 | EW | 14.76 | 14.98 | CV | 0.352926 | 2457624.5463 |

Figure 1. Observations were obtained using this homemade 255-mm F/4.7 Newton telescope, equipped with Starlight Xpress Trius-SX9 CCD camera, with a sensor area of 1392 × 1040 pixels (Pixel size: 6.45 x 6.45 µM).

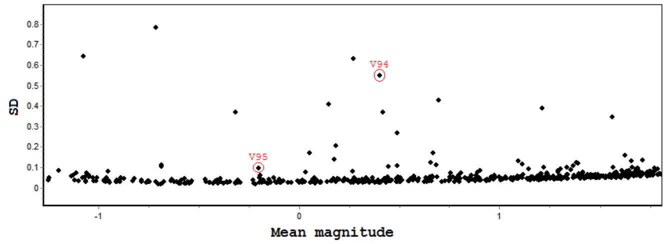

Figure 2. Magnitude-RMS scatter diagram. This a plot (SD Plot) of the Mean Magnitude (x-axis) and the standard deviation (y-axis) for each candidate, and is the discovery graph for VESPA_V94 and V95. The zero in the x-axis represents the mean of magnitudes. Values < zero are for the stars brighter than mean and the values > zero are for the stars fainter than the mean.

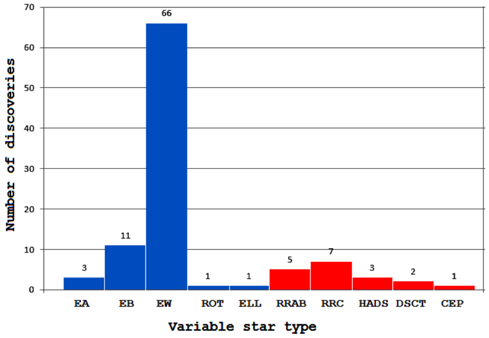

Figure 3. Variable stars discovered in this project, by type.

*Table 3. Cross identification.*

VESPA_V1 = 2MASS J22024225+2756117 = UCAC4 590-132222
VESPA_V2 = 2MASS J20295917+1613248 = UCAC4 532-128317
VESPA_V3 = 2MASS J20305765+1620182 = UCAC4 532-128620
VESPA_V4 = 2MASS J20332757+1633491 = UCAC4 533-132584
VESPA_V5 = 2MASS J20335203+1637161 = UCAC4 534-128918
VESPA_V6 = 2MASS J20333100+1645306 = UCAC4 534-128825
VESPA_V7 = 2MASS J20281070+1557483 = UCAC4 530-133575
VESPA_V8 = 2MASS J20290495+162054 = UCAC4 532-128061
VESPA_V9 = 2MASS J22143494+4110292 = UCAC4 656-106683
VESPA_V10 = 2MASS J22150137+4055416 = UCAC4 655-109319
VESPA_V11 = 2MASS J22153246+4202214 = UCAC4 661-108309
VESPA_V12 = 2MASS J22005064+4328054 = UCAC4 668-108654
VESPA_V13 = 2MASS J22161133+4144343 = UCAC4 659-105178
VESPA_V14 = 2MASS J21593423+4344200 = UCAC4 669-105250
VESPA_V15 = 2MASS J22015659+4338143 = UCAC4 669-105729
VESPA_V16 = 2MASS J22010139+4307474 = UCAC4 666-109206
VESPA_V17 = 2MASS J22002275+4247162 = UCAC4 664-106603
VESPA_V18 = 2MASS J21592172+4255596 = GSC 03193-01009
VESPA_V19 = 2MASS J01215775+4749332 = GSC 03269-00586
VESPA_V20 = 2MASS J21574764+4312521 = UCAC4 667-104920
VESPA_V21 = 2MASS J01555975+5143067 = GSC 03292-02057
VESPA_V22 = 2MASS J01543649+5140257 = GSC 03292-02037
VESPA_V23 = 2MASS J01561556+5226548 = GSC 03292-01328
VESPA_V24 = 2MASS J01560166+5220266 = USNO-B1.0 1423-0062011
VESPA_V25 = 2MASS J05291136+3618531 = GSC 02415-01387
VESPA_V26 = 2MASS J05290770+3707190 = UCAC4 636-026479
VESPA_V27 = GSC 03047-01108 = UCAC4 651-054439
VESPA_V28 = GSC 03047-00740 = UCAC4 662-058379
VESPA_V29 = GSC 03038-00203 = UCAC4 653-056492
VESPA_V30 = UCAC4 536-132799 = USNO-B1.0 1070-0618597
VESPA_V31 = UCAC4 536-132889 = USNO-B1.0 1070-0618935
VESPA_V32 = CMC15 J202835.9+162950 = UCAC4 533-131232
VESPA_V33 = CMC15 J202810.7+165828 = UCAC4 535-129895
VESPA_V34 = 2MASS J20282292+1725258 = CMC15 J202822.9+172525
VESPA_V35 = 2MASS J20265265+1607383 = CMC15 J202652.6+160738
VESPA_V36 = 2MASS J20284763+1727519 = CMC15 J202847.6+172751
VESPA_V37 = CMC15 J202552.4+155909 = UCAC4 530-132810
VESPA_V38 = 2MASS J20255544+1555036 = CMC15 J202555.4+155503
VESPA_V39 = 2MASS J20262608+1613294 = CMC15 J202626.0+161329
VESPA_V40 = 2MASS J20252969+1555353 = CMC15 J202529.7+155535
VESPA_V41 = 2MASS J20260198+1716055 = CMC15 J202601.9+171605
VESPA_V42 = 2MASS J20255536+1712004 = CMC15 J202555.3+171200
VESPA_V43 = 2MASS J20255886+1604597 = CMC15 J202558.8+160459
VESPA_V44 = 2MASS J20254596+1556505 = CMC15 J202545.9+155650
VESPA_V45 = 2MASS J20245629+1634209 = CMC15 J202456.2+163420
VESPA_V46 = 2MASS J20252674+1648434 = CMC15 J202526.7+164843
VESPA_V47 = 2MASS J20244451+1648594 = CMC15 J202444.5+164859
VESPA_V48 = 2MASS J21572320+4343446 = CMC15 J215723.2+434344
VESPA_V49 = 2MASS J21550937+4311599 = CMC15 J215509.3+431159
VESPA_V50 = 2MASS J21561748+4306299 = CMC15 J215617.4+430629
VESPA_V51 = 2MASS J21551852+4343504 = CMC15 J215518.5+434350
VESPA_V52 = 2MASS J21553378+4313402 = UCAC4 667-104506
VESPA_V53 = 2MASS J21551650+4338246 = CMC15 J215516.5+433824
VESPA_V54 = 2MASS J21555907+4352473 = CMC15 J215559.0+435247
VESPA_V55 = 2MASS J21585137+4403143 = CMC15 J215851.3+440314
VESPA_V56 = 2MASS J21582830+4402398 = CMC15 J215828.3+440239
VESPA_V57 = 2MASS J21562051+4400505 = CMC15 J215620.5+440050
VESPA_V58 = 2MASS J23060071+5248286 = UCAC4 715-107866
VESPA_V59 = 2MASS J23074721+5308326 = UCAC4 716-108199
VESPA_V60 = 2MASS J23070597+5315072 = UCAC4 717-106819
VESPA_V61 = 2MASS J23065483+5301137 = UCAC4 716-108055
VESPA_V62 = 2MASS J21573258+4411532 = CMC15 J215732.5+441153
VESPA_V63 = 2MASS J22153602+4957262 = CMC15 J221536.0+495726
VESPA_V64 = 2MASS J06200295+2431004 = CMC15 J062002.9+243100
VESPA_V65 = 2MASS J05262565+3718591 = CMC15 J052625.6+371859
VESPA_V66 = 2MASS J21575805+4414254 = CMC15 J215758.0+441425
VESPA_V67 = 2MASS J04423923+2020360 = CMC15 J044239.2+202035
VESPA_V68 = 2MASS J04404761+2038589 = CMC15 J044047.6+203858
VESPA_V69 = 2MASS J05553235+1013397 = CMC15 J055532.3+101339
VESPA_V70 = 2MASS J05560959+1019447 = CMC15 J055609.5+101944
VESPA_V71 = 2MASS J05555569+1025402 = CMC15 J055555.6+102540
VESPA_V72 = 2MASS J05553591+1010410 = CMC15 J055535.9+101041
VESPA_V73 = 2MASS J07092907+2402152 = CMC15 J070929.0+240215
VESPA_V74 = 2MASS J07094640+2412002 = CMC15 J070946.3+241200
VESPA_V75 = 2MASS J07094011+2413031 = CMC15 J070940.1+241303
VESPA_V76 = 2MASS J15012728+1902426 = CMC15 J150127.2+190242
VESPA_V77 = 2MASS J19295526+4359325 = CMC15 J192955.2+435932
VESPA_V78 = 2MASS J20240071+1605136 = CMC15 J202400.7+160513
VESPA_V79 = 2MASS J20221915+1609094 = CMC15 J202219.1+160909
VESPA_V80 = 2MASS J20222650+1630577 = CMC15 J202226.5+163057
VESPA_V81 = 2MASS J20222640+1636007 = CMC15 J202226.3+163600
VESPA_V82 = 2MASS J20230947+1643214 = CMC15 J202309.4+164321
VESPA_V83 = 2MASS J20225805+1638384 = CMC15 J202258.0+163838
VESPA_V84 = 2MASS J20223442+1630393 = CMC15 J202234.4+163039
VESPA_V85 = 2MASS J20230080+1717184 = CMC15 J202300.8+171718
VESPA_V86 = 2MASS J20222860+1657210 = CMC15 J202228.6+165721
VESPA_V87 = 2MASS J20220051+1700593 = CMC15 J202200.5+170059
VESPA_V88 = 2MASS J20215918+1710365 = CMC15 J202159.1+171036
VESPA_V89 = 2MASS J20245192+1724410 = CMC15 J202451.9+172441
VESPA_V90 = 2MASS J20235827+1744303 = CMC15 J202358.2+174430
VESPA_V91 = 2MASS J20232990+1734564 = CMC15 J202329.9+173456
VESPA_V92 = 2MASS J20231671+1735267 = CMC15 J202316.7+173526
VESPA_V93 = 2MASS J20241113+1736579 = CMC15 J202411.1+173657
VESPA_V94 = 2MASS J20195774+1658505 = CMC15 J201957.7+165850
VESPA_V95 = 2MASS J20202748+1648482 = CMC15 J202027.4+164848
VESPA_V96 = 2MASS J20203203+1735574 = CMC15 J202032.0+173557
VESPA_V97 = 2MASS J20220407+1640442 = CMC15 J202204.0+164044
VESPA_V98 = 2MASS J20214204+1714445 = CMC15 J202142.0+171444
VESPA_V99 = 2MASS J20211865+1741371 = CMC15 J202118.6+174137
VESPA_V100 = 2MASS J20202638+1719268 = CMC15 J202026.3+171926

We used POLYPUS software release 1.9 (Bassano Bresciano Observatory 2013) to control the robotic observations and astrometrical pointing system. We took exposures when the target's altitude was more than 30 degrees. Raw images were processed with flat field and dark frames.

We used the variable star search utility of MPO CANOPUS version 10.4.0.20 (Minor Planet Observer 2010) to search for new variable stars. This utility uses a magnitude-RMS scatter diagram. Figure 2 is a plot (SD Plot) of the Mean Magnitude (x-axis) and the standard deviation (y-axis) for each candidate, and is the discovery graph for VESPA_V94 and V95. The zero in the x-axis represents the mean of magnitudes. Values < zero are for the stars brighter than mean and the values > zero are for the stars fainter than the mean.

Usually, for our system, the discoveries are in the 0.05 < SD < 1 range. Other stars have SD in this range for other (non-variable) reasons.

We also used MPO CANOPUS to perform differential photometry on the reduced images. PERANSO software version 2.51 (Vanmunster 2013) was used for period analysis (using generally the ANOVA method) and to determine the epoch and the amplitude.

In a typical observing session, one or two fields in succession are imaged for the duration of the night, in order to have a continuous coverage of a 0.13 or 0.27 square degree area for each observing session, with a typical exposure time of 2 minutes. The exposure time was chosen in order to measure photometrically stars between magnitudes 13.5 and 16.5.

To increase the probability of finding new stars, the fields were chosen in the vicinity of the Milky Way in areas not yet covered by professional surveys to avoid discovering stars already known. Generally, the fields were chosen from the +10 < declination < +60 range due to obstacles on the ground. In some cases, the fields were those crossed by some asteroids of which we studied photometrically the rotation period. For the choice of the fields we have used the AAVSO Variable Star Plotter (VSP; AAVSO 2016) service of the AAVSO.

The methodology involves a discovery phase in which we scanned the fields in search of new stars, and a followup phase in which we obtained the complete light curves.

We used comparison stars of similar color to that of the variable so as to minimize errors due to atmospheric refraction. To improve the parameters of these stars we have also used, if possible, data of the CRTS, SWASP, ASAS-3, APASS, and NSVS surveys. The coordinates of new variable stars (Table 2) were obtained from the UCAC4 catalogue (Zacharias *et al.* 2012).

## 3. Discussion

For every star we have proposed a type of variability based on the characteristics shown by its differential light curve, its amplitude, period, and spectral class (Tables 1 and 3; Figure 3).

We have determined the spectral class from the APASS, 2MASS, and CMC 15 catalogues, using tables contained in *A Stellar Spectral Flux Library: 1150–25000 A°* (Pickles 1998).

For the eclipsing stars we have also used *Binary Stars–A Pictorial Atlas* (Terrell *et al.* 1992). For pulsating stars we have used the text: "Variable Star Type Designations in VSX" (Watson *et al.* 2014), based on the *General Catalogue of Variable Stars* (GCVS; Samus *et al.* 2009) description of variable star type designations, and *Variable Star Classification and Light Curves* (AAVSO 2012).

We have submitted all stars to AAVSO/VSX, which has approved and registered these stars.

## 4. Co-discovery

In some cases the discoveries were made thanks to the collaboration of other people so we included them as discoverers, with us, in the VSX record: Sebastian Otero, co-discoverer of VESPA_V39 and VESPA_V76; Giorgio Bianciardi, co-discoverer of VESPA_V1 and VESPA_V2; and Bruce McMath, co-discoverer of VESPA_V20 and VESPA_V57.

## 5. Acknowledgements

Our thanks to Sebastian Otero (VSX Team) for his extremely valuable comments and help in resolving the intricate cases in variable star identification. Many of our discoveries have been resolved with the help of Sebastian's vast knowledge and his experience.

This research has made use of the follow sources and services: International Variable Star Index (VSX) database, operated at AAVSO,Cambridge, Massachusetts, USA; the AAVSO Photometric All-Sky Survey (APASS; Henden *et al.* 2015), funded by the Robert Martin Ayers Sciences Fund; VizieR catalogue access tool, CDS, Strasbourg, France; the Two Micron All Sky Survey, which is a joint project of the University of Massachusetts and the Infrared Processing and Analysis Center/California Institute of Technology, funded by the National Aeronautics and Space Administration and the National Science Foundation; the CMC15 Data Access Service at CAB (INTA-CSIC); the CSS survey funded by the National Aeronautics and Space Administration under Grant No. NNG05GF22G issued through the Science Mission Directorate Near-Earth Objects Observations Program; the CRTS survey is supported by the U.S. National Science Foundation under grants AST-0909182 and AST-1313422; The All Sky Automated Survey (Pojmański 1997); the Northern Sky Variability Survey created jointly by the Los Alamos National Laboratory and University of Michigan, funded by the U.S. Department of Energy, the National Aeronautics and Space Administration and the National Science Foundation; SuperWASP Public Archive operated by the WASP consortium; observations obtained with XMM-Newton, an ESA science mission with instruments and contributions directly funded by ESA Member States and the USA (NASA); U.S. Naval Observatory CCD Astrograph Catalog (UCAC4).

## References

AAVSO. 2016, Variable Star Plotter (VSP; https://www.aavso.org/apps/vsp/).

AAVSO. 2012, Variable Star Classification and Light Curves, AAVSO, Cambridge, MA (https://www.google.com/url?q=https://www.aavso.org/files/Variable%2520Star%2520Classification%2520and%2520Light%2520Curves%2520Manual%25202.1.pdf&sa=U&ved=0ahUKEwipzeeU4qPRAhUG6YMKHVh1A2AQFggEMAA&client=internal-uds-cse&usg=AFQjCNFWhsdQQocyTci_g3p4PZt3uREptw).

Bassano Bresciano Observatory. 2013, POLYPUS software release 1.9 (http://www.osservatoriobassano.org/Software.asp).

Henden, A. A., *et al.* 2015, AAVSO Photometric All-Sky Survey, data release 9 (https://www.aavso.org/apass).

Minor Planet Observer. 2010, MPO Software Suite (http://www.minorplanetobserver.com), BDW Publishing, Colorado Springs.

Pickles, A. J. 1998, *Publ. Astron. Soc. Pacific*, **110**, 863.

Pojmański, G. 1997, *Acta Astron.*, **47**, 467.

Samus, N. N., *et al.* 2009, *General Catalogue of Variable Stars*, VizieR On-line Data Catalog (http://cdsarc.u-strasbg.fr/viz-bin/Cat?B/gcvs).

Terrell, D., Mukherjee, J., and Wilson, R. E. 1992, *Binary Stars. A Pictorial Atlas*, Kriegar, Malabar.Vanmunster, T. 2013, light curve and period analysis software, PERANSO (http://www.peranso.com/).

Watson, C., Henden, A. A., and Price, C. A. 2014, AAVSO International Variable Star Index VSX (Watson+, 2006–2014; https://www.aavso.org/vsx).

Zacharias, N., Finch, C. T., Girard, T. M., Henden, A., Bartlett, J. L., Monet, D. G., and Zacharias, M. I. 2012, *The Fourth U.S. Naval Observatory CCD Astrograph Catalog* (UCAC4), VizieR On-line Data Catalog (http://cdsarc.u-strasbg.fr/viz-bin/Cat?I/322).

Table 4. Variable stars by type.

| *Extrinsic* | | *Intrinsic* | |
|---|---|---|---|
| *Type* | *Number* | *Type* | *Number* |
| EA | 3 | RRAB | 5 |
| EB | 11 | RRC | 7 |
| EW | 66 | HADS | 3 |
| ELL | 1 | DSCT | 2 |
| ROT | 1 | CEP | 1 |

Table 5. Key to the sources of observations shown in Figure 4 (from VSX, Watson *et al.* 2014).

| *Vespa* | *Use of Colors in the Light Curves* |
|---|---|
| V1 | Green = UAI_Astra/Skylive 2014-08-16, all other VESPA at Bassano Observatory |
| V2 | Green = UAI_Astra/Skylive 2014-08-21, all other VESPA at Bassano Observatory |
| V3 | All VESPA at Bassano Observatory |
| V4 | All VESPA at Bassano Observatory |
| V5 | All VESPA at Bassano Observatory |
| V6 | All VESPA at Bassano Observatory |
| V7 | All VESPA at Bassano Observatory |
| V8 | Black = VESPA, yellow = ASAS-3, pink = APASS |
| V9 | All VESPA at Bassano Observatory |
| V10 | All VESPA at Bassano Observatory |
| V11 | All VESPA at Bassano Observatory |
| V12 | All VESPA at Bassano Observatory |
| V13 | All VESPA at Bassano Observatory |
| V14 | All VESPA at Bassano Observatory |
| V15 | All VESPA at Bassano Observatory |
| V16 | All VESPA at Bassano Observatory |
| V17 | All VESPA at Bassano Observatory |
| V18 | Blue = VESPA, green = SWASP, black = APASS |
| V19 | Black = VESPA, green = SWASP |
| V20 | Blue = VESPA, black = Bruce McMath |
| V21 | Grey = NSVS, all other VESPA at Bassano Observatory |
| V22 | Grey = NSVS, all other VESPA at Bassano Observatory |
| V23 | grey = NSVS, all other VESPA at Bassano Observatory |
| V24 | All VESPA at Bassano Observatory |
| V25 | Black = VESPA, red = NSVS, green = SWASP |
| V26 | All VESPA at Bassano Observatory |
| V27 | Grey = CRTS, all other VESPA at Bassano Observatory |
| V28 | Grey = CRTS, all other VESPA at Bassano Observatory |
| V29 | Red = VESPA, grey = CRTS |
| V30 | All VESPA at Bassano Observatory |
| V31 | All VESPA at Bassano Observatory |
| V32 | Yellow = ASAS-3, red = APASS, all other VESPA at Bassano Observatory |
| V33 | All VESPA at Bassano Observatory |
| V34 | All VESPA at Bassano Observatory |
| V35 | All VESPA at Bassano Observatory |
| V36 | All VESPA at Bassano Observatory |
| V37 | All VESPA at Bassano Observatory |
| V38 | All VESPA at Bassano Observatory |
| V39 | Blue = VESPA, red = APASS, light green = NSVS, green = ASAS-3 + Sebastian Otero |
| V40 | All VESPA at Bassano Observatory |
| V41 | All VESPA at Bassano Observatory |
| V42 | All VESPA at Bassano Observatory |
| V43 | All VESPA at Bassano Observatory |
| V44 | All VESPA at Bassano Observatory |
| V45 | All VESPA at Bassano Observatory |
| V46 | All VESPA at Bassano Observatory |
| V47 | All VESPA at Bassano Observatory |
| V48 | All VESPA at Bassano Observatory |
| V49 | All VESPA at Bassano Observatory |
| V50 | Yellow = SWASP, all other VESPA at Bassano Observatory |
| V51 | Yellow = SWASP, all other VESPA at Bassano Observatory |
| V52 | All VESPA at Bassano Observatory |
| V53 | All VESPA at Bassano Observatory |
| V54 | All VESPA at Bassano Observatory |
| V55 | All VESPA at Bassano Observatory |
| V56 | All VESPA at Bassano Observatory |
| V57 | Red = VESPA, blue = Bruce McMath |
| V58 | Blue = VESPA, yellow = SWASP |
| V59 | All VESPA at Bassano Observatory |
| V60 | All VESPA at Bassano Observatory |
| V61 | Yellow = SWASP, green = APASS, all other VESPA at Bassano Observatory |
| V62 | Blue = VESPA, red = APASS |
| V63 | All VESPA at Bassano Observatory |
| V64 | Yellow = SWASP, all other VESPA at Bassano Observatory |
| V65 | Blue = VESPA, yellow = SWASP |
| V66 | All VESPA at Bassano Observatory |
| V67 | Blue = VESPA, green = CRTS |
| V68 | Blue = VESPA, light grey = SWASP, grey = CRTS |
| V69 | Blue = VESPA, red = APASS |
| V70 | All VESPA at Bassano Observatory |
| V71 | All VESPA at Bassano Observatory |
| V72 | All VESPA at Bassano Observatory |
| V73 | Blue = VESPA, green = CRTS |
| V74 | Black = VESPA, red = CRTS |
| V75 | Black = VESPA,grey = SWASP |
| V76 | Grey = CRTS, all other VESPA at Bassano Observatory + Sebastian Otero |
| V77 | All VESPA at Bassano Observatory |
| V78 | All VESPA at Bassano Observatory |
| V79 | All VESPA at Bassano Observatory |
| V80 | All VESPA at Bassano Observatory |
| V81 | All VESPA at Bassano Observatory |
| V82 | All VESPA at Bassano Observatory |
| V83 | All VESPA at Bassano Observatory |
| V84 | All VESPA at Bassano Observatory |
| V85 | All VESPA at Bassano Observatory |
| V86 | All VESPA at Bassano Observatory |
| V87 | All VESPA at Bassano Observatory |
| V88 | All VESPA at Bassano Observatory |
| V89 | All VESPA at Bassano Observatory |
| V90 | All VESPA at Bassano Observatory |
| V91 | All VESPA at Bassano Observatory |
| V92 | All VESPA at Bassano Observatory |
| V93 | All VESPA at Bassano Observatory |
| V94 | All VESPA at Bassano Observatory |
| V95 | All VESPA at Bassano Observatory |
| V96 | All VESPA at Bassano Observatory |
| V97 | All VESPA at Bassano Observatory |
| V98 | All VESPA at Bassano Observatory |
| V99 | All VESPA at Bassano Observatory |
| V100 | All VESPA at Bassano Observatory |

*Color versions of the plots shown in Figure 4 (published grayscale in print) may be viewed at https://www.aavso.org/apps/jaavso/article/3234/ .*

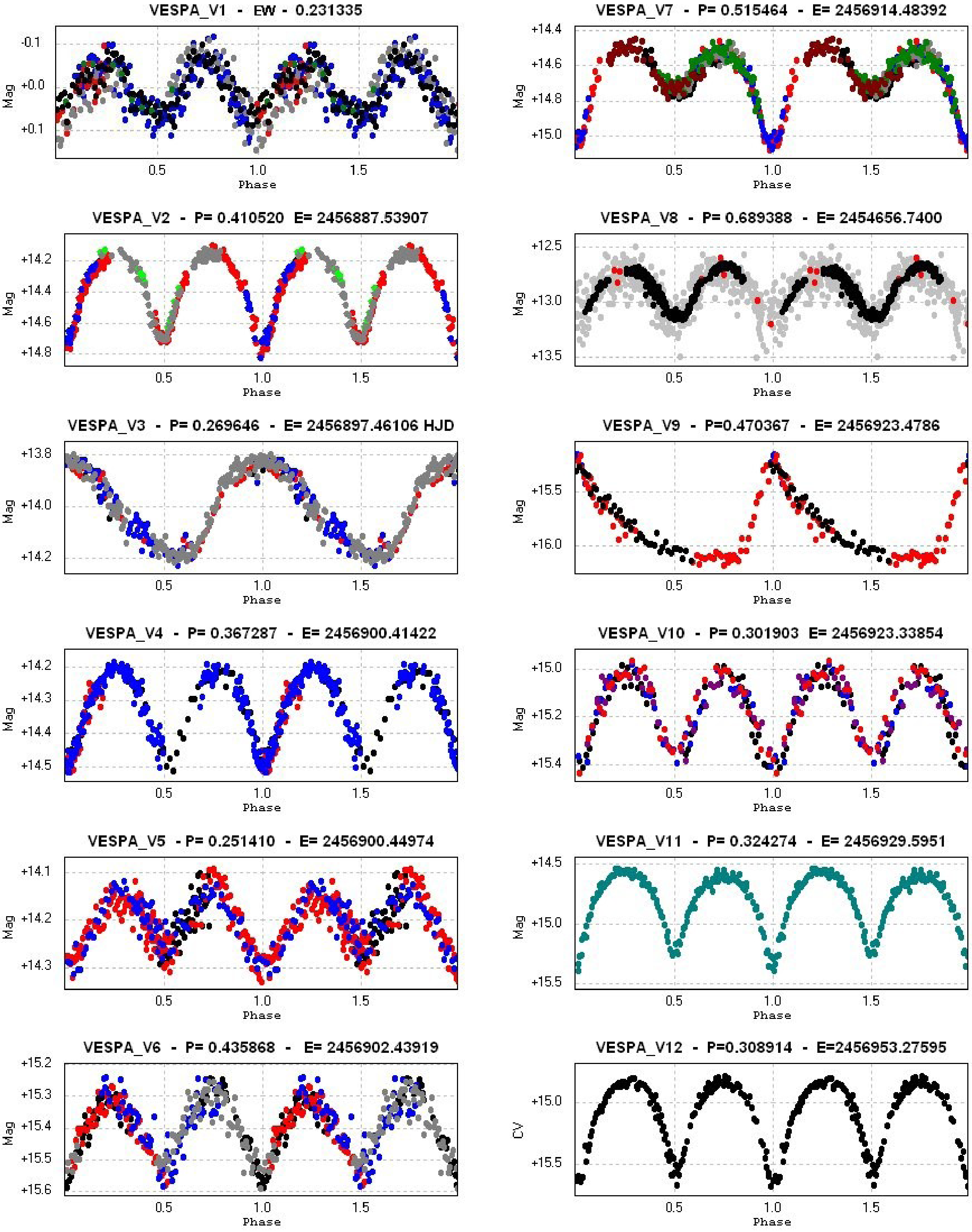

Figure 4. Light curves of the 100 discovered variable stars. In the following pages we present the light curves of all variable stars, presented in the order given in Table 2. Explanation of the colors used in the light curves: Generally each color represents an observing session. In some cases the different colors are used for the various survey (CRTS, SWASP, ASAS-3, APASS, NSVS, etc.) used to better determine the period of the variableas as described in Table 5. In the AAVSO-VSX, for each variable star there is a light curve with a legend that best explains the colors used.

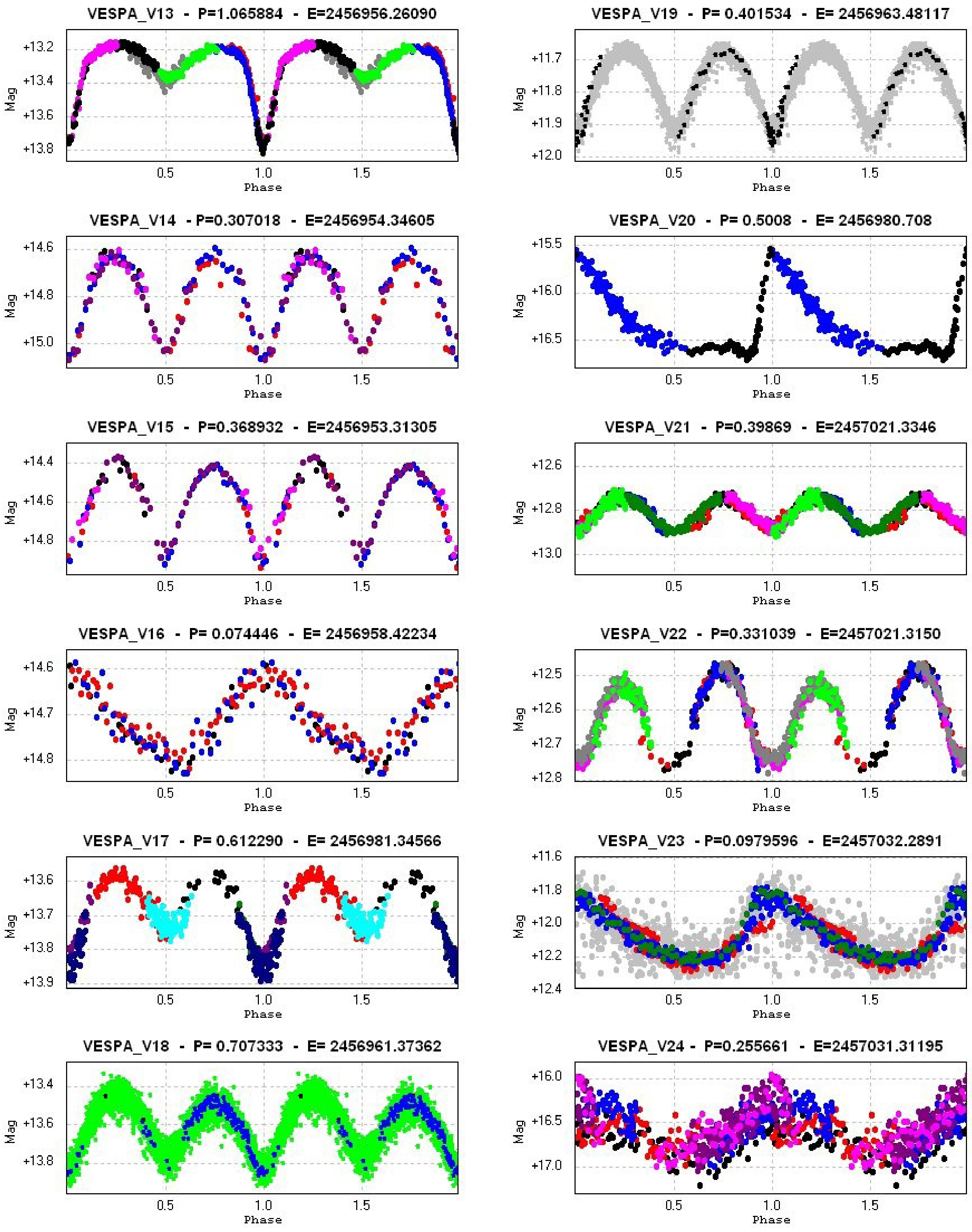

Figure 4. Light curves of the 100 discovered variable stars, cont.

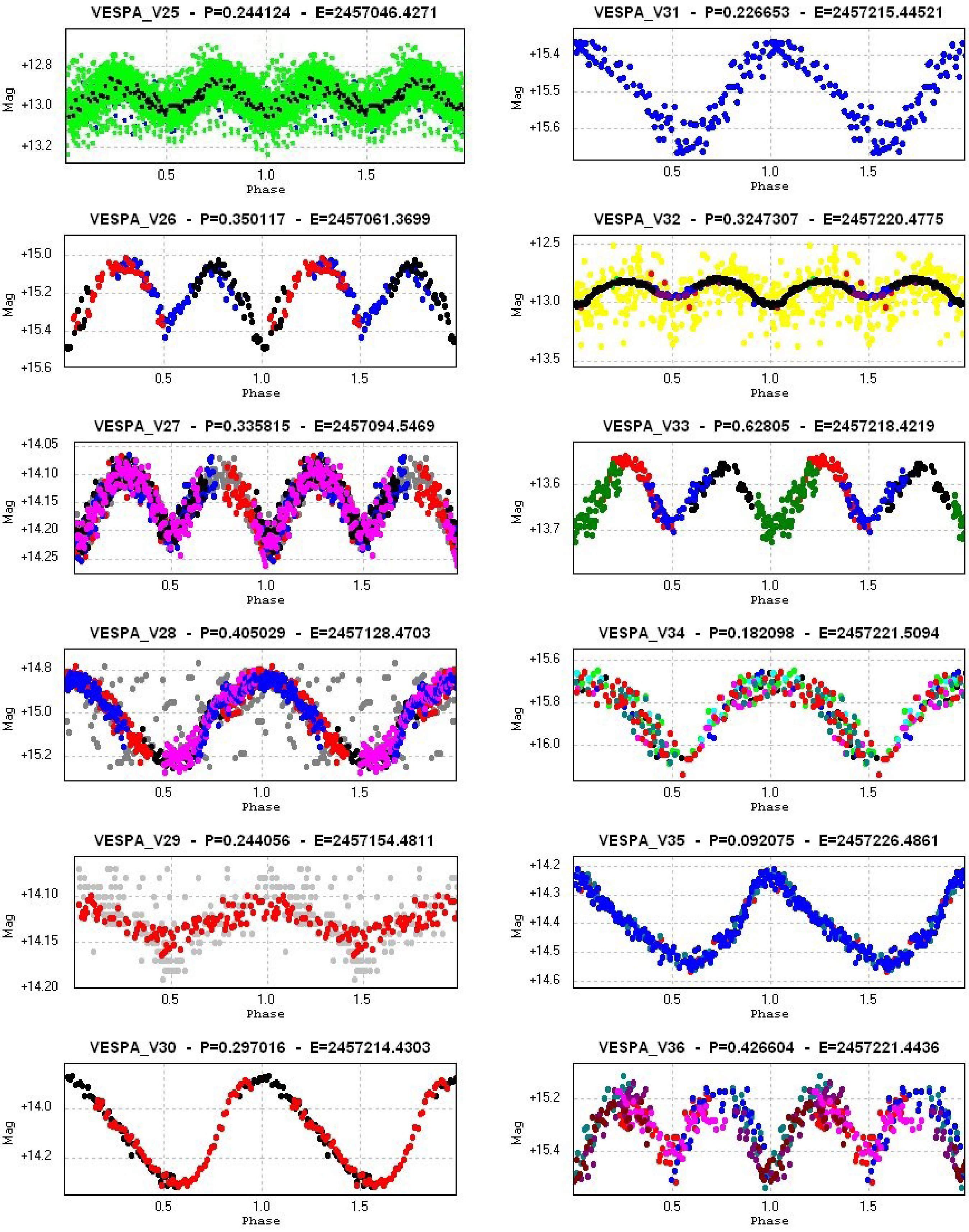

VESPA_V25 - P=0.244124 - E=2457046.4271

VESPA_V26 - P=0.350117 - E=2457061.3699

VESPA_V27 - P=0.335815 - E=2457094.5469

VESPA_V28 - P=0.405029 - E=2457128.4703

VESPA_V29 - P=0.244056 - E=2457154.4811

VESPA_V30 - P=0.297016 - E=2457214.4303

VESPA_V31 - P=0.226653 - E=2457215.44521

VESPA_V32 - P=0.3247307 - E=2457220.4775

VESPA_V33 - P=0.62805 - E=2457218.4219

VESPA_V34 - P=0.182098 - E=2457221.5094

VESPA_V35 - P=0.092075 - E=2457226.4861

VESPA_V36 - P=0.426604 - E=2457221.4436

Figure 4. Light curves of the 100 discovered variable stars, cont.

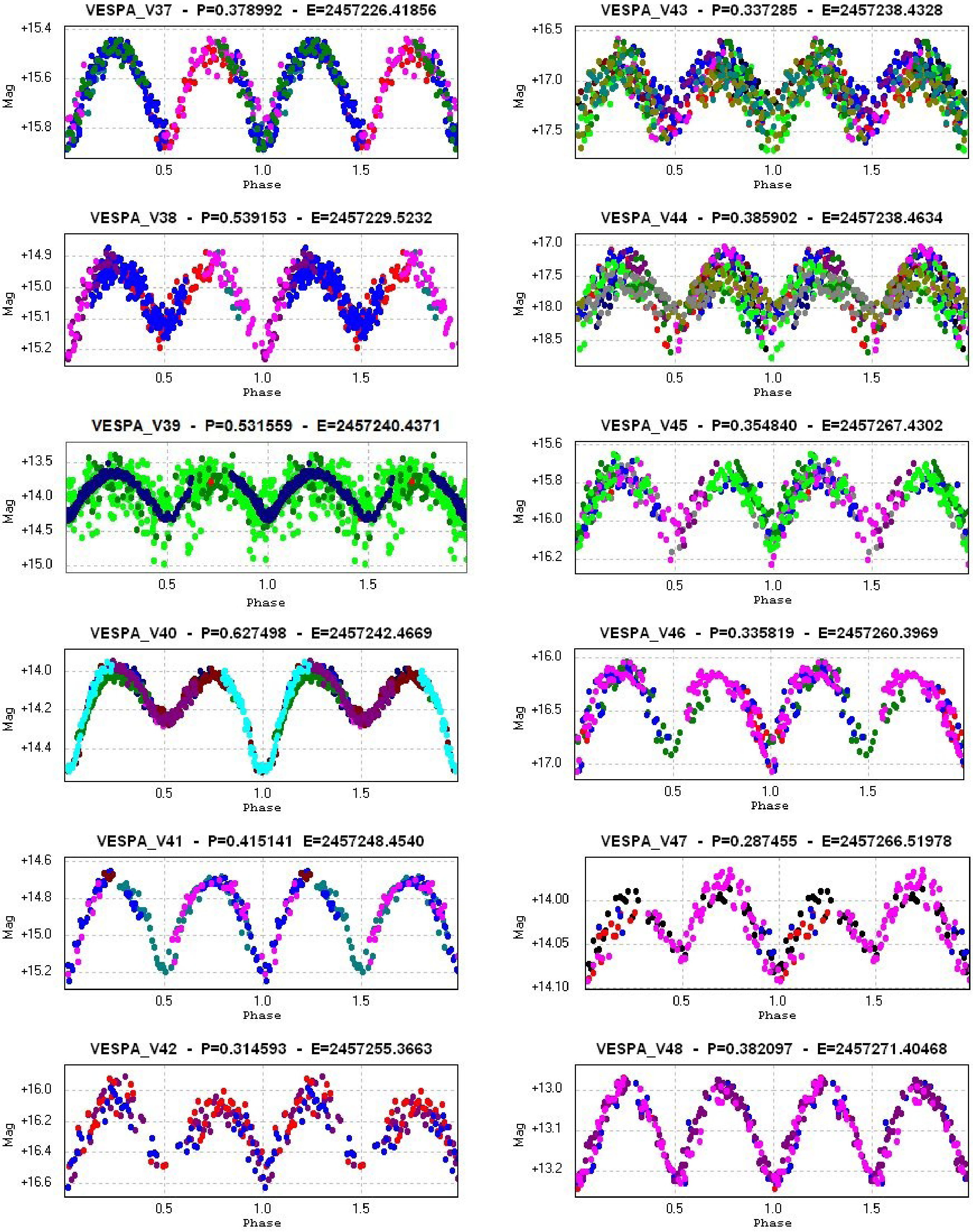

VESPA_V37 - P=0.378992 - E=2457226.41856

VESPA_V38 - P=0.539153 - E=2457229.5232

VESPA_V39 - P=0.531559 - E=2457240.4371

VESPA_V40 - P=0.627498 - E=2457242.4669

VESPA_V41 - P=0.415141 E=2457248.4540

VESPA_V42 - P=0.314593 - E=2457255.3663

VESPA_V43 - P=0.337285 - E=2457238.4328

VESPA_V44 - P=0.385902 - E=2457238.4634

VESPA_V45 - P=0.354840 - E=2457267.4302

VESPA_V46 - P=0.335819 - E=2457260.3969

VESPA_V47 - P=0.287455 - E=2457266.51978

VESPA_V48 - P=0.382097 - E=2457271.40468

Figure 4. Light curves of the 100 discovered variable stars, cont.

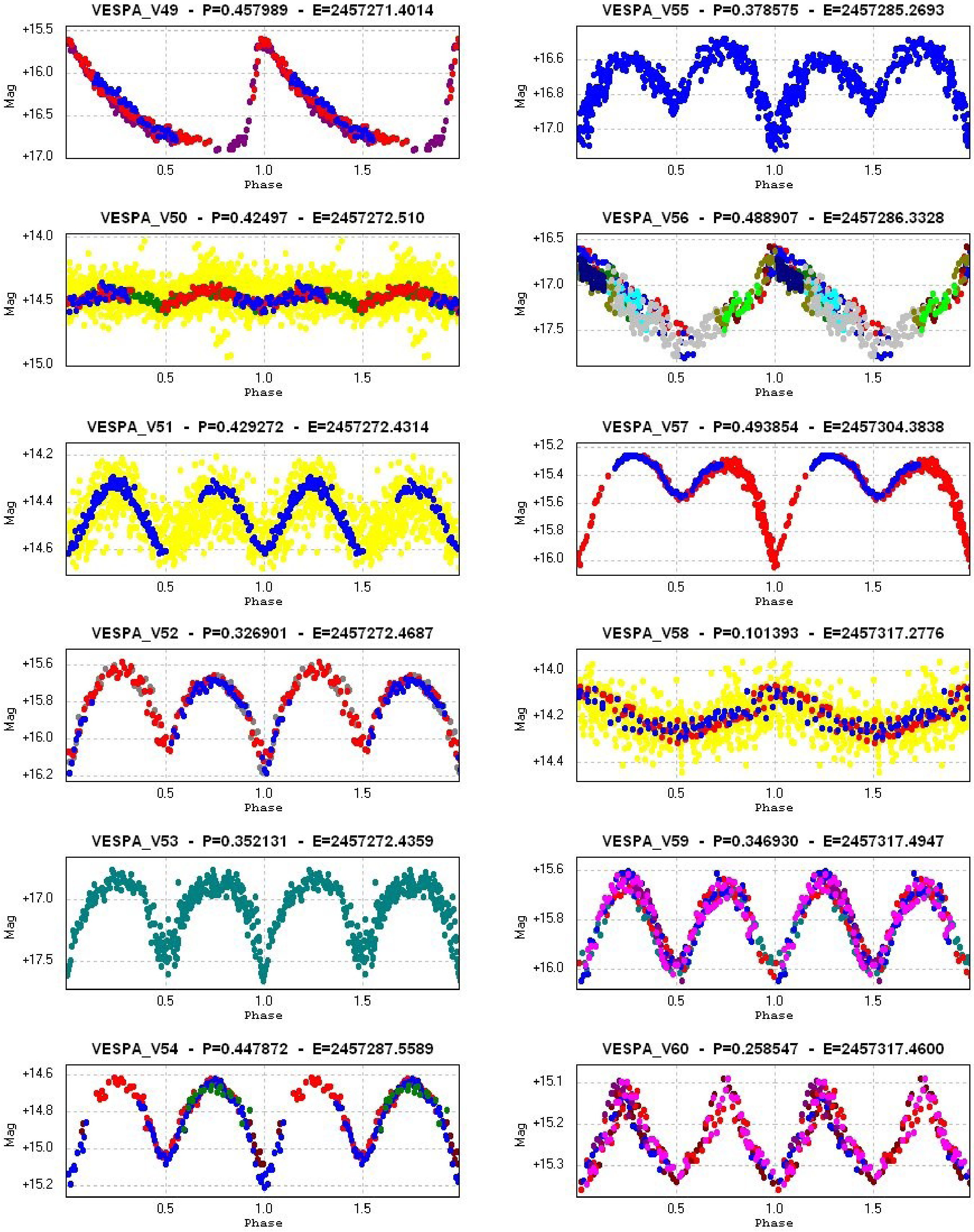

Figure 4. Light curves of the 100 discovered variable stars, cont.

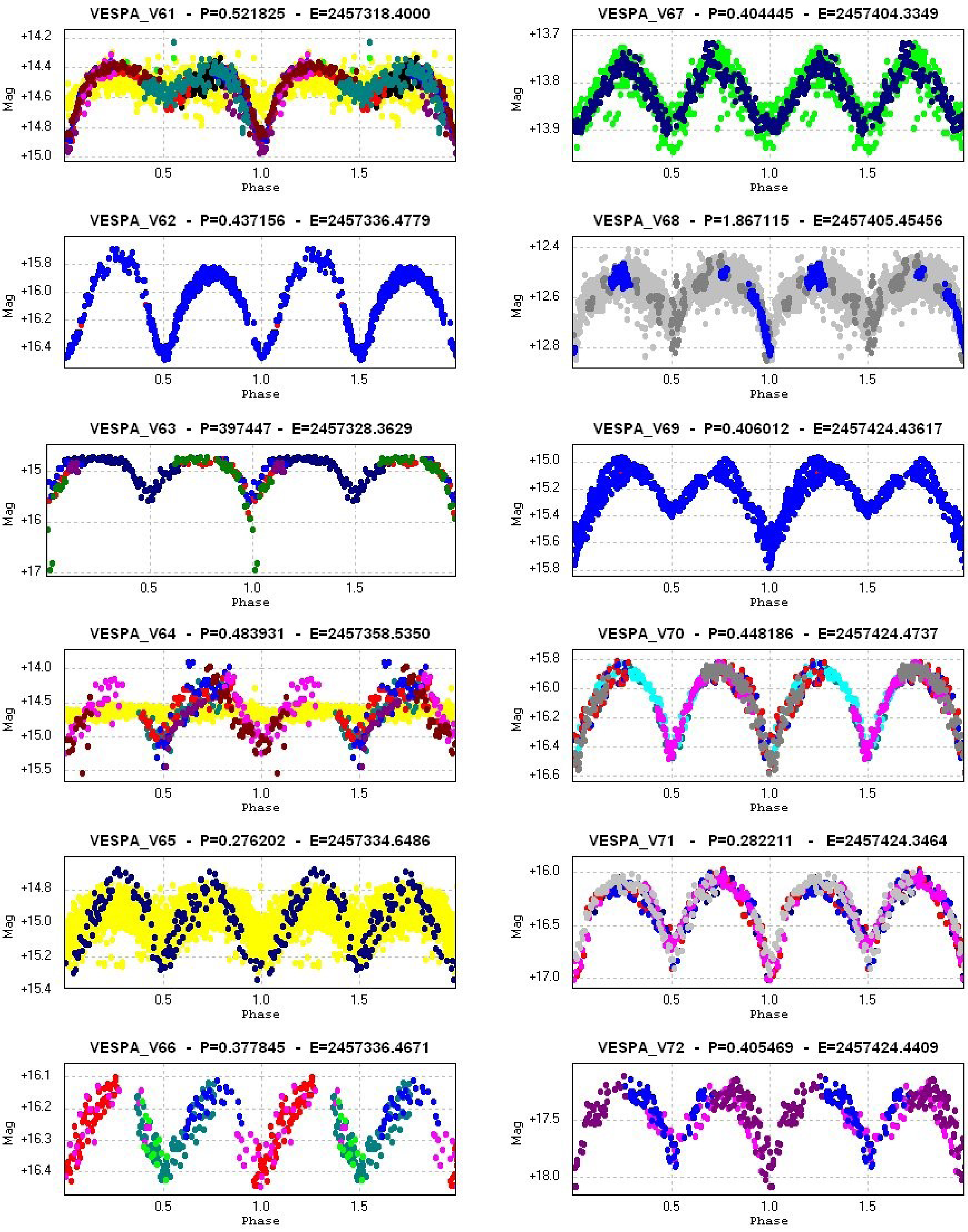

VESPA_V61 - P=0.521825 - E=2457318.4000

VESPA_V67 - P=0.404445 - E=2457404.3349

VESPA_V62 - P=0.437156 - E=2457336.4779

VESPA_V68 - P=1.867115 - E=2457405.45456

VESPA_V63 - P=397447 - E=2457328.3629

VESPA_V69 - P=0.406012 - E=2457424.43617

VESPA_V64 - P=0.483931 - E=2457358.5350

VESPA_V70 - P=0.448186 - E=2457424.4737

VESPA_V65 - P=0.276202 - E=2457334.6486

VESPA_V71 - P=0.282211 - E=2457424.3464

VESPA_V66 - P=0.377845 - E=2457336.4671

VESPA_V72 - P=0.405469 - E=2457424.4409

Figure 4. Light curves of the 100 discovered variable stars, cont.

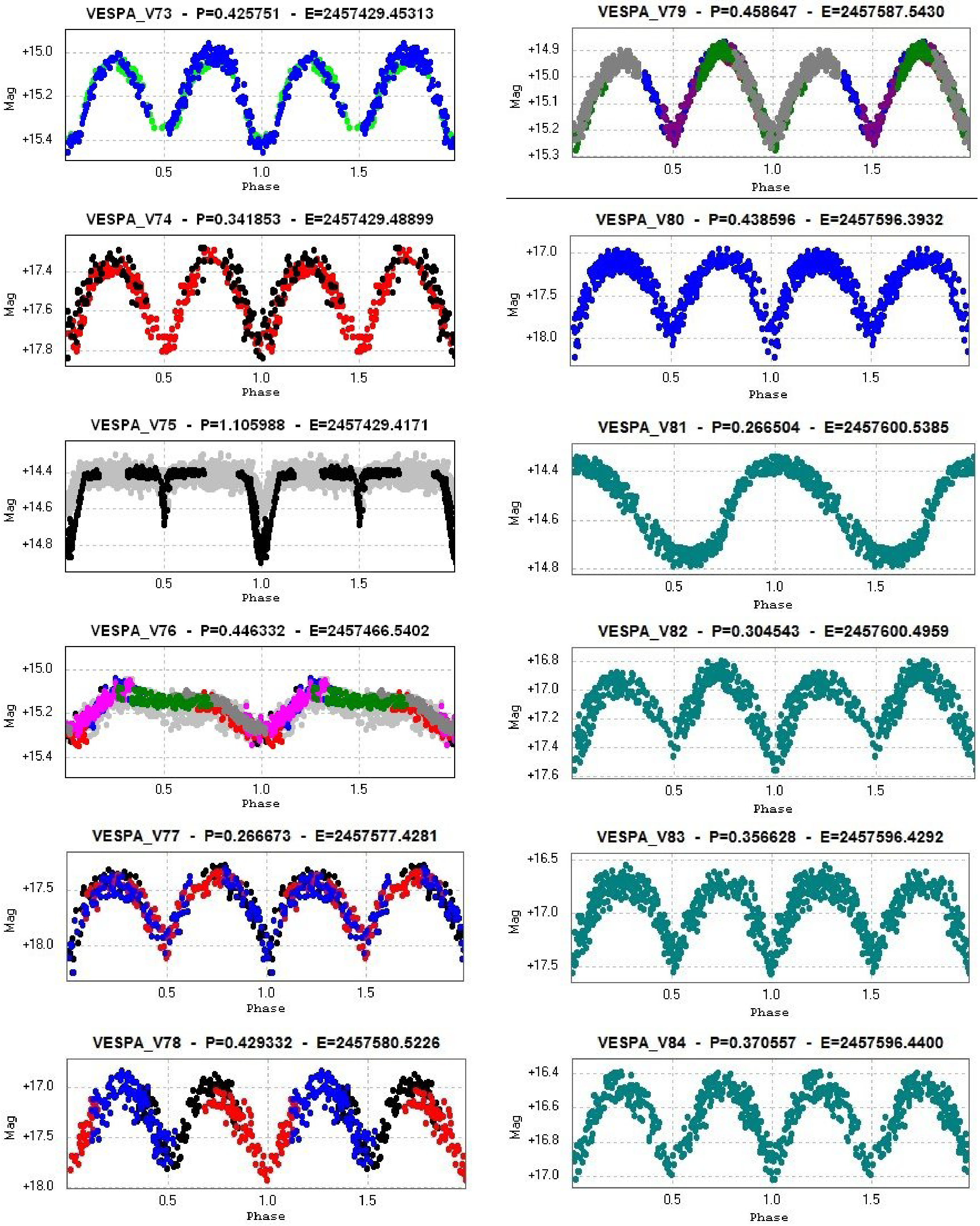

VESPA_V73 - P=0.425751 - E=2457429.45313

VESPA_V74 - P=0.341853 - E=2457429.48899

VESPA_V75 - P=1.105988 - E=2457429.4171

VESPA_V76 - P=0.446332 - E=2457466.5402

VESPA_V77 - P=0.266673 - E=2457577.4281

VESPA_V78 - P=0.429332 - E=2457580.5226

VESPA_V79 - P=0.458647 - E=2457587.5430

VESPA_V80 - P=0.438596 - E=2457596.3932

VESPA_V81 - P=0.266504 - E=2457600.5385

VESPA_V82 - P=0.304543 - E=2457600.4959

VESPA_V83 - P=0.356628 - E=2457596.4292

VESPA_V84 - P=0.370557 - E=2457596.4400

Figure 4. Light curves of the 100 discovered variable stars, cont.

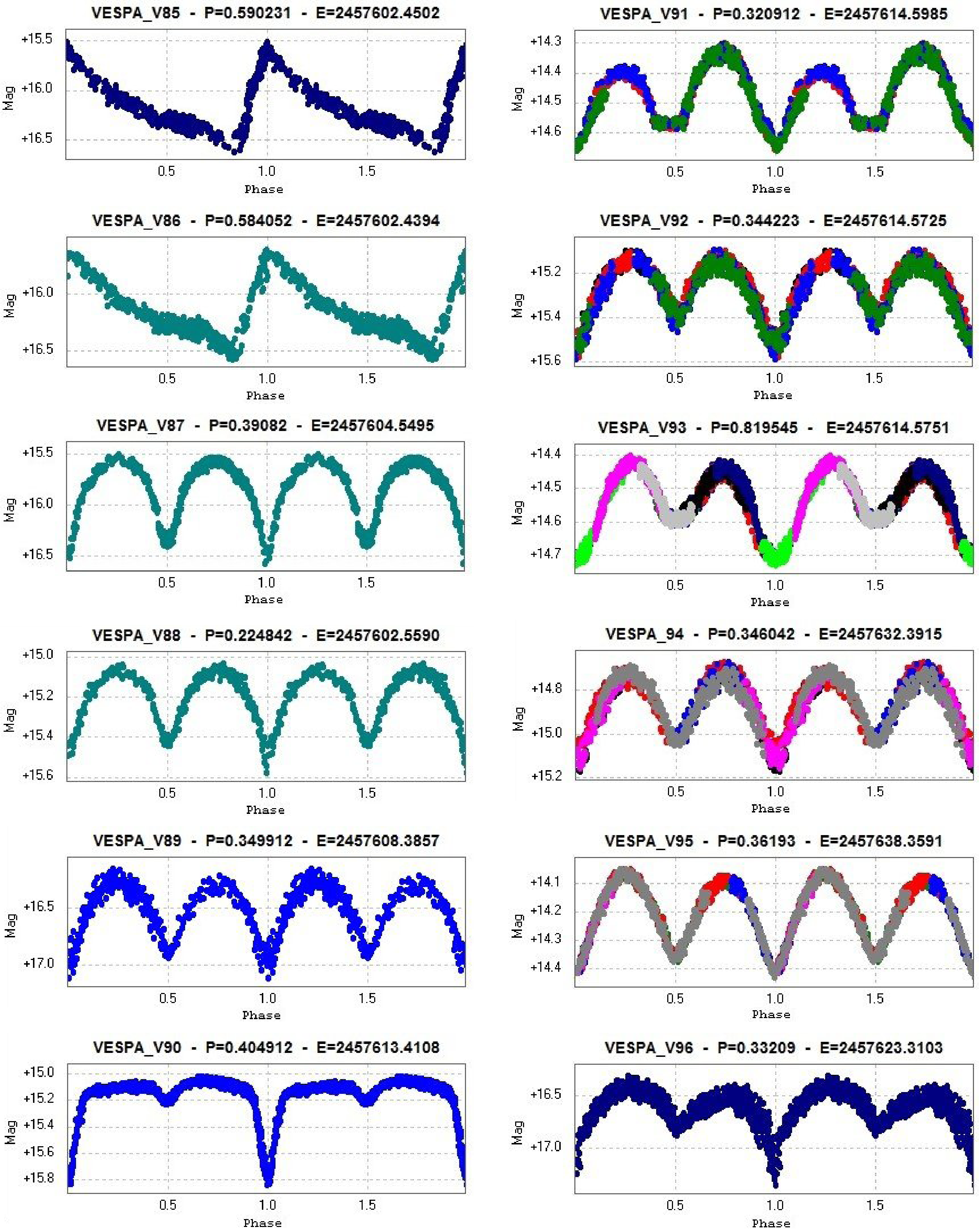
VESPA_V85 - P=0.590231 - E=2457602.4502

VESPA_V91 - P=0.320912 - E=2457614.5985

VESPA_V86 - P=0.584052 - E=2457602.4394

VESPA_V92 - P=0.344223 - E=2457614.5725

VESPA_V87 - P=0.39082 - E=2457604.5495

VESPA_V93 - P=0.819545 - E=2457614.5751

VESPA_V88 - P=0.224842 - E=2457602.5590

VESPA_94 - P=0.346042 - E=2457632.3915

VESPA_V89 - P=0.349912 - E=2457608.3857

VESPA_V95 - P=0.36193 - E=2457638.3591

VESPA_V90 - P=0.404912 - E=2457613.4108

VESPA_V96 - P=0.33209 - E=2457623.3103

Figure 4. Light curves of the 100 discovered variable stars, cont.

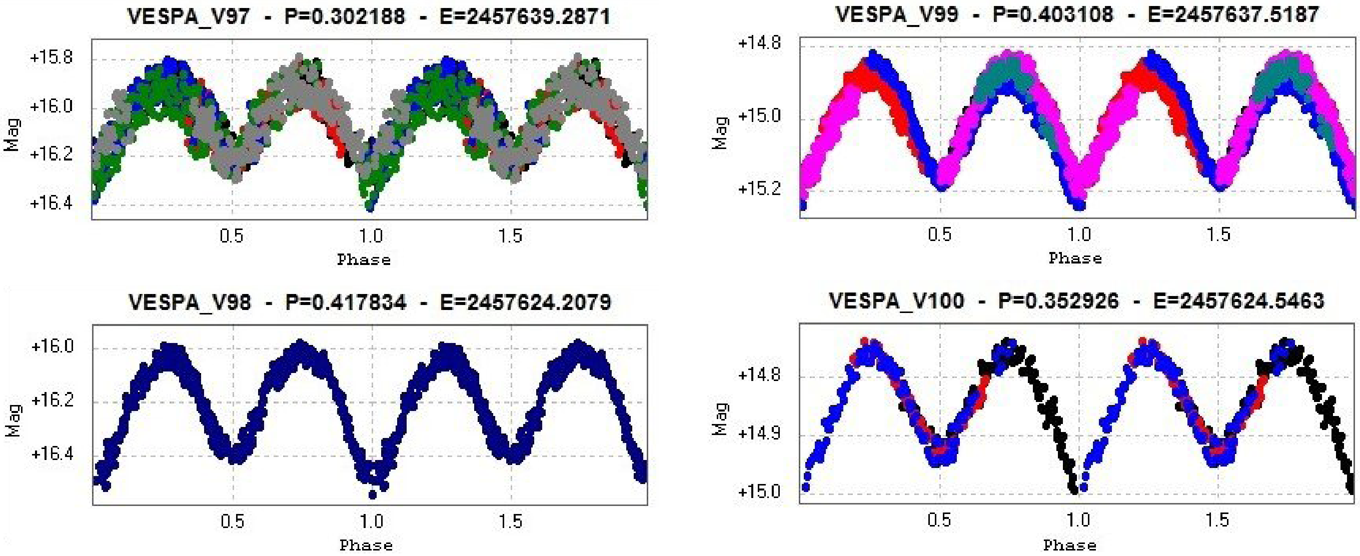

VESPA_V97 - P=0.302188 - E=2457639.2871

VESPA_V99 - P=0.403108 - E=2457637.5187

VESPA_V98 - P=0.417834 - E=2457624.2079

VESPA_V100 - P=0.352926 - E=2457624.5463

Figure 4. Light curves of the 100 discovered variable stars, cont.

# Studies of the Long Secondary Periods in Pulsating Red Giants. II. Lower-Luminosity Stars

**John R. Percy**
**Henry Wai-Hin Leung**
*Department of Astronomy and Astrophysics, and Dunlap Institute of Astronomy and Astrophysics, University of Toronto, Toronto, ON M5S 3H4, Canada; john.percy@utoronto.ca*

*Received November 8, 2016; revised January 10, 2017; accepted January 19, 2017*

**Abstract** We have used AAVSO visual and photoelectric V data and the AAVSO time-series package VSTAR and the Lomb-Scargle time-series algorithm to determine improved pulsation periods, "long secondary periods" (LSPs), and their amplitudes in 51 shorter-period pulsating red giants in the AAVSO photoelectic photometry program and in the AAVSO LPV (long period variable) binocular program. As is well known, radial pulsation becomes detectable in red giants at about spectral type M0, with periods of about 20 days. We find that the LSP phenomenon is also first detectable at about M0. Pulsation and LSP visual or V amplitudes increase from near zero to about 0.1 magnitude at periods of 100 days. At longer periods, the pulsation amplitudes continue to increase, but the LSP amplitudes are generally between 0.1 and 0.2 magnitude on average. The ratios of LSP to pulsation period cluster around 5 and 10, presumably depending on whether the pulsation period is the fundamental or first overtone. The pulsation and LSP phase curves are generally close to sinusoidal, except when the amplitude is small, in which case they may be distorted by observational scatter or, in the case of the LSP amplitude, by the pulsational variability. As with longer-period stars, the LSP amplitude increases and decreases by a factor of two or more, for unknown reasons, on a median time scale of about 20 LSPs. The LSP phenomenon is thus present and similar in radially pulsating red giants of all periods. Its cause remains unknown.

## 1. Introduction

In a previous paper (Percy and Deibert 2016), which is one of a series of our papers about pulsating red giants, we addressed the question of the nature and cause of the "long secondary periods" (LSPs) which occur in about a third of these stars, and whose cause is unknown. In the present paper, we look especially at shorter-period pulsating red giants in two samples: (1) stars in the AAVSO photoelectric photometry (PEP) program, which have both visual and PEP data; (2) shorter-period stars in the AAVSO LPV Binocular Program (www.aavso.org/lpv-section-file-downloads). These data, though not as precise as, for instance, MACHO and OGLE data, have the advantage that they have been sustained over many decades.

AAVSO PEP observations of pulsating red giants have already been analyzed by Percy *et al.* (1996). Now, there are an additional two decades of data. Robotic telescope PEP observations of similar stars were analyzed by Percy *et al.* (2001), and merged AAVSO and robotic observations were analyzed by Percy *et al.* (2008).

We hope to address scientific questions such as whether the LSPs occur in shorter-period, lower-luminosity red giants, and whether their amplitudes, and their ratio to the fundamental pulsation period are the same as in longer-period stars. Shorter-period stars have smaller pulsation and LSP amplitudes but, for the same length of dataset, yield more accurate values of the LSP, and the timescale of its amplitude variation. Since the pulsation periods are much less than a year, they are slightly less likely to be complicated by one-cycle-per-year aliases. Ultimately, we would like to make progress in identifying the nature and cause of the LSP phenomenon.

## 2. Data and Analysis

We used visual and PEP V observations from the AAVSO International Database (AID; Kafka 2016), and the AAVSO VSTAR time-series analysis package (Benn 2013), which includes both a Fourier and a wavelet analysis routine. Co-author HL was interested in comparing the results of VSTAR with those from the Lomb-Scargle algorithm (implemented here with the astropy.stats.LombScargle routine within PYTHON (www.python.org)) so we used that also for some of the analysis. Figure 1 shows the period spectrum of the visual data on T Cen, obtained with the Lomb-Scargle algorithm. The best period, the one-year aliases, and the harmonics are present and marked.

Our two samples of stars have some selection effects. Those in the PEP program were pulsating red giants which were in the AAVSO visual program in the early 1980s, but had small

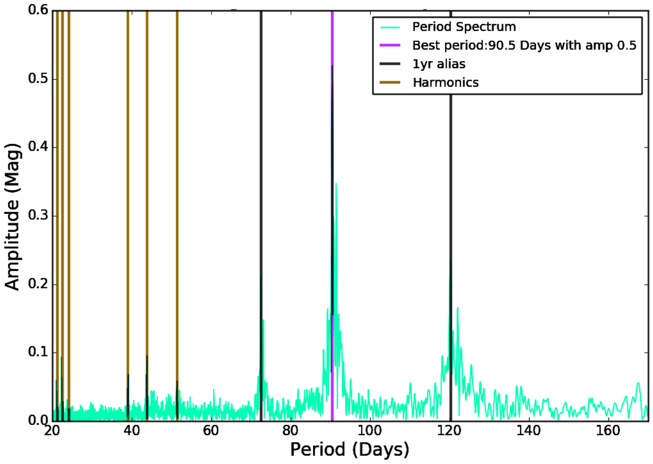

Figure 1. The Lomb-Scargle period spectrum for T Cen visual data, showing the best period (90.5 days), the one-year aliases, and the harmonics.

amplitudes, and would therefore benefit from PEP observations. The stars in the binocular program were presumably stars which were reasonably bright, and had moderate to high amplitudes. We chose to analyze stars from this program with shorter periods, since we were especially interested in the LSP phenomenon in such stars.

## 3. Results

### 3.1. Periods and amplitudes

We have determined improved periods and amplitudes in these 43 stars. Table 1 lists stars in the AAVSO LPV Binocular Program with periods less than about 120 days, for which there were sufficient data for analysis, along with our results. The columns give: the star name, the pulsation period PP, the LSP, the ratio of LSP to PP, and the pulsation and LSP visual amplitudes in magnitudes. In this and Table 2, some LSPs are close to one year and, if their amplitudes are small, there is some possibility that they are spurious (Percy 2015). Table 2 lists stars in the AAVSO PEP program for which there were sufficient visual and PEP V data to determine periods (see Notes on Individual Stars), along with our results. The columns give: the star name, the pulsation period PP, the LSP, the ratio of LSP to PP, and the pulsation and LSP amplitudes. In deciding on the value of the amplitude, we have usually given greater weight to the photoelectric V data. In any case, the PP and LSP amplitudes of these stars vary with time (Percy and Abachi 2013). Note that, although we concentrated on stars with shorter periods, there were stars in the PEP program (RS Cnc, η Gem, and SW Vir) which had longer periods. In the binocular program, X Her was listed as having a period of 102 days, but was found to have a longer one; Y Lyn was listed as having a period of 110 days, but was also found to have a longer one.

There were six stars (TV Psc, Z Eri, RR Eri, TV UMa, FP Vir, and V1070 Cyg) which were common to both programs. The two authors decided to analyze them independently. For Z Eri, this yielded two different results for the pulsation period —78.5 and 118.4 days. For this star, the Fourier spectrum yielded *several* peaks of comparable height, including those mentioned. In the V data, the highest was 239–243 days. We conclude that, with the present data, the pulsation period is indeterminate. For RR Eri, we obtained two different results for the LSP—366 and 742 days. In the Fourier spectrum of the V data, 742 days is marginally higher, whereas 366 days could well be a spurious period. Aside from these marginal differences, VSTAR and Lomb-Scarge gave equivalent results.

### 3.2. Long secondary periods

For the stars in Table 1, Figure 2 plots the ratio of LSP to pulsation period LSP/PP against PP. The shaded area is a histogram projected on the y-axis, with the scale on the top. Percy and Deibert (2016) found the ratio LSP/PP to be about 5 when the pulsation period was the fundamental period, and about 10 when the pulsation period was the first overtone. Figure 2 also shows clustering at about 5–6 and 8–10 and also some stars with a ratio of 12–14. The latter have short pulsation periods, and may be pulsating in the second overtone. This is consistent with previous studies of pulsation modes in short-

Table 1. Shorter-period stars in the AAVSO LPV binocular program.

| *Star* | *PP (d)* | *LSP (d)* | *LSP/PP* | *PP amp (mag)* | *LSP amp (mag)* |
|---|---|---|---|---|---|
| θ Aps | 108.8 | 1023 | 9.4 | 0.14 | 0.11 |
| RT Cnc | 89.3 | 371: | 4.1 | 0.06 | 0.10 |
| TU CVn | 44.8 | 363: | 8.1 | 0.03 | 0.03 |
| V465 Cas | 97.2 | 895 | 9.3 | 0.07 | 0.18 |
| T Cen | 90.5 | — | — | 0.54 | — |
| SS Cep | 100.3 | 958 | 9.5 | 0.06 | 0.09 |
| RR CrB | 55.5 | 630 | 11.3 | 0.04 | 0.05 |
| AF Cyg | 94 | 1439 | 15.3 | 0.13 | 0.08 |
| V1070 Cyg | 62.4 | 640 | 10.3 | 0.04 | 0.05 |
| U Del | 118 | 1166 | 9.9 | 0.05 | 0.21 |
| CT Del | 80.7 | 372: | 4.6 | 0.06 | 0.12 |
| TX Dra | 77.5 | 712 | 9.2 | 0.09 | 0.15 |
| Z Eri | 118.4 | 725 | 6.2 | 0.05 | 0.11 |
| RR Eri | 92.6 | 366: | 3.9 | 0.06 | 0.10 |
| X Her | 176.0 | 667 | 3.8 | 0.06 | 0.08 |
| g Her | 87.6 | 877 | 10.0 | 0.03 | 0.16 |
| UW Her | 106.8 | 985 | 9.3 | 0.09 | 0.07 |
| IQ Her | 76.1 | 624 | 8.2 | 0.05 | 0.12 |
| RX Lep | 100.7 | 572 | 5.6 | 0.06 | 0.07 |
| Y Lyn | 133.2 | 1257 | 9.5 | 0.08 | 0.33 |
| SV Lyn | 67.6 | 545 | 8.1 | 0.06 | 0.08 |
| XY Lyr | 121.4 | 1235 | 10.2 | 0.04 | 0.04 |
| GO Peg | 74.9 | 473 | 6.3 | 0.05 | 0.07 |
| TV Psc | 55.1 | 403 | 7.4 | 0.03 | 0.04 |
| τ4 Ser | 111.1 | 1159 | 10.5 | 0.04 | 0.11 |
| W Tri | 105.5 | 765 | 7.3 | 0.05 | 0.08 |
| ST UMa | 90.2 | 625 | 6.9 | 0.04 | 0.07 |
| TV UMa | 53.8 | 653 | 12.2 | 0.03 | 0.06 |
| V UMi | 72.9 | 759 | 10.5 | 0.12 | 0.08 |
| FP Vir | 62.8 | 384 | 6.1 | 0.08 | 0.11 |

Table 2. Red giants in the AAVSO PEP program.

| *Star* | *PP (d)* | *LSP (d)* | *LSP/PP* | *PP amp (mag)* | *LSP amp (mag)* |
|---|---|---|---|---|---|
| χ Aqr | 40.2 | 229 | 5.7 | 0.03 | 0.03 |
| RZ Ari | 56.5 | 507 | 9.0 | 0.05 | 0.05 |
| W Boo | 25 | 360:: | 14.4 | 0.02 | 0.04 |
| RS Cnc | 240.8 | 2050 | 8.5 | 0.19 | 0.12 |
| FZ Cep | 81.8 | 743 | 9.1 | 0.11 | 0.10 |
| FS Com | 55.7 | 680 | 12.2 | 0.06 | 0.06 |
| W Cyg | 132 | (259) | (2) | 0.20 | 0.17 |
| AB Cyg | 69 | 525 | 7.6 | 0.10 | 0.13 |
| V1070 Cyg | 62.8 | 639 | 10.2 | 0.04 | 0.05 |
| V1339 Cyg | 34.1 | — | — | 0.04 | — |
| EU Del | 62.5 | 626 | 10.0 | 0.12 | 0.08 |
| AZ Dra | 44 | 359: | 8.2 | 0.04: | 0.10: |
| Z Eri | 78.5 | 730 | 9.3 | 0.10 | 0.13 |
| RR Eri | 92.5 | 742 | 8.0 | 0.12 | 0.10 |
| η Gem | 232 | — | — | 0.07 | — |
| IN Hya | 87.8 | 693: | 7.9 | 0.09 | 0.10 |
| R Lyr | 53 | 380: | 7.2 | 0.04 | 0.04 |
| V533 Oph | 58 | 400 | 6.9 | 0.08 | 0.10 |
| ρ Per | 55 | 723 | 13.1 | 0.05 | 0.06 |
| TV Psc | 55.0 | 400: | 7.3 | 0.03 | 0.04 |
| CE Tau | 105 | 1280 | 12.2 | 0.03 | 0.08 |
| TV UMa | 54 | 640 | 11.9 | 0.06: | 0.07 |
| VW UMa | 66 | 621 | 9.4 | 0.06 | 0.07 |
| VY UMa | 122 | 1180 | 9.7 | 0.05 | 0.06 |
| SW Vir | 155 | 1647 | 10.6 | 0.50 | 0.21 |
| FH Vir | 59.6 | 360: | 6.0 | 0.09 | 0.15: |
| FP Vir | 65 | 375: | 5.8 | 0.07 | 0.10 |

period, small-amplitude red giants, which showed that many of these pulsate in the first or second overtone (e.g. Percy and Bakos 2003).

### 3.3. Amplitudes

Figure 3 plots the visual or V pulsation amplitude in magnitudes against the pulsation period. As is well-known (see Percy and Guler 1999 and the review by Kiss and Percy 2012, for instance), pulsation sets in at about M0 spectral type, which corresponds to periods of about 20 days. The pulsation amplitude then increases with period, as seen in Figure 4.

Figure 4 plots the PP amplitude against the LSP amplitude, both visual or V, in magnitudes. The two are approximately equal for periods less than about 100 days. For longer periods, the LSP amplitude is typically 0.05–0.2 magnitude (Percy and Deibert 2016). The LSP phenomenon thus becomes detectable at the same spectral type as radial pulsation.

### 3.4. Phase curves

For the stars in Table 1, the shape of the pulsation phase curve and the LSP phase curve were investigated by fitting them with a fifth-degree polynomial, and comparing the result to a sine curve using the scipy.stats.pearsonr module in PYTHON. The results are shown in figures 5 and 6. For the pulsation phase curves, there is a small dissimilarity for stars with visual amplitudes less than 0.1 magnitude. The simplest explanation is that, for these, the shape of the true (sinusoidal?) phase curve is being distorted by observational scatter. The LSP phase curves also tend to be less sinusoidal if the amplitude is less than 0.1 magnitude; again, the simplest explanation is that this is due to the distorting effect of observational scatter and of the pulsational variability. For the following stars, the LSP phase curve was flagged as being non-sinusoidal: V1070 Cyg, Z Eri, RX Lep, and XY Lyr. Only two of the four have amplitudes less than 0.10 magnitude. Percy and Deibert (2016) found, from visual inspection, that the LSP phase curve of Y Lyn was clearly sawtooth, rather than sinusoidal; here, we find it to be sinusoidal.

### 3.5. Amplitude variations

Table 3 lists stars from Table 1 which had sufficient data to investigate variations in the LSP amplitude using the wavelet routine in VSTAR. The columns list: the name of the star, the range of the LSP amplitude in magnitudes, the number N of cycles of LSP amplitude increase and decrease, and the ratio of the length L of these cycles to the LSP, where L is the length of the dataset divided by N. See our previous papers, especially Percy and Abachi (2013), for more discussion of the determination of these. In particular: note that N and L are very approximate, because there is often less than one cycle of increase and decrease in the dataset—even though the dataset may be many decades long.

The median ratio of cycle length L to LSP is 21, slightly lower than the value 30 found by Percy and Abachi (2013); the difference is probably not significant. The LSP amplitudes vary by typically a factor of two, again in agreement with the values found by Percy and Abachi (2013). Combining our results with those of Percy and Abachi (2013), there is no obvious correlation between L/LSP and pulsation period, i.e. with the radius of the star.

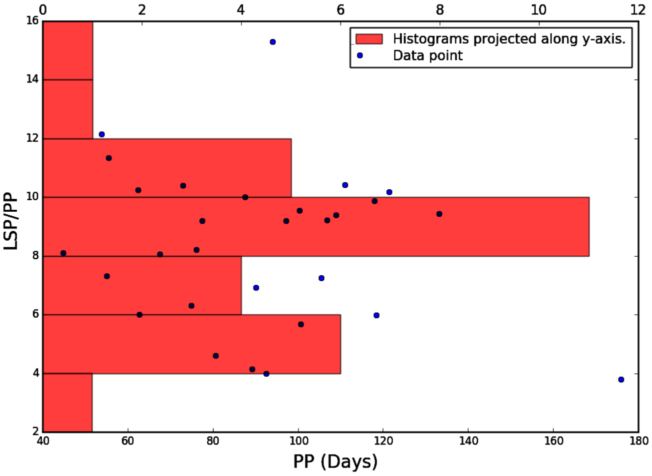

Figure 2. The ratio of LSP to pulsation period PP, as a function of PP, for the stars in Table 1. The shaded area represents a histogram of the data, with the scale at the top. The results are consistent with those of Percy and Deibert (2016), namely that the values cluster about 5 and 10, depending on whether the pulsation period is the fundamental period or the first overtone.

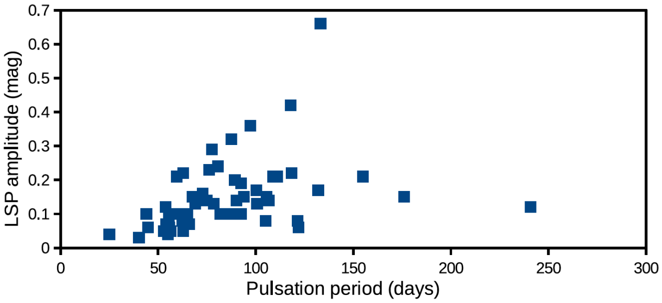

Figure 3.The visual or V pulsation amplitude in magnitudes versus pulsation period. As is well known from previous studies (reviewed by Kiss and Percy 2012), the shortest-period stars have the smallest amplitudes; radial pulsational instability sets in at spectral type approximately M0III.

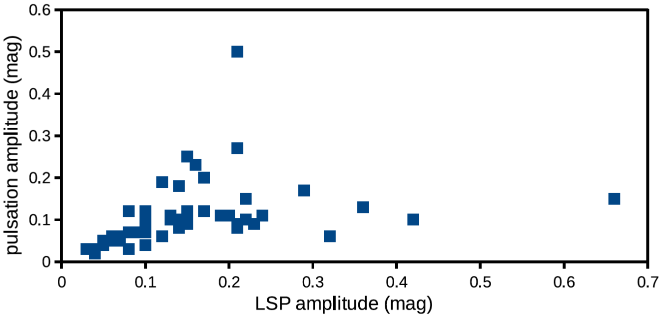

Figure 4. The PP amplitude as a function of LSP amplitude (both visual or V, in magnitudes), for the stars in Table 2. For longer-period stars, Percy and Deibert (2016) found that the LSP amplitude was typically 0.2 magnitude. For the shorter-period stars, both the LSP amplitude and the pulsation amplitude are approximately equal. Both radial pulsation and the LSP phenomenon set in at spectral type about M0III.

### 3.6. Notes on individual stars

*$\chi$ Aqr* The V data give periods of 40.2 and 229 days, but the amplitudes are small. The visual data do not give reliable periods.

*RZ Ari* The visual and V data give the same pulsation period (56.5 days) but the LSP (507 days) is present in the V data only.

*W Boo* This star switches modes between 25 and 50 days (Percy and Desjardins 1996). The present V data give a strongest period of 25.7 days. The visual and V data both give an LSP of 358–365 days, with small amplitude; it is suspiciously close to one year, and may be spurious.

*VZ Cam* There are no significant peaks in the visual or V data.

*RS Cnc* The pulsation period of 240.8 days is present in both the visual and V data. There is a possible LSP of 2,050 ± 100 days.

*DM Cep* No periods could be found.

*FZ Cep* The V data give periods of 81.8 and 743 days. The visual data are inconclusive.

*T Cet* The pulsation period may be 161 or 288 days; these are aliases. The LSP may be 1,908 days, but this too may be an alias.

*FS Com* The visual and V data both give a pulsation period of 55.7 days. The V data give an LSP of 689 days, in agreement with the result of Percy *et al.* (2008). The visual data do not show an LSP.

*GK Com* The results are uncertain.

*W Cyg* The visual data give periods of 132 and 259 days, as do the V data. We assume these to be the fundamental and first overtone periods. There is no evidence for an LSP.

*AB Cyg* The V data give periods of 69.3 and 521 days. The visual data give an LSP of 529 days, but the pulsation period is uncertain.

*V973 Cyg* The visual data give periods of 40.5 and 362 or 394 days. The V data give periods of 36.5 and 391 days. In each case, the amplitude is small.

*V1070 Cyg* The visual data give periods of 62.8 and 639 days. The V data are inconclusive.

*V1339 Cyg* The visual and V data both give pulsation periods of 34.06 days. The visual data give an LSP of 339 days, but the amplitude is only 0.02 magnitude, so it is uncertain.

*EU Del* The visual data give periods of 62.55 and 623.8 days. The V data give periods of 62.52 and 629.3 days. This star is a "prototype" of small-amplitude pulsating red giants.

*VW Dra* The data are noisy.

*AT Dra* Data are plentiful, but somewhat noisy. There are no significant peaks.

*AZ Dra* The visual data give a pulsation period of 44.4 days. The visual and V data both give an LSP of 357–360 days, with amplitudes about 0.10 magnitude. The period may be spurious.

*Z Eri* Both the visual and V data give periods of 78.5 and 730 days.

*RR Eri* The V data give periods of 92.5 and 742 days. The former is weakly present in the visual data, but not the latter. The GCVS period is 97 days.

*IS Gem* Non-variable.

*η Gem* The pulsation period (232 days) is present in both the visual and V data, but there is no obvious LSP.

*X Her* *The General Catalogue of Variable Stars* (GCVS; Samus *et al.* 2012) gives a period of 95 days; we find 176 days.

*ST Her* Both the visual and V data give periods of 151 or 257 days. These are aliases, and we cannot choose between them.

*AK Hya* The data are noisy; there are no convincing peaks.

Table 3. Amplitude variations in the LSPs in shorter-period red giant stars.

| *Star* | *LSP amp* | *N cycles* | *L/LSP* |
|---|---|---|---|
| θ Aps | 0.07–0.17 | 0.75 | 34 |
| RT Cnc | 0.05–0.15 | 4 | 8 |
| TU CVn | 0.02–0.06 | 2 | 50 |
| SS Cep | 0.07–0.16 | 1.5 | 26 |
| AF Cyg | 0.05–0.11 | 1.5 | 21 |
| V1070 Cyg | 0.04–0.06 | 1.5 | 16 |
| U Del | 0.14–0.26 | 0.5 | 21 |
| CT Del | 0.02–0.18 | 1.7 | 20 |
| Z Eri | 0.08–0.19 | 2 | 21 |
| X Her | 0.04–0.25 | 1 | 60 |
| g Her | 0.08–0.22 | 0.5 | 46 |
| RX Lep | 0.05–0.13 | 2 | 18 |
| Y Lyn | 0.15–0.40 | 0.5 | 32 |
| SV Lyn | 0.03–0.10 | 2 | 18 |
| XY Lyr | 0.03–0.07 | 1 | 16 |
| TV Psc | 0.02–0.10 | 1.25 | 40 |
| τ4 Ser | 0.07–0.12 | 1.25 | 17 |
| W Tri | 0.06–0.10 | 1.75 | 20 |
| ST UMa | 0.03–0.12 | 2 | 24 |
| TV UMa | 0.03–0.06 | 2 | 15 |
| V UMi | 0.03–0.20 | 0.75 | 26 |
| FP Vir | 0.06–0.17 | 1.5 | 33 |

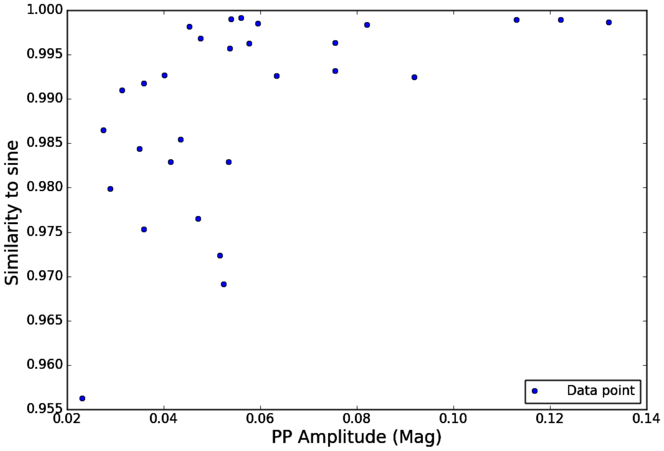

Figure 5. The similarity of the pulsation phase curve to a sine curve, as a function of pulsation amplitude in magnitudes. Stars with small pulsation amplitudes may have phase curves which differ slightly from sine curves, perhaps because observational scatter distorts the phase curve.

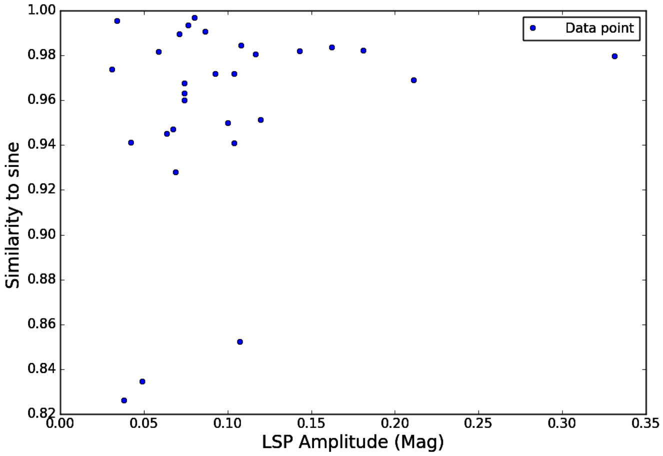

Figure 6. The similarity of the LSP phase curve to a sine curve, as a function of the LSP amplitude in magnitudes. Stars with smaller LSP amplitudes may have LSP phase curves which differ slightly from sine curves, perhaps because observational scatter and the pulsational variability distort the LSP phase curve.

*IN Hya* The V data suggest a pulsation period of 87.9 days and an LSP of 693 days. The visual data are less clear, but may indicate a pulsation period of 85.8 days.

*SS Lep* Probably non-variable.

*Y Lyn* GCVS gives a period of 110 days; we get 133.2 days.

*R Lyr* The visual and V data give a period of 53 ± 10 days. There is no LSP (Percy *et al.* 2008).

*V614 Mon* The pulsation period is unclear, and the LSP in both the visual and V data is dangerously close to one year.

*V533 Oph* The visual data give periods of 55.3 and 398 days. The V data give periods of 60.0 and 405 days.

*ρ Per* The visual and V data give the same pulsation period (55 ± 0.5 days) but the LSP (723 days) is visible in the V data only.

*TV Psc* The periods from the visual (55.1 days) and V data (55.0 days) are consistent, even though the amplitudes are small—0.06 and 0.02 magnitude, respectively—but the LSP is uncertain: 403 days from the visual data, and 546 days from the V data, both seemingly well-determined.

*TX Psc* No reliable periods could be found.

*XZ Psc* No reliable periods could be found.

*V449 Sco* There are no significant peaks.

*CE Tau* The pulsation period (105 ± 2 days) and the LSP (1280 ± 10 days) are present in both the visual and V data.

*TV UMa* The visual data give periods of 53.8 and 656 days; the V data give periods of 50–60 and 627 days.

*VW UMa* The visual data give periods of 65.9 and 624 days; the V data give periods of 66.2 and 618 days.

*VY UMa* The visual data give periods of 121.8 and 1,200 days. The V data are less certain, but suggest periods of 125 and 1,160 days.

*SW Vir* The visual and V data give pulsation periods of 155.3 and 154 days, respectively. The LSP is uncertain, but may be 1647 days.

*EV Vir* The data are too sparse to yield a result.

*FH Vir* The V data give a pulsation period of 59.6 days, in reasonable agreement with the GCVS period of 70 days. The LSP may be about 350–370 days, but this is dangerously close to a year.

*FP Vir* The visual data give periods of 62.8 and 383 days; the V data give periods of 67.0 and 369 days.

## 4. Discussion

We must emphasize the challenges and consequent uncertainties of our work: the amplitudes of our stars are small; the data are primarily visual, so they have limited accuracy and the possibility of spurious signals. Despite the decades-long database, some of the phenomena that we are studying would benefit from an even longer one.

Our results should provide additional constraints on the cause of the LSP phenomenon. That cause must be able to act in lower-luminosity stars as well as higher-luminosity ones. At the same time, its amplitude must approach zero in the lowest-luminosity pulsators, as the pulsation amplitude does. And, whatever causes the cyclic changes in LSP *amplitudes* must operate over the entire period/luminosity range. Wood (2015) also shows (his Figure 1) that LSPs extend to the lowest luminosities—though sparsely—in the Large Magellanic Cloud. It also appears that LSPs occur on both the red giant branch and on the asymptotic giant branch. The LSP mechanism must explain the tight correlation between the LSP and the fundamental pulsation period, and the consistency of the LSP amplitude variations over the entire LSP range. It must also explain the large prevalence of LSPs—over 30 percent at all luminosities. It cannot be dependent on some rare process or configuration in the star.

Several possible causes of LSPs have been suggested in the literature e.g. Nicholls *et al.* (2009). Some do not match all of the observations. Others are inconsistent with theoretical predictions, in their present form. Percy and Diebert (2016) discussed the possibility of some form of rotational variability, but there were significant problems with that hypothesis. It is possible, of course, that different mechanisms act in different stars. V Hya, for instance, may be a form of eclipsing binary.

Saio *et al.* (2015) proposed that oscillatory convective pulsation modes might be a possible explanation for the LSPs. This hypothesis had some problems, but they might be overcome by a better treatment of convection; the authors used the standard mixing-length theory of convection. Based on the constraints listed above, this hypothesis is very attractive, but the “problem of the LSPs” must be considered unsolved at this point in time.

Are there red giants with LSPs but no primary (pulsation) periods? Probably not, because almost all red giants cooler than M0III are unstable to pulsation. But it might be worth looking at late K giants to see if any of them varied with periods 5–10 times greater than the expected fundamental mode period.

## 5. Conclusions

We have used AAVSO visual and PEP data to determine improved periods and amplitudes of lower-luminosity, shorter-period pulsating red giants. Our results extend those of Percy and Deibert (2016) to stars with shorter periods—down to 20–30 days. As red giants expand, radial pulsation becomes detectable in early type giants, with periods of about 20 days. So does the LSP phenomenon. With increasing period, the pulsation and LSP amplitudes both increase, and are approximately equal on average. When the period is longer than about 100 days, the LSP amplitude levels off at 0.1 to 0.2 magnitude. The LSP is about five times the fundamental pulsation period in these shorter-period stars, as it is in longer-period ones, and the LSP amplitude rises and falls on a time scale of about 20 LSPs. The LSP phenomenon thus extends to the shortest periods. Its nature and cause, however, are still unknown, but it must be able to operate in stars with shorter periods, warmer temperatures, and lower luminosities.

## 6. Acknowledgements

We thank the AAVSO observers who made the observations on which this project is based, the AAVSO staff who archived them and made them publicly available, and the developers of the VSTAR package which we used for analysis. This paper is based, in part, on a short summer research project by undergraduate astronomy and physics student co-author HL.

We acknowledge and thank the University of Toronto Work-Study Program for financial support. This project made use of the SIMBAD database, maintained in Strasbourg, France.

## References

Benn, D. 2013, VSTAR data analysis software (http://www.aavso.org/node/803).

Kafka, S. 2016, observations from the AAVSO International Database (https://www.aavso.org/aavso-international-database).

Kiss, L. L., and Percy, J. R. 2012, *J. Amer. Assoc. Var. Star Obs.*, **40**, 528.

Nicholls, C. P., Wood, P. R., Cioni, M.-R. L., and Soszyński 2009, *Mon. Not. Roy. Astron. Soc.*, **399**, 2063.

Percy, J. R. 2015, *J. Amer. Assoc. Var. Star Obs.*, **43**, 223.

Percy, J. R., and Abachi, R. 2013, *J. Amer. Assoc. Var. Star Obs.*, **41**, 193.

Percy, J. R., and Bakos, A. G. 2003, in *The Garrison Festschrift*, ed. R. O. Gray, C. J. Corbally, and A. G. D. Philip, L. Davis Press, Schenectady, NY, 49.

Percy, J. R., and Deibert, E. 2016, *J. Amer. Assoc. Var. Star Obs.*, **44**, 94.

Percy, J. R., and Desjardins, A. 1996, *Publ. Astron. Soc. Pacific*, **108**, 847.

Percy, J. R., Desjardins, A., Yu, L., and Landis, H. J. 1996, *Publ. Astron. Soc. Pacific*, **108**, 139.

Percy, J. R., and Guler, M. 1999, *J. Amer. Assoc. Var. Star Obs.*, **27**, 1.

Percy, J. R., Mashintsova, M., Nasui, C. O., Palaniappan, R., Seneviratne, R., and Henry, G. W. 2008, *Publ. Astron. Soc. Pacific*, **120**, 523.

Percy, J. R., Wilson,, J. B., and Henry, G. W. 2001, *Publ. Astron. Soc. Pacific*, **113**, 983.

Saio, H., Wood, P. R., Takayama, M., and Ita, Y. 2015, *Mon. Not. Roy. Astron. Soc.*, **452**, 3863.

Samus, N. N., *et al.* 2012, *General Catalogue of Variable Stars*, Sternberg Astronomical Institute, Moscow (GCVS database, http://www.sai.msu.su/gcvs/gcvs/index.htm).

Wood, P. R. 2015, *Mon. Not. Roy. Astron. Soc.*, **448**, 3829.

# High-Cadence B-Band Search for Optical Flares on CR Draconis

**Gary A. Vander Haagen**
*Stonegate Observatory, 825 Stonegate Road, Ann Arbor, MI; garyvh2@gmail.com*

*Received November 22, 2016; revised December 16, 2016, January 12, 2017; accepted January 12, 2017*

**Abstract** The high-cadence search at 50 samples/sec of CR Dra revealed one B-band flare of 560 ± 30 seconds' duration, and 30-mmag peak above the mean. Three additional potential low-level flares could not be confirmed. The search for fast sub-second flares was conducted with negative results. The study collected $1.15 \times 10^7$ photometric measurements over 64.16 hours on 27 nights from May 6, 2016, through October 25, 2016. This represents a flare rate of 0.016 flare/hour. The CR Dra binary has resolved orbital components with established orbital elements. From this flare and historical flare events, any correlation between the system components' calculated linear separation and flare activity level could not be confirmed.

## 1. Introduction

CR Draconis is one of approximately 100 nearby flare stars within 25 pc, a short period young Me dwarf binary type M5.6V (Simbad 2016), B-magnitude 10.92, HIP 79796. The flaring of the young Me dwarf star systems is related to their stage of evolution. That is, almost all dwarf stars possess the ability to flare during an early portion of their evolution and some of low luminosity can stay in this stage for $10^{10}$ years or longer (Mirzoyan 1990). Factors influencing this evolutionary process are still under study, with stellar rotation, magnetic fields, total mass, and potentially their component separation being contributors. Tamazian *et al.* (2008) presents a good summary of the current theories for flaring of these systems. One recent study area is the relationship between flares and the rapid changes in their stellar magnetic field configuration and coronal mass ejections (CME). Manchester *et al.* (2005) describes a model whereby the CME drives "fast-mode" shock from the stellar surface to distances of approximately 1 AU with consequent plasma and magnetic field changes, which may affect flare activity. This theory has researchers looking for nearby binaries with short periods and known orbits to look for correlation between component separation within ~ 2 AU or less and increased flare rates or flux energy levels. For this reason alone, the short period binary CR Dra is of interest in understanding the relationship, if any, between flaring and magnetic field interaction of close partners.

CR Dra is one of a small number of nearby flare stars less than 25 pc distant with the potential for resolving the individual bodies and calculating orbit and dynamical mass. Tamazian *et al.* (2008) used speckle measurements to refine the previous work of Blazit *et al.* (1987) to resolve the two-body system. These data revealed a highest probability mass sum of 1.00 Ms, a dynamical parallax of 58.43 mas or 17.4 pc, an orbital period of 4.040 ± 0.005 years, and orbital elements with ephemeris for the years 2008–2013. With these data the correlation between the bodies' orbital separation and flaring were studied as proposed by Manchester *et al.* (2005). The very limited historical flare data (Table 1) were superimposed on the calculated orbital positions (Tamazian *et al.* 2008), and revealed "no plausible correlation between flaring activity and linear distance between components."

The objective of this search was to conduct a high-cadence photometric study to capture conventional longer flares and also any solo or short duration sub-second flares preceeding, during, or following the main outburst. Such data should improve the granularity of knowledge of an outburst event and potentially capture very fast solo events missed by conventional long integration photometry (Vander Haagen 2013, 2015). These data will also be resampled for longer flare analysis. In addition, any flare data will be correlated with the component orbital position.

## 2. Optical system, data collection, and analysis tools

The optical system consisted of a 43-cm corrected Dall-Kirkham scope, a high-speed silicon photomultiplier (SPM), and a data acquisition system capable of sub-millisecond data collection times. The SPM was chosen for this application

Table 1. The historical data for CR Dra flares show the observation time span, detection results, linear separation distance (d) in AU, and flare rates. Flare rates were generally not cited (—) or total observing time was not provided to enable calculation.

| *Observation Date* | *Flares Detected* | *Distance (d) AU* | *Flare Rate* | *Reference* |
|---|---|---|---|---|
| 1968 May 28–July 14 | none | 2.59–2.34 | 0 | Cristaldi and Rodono (1970) |
| 1970 May 11–June 18 | 1 flare | 2.45–2.52 | — | Cristaldi and Longhitano (1979) |
| 1971 July 1 | 1 flare | 2.95 | — | Cristaldi and Rodono (1973) |
| 1974 June 7 | 1 flare | 2.47 | 0.025 flares/hour | Kareklidis *et al.* (1977) |
| 1974 June | low activity | 2.47 | — | Mahmoud (1991) |
| 1975 June–August | none | 2.96–2.93 | 0 flares, 46.9 hours | Mahmoud *et al.* (1980) |
| 1978 May 10–17 | 1 flare | 2.41 | — | Anderson (1979) |
| 1980 July 19–20 | none (Einstein) | 2.41 | 0 | Ambruster *et al.* (1987) |
| 1991 June | none (ROSAT) | 2.95 | 0 | Tsikoudi and Kellett (1997) |
| 2007 March–July | none | 2.78–2.93 | 0 | Tamazian *et al.* (2008) |
| 2007 April–July | 20 flares | 2.83–2.92 | — | Dal (2012) |

because it has sensitivity comparable to a standard single channel vacuum photomultiplier yet a more robust mechanical and electrical design with the disadvantage of higher dark counts (Vander Haagen 2011).

The optical system is shown in Figure 1. The incoming beam is split approximately 85/4 with the reflected portion passing through the optical filter, an f-stop yielding a 57 arc-second field, and onto the SPM detector. A wide bandwidth pulse amplifier amplifies the SPM signal, producing a 2–3 volt pulse of approximately 50ns for each converted photon. The photon pulses are sent to a PC-based data acquisition system where they are gated and counted based upon the collection rate. A 20-ms gate was used for measurements, generating a 50 Hz data collection rate or 50 samples/second. The balance of the incoming beam passes through the beam splitter to a conventional CCD camera used for initial alignment, guiding, and measurement of both the guide star flux and background flux. The target flux counts along with GPS 1-second time stamps are recorded in the DAQ Log File by the data acquisition system (Vander Haagen and Owings 2014). The CCD Data and Control stream consists of reference and background flux values plus pixel counts for each guide star sample, typically every 5 seconds. These values are stored in the AG (auto-guider) Tracker Log file.

Upon completion of the night's search the DAQ Log File and the CCD's AG Tracker Log File are merged and parsed so every target data point is matched to the time Tracker data with the target counts corrected for the SPM dark counts and sky background in a quadrature calculation, and each sample GPS time-stamped. This parsing operation results in an integrated file with all constituents ready for analysis, with each file containing up to one million sample lines each containing target, reference, and background data. Files of this size are too large for spreadsheet analysis but are easily analyzed using signal processing software such as SIGVIEW (SignalLab 2016). The files are reviewed and can be processed using a variety of filters, time domain transforms, and statistical tools. After reviewing the high speed data for fast flares the data were resampled using SIGVIEW to 2-second bins for the longer flare search. The same reference star is used for each run. Since the prime flare attributes for analysis are the ratio of peak flux to mean flux, duration, and the flare profile, the data are not corrected for air mass.

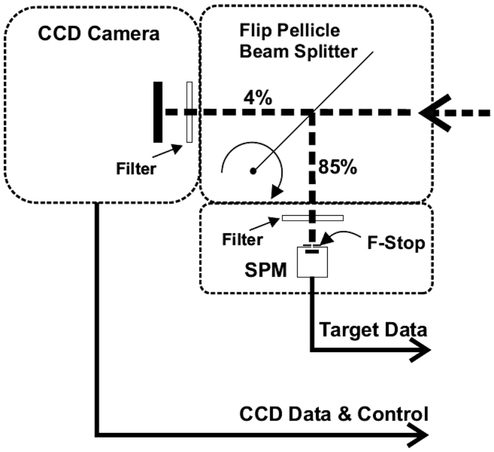

Figure 1. The optical train pictorial shows the pellicle beam splitter with both reflected and pass-through beams. The reflected beam passes through the narrow band filter, aperture, and onto the silicon photomultiplier (SPM). The pellicle can be flipped to allow 100% light transmission for initial target alignment using the CCD camera. The SPM is mounted on a X-Y stage for precise centering of detector to the centerline of the CCD camera. Guiding is provided with pellicle in position shown.

## 3. Flare search

The study objective was capturing high time-resolution flaring activity connected with longer duration conventional flares and short duration solo flares. Very short flares of 10 to 100 ms duration have been observed unconnected with conventional flaring activity. These very short flares generally consisted of one or more points at 3σ or higher with a peak at 4–10σ. A 50ms duration flare was reported for EV Lac in the U–B band by Zhilyaev and Romanjuk (1990) and simultaneous U and B-band flares on BY Dra (Zalinian and Tovmassian 1987). Vander Haagen (2013) also reported very short duration flares on AR Lac, II Peg, and UX Ari of 30 to 85 ms duration with peaks 0.29–0.51 magnitude above the mean.

A criterion was developed to isolate these short duration flares in very large sample sizes: flares must consist of a minimum of three consecutive data points, two at or above 3σ and one at or above 5σ. Since the minimum number of photons per gate was always 100 or more, normal distribution statistics were used to compute the standard deviation. Statistics were collected 600 seconds prior to the event where possible using digital signal processing software (SignalLab 2016). This process is similar in direction to that followed by flare searches (Byrne *et al.* 1994) and as described by Vander Haagen (2015). The probability of this sequence being a random event is $5.2 \times 10^{-13}$ N, where N is the number of integrations or samples taken during the observing interval and σ is for the positive events only. With N ranging from 1 to $2 \times 10^{6}$ samples during an observing interval the probability of the event sequence being random is appropriately small. This criterion was used for each of the data sets to isolate potential short duration flares.

The search for slower or longer flares with small flux change was best served by resampling to a longer gating period of two seconds. Searching for such signals in the 100 mmag or lower range with durations of minutes or longer at low S/N ratios is difficult amidst all high frequency noise. All the data groups were reviewed at both the 50 s/sec and the resampled 0.5 s/sec rates.

## 4. CR Dra data collection and results

Data collection was conducted over 27 nights from May 6, 2016, through October 25, 2016 (Figure 2). The total data collection time was 64.16 hours, or 231 Ksec at 50 samples/sec. Using a 500-nm low pass filter combined with the SPM response the resultant band pass approximates standard B-band. B-band was chosen since CR Dra emits greater flare energy at shorter wavelengths (Cristaldi and Longhitano 1979). The U-band would have been the best choice for low-level flare detection but the SPM detector has very little response in that region.

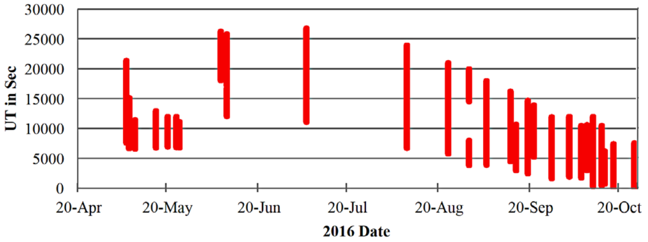

Figure 2. CR Dra data collection span of 27 nights from May 6 through October 25, 2106. The y-axis is in UT (seconds) for the date specified, showing the nightly time span when data were acquired, e.g., 7201 sec UT = 02:00:01 UT.

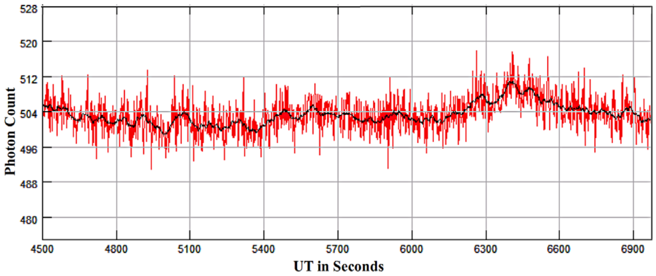

Figure 3. 2016-09-27, CR Dra data resampled at 0.5 s/sec (2 sec gating period) showing 30 mmag, 560 ± 30 seconds duration flare with 503 mean and 517 peak (4.1σ). The solid black line is a 20-sample running-average plot. CR Dra is a steady 10.92 B-mag star under non-flaring conditions. The time axis is in UT (seconds) for the date specified, e.g., 7201 sec UT = 02:00:01 UT.

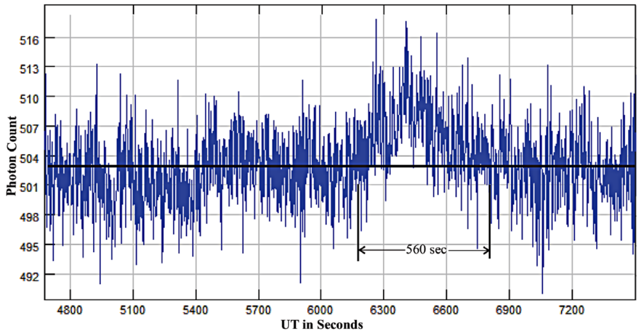

Figure 4. 2016-09-27 CR Dra axis expanded to show greater flare detail and the duration measurement. Sample rate is 50s/sec. Duration is measured between the approximate points where flux exits and returns to the mean value of 503 counts (horizontal line) or 560 ± 30 sec. The time axis is in UT (seconds) for the date specified, e.g., 7201 sec UT = 02:00:01 UT.

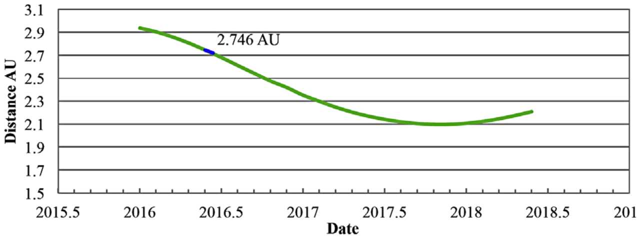

Figure 5, binary component linear separation calculated using the orbital elements from Tamazian *et al.* (2008). Highlight shows orbital position of 2016-09-27 flare at 2.75 AU.

No short duration flares were detected using the statistical criteria over the full $1.15 \times 10^7$ measurement data set.

All data sets were resampled using two-second gating, 0.5 s/sec, and reviewed for flare activity. Figure 3 shows a 2016-09-27 flare of 30 mmag, 4.1σ, and 560 ± 30 seconds' duration. The graph scale is expanded in Figure 4 to show greater instantaneous detail and the flare duration as measured at the mean quiescent flux crossing line. The flare occurred at the two-body linear separation of 2.75 AU as shown in the orbital plot (Figure 5). There were three other potential low level flares, two on 2016-10-09 and one on 2016-08-23, that could not be confirmed due to unstable atmospheric conditions and the poor S/N of the target and reference data.

## 5. Conclusions

In conclusion, a statistical criterion was used to isolate short duration optical flares from random photon events. No short duration flares were detected over the 64.16-hour observing period. One 560-second duration flare was detected with peak 30 mmag above the mean yielding a flare rate of 0.016 flare/hour. The flare rate is the prime indicator of activity and there are insufficient data for statistical analysis. However, the flare rate and magnitude are consistent with those reported by Kareklidis *et al.* (1977) at 2.47 AU linear separation, but likely a substantially lower rate than Dal (2012) at 2.83–2.92 AU, should the rate been provided.

The 0.016 flare/hour does not confirm or disapprove the conclusion of Tamazian *et al.* 2008 that there is no correlation between activity level and component separation. The activity level from the Dal (2012) search in which 20 flares were detected at 2.83-2.92 AU does help the argument. However, until a search is conducted close to the minimum body separation of 2.1 AU, where flare rates and/or flux increases are theorized, a firm conclusion seems premature. There will be an opportunity early in the fall of 2017 when the binary is at minimum linear separation to test the fast-mode shock hypothesis.

## 6. Acknowledgements

Thanks are expressed to L. E. Owings for his collaboration on the data pipeline and writing of the two software programs necessary for data reduction.

## References

Ambruster, C. W., Sciortino, S., and Golub, L. 1987, *Astrophys. J., Suppl. Ser.*, **65**, 273.
Anderson, C. M. 1979, *Publ. Astron. Soc. Pacific*, **91**, 202.
Blazit, A., Bonneau, D., and Foy, R. 1987, *Astron. Astrophys., Suppl. Ser.*, **71**, 57.
Byrne, P. B., Lanzafame, A. C., Sarro, L. M., and Ryans, R. 1994, *Mon. Not. Roy. Astron. Soc.*, **270**, 427.
Cristaldi, S., and Longhitano, M. 1979, *Astron. Astrophys., Suppl. Ser.*, **38**, 175.
Cristaldi, S., and Rodono, M. 1970, *Astron. Astrophys., Suppl. Ser.*, **2**, 223.
Cristaldi, S., and Rodono, M. 1973, *Astron. Astrophys., Suppl. Ser.*, **10**, 47.

Dal, H. A. 2012, *Publ. Astron. Soc. Japan*, **64**, 82.

Kareklidis, G., Mavridis, L. N., and Stavridis, D. C. 1977, *Inf. Bull. Var. Stars*, No. 1356, 1.

Mahmoud, F. M. 1991, *Astrophys. Space Sci.*, **186**, 113.

Mahmoud, F. M., Mavridis, L. N., Stavridis, D., and Varvoglis, P. 1980, *Inf. Bull. Var. Stars*, No. 1799, 1.

Manchester, W. B. IV, *et al.* 2005, *Astrophys. J.*, **622**, 1225.

Mirzoyan, L. V. 1990, in *Flare Stars in Star Clusters, Associations and the Solar Vicinity*, ed. L. V. Mirzoyan, B. R. Pettersen, M. K. Tsvetkov, IAU Symp. 137, Kluwer Academic Publishers, Dordrecht, 1.

SignalLab. 2016, SIGVIEW 2.8 software for DSP applications (http://www.sigview.com/index.htm).

Simbad Astromical Database. 2016, (http://simbad.u-strasbg.fr/simbad/).

Tamazian, V. S., Docobo, J. A., Balega, Y. Y., Melikian, N. D., Maximov, A. F., and Malogolovets, E. V. 2008, *Astron. J.*, **136**, 974.

Tsikoudi, V., and Kellett, B. J. 1997, *Mon. Not. Roy. Astron. Soc.*, **285**, 759.

Vander Haagen, G. A., 2011, in *The Society for Astronomical Sciences 30th Annual Symposium on Telescope Science*, Society for Astronomical Sciences, Rancho Cucamonga, CA, 87.

Vander Haagen, G. A. 2013, *J. Amer. Assoc. Var. Star Obs.*, **41**, 114.

Vander Haagen, G. A. 2015, *J. Amer. Assoc. Var. Star Obs.*, **43**, 219.

Vander Haagen, G. A., and Owings, L. E. 2014, in *The Society for Astronomical Sciences 33rd Annual Symposium on Telescope Science*, Society for Astronomical Sciences, Rancho Cucamonga, CA, 191.

Zalinian, V. P., and Tovmassian, H. M. 1987, *Inf. Bull. Var. Stars*, No. 2992, 1.

Zhilyaev, B. E., and Romanjuk, Ya. O. 1990, in *Flare Stars in Star Clusters, Associations and the Solar Vicinity*, ed. L. V. Mirzoyan, B. R. Pettersen, M. K. Tsvetkov, IAU Symp. 137, Kluwer Academic Publishers, Dordrecht, 35.

# Photometric Analysis of HD 213616: a Multi-modal δ Scuti Variable Star

**Vance Petriew**
*P.O. Box 9 Station main, White City, SK S4L 5B1, Canada; vance.petriew@sasktel.net*

**Horace A. Smith**
*Department of Physics and Astronomy, Michigan State University, East Lansing, MI 48824, USA; smith@pa.msu.edu*

*Received November 28, 2016; Revised December 15, 2016; accepted December 16, 2016*

**Abstract** We analyzed new photometry of HD 213616, showing that, instead of being a W Ursae Majoris eclipsing binary, it is a multimode δ Scuti star of relatively high amplitude. Three independent pulsation modes were identified in a Fourier analysis of the photometry, in addition to several combination pulsation frequencies.

## 1. Introduction

In a quest for brighter eclipsing binary targets from the online AAVSO's Variable Star Index (VSX; Watson *et al.* 2014), the star HD 213616 (R.A. $22^h\ 32^m\ 07.8^s$, Dec. +39° 47' 56.2" (2000.0)) was randomly selected for an all-night time series run. After one night of photometry, it was clear that the current VSX classification of HD 213616 as an EW (W Ursae Majoris) eclipsing variable was incorrect. As we will show in the remainder of this paper, HD 213616 instead appears to be a δ Scuti (DSCT) type variable.

## 2. Data

To better capture this variable star's behavior, multiple nights of data were collected during the 2015 and 2016 observing seasons. Data were collected late into season one using an SBIG ST7-XME CCD camera coupled to a Celestron CPC-800 GPS telescope. The CCD camera is equipped with a single Johnson V filter which was employed for all observations. The effective focal length is 906 mm. The 9-µm pixels of the SBIG camera provide an image scale of 2.05 arcseconds per pixel.

In 2016, the same telescope and CCD camera were used to collect more data, bringing the total number of aperture photometry data points used in this analysis to 10,524. The date range of the observations is HJD 2457291 to HJD 2457635.

The reference star used for photometry was TYC 3205-1759-1 (R.A. $22^h\ 30^m\ 28.4^s$, Dec. +39° 46' 09.5" (2000.0)). When the photometry was entered into the AAVSO International Database (AID; Kafka 2016), a V magnitude of 9.08 was adopted for the reference star. As of Data Release 9, the V magnitude for TYC 3205-1759-1 from the APASS catalogue (Henden and Munari 2014) is 9.087 ± 0.057. Note that the comparison star is quite red, with an APASS B–V value around 1.4. The check star used was TYC 3205-1808-1 (R.A. $22^h\ 30^m\ 11.1^s$, Dec. +39° 36' 28.6" (2000.0)). Integration times for each frame were 30 seconds, which produced SNR values above 300 for both the variable and the reference star. The software MAXIM DL version 5.01 (Diffraction Limited 2012) was used to perform differential aperture photometry of the dataset. Typical aperture sizes are 7 to 9 pixels in size with a gap of 8 and an annulus of 10 pixels. All frames were bias, dark, and flat field corrected. Data were exported from MAXIM DL and into MICROSOFT EXCEL to calculate error bars for the data based on the formula

$$\text{Error} = [(\sigma(k-c))^2 + (1/\text{SNR})^2]^{0.5} \quad (1)$$

following the recommendation of Koppleman (2005), where σ(k−c) is the standard deviation for the comparison star minus check star magnitudes and SNR is the signal-to-noise ratio of the measurement.

The typical uncertainty of differential V magnitudes for a single observing session is 0.008 magnitude, with the largest uncertainty being around 0.014 magnitude. There may be slight offsets from night to night but these typically run in the range of 0.01 magnitude and were not accounted for in the dataset. The photometric data points were not extinction corrected. The distribution of the observations over time is shown in Figure 1. Figure 2 illustrates the variation of HD 213616 during four nights of observation. The photometry of HD 213616 has been entered into the AAVSO International Database.

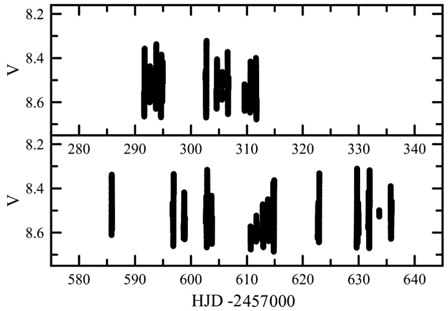

Figure 1. Light curve for HD 213616 from 2015 (top panel) and 2016 (bottom panel).

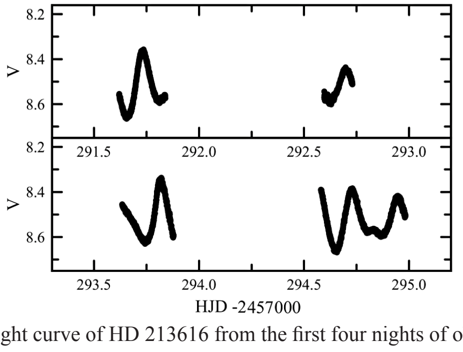

Figure 2. Light curve of HD 213616 from the first four nights of observation.

In the remainder of this paper we present a Fourier analysis of the new photometry that supports the DSCT classification for this star. We also discuss the earlier observations of HD 213616 that suggested that the star was instead an EW variable.

## 3. Analysis

We Fourier-analyzed the photometric observations using the PERIOD04 routine (Lenz and Breger 2005). Scans were performed for the frequency range 0–50 cycles / day for the 2015 and 2016 datasets individually (frequency resolution $\Delta\nu = 10^{-4}$ d$^{-1}$) and for the entire 2015–2016 dataset (frequency resolution $\Delta\nu = 10^{-5}$ d$^{-1}$). Because the observations were obtained from a single site, we also inspected the spectral windows of the observations to gain insight into possible aliasing problems. We adopted an iterative approach to find significant frequencies, using PERIOD04 to identify the strongest frequency, cleaning the data to remove that frequency, rescanning, identifying the next strongest frequency, and repeating until we detected all the frequencies with amplitudes greater than about 4 times the typical noise in the spectrum. Results are shown in Table 1 for the frequencies detected and their amplitudes and phases. The numbers in parentheses are an estimate of the uncertainty in each quantity. PERIOD04 offers two ways of estimating uncertainties of derived parameters, a least squares error calculation and a monte carlo simulation. If one of these approaches gave a significantly larger uncertainty than the other, we adopted the larger uncertainty in Table 1. We also examined the effects that small changes in the PERIOD04 scanning parameters had upon the derived frequencies, amplitudes, and phases. In a few instances this suggested that the actual uncertainties should be slightly larger than the formal uncertainties returned by the PERIOD04 routine. If so, we chose the larger, more conservative, estimate of error.

In all of the analyses, three frequencies, f1, f2, and f3, were dominant. The frequency near 10.67 c / d could be interpreted as 2f1, a harmonic of the f1 frequency. Four other frequencies could be interpreted as combinations of the first three frequencies. In addition, for the entire 2015–2016 dataset, some power (amplitude 0.007 magnitude) was found at a frequency of 0.03905 d$^{-1}$, corresponding to a period of 25.61 days. We are not certain of the reality of this frequency, since it is not seen in the separate analyses of the 2015 and 2016 observations, and because the corresponding period is within a factor of 1 or 2 of the total time spans covered by the 2015 and 2016 observations, taking each year separately.

Including just the f1, f2, f3, and 2f1 components in an analysis reduces the root mean square scatter in the 2015–2016 magnitudes from 0.083 mag. to a residual scatter of 0.017 mag. Including all of the components in the analysis further reduces the residuals to 0.011 magnitude, close to the expected observational uncertainty. For the 2015 observations alone, the corresponding numbers are 0.079 mag., 0.014 mag., and 0.010 mag. For the 2016 observations only, the corresponding numbers are 0.085 mag., 0.017 mag., and 0.011 mag.

To illustrate the appearance of the Fourier spectrum, in Figure 3 we show a portion of the spectrum for the 2015–2016 observations. In Figure 4, we show the spectrum after the data have been prewhitened to remove the significant frequencies.

Table 1. Fourier analysis.

| *Frequency (c/d)* | *V (amplitude)* | *Phase* | *Identification* |
|---|---|---|---|
| 2015–2016 | | | |
| 5.33800(1) | 0.0946(1) | 0.374(1) | f1 |
| 6.68087(1) | 0.0289(1) | 0.200(1) | f2 |
| 8.02710(1) | 0.0429(1) | 0.402(1) | f3 |
| 10.67595(2) | 0.0111(2) | 0.922(2) | 2f1 |
| 1.34308(2) | 0.0095(2) | 0.442(2) | f2-f1 |
| 2.68890(2) | 0.0093(2) | 0.119(3) | f3-f1 |
| 12.01582(3) | 0.0061(2) | 0.272(3) | f1+f2 |
| 13.36507(3) | 0.0077(2) | 0.906(3) | f1+f3 |
| 2015 | | | |
| 5.3381(1) | 0.0948(3) | 0.641(1) | f1 |
| 6.6798(2) | 0.0282(2) | 0.509(1) | f2 |
| 8.0275(1) | 0.0415(2) | 0.189(1) | f3 |
| 10.6711(4) | 0.0118(2) | 0.837(3) | 2f1 |
| 1.3463(10) | 0.0060(2) | 0.950(6) | f2-f1 |
| 2.6890(6) | 0.0093(2) | 0.366(4) | f3-f1 |
| 12.0179(14) | 0.0039(2) | 0.391(8) | f1+f2 |
| 13.3670(6) | 0.0070(3) | 0.307(5) | f1+f3 |
| 2016 | | | |
| 5.3380(1) | 0.0942(1) | 0.374(1) | f1 |
| 6.6809(1) | 0.0294(1) | 0.472(1) | f2 |
| 8.0268(1) | 0.0437(1) | 0.688(1) | f3 |
| 10.6770(2) | 0.0116(1) | 0.422(3) | 2f1 |
| 1.3446(2) | 0.0125(1) | 0.890(3) | f2-f1 |
| 2.6885(2) | 0.0091(1) | 0.157(4) | f3-f1 |
| 12.0168(3) | 0.0069(1) | 0.116(5) | f1+f2 |
| 13.3657(3) | 0.0078(1) | 0.606(3) | f1+f3 |

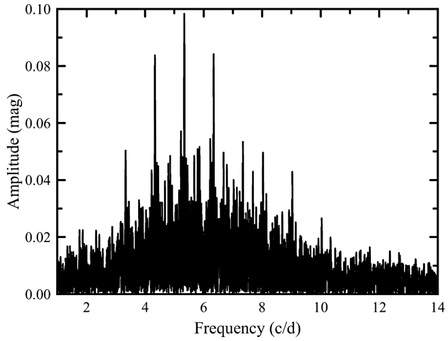

Figure 3. A portion of the Fourier spectrum for the 2015–2016 observations before any frequency has been cleaned.

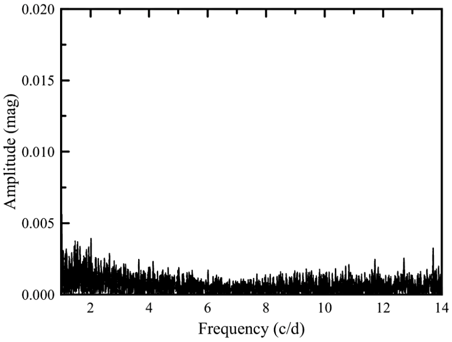

Figure 4. The residual Fourier spectrum for the 2015-2016 observations after the frequencies of Table 1 have been cleaned. Note that the amplitude scale is different from that of Figure 3.

Although the frequencies and amplitudes for the components in Table 1 are similar for the 2015–2016, 2015, and 2016 data, they are not identical, and, in fact, they sometimes differ by more than the adopted error bars. However, given the problems inherent when observations are from a single location, we hesitate to conclude that the year-to-year differences are real. New observations, particularly from multiple longitudes, would help in evaluating the stability of the frequency components observed in HD 213616.

## 4. Discussion

As noted above, the Variable Star Index (VSX) lists HD 213616 as a probable W Ursae Majoris eclipsing variable. The VSX lists a frequency of 2.6690 c/d, which is half the frequency of the f1 component found in this analysis. That result is based upon data from the WASP survey (Butters *et al.* 2010) that was obtained between HJD 2453154 and 2454669. There are 4,721 photometric points for HD 213616 listed in the SuperWASP public archive (http://www.superwasp.org/), although a few of these show large deviations from the others and are likely erroneous. HD 213616 is also identified as variable in the Chandra Variable Guide Star Catalog (Nichols *et al.* 2010), but with less than a day of observation those data are not sufficient for a period determination.

A period search analysis of the SuperWASP data using the PERIODOGRAM software available on the NASA Exoplanet Archive (2016) website (http://exoplanetarchive.ipac.caltech.edu/) with a resolution of 0.0001 does, however, reveal the three dominant frequencies of Table 1, as well as aliases that differ by one or more cycles per day from those frequencies. In the analysis of the SuperWASP data the frequencies recovered that appear to correspond to f1, f2, and f3 are: 5.3380 c/d, 6.6811 c/d, and 8.0272 c/d. Although the SuperWASP data cover a longer time interval than the data in Table 1, there are fewer observations per day, raising the susceptibility to aliases with a different number of cycles per day.

The existence of three independent frequencies plus combination terms in the light curve of HD 213616 indicates that it is not a W UMa binary. Instead, it strongly indicates that HD 213616 is a high amplitude δ Scuti pulsator (HADS). HADS variables generally have one or more frequencies greater than 5 c/d and amplitudes greater than 0.3 magnitude. The magnitude range in Figure 1 and our derived periods would thus place HD 213616 within the HADS class. The F5 spectral type of HD 213616 in the SIMBAD database would be consistent with a δ Scuti identification, although it would be near the cool limit for such stars (Catelan and Smith 2015). Many HADS stars have one or two main periods which are often interpreted as being the radial fundamental and first overtone modes (Templeton 2000; Balona 2016). In double-mode HADS stars, the ratio of the periods is usually in the range 0.76–0.78 (Furgoni 2016). In the case of HD 213616, however, we have three apparently independent frequencies, suggesting the existence of three modes. Nor do the period ratios of any combination of f1, f2, and f3 fall within the 0.76 to 0.78 range.

HADS stars with three modes are not unknown. For example, KIC 6382916 was found to have modes with frequencies of 4.9107, 6.4314, and 8.0350 c/d, reminiscent of the three possible modes in HD 213616 (Ulusoy *et al.* 2013). However, for KIC 6382916, the amplitudes of the first two modes were comparable, while the third had a much smaller amplitude. The f1 frequency for HD 213616 has the largest amplitude but the amplitudes of f2 and f3 are not very different from one another and only 2 or 3 times smaller than the amplitude of f1. If the two smallest frequencies for HD 213616 are interpreted as being the fundamental and first overtone radial modes, the period ratio of 0.799 would be within the range of period ratios observed for the two largest amplitude modes within δ Scuti stars observed by the Kepler mission that have five or more combination frequencies (Balona 2016). However, it is by no means certain that we can interpret f1 and f2 as fundamental and first overtone radial modes. HD 213616 might thus repay further study.

## 5. Acknowledgements

This research has made use of the NASA Exoplanet Archive, which is operated by the California Institute of Technology, under contract with the National Aeronautics and Space Administration under the Exoplanet Exploration Program. This research was made possible through the use of the AAVSO Photometric All-Sky Survey (APASS), funded by the Robert Martin Ayers Sciences Fund. We would also like to thank Matthew Templeton, Gerry Samolyk, Richard Huziak, and Gary Billings for their encouragement and for valuable discussions about this star.

## References

Balona, L. A. 2016, *Mon. Not. Roy. Astron. Soc.*, **459**, 1097.

Butters, O. W., *et al.* 2010, *Astron. Astrophys.*, **520**, L10.

Catelan, M., and Smith, H. A. 2015, *Pulsating Stars*, Wiley-VCH, Weinheim, Germany.

Diffraction Limited. 2012, MAXIMDL image processing software (http://www.cyanogen.com).

Furgoni, R. 2016, *J. Amer. Assoc. Var. Star Obs.*, **44**, 6.

Henden, A., and Munari, U. 2014, *Contrib. Astron. Obs. Skalnaté Pleso*, **43**, 518.

Kafka, S. 2016, variable star observations from the AAVSO International Database (https://www.aavso.org/aavso-international-database).

Koppleman, M. 2005, in *The Society for Astronomical Sciences 24th Annual Symposium on Telescope Science*, Society for Astronomical Sciences, Rancho Cucamonga, CA, 107.

Lenz, P., and Breger, M. 2005, *Commun. Asteroseismology*, **146**, 53.

NASA Exoplanet Archive. 2015, PERIODOGRAM (http://exoplanetarchive.ipac.caltech.edu/).

Nichols, J. S., Henden, A. A., Huenemoerder, D. P., Lauer, J. L., Martin, E., Morgan, D. L., and Sundheim, B. A. 2010, *Astrophys. J., Suppl. Ser.*, **188**, 473.

Templeton, M. 2000, Ph.D. Thesis, New Mexico State Univ.

Ulusoy, C., *et al.* 2013, *Mon. Not. Roy. Astron. Soc.*, **433**, 394.

Watson, C., Henden, A. A., and Price, C. A. 2014, AAVSO International Variable Star Index VSX (Watson+, 2006–2014; http://www.aavso.org/vsx).

# A Photometric Study of the Near-Contact Binary XZ Persei

**Edward J. Michaels**
*Stephen F. Austin State University, Department of Physics, Engineering, and Astronomy, P.O. Box 13044, Nacogdoches, TX 75962; emichaels@sfasu.edu*

*Received February 6, 2017; revised March 1, 2017; accepted March 1, 2017*

**Abstract** Presented are two sets of multi-band CCD photometry of the Algol-type binary XZ Persei. Photometric solutions were derived using the Wilson-Devinney program for each dataset. The solution results indicate XZ Per is a semi-detached, near-contact binary whose less-massive secondary star fills its Roche lobe. Asymmetries in the light curves were modeled by including a hot spot on the primary star. This spot is likely caused by impact heating from mass transfer. The orbital period was analyzed using 473 light minima spanning 90 years. Several alternating period changes were found superimposed on a long term secular period decrease. With continued mass and angular momentum loss, the separation between the stars will likely decrease until the primary fills its Roche lobe forming a contact binary.

## 1. Introduction

The *General Catalogue of Variable Stars* (GCVS; Samus *et al.* 2017) identifies XZ Persei (TYC 3328-3186-1, GSC 3328-3186) as a semi-detached Algol eclipsing system with an orbital period of 1.15163412 days and a spectral type of G1. Photometric orbital elements were first determined by Lavrov (1971). Geometric and physical parameters for this system were computed by Brancewicz and Dworak (1980) using an iterative method which indicated a semi-detached configuration. XZ Per is also included in a catalogue of 411 Algol-type binary stars (Budding *et al.* 2004). This catalogue gives an orbital inclination of 88°, a mass ratio of 0.69, a distance of 250 pc, and spectral types for the primary and secondary stars of G1+[K1IV]. In a spectroscopic survey of late F-K eclipsing binaries, Popper (1996) found the primary star's spectral type to be F2-5. Many primary minima timings have been published going back to 1927. Several period studies have been completed on this system (Whitney 1959; Szafraniec 1960; Wood and Forbes 1963; Kreiner 1971; Mallama 1980; Qian 2001a). It has also been surveyed for a gaseous disk using time-resolved spectroscopy (Kaitchuck and Honeycutt 1982; Kaitchuck *et al.* 1985).

In this paper a photometric study of XZ Per is presented. The paper is organized into sections. The first complete set of multi-wavelength photometric observations for this star is presented in section 2. Orbital period changes are investigated in section 3, a light curve analysis is presented in section 4, results from the period study and light curve analysis are discussed in section 5, and conclusions are stated in section 6.

## 2. Observations

XZ Per was observed photometrically with the 0.31-m Ritchey-Chrétien telescope located at the Waffelow Creek Observatory (http://obs.ejmj.net/index.php). Images were acquired with a SBIG-STXL camera equipped with a KAF-6303E CCD (9µm pixels). Two complete data sets were collected. Images that comprise Data Set 1 (DS1) were taken in the Sloan g', r', and i' passbands on fifteen nights in January and February 2016. Data Set 2 (DS2) images were acquired in the Johnson B and V passbands on eight nights in September and October 2016. A total of 7,226 images were acquired, 4,648 in the Sloan passbands and 2,578 in the Johnson passbands. All the images were calibrated with bias, dark, and flat field frames taken before each night's observing run. MIRA software was used for calibration and ensemble differential aperture photometry of the light images (Mirametrics 2015). The instrumental magnitudes of XZ Per were converted to standard magnitudes using comparison star magnitudes taken from the AAVSO Photometric All-Sky Survey (APASS; Henden *et al.* 2014). The comparison and check stars used in this study are shown in Table 1. The finder chart in Figure 1 shows a nearby field star 8.1" to the ENE of XZ Per. The light contribution from this star was easily removed by proper sizing of the rings when performing the aperture photometry. After converting the Heliocentric Julian Day (HJD) of each observation to orbital phase the folded light curves were plotted (see Figure 2). All light curves in this paper are plotted from phase –0.6 to 0.6, with negative phase defined as φ –1. The check star's V passband observations are shown in the bottom panel of Figure 2 with the standard deviations shown in Table 1. The check star magnitudes were inspected each night and no significant variability was found. The observations have been archived and are accessible from the AAVSO International Database (Kafka 2015).

## 3. Analysis

### 3.1. Period study and ephemerides

The most recent study of orbital period changes for XZ Per was done by Qian (2001a). Since that study, many additional minimum timings have become available and were used in the present analysis. From the literature, 488 minima were found spanning the years 1927–2016. From the observations in this study, an additional seven new primary minima were obtained (Table 2). Using the linear ephemeris of Mallama (1980),

$$\text{HJD Min I} = 2443507.47742 + 1.15163412\ E, \qquad (1)$$

the *(O–C)* values were computed. All the minima timings and *(O–C)* values are listed in Tables 2 and 3. The ephemeris diagram is shown in Figure 3. From the full set of minima, fifteen timings identified in Table 3 showed significant deviations from the

Table 1. Variable (V), comparison (C), and check (K) stars in this study.

| *Star* | *R.A. (2000)* *h* | *Dec. (2000)* *°* | *B* | *V* | *g'* | *r'* | *i'* | *(B–V)* |
|---|---|---|---|---|---|---|---|---|
| XZ Per (V) | 4.15768 | +46.56686 | | | | | | |
| GSC3328-1649 (C1) | 4.17230 | +46.48831 | 11.295<br>± 0.076 | 10.570<br>± 0.059 | 10.882<br>± 0.052 | 10.372<br>± 0.065 | 10.239<br>± 0.043 | 0.725 |
| GSC3328-1055 (C2) | 4.16805 | +46.60359 | 11.662<br>— | 10.746<br>± 0.012 | 11.167<br>± 0.049 | 10.456<br>± 0.012 | 10.116<br>± 0.034 | 0.916 |
| GSC3328-2924 (C3) | 4.16396 | +46.50468 | 11.410<br>— | 10.911<br>± 0.019 | 11.118<br>± 0.037 | 10.795<br>± 0.015 | 10.639<br>± 0.039 | 0.499 |
| GSC3328-2029 (C4) | 4.15812 | +46.62578 | 11.837<br>— | 11.181<br>± 0.025 | 11.447<br>± 0.032 | 10.982<br>± 0.010 | 10.761<br>± 0.028 | 0.656 |
| GSC3328-985 (C5) | 4.17478 | +46.52096 | 12.374<br>± 0.008 | 11.386<br>± 0.045 | 11.866<br>± 0.010 | 10.957<br>± 0.017 | 10.419<br>± 0.000 | 0.998 |
| GSC3328-1883 (C6) | 4.16236 | +46.67258 | 12.291<br>± 0.008 | 11.725<br>± 0.030 | 11.966<br>± 0.035 | 11.574<br>± 0.006 | 11.391<br>± 0.033 | 0.566 |
| GSC3328-1869 (C7) | 4.14996 | +46.46364 | 12.497<br>± 0.038 | 11.810<br>± 0.059 | 12.085<br>± 0.034 | 11.601<br>± 0.034 | 11.415<br>± 0.059 | 0.687 |
| GSC3328-2491 (C8) | 4.13869 | +46.45859 | 12.681<br>± 0.049 | 12.064<br>± 0.060 | 12.303<br>± 0.033 | 11.921<br>± 0.029 | 11.764<br>± 0.067 | 0.617 |
| GSC3328-2529 (C9) | 4.16223 | +46.66057 | 13.079<br>± 0.006 | 12.260<br>± 0.034 | 12.603<br>± 0.029 | 11.982<br>± 0.006 | 11.655<br>± 0.020 | 0.819 |
| GSC3328-1641 (K) | 4.14319 | +46.54925 | 13.418<br>— | 11.829<br>± 0.017 | 12.553<br>± 0.025 | 11.244<br>± 0.000 | 10.606<br>± 0.020 | 1.589 |
| Standard deviation of check star magnitudes | | | ± 0.016 | ± 0.008 | ± 0.008 | ± 0.006 | ± 0.006 | |
| Observed check star magnitudes (K) | | | 13.421<br>± 0.049 | 11.815<br>± 0.023 | 12.532<br>± 0.029 | 11.247<br>± 0.023 | 10.607<br>± 0.023 | |

*APASS comparison and check star magnitudes and errors. The observed check star magnitudes are the averages over all nights for each passband.*

Table 2. New times of minima for XZ Per.

| *Epoch* *HJD 2400000+* | *Error* | *Type* | *Cycle* | *O–C* |
|---|---|---|---|---|
| 57400.7189 | 0.00012 | ccd | 12064.0 | –0.07256 |
| 57422.5998 | 0.00010 | ccd | 12083.0 | –0.07264 |
| 57423.7515 | 0.00013 | ccd | 12084.0 | –0.07258 |
| 57430.6614 | 0.00010 | ccd | 12090.0 | –0.07251 |
| 57666.7458 | 0.00004 | ccd | 12295.0 | –0.07309 |
| 57667.8977 | 0.00006 | ccd | 12296.0 | –0.07283 |
| 57689.7785 | 0.00005 | ccd | 12315.0 | –0.07314 |

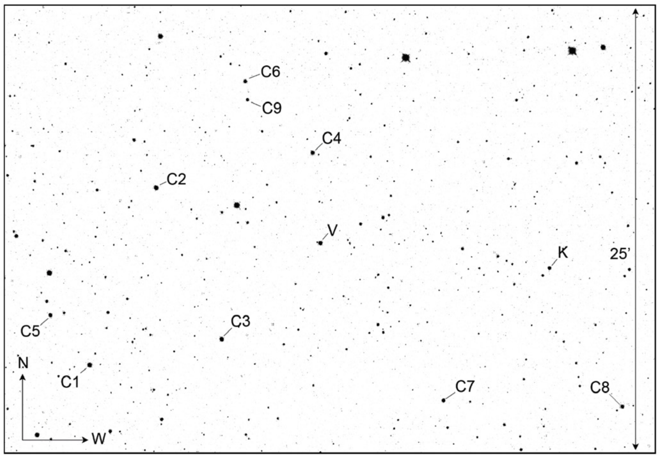

Figure 1. Finder chart for XZ Per (V), comparison (C1–C9), and check (K) stars.

trend and were therefore not used in the analysis.

Using the *(O–C)* residuals from Equation 1, a new linear ephemeris was computed by weighted least-squares solution. A weight of 1 was applied to visual and photographic timings, and 10 to PE and CCD observations. The new linear ephemeris is given by

$$\text{HJD Min I} = 2457689.78840(8) + 1.15163048(9)\,E, \tag{2}$$

and is shown overlaid on the O–C data in Figure 3 (dashed line). The general *(O–C)* trend indicates the orbital period appears to be slowly decreasing with embedded sudden alternating period jumps. This behavior was first noted by Qian (2001a), who found the period variation to consist of a secular period decrease with two superposed period jumps. Since that study, it appears several additional period jumps have occurred (see Figure 3). Assuming the *(O–C)* data trend has a parabolic variation that is not a part of a longer repeating cycle, a weighted least-squares

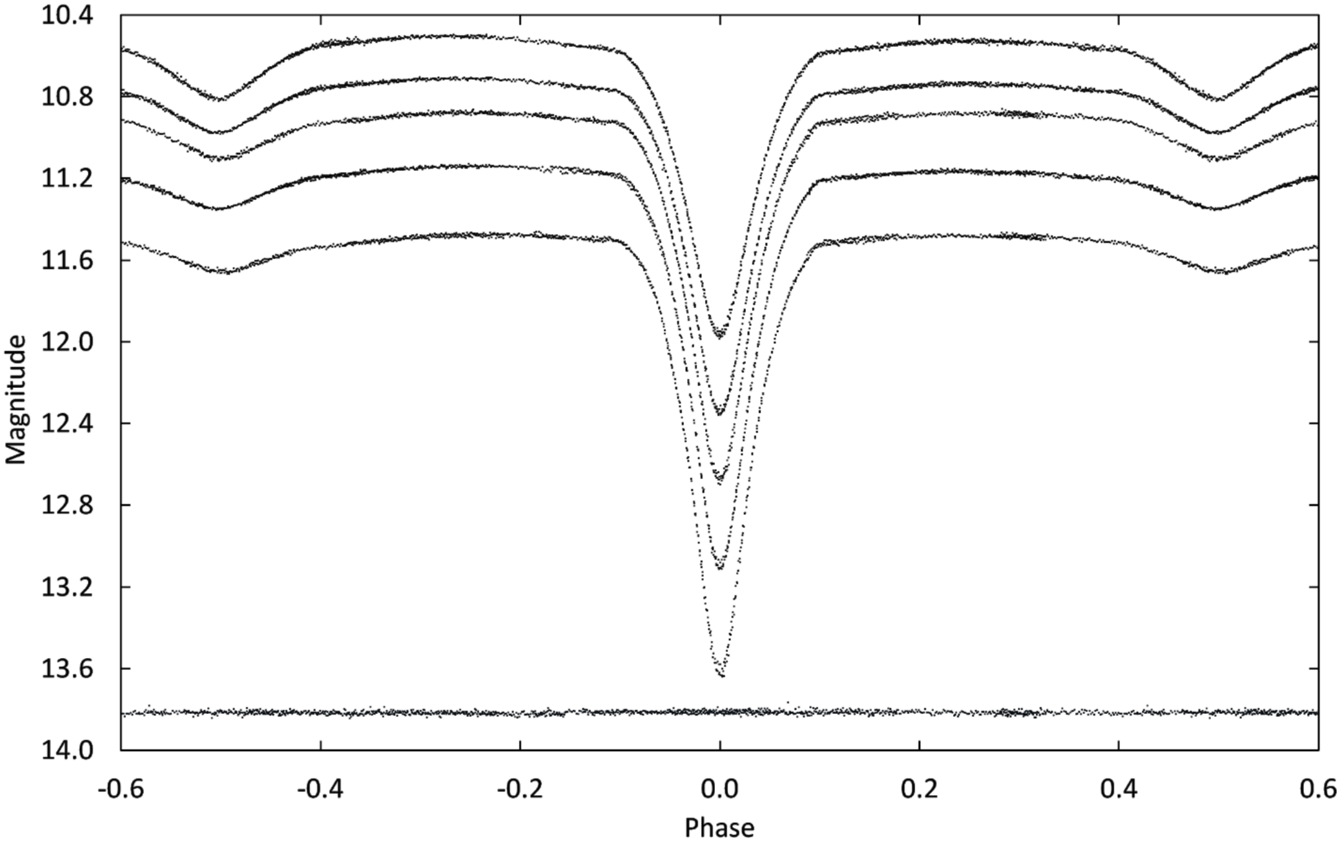

Figure 2. Folded light curves for each observed passband. The differential magnitudes of the variable were converted to standard magnitudes using the calibrated magnitudes of the comparison stars. From top to bottom the light curve passbands are Sloan i', Sloan r', Johnson V, Sloan g', and Johnson B. The bottom curve shows the standard Johnson V magnitudes of the check star (offset +2.0 magnitude). The standard deviations of the check star magnitudes are shown in Table 1. Error bars are not shown for clarity.

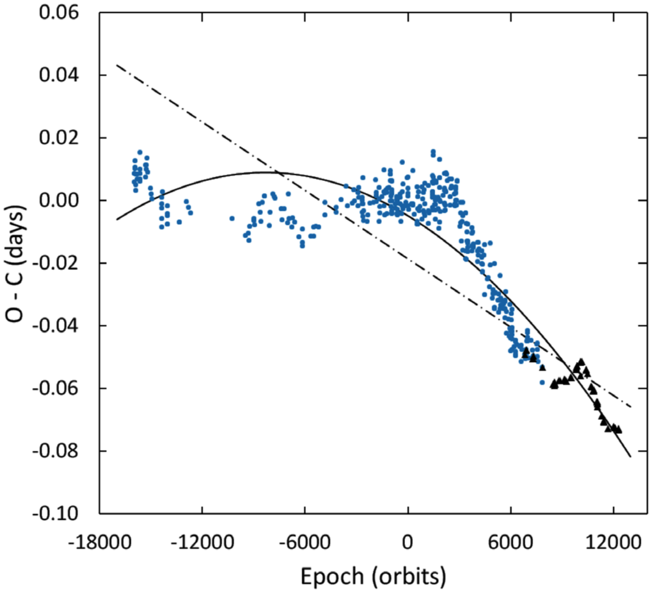

Figure 3. (*O–C)* residuals from the linear ephemeris of Equation 1. The dashed line is the new linear fit of Equation 2 and the solid line the quadratic fit of Equation 3. Circles refer to visual and photographic data and triangles the PE and CCD data.

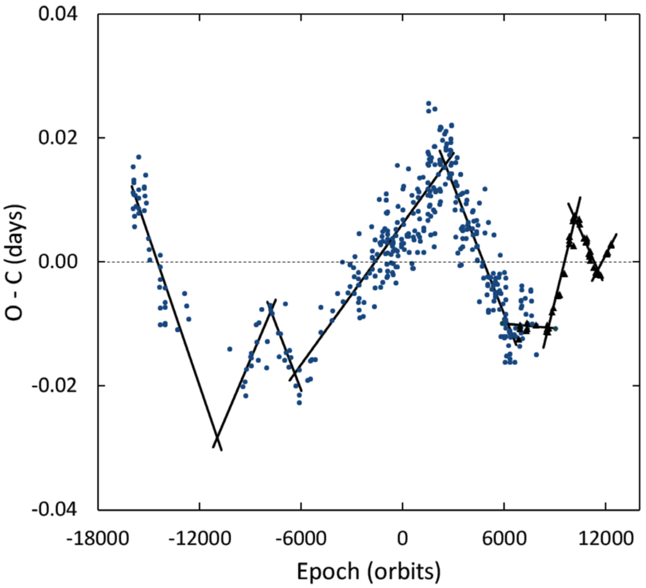

Figure 4. *(O–C)$_Q$* residuals from the quadratic ephemeris fit. The line segments are several linear ephemerides that were fit to the residuals. Circles refer to visual and photographic data and triangles the PE and CCD data.

solution yields the following quadratic ephemeris:

$$\text{HJD Min I} = \\ 2457689.7909(7) + 1.15162587(6)\,\text{E} - 3.48(12) \times 10^{-10}\,\text{E}^2. \quad (3)$$

The quadratic fit to the *(O–C)* observations is shown in Figure 3 (solid line) and the $(O–C)_Q$ residuals from the quadratic ephemeris are presented in Figure 4.

The $(O–C)_Q$ residuals clearly show the decreasing period is not smooth but punctuated by several alternating period changes. It is assumed that between the period jumps the orbital period is undergoing a steady decrease. From inspection of Figure 4, there appear to be 8 period jumps. To better characterize the period jumps, the $(O–C)_Q$ residuals were divided into nine segments (see Figure 4). Using the method of least-squares, a linear function given by

$$(O–C)_Q = \Delta T + \Delta P E\,, \quad (4)$$

was found for each segment to obtain the best fit to the $(O–C)_Q$ values. The computed ΔT and ΔP values for each segment are listed in Table 4. For any cycle E the orbital period, P(E), can be computed by summing the ephemeris period ($P_E$ = 1.15163412 days), the period jump for the segment in which the cycle is located (ΔT), and the contribution from the secular period decrease using dP/dt in units of days/day ($dP/dt = –3.48 \times 10^{-10}$ d $d^{-1}$). Using the following equation,

$$P(E) = P_E + \Delta P + \frac{dP}{dt} EP\,, \quad (5)$$

the differences between the actual period P(E) and the ephemeris period $P_E$ for each segment were computed and the results plotted in Figure 5. It is possible some of the early jumps located between cycles –16,000 and –6,000 are not real. This cycle interval has fewer observations, the visual minima have a large amount of scatter, and a large data gap exists for the years 1938–1945. More precise CCD minima timings became available beginning about the year 1999 (cycle count 7,000). Between cycles 7,000 and 15,000 a few sudden period changes are well documented by these precision timings, leaving little doubt that period jumps are occurring in this system.

### 3.2. Temperature, spectral type

Popper (1996) obtained three high-resolution spectra of XZ Per and found a spectral type of F2-5. The spectral lines of only the primary star were seen. For light curve modeling an effective temperature for the primary was selected midway between the spectral types F2 and F5 with an error estimate taken from that range. Using Table 5 of Pecaut and Mamajek (2013) gives an effective temperature for the primary star of $T_{eff}$ = 6680 ± 170K and a color index of *B–V* = 0.40 ± 0.05. To measure the changing color of XZ Per over its entire phase range, the Johnson *V* and *B* passband observations were binned with a phase width of 0.005. Both phase and magnitude were averaged in each bin interval. Figure 6 shows the binned V magnitude light curve and in the bottom panel the *(B–V)* color index. The significant reddening of the light at primary eclipse indicates a large temperature difference between the primary and secondary stars. The observed color over the entire phase range may also be reddened due to interstellar dust. XZ Per is located 3° south of the galactic equator, therefore a significant amount of interstellar extinction is possible. Extinction will be discussed further in section 4.

### 3.3. Synthetic light curve modeling

Photometric models of XZ Per were obtained for each of the two sets of data, DS1 (g', r', and i' observations) and DS2 (*B* and *V* observations). The observations were binned in both phase and magnitude with a phase interval of 0.005. The average number of observations per bin was eight for DS1 and six for DS2. The binned magnitudes were converted to relative flux for modeling. Preliminary fits to each light curve were made using the BINARY MAKER 3.0 program (BM3; Bradstreet and Steelman 2002). The initial mass ratio for this modeling was taken from a catalogue of eclipsing binary parameters (Brancewicz and Dworak 1980); standard convective parameters were used for both stars and limb darkening coefficients were from Van Hamme's (1993) tabular values. The resulting BM3 synthetic light curves for each color fit the observations well and were consistent for each data set. The stellar parameters from the light curve fits were independently averaged for each model, DS1 and DS2. These values were used as the initial input parameters for computation of simultaneous three-color (DS1) and two-color (DS2) light curve solutions with the 2013 version of the Wilson-Devinney program (WD; Wilson and Devinney 1971; Van Hamme and Wilson 1998). There are two mass ratios published for this system, 0.69 (Brancewicz and Dworak 1980) and 0.50 (Malkov *et al.* 2006). A derived mass ratio from a WD solution would only have reasonable accuracy if the eclipses are total (Wilson 1978; Terrell and Wilson 2005). The eclipses of XZ Per are not total, and combined with the inconsistent published mass ratios, a q-search would be required. For fixed inputs, the effective temperature of the primary was set to $T_1$ = 6680 K (see section 3.2) and standard convective values for gravity darkening and albedo, $g_1 = g_2 = 0.32$ (Lucy 1968) and $A_1 = A_2 = 0.5$ (Ruciński 1969), respectively. The logarithmic limb darkening coefficients were interpolated from tabulated values using the method of Van Hamme (1993). The Kurucz (1993) stellar atmosphere model was applied and detailed reflection was utilized in modeling. The adjustable parameters include the inclination (i), mass ratio ($q = M_2 / M_1$), potential (Ω), temperature of the secondary star ($T_2$), the normalized flux for each wavelength (L), and third light ($\ell$).

Mode 2 (detached configuration) was used initially but every solution attempt converged quickly to a semi-detached configuration. This indicates the secondary star fills its Roche lobe. Mode 5 (semi-detached configuration) was therefore used on subsequent iterations and the final solutions. Using the DS1 light curves, a series of solutions were made using fixed mass ratios from 0.30 to 1.00 with a step of 0.05. This q-search had minimum residual value at about q = 0.64 (see Figure 7) and was used as the initial mass ratio for the final solution attempts for each data set. With the mass ratio as a free parameter, the resulting best-fit final solution parameters are shown in columns

Table 3. Available times of minima and O–C residuals from Equation 1.

| *Epoch HJD 2400000+* | *Type* | *Cycle* | *O–C* | *Reference* |
|---|---|---|---|---|
| 25150.438 | vis | –15940.0 | 0.00847 | BAV Lichten. DB |
| 25151.587 | vis | –15939.0 | 0.00584 | BAV Lichten. DB |
| 25157.352 | vis | –15934.0 | 0.01267 | BAV Lichten. DB |
| 25187.292 | vis | –15908.0 | 0.01018 | BAV Lichten. DB |
| 25188.444 | vis | –15907.0 | 0.01055 | BAV Lichten. DB |
| 25216.081 | vis | –15883.0 | 0.00833 | BAV Lichten. DB |
| 25234.502 | vis | –15867.0 | 0.00318 | BAV Lichten. DB |
| 25249.475 | vis | –15854.0 | 0.00494 | BAV Lichten. DB |
| 25301.302 | vis | –15809.0 | 0.00840 | BAV Lichten. DB |
| 25324.333 | vis | –15789.0 | 0.00672 | BAV Lichten. DB |
| 25506.293 | vis | –15631.0 | 0.00853 | BAV Lichten. DB |
| 25514.352 | vis | –15624.0 | 0.00609 | BAV Lichten. DB |
| 25520.114 | vis | –15619.0 | 0.00992 | BAV Lichten. DB |
| 25529.324 | vis | –15611.0 | 0.00685 | BAV Lichten. DB |
| 25530.484 | vis | –15610.0 | 0.01521 | BAV Lichten. DB |
| 25886.335 | vis | –15301.0 | 0.01127 | BAV Lichten. DB |
| 25893.241 | vis | –15295.0 | 0.00747 | BAV Lichten. DB |
| 25917.429 | vis | –15274.0 | 0.01115 | BAV Lichten. DB |
| 25945.067 | vis | –15250.0 | 0.00993 | BAV Lichten. DB |
| 26000.349 | vis | –15202.0 | 0.01349 | BAV Lichten. DB |
| 26030.287 | vis | –15176.0 | 0.00901 | BAV Lichten. DB |
| 26208.785 | vis | –15021.0 | 0.00372 | BAV Lichten. DB |
| 26257.152 | vis | –14979.0 | 0.00208 | BAV Lichten. DB |
| 26305.519 | vis | –14937.0 | 0.00045 | BAV Lichten. DB |
| 26957.341 | vis | –14371.0 | –0.00246 | BAV Lichten. DB |
| 26979.216 | vis | –14352.0 | –0.00851 | BAV Lichten. DB |
| 26980.375 | vis | –14351.0 | –0.00114 | BAV Lichten. DB |
| 26980.377 | vis | –14351.0 | 0.00086 | BAV Lichten. DB |
| 26981.522 | vis | –14350.0 | –0.00578 | BAV Lichten. DB |
| 27002.260 | vis | –14332.0 | 0.00281 | BAV Lichten. DB |
| 27337.375 | vis | –14041.0 | –0.00772 | BAV Lichten. DB |
| 27343.136 | vis | –14036.0 | –0.00489 | BAV Lichten. DB |
| 27344.285 | vis | –14035.0 | –0.00753 | BAV Lichten. DB |
| 27345.440 | vis | –14034.0 | –0.00416 | BAV Lichten. DB |
| 27346.594 | vis | –14033.0 | –0.00179 | BAV Lichten. DB |
| 28151.581 | vis | –13334.0 | –0.00704 | BAV Lichten. DB |
| 28151.581 | vis | –13334.0 | –0.00704 | BAV Lichten. DB |
| 28635.274 | vis | –12914.0 | –0.00037 | BAV Lichten. DB |
| 28783.833 | vis | –12785.0 | –0.00218 | BAV Lichten. DB |
| 28932.392 | vis | –12656.0 | –0.00398 | BAV Lichten. DB |
| 31712.435 | vis | –10242.0 | –0.00574 | BAV Lichten. DB |
| 32623.372 | vis | –9451.0 | –0.01133 | BAV Lichten. DB |
| 32770.782 | vis | –9323.0 | –0.01050 | BAV Lichten. DB |
| 32820.300 | vis | –9280.0 | –0.01277 | BAV Lichten. DB |
| 32868.673 | vis | –9238.0 | –0.00840 | BAV Lichten. DB |
| 33155.432 | vis | –8989.0 | –0.00630 | BAV Lichten. DB |
| 33183.071 | vis | –8965.0 | –0.00651 | BAV Lichten. DB |
| 33185.375 | vis | –8963.0 | –0.00578 | BAV Lichten. DB |
| 33207.254 | vis | –8944.0 | –0.00783 | BAV Lichten. DB |
| 33505.534 | vis | –8685.0 | –0.00107 | BAV Lichten. DB |
| 33581.539 | vis | –8619.0 | –0.00392 | BAV Lichten. DB |
| 33657.544 | vis | –8553.0 | –0.00677 | BAV Lichten. DB |
| 33717.435 | P | –8501.0 | –0.00075 | BAV Lichten. DB |
| 33900.547 | vis | –8342.0 | 0.00143 | BAV Lichten. DB |
| 33900.547 | vis | –8342.0 | 0.00143 | BAV Lichten. DB |
| 34226.450 | vis | –8059.0 | –0.00803 | BAV Lichten. DB |
| 34271.368 | vis | –8020.0 | –0.00376 | BAV Lichten. DB |
| 34284.334* | vis | –8008.5 | –0.28155 | BAV Lichten. DB |
| 34453.332 | vis | –7862.0 | 0.00205 | BAV Lichten. DB |
| 34529.339 | vis | –7796.0 | 0.00120 | BAV Lichten. DB |
| 34606.498 | vis | –7729.0 | 0.00071 | BAV Lichten. DB |
| 35008.415 | vis | –7380.0 | –0.00259 | BAV Lichten. DB |
| 35008.415 | vis | –7380.0 | –0.00259 | BAV Lichten. DB |
| 35062.538 | P | –7333.0 | –0.00640 | Whitney 1959 |
| 35190.373 | P | –7222.0 | –0.00279 | BAV Lichten. DB |
| 35450.638 | P | –6996.0 | –0.00710 | Whitney 1959 |
| 35510.532 | P | –6944.0 | 0.00193 | Whitney 1959 |
| 35539.315 | P | –6919.0 | –0.00592 | BAV Lichten. DB |
| 35745.455 | vis | –6740.0 | –0.00843 | BAV Lichten. DB |
| 35782.310 | vis | –6708.0 | –0.00572 | BAV Lichten. DB |
| 35904.382 | vis | –6602.0 | –0.00694 | BAV Lichten. DB |
| 36194.589 | P | –6350.0 | –0.01174 | Whitney 1959 |
| 36452.552 | vis | –6126.0 | –0.01458 | BAV Lichten. DB |
| 36452.553 | vis | –6126.0 | –0.01338 | BAV Lichten. DB |
| 36452.558 | vis | –6126.0 | –0.00928 | BAV Lichten. DB |
| 37020.311 | vis | –5633.0 | –0.01140 | BAV Lichten. DB |
| 37196.511 | vis | –5480.0 | –0.01142 | BAV Lichten. DB |
| 37196.514 | vis | –5480.0 | –0.00842 | BAV Lichten. DB |
| 37316.284 | vis | –5376.0 | –0.00837 | BAV Lichten. DB |
| 37545.459 | vis | –5177.0 | –0.00856 | BAV Lichten. DB |
| 37932.412 | vis | –4841.0 | –0.00463 | BAV Lichten. DB |
| 37932.416 | vis | –4841.0 | –0.00063 | BAV Lichten. DB |
| 38684.430 | P | –4188.0 | –0.00371 | Todoran 1967 |
| 38714.374 | P | –4162.0 | –0.00219 | Todoran 1967 |
| 39033.379 | vis | –3885.0 | 0.00016 | BAV Lichten. DB |
| 39390.390 | P | –3575.0 | 0.00458 | Todoran 1967 |
| 39445.662 | vis | –3527.0 | –0.00186 | Robinson 1967 |
| 39772.727 | vis | –3243.0 | –0.00095 | Baldwin 1974 |
| 39886.743 | vis | –3144.0 | 0.00327 | Baldwin 1974 |
| 39893.653 | vis | –3138.0 | 0.00347 | Baldwin 1974 |
| 39916.682 | vis | –3118.0 | –0.00021 | Baldwin 1974 |
| 40151.618 | vis | –2914.0 | 0.00243 | BAV Lichten. DB |
| 40151.618 | P | –2914.0 | 0.00243 | Baldwin 1974 |
| 40188.466 | vis | –2882.0 | –0.00187 | Flin 1969 |
| 40203.440 | vis | –2869.0 | 0.00089 | Flin 1969 |
| 40232.234 | vis | –2844.0 | 0.00404 | Flin 1969 |
| 40471.766 | vis | –2636.0 | –0.00386 | Baldwin 1974 |
| 40477.527 | vis | –2631.0 | –0.00103 | BAV Lichten. DB |
| 40477.528 | vis | –2631.0 | –0.00003 | BAV Lichten. DB |
| 40477.529 | vis | –2631.0 | 0.00097 | BAV Lichten. DB |
| 40499.404 | vis | –2612.0 | –0.00508 | BAV Lichten. DB |
| 40499.408 | vis | –2612.0 | –0.00108 | BAV Lichten. DB |
| 40500.568 | vis | –2611.0 | 0.00729 | BAV Lichten. DB |
| 40539.713 | vis | –2577.0 | –0.00327 | Baldwin 1974 |
| 40554.681 | vis | –2564.0 | –0.00652 | Baldwin 1974 |
| 40796.524 | vis | –2354.0 | –0.00668 | BAV Lichten. DB |
| 40856.411 | vis | –2302.0 | –0.00466 | Baldwin 1975 |
| 40969.275 | vis | –2204.0 | –0.00080 | Baldwin 1976a |
| 41221.483 | vis | –1985.0 | –0.00067 | BAV Lichten. DB |
| 41357.383 | vis | –1867.0 | 0.00650 | Klimek 1972 |
| 41395.380 | vis | –1834.0 | –0.00042 | Klimek 1973 |
| 41395.382 | vis | –1834.0 | 0.00158 | BBSAG No. 2 |
| 41395.383 | vis | –1834.0 | 0.00258 | Baldwin 1976a |
| 41410.353 | vis | –1821.0 | 0.00133 | BBSAG No. 3 |
| 41570.422 | vis | –1682.0 | –0.00681 | BBSAG No. 5 |
| 41585.404 | vis | –1669.0 | 0.00395 | BBSAG No. 5 |
| 41593.462 | vis | –1662.0 | 0.00051 | BBSAG No. 6 |
| 41623.400 | vis | –1636.0 | –0.00398 | BBSAG No. 6 |
| 41623.402 | vis | –1636.0 | –0.00198 | Baldwin 1976a |
| 41759.298 | vis | –1518.0 | 0.00119 | BBSAG No. 8 |
| 41905.564 | vis | –1391.0 | 0.00966 | BBSAG No. 11 |
| 41913.614 | vis | –1384.0 | –0.00178 | BBSAG No. 11 |
| 41927.438 | vis | –1372.0 | 0.00261 | BBSAG No. 11 |
| 41982.716 | vis | –1324.0 | 0.00217 | Baldwin 1976b |
| 41989.619 | vis | –1318.0 | –0.00463 | Baldwin 1976b |
| 42071.393 | vis | –1247.0 | 0.00335 | BBSAG No. 13 |
| 42109.396 | vis | –1214.0 | 0.00242 | BBSAG No. 14 |
| 42132.422 | vis | –1194.0 | –0.00426 | BBSAG No. 14 |
| 42139.340 | vis | –1188.0 | 0.00393 | BBSAG No. 15 |
| 42262.565 | vis | –1081.0 | 0.00408 | BBSAG No. 17 |
| 42337.417 | vis | –1016.0 | –0.00013 | BBSAG No. 18 |
| 42367.366 | vis | –990.0 | 0.00638 | BAV Lichten. DB |
| 42367.368 | vis | –990.0 | 0.00838 | BAV Lichten. DB |
| 42367.368 | vis | –990.0 | 0.00838 | BAV Lichten. DB |

*table continued on following pages*

Table 3. Available times of minima and O–C residuals from Equation 1, cont.

| *Epoch HJD 2400000+* | *Type* | *Cycle* | *O–C* | *Reference* |
|---|---|---|---|---|
| 42367.369 | vis | –990.0 | 0.00938 | BAV Lichten. DB |
| 42391.542 | vis | –969.0 | –0.00194 | Baldwin 1977 |
| 42405.365 | vis | –957.0 | 0.00145 | BBSAG No. 19 |
| 42428.392 | vis | –937.0 | –0.00423 | BBSAG No. 20 |
| 42429.554 | vis | –936.0 | 0.00614 | BAV Lichten. DB |
| 42435.302 | vis | –931.0 | –0.00403 | BBSAG No. 20 |
| 42435.308 | vis | –931.0 | 0.00197 | BBSAG No. 20 |
| 42450.274 | vis | –918.0 | –0.00328 | BBSAG No. 21 |
| 42450.277 | vis | –918.0 | –0.00028 | BBSAG No. 21 |
| 42450.280 | vis | –918.0 | 0.00272 | BBSAG No. 21 |
| 42458.342 | vis | –911.0 | 0.00328 | BBSAG No. 21 |
| 42458.345 | vis | –911.0 | 0.00628 | BBSAG No. 21 |
| 42688.663 | vis | –711.0 | –0.00254 | BAV Lichten. DB |
| 42689.816 | vis | –710.0 | –0.00117 | BAV Lichten. DB |
| 42754.309 | vis | –654.0 | 0.00031 | BBSAG No. 25 |
| 42777.337 | vis | –634.0 | –0.00437 | BBSAG No. 25 |
| 42785.404 | vis | –627.0 | 0.00119 | BBSAG No. 26 |
| 42809.587 | vis | –606.0 | –0.00012 | Baldwin and Samolyk 1993 |
| 42830.317 | vis | –588.0 | 0.00046 | BBSAG No. 26 |
| 42832.615 | vis | –586.0 | –0.00481 | Baldwin and Samolyk 1993 |
| 42832.620 | vis | –586.0 | 0.00019 | Baldwin and Samolyk 1993 |
| 42838.375 | vis | –581.0 | –0.00298 | BBSAG No. 26 |
| 42838.377 | vis | –581.0 | –0.00098 | BBSAG No. 26 |
| 42985.786 | vis | –453.0 | –0.00114 | Baldwin and Samolyk 1993 |
| 43014.580 | vis | –428.0 | 0.00200 | BBSAG No. 29 |
| 43023.787 | vis | –420.0 | –0.00407 | Baldwin and Samolyk 1993 |
| 43023.792 | vis | –420.0 | 0.00093 | BAV Lichten. DB |
| 43037.604 | vis | –408.0 | –0.00668 | BBSAG No. 30 |
| 43098.643 | vis | –355.0 | –0.00429 | Baldwin and Samolyk 1993 |
| 43128.588 | vis | –329.0 | –0.00177 | Baldwin and Samolyk 1993 |
| 43134.360 | vis | –324.0 | 0.01205 | BAV Lichten. DB |
| 43136.654 | vis | –322.0 | 0.00279 | Baldwin and Samolyk 1993 |
| 43188.472 | vis | –277.0 | –0.00275 | BBSAG No. 32 |
| 43188.480 | vis | –277.0 | 0.00525 | BBSAG No. 32 |
| 43393.465 | vis | –99.0 | –0.00062 | BBSAG No. 35 |
| 43395.767 | vis | –97.0 | –0.00189 | Baldwin and Samolyk 1993 |
| 43409.587 | vis | –85.0 | –0.00150 | BBSAG No. 35 |
| 43493.665 | vis | –12.0 | 0.00721 | Baldwin and Samolyk 1993 |
| 43506.328 | vis | –1.0 | 0.00223 | BBSAG No. 36 |
| 43514.391 | vis | 6.0 | 0.00380 | BBSAG No. 36 |
| 43538.579 | vis | 27.0 | 0.00748 | Baldwin and Samolyk 1993 |
| 43544.328 | vis | 32.0 | –0.00169 | BBSAG No. 36 |
| 43544.331 | vis | 32.0 | 0.00131 | BBSAG No. 36 |
| 43575.421 | vis | 59.0 | –0.00281 | BBSAG No. 37 |
| 43788.475 | vis | 244.0 | –0.00113 | BBSAG No. 39 |
| 43803.446 | vis | 257.0 | –0.00137 | BBSAG No. 39 |
| 43865.645 | vis | 311.0 | 0.00939 | Baldwin and Samolyk 1993 |
| 43870.241 | vis | 315.0 | –0.00115 | BBSAG No. 41 |
| 43878.302 | vis | 322.0 | –0.00159 | BBSAG No. 41 |
| 43932.426 | vis | 369.0 | –0.00439 | BBSAG No. 42 |
| 44132.808 | vis | 543.0 | –0.00673 | Baldwin and Samolyk 1993 |
| 44132.819 | vis | 543.0 | 0.00427 | Baldwin and Samolyk 1993 |
| 44139.717 | vis | 549.0 | –0.00753 | Baldwin and Samolyk 1993 |
| 44189.246 | vis | 592.0 | 0.00120 | BBSAG No. 45 |
| 44192.692 | vis | 595.0 | –0.00770 | Baldwin and Samolyk 1993 |
| 44214.578 | vis | 614.0 | –0.00275 | Baldwin and Samolyk 1993 |
| 44222.645 | vis | 621.0 | 0.00281 | Baldwin and Samolyk 1993 |
| 44266.401 | vis | 659.0 | –0.00329 | BBSAG No. 46 |
| 44267.538* | vis | 660.0 | –0.01792 | BAV Lichten. DB |
| 44311.316 | vis | 698.0 | –0.00202 | BBSAG No. 47 |
| 44449.509* | vis | 818.0 | –0.00511 | BBSAG No. 49 |
| 44472.551 | vis | 838.0 | 0.00421 | BBSAG No. 49 |
| 44474.844 | vis | 840.0 | –0.00606 | Baldwin and Samolyk 1993 |
| 44539.342 | vis | 896.0 | 0.00043 | BBSAG No. 51 |
| 44549.703 | vis | 905.0 | –0.00328 | Baldwin and Samolyk 1993 |
| 44555.467 | vis | 910.0 | 0.00255 | BBSAG No. 51 |
| 44608.443 | vis | 956.0 | 0.00338 | BBSAG No. 52 |
| 44638.378 | vis | 982.0 | –0.00411 | BAV Lichten. DB |
| 44646.449 | vis | 989.0 | 0.00546 | BBSAG No. 53 |
| 44647.594 | vis | 990.0 | –0.00118 | Baldwin and Samolyk 1993 |
| 44683.291 | vis | 1021.0 | –0.00484 | BBSAG No. 53 |
| 44881.358* | vis | 1193.0 | –0.01891 | BAV Lichten. DB |
| 44883.685 | vis | 1195.0 | 0.00483 | BBSAG No. 57 |
| 44884.839* | vis | 1196.0 | 0.00719 | Baldwin and Samolyk 1993 |
| 44898.648 | vis | 1208.0 | –0.00342 | Baldwin and Samolyk 1993 |
| 44911.312 | vis | 1219.0 | –0.00739 | BBSAG No. 57 |
| 44934.348 | vis | 1239.0 | –0.00407 | BBSAG No. 57 |
| 45201.528 | vis | 1471.0 | –0.00319 | BAV Lichten. DB |
| 45201.529 | vis | 1471.0 | –0.00219 | BAV Lichten. DB |
| 45201.532 | vis | 1471.0 | 0.00081 | BAV Lichten. DB |
| 45201.532 | vis | 1471.0 | 0.00081 | BAV Lichten. DB |
| 45201.533 | vis | 1471.0 | 0.00181 | BAV Lichten. DB |
| 45201.533 | vis | 1471.0 | 0.00181 | BAV Lichten. DB |
| 45201.534 | vis | 1471.0 | 0.00281 | BAV Lichten. DB |
| 45201.534 | vis | 1471.0 | 0.00281 | BAV Lichten. DB |
| 45201.534 | vis | 1471.0 | 0.00281 | BAV Lichten. DB |
| 45201.537 | vis | 1471.0 | 0.00581 | BAV Lichten. DB |
| 45201.537 | vis | 1471.0 | 0.00581 | BAV Lichten. DB |
| 45201.539 | vis | 1471.0 | 0.00781 | BAV Lichten. DB |
| 45231.481 | vis | 1497.0 | 0.00732 | BBSAG No. 62 |
| 45247.602 | vis | 1511.0 | 0.00544 | BBSAG No. 63 |
| 45247.612 | vis | 1511.0 | 0.01544 | BBSAG No. 63 |
| 45253.369 | vis | 1516.0 | 0.01427 | BBSAG No. 63 |
| 45313.246 | vis | 1568.0 | 0.00630 | BBSAG No. 64 |
| 45314.390 | vis | 1569.0 | –0.00133 | BBSAG No. 64 |
| 45352.394 | vis | 1602.0 | –0.00126 | BBSAG No. 64 |
| 45359.306 | vis | 1608.0 | 0.00094 | BBSAG No. 64 |
| 45368.512 | vis | 1616.0 | –0.00614 | BBSAG No. 65 |
| 45390.396 | vis | 1635.0 | –0.00319 | BBSAG No. 65 |
| 45397.309 | vis | 1641.0 | 0.00001 | BBSAG No. 65 |
| 45405.376 | vis | 1648.0 | 0.00557 | BBSAG No. 66 |
| 45435.319 | vis | 1674.0 | 0.00608 | BBSAG No. 66 |
| 45558.535 | vis | 1781.0 | –0.00277 | BAV Lichten. DB |
| 45566.600 | vis | 1788.0 | 0.00079 | BBSAG No. 68 |
| 45611.504 | vis | 1827.0 | –0.00894 | BBSAG No. 69 |
| 45640.311 | vis | 1852.0 | 0.00721 | BBSAG No. 69 |
| 45649.510 | vis | 1860.0 | –0.00686 | BBSAG No. 69 |
| 45671.398 | vis | 1879.0 | 0.00009 | BAV Lichten. DB |
| 45671.402 | vis | 1879.0 | 0.00409 | BAV Lichten. DB |
| 45671.405 | vis | 1879.0 | 0.00709 | BAV Lichten. DB |
| 45671.411 | vis | 1879.0 | 0.01309 | BAV Lichten. DB |
| 45672.550 | vis | 1880.0 | 0.00005 | BAV Lichten. DB |
| 45694.427 | vis | 1899.0 | –0.00359 | BBSAG No. 70 |
| 45701.340 | vis | 1905.0 | –0.00040 | BBSAG No. 70 |
| 45915.546 | vis | 2091.0 | 0.00166 | BBSAG No. 73 |
| 45993.864 | vis | 2159.0 | 0.00853 | Baldwin and Samolyk 1993 |
| 45998.461 | vis | 2163.0 | –0.00100 | BBSAG No. 74 |
| 46000.769 | vis | 2165.0 | 0.00373 | Baldwin and Samolyk 1993 |
| 46005.375 | vis | 2169.0 | 0.00319 | BBSAG No. 74 |
| 46006.520 | vis | 2170.0 | –0.00344 | BBSAG No. 74 |
| 46007.674 | vis | 2171.0 | –0.00107 | Baldwin and Samolyk 1993 |
| 46029.553 | vis | 2190.0 | –0.00312 | Baldwin and Samolyk 1993 |
| 46050.284 | vis | 2208.0 | –0.00154 | BBSAG No. 75 |
| 46052.592 | vis | 2210.0 | 0.00319 | Baldwin and Samolyk 1993 |
| 46060.653 | vis | 2217.0 | 0.00276 | Baldwin and Samolyk 1993 |
| 46060.659 | vis | 2217.0 | 0.00876 | BAV Lichten. DB |
| 46119.392 | vis | 2268.0 | 0.00842 | BBSAG No. 76 |
| 46172.365 | vis | 2314.0 | 0.00625 | BBSAG No. 76 |
| 46318.623 | vis | 2441.0 | 0.00671 | BBSAG No. 78 |
| 46357.773 | vis | 2475.0 | 0.00115 | Baldwin and Samolyk 1993 |
| 46377.348 | vis | 2492.0 | –0.00163 | BBSAG No. 79 |
| 46416.509 | vis | 2526.0 | 0.00381 | BBSAG No. 79 |
| 46439.542 | vis | 2546.0 | 0.00413 | Baldwin and Samolyk 1993 |
| 46447.606 | vis | 2553.0 | 0.00669 | Baldwin and Samolyk 1993 |

*table continued on following pages*

Table 3. Available times of minima and O–C residuals from Equation 1, cont.

| *Epoch HJD 2400000+* | *Type* | *Cycle* | *O–C* | *Reference* |
|---|---|---|---|---|
| 46478.698 | vis | 2580.0 | 0.00457 | Baldwin and Samolyk 1993 |
| 46629.556 | vis | 2711.0 | –0.00150 | BBSAG No. 80 |
| 46659.502 | vis | 2737.0 | 0.00201 | BBSAG No. 81 |
| 46681.380 | vis | 2756.0 | –0.00103 | BBSAG No. 81 |
| 46713.625 | vis | 2784.0 | –0.00179 | Baldwin and Samolyk 1993 |
| 46736.662 | vis | 2804.0 | 0.00253 | Baldwin and Samolyk 1993 |
| 46742.422 | vis | 2809.0 | 0.00436 | BBSAG No. 82 |
| 46744.721 | vis | 2811.0 | 0.00009 | Baldwin and Samolyk 1993 |
| 46764.301 | vis | 2828.0 | 0.00231 | BBSAG No. 82 |
| 46765.454 | vis | 2829.0 | 0.00367 | BBSAG No. 82 |
| 46804.606 | vis | 2863.0 | 0.00011 | Baldwin and Samolyk 1993 |
| 46805.756 | vis | 2864.0 | –0.00152 | Baldwin and Samolyk 1993 |
| 46817.280 | vis | 2874.0 | 0.00614 | BBSAG No. 83 |
| 46820.735 | vis | 2877.0 | 0.00624 | Baldwin and Samolyk 1993 |
| 47001.557* | vis | 3034.0 | 0.02168 | BAV Lichten. DB |
| 47039.531 | vis | 3067.0 | –0.00825 | BBSAG No. 85 |
| 47063.711* | vis | 3088.0 | –0.01256 | Baldwin and Samolyk 1993 |
| 47069.481 | vis | 3093.0 | –0.00073 | BBSAG No. 87 |
| 47084.449 | vis | 3106.0 | –0.00398 | BBSAG No. 86 |
| 47086.749 | vis | 3108.0 | –0.00724 | Baldwin and Samolyk 1993 |
| 47109.776 | vis | 3128.0 | –0.01293 | Baldwin and Samolyk 1993 |
| 47185.790 | vis | 3194.0 | –0.00678 | Baldwin and Samolyk 1993 |
| 47200.763 | vis | 3207.0 | –0.00502 | Baldwin and Samolyk 1993 |
| 47205.374 | vis | 3211.0 | –0.00056 | BBSAG No. 87 |
| 47235.301 | vis | 3237.0 | –0.01605 | BBSAG No. 88 |
| 47390.769 | vis | 3372.0 | –0.01865 | Baldwin and Samolyk 1993 |
| 47411.513 | vis | 3390.0 | –0.00407 | BBSAG No. 89 |
| 47411.513 | vis | 3390.0 | –0.00407 | Baldwin and Samolyk 1993 |
| 47420.714 | vis | 3398.0 | –0.01614 | Baldwin and Samolyk 1993 |
| 47435.694 | vis | 3411.0 | –0.00738 | BAV Lichten. DB |
| 47456.412 | vis | 3429.0 | –0.01880 | BBSAG No. 90 |
| 47480.602 | vis | 3450.0 | –0.01311 | Baldwin and Samolyk 1993 |
| 47524.367 | vis | 3488.0 | –0.01021 | BBSAG No. 90 |
| 47554.306 | vis | 3514.0 | –0.01370 | BBSAG No. 91 |
| 47554.312 | vis | 3514.0 | –0.00770 | BBSAG No. 91 |
| 47556.608 | vis | 3516.0 | –0.01497 | Baldwin and Samolyk 1993 |
| 47562.368 | vis | 3521.0 | –0.01314 | BBSAG No. 91 |
| 47564.668 | vis | 3523.0 | –0.01640 | Baldwin and Samolyk 1993 |
| 47822.640 | vis | 3747.0 | –0.01045 | Baldwin and Samolyk 1993 |
| 47823.786 | vis | 3748.0 | –0.01608 | Baldwin and Samolyk 1993 |
| 47837.607 | vis | 3760.0 | –0.01469 | Baldwin and Samolyk 1993 |
| 47850.281 | vis | 3771.0 | –0.00867 | BBSAG No. 94 |
| 47858.341 | vis | 3778.0 | –0.01011 | BBSAG No. 93 |
| 47911.312 | vis | 3824.0 | –0.01427 | BBSAG No. 94 |
| 47934.345 | vis | 3844.0 | –0.01396 | BBSAG No. 94 |
| 47943.557 | vis | 3852.0 | –0.01503 | Baldwin and Samolyk 1993 |
| 48209.580 | vis | 4083.0 | –0.01951 | Baldwin and Samolyk 1993 |
| 48222.254 | vis | 4094.0 | –0.01349 | BBSAG No. 97 |
| 48232.616 | vis | 4103.0 | –0.01619 | Baldwin and Samolyk 1993 |
| 48260.254 | vis | 4127.0 | –0.01741 | BBSAG No. 97 |
| 48260.258 | vis | 4127.0 | –0.01341 | BBSAG No. 97 |
| 48329.354 | vis | 4187.0 | –0.01546 | BBSAG No. 97 |
| 48490.578 | vis | 4327.0 | –0.02024 | BBSAG No. 98 |
| 48506.705 | vis | 4341.0 | –0.01611 | Baldwin and Samolyk 1993 |
| 48512.461 | vis | 4346.0 | –0.01829 | BAV Lichten. DB |
| 48512.461 | vis | 4346.0 | –0.01789 | Baldwin and Samolyk 1993 |
| 48534.340 | vis | 4365.0 | –0.02033 | BBSAG No. 99 |
| 48536.641 | vis | 4367.0 | –0.02260 | Baldwin and Samolyk 1993 |
| 48564.280 | vis | 4391.0 | –0.02282 | BBSAG No. 99 |
| 48625.322 | vis | 4444.0 | –0.01743 | BBSAG No. 100 |
| 48686.346 | vis | 4497.0 | –0.03004 | BBSAG No. 100 |
| 48686.362 | vis | 4497.0 | –0.01404 | BBSAG No. 101 |
| 48893.645 | vis | 4677.0 | –0.02518 | Baldwin and Samolyk 1997 |
| 48923.588 | vis | 4703.0 | –0.02467 | Baldwin and Samolyk 1997 |
| 49005.351 | vis | 4774.0 | –0.02769 | BBSAG No. 103 |
| 49066.395 | vis | 4827.0 | –0.02060 | BAV Lichten. DB |
| 49066.402 | vis | 4827.0 | –0.01360 | BAV Lichten. DB |
| 49220.703 | vis | 4961.0 | –0.03127 | Baldwin and Samolyk 1997 |
| 49243.737 | vis | 4981.0 | –0.02995 | Baldwin and Samolyk 1997 |
| 49250.647 | vis | 4987.0 | –0.02976 | Baldwin and Samolyk 1997 |
| 49266.771 | vis | 5001.0 | –0.02863 | Baldwin and Samolyk 1997 |
| 49326.650 | vis | 5053.0 | –0.03461 | Baldwin and Samolyk 1997 |
| 49327.802 | vis | 5054.0 | –0.03424 | Baldwin and Samolyk 1997 |
| 49331.271 | vis | 5057.0 | –0.02014 | BBSAG No. 105 |
| 49333.560 | vis | 5059.0 | –0.03441 | Baldwin and Samolyk 1997 |
| 49384.237 | vis | 5103.0 | –0.02931 | BBSAG No. 106 |
| 49455.638 | vis | 5165.0 | –0.02963 | Baldwin and Samolyk 1997 |
| 49561.586 | vis | 5257.0 | –0.03197 | BBSAG No. 107 |
| 49637.594 | vis | 5323.0 | –0.03182 | Baldwin and Samolyk 1997 |
| 49637.596 | vis | 5323.0 | –0.02982 | Baldwin and Samolyk 1997 |
| 49650.258 | vis | 5334.0 | –0.03580 | BBSAG No. 108 |
| 49713.599 | vis | 5389.0 | –0.03467 | Baldwin and Samolyk 1997 |
| 49713.602 | vis | 5389.0 | –0.03167 | Baldwin and Samolyk 1997 |
| 49715.913 | vis | 5391.0 | –0.02394 | Saijo 1997 |
| 49774.636 | vis | 5442.0 | –0.03428 | Baldwin and Samolyk 1997 |
| 49787.307 | vis | 5453.0 | –0.03126 | BBSAG No. 108 |
| 49789.608 | vis | 5455.0 | –0.03352 | Baldwin and Samolyk 1997 |
| 49810.337 | vis | 5473.0 | –0.03394 | BBSAG No. 109 |
| 49810.339 | vis | 5473.0 | –0.03194 | BBSAG No. 109 |
| 49948.534 | vis | 5593.0 | –0.03303 | BBSAG No. 110 |
| 49965.807 | vis | 5608.0 | –0.03454 | Baldwin and Samolyk 1997 |
| 50041.817 | vis | 5674.0 | –0.03240 | Baldwin and Samolyk 1997 |
| 50047.570 | vis | 5679.0 | –0.03757 | Baldwin and Samolyk 1997 |
| 50047.573 | vis | 5679.0 | –0.03457 | Baldwin and Samolyk 1997 |
| 50068.305 | vis | 5697.0 | –0.03198 | BBSAG No. 111 |
| 50099.402 | vis | 5724.0 | –0.02910 | BBSAG No. 111 |
| 50154.674 | vis | 5772.0 | –0.03554 | Baldwin and Samolyk 1997 |
| 50167.335 | vis | 5783.0 | –0.04252 | BBSAG No. 111 |
| 50313.597 | vis | 5910.0 | –0.03805 | BBSAG No. 113 |
| 50337.776 | vis | 5931.0 | –0.04337 | Baldwin and Samolyk 1997 |
| 50380.389 | vis | 5968.0 | –0.04083 | BBSAG No. 113 |
| 50397.671 | vis | 5983.0 | –0.03334 | Baldwin and Samolyk 1997 |
| 50420.693 | vis | 6003.0 | –0.04402 | Baldwin and Samolyk 1997 |
| 50427.605 | vis | 6009.0 | –0.04183 | Baldwin and Samolyk 1997 |
| 50433.357 | vis | 6014.0 | –0.04800 | BBSAG No. 114 |
| 50486.342 | vis | 6060.0 | –0.03817 | BBSAG No. 114 |
| 50488.642 | vis | 6062.0 | –0.04144 | Baldwin and Samolyk 1997 |
| 50495.557 | vis | 6068.0 | –0.03624 | Baldwin and Samolyk 1997 |
| 50509.371 | vis | 6080.0 | –0.04185 | BBSAG No. 114 |
| 50509.378 | vis | 6080.0 | –0.03485 | BBSAG No. 114 |
| 50516.282 | vis | 6086.0 | –0.04065 | BBSAG No. 114 |
| 50517.430 | vis | 6087.0 | –0.04429 | BBSAG No. 114 |
| 50518.583 | vis | 6088.0 | –0.04292 | Baldwin and Samolyk 1997 |
| 50541.611 | vis | 6108.0 | –0.04760 | Baldwin and Samolyk 1997 |
| 50692.476 | vis | 6239.0 | –0.04667 | BBSAG No. 115 |
| 50752.363 | vis | 6291.0 | –0.04465 | BBSAG No. 116 |
| 50761.571 | vis | 6299.0 | –0.04972 | Baldwin and Samolyk 2002 |
| 50762.724 | vis | 6300.0 | –0.04836 | Baldwin and Samolyk 2002 |
| 50769.633 | vis | 6306.0 | –0.04916 | Baldwin and Samolyk 2002 |
| 50774.244 | vis | 6310.0 | –0.04470 | BBSAG No. 116 |
| 50782.305 | vis | 6317.0 | –0.04514 | BBSAG No. 116 |
| 50845.644 | vis | 6372.0 | –0.04601 | Baldwin and Samolyk 2002 |
| 51057.544 | vis | 6556.0 | –0.04669 | BBSAG No. 118 |
| 51133.547 | vis | 6622.0 | –0.05154 | Baldwin and Samolyk 2002 |
| 51156.585 | vis | 6642.0 | –0.04623 | Baldwin and Samolyk 2002 |
| 51177.313 | vis | 6660.0 | –0.04764 | BBSAG No. 119 |
| 51383.4540 | CCD | 6839.0 | –0.04915 | BAV Lichten. DB |
| 51438.731 | vis | 6887.0 | –0.05058 | Baldwin and Samolyk 2002 |
| 51469.8278 | PE | 6914.0 | –0.04791 | Nelson 2000 |
| 51490.5576 | CCD | 6932.0 | –0.04752 | Baldwin and Samolyk 2002 |
| 51513.589 | vis | 6952.0 | –0.04880 | Baldwin and Samolyk 2002 |
| 51544.687 | vis | 6979.0 | –0.04492 | Baldwin and Samolyk 2002 |
| 51551.598 | vis | 6985.0 | –0.04373 | Baldwin and Samolyk 2002 |
| 51557.356 | vis | 6990.0 | –0.04390 | BBSAG No. 122 |

*table continued on next page*

Table 3. Available times of minima and O–C residuals from Equation 1, cont.

| *Epoch HJD 2400000+* | *Type* | *Cycle* | *O–C* | *Reference* |
|---|---|---|---|---|
| 51580.391 | vis | 7010.0 | –0.04158 | BBSAG No. 122 |
| 51581.542 | vis | 7011.0 | –0.04222 | Baldwin and Samolyk 2002 |
| 51582.691 | vis | 7012.0 | –0.04485 | Baldwin and Samolyk 2002 |
| 51625.296 | vis | 7049.0 | –0.05031 | BBSAG No. 122 |
| 51809.563 | vis | 7209.0 | –0.04477 | BBSAG No. 123 |
| 51870.594 | vis | 7262.0 | –0.05038 | Baldwin and Samolyk 2002 |
| 51878.658 | vis | 7269.0 | –0.04782 | Baldwin and Samolyk 2002 |
| 51893.6265 | CCD | 7282.0 | –0.05056 | Baldwin and Samolyk 2002 |
| 51913.219* | vis | 7299.0 | –0.03584 | BBSAG No. 124 |
| 51946.6017 | CCD | 7328.0 | –0.05053 | Baldwin and Samolyk 2002 |
| 51952.3600* | PE | 7333.0 | –0.05040 | BBSAG No. 124 |
| 51961.5738 | CCD | 7341.0 | –0.04967 | Baldwin and Samolyk 2002 |
| 52205.724 | vis | 7553.0 | –0.04591 | Baldwin and Samolyk 2002 |
| 52212.634 | vis | 7559.0 | –0.04571 | BBSAG No. 126 |
| 52227.601 | vis | 7572.0 | –0.04996 | Baldwin and Samolyk 2002 |
| 52250.636 | vis | 7592.0 | –0.04764 | Baldwin and Samolyk 2002 |
| 52265.589* | vis | 7605.0 | –0.06588 | BAV Lichten. DB |
| 52279.423 | vis | 7617.0 | –0.05149 | BBSAG No. 127 |
| 52530.479* | vis | 7835.0 | –0.05173 | Diethelm 2003 |
| 52555.8134 | PE | 7857.0 | –0.05328 | Nelson 2003 |
| 52585.751 | vis | 7883.0 | –0.05817 | BAV Lichten. DB |
| 52637.572 | vis | 7928.0 | –0.06070 | BAV Lichten. DB |
| 52637.575 | vis | 7928.0 | –0.05770 | BAV Lichten. DB |
| 52652.550 | vis | 7941.0 | –0.05415 | BAV Lichten. DB |
| 52658.3078 | PE | 7946.0 | –0.05432 | Diethelm 2003 |
| 52902.454 | vis | 8158.0 | –0.05455 | Diethelm 2004 |
| 52966.940 | vis | 8214.0 | –0.06006 | BAV Lichten. DB |
| 53290.5507 | CCD | 8495.0 | –0.05855 | Zejda *et al.* 2006 |
| 53326.2516 | CCD | 8526.0 | –0.05831 | Nagai 2004a |
| 53342.375 | vis | 8540.0 | –0.05778 | Locher 2005 |
| 53351.5880 | CCD | 8548.0 | –0.05786 | BAV Lichten. DB |
| 53359.6483 | CCD | 8555.0 | –0.05900 | BAV Lichten. DB |
| 53410.3205 | PE | 8599.0 | –0.05870 | Hübscher *et al.* 2005 |
| 53594.576* | vis | 8759.0 | –0.06466 | Locher 2005 |
| 53654.4681 | CCD | 8811.0 | –0.05753 | Hübscher *et al.* 2006 |
| 53733.938* | vis | 8880.0 | –0.05039 | Nagai 2004b |
| 53755.8120 | CCD | 8899.0 | –0.05743 | BAV Lichten. DB |
| 53761.5703* | CCD | 8904.0 | –0.05730 | BAV Lichten. DB |
| 54044.8725 | CCD | 9150.0 | –0.05710 | BAV Lichten. DB |
| 54059.8435 | CCD | 9163.0 | –0.05734 | BAV Lichten. DB |
| 54116.2733 | CCD | 9212.0 | –0.05761 | Doğru *et al.* 2009 |
| 54172.7032 | CCD | 9261.0 | –0.05779 | BAV Lichten. DB |
| 54476.7360 | CCD | 9525.0 | –0.05639 | Samolyk 2008 |
| 54521.6495 | CCD | 9564.0 | –0.05662 | Samolyk 2008 |
| 54830.2903 | CCD | 9832.0 | –0.05377 | Hübscher *et al.* 2009 |
| 54830.2909 | CCD | 9832.0 | –0.05317 | Hübscher *et al.* 2009 |
| 54848.7164 | CCD | 9848.0 | –0.05381 | Diethelm 2009 |
| 54863.6886 | CCD | 9861.0 | –0.05286 | Samolyk 2009 |
| 54863.6887 | CCD | 9861.0 | –0.05276 | Samolyk 2009 |
| 54868.2952 | CCD | 9865.0 | –0.05279 | Doğru *et al.* 2009 |
| 55105.5329 | CCD | 10071.0 | –0.05172 | Erkan *et al.* 2010 |
| 55122.8078 | CCD | 10086.0 | –0.05133 | Samolyk 2010 |
| 55127.4097 | CCD | 10090.0 | –0.05597 | Erkan *et al.* 2010 |
| 55130.8691 | CCD | 10093.0 | –0.05147 | Samolyk 2010 |
| 55205.7253 | CCD | 10158.0 | –0.05149 | Diethelm 2010 |
| 55500.5411 | CCD | 10414.0 | –0.05403 | Doğru *et al.* 2011 |
| 55501.6927 | CCD | 10415.0 | –0.05406 | Samolyk 2011 |
| 55502.8443 | CCD | 10416.0 | –0.05409 | Diethelm 2011 |
| 55571.9411 | CCD | 10476.0 | –0.05534 | Nagai 2012 |
| 55579.4331* | CCD | 10482.5 | –0.04896 | Hübscher 2011 |
| 55837.9646 | CCD | 10707.0 | –0.05932 | Samolyk 2012 |
| 55867.9069 | CCD | 10733.0 | –0.05951 | Diethelm 2012 |
| 55970.4010 | CCD | 10822.0 | –0.06085 | Hoňková *et al.* 2013 |
| 55970.4011 | CCD | 10822.0 | –0.06075 | Hoňková *et al.* 2013 |
| 55970.4011 | CCD | 10822.0 | –0.06075 | Hoňková *et al.* 2013 |
| 56015.3147 | CCD | 10861.0 | –0.06088 | Hoňková *et al.* 2013 |
| 56015.3151 | CCD | 10861.0 | –0.06053 | Hoňková *et al.* 2013 |
| 56186.9049 | CCD | 11010.0 | –0.06416 | Samolyk 2013a |
| 56230.6663 | CCD | 11048.0 | –0.06486 | Samolyk 2013a |
| 56238.7280 | CCD | 11055.0 | –0.06460 | Samolyk 2013a |
| 56262.9112 | CCD | 11076.0 | –0.06571 | Nagai 2013 |
| 56262.9126 | CCD | 11076.0 | –0.06431 | Samolyk 2015 |
| 56520.8743 | CCD | 11300.0 | –0.06866 | Samolyk 2013b. |
| 56654.4619 | CCD | 11416.0 | –0.07061 | Hoňková *et al.* 2015 |
| 56654.4622 | CCD | 11416.0 | –0.07031 | Hoňková 2*et al.* 015 |
| 56692.4656 | CCD | 11449.0 | –0.07084 | Hoňková *et al.* 2015 |
| 56692.4659 | CCD | 11449.0 | –0.07054 | Hoňková *et al.* 2015 |
| 56953.8846 | CCD | 11676.0 | –0.07279 | Samolyk 2015 |
| 57355.8055 | CCD | 12025.0 | –0.07219 | Samolyk 2016 |

**These minima timings deviated significantly for the O–C trend and were not used in the period analysis.*

Table 4. Orbital period jumps of XZ Per.

| *Cycle Interval* | *ΔT (days)* | *ΔP ($10^{-5}$ days)* | *ΔP (seconds)* |
|---|---|---|---|
| –16000 to –9900 | –0.1163 ± 0.0106 | –0.80 ± 0.07 | –0.69 ± 0.06 |
| –9900 to –7200 | –0.0422 ± 0.0152 | 0.64 ± 0.18 | 0.56 ± 0.15 |
| –7200 to –6400 | 0.0641 ± 0.0087 | –0.72 ± 0.13 | –0.62 ± 0.11 |
| –6400 to 2600 | –0.0063 ± 0.0003 | 0.38 ± 0.01 | 0.33 ± 0.01 |
| 2600 to 6700 | 0.0332 ± 0.0018 | –0.70 ± 0.04 | –0.60 ± 0.03 |
| 6700 to 8600 | –0.0087 ± 0.0050 | –0.02 ± 0.07 | –0.02 ± 0.06 |
| 8600 to 10100 | –0.1055 ± 0.0044 | 1.10 ± 0.05 | 0.95 ± 0.04 |
| 10100 to 11500 | 0.0704 ± 0.0080 | –0.62 ± 0.08 | –0.54 ± 0.07 |
| 11500 to 12400 | –0.0632 ± 0.0044 | 0.54 ± 0.04 | 0.46 ± 0.03 |

2 and 3 of Table 5. No appreciable third light contribution was seen in the lights. The values for the g' and B passbands were very small, while the longer wavelengths, r', i', and V, were both small and negative. The normalized light curves for each passband, overlaid by the synthetic solution curves, are shown in Figure 8 with the residuals in Figure 9.

### 3.4. Spot model

The asymmetries in the light curves seen in Figures 8 and 9 are usually attributed to cool spots, hot regions such as faculae, or gas streams that impact one of the stars. At orbital phase 0.9 there is an excess of light seen in all the light curves. The residuals in Figure 9 show a sharp cutoff in this excess light when the stars approach primary eclipse. This feature is most likely caused by a hot spot on the primary star. Mass transferred from the Roche lobe filling secondary star would impact the primary star on its trailing side close to the equator (Zhang *et al.* 2014). An additional feature seen in the light curve residuals of Figure 9 is a light loss centered between orbital phase 0.3 to 0.4 for the DS1 observations. This indicates an under luminous region (cool spot) on the larger secondary star at the time the DS1 observations were acquired. This feature is not apparent in the DS2 data that were obtained six months later. Using BM3, a hot and cool spot were modeled for the DS1 observations and a single hot spot for DS2. The spot parameter's latitude,

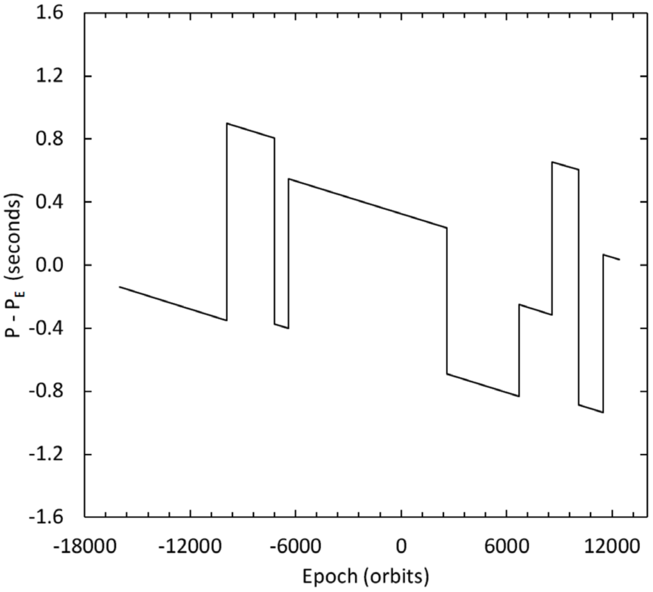

Figure 5. Orbital period changes of XZ Per as a function of time.

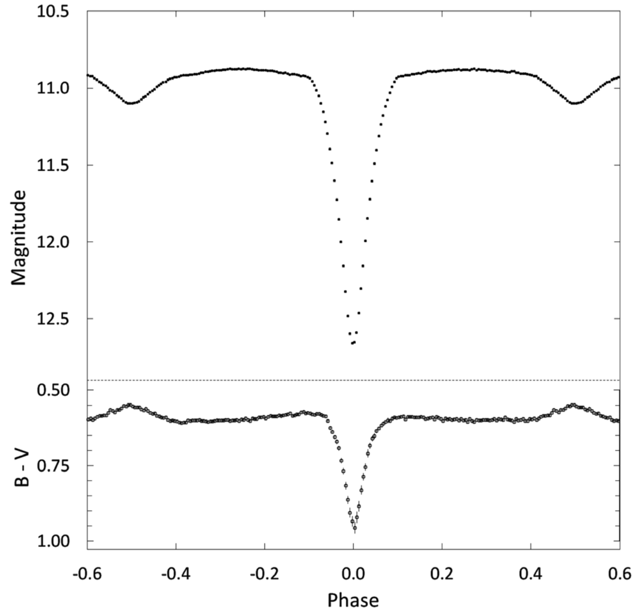

Figure 6. Light curve of all V-band observations in standard magnitudes (top panel). The observations were binned with a phase width of 0.005. The errors for each binned point are about the size of the plotted points. The B–V colors were calculated by subtracting the binned V magnitudes from the linearly interpolated binned B magnitudes.

longitude, size, and temperature were adjusted until a good fit resulted between the synthetic and observed light curves. New WD solutions were then made using the spot parameters from the BM3 fits. The best-fit WD spotted solution parameters are shown in columns 4 and 5 in Table 5. Figure 10 shows the final spotted model fits (solid lines) to the observed light curves and Figure 11 the residuals. For the DS1 solutions the sum of the residuals squared was 0.52 for the spotted model and 0.77 for the unspotted model (1.5 times larger) and for the DS2 solutions 0.26 for the spotted model and 0.54 for the unspotted model (2.1 times larger). A graphical representation of the spotted DS1 model is shown in Figure 12.

## 4. Discussion

The WD solutions indicate XZ Per is an evolved semi-detached system with the less massive secondary star filling its Roche lobe. Figure 13 compares the mass and radius of both stars with 61 semi-detached systems with well determined absolute parameters (Ibanoğlu *et al.* 2006). The primary star of XZ Per is close to the ZAMS like most of the other primaries in this group. The secondary along with all the other secondary stars in the sample are located on or above the TAMS line. The absolute stellar parameters of XZ Per can now be estimated. A main-sequence star with an effective temperature of 6680 K gives a mass of 1.41 ± 0.08 $M_\odot$ (Pecaut and Mamajeck 2013). Using the mass ratio from the WD solution gives the secondary star's mass as 0.92 ± 0.06 $M_\odot$ and applying Kepler's Third Law gives a distance between the mass centers of 6.125 ± 0.005 $R_\odot$. The mean stellar densities, $\bar{\rho}_1 = 0.39 \pm 0.01$ g cm$^{-3}$ and $\bar{\rho}_2 = 0.14 \pm 0.03$ g cm$^{-3}$, were found using Mochnacki's (1981) empirical relationship

$$\bar{\rho}_1 = \frac{0.0189}{r_1^3(1 + q)\, P^2} \text{ and } \bar{\rho}_2 = \frac{0.0189q}{r_2^3\,(1 + q)\, P^{2'}}, \qquad (6)$$

where the stellar radius is normalized to the semi-major axis and P is in days. The visual luminosities, $L_{1V} = 5.87 \pm 0.56\ L_\odot$ and $L_{2V} = 1.20 \pm 0.30\ L_\odot$, were calculated using the bolometric magnitudes from the WD light curve program (LC) and bolometric corrections (Pecaut and Mamajek 2013). The LC output also provided the stellar radii and surface gravities of each star. All the estimated stellar parameters have been collected in Table 6. The distance to this system was determined from the precision parallax measurements of the Gaia spacecraft (Gaia 2016). The measured parallax is p = 0.00234 ± 0.00023, which gives a distance of d = 427 ± 48 pc. Assuming no interstellar extinction, this distance combined with the apparent V magnitude at orbital phase 0.25 gives an absolute magnitude of $M_V = 2.73 \pm 0.05$. This value compares well with the absolute magnitudes from the DS1 and DS2 model solutions, $M_V = 2.74 \pm 0.10$ and $M_V = 2.77 \pm 0.10$, respectively. If the spectroscopically determined effective temperature for the primary star is accurate, these values indicate the interstellar extinction is likely small (a few hundredths of a magnitude). A higher temperature primary, on the other hand, would point to a larger extinction value. A precision spectroscopic study would be necessary to confirm the temperature of the primary star as well as provide direct determination of the stellar masses.

Mass transfer can occur in semi-detached systems when the secondary star fills its Roche lobe. The main-sequence primary is on the receiving end of the matter stream. Given the short orbital period of XZ Per, the distance between the two stars is small compared to their radii. The mass stream would likely be narrow and would directly impact the primary star near its equator, creating a small hot spot due to impact heating (Zhang *et al.* 2014; Ibanoğlu *et al.* 2006). The locations and sizes of the hot spots modeled in both WD solutions are consistent with an active mass stream from the secondary to the primary star. Additional small distortions in the light

Table 5. XZ Per synthetic light curve solutions.

| *parameter* | *DS1–g', r', i'* *no spots* | *DS2–B,V* *no spots* | *DS1–g', r', i'* *with spots* | *DS2–B,V* *with spots* |
|---|---|---|---|---|
| i (°) | 85.05 ± 0.42 | 84.97 ± 0.08 | 85.15 ± 0.11 | 85.03 ± 0.05 |
| $T_1$ (K) | [1]6680 | [1]6680 | [1]6680 | [1]6680 |
| $T_2$ (K) | 4624 ± 7 | 4636 ± 8 | 4628 ± 11 | 4636 ± 5 |
| $q(M_2/M_1)$ | 0.638 ± 0.013 | 0.629 ± 0.004 | 0.647 ± 0.005 | 0.637 ± 0.003 |
| $\Omega_1$ | 4.195 ± 0.038 | 4.272 ± 0.017 | 4.195 ± 0.013 | 4.247 ± 0.012 |
| $\Omega_2$ | 3.131 | 3.116 | 3.149 | 3.131 |
| $L_1/(L_1+L_2)$ (B) | — | 0.8906 ± 0.0002 | — | 0.8949 ± 0.0002 |
| $L_1/(L_1+L_2)$ (V) | — | 0.8185 ± 0.0005 | — | 0.8244 ± 0.0003 |
| $L_1/(L_1+L_2)$ (g') | 0.8650 ± 0.0023 | — | 0.8644 ± 0.0004 | — |
| $L_1/(L_1+L_2)$ (r') | 0.7802 ± 0.0035 | — | 0.7788 ± 0.0007 | — |
| $L_1/(L_1+L_2)$ (i') | 0.7337 ± 0.0041 | — | 0.7318 ± 0.0008 | — |
| $r_1$ pole | 0.2703 ± 0.0020 | 0.2724 ± 0.0013 | 0.2818 ± 0.0011 | 0.2779 ± 0.0010 |
| $r_1$ point | 0.2813 ± 0.0022 | 0.2848 ± 0.0016 | 0.2964 ± 0.0014 | 0.2918 ± 0.0012 |
| $r_1$ side | 0.2747 ± 0.0021 | 0.2771 ± 0.0014 | 0.2872 ± 0.0012 | 0.2831 ± 0.0011 |
| $r_1$ back | 0.2790 ± 0.0022 | 0.2821 ± 0.0015 | 0.2930 ± 0.0013 | 0.2887 ± 0.0012 |
| $r_2$ pole | 0.3095 ± 0.0019 | 0.3179 ± 0.0006 | 0.3185 ± 0.0006 | 0.3198 ± 0.0004 |
| $r_2$ point | 0.4417 ± 0.0019 | 0.4524 ± 0.0006 | 0.4530 ± 0.0006 | 0.4547 ± 0.0004 |
| $r_2$ side | 0.3234 ± 0.0020 | 0.3324 ± 0.0006 | 0.3330 ± 0.0007 | 0.3344 ± 0.0004 |
| $r_2$ back | 0.3557 ± 0.0020 | 0.3646 ± 0.0006 | 0.3651 ± 0.0006 | 0.3665 ± 0.0004 |
| $\sum res^2$ | 0.77 | 0.52 | 0.54 | 0.26 |
| *spot parameters* | | | *Star 1-Hot Spot* | *Star 1-Hot Spot* |
| colatitude (°) | — | — | 90 ± 14 | 72 ± 2 |
| longitude (°) | — | — | 21 ± 3 | 10 ± 1 |
| spot radius (°) | — | — | 10 ± 3 | 10 ± 2 |
| temp.-factor | — | — | 1.13 ± 0.07 | 1.17 ± 0.04 |
| | | | *Star 2-Cool Spot 1* | |
| colatitude (°) | — | — | 46 ± 18 | — |
| longitude (°) | — | — | 73 ± 4 | — |
| spot radius (°) | — | — | 24 ± 8 | — |
| temp.-factor | — | — | 0.85 ± 0.09 | — |

*[1] Assumed.*

*Note: The errors in the stellar parameters result from the least–squares fit to the model. The actual uncertainties of the parameters are considerably larger (ex. $T_1$ and $T_2$ have uncertainties of about ± 180 K).*

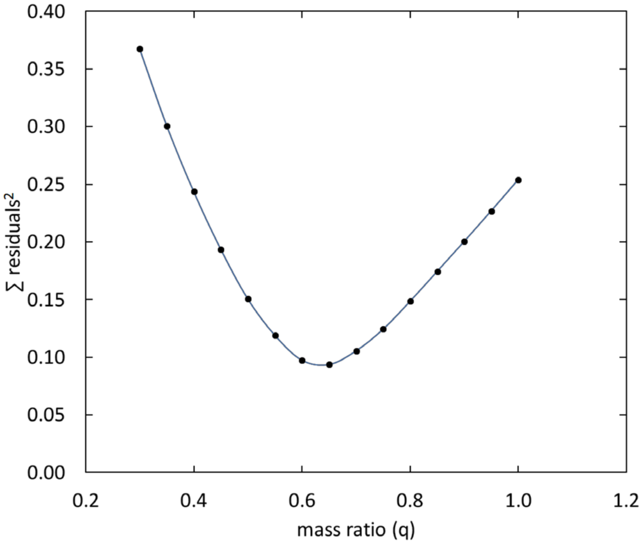

Figure 7. Results of the q-search showing the relation between the sum of the residuals squared and the mass ratio q.

curves at other orbital phases may also be effects of the impact heating, as diffusion and convection transport energy beyond the impact region.

The conservative mass transfer supported by the impact heating on the primary star would result in the widening of the orbit and an increasing period (Huang 1963). The least-squares solution for the quadratic ephemeris (section 3) gives a secular period decrease of $dP/dt = -1.27 \times 10^{-7}$ d $yr^{-1}$. This observed period decrease indicates the mass and angular momentum for the two stars is not conserved. Magnetic braking, which requires a stellar wind and a stellar magnetic field, is a possible cause of the angular momentum loss. XZ Per has a late-type secondary (spectral type K4) with a deep convective envelope. This convection combined with its rapid rotation should make the star magnetically active. The dark spot modeled on the secondary star and the changes in spot configuration between the two observational data sets is a good indication of magnetic activity. This could be the mechanism causing the mass and angular momentum loss and the resulting decrease in the orbital period (Hall 1989). There are a number of other Algols that have decreasing orbital periods with comparable dP/dt values (21 in Table 6 of Yang and Wei 2009). In addition, a

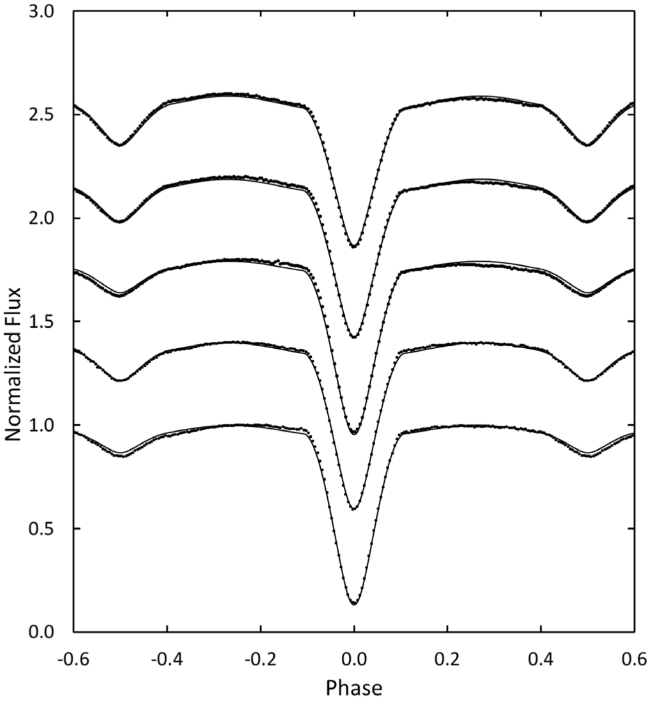

Figure 8. The WD model fit without spots (solid curve) to the observed normalized flux curves for each passband. From top to bottom the passbands are Sloan i', Sloan r', Sloan g', Johnson V, and Johnson B. Each curve is offset by 0.2 for this combined plot. The best-fit parameters are given in columns 2 and 3 of Table 5. Error bars are omitted from the points for clarity.

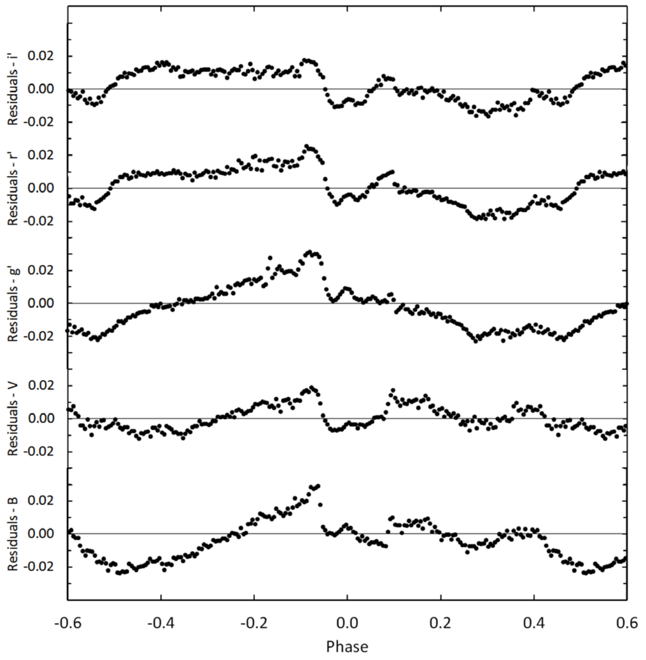

Figure 9. The residuals for the best-fit WD model without spots. Error bars are omitted from the points for clarity.

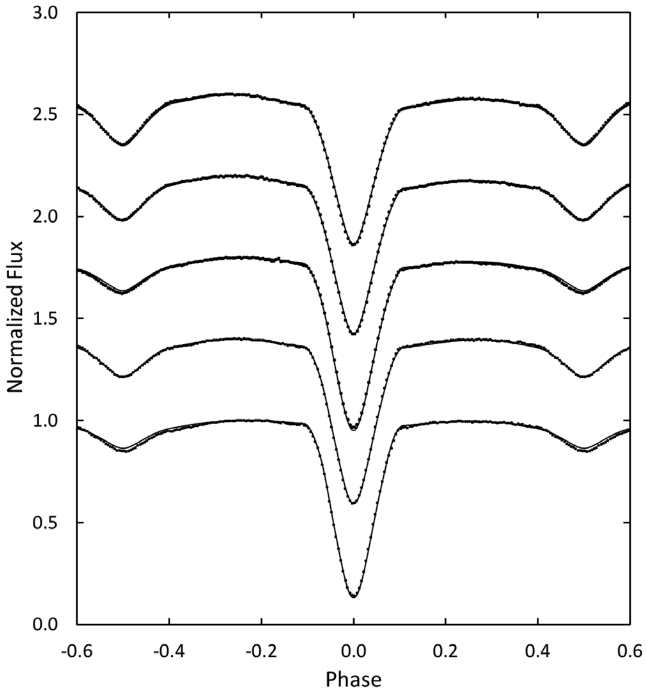

Figure 10. The WD model fit with spots (solid curve) to the observed normalized flux curves for each passband. From top to bottom the passbands are Sloan i', Sloan r', Sloan g', Johnson V, and Johnson B. Each curve is offset by 0.2 for this combined plot. The best-fit parameters are given in columns 4 and 5 of Table 5. Error bars are omitted from the points for clarity.

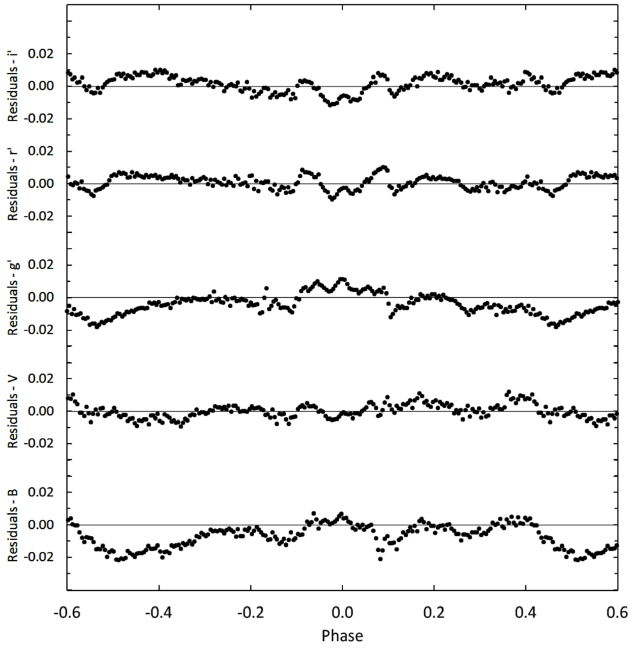

Figure 11. The residuals for the best-fit WD models with spots. Error bars are omitted from the points for clarity.

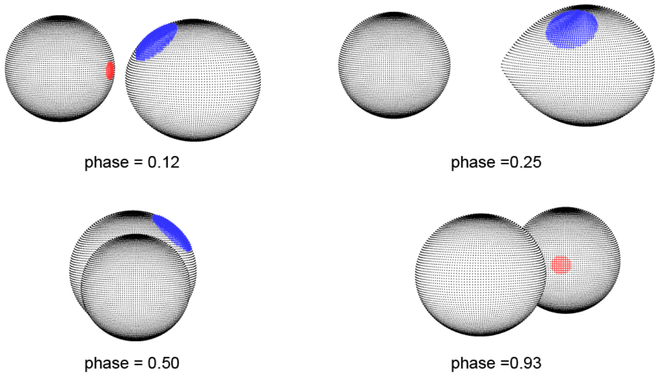
phase = 0.12

phase =0.25

phase = 0.50

phase =0.93

Figure 12. Roche Lobe surfaces of the best-fit WD spot DS1 model with orbital phase shown below each diagram.

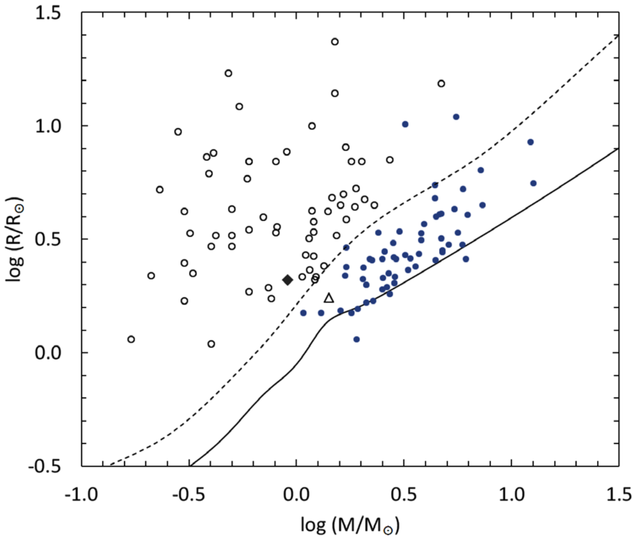

Figure 13. Positions of both components of XZ Per on the Mass–Radius diagram of 62 semi-detached Algol systems with well determined parameters. Closed circles are the primary stars and open circles the secondary stars. The triangle and the diamond are the primary and the secondary of XZ Per, respectively. Solid and dotted lines refer to ZAMS and TAMS, respectively, calculated from Tout *et al.* (1996).

number of Algol systems (RW CrB, TU Her, BO Mon, Y Psc, AY Gem, UU And, TY Peg, X Tri, and Z Per) also show sudden period jumps superimposed on secular decreasing periods that are similar to XZ Per (Qian 2000a, 2000b, 2001a, 2001b, 2002). The possible mechanism for the observed alternating period changes in semi-detached binaries was discussed by van 'T Veer (1993) and investigated by Qian (2002), who finds both the secular period decrease and the irregular period jumps can be explained by the variable interplay between magnetic coupling and spin orbit coupling. A secular period decrease could also result from a small fraction of the transferred mass forming a circumbinary disk (Chen *et al.* 2006). Detailed calculations indicate the orbital angular momentum can be efficiently removed by a thin disk surrounding both stars, but observations of XZ Per with time-resolved spectroscopy found no evidence of emission from a gaseous disk (Kaitchuck and Honeycutt 1982).

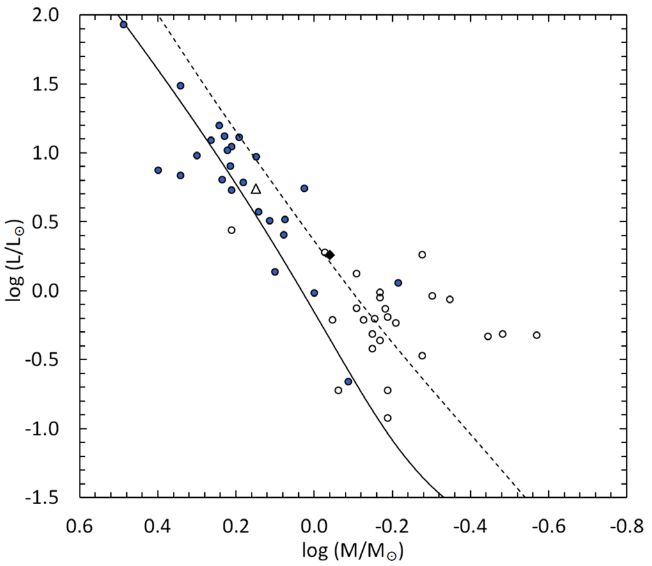

Figure 14. Positions of both components of XZ Per on the Mass–Luminosity diagram of 25 semi-detached NCB Algol systems with well determined parameters. Closed circles are the primary stars and open circles the secondary stars. The triangle and diamond are the primary and the secondary of XZ Per, respectively. Solid and dotted lines refer to ZAMS and TAMS, respectively, calculated from Tout *et al.* (1996).

Table 6. Provisional stellar parameters for XZ Per.

| *Parameter* | *Symbol* | *Value* |
|---|---|---|
| Stellar masses | $M_1 (M_\odot)$ | 1.41±0.08 |
| | $M_2 (M_\odot)$ | 0.91±0.06 |
| Semi-major axis | $a (R_\odot)$ | 6.120±0.005 |
| Stellar radii | $R_1 (R_\odot)$ | 1.75±0.03 |
| | $R_2 (R_\odot)$ | 2.09±0.12 |
| Surface gravity | $\log g_1$ (cgs) | 4.10±0.03 |
| | $\log g_2$ (cgs) | 3.76 ± 0.04 |
| Mean density | $\bar{\rho}_1$ (g cm$^{-3}$) | 0.37±0.01 |
| | $\bar{\rho}_2$ (g cm$^{-3}$) | 0.14±0.03 |
| Stellar luminosity | $L_{1V} (L_\odot)$ | 5.9±0.6 |
| | $L_{2V} (L_\odot)$ | 1.2±0.3 |
| Bolometric magnitude | $M_{bol,1}$ | 2.9±0.1 |
| | $M_{bol,2}$ | 4.1±0.2 |

*Values in this table are provisional. Radial velocity observations are necessary for direct determination of $M_1$, $M_2$, and a.*

The observed light curves and photometric solutions of XZ Per look very similar to EP Cas, AK CMi, FG Gem, and DF Pup, which were classified as near contact binaries (NCB) (Yang *et al.* 2013) where the secondary star fills the Roche lobe and the primary is inside one. Yakut and Eggleton (2005) compiled a list of 25 NCBs with well determined parameters. Figure 14 shows a mass luminosity diagram (M-L) of the components of these binaries with XZ Per included. The primary star of XZ Per (open triangle in Figure 14) lies about midway between the zero-age main-sequence (ZAMS) line and the terminal-age main-sequence (TAMS), as do most of the other NCB primary stars. XZ Per's secondary star (filled diamond in Figure 14) lies close to the TAMS, again indicating it has evolved. Most of the other secondary stars in this NCB sample are at a similar point in their evolution. The filling factor for the primary star can determine how close the star is to filling its lobe. It is defined as $f_1 = R_1 / R_L$, where $R_1$ is the radius of the primary star and $R_L$ is the volume radius of the Roche lobe. Eggleton's (1983) formula gives $R_L/a$ as a function of mass ratio (q),

$$\frac{R_L}{a} = \frac{0.49q^{2/3}}{0.6q^{2/3} + \ln(1 + q^{1/3})'}, \tag{7}$$

where a is the separation between the star's mass centers. Using the photometric solution from DS1 gives a value of $f_1 = 84\%$, which is higher than many semi-detached binaries that show a secular period decrease (Yang and Wei 2009). XZ Per appears to be at an intermediate evolutionary state, beginning life as a close detached binary and eventually, with additional mass and angular momentum loss, becoming a W UMa contact binary (Yakut and Eggleton 2005). Model calculations indicate XZ Per should start its contact phase 4–5 Gyr after its formation with the two stars ultimately coalescing into a single star (Gazeas and Stępień 2008).

## 5. Conclusions

Two new sets of photometric observations of XZ Per resulted in five complete light curves that were used for investigation of this system. Based on these observations, photometric solutions were obtained for both data sets. The results of a detailed analysis of the DS1 observations and the period study gave the following results:

1. XZ Per is a semi-detached Algol-type eclipsing binary with a mass ratio of q = 0.647 and an orbital inclination of i = 85.2°. The effective temperature of the primary star is $T_1 = 6680$ K, and the secondary $T_2 = 4628$ K. The primary is a F3 main-sequence star and the secondary an evolved K4 star (possibly a subgiant). No third light was found in the system but a hot spot was modeled on the primary star and a large cool spot on the secondary. Mass transferred from the secondary star is the likely cause of the hot spot on the primary. The cool spot was not necessary for the DS2 solution, indicating a changing spot configuration and therefore a magnetically active secondary star.

2. The period study found a secular decrease in the orbital period at a rate of $dP/dt = -1.27 \times 10^{-7}$ d yr$^{-1}$. Magnetic braking is likely the mechanism causing mass and angular momentum loss. In addition, the *(O–C)* data displayed several alternating period jumps superimposed on the secular decrease. The fill-out of 84% for the primary star indicates a near contact configuration. With additional angular momentum and mass loss, the fill-out of the primary star will continue to increase as the orbital period decreases until it eventually fills its Roche lobe.

Future spectroscopic and precision photometric observations would be important in monitoring orbital period changes and would allow determination of absolute parameters.

## 6. Acknowledgements

This research was made possible through the use of the AAVSO Photometric All-Sky Survey (APASS), funded by the Robert Martin Ayers Sciences Fund. This research has made use of the VizieR catalogue access tool and data from the SIMBAD database (operated at CDS, Strasbourg, France), the European Space Agency (ESA) mission Gaia (http://www.cosmos.esa.int/gaia), and the Lichtenknecker-Database of the BAV. The author would especially like to acknowledge the observers of AAVSO, BAV, VSOLJ, and other organizations that provided observations spanning several decades. Without their tireless efforts, the period study in this paper would not have been possible. The author is grateful to Norman Markworth for his careful reading of the manuscript and his valuable comments and suggestions.

## References

Baldwin, M. 1974, *J. Amer. Assoc. Var. Star Obs.*, **3**, 60.
Baldwin, M. 1975, *J. Amer. Assoc. Var. Star Obs.*, **4**, 86.
Baldwin, M. 1976a, *J. Amer. Assoc. Var. Star Obs.*, **5**, 29.
Baldwin, M. 1976b, *J. Amer. Assoc. Var. Star Obs.*, **5**, 84.
Baldwin, M. 1977, *J. Amer. Assoc. Var. Star Obs.*, **6**, 24.
Baldwin, M. E., and Samolyk, G. 1993, *Observed Minima Timings of Eclipsing Binaries, Number 1*, (https://www.aavso.org/observed-minima-timings-eclipsing-binaries)
Baldwin, M. E., and Samolyk, G. 1997, *Observed Minima Timings of Eclipsing Binaries, Number 4*, (https://www.aavso.org/observed-minima-timings-eclipsing-binaries)
Baldwin, M. E., and Samolyk, G. 2002, *Observed Minima Timings of Eclipsing Binaries, Number 7*, (https://www.aavso.org/observed-minima-timings-eclipsing-binaries)
Beob. der Schweizerischen Astron. Ges. (BBSAG). 1972–2002, *BBSAG Bull.,* Nos. 2–127 (https://www.calsky.com/cs.cgi/Deep-Sky/8/3?&lang=en).
Berliner Arb. Veränderl. Sterne. 2015, Lichtenknecker-Database of the BAV (http://www.bav-astro.eu/index.php/veroeffentlichungen/lichtenknecker-database)
Bradstreet, D. H., and Steelman, D. P. 2002, *Bull. Amer. Astron. Soc.*, **34**, 1224.
Brancewicz, H. K., and Dworak, T. Z. 1980, *Acta Astron.*, **30**, 501.
Budding, E., Erdem, A., Çiçek, C., Bulut, I., Soydugan, F., Soydugan, E., Bakiş, V., and Demircan, O. 2004, *Astron. Astrophys.*, **417**, 263.
Chen, W.-C., Li, Z.-D., and Qian, S.-B. 2006, *Astrophys. J.*, **649**, 973.
Diethelm, R. 2003, *Inf. Bull. Var. Stars*, No. 5438, 1.
Diethelm, R. 2004, *Inf. Bull. Var. Stars*, No. 5543, 1.
Diethelm, R. 2009, *Inf. Bull. Var. Stars*, No. 5894, 1.
Diethelm, R. 2010, *Inf. Bull. Var. Stars*, No. 5945, 1.
Diethelm, R. 2011, *Inf. Bull. Var. Stars*, No. 5960, 1.
Diethelm, R. 2012, *Inf. Bull. Var. Stars*, No. 6011, 1.
Doğru, S. S., Erdem, A., Aliçavuş, F., Akin, T., and Kanvermez, C. 2011, *Inf. Bull. Var. Stars*, No. 5988, 1.
Doğru, S. S., Erdem, A., Donmez, A., Bulut, A., Akin, T., Dogru, D., Çiçek, C., and Soydugan, F. 2009, *Inf. Bull. Var. Stars*, No. 5893, 1.
Eggleton, P. P. 1983, *Astrophys. J.*, **268**, 368.
Erkan, N., Erdem, A., Akin, T., Aliçavuş, F., and Soydugan, F. 2010, *Inf. Bull. Var. Stars*, No. 5924, 1.

Flin, P. 1969, *Inf. Bull. Var. Stars*, No. 328, 1.

Gaia Collaboration, *et al.* 2016, *Astron. Astrophys.*, **595A**, 2 (Gaia Data Release 1).

Gazeas, K., and Stepień, K. 2008, *Mon. Not. Roy. Astron. Soc.*, **390**, 1577.

Hall, D. S. 1989, *Space Sci. Rev.*, **50**, 219.

Henden, A. A., *et al.* 2014, AAVSO Photometric All-Sky Survey, data release 9, (https://www.aavso.org/apass).

Hoňková, K. *et al.* 2013, *Open Eur. J. Var. Stars*, No. 160, 1.

Hoňková, K. *et al.* 2015, *Open Eur. J. Var. Stars*, No. 168, 1.

Huang, S. S. 1963, *Astrophys. J.*, **138**, 471

Hübscher, J. 2011, *Inf. Bull. Var. Stars*, No. 5984, 1.

Hübscher, J., Paschke, A., and Walter, F. 2005, *Inf. Bull. Var. Stars*, No. 5657, 1.

Hübscher, J., Paschke, A., and Walter, F. 2006, Inf. Bull. Var. Stars, No. 5731, 1.

Hübscher, J., Steinbach, H.-M., and Walter, F. 2009, *Inf. Bull. Var. Stars*, No. 5889, 1.

Ibanoğlu, C. *et al.* 2006, *Mon. Not. Roy. Astron. Soc.*, **373**, 435.

Kafka, S. 2015, variable star observations from the AAVSO International Database (https://www.aavso.org/aavso-international-database).

Kaitchuck, R. H., and Honeycutt, R. K. 1982, *Publ. Astron. Soc. Pacific*, **94**, 532.

Kaitchuck, R. H., Honeycutt, R. K., and Schlegel, E. M. 1985, *Publ. Astron. Soc. Pacific*, **97**, 1178.

Klimek, Z. 1972, *Inf. Bull. Var. Stars*, No. 637, 1.

Klimek, Z. 1973, *Inf. Bull. Var. Stars*, No. 779, 1.

Kreiner, J. M. 1971, *Acta Astron.*, **21**, 365.

Kurucz, R. L. 1993, in *Light Curve Modeling of Eclipsing Binary Stars*, ed. E. F. Milone, IAU Symp. 151, Springer, New York, 93.

Lavrov, M. I. 1971, *Soviet Astron.*, **15**, 2, 236.

Locher, K. 2005, *Open Eur. J. Var. Stars*, No. 3, 1.

Lucy, L. B. 1968, *Astrophys. J.*, **151**, 1123.

Malkov, O. Yu., Oblak, E., Snegireva, E. A., and Torra, J. 2006, *Astron. Astrophys.*, **446**, 785.

Mallama, A. D. 1980, *Astrophys. J., Suppl. Ser.*, **44**, 241.

Mirametrics. 2015, Image Processing, Visualization, Data Analysis, (http://www.mirametrics.com)

Mochnacki, S. W. 1981, *Astrophys. J.*, **245**, 650.

Nagai, K. 2004a, *Bull. Var. Star Obs. League Japan*, No. 43, 5.

Nagai, K. 2004b, *Bull. Var. Star Obs. League Japan*, No. 44, 7.

Nagai, K. 2012, *Bull. Var. Star Obs. League Japan*, No. 53, 6.

Nagai, K. 2013, *Bull. Var. Star Obs. League Japan*, No. 55, 6.

Nelson, R. 2000, *Inf. Bull. Var. Stars*, No. 4840, 1.

Nelson, R. 2003, *Inf. Bull. Var. Stars*, No. 5371, 1.

Pecaut, M. J., and Mamajek, E. E. 2013, *Astrophys. J., Suppl. Ser.*, **208**, 9 (http://www.pas.rochester.edu/~emamajek/EEM_dwarf_UBVIJHK_colors_Teff.txt).

Popper, D. M. 1996, *Astrophys. J., Suppl. Ser.*, **106**, 133.

Qian, S. 2000a, *Astron. J.*, 119, 901.

Qian, S. 2000b, *Astron. J.*, 119, 3064.

Qian, S. 2001a, *Astron. J.*, 121, 1614.

Qian, S. 2001b, *Astron. J.*, 122, 1561.

Qian, S. 2002, *Publ. Astron. Soc. Pacific*, **114**, 650.

Robinson, I. J. 1967, *Inf. Bull. Var. Stars*, No. 221, 3.

Ruciński, S. M. 1969, *Acta Astron.*, **19**, 245.

Saijo, K. 1997, *Bull. Var. Star Obs. League Japan*, No. 23, 1.

Samolyk, G. 2008, *J. Amer. Assoc. Var. Star Obs.*, **36**, 171.

Samolyk, G. 2009, *J. Amer. Assoc. Var. Star Obs.*, **37**, 44.

Samolyk, G. 2010, *J. Amer. Assoc. Var. Star Obs.*, **38**, 183.

Samolyk, G. 2011, *J. Amer. Assoc. Var. Star Obs.*, **39**, 177.

Samolyk, G. 2012, *J. Amer. Assoc. Var. Star Obs.*, **40**, 975.

Samolyk, G. 2013, *J. Amer. Assoc. Var. Star Obs.*, **41**, 122.

Samolyk, G. 2013, *J. Amer. Assoc. Var. Star Obs.*, **41**, 328.

Samolyk, G. 2015, *J. Amer. Assoc. Var. Star Obs.*, **43**, 77.

Samolyk, G. 2016, *J. Amer. Assoc. Var. Star Obs.*, **44**, 69.

Samus, N. N., Kazarovets, E. V., Durlevich, O. V., Kireeva, N. N., and Pastukhova, E. N. 2017, *Astron. Rep.*, **61**, 80 (*General Catalogue of Variable Stars*, version GCVS 5.1.; http://www.sai.msu.su/gcvs/gcvs/index.htm).

Szafraniec, R. 1960, *Acta Astron.*, **10**, 99.

Terrell, D., and Wilson, R. E. 2005, *Astrophys. Space Sci.*, **296**, 221.

Todoran, I. 1967, *Inf. Bull. Var. Stars*, No. 187, 1.

Tout, C. A., Pols, O. R., Eggleton, P. P., and Han, Z. 1996, *Mon. Not. Roy. Astron. Soc.*, **281**, 257.

van Hamme, W. 1993, *Astron. J.*, **106**, 2096.

van Hamme, W., and Wilson, R. E. 1998, *Bull. Amer. Astron. Soc.*, 30, 1402.

Van 'T Veer, F. 1993, in *New Frontiers in Binary Star Research*, ed. K.-C. Leung, I.-S. Nha, ASP Conf. Ser. 38, 229.

Whitney, B. S. 1959, *Astron. J.*, **64**, 258**.**

Wilson, R. E. 1978, *Astrophys. J.*, **224**, 885.

Wilson, R. E., and Devinney, E. J. 1971, *Astrophys. J.*, **166**, 605.

Wood, B. D., and Forbes, J. E. 1963, *Astron. J.*, **68**, 257.

Yakut, K., and Eggleton, P. P. 2005, *Astrophys. J.*, **629**, 1055.

Yang, Y.-G., Dai, H.-F., He, J.-J., Zhang, J., and Ding, W. 2013, *Publ. Astron. Soc. Japan*, **65**, 45.

Yang, Y.-G., and Wei, J.-Y. 2009, *Astron. J.*, **137**, 226.

Zejda, M., Mikulasek, Z., and Wolf, M. 2006, *Inf. Bull. Var. Star*s, No. 5741, 1.

Zhang, J., Qian, S.-B., and Jiang, L.-Q. 2014, *Res. Astron. Astrophys.*, **14**, 179.

# Observation of a Deep Visual "Eclipse" in the WC9-Type Wolf-Rayet Star, WR 76

**Rod Stubbings**
*Tetoora Road Observatory, 2643 Warragul-Korumburra Road, Tetoora Road, 3821, Victoria, Australia; stubbo@sympac.com.au*

**Peredur Williams**
*Institute for Astronomy, Royal Observatory, Blackford Hill, Edinburgh, EH9 3HJ, United Kingdom; pmw@roe.ac.uk*

*Received February 27, 2017; revised March 22, 2017; accepted March 23, 2017*

**Abstract** The WC9-Type Wolf-Rayet star WR 76 is one of the most prolific dust makers identified from its infrared emission. WR 76 experienced a deep fading eclipse in 2016. The ~3.1 magnitude depth of the eclipse exceeds fadings in similar eclipses observed in WR stars thus far. Conclusions from recent and earlier analyses of eclipses observed suggests that WR 76 may be a prolific eclipser.

## 1. Introduction

Abrupt visual transient fading events, sometimes referred to as "eclipses," a term that will be used throughout this paper, can be caused by the obscuration by dust in the line of sight. Such eclipses have been observed in R Coronae Borealis (R CrB) stars (Loreta 1934; O'Keefe 1939) and classical novae (Gehrz 1988) for many decades, and more recently in WC-type Wolf-Rayet stars (Veen *et al.* 1998). All three sub-classes also frequently exhibit infrared (IR) emission from dust heated by the stellar radiation (Feast and Glass 1973; Williams *et al.* 1987), These two manifestations of dust formation are complementary in the information they convey. The IR emission measures all the dust, not restricted to that in the line of sight, and can indicate the dust grain temperature and chemistry, which is usually carbon, but sometimes can be more complex. This is evident in the following subclasses: R CrB stars (García-Hernández *et al.* 2013), novae (Helton *et al.* 2014), and WR stars (Chiar and Tielens 2001). On the other hand, the eclipses can give an indication of the sizes of grains if they have been observed in more than one passband (Veen *et al.*1998; Fahed *et al.* 2009).

From the IR light curves that show periodic outbursts, such as the prototype WR 140 (Williams *et al.* 1990), and IR imaging that shows rotating "pinwheel" structures in the prototype WR 104 (Tuthill *et al.* 1999), dust formation is found to be related to wind interactions in WR+OB binary systems. The WR numbers for the Wolf-Rayet stars in this paper were assigned by van der Hucht *et al.* (1981) and van der Hucht (2001), who also give alternative designations. In contrast, the incidence of eclipses by WR stars appears to be sporadic. The suggestion that the eclipses of WR 104 had the same period as the rotating dust pinwheel (Kato *et al.* 2002a) was not supported in a long-term monitoring study (Williams 2014) of dust-making WC stars based on the V-band photometry in the ASAS-3 survey (Pojmański 2002). The ASAS-3 data were accumulated from 2001 to 2009, which, allowing for seasonal and other gaps, provided data equivalent to around four years of continuous coverage for each star. The highest frequency of eclipse events was shown by WR 104, amounting to 7/8 of the time, but the IR images of the dust pinwheel (Tuthill *et al.* 2008) indicate that eclipse-made dust was not an important contributor to its dust cloud. Several eclipses were also observed from WR 106 and other WC type stars in the ASAS-3 data.

WR 53 showed no optical eclipses in the 2001–2009 ASAS-3 data, and exhibited no variation or shallow eclipse activity. Independent visual and additional photometric monitoring of WR 53 commenced in 2011 to look for variations, and surprisingly a deep 1- magnitude eclipse in 2015 was discovered (Stubbings 2015). WR 53 was also one of the WC8-9 stars known from its IR emission to be a dust maker (Williams *et al.* 1987), re-radiating about 3.6% of its UV-optical flux in the IR. The corresponding fraction for WR 104 was 60%, which led to the suggestion of a possible correlation between dust luminosity of the IR and the frequency of eclipses (Williams 2014). Other stars known to be prolific dust makers from their IR emissions, WR 48a, WR76, and WR118, were too faint for the ASAS-3 survey to detect eclipses (Williams 2014). These stars were proposed for monitoring for visual eclipses to test the suggested correlation concerning dust luminosity of the IR and eclipses (Williams 2014). The brightest of these WR stars for visual monitoring is WR 76, (J2000: R.A. $16^h$ $40^m$ $05.25^s$, Dec. –45° 41' 12.7"), and was measured at $V_o = 15.46$ (Fahed *et al.* 2009). WR 76 is a WC9 star (Torres *et al.* 1986) which re-radiates ~68% of its optical-UV luminosity in the IR (Williams *et al.* 1987), and this was selected for concentrated monitoring to search for eclipses in the present study.

## 2. Observations

WR 76 has a visual observing window from February to November. A visual monitoring program commenced in April 2016 to search for eclipses. A visual chart with comparison stars of 15.2, 15.5, and 16.1 was used for reference. After months of monitoring WR76, which remained at around 15.2, a small dip was noticed on JD 2457606 (August 4) at a visual magnitude of 15.5. One of the authors (RS) contacted Peter Nelson to check WR 76 with a V-band image; he was able to obtain an image and time series observations 3 days later, giving V = 14.7 with no fading trend apparent. On the same night the author noticed WR 76 had returned back to around 15.3 visually. WR 76 remained at a visual magnitude of 15.3 until JD 2457653 (September 26), when again it declined to 15.5 and remarkably fainter to 16.0

the following night. A V-band image was obtained four days later on JD 2457658 at V = 15.29. The data indicated a ~ 0.6 magnitude drop in V and ~ 0.7 visually, therefore a definite eclipse event was in progress. The fading trend continued and on JD 2457667 (October 6) a visual magnitude of 16.8 was recorded. At this point communication was made with Nidia Morrell (2016) to see if spectroscopy could be obtained from the El Leoncito Astronomical Complex astronomical observatory in Argentina. Unfortunately the elevation of WR 76 was then below the limit of their telescope. An additional V-band image was taken by Nelson on JD 2457773 (October 12) indicating WR 76 was now in a deep eclipse at V = 17.7.

With the full Moon and cloud cover making it difficult to observe visually, the next available observations were obtained on JD 2457685 (October 24) at a visual magnitude of 17.3 and also a V-band image at V =17.4. The rising branch of the eclipse progressed to maximum light on JD 2457702 (November 10) at a visual magnitude of 15.0. The eclipse had commenced on JD 2457653 (September 22) and recovered on JD 2457702 (November 10) with a duration of ~ 49 days and a depth of ~ 3.1 magnitudes in V and perhaps quite fainter due to the gap in data. The possibility of a slight minor eclipse on JD 2457606 (August 4) could also be linked to the main eclipse event. The light curve is presented in Figure 1. The visual difference of 0.5 - 0.6 mag. at maximum from Johnson V could be due to spectral aspects of the variable's light and does not affect the result.

## 3. Discussion

The eclipse in WR76 observed in 2016 is deeper than those observed in WR 104 (Kato *et al.* 2002a; Williams 2014) and comparable to a 2.9-magnitude eclipse observed in WR 106 by Kato *et al.* (2002b) throughout an eight-year monitoring period. Low level variation of σ(v) = 0.06 during a one-month observing run had been observed in WR 76 by Fahed *et al.* (2009) and from comparison with variation in (v–i) was interpreted in terms of variable extinction by dust. Observations of WR 76 in the Bochum Galactic Disk Survey (Hackstein *et al.* 2015) showed a well-defined Δ r ~ 0.4-magnitude eclipse in mid-2013 followed by another fading into a deeper eclipse at Δ r ~ 1.7 magnitude and parts of other eclipses in shorter observing runs in 2012 and 2014, all of which are presented in Figure 2. Unfortunately, the cadence of the observations, which was not dedicated to this star but was surveying the whole field for variables, has not allowed for the deeper eclipse to be defined. The relative amplitudes Δr / Δi ~ 1.2 are also consistent with eclipsing by sub-micron particles (cf. Veen *et al.* 1998; Fahed *et al.* 2009), suggesting that the visual eclipse reported in this paper has a similar origin.

In this case, the fading by about 3 mag. over approximately 25 days from JD 2457650 would have been caused by the rapid formation of a cloud of dust particles in the line of sight, which covered the stellar disk. The dust that would have formed in the stellar wind of WR 76 is expected to have a terminal velocity near 1000 km/s (van der Hucht 2001), which would have dissipated the cloud and reduced its extinction. While WR 76 was fading, the formation rate of the dust must have been high enough to more than compensate for its dissipation. When dust formation ceased and the existing dust was dissipated, the extinction fell and the flux recovered to its pre-eclipse level over a period of about 20 days. Veen *et al.* (1998) developed models to fit the eclipse light curves of three other WR stars, WR 103, WR 121, and WR 113, and found that the dust was forming significantly closer to the stars than the amorphous carbon dust clouds modelled from IR photometry by Williams *et al.* (1987). Support for the scale of the IR dust cloud models comes from detailed modelling of the dust pinwheel around WR 104 by Harries *et al.* (2004). This suggests that the dust grains modelled by Veen *et al.* (1998) would not have been able to survive heating in the stellar radiation field. On the other hand, independent evidence for the presence of scattering particles extremely close to the WC star component of WR 113 was provided by the observations of David-Uraz *et al.* (2012). This suggests that the particles responsible for the eclipses observed from WR stars may be more refractory and have optical properties very different from those of the amorphous carbon grains believed to be responsible for the IR emission. Further study of these phenomena would be helpful in understanding the formation of dust in the most hostile environments.

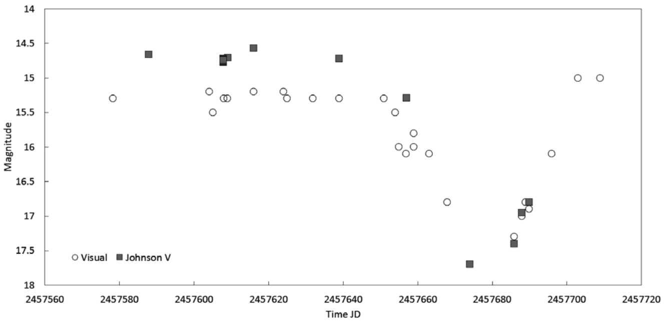

Figure 1. AAVSO light curve showing the deep ~3.1 magnitude eclipse beginning on JD 2457653–2457702 (September 22–November 10) and lasting for 49 days before returning to maximum light. Black circles are visual data, green squares are Johnson V.

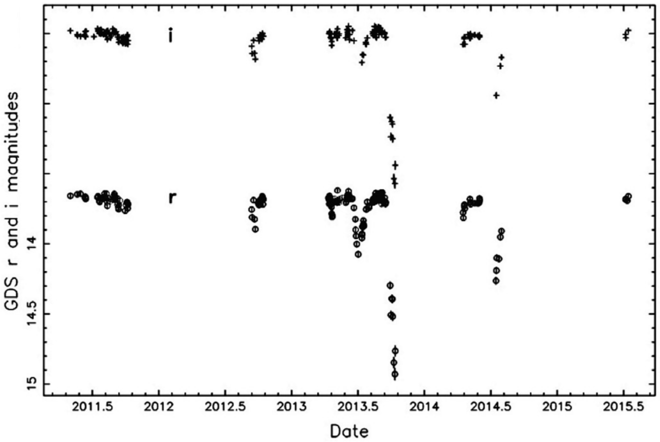

Figure 2. Observations of WR 76 in the Bochum Galactic Disk Survey showing recorded eclipses in r and i magnitudes.

## 4. Conclusion

The combined results from recent and earlier studies of the deep eclipse observed only during one season of monitoring suggests that WR 76 may be a prolific eclipser, but further observations are required in order to test this and characterize these events.

In the four seasons in which WR 76 was observed in the Bochum Galactic Disk Survey, eclipses or parts of eclipses were observed in three out of the four, which also implies that eclipses may be rather frequent. The eclipse observed in WR 76 is one of the deepest known thus far compared to deep eclipses observed in WR 104 and WR 106. Eclipses found in WR stars are generally rare, with only one detected eclipse from WR 53 in fourteen years observing, apart from the heavier dust makers, suggesting WR 76 could be an excellent subject for the further study of this phenomenon.

## 5. Acknowledgements

We acknowledge with thanks the variable star observations from the AAVSO International Database (Kafka 2016) contributed by observers worldwide and used in this research. This research has made use of the International Variable Star Index (VSX) database (Watson *et al.* 2015), operated at AAVSO, Cambridge, Massachusetts, USA, and the Bochum Galactic Disk Survey. We would like to thank Peter Nelson for providing V-band images. We would also like to thank the anonymous referee whose comments and suggestions were helpful.

## References

Chiar, J. E., and Tielens, A. G. G. M. 2001, *Astrophys. J.*, **550**, L207.

David-Uraz, A., *et al.* 2012, *Mon. Not. Roy. Astron. Soc.*, **426**, 1720.

Fahed, R., Moffat, A. F. J., and Bonanos, A. Z. 2009, *Mon. Not. Roy. Astron. Soc.*, **392**, 376

Feast, M. W., and Glass, I. S. 1973, *Mon. Not. Roy. Astron. Soc.*, **161**, 293.

García-Hernández, D. A., Rao, N. K., and Lambert, D. L. 2013, *Astrophys. J.*, **773**, 107.

Gehrz, R., D. 1988, *Ann. Rev. Astron. Astrophys.*, **26**, 377.

Hackstein, M., *et al.* 2015, *Astron. Nachr.*, **336**, 590 (data retrieved from table J/AN/336/590 at http://vizier.u-strasbg.fr).

Harries, T. J., Monnier, J. D., Symington, N. H., and Kurosawa, R. 2004, *Mon. Not. Roy. Astron. Soc.*, **350**, 565.

Helton, L. A., Evans, A., Woodward, C. E., Gehrz, R. D., and Vacca, W. 2014, in *Stella Novae: Past and Future Decades*, ed. P. A. Woudt, V. A. R. M. Ribeiro, ASP Conf. Ser. 490, Astronomical Society of the Pacific, San Francisco, 261.

Kafka, S. 2016, variable star observations from the AAVSO International Database (https://www.aavso.org/aavso-international-database).

Kato, T., Haseda, K., Yamaoka, H., and Takamizawa, K. 2002a, *Pub. Astron. Soc. Japan*, **54**, L51.

Kato, T., Haseda, K., Takamizawa, K., and Yamaoka, H. 2002b, *Astron. Astrophys.*, **393**, L69.

Loreta, E. 1934, *Astron. Nachr.*, **254**, 151.

Morrell, N. 2016, private communication.

O'Keefe, J. A. 1939, *Astrophys. J.*, **90**, 294.

Pojmański, G. 2002, *Acta Astron.*, **52**, 397.

Stubbings, R. 2015, *J. Amer. Assoc. Var. Star Obs.*, **43**, 163.

Torres, A. V., Conti, P. S., and Massey, P. 1986, *Astrophys. J.*, **300**, 379.

Tuthill, P. G., Monnier, J. D., and Danchi, W. C. 1999, *Nature*, **398**, 487.

Tuthill, P. G., Monnier, J. D., Lawrance, N., Danchi, W. C., Owocki, S. P., and Gayley, K. G. 2008, *Astrophys. J.*, **675**, 698.

van der Hucht, K. A. 2001, *New Astron. Rev.*, **45**, 135.

van der Hucht, K. A., Conti, P. S., Lundstrom, I., and Stenholm, B. 1981, *Space Sci. Rev.*, **28**, 227.

Veen, P. M., van Genderen, A. M., van der Hucht, K. A., Li, A., Sterken, C., and Dominik, C. 1998, *Astron. Astrophys.*, **329**, 199.

Watson, C., Henden, A. A., and Price, C. A. 2015, AAVSO International Variable Star Index VSX (Watson+, 2006–2015; http://www.aavso.org/vsx).

Williams, P. M., van der Hucht, K. A., and Thé, P. S. 1987, *Astron. Astrophys.*, **182**, 91.

Williams, P. M., van der Hucht, K. A., Pollock, A. M. T., Florkowski, D. R., van der Woerd, H., and Wamstecker, W. M. 1990, *Mon. Not. Roy. Astron. Soc.*, **243**, 662.

Williams, P. M. 2014, *Mon. Not. Roy. Astron. Soc.*, **445**, 1253.

# HD 46487 is Now a Classical Be Star

**David G. Whelan**
**R. David Baker**
*Department of Physics, Austin College, 900 N. Grand Avenue, Sherman, TX 75090; dwhelan@austincollege.edu*

*Received March 13, 2017; revised May 15, 2017; accepted May 23, 2017*

**Abstract** We present the first observations of hydrogen line emission detected around the B-type star HD 46487, a well-studied star in the CoRoT field of view. The emission is only evident in the Hα line, for which the observed violet-red peak separation ($\Delta \upsilon_p$) is typical of a Be star with a circumstellar disk. The absence of dust emission from the infrared spectral energy distribution excludes the possibility of a very young star. The star's magnitude (V = 5.079) and regular use in the literature for a variety of studies suggests that the line emission had a high probability of being found previously, had it been evident; since such was not the case, we believe that the Be phenomenon for HD 46487 has only very recently "turned on." We therefore recommend that this star be spectroscopically and photometrically monitored to track continued changes to its circumstellar morphology.

## 1. Introduction

Main sequence and giant B-type stars are often fast rotators. Classical Be stars are universally so, and most are believed to rotate at speeds near critical (Townsend *et al.* 2004). Unlike "normal" B-type stars, however, Be stars experience nonradial pulsational modes that eject matter from the surface, allowing them to form a circumstellar decretion disk at the star's equator (Rivinius *et al.* 2013). It is therefore interesting that stars have become Be stars after decades of appearing normal, or else have ceased to exhibit the Be phenomenon (Chojnowski *et al.* 2015, 2017). In fact, observations of the transition between normal B-type and Be star are becoming quite common; many examples exist in the more than decade-long archive of the Be Star Spectra (BeSS) Database. (BeSS may be accessed online at http://basebe.obspm.fr/basebe/Accueil.php?flag_lang=en) (Neiner *et al.* 2011). With the help of BeSS, data are being collected that illustrate the timescales on which disks build up and decrete, track violet-to-red emission peak separation (VR) variability due to one-armed global oscillations (Okazaki 1991), and variability due to outbursts.

But in spite of this growing collection of data, little is known about why they begin to exhibit emission when they do (Porter and Rivinius 2003). McSwain *et al.* (2009) showed that Be stars rotate faster on average than normal B-type stars, and their near-critical speeds make it easier for Be stars to lose mass to their surroundings. The difference in rotation rate for roughly 75% of Be stars is likely due to the transfer of angular momentum during binary interactions (McSwain and Gies 2005; deMink *et al.* 2013), and evidence suggests that such interactions are most common within the first 100 Myr of the star's life.

HD 46487, unlike many recently discovered Be stars, has been well-studied of late; partly this is because it is a bright source (V = 5.079) but also because it resides in the CoRoT field of view, which was targeted for exoplanet discoveries and asterseismology studies (Auvergne *et al.* 2009). At the time that the CoRoT field of view was being searched for Be stars, HD 46487 was not one, and so was not included in Neiner *et al.* (2005) or Frémat *et al.* (2006). However, other publications from this time allow us to search for any evidence of extant or forming circumstellar matter in the past couple of decades. Its far-ultraviolet (FUV) spectrum exhibited no resonance lines in 2003, as we might have expected for a Be star (Jo *et al.* 2016; Rountree and Sonneborn 1991). It also showed no evidence of any photospheric pulsation (Lefever *et al.* 2010); photometric variability, due to either periodic variability or outbursts, is a common feature of Be stars (Labadie-Bartz *et al.* 2017; Rivinius 2013). Other more recent uses for HD 46487 in the literature, such as being used as a calibrator in interferometric observations (e.g. Ellerbroek *et al.* 2015), further suggest that the star was still normal until as late as 2013.

Several studies have provided us with fundamental physical parameters. HD 46487 was classified as a B5 Vn star in Abt *et al.* (1990), where the "n" designation suggests broad absorption lines. Its projected rotational speed, $v \sin i$ where i is the inclination angle, is likely between 285–300 km/s (Abt *et al.* 2002; Huang *et al.* 2010). This high speed has lead to a bulging out of the equator, such that the equator has a substantially lower surface gravity than its poles ($\log(g)$ of 3.63 at the equator, compared to 3.95 at the poles (Huang *et al.* 2010)). There is no observed binary companion (Abt *et al.* 1990; Eggleton and Tokovinin 2008; Gullikson *et al.* 2016b). Recent spectra of HD 46487 are reported in Gullikson *et al.* (2016a, 2016b). Presented in these works there is a high-resolution (R ~ 60,000) spectrum in the wavelength range 3400–10000 Å taken with the cross-dispersed echelle spectrograph (TS23) at the Harlan J. Smith 2.7-meter telescope (http://www.as.utexas.edu/mcdonald/facilities/2.7m/cs2.html) on 2014-01-11, as well as two near-infrared (1.45–2.5μm) spectra taken with IGRINS (Park *et al.* 2014) on the same telescope taken on 2014-10-16 and 2015-03-03. These three spectra together cover wavelengths for Balmer, Paschen, and Brackett series hydrogen lines, and would all have clearly exhibited that HD 46487 was an emission-line source, had it been evident.

We present the first known observations, taken in March 2017, of the onset of the Be phenomenon in the well-studied star HD 46487. We will describe our observations and data reduction in section 2, present and analyze our spectra in section 3, briefly discuss the results in section 4, and then conclude in section 5.

## 2. Observations and data reduction

The Adams Observatory sits atop the IDEA Center science building at Austin College in Sherman, Texas. This facility provides opportunities for research, introductory and advanced astronomy classes, and public star-gazing events. Built by DFM Engineering in 2013, the 0.61-m f/8 Ritchey-Chrétien telescope is used primarily for spectroscopy, photometry, and imaging. Instruments are located at Cassegrain focus.

The spectrograph used for these observations is a long-slit LhiresIII spectrograph designed for commercial sale by Shelyak Instruments. It is a modular spectrograph for which the dispersion grating can easily be switched. Collimation and focusing are performed by the same optic, a simple doublet with f/6.67 and a diameter of 30 mm.

The CCD camera being used is a Finger Lakes Instrumentation (FLI) Microline with a thermoelectric cooler that can reach 60° C below ambient. It contains a back-illuminated e2V 42-10 CCD that is coated for enhanced broadband transmittance (~75–95% quantum efficiency from λ = 3800–7000Å) and the array of 512 × 2048 pixels are each 13.5µm square. Considering the demagnification of the spectrograph camera, the effective pixel size at the slit mask is 16µm. We therefore choose a 35µm slit as the best resolution match (a 32µm slit is not available for sale through Shelyak). The camera and spectrograph can be used to observe stars as faint as V ~ 10.

Dispersion with the 2400 gr/mm dispersion grating is 0.168Å per pixel around 6500Å, and 0.235Å per pixel around 4300Å. The resultant resolutions vary with wavelength. Typically we see resolutions in the range $7{,}500 \lesssim R \lesssim 9{,}500$ around Hγ (4341Å) and $14{,}000 \lesssim R \lesssim 20{,}000$ around Hα (6563Å). With the 1200 gr/mm grating, dispersion is 0.54Å per pixel in between ~3800Å and 5000Å, with the resolution varying between $3{,}000 \lesssim R \lesssim 4{,}500$.

A log of observational data, including exposure times and signal-to-noise ratios (SNR), is provided in Table 1. HD 46487 was first observed as a telluric standard for another project, so only a single spectrum was acquired on the first night. Flatfield, dark current, bias, and neon-argon lamp images are observed every night. The gain and read noise are computed using the bias and flatfield images; gain is 1.5 $e^-$/ADU and read noise is 13.1 $e^-$/pixel. Dark current and bias are removed from the science images, and they are then divided by the normalized flatfield. All data reduction and spectral extraction is performed in PYTHON using the author's own routines.

The reduced science images are collapsed in the wavelength direction, and the star's dispersion is fit with a Gaussian to determine an extraction center and width. The spectrum is then extracted between 2σ of the Gaussian's center, rounded out to the nearest pixel. The pixels on either side of the spectrum's extraction window are used to compute a local sky value that is then subtracted away from the star's spectrum, removing any background. Wavelength values are determined using known lines from the neon-argon lamp spectrum. The SNR is computed at every pixel using the CCD equation from Merline and Howell (1995), and are then propagated to compute errors at every wavelength value in the spectrum.

Table 1. HD 46487 observations data.

| *MJD* | *Dispersion (Å/pixel)* | *Wavelength Range (Å)* | *Exposure Time (seconds)* | *Airmass* | *Average SNR* |
|---|---|---|---|---|---|
| 57826.098 | 0.168 | 6380–6722 | 1800 | 1.3 | 196 |
| 57827.054 | 0.168 | 6380–6722 | 1800 | 1.2 | 151 |
| 57827.103 | 0.235 | 4182–4673 | 1800 | 1.3 | 339 |
| 57827.141 | 0.543 | 3820–4942 | 900 | 1.4 | 304 |

## 3. Analysis

### 3.1. Disk emission

The Hα spectrum of HD 46487 is shown in Figure 1, as it was observed on the nights of 13 and 14 March 2017. There are noticeable differences between the two spectra. The telluric absorption features are substantially stronger in the second observation. The hydrogen emission is markedly more pronounced as well. Variations in emission strength on the order of days is not uncommon for Be stars, particularly during a phase of disk build-up (e.g. Rivinius *et al.* (2013) and references therein).

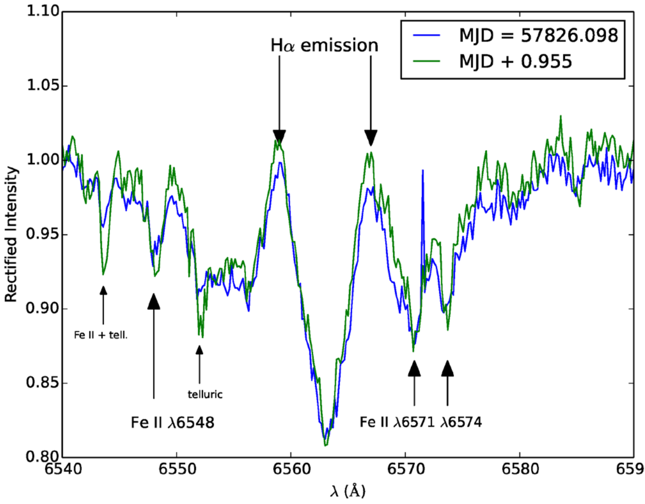

Figure 1. Two spectra observed on consecutive nights show Hα emission inside the photospheric absorption line. Various Fe II lines are evident, as well as some telluric absorption lines. Modified Julian dates are shown.

The peak separation in the Hα emission is ~7.9Å, which translates to an orbital speed of ~180 km/s. If we take v sin i = 290 km/s as a rough average of the available literature values (see section 1), then according to Huang's Law (Huang 1972):

$$r_d = \left( \frac{2 \times v \sin i}{\Delta v_p} \right)^2 \qquad (1)$$

where $\Delta v_p$ is the emission peak separation, then the Hα line-emitting radius is 19 $R_*$.

### 3.2. Spectral typing

The optical spectrum of HD 46487 in the wavelength range 3820–4950Å is shown in Figure 2 at two resolutions. The strengths of the He I λ4009/4026 lines, the presence of Si II λ4128–4130, its strength relative to He I λ4121, 4144, and the He I λ4471/Mg II λ4481 ratio all confirm a spectral type of B5.

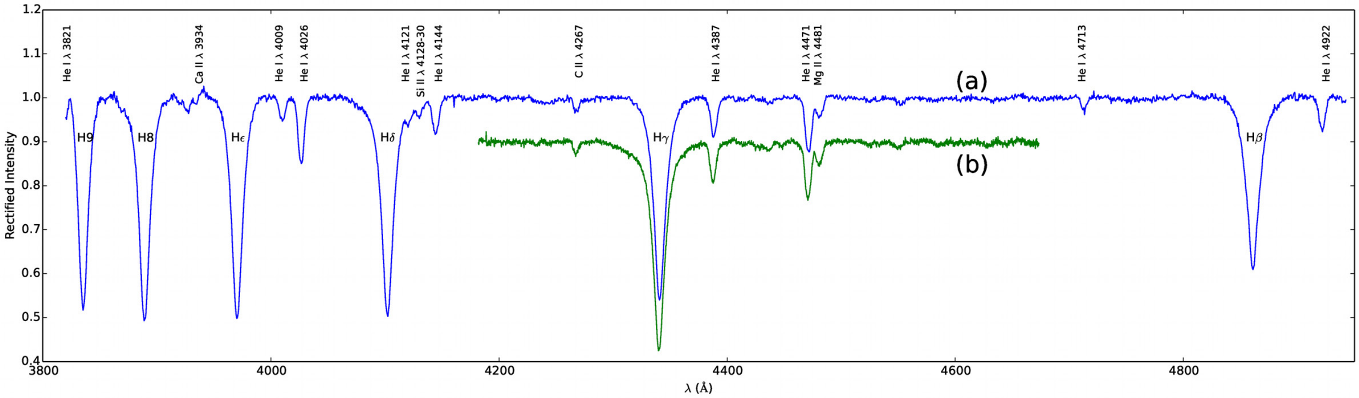

Figure 2. The violet-blue-green spectrum of HD 46487 taken on the night of 14 March 2017, with hydrogen, He I, and various metal absorption lines labeled. Spectrum (a) was obtained using the 1200 gr/mm dispersion grating, (R ~ 4,000) while spectrum (b) was obtained using the 2400 gr/mm grating (R ~ 9,000).

Table 2. Equivalent width measurements.

| *Line Identification* | *Low-res*[a] | *Equivalent Widths (mÅ)* *Med-res*[b] | *B2V*[c] | *B5V*[c] |
|---|---|---|---|---|
| He I λ4009 | 324 ± 19 | — | 613 | 217 |
| He I λ4026 | 977 ± 20 | — | 1541 | 878 |
| He I λ4144 | 524 ± 20 | — | 765 | 322 |
| C II λ4267 | 144 ± 13 | 145 ± 17 | 270 | 97 |
| He I λ4387 | 612 ± 16 | 563 ± 23 | 950 | 378 |
| He I λ4471 | 683 ± 33 | 742 ± 34 | 1442 | 667 |
| Mg II λ4481 | 193 ± 33 | 225 ± 30 | 198 | 272 |

*Notes: a. Data taken with the 1200 gr/mm dispersion grating. b. Data taken with the 2400 gr/mm dispersion grating. c. Model values from Frémat* et al. *(2006).*

The lines are very broad, suggesting that this is a main sequence star, and that the "nebular" designation is justified. We conclude that the spectral type based on visual inspection is B5 Vn, and that emission is not evident in the optical spectrum.

We measured the equivalent widths for the helium and metal absorption lines observed in the optical spectra. Results are given in Table 2, along with plane-parallel model predictions from Frémat *et al.* (2006) for comparison. Most notably, all of the line equivalent widths would suggest an earlier spectral type than what is visually observed.

### 3.3. The spectral energy distribution

The spectral energy distribution (SED) from ultraviolet to infrared is plotted against a B5 V stellar template in Figure 3. The stellar template is taken from Castelli and Kurucz (2003). Data points were collected using VizieR and sources include Thompson *et al.* (1978) for the ultraviolet, Crawford *et al.* (1971), and Høg *et al.* (2000) for the optical, and the 2MASS survey (Skrutskie *et al.* 2006), the WISE Survey (Wright *et al.* 2010), the AKARI All-Sky Survey (Ishihara *et al.* 2010), and the IRAS survey (Neugebauer *et al.* 1984) for the infrared. The IRAS data points suffer from a very large point spread function (~5 arcmin) and it is no surprise that they contain emission from nearby interstellar gas; this is the source of the discrepancy between the IRAS and WISE data points. There is no evidence of dust emission around HD 46487, and out to 22 µm, there is no substantial deviation from the stellar Rayleigh-Jeans tail.

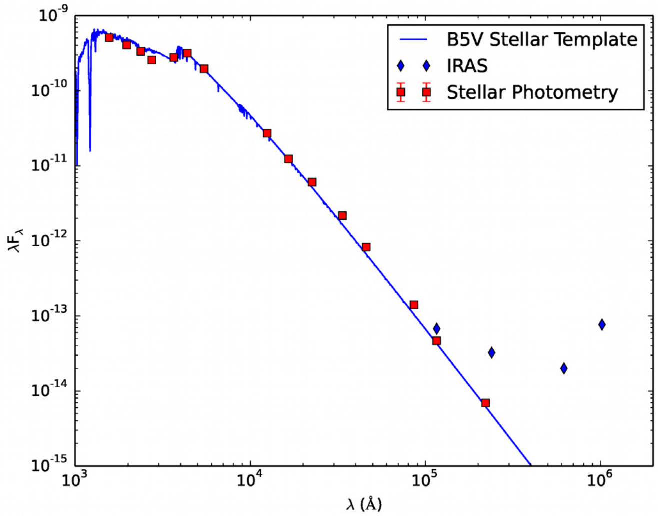

Figure 3. The infrared SED for HD 46487 is plotted against a B5V stellar template for comparison. IRAS data points (diamonds) have a point spread function that includes nearby diffuse dust emission. Error bars are smaller than the symbol size.

## 4. Discussion

The Hα line-emitting radius is calculated to be 19 $R_*$, as discussed in section 3.1. This is consistent with the average Hα line-emitting radii for Be stars in Hanuschik (1988) and in Slettebak *et al.* (1992), which quote ~ 20 $R_*$ and ~19 $R_*$, respectively.

The spectral type determined upon visual inspection should be treated with skepticism. Fast-rotating stars bulge at the equator, which both increases their surface area and creates a gradient in surface temperature from equator to pole. As a result, fast-rotating stars have higher luminosities and lower average surface temperatures (i.e., later spectral types) than their slow-rotating counterparts (Gray and Corbally 2009). There is also the effect of rotation on the perceived depths of the absorption lines themselves. Fast rotation will broaden the helium and metal absorption lines, so that they appear shallower than they would for another star of the same spectral type. These broadening effects are, in some cases, asymmetric, as is the case with the Mg II λ4481 line, which is intrinsically narrower than the He I λ4471 line. The Mg II λ4481/He I λ4471 line ratio is one of several used in spectral typing for which intrinsic line width differences can be an issue. Since issues related to rapid rotation affect our perception of a star's intrinsic spectral type, some work has been done to spectral type fast-rotating stars (e.g. Garrison and Gray 1994). At this time, however, there exist no fast-rotating spectroscopic standards earlier than B7 in the literature that can be used for visual comparisons.

The spectral type inferred from equivalent width measurements can also be problematic for Be stars. Continuum emission originating within the disk can partially fill in the absorption lines in a process known as line damping. This means that a Be star's actual spectral type will be earlier than that measured. This is in addition to the effects of scattered light from within the spectrograph itself, which will also fill in absorption signatures. Since the equivalent width measurements in Table 2 already suggest that the spectral type is earlier than what is inferred from visual inspection, we may consider line damping and scattered light as exaggerating effects, and can confidently conclude that HD 46487 has an earlier spectral type (B4 or B3) than is determined from visual inspection.

Pre-main sequence stars such as Herbig Be stars exhibit hydrogen line emission due to a circumstellar disk just like classical Be stars (Herbig 1960). They should additionally possess a broad infrared excess due to circumstellar free-free emission (which is expected for classical Be stars as well; Gehrz *et al.* 1974) and thermally-radiating dust (Malfait *et al.* 1998). Indeed, McDonald *et al.* (2012) found 1 magnitude of infrared excess for HD 46487 out to 22 µm. As illustrated in Figure 3, we cannot confirm such a large infrared excess, and what little infrared excess is seen is certainly not due to dust emission. HD 46487 is therefore not a pre-main sequence source, and what infrared excess exists is most likely due to circumstellar gaseous material and/or winds that would be responsible for free-free emission.

Due to the recent IGRINS and TS23 spectra of HD 46487 published in Gullikson *et al.* (2016b), we can state that HD 46487 was observed to be a normal main sequence B-type star as late as March 2015. All of the data used to compile the SED in Figure 3 was published earlier than 2013. It was additionally used in 2013 as a calibrator for interferometric observations in Brγ (Ellerbroek *et al.* 2015), an unsatisfactory choice had it exhibited a substantial gaseous circumstellar disk. It therefore seems likely that the Be phenomenon became evident no earlier than March 2015.

## 5. Conclusion

HD 46487 (V = 5.079) makes an excellent target for small aperture telescopes. Now that it exhibits the Be phenomenon, we should expect it to vary like other Be stars: with periodic photometric variability, the occasional small outburst, and variations in its line emission on timescales anywhere from hours to years. There are three specific areas that will be most useful for continued studies of this source.

*Spectroscopic observations of Hα.* Such observations would be useful to track the changing line emission, whether it be due to small outbursts and resultant pockets of gas rotating within the disk, or else long-scale global one-armed oscillations. Spectra submitted to BeSS (as we plan to do) would then be available to the entire community of Be star observers.

*Photometric observations at optical wavelengths.* Such observations may be useful for tracking periodicity, which is common in Be star atmospheres, and may also be useful for catching outbursts.

*Near-infrared photometric observations.* Most Be stars show an infrared excess due to free-free emission. Now that HD 46487 exhibits the Be phenomenon, we expect to see this change mostly to its near-infrared SED.

We recognize the need for collaboration on these observations. Interested parties are encouraged to contact the authors.

## 6. Acknowledgements

This work would not have been possible without the Adams Observatory at Austin College, made possible by the generosity of the John and Patricia Adams Foundation of Bedford, Texas. DGW would like to thank Michael Joner for his critical read of the manuscript before submission, and for the helpful feedback of the anonymous referee.

## References

Abt, H. A., Gomez, A. E., and Levy, S. G. 1990, *Astrophys. J. Suppl. Ser.*, **74**, 551.

Abt, H. A., Levato, H., and Grosso, M. 2002, *Astrophys. J.*, **573**, 359.

Auvergne, M., *et al.* 2009, *Astron. Astrophys.*, **506**, 411.

Castelli, F., and Kurucz, R. L. 2003, in *Modelling of Stellar Atmospheres, Poster Contributions.*, IAU Symp. 210, A20.

Chojnowski, S. D., *et al.* 2015, *Astron. J.*, **149**, 7.

Chojnowski, S. D., *et al.* 2017, *Astron. J.*, **153**, 174.

Crawford, D. L., Barnes, J. V., and Golson, J. C. 1971, *Astron. J.*, **76**, 1058.

de Mink, S. E., Langer, N., Izzard, R. G., Sana, H., and de Koter, A. 2013, *Astrophys. J.*, **764**, 166.

Eggleton, P. P., and Tokovinin, A. A. 2008, *Mon. Not. Roy. Astron. Soc.*, **389**, 869.

Ellerbroek, L. E., *et al.* 2015, *Astron. Astrophys.*, **573**, 77.

Frémat, Y., Neiner, C., Hubert, A.-M., Floquet, M., Zorec, J., Janot-Pacheco, E., and Renan de Medeiros, J. 2006, *Astron. Astrophys.*, **451**, 1053.

Garrison, R. F., and Gray, R. O. 1994, *Astron. J.*, **107**, 1556.

Gehrz, R. D., Hackwell, J. A., and Jones, T. W. 1974, *Astrophys. J.*, **191**, 675.

Gray, R. O., and Corbally, C. J. 2009, *Stellar Spectral Classification*, Princeton University Press, Princeton.

Gullikson, K., Kraus, A., and Dodson-Robinson, S. 2016a, *Astron. J.*, **152**, 40.

Gullikson, K., *et al.* 2016b, *Astron. J.*, **151**, 3.

Hanuschik, R. W. 1988, *Astron. Astrophys.*, **190**, 187.

Herbig, G. H. 1960, *Astrophys. J., Suppl. Ser.*, **4**, 337.

Høg, E., *et al.* 2000, *Astron. Astrophys.*, **355**, 27.

Huang, S.-S. 1972, *Astrophys. J.*, **171**, 549.

Huang, W., Gies, D. R., and McSwain, M. V. 2010, *Astrophys. J.*, **722**, 605.

Ishihara, D., *et al.* 2010, *Astron. Astrophys.*, **514**, 1.

Jo, Y.-S., Seon, K.-I., Min, K.-W., Choi, Y.-J., Lim, T.-H., Lim, Y.-M., Edelstein, J., and Han, W. 2016, *Mon. Not. Roy. Astron. Soc.*, **456**, 417.

Labadie-Bartz, J., *et al.* 2017, *Astron. J.*, **153**, 252.

Lefever, K., Puls, J., Morel, T., Aerta, C., Devin, L., and Briquet, M. 2010, *Astron. Astrophys.*, **515**, 74.

Malfait, K., Bogaert, E., and Waelkens, C. 1998, *Astron. Astrophys.*, **331**, 211.

McDonald, I., Zijlstra, A. A., and Boyer, M. L. 2012, *Mon. Not. Roy. Astron. Soc.*, **427**, 343.

McSwain, M. V., and Gies, D. R. 2005, *Astrophys. J., Suppl. Ser.*, **161**, 118.

McSwain, M. V., Huang, W., and Gies, D. R. 2009, *Astrophys. J.*, 700, 1216.

Merline, W. J., and Howell, S. B. 1995, *Exp. Astron.*, **6**, 163.

Neiner, C., de Batz, B., Cochard, F., Floquet, M., Mekkas, A., and Desnoux, V. 2011, *Astron. J.*, **142**, 149.

Neiner, C., Hubert, A.-M., and Catala, C. 2005, *Astrophys. J., Suppl. Ser.*, **156**, 237.

Neugebauer, G., *et al.* 1984, *Astrophys. J.*, **278**, 1.

Okazaki, A. T. 1991, *Publ. Astron. Soc. Japan*, **43**, 75.

Park, C., *et al.* 2014, *Proc. SPIE*, **9147**, 1.

Porter, J. M., and Rivinius, T. 2003, *Publ. Astron. Soc. Pacific*, **115**, 1153.

Rivinius, T. 2013, in *Stellar Pulsations*, Astrophys. Space Sci. Proc., 31, 253.

Rivinius, T., Carciofi, A. C., and Martayan, C. 2013, *Ann. Rev. Astron. Astrophys.*, **21**, 69.

Rountree, J., and Sonneborn, G. 1991, *Astrophys. J.*, **369**, 515.

Skrutskie, M. F., *et al.* 2006, *Astron. J.*, **131**, 1163.

Slettebak, A., Collins, G. W., and Truax, R. 1992, *Astrophys. J., Suppl. Ser.*, **81**, 335.

Thompson, G. I., Nandy, K., Jamar, C., Monfils, A., Houziaux, L., Carnochan, D. J., and Wilson, R. 1978, *Catalogue of Stellar Ultraviolet Fluxes*, Liege University, Liege, Belgium.

Townsend, R. H. D., Owocki, S. P., and Howarth, I. D. 2004, *Mon. Not. Roy. Astron. Soc.*, **350**, 189.

Wright, E. L., *et al.* 2010, *Astron. J.*, **140**, 1868.

# BVRI Photometry of SN 2016coj in NGC 4125

**Michael Richmond**
*School of Physics and Astronomy, Rochester Institute of Technology, Rochester, NY 14623, mwrsps@rit.edu*

**Brad Vietje**
*Northeast Kingdom Astronomy Foundation, PO Box 173, Peacham, VT 05862, brad@nkaf.org*

*Received April 12, 2017; revised June 6, 2017; accepted June 6, 2017*

**Abstract** We present BVRI photometry of supernova (SN) 2016coj in NGC 4125 from 9 days before to 57 days after its *B*-band maximum light. Our light curves and color curves suggest that this event belongs to the "normal" class of type Ia SNe, with a decline rate parameter $\Delta m_{15}(B) = 1.32 \pm 0.10$, and that it suffers little extinction. Adopting a distance modulus to its host galaxy of $(m - \mathrm{M}) = 31.89$ mag, we compute extinction-corrected peak absolute magnitudes of $M_B = –19.01$, $M_V = –19.05$, $M_R = –19.03$, and $M_I = –18.79$. The explosion occurred close enough to the nucleus of NGC 4125 to hinder the measurement of its brightness. We describe our methods to reduce the effect of such host-galaxy contamination, but it is clear that our latest values suffer from systematic bias.

## 1. Introduction

Supernova (SNe) of type Ia are thought to originate in close binary systems, consisting of either a single white dwarf and a main-sequence companion, or two white dwarfs. When one white dwarf accretes enough material to exceed the Chandrasekhar limit (Chandrasekhar 1931), either by long-term transfer from a main sequence companion, or by a violent merger with another white dwarf, a runaway thermonuclear reaction propagates through it, disrupting the entire white dwarf, heating the ejecta to hundreds of thousands of degrees and blowing it out into space at thousands of kilometers per second. The expanding cloud of hot gas radiates energy for several months, reaching absolute magnitudes in the optical of order –18 to –20. Many (but not all) type Ia SNe exhibit similar properties, with a correlation between the shape of the light curve and the absolute magnitude at peak (Phillips 1993). When events are observed in sufficient detail, one can use the shape of the light curve to compute the absolute magnitude (Prieto *et al.* 2006; Guy *et al.* 2005), and so use these SNe as "standard-izable candles" to determine distances.

Supernova 2016coj in the galaxy NGC 4125, a peculiar elliptical of class E6 (de Vaucouleurs *et al.* 1991), was discovered by the Lick Observatory Supernova Search (Filippenko *et al.* 2001; Leaman *et al.* 2011) on UT 2016 May 28 (Zheng *et al.* 2016) and quickly identified as a type Ia explosion. Since its host galaxy is relatively close to our Milky Way, at a redshift of only z = 0.004523 according to the NASA Extragalactic Database (NED; see https://ned.ipac.caltech.edu), this event promised to provide a wealth of high-precision information. However, since the supernova occurred not far from the galaxy's nucleus, disentangling its light from that of the surrounding stars turns out to be a difficult task.

In this paper, we describe photometry of SN 2016coj in the BVRI passbands acquired at two locations, starting on UT 2016 May 30 and ending UT 2016 Aug 4, an interval of 66 days. Section 2 describes our observational methods, the cleaning of the raw CCD images, and the techniques we used to extract instrumental magnitudes. We explain our photometric calibration of the raw measurements onto the standard Johnson-Cousins system in section 3. The light curves and color curves of the event are shown in section 4; we comment briefly on their properties and the effect of extinction along the line of sight. We present our conclusions in section 5. In an appendix, we discuss the difficulties of measuring the light of a point source immersed in a non-uniform background, and use simple simulations to estimate the nature of systematic biases that appear in our data.

## 2. Observations

We present herein data acquired at the RIT Observatory, near Rochester, New York, and at the Northern Skies Observatory (NSO), in Peacham, Vermont. We will describe below the procedures by which we acquired and reduced the images from each observatory in turn.

The RIT Observatory is located on the southeastern corner of the Rochester Institute of Technology campus, at longitude 77:39:53 West, latitude +43:04:33 North, and an altitude of 168 meters. Our Meade LX200 f/10 30-cm telescope provides a plate scale of 1.38" per pixel at the focus of our SBIG ST-9 camera, which has BVRI filters built to the Bessell prescription. When observing SN 2016coj, we acquired a series of 5 to 20 short exposures (exposure times 30 seconds each up to 2016 July 19 = JD 2457588, 120 seconds each after that date), discarding those with trailing or extinction by clouds. We acquired dark and flatfield images each night, creating master frames from the median of 10 individual images. Flatfields were based on images of the twilight sky, with the exception of UT June 13, when bad conditions forced us to use dome flats. After subtracting the master dark from each target frame and dividing it by the normalized master flatfield, we examined each resulting "clean" image by eye, discarding those with poor quality.

Before extracting instrumental magnitudes, we combined all the images in a particular passband using a median technique, in order to increase the signal-to-noise ratio and eliminate cosmic rays. Figure 1 shows an example of such a combined image, with labels indicating stars used for calibration.

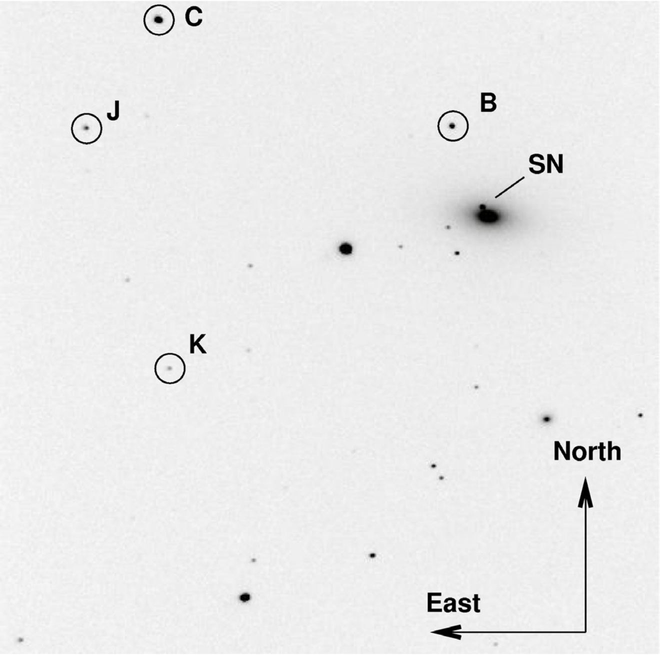

Figure 1. R-band composite (16 images of 30 seconds each) of SN 2016coj from RIT, showing stars used to calibrate measurements. North is up, East to the left. The field of view is roughly 12 by 12 arcminutes.

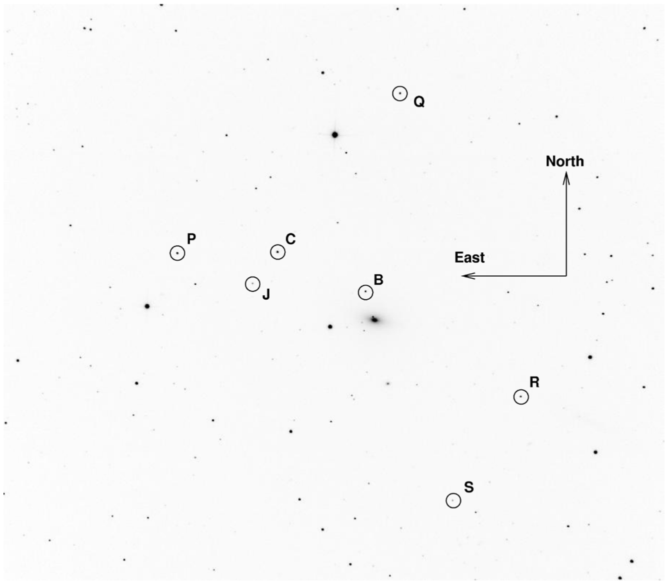

Figure 3. R-band composite (5 images of 45 seconds each) of SN 2016coj from NSO, showing stars used to calibrate measurements. North is up, East to the left. The field of view is roughly 30 by 30 arcminutes.

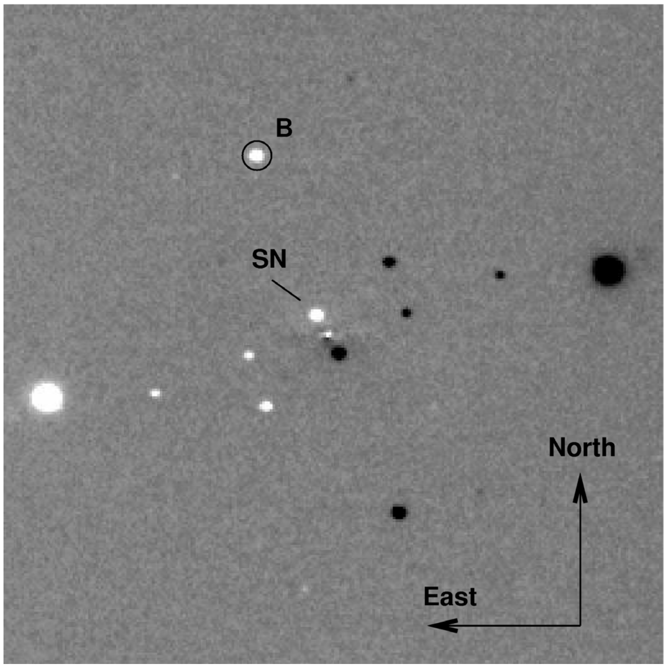

Figure 2. The residual after rotation and subtraction of an image from RIT taken UT 2016 June 24. Positive residuals are bright and negative dark. North is up, East to the left; the galaxy's nucleus appears at the center. The field of view is roughly 7 by 7 arcminutes.

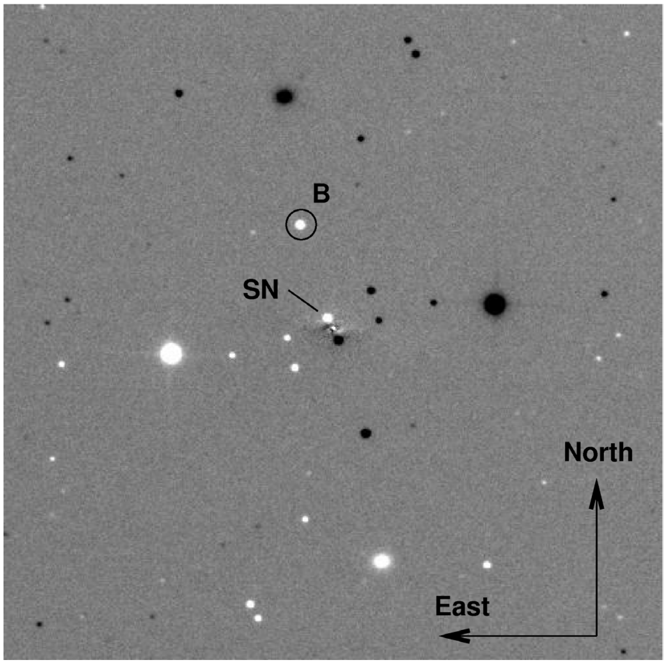

Figure 4. The residual after rotation and subtraction of an image from NSO taken UT 2016 June 26. Positive residuals are bright and negative dark. North is up, East to the left; the galaxy's nucleus appears at the center. The field of view is roughly 10 by 10 arcminutes.

Table 1. Photometry of comparison stars.

| *Star* | *R.A. (J2000)*<br>*h m s* | *Dec. (J2000)*<br>*° ′ ″* | *B* | *V* | *R* | *I* |
|---|---|---|---|---|---|---|
| B | 12 08 11.72 | +65 12 04.7 | 15.198 ± 0.086 | 14.133 ± 0.052 | 13.627 ± 0.116 | 13.155 ± 0.156 |
| C | 12 09 01.20 | +65 14 03.5 | 13.317 ± 0.093 | 12.673 ± 0.058 | 12.316 ± 0.121 | 11.980 ± 0.161 |
| J | 12 09 13.84 | +65 12 09.7 | 15.607 ± 0.109 | 14.956 ± 0.065 | 14.603 ± 0.136 | 14.271 ± 0.182 |
| K | 12 09 00.39 | +65 07 51.9 | 16.573 ± 0.123 | 15.975 ± 0.082 | 15.547 ± 0.174 | 15.147 ± 0.231 |
| P | 12 09 56.10 | +65 13 37.8 | 13.778 ± 0.095 | 13.113 ± 0.058 | 12.750 ± 0.116 | 12.409 ± 0.154 |
| Q | 12 08 11.72 | +65 12 04.7 | 15.198 ± 0.086 | 14.133 ± 0.052 | 13.627 ± 0.116 | 13.155 ± 0.156 |
| R | 12 06 43.72 | +65 06 30.3 | 15.392 ± 0.097 | 14.424 ± 0.058 | 13.911 ± 0.119 | 13.432 ± 0.158 |
| S | 12 07 17.93 | +65 00 19.8 | 15.929 ± 0.108 | 15.246 ± 0.065 | 14.869 ± 0.128 | 14.515 ± 0.169 |

The Point Spread Function (PSF) of these combined images had a typical Full Width at Half Maximum (FWHM) of 3.5" to 4.1".

Since the supernova lies only about 12 arcseconds from the nucleus of its host galaxy (Zheng *et al.* 2016), simple aperture photometry will yield poor results. A systematic error can appear in such measurements due to imperfect background subtraction; the size of the error will grow as the supernova fades. A standard technique in such cases is to match each target image to a template of the same galaxy taken some time before or after the event, in which the supernova does not appear, and then to subtract the template from the target image. However, since we lacked template images, we adopted a technique which does not require them; the drawback is that its results are less accurate, and can still suffer from systematic effects. See the Appendix for a detailed explanation.

The basic idea of the method is to use the symmetry of the elliptical galaxy host to provide a pseudo-template. We identified the center of the host galaxy, rotated the image by 180° around this point, then subtracted the rotated version from the original. An example of the results, starting with the same image shown in Figure 1, is displayed in Figure 2; we have zoomed in to show details near the nucleus more clearly. The subtraction is not perfect: small positive and negative residuals remain near the center of the galaxy. However, the residuals decrease rapidly with radius, and near the position of the supernova they are typically much smaller than the peak of the supernova's light. Moreover, the background around and underneath the supernova is much more uniform than in the original image, removing the main source of error in the aperture photometry.

After creating these residual images, we performed standard aperture photometry of the SN and reference stars, using the XVista (Treffers and Richmond 1989) routines STARS and PHOT. We chose to measure light within circular apertures of a fixed radius, a bit larger than the usual FWHM: 4 pixels = 5.5". A local sky background was estimated for each star using an annulus with radii of 6.9" and 13.8".

The Northern Skies Observatory is located in Peacham, Vermont, at longitude 72:09:57 West, latitude +44:19:30 North, and an elevation of 384 meters above sea level. Images of SN 2016coj were acquired through a 43-cm f/6.8 corrected Dall-Kirkham astrograph made by PlaneWave Instruments. Light passes through Johnson-Cousins BVRI filters before reaching an Apogee Alta U16M CCD camera; we bin the chip 2 × 2 to produce a plate scale of 1.26" per pixel. We acquire new flatfield images for each observing session, but re-use bias and dark frames for a month or so. We acquired 5 unguided images in each passband, using exposure times of 45 to 60 seconds each. After using MAXIMDL (Diffraction Ltd. 2012) to subtract master bias and master dark frames, and divide by a master flatfield frame, we combined the images in each passband using a median technique. These combined images typically had a FWHM ranging between 3.1" and 3.9", with most lying near the low end of this range. A sample composite R-band image is shown in Figure 3.

We applied the rotation technique described above to each combined image before extracting photometry using circular apertures of radius 3 pixels = 3.8". The local background was measured for each star using an annulus of radii 12.6" and 25.2". Figure 4 shows one such residual image from the NSO dataset.

## 3. Photometric calibration

In order to transform our instrumental measurements onto the standard Johnson-Cousins BVRI system, we used a set of local reference stars (Table 1) provided by the American Association of Variable Star Observers (AAVSO; https://www.aavso.org) in their sequence X18345FX. These stars are labelled in all figures showing the supernova and its surroundings. Given our relatively small fields of view and shallow limiting magnitudes, we did not select comparison stars on the basis of color, but accepted them all. The color range covered is relatively small: $0.598 \leq (B–V) \leq 1.065$. SN 2016coj has a color of $(B–V) \simeq 0.0$ near maximum light, and does not redden to match the comparison stars until about 15 days later. Of course, the spectrum of this type Ia SN is so distinct from that of the comparison stars that color corrections must be approximate in any case.

In order to convert the RIT measurements to the Johnson-Cousins system, we analyzed images of the standard fields PG1633+009 and PG2213-006 (Landolt 1992) taken on five nights between June and August 2016. Comparing our instrumental values to the standard magnitudes, we determined transformation equations

$$B = b + 0.2016(0134) \times (b-v) + Z_B \tag{1}$$

$$V = v - 0.0920(0063) \times (v-r) + Z_V \tag{2}$$

$$R = r - 0.1137\ (0058) \times (r–i) + Z_R \tag{3}$$

$$I = i - 0.0174\ (0034) \times (r–i) + Z_I \tag{4}$$

Table 2. RIT photometry of SN 2016coj.

| *JD−2457530* | *B* | *V* | *R* | *I* | *Comments* |
|---|---|---|---|---|---|
| 9.64 | 14.108 ± 0.040 | 13.960 ± 0.029 | 13.811 ± 0.067 | 13.866 ± 0.085 | |
| 10.61 | 13.816 ± 0.042 | 13.760 ± 0.021 | 13.657 ± 0.020 | 13.677 ± 0.040 | |
| 11.61 | 13.663 ± 0.067 | 13.556 ± 0.028 | 13.432 ± 0.104 | 13.484 ± 0.125 | cirrus |
| 19.60 | 13.231 ± 0.062 | 13.072 ± 0.038 | 13.061 ± 0.021 | 13.426 ± 0.073 | |
| 20.59 | 13.371 ± 0.090 | 13.109 ± 0.057 | 13.070 ± 0.038 | 13.503 ± 0.105 | cirrus |
| 21.58 | 13.244 ± 0.077 | 13.139 ± 0.049 | 13.161 ± 0.040 | 13.548 ± 0.049 | light clouds |
| 22.64 | 13.368 ± 0.058 | 13.196 ± 0.057 | 13.268 ± 0.077 | 13.822 ± 0.136 | |
| 23.59 | 13.415 ± 0.027 | 13.179 ± 0.029 | 13.212 ± 0.021 | 13.714 ± 0.059 | |
| 24.59 | 13.480 ± 0.049 | 13.232 ± 0.029 | 13.369 ± 0.046 | 13.837 ± 0.101 | cirrus |
| 27.60 | 13.884 ± 0.045 | 13.409 ± 0.027 | 13.544 ± 0.061 | 13.970 ± 0.065 | |
| 28.60 | 13.998 ± 0.050 | 13.440 ± 0.022 | 13.632 ± 0.059 | 13.984 ± 0.063 | cirrus |
| 29.61 | 13.975 ± 0.096 | 13.472 ± 0.030 | 13.543 ± 0.065 | 13.859 ± 0.088 | bright moon |
| 31.61 | 14.270 ± 0.072 | 13.586 ± 0.028 | 13.648 ± 0.079 | 13.719 ± 0.111 | |
| 32.59 | 14.436 ± 0.049 | 13.639 ± 0.023 | 13.648 ± 0.072 | 13.750 ± 0.085 | |
| 33.60 | 14.535 ± 0.088 | 13.650 ± 0.024 | 13.675 ± 0.057 | 13.723 ± 0.087 | |
| 36.59 | 15.166 ± 0.222 | 13.865 ± 0.048 | 13.656 ± 0.088 | 13.608 ± 0.085 | clouds |
| 37.59 | 15.129 ± 0.091 | 13.964 ± 0.052 | 13.670 ± 0.066 | 13.572 ± 0.099 | fewer images |
| 39.60 | 15.400 ± 0.115 | 14.061 ± 0.030 | 13.737 ± 0.069 | 13.516 ± 0.086 | |
| 40.60 | 15.370 ± 0.069 | 14.155 ± 0.043 | 13.795 ± 0.061 | 13.418 ± 0.104 | |
| 42.60 | 15.678 ± 0.119 | 14.349 ± 0.044 | 13.948 ± 0.072 | 13.593 ± 0.086 | |
| 43.60 | 15.722 ± 0.078 | 14.421 ± 0.040 | 14.034 ± 0.081 | 13.705 ± 0.095 | |
| 45.60 | 15.938 ± 0.079 | 14.586 ± 0.044 | 14.248 ± 0.078 | 13.840 ± 0.082 | haze |
| 50.60 | 16.026 ± 0.117 | 14.822 ± 0.069 | 14.462 ± 0.093 | 14.372 ± 0.106 | cirrus |
| 51.60 | 15.844 ± 0.189 | 14.897 ± 0.049 | 14.578 ± 0.085 | 14.272 ± 0.113 | cirrus |
| 53.60 | 16.265 ± 0.107 | 14.926 ± 0.062 | 14.654 ± 0.081 | 14.414 ± 0.107 | haze, old flats |
| 56.60 | 16.193 ± 0.117 | 15.100 ± 0.055 | 14.799 ± 0.082 | 14.596 ± 0.098 | |
| 58.60 | 16.002 ± 0.113 | 15.111 ± 0.058 | 14.796 ± 0.086 | 14.609 ± 0.113 | |
| 59.60 | 16.202 ± 0.102 | 15.069 ± 0.047 | 14.815 ± 0.064 | 14.623 ± 0.084 | start longer exp |
| 62.60 | — | 15.188 ± 0.035 | 14.915 ± 0.084 | 14.686 ± 0.110 | |
| 63.61 | — | 15.222 ± 0.063 | 15.032 ± 0.090 | 14.824 ± 0.124 | cirrus |
| 65.60 | — | 15.257 ± 0.038 | 15.020 ± 0.062 | 14.840 ± 0.082 | |
| 66.60 | — | 15.289 ± 0.049 | 15.061 ± 0.082 | 14.839 ± 0.125 | cirrus |
| 69.62 | — | 15.374 ± 0.041 | 15.176 ± 0.087 | 14.928 ± 0.083 | light clouds |
| 72.60 | — | 15.433 ± 0.036 | 15.211 ± 0.083 | 14.949 ± 0.089 | |
| 73.59 | — | 15.451 ± 0.039 | 15.235 ± 0.069 | 15.118 ± 0.090 | |
| 75.61 | — | 15.503 ± 0.092 | 15.421 ± 0.108 | 15.054 ± 0.126 | light clouds |

In the equations above, lower-case symbols represent instrumental magnitudes, upper-case symbols Johnson-Cousins magnitudes, terms in parentheses the uncertainties in each coefficient, and Z the zeropoint in each band. The relatively small field of view of the RIT images allowed us to use only a few stars for calibration: B, C, J, and, in some cases, K.

In mid-June 2016, we noticed that images in the *B*-band from RIT had a low signal-to-noise ratio, even after coaddition; this is largely a function of the relatively low sensitivity of our camera's sensor at short wavelengths. The *B*-band measurements showed a large scatter from night to night, making real trends in the light curve hard to discern. Therefore, after UT 2016 June 20, we stopped taking images at RIT in the *B*-band.

We present our calibrated measurements of SN 2016coj made at RIT in Table 2. The first column shows the mean Julian Date of all the exposures taken during each night; we have subtracted the arbitrary constant 2457530 from all Julian Dates for convenience. The uncertainties listed in Table 2 incorporate the uncertainties in instrumental magnitudes and in the offset to shift the instrumental values to the standard scale, added in quadrature.

We determined linear transformations between the instrumental NSO measurements and the standard scale using images of the open cluster M67 and photometry provided by the AAVSO. The transformation equations for NSO were

$$B = b - 0.164(0.033) \times (b-v) + Z_B \tag{5}$$

$$V = v - 0.109(0.023) \times (b-v) + Z_V \tag{6}$$

$$V = v - 0.197(0.050) \times (v-r) + Z_V \tag{7}$$

$$R = r - 0.205(0.052) \times (r-i) + Z_R \tag{8}$$

$$I = i - 0.238(0.073) \times (r-i) + Z_I \tag{9}$$

In the equations above, lower-case symbols represent instrumental magnitudes, upper-case symbols Johnson-Cousins magnitudes, terms in parentheses the uncertainties in each coefficient, and *Z* the zeropoint in each band. We list two equations for the *V*-band; on nights when we acquired *R* images, we used the ($v$–$r$) equation, but on nights when we measured only *B* and *V*, we used the ($b$–$v$) version.

Table 3 lists our calibrated measurements of SN 2016coj made at Northern Skies Observatory.

## 4. Light curves

In order to determine the time and magnitude at peak brightness, we fit polynomials of order 3 to the light curves near maximum, using data from the period 0 < (JD – 2457530)

Table 3. NSO photometry of SN 2016coj.

| *JD – 2457530* | *B* | *V* | *R* | *I* |
|---|---|---|---|---|
| 20.64 | 13.307 ± 0.023 | 13.073 ± 0.027 | 13.121 ± 0.037 | 13.570 ± 0.057 |
| 25.64 | 13.606 ± 0.056 | 13.242 ± 0.015 | — | — |
| 33.65 | 14.565 ± 0.038 | 13.791 ± 0.017 | 13.773 ± 0.035 | 13.967 ± 0.056 |
| 34.63 | 14.682 ± 0.025 | 13.845 ± 0.026 | 13.769 ± 0.034 | 13.824 ± 0.047 |
| 35.64 | 14.785 ± 0.058 | 13.807 ± 0.032 | — | — |
| 39.61 | 15.195 ± 0.067 | 14.037 ± 0.032 | — | — |
| 42.61 | 15.487 ± 0.034 | 14.369 ± 0.028 | 14.000 ± 0.036 | 13.687 ± 0.065 |
| 43.66 | 15.626 ± 0.047 | 14.461 ± 0.030 | 14.110 ± 0.039 | 13.729 ± 0.058 |
| 45.59 | 15.729 ± 0.043 | 14.632 ± 0.031 | — | — |
| 73.59 | 16.423 ± 0.058 | 15.590 ± 0.038 | 15.456 ± 0.042 | 15.535 ± 0.075 |

Table 4. Apparent magnitudes at maximum light.

| *Passband* | *JD – 2457530* | *Magnitude* |
|---|---|---|
| B | 18.1 ± 0.4 | 13.16 ± 0.07 |
| V | 18.7 ± 0.2 | 13.06 ± 0.01 |
| R | 18.0 ± 0.4 | 13.04 ± 0.03 |
| I | 16.2 ± 2.9 | 13.23 ± 0.10 |
| I (sec) | 39.0 ± 0.7 | 13.50 ± 0.05 |

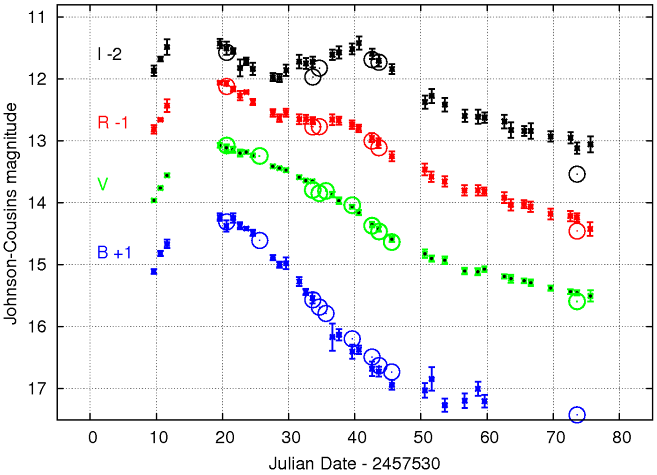

Figure 5. Light curves of SN 2016coj in BVRI. The data for each passband have been offset vertically for clarity. Small symbols represent measurements from RIT, large symbols those from NSO; uncertainties in the latter are smaller than the symbols.

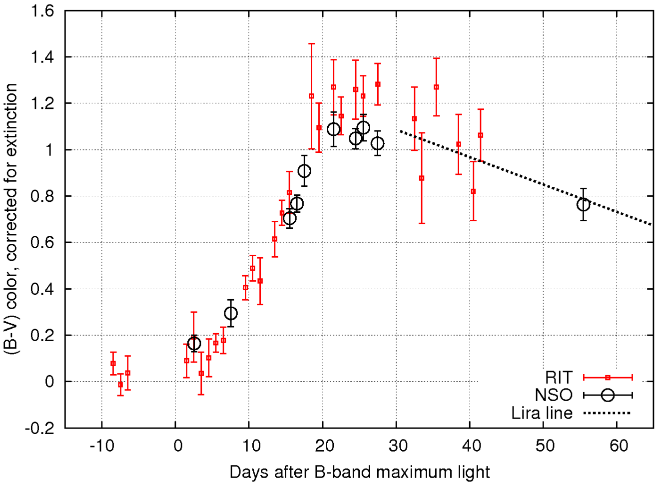

Figure 6. (B–V) color evolution of SN 2016coj, after correcting for extinction.

< 30 in each passband, weighting the fits by the uncertainties in each measurement. We list the results in Table 4. For the secondary maximum in *I*-band, we found that polynomials of order 2 provided better fits; we averaged the results from several intervals during during the period 30 < (JD – 2457530) < 50 to produce the value in the table. Note that the *I*-band magnitude at its primary maximum is particularly uncertain, as it falls farther within the gap in our measurements than the peaks in other passbands.

Using a second-order polynomial to interpolate in the B-band observations exactly 15 days after the time of B-band maximum light, we compute $\Delta_{15}(B) = 1.32 \pm 0.10$. By this measure, SN 2016coj lies in the range of "normal" type Ia SNe, such as 1980N (Hamuy *et al.* 1991), 1989B (Wells *et al.* 1994), 1994D (Richmond *et al.* 1995), 2003du (Stanishev *et al.* 2007), and 2011fe (Richmond and Smith 2012; Parrent *et al.* 2012). The secondary peak in *I*-band, which lies 22.8 ± 1.0 days after and 0.27 ± 0.07 magnitude below the primary peak, is also typical of "normal" type Ia events.

Our values of the apparent magnitude at *B*-band maximum light and the $\Delta_{15}(B)$ parameter agree with those measured by Zheng *et al.* (2016). Those authors also provide spectroscopic evidence to support a "normal" classification for SN 2016coj.

In order to compute absolute magnitudes and intrinsic colors for SN 2016coj, we must remove the extinction due to any intervening material. Fortunately, there appears to be very little dust in its direction. Our own Galaxy's contribution is small: Schlegel *et al.* (1998) use infrared maps of the Milky Way to estimate $E(B\text{–}V)_{\mathrm{MW}} = 0.017$ in the direction of NGC 4125. Zheng *et al.* (2016) examine high-resolution spectra of SN 2016coj to look for absorption lines caused by interstellar material in the host galaxy. Finding none, they employ several methods to place upper limits on the reddening of $E(B\text{–}V)_{\mathrm{host}} \lesssim 0.05$ or $E(B\text{–}V)_{\mathrm{host}} \lesssim 0.09$. We will adopt a host value of $\mathrm{E}(B\text{–}V)_{\mathrm{host}} = 0.05$ for the color curves we present below, yielding a total reddening of $E(B\text{–}V)_{\mathrm{tot}} = 0.067$. Following the conversions from reddening to extinction given in Schlafly and Finkbeiner (2011), we derive the extinction to SN 2016coj to be $A_B = 0.24$, $A_V = 0.18$, $A_R = 0.15$, and $A_I = 0.10$.

After removing this extinction from each passband, we calculate the evolution of the event in each color; see Figure 6 for (*B–V*), Figure 7 for (*V–R*), and Figure 8 for (*R–I*). The (*B–V*) color shows a value of zero at maximum light, typical for a normal type Ia. In the same figure, we have drawn a line which

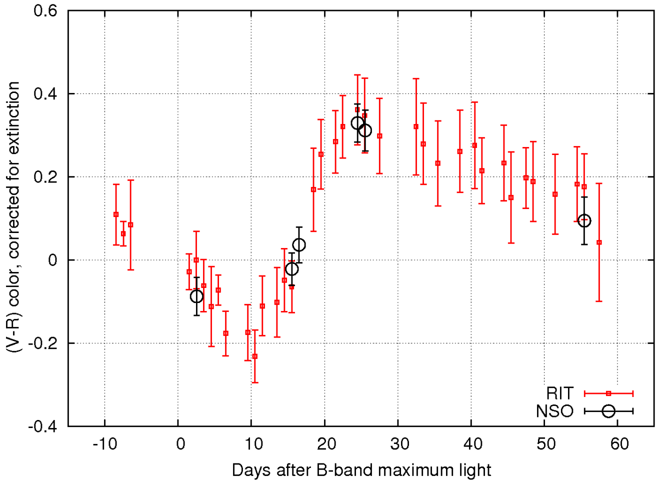

Figure 7. (V–R) color evolution of SN 2016coj, after correcting for extinction.

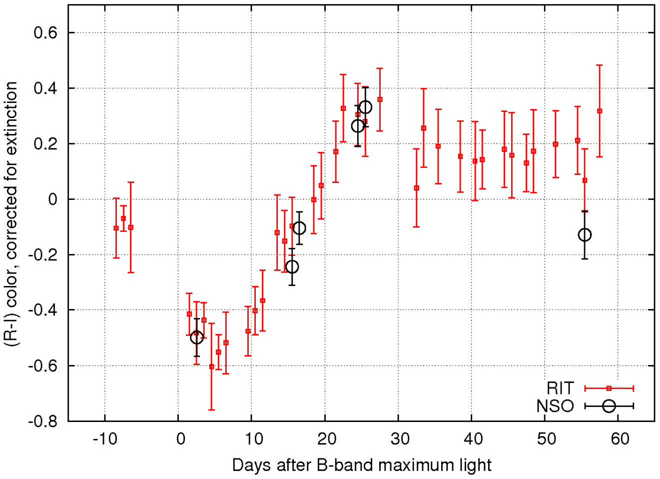

Figure 8. (R–I) color evolution of SN 2016coj, after correcting for extinction.

represents the late-time $(B–V)$ evolution of a set of normal type Ia SNe with little or no extinction (Lira 1995; Phillips *et al.* 1999). Although our measurements are sparse and noisy at late times, due to the low signal in the $B$ band, they suggest that SN 2016coj followed the same evolution as other normal events. In Figure 7, we see that SN 2016coj reaches a minimum $(V–R)$ color about 10 days after $B$-band maximum, then increases to a maximum $(V–R) = 0.35$. The time of minimum is a few days earlier in $(R–I)$, which then rises to a maximum of $(R–I) = 0.35$. All these properties are similar to those in the color curves of the normal SNe Ia 1994D (Richmond *et al.* 1995), 2003du (Stanishev *et al.* 2007), 2009an (Sahu *et al.* 2013), and 2011fe (Richmond and Smith 2012). The only significant difference in the late-time behavior of SN 2016coj is in $(R–I)$, which appears to have a relatively constant value of $(R–I) \sim 0.2$. However, we believe that this color in particular suffers from a systematic bias in the RIT $I$-band measurements (see the Appendix); note the position of the single late-time NSO datum, at a negative color more typical of normal SNe.

## 5. Absolute magnitudes

What was the absolute magnitude of SN 2016coj? In order to convert our apparent magnitudes to the absolute scale, we need to account for extinction and the distance to the host galaxy (Table 5). As mentioned earlier, Zheng *et al.* (2016) place only upper limits on the extinction due to material in the host galaxy. In the discussion which follows, we will compute two values of absolute magnitude, one assuming no extinction in the host galaxy, the other corresponding to the upper limit of $E(B–V) = 0.05$ derived in Zheng *et al.* (2016). The distance to NGC 4125 has been measured a number of times, but none are very recent. We will adopt the measurement based on Surface Brightness Fluctuations (SBF) by Tonry *et al.* (2001) of $(m – \mathrm{M}) = 31.89 \pm 0.25$.

Table 5. Absolute magnitudes of SN 2016coj at maximum light, corrected for extinction.

| *Passband* | *E (B − V ) = 0 in host* | *E (B − V ) = 0.05 in host* | *based on $\Delta m_{15}(B)^{a}$* |
|---|---|---|---|
| B | −18.79 ± 0.26 | −18.97 ± 0.26 | −19.19 ± 0.10 |
| V | −18.88 ± 0.26 | −19.01 ± 0.26 | −19.12 ± 0.09 |
| R | −18.89 ± 0.26 | −18.99 ± 0.26 | −19.14 ± 0.07 |
| I | −18.68 ± 0.27 | −18.76 ± 0.27 | −18.87 ± 0.08 |
| I (sec) | −18.41 ± 0.26 | −18.49 ± 0.26 | — |

*a. Using the relationship from Prieto et al. (2006).*

A connection between the absolute magnitude of a type Ia SN and its rate of decline after maximum was first noted by Phillips (1993) and has since been refined by a number of authors (Hamuy *et al.* 1996; Riess *et al.* 1996; Perlmutter *et al.* 1997). We choose the relationships derived by Prieto *et al.* (2006) which are based on the fading in $B$-band in the first 15 days after maximum light, the $\Delta m_{15}(B)$ parameter. In the case of SN 2016coj, we measure $\Delta m_{15}(B) = 1.32 \pm 0.10$. Inserting that into the equations in Table 3 of Prieto *et al.* (2006) for events in environments with low extinction, we derive the absolute magnitudes shown in the rightmost column of Table 3. With the exception of the $B$-band measurement assuming no host extinction, all measurements agree with the predictions of the decline-rate method, supporting further the classification of SN 2016coj as normal. The slight improvement offered by assuming a small host extinction provides weak evidence that it may be close to the upper limits derived by Zheng *et al.* (2016).

## 6. Conclusion

Our measurements of SN 2016coj show that its photometric behavior at early times (within 60 days of maximum light) follows that of “normal” type Ia SNe. We compute a decline parameter of $\Delta m_{15}(B) = 1.32 \pm 0.10$ magnitude, placing it in the middle of the distribution of normal events. Adopting a distance modulus to NGC 4125 of $(m – \mathrm{M}) = 31.89$ and correcting for a total of $E(B–V) = 0.067$ of extinction, we derive absolute magnitudes of $M_B = –19.01$, $M_V = –19.05$, $M_R = –19.03$, and $M_I = –18.79$.

We have shown that correcting for contamination of SN measurements by the background light of the host galaxy is a difficult issue for this event. While our measurements at early times—upon which the above conclusions are based—are reliable, those at late times must be treated with caution. The simple procedure we used for this dataset does not require template images of the host galaxy alone, but can leave a systematic error which grows as the target object fades.

## 7. Acknowledgements

We thank the staff at AAVSO for their finding charts, sequences of comparison stars, and endless support of observers. MWR is grateful for the continued support of the RIT Observatory by RIT and its College of Science. BV thanks the Northeast Kingdom Astronomy Foundation for allowing him to use their facility. The Lick Observatory Supernova Search noticed this event and quickly alerted the rest of the community, permitting us to begin our study while the supernova was still on the rise. This research has made use of the "Aladin Sky Atlas" and SIMBAD database (Wenger *et al.* 2000), developed and operated at the CDS, Strasbourg Observatory, France, We have also made use of the NASA/IPAC Extragalactic Database (NED) which is operated by the Jet Propulsion Laboratory, California Institute of Technology, under contract with the National Aeronautics and Space Administration. This paper (and many others) has made use of NASA's Astrophysics Data System. Facility: AAVSO.

## References

Chandrasekhar, S. 1931, *Astrophys. J.*, **74**, 81.

de Vaucouleurs, G., de Vaucouleurs, A., Corwin, H. G., Jr., Buta, R. J., Paturel, G., and Fouqué, P. 1991, *Third Reference Catalog of Bright Galaxies*, Springer, New York.

Diffraction Limited. 2012, MAXIMDL image processing software (http://www.cyanogen.com).

Filippenko, A. V., Li, W. D., Treffers, R. R., and Modjaz, M. 2001, in *Small Telescope Astronomy on Global Scales*, eds. B. Paczynski, W.-P. Chen, and C. Lemme, ASP Conf. Ser. 246, Astronomical Society of the Pacific, San Francisco, 121.

Guy, J., Astier, P., Nobili, S., Regnault, N., and Pain, R. 2005, *Astron. Astrophys.*, **443**, 781.

Hamuy, M., Phillips, M. M., Maza, J., Wischnjewsky, M., Uomoto, A., Landolt, A. U., and Khatwani, R. 1991, *Astron. J.*, **102**, 208.

Hamuy, M., Phillips, M. M., Suntzeff, N. B., Schommer, R. A., Maza, J., and Aviles, R. 1996, *Astron. J.*, **112**, 2391.

Landolt, A. U. 1992, *Astron. J.*, **104**, 340.

Leaman, J., Li, W., Chornock, R., and Filippenko, A. V. 2011, *Mon. Not. Roy. Astron. Soc.*, **412**, 1419.

Lira, P. 1995, Master's thesis, Univ. Chile.

Parrent, J. T., *et al.* 2012, *Astrophys. J., Lett.*, **752**, L26.

Perlmutter, S., *et al.* 1997, *Astrophys. J.*, **483**, 565.

Phillips, M. M. 1993, *Astrophys. J., Lett.*, **413**, L105.

Phillips, M. M., Lira, P., Suntzeff, N. B., Schommer, R. A., Hamuy, M., and Maza, J. 1999, *Astron. J.*, **118**, 1776.

Prieto, J. L., Rest, A., and Suntzeff, N. B. 2006, *Astrophys. J.*, **647**, 501.

Richmond, M. W., *et al.* 1995, *Astron. J.*, **109**, 2121.

Richmond, M. W., and Smith, H. A. 2012, *J. Amer. Assoc. Var. Star Obs.*, **40**, 872.

Riess, A. G., Press, W. H., and Kirshner, R. P. 1996, *Astrophys. J.*, **473**, 88.

Sahu, D. K., Anupama, G. C., and Anto, P. 2013, *Mon. Not. Roy. Astron. Soc.*, **430**, 869.

Schlafly, E. F., and Finkbeiner, D. P. 2011, *Astrophys. J.*, **737**, 103.

Schlegel, D. J., Finkbeiner, D. P., and Davis, M. 1998, *Astrophys J.*, **500**, 525.

Stanishev, V. *et al.* 2007, *Astron. Astrophys.*, **469**, 645.

Tonry, J. L., Dressler, A., Blakeslee, J. P., Ajhar, E. A., Fletcher, A. B., Luppino, G. A., Metzger, M. R., and Moore, C. B. 2001, *Astrophys. J.*, **546**, 681.

Treffers, R. R., and Richmond, M. W. 1989, *Publ. Astron. Soc. Pacific*, **101**, 725.

Wells, L. A., *et al.* 1994, *Astron. J.*, **108**, 2233.

Wenger, M., *et al.* 2000, *Astron. Astrophys., Suppl. Ser.*, **143**, 9.

Zheng, W., Yuk, H., Manzano-King, C., Canalizo, G., Sexton, R., Barth, A., Shivvers, I., and Filippenko, A. V. 2016, *Astron. Telegram*, No. 9095, 1.

## Appendix: Bias in photometry

The location of SN 2016coj in its host galaxy presents the observer with good news and bad news. The good news is that NGC 4125 is an elliptical galaxy, and therefore likely contains relatively little gas and dust, as the spectroscopic measurements of Zheng *et al.* (2016) confirm. It is therefore not necessary to make large corrections for extinction. But the bad news is that the supernova is close enough to the bright core of its host, offset by only 5.0" east and 10.8" north (Zheng *et al.* 2016), that the light of the nucleus and the surrounding stars provides a significant background to measurements of the SN. Moreover, at this location, the light of the galaxy has a strong radial gradient, making it very difficult to subtract its contribution accurately.

Since other observers may encounter similar situations, we describe in some detail below our investigation of the likely systematic errors that can arise when one attempts to perform photometry on such images.

It became clear to us that simple aperture photometry methods would yield poor results in this case. Since we did not have template images of the galaxy to use as references for subtraction in the standard manner, we settled upon a method which would provide better (but not perfect) results: making a copy of each image, rotating the copy by 180° around the center of the galaxy, then subtracting the copy from the original. As shown in Figure 2, the resulting residual image has a background near the location of the supernova which is both much lower, and much more uniform, than the original image. We used these residual images to derive the measurements presented in this paper.

However, we suspected that there remained a sometimes significant systematic error in the photometry produced by this method, for two reasons. First, when comparing the decline of SN 2016coj against that of other type Ia SNe, such as SN 2011fe, we noticed that this event faded less quickly at late times—by an amount which appeared to grow with time. Second, we noticed a difference between measurements from our two sites: measurements from NSO, which typically have a smaller PSF and higher signal-to-noise than those from RIT, showed the SN as slightly fainter, and this difference also grew with time.

Could there be a reason why measurements of faint point sources immersed in a noisy (and possibly non-uniform) background should show a systematic error? Our technique of identifying and measuring both reference stars and the supernova in images was a simple one: we searched through each image independently to identify peaks above the local sky background, measured their properties, and kept as "good" sources those which had shapes consistent with the expected PSF. We used the pixels around each of these sources to compute its center, placed a circular aperture at this position, and integrated the light within the aperture; finally, we subtracted the contribution from the local background light within the aperture.

The important feature of this standard method is that the position of the aperture used to measure the SN (and reference stars) is not fixed in any way: it may be influenced independently by noise in each image, especially when the source is faint and the noise is high. A better technique, one which is natural when using a template, is to align images, co-add them to improve signal-to-noise, and measure relative positions for the SN and several reference stars; then, in each individual image, measure the position of bright reference stars and use them to *infer* the position of the SN using a fixed offset, rather than computing it based on the possibly noisy data at its location in each image. The method we employed is likely to shift the center of the SN's aperture slightly to follow positive noise peaks, which could yield measurements slightly higher than they ought to be.

In short, we suspect that our measurements, especially those made at RIT, contain a systematic positive bias: the SN appears brighter than it actually is, by an amount which increases as the SN fades.

To test this hypothesis, we created a set of simulated images with properties similar to those acquired at RIT, and subjected them to exactly the same measurement methods as we used on our actual images. We started with a simplified situation: a set of reference stars of identical brightness on a uniform background, and a single "supernova" immersed in a "square galaxy" region of uniform higher intensity; see Figure 9. The stars are modeled as gaussians of FWHM 3.0 pixels, matching the typical seeing at RIT, and the gain in the image is set to 2.2 electrons per count, matching the properties of the SBIG ST-9E camera. The brightness of the "square galaxy" is set to 620 counts, typical for the region near SN 2016coj in *R*-band images. Note that the stars are placed at intervals with small random variations, ensuring that they appear at a wide range of sub-pixel locations. We ran a number of instances of each simulation, shifting both the reference stars and the "supernova" by small random sub-pixel positions each time.

In this simplified situation, we chose as the center of rotation the geometric center of the image. After making a copy and rotating it around this center by 180°, we subtracted the copy from the original, leaving both reference stars and "supernova" in a near-zero background; but the pixels surrounding the supernova might be noisier than those surrounding the reference stars. As a sanity check that our software was not introducing errors of its own, we ran simulations in which no photon noise was added to the images: the background value was some fixed value in all pixels, and the model gaussian for each star was similarly exact. Over a series of trials, the reference stars and "supernova" were all set to the same input brightness, increasing gradually throughout the trials until their centers reached a value of 30,000 counts (similar to the limit of linearity on our camera). We would expect the stars and "supernova" all to have exactly the same magnitude in this noiseless simulation. The magenta symbols in Figure 10 show that the difference between the average reference star magnitude, and the "supernova" magnitude, is indeed zero under these conditions.

However, when we add photon noise to our simulations, we find some differences between the magnitude of the reference stars and the "supernova." We ran simulations with two background levels, 100 and 1,000 counts per pixel, roughly bracketing the range of sky levels in real RIT images (which varies due to clouds, haze, and the aspect of the Moon). Consider first the red asterisk symbols, which show the results under low sky conditions: when the SN and stars are bright, there is no significant difference in their measured magnitudes. But when the stars are faint, noise in the sky background and in their own signal leads both to increased scatter and to discrepancy between the average value of the reference stars and that of the "supernova"; the SN tends to be measured as brighter than the reference stars. The amplitude of the difference grows to roughly 0.1 magnitude by the time the stars are too faint to detect reliably. The blue circular symbols, corresponding to higher and so noisier background sky levels, show the same trend, but at an increased amplitude.

We conclude that point sources simply immersed in a higher background of light will suffer from a systematic bias under our measurement procedure, appearing brighter than they ought to be. However, the situation of SN 2016coj is even worse: not only is it in a region of higher background level than the comparison stars, but it sits in a strong spatial gradient. What effect will this additional complication have on our measurements?

We performed a very simple test by creating a toy model of our real images. We created an artificial galaxy by superposing a central gaussian (FWHM = 3.0 pixels) and an extended and flattened component (FWHM = 8.0 pixels, convolved with a kernel of FWHM = 6 along rows and FWHM = 12 along columns), scaling the result so that it resembled the appearance of NGC 4125 in our *R*-band images. We then placed the "supernova" at an offset from the galaxy similar to its actual offset. Both the galaxy and the "supernova" were shifted in position by small random sub-pixel amounts in each realization of our simulations. Figure 11 shows an example of these artificial images, one in which the reference stars and SN are all at the maximum brightness.

We then carried out a series of instances, changing the brightness of the stellar objects over a wide range; at each level of brightness, we ran ten realizations, varying the positions of each source at the sub-pixel level and generating different random values of photon noise. For each realization, we carried out exactly the same measurement procedure as we used for the real images:

- a copy of the image was displayed on a computer screen

- the user moved a cursor to the center of the galaxy, pressed

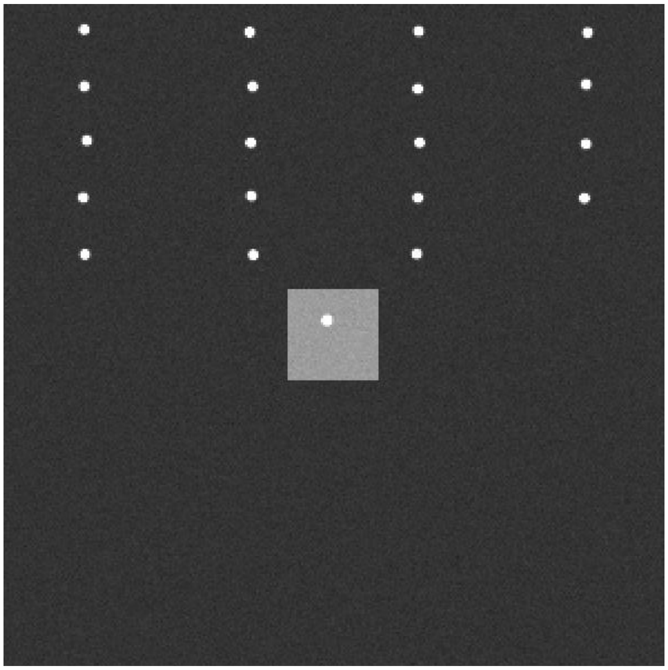

Figure 9. Simulated image with 19 reference stars in a low background and a “supernova” immersed in a “square galaxy.”

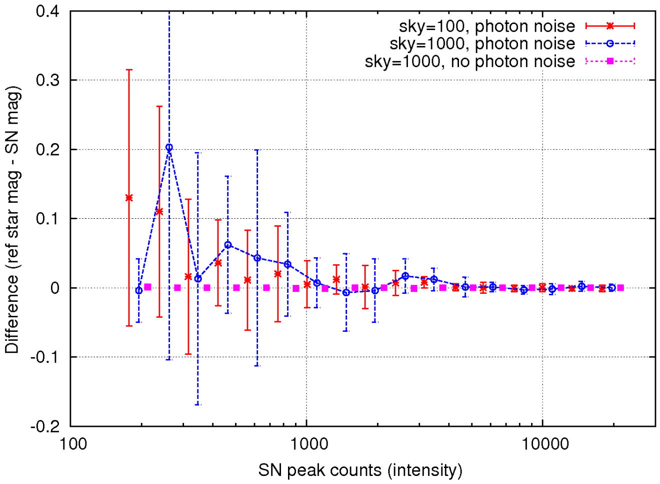

Figure 10. Results of photometry after rotation and subtraction of the simulated images with a “square galaxy.”

a key to initiate a calculation of the local centroid and display a radial profile, made adjustments to initial position until satisfied that the center had been found correctly

- a copy of the image was rotated around this position

- the copy was subtracted from the original image

- point sources in the residual image were automatically found and measured via aperture photometry

An example of one residual image is shown in Figure 12. There is clearly imperfect subtraction of the galaxy’s light at its very center, as is seen in most of the real images after this procedure.

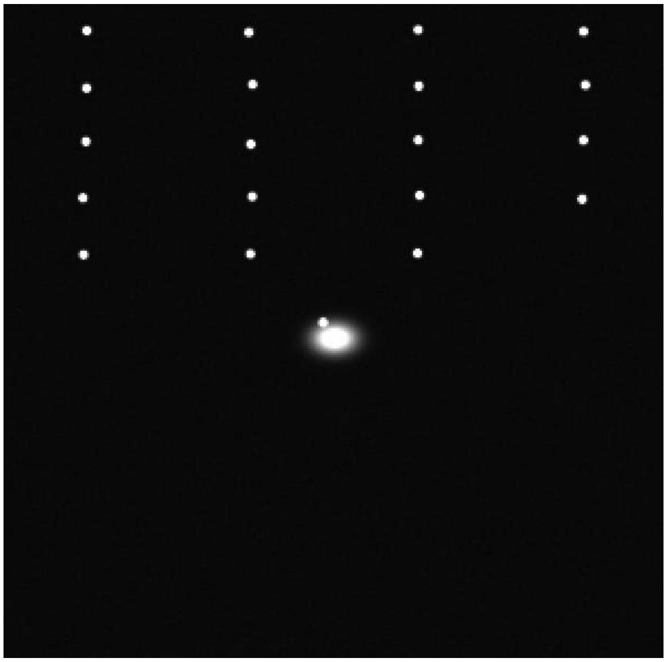

Figure 11. Simulated image with 19 reference stars in a low background and a “supernova” placed close to an artificial galaxy.

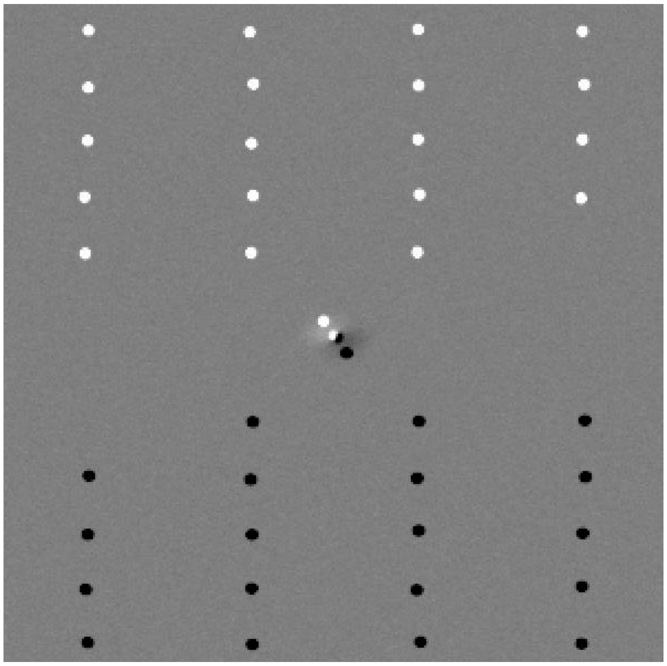

Figure 12. Simulated image with artificial galaxy after rotation and subtraction.

The results of photometry on these images are display in Figure 13. In this case, we fixed the brightness of the overall sky background to 100 counts for all realizations, so it represents the optimistic end of the spectrum of real conditions. The general trend is similar to that in the “square galaxy” simulations: measurements of the SN appear brighter than those of the reference stars, by an amount which increases as the SN fades. However, there are important differences: first, this systematic difference appears even in the absence of photon noise; this indicates that the software used to perform the image analysis (xvista; Treffers and Richmond 1989) is unable to compute the center of the galaxy accurately enough, or perform the image rotation accurately enough, or both. Second, note that the *amplitude* of the systematic difference is much larger than in the "square galaxy" simulations: the SN can appear about 1.0 magnitude brighter it ought to be, instead of just 0.1 magnitude.

In order to reduce these systematic errors, one must improve the method of subtracting the background contribution to the total light within the photometric aperture. Given the large FWHM of our images, we could not decrease the size of the photometric aperture significantly; given the location of the SN, close to the galaxy's nucleus, increasing the size of the background annulus would make matters worse, and, given the large FWHM, decreasing the size of the background annulus is not possible. Rather than choosing some constant value per pixel for the background contribution, one could do better by making a model of the galaxy's light within the photometric aperture. We will investigate this technique in the future; it would require a substantial effort to modify the existing software. The difficulty of proper background subtraction is, of course, the reason that many astronomers adopt the "template subtraction" method.

Now, in light of this information, let us review the light curves shown in Figure 5. When the SN is bright, measurements from RIT and NSO agree well; but as the SN fades, an offset between the two datasets appears, with the NSO measurements slightly fainter. The offset is largest in the *I*-band and smallest in the *B*-band; we ascribe this trend with wavelength to the color of the galaxy's light. The starlight of NGC 4125 is more prominent at long wavelengths, making the background at the location of SN 2016coj brightest (relative to the SN) in the *I*-band. Since the NSO data have both a smaller PSF and a higher signal-to-noise ratio, they suffer from less contamination by the galaxy's light.

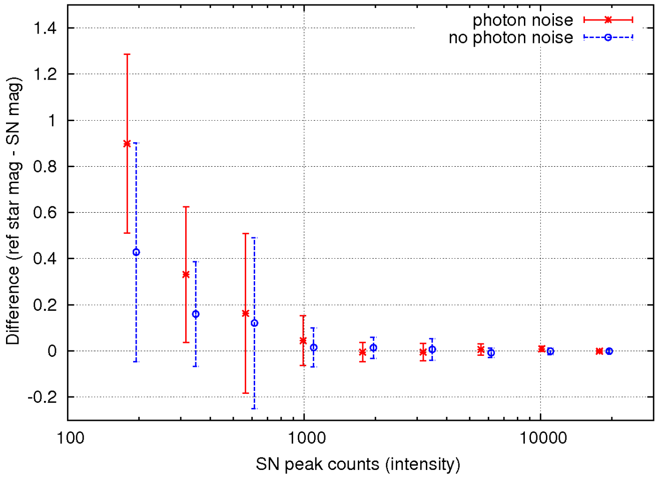

Figure 13. Results of photometry after rotation and subtraction of the simulated images with a realistic galaxy model.

At early times, the SN was bright enough that any systematic bias was at most comparable to the random uncertainties in each measurement; but that is certainly not true for the late times. We recommend that readers use with caution the latest measurements presented here. We suggest that greater weight be given to the NSO values at late times; it might be profitable to "warp" the RIT measurements at late times to match the final NSO magnitudes.

# Using Unfiltered Images to Perform Standard Filter Band Photometry

**Joe Garlitz**
*1155 Harford Street, Elgin, OR 97827; garlitzj@eoni.com*

*Received May 24, 2016; revised July 7, October 24, 2016, February 17, 2017; accepted February 20, 2017*

**Abstract** This paper demonstrates that raw instrumental magnitudes of stars measured from a single unfiltered CCD image can be transformed into standard passband magnitudes. Star fields that have good catalogued photometric magnitudes can be used as a reference to transform unfiltered instrumental magnitudes into a standard system. To demonstrate this, the AAVSO (VSP) M-67 catalogued stars are used. It is shown that, within certain constraints, the standard B, V, Rc, and Ic magnitudes can be accurately determined from unfiltered instrumental magnitudes. For well behaved, well calibrated stars, the transformations to standard magnitudes can be done within a standard deviation of better than 0.021 magnitude. The paper further presents a simple spreadsheet tool to automatically derive the "standard" magnitudes from the raw instrumental magnitudes. This greatly simplifies the task of calculating transformation coefficients, and makes it possible to calibrate a CCD imaging system on an image-by-image basis.

## 1. Introduction

A variety of differential photometric measurements are made by amateur astronomers, such as: light curves of variable stars, the rotational periods of asteroids, and transit timing of exoplanets. Many projects, however, require photometric measurements referenced to "standard" filter passbands. Due to the added work required and the use of filters that reduce the signal of the image, many amateurs do not attempt to make such measurements.

With the advent of all-sky catalogues such as the Guide Star Catalog (GSC; Space Telescope Science Institute 2001), AAVSO Photometric All-Sky Survey (APASS; Henden *et al.* 2015), Carlsberg Meridian Catalogue 14 (CMC14; Copenhagen University Observatory 2006), and others, nearly any image field will contain a number of cataloged stars having standard magnitudes. As high quality all-sky photometric catalogues become available, single-image transformation of instrumental magnitudes to "standard" systems can become a common practice.

## 2. Previous work

Henden (2000) presented an experiment using 64 calibrated stars in M67 to determine the practicality of making standard photometric measurements from unfiltered CCD images. Henden has shown that unfiltered images can be used to make some standard photometric measurements. The color response of the camera is determined and used to transform unfiltered instrumental magnitudes to standard magnitudes. The accuracy of the transformation is dependent primarily on obtaining the photometric response of the imaging system and the color index of the target star. He determined the V and R color coefficients for six different CCD sensors. Using these he presented a sample transformation of the unfiltered instrumental magnitude of a star to the standard V magnitude. He demonstrated that by determining the color response of the CCD and the color index of the subject star, the unfiltered instrumental magnitude transformed to the known standard V magnitude of the star within 0.06 magnitude.

Gary (2009) has developed a novel method to do all-sky photometry using unfiltered images. Predetermined zero-point adjustments for his imaging system and the cataloged 2MASS J and K magnitudes of the subject star are used to derive proper transform coefficients to calculate V, R, and r' standard magnitudes.

Dymock and Miles (2009) described a method of determining the V magnitude of an asteroid using differential photometry with the magnitudes of comparison stars selected from the CMC14 catalogue data. They made use of the availability of a large number of suitable CMC14 stars within the data image to make "reasonably accurate magnitude" measurements without resorting to all-sky photometry. This method is basically the same as presented here. Dymock and Miles limited their presentation to "V" magnitudes of asteroids using the CMC14 catalogue as reference. Their procedure, however, is applicable to any other available catalogue and can be used for stars as well as asteroids.

Yoshida (2010) provides a series of conversion coefficients to transform unfiltered instrumental magnitudes of six different CCD chips, as in Henden (2000).

Dunckel (2014) presented a method to obtain calibrated standard magnitudes from measurements of filtered images using APASS magnitudes as reference. This method parallels the procedure presented in this paper, the difference being that Dunckel uses filtered images, while this presentation uses unfiltered images. The results of Dunckel using filtered images, all things being the same, will be more accurate than the use of unfiltered images, but with the disadvantage of signal reduction due to filtering.

The AAVSO Transform Generator (TG; AAVSO 2016) project is a recently developed online tool that allows the easy calibration of a filtered imaging system and the calculation of standard magnitudes of stars imaged by a CCD camera. It is available for use by amateur astronomers. This provides an easy method to generate photometric measurements suitable for AAVSO observing programs.

## 3. Acquiring instrumental magnitudes

Images of the M-67 star field were made using a 12-inch diameter f/5 Newtonian reflector with an SBIG ST402me CCD camera. The camera was mounted at prime focus. A series of images of M-67 was made in a single night spanning air masses 1.2 to 2.0. The images were 20-second exposures without filter.

Each image was dark- and flat-field calibrated using the AIP4WIN magnitude measurement tool (Berry and Burnell 2005). The stars measured for this exercise were 63 of the 64 Henden (2000) M-67 stars. Star number 56 was out of the image frame and was not measured. The instrumental magnitudes (Imag) of the 63 stars were measured at air masses of 1.2, 1.4, 1.6, and 2.0. To increase the data quality, the instrumental magnitudes of 6 consecutive images were averaged to give the approximate equivalent of 120 seconds of exposure.

AAVSO has expanded and refined the M-67 star chart to over 170 calibrated stars. The current AAVSO VSP star chart magnitudes of the 64 Boulder swri numbers (Henden 2000) M-67 stars were obtained from Myers (2012). The finder chart, Appendix A, identifies these 64 stars with their Boulder swri numbers. Of the original 64 Henden (2000) stars, fifteen have been culled from the current AAVSO-VSP list, leaving 49 Boulder swri calibrated stars. A key correlating the 64 swri numbers to the AAVSO-VSP AUIDs is given in Appendix B (Myers 2016). The measured instrumental magnitudes, and the corresponding AAVSO catalogue magnitudes and AUID numbers for the 48 measured stars are given in Appendix C.

## 4. Determining the color response of the imaging system

For clarity, catalogued reference magnitudes will be designated using upper case, such as “B” and “V”. Calculated standard magnitudes derived from measuring an image are designated using lower case, such as “b” and “v”. As a general designation, “F” is used to refer to a catalogue magnitude, and “f” designates a calculated magnitude for a generic passband.

To determine the imaging system’s color response, the M-67 catalogued magnitudes (B, V, Rc, Ic) were plotted against the measured unfiltered raw instrumental magnitudes (Imag) of the 48 measured stars. Figure 1 shows the B, V, Rc, Ic magnitudes (y-axis) plotted against the unfiltered raw instrumental magnitudes (x-axis) for air mass 1.2. It is seen that the Rc magnitudes are nearly linear. Figure 2 shows the residuals (“F” – Imag), that is, the cataloged M-67 magnitudes minus the measured instrumental magnitudes (Imag) plotted against the color index (B–V), for these four filter passbands at air mass 1.2. The plotted data demonstrate that the imaging system used is consistent with the Rc filter band. This is good information for the general use of this particular system and replicates the results of Henden (2000).

### 4.1. Calculating transforms: strategy

Using a photometry processing software, the unfiltered CCD image is measured to obtain the raw instrumental magnitudes (Imag) of the target and comparison stars. The several passband magnitudes of the comparison stars are obtained from a suitable photometric catalogue for stars in the image field: APASS, CMC14, or AAVSO star charts, for example. Finally, using the spreadsheet numerical tool “solver,” the transformation coefficients of the imaging system for each filter passband of interest are calculated. The spreadsheet automatically applies the calculated transformation coefficients to the raw instrumental magnitudes of the measured stars, calculating their derived standard magnitudes, “f”, for the selected filter band.

The method presented short-cuts the normal photometric procedure which generally requires measuring nearby, out of frame, calibrated reference stars. By using catalogued reference stars within the data image, the reference stars are measured simultaneously with the target star, through the same system, the same atmosphere, and at the same time. This all but eliminates the system and environmental variations of the reference stars with respect to the target star for the image being measured.

### 4.2. Calculating transforms: calculation equation

The equation used to determine the transformation coefficients is the standard photometric equation. Using the default nomenclature (Boyd 2012), and modified for a generic passband (F), the equation is:

$$f = Imag - (k'_{F} \times X) - (k''_{F(Ci)} \times X \times Ci) + (T_{F(Ci)} \times Ci) + Z_{F}. \quad (1)$$

where:

f = Standard magnitude calculated for the “F” filter passband,

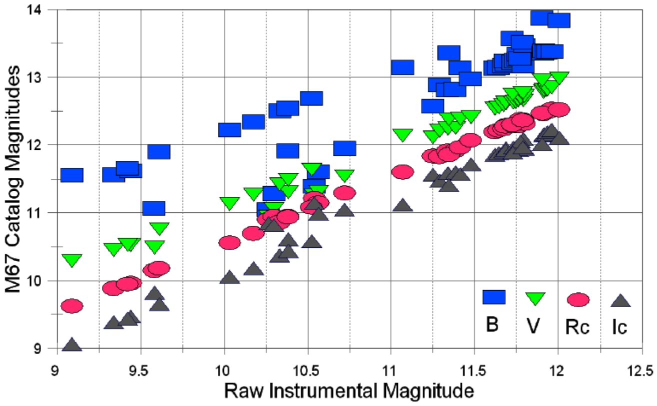

Figure 1. B, V, Rc, Ic magnitudes (y-axis) compared to the unfiltered raw instrumental magnitudes (x-axis) for air mass 1.2.

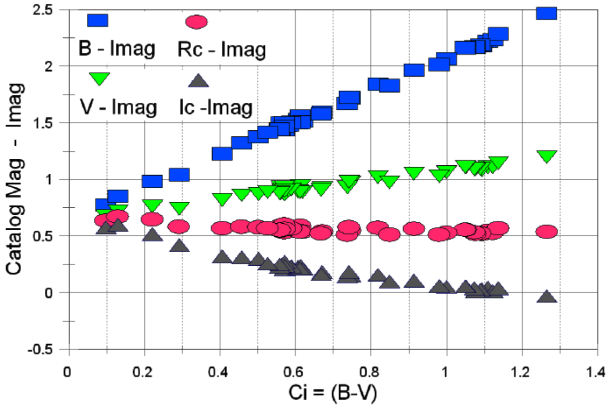

Figure 2. The catalogued M-67 magnitudes minus the measured instrumental magnitudes (Imag) plotted against the color index (B–V), for four filter passbands at air mass 1.2.

Imag = Measured unfiltered raw instrumental magnitude,
$k'_F$ = Atmospheric extinction coefficient at the observatory,
X = Air mass of the image at the observatory when the image was taken,
$k''_{F(Ci)}$ = Second order color extinction coefficient,
Ci = Color index of the measured stars calculated using the reference catalogue, e.g. (B–V)
$T_{F(Ci)}$ = Instrumental transformation coefficient for the color index Ci,
$Z_F$ = Zero point offset of the instrumental magnitude.

It is assumed for the purpose of these calculations that all the stars in a single narrow field image (30 × 30 arc min) have nominally the same air mass and attenuation at elevations above 30 degrees. The users of this procedure should determine the validity of this assumption for their own conditions; see Dunckel (2014, page 109). With this supposition, the values of X, and Z, and the coefficients k' and k" for a given passband are essentially constant for all stars in the subject image. Consolidating constants, the working equation to calculate the derived standard magnitudes in filter band "F" becomes:

$$f = Imag + Ci \times T' + Z' \qquad (2)$$

where:

$T' = T_{F(Ci)} - k''_{F(Ci)} \times X$ and
$Z' = Z_F - k'_F \times X$.

It is to be noted that in making these calculations, the transformation coefficients are applicable only to the image from which they were derived. While this procedure does determine the static instrumental constants of the imaging system, these constants are combined with X in both T' and Z' where X is changing with time.

### 4.3. Calculating transforms: source of data

The data required to make the transformations from instrumental magnitudes to standard magnitudes come from five sources:

1. The star field containing the object of interest is imaged and measured to obtain the raw instrumental magnitudes (Imag) of the target star(s) and the several catalogued reference stars.

2. The standard magnitudes for each of the measured reference stars are extracted from a photometric catalogue for all filter passbands of interest (B, V, Rc, Ic, for example).

3. The color indices (Ci) of each measured star are calculated from the catalogued reference data (Ci = (B–V), for example).

4. The sky and system transformation coefficients ( T' and Z') for the image are determined by the spreadsheet.

5. Finally, the color index, Ci, of the target star must be determined. The Ci depends on the nature of the target. For asteroids or comets, Ci may be estimated based on the solar spectrum. Variable stars generally have variable color indices. Each type of star will present a different challenge to obtaining a proper Ci (see Henden 2000, section 3.0, page 40). Appendix E presents a quick method to determine the color index of a star. Note that it is necessary that the color of the target star be within the color response of the imaging camera; see section 6, Conclusions, for an expanded comment.

### 4.4. Calculating transforms: spreadsheet

For this procedure, Equation 2 is used to calculate the values of the "derived" standard magnitudes of each measured star in the subject image, (b, v, r, i, for example). The "solver" or "optimize" spreadsheet tool will calculate an optimum set of constants that satisfy a given set of boundary conditions. Within the spreadsheet algorithm, the constants T' and Z' are repeatedly changed until the algorithm returns a solution that best meets the boundary conditions. Thus the transformation constants T' and Z' for any given image are directly calculated using the spreadsheet.

The boundary conditions for the calculations are defined in terms of the residual value R', of each measured star, where R' = (F – f ); for example, R' = (B–b). The boundary conditions are:

1. The standard deviation of the set of R'(n) for n measured stars is minimized, which sets the color and air mass coefficients.

2. The average of the set of R'(n) values is zero, which sets the zero point adjustment. Using data from the M-67 star field and for the B-filter passband, the spreadsheet appears as in Figure 3.

Two cells are set up to hold the constants T' and Z', {C14, C15}. (These are "fixed" cells and are used in each calculation made in row 10). A third cell is set up to calculate the Standard Deviation of the residuals, StdDev(R'(n)), {C12}, and a fourth cell is set up to calculate the average of the residuals Avg(R'(n)), {C13}. Rows 4 through 7 contain the catalogued standard magnitudes for the several filter bands of interest for each measured star. Row 8 is the color index calculated for each reference star (B–V).

Note that the target star, as shown, does not have cataloged magnitudes; thus, Ci for the target must be determined from another source and inserted at {C8} (see section 4.3, item 5). Row 9 is the raw instrumental magnitudes (Imag) of the measured stars. Row 10 is the derived magnitudes; "b" for the "B" passband being used in this example. Row 11 is the calculated residual for each star, (B–b). The "Solver" insert sets the boundary conditions, which are: 1) minimize the standard deviation of the residuals, and 2) make the average of the residuals equal zero. With the spreadsheet set up, clicking "solve" automatically calculates the image transformation coefficients, T' and Z', and the derived standard magnitude "b" for each star.

The derived magnitudes for an image can be calculated for any filter band. Figure 3 shows the B-filter band calculation. This is determined by using (B–b)n for the values of R'(n). To select the "V" filter band, the R'(n) values used are (V–v)n. A sample spreadsheet is available at: http://users.eoni.com/~garlitzj/Sample_Unfiltered_1.xls .

### 4.5. Calculating transforms: derived b, v, r, i magnitudes

Using the procedure described, the derived magnitudes (b, v, r, i) for the standard passbands (B, V, Rc, Ic) were calculated for the 48 M-67 stars described in section 2. These 48 reference stars with their corresponding measured unfiltered instrumental

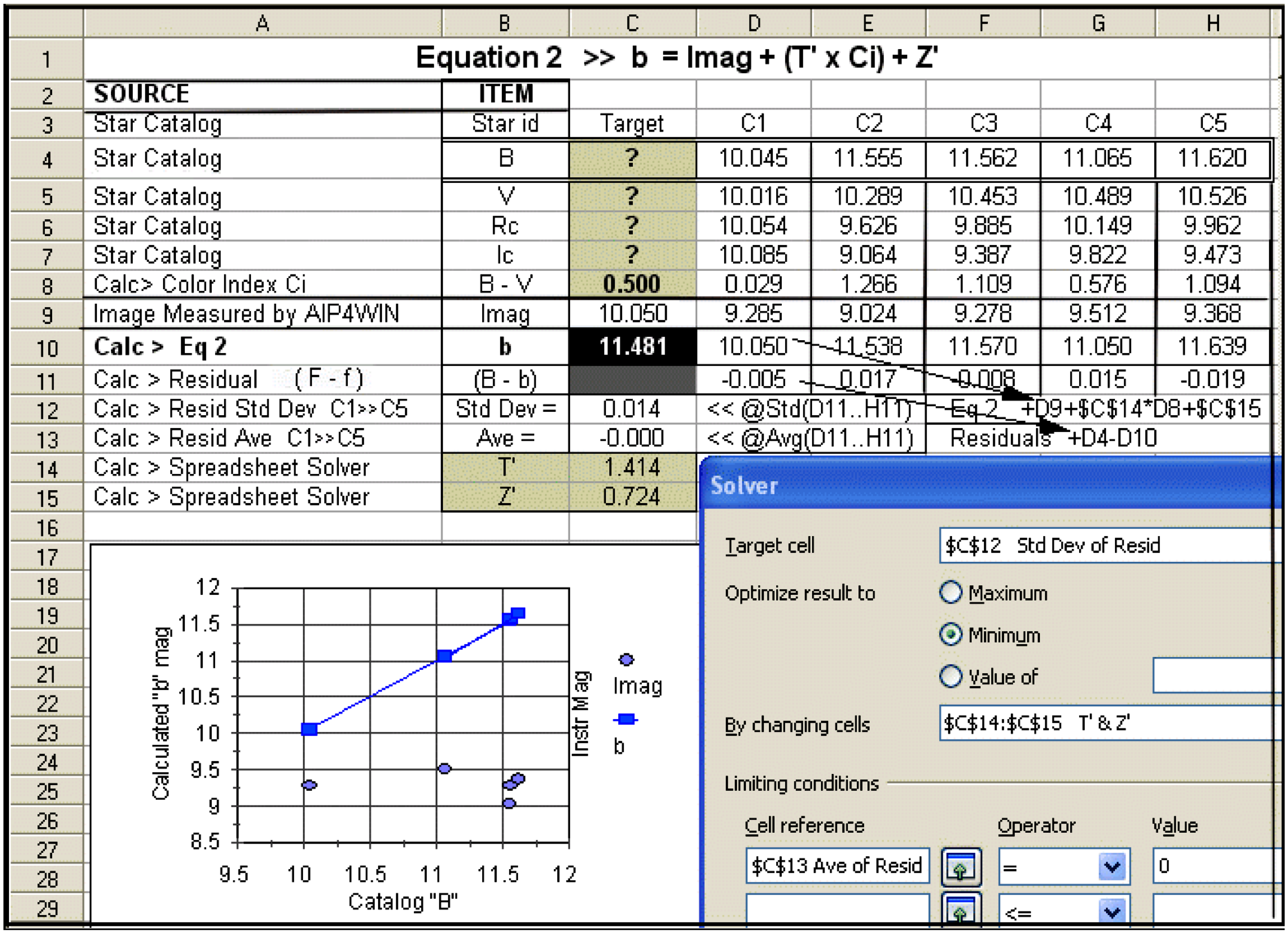

| | A | B | C | D | E | F | G | H |
|---|---|---|---|---|---|---|---|---|
| 1 | Equation 2 >> b = Imag + (T' x Ci) + Z' | | | | | | | |
| 2 | SOURCE | ITEM | | | | | | |
| 3 | Star Catalog | Star id | Target | C1 | C2 | C3 | C4 | C5 |
| 4 | Star Catalog | B | ? | 10.045 | 11.555 | 11.562 | 11.065 | 11.620 |
| 5 | Star Catalog | V | ? | 10.016 | 10.289 | 10.453 | 10.489 | 10.526 |
| 6 | Star Catalog | Rc | ? | 10.054 | 9.626 | 9.885 | 10.149 | 9.962 |
| 7 | Star Catalog | Ic | ? | 10.085 | 9.064 | 9.387 | 9.822 | 9.473 |
| 8 | Calc> Color Index Ci | B - V | 0.500 | 0.029 | 1.266 | 1.109 | 0.576 | 1.094 |
| 9 | Image Measured by AIP4WIN | Imag | 10.050 | 9.285 | 9.024 | 9.278 | 9.512 | 9.368 |
| 10 | Calc > Eq 2 | b | 11.481 | 10.050 | 11.538 | 11.570 | 11.050 | 11.639 |
| 11 | Calc > Residual ( F - f ) | (B - b) | | -0.005 | 0.017 | -0.008 | 0.015 | -0.019 |
| 12 | Calc > Resid Std Dev C1>>C5 | Std Dev = | 0.014 | << @Std(D11..H11) | | Eq 2 +D9+$C$14*D8+$C$15 | | |
| 13 | Calc > Resid Ave C1>>C5 | Ave = | -0.000 | << @Avg(D11..H11) | | Residuals +D4-D10 | | |
| 14 | Calc > Spreadsheet Solver | T' | 1.414 | | | | | |
| 15 | Calc > Spreadsheet Solver | Z' | 0.724 | | | | | |
| 16 | | | | | | | | |

Solver

Target cell $C$12 Std Dev of Resid

Optimize result to ○ Maximum ● Minimum ○ Value of

By changing cells $C$14:$C$15 T' & Z'

Limiting conditions

| Cell reference | Operator | Value |
|---|---|---|
| $C$13 Ave of Resid | = | 0 |
| | <= | |

Figure 3. Spreadsheet using data from the M-67 star field and for the B-filter passband.

magnitudes are listed in Appendix C. The derived (b, v, r, i) magnitudes for air masses 1.2, 1.4, 1.6, and 2.0 for each passband (B, V, Rc, Ic) are listed in Appendix D.

Figures 4 and 5 show the raw instrumental magnitudes (Imag) and the “b” and “r” derived magnitudes respectively, plotted against their corresponding catalogued B and Rc magnitudes at air mass 1.2. It is evident from these plots that the calculated magnitudes “b” and “r” are consistent with the catalogued magnitudes B and Rc for these two filter bands. This is especially evident for the B band where the instrumental magnitudes are very widely scattered.

Figures 6 and 7 present the residuals (B–b) and (Rc–r) plotted against their respective color indices (B–V) and (Rc–Ic) at air mass 1.2. The standard deviation of these residuals is 0.016 magnitude for (B–b) and 0.018 magnitude for (Rc–r).

Table 1 presents the transformation coefficients for the B, V, Rc, Ic filter passbands at air masses of 1.2 and 2.0 for the 48 measured M-67 stars. These coefficients were derived from the unfiltered images of M-67 calculated by the spreadsheet using Equation 2. The color indexes used for the calculations were (B–V) and (Rc–Ic) as listed.

## 5. Assessing the accuracy of the derived magnitudes

For each of the 48 measured stars, the residuals (B–b), (V–v), (Rc–r), and (Ic–i) were calculated at each air mass. Calculating the standard deviation of these residuals gives the results shown in Table 2. For this star field of 48 well calibrated reference stars, the plots in Figures 4, 5, 6, 7, and the standard deviation values in Table 2 demonstrate that standard magnitudes (B, V, Rc, Ic) can be accurately derived from a single unfiltered image. The derived (b, v, r, i) magnitudes are accurate to a standard deviation of 0.021 magnitude or better for air mass 1.2 through 2.0.

The standard deviations of the residuals in Table 2 are comparable to the average of the errors reported for the calibrated AAVSO M-67 stars as shown in Table 3 and listed in Appendix C. This indicates that the quality of the derived magnitudes is comparable to the quality of the reference magnitudes.

## 6. Conclusions

An imaging system’s color response can be readily demonstrated by plotting the measured unfiltered instrumental magnitudes of a star field of well-behaved stars against the catalogued standard magnitudes of those stars (section 3). The imaging system used in the work for this paper is seen to respond very much like an Rc filter. Thus, for this system, the magnitudes derived from the unfiltered instrumental magnitudes

Table 1. Transformation coefficients Z' and T' for B, V, Rc, Ic passbands using 48 M–67 stars.

| | *Airmass = 1.2* | | | | *Airmass = 2.0* | | | |
|---|---|---|---|---|---|---|---|---|
| *Passband and [Ci]* | *B [B–V]* | *V [B–V]* | *Rc [B–V]* | *Ic [Rc–Ic]* | *B [B–V]* | *V [B–V]* | *Rc [B–V]* | *Ic [Rc–Ic]* |
| Z’ | 0.720 | 0.720 | 0.817 | 0.817 | 0.264 | 0.264 | 0.402 | 0.376 |
| T’ | 1.407 | 0.407 | –0.239 | –1.239 | 1.451 | 0.451 | –0.061 | –1.135 |

Table 2. Standard deviations for 48 AAVSO M-67 stars.

| *Filter Band Residuals* | *B (B–b)* | *V (V–v)* | *Rc (Rc–r)* | *Ic (Ic–i)* | *Air Mass* |
|---|---|---|---|---|---|
| Standard Deviation | 0.016 | 0.016 | 0.018 | 0.018 | 1.2 |
| | 0.016 | 0.016 | 0.017 | 0.017 | 1.4 |
| | 0.018 | 0.018 | 0.018 | 0.019 | 1.6 |
| | 0.020 | 0.020 | 0.021 | 0.021 | 2.0 |

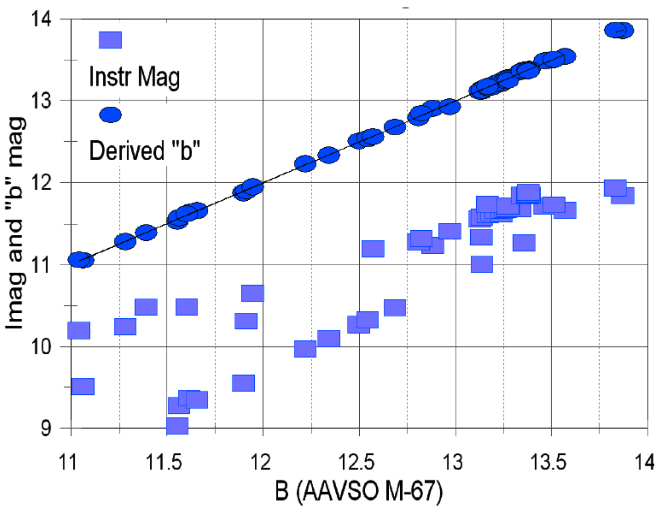

Figure 4. Raw instrumental magnitudes transformed to standard B magnitudes.

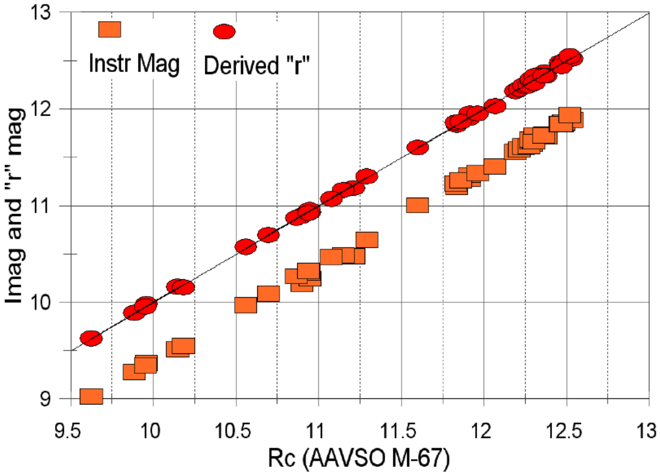

Figure 5. Raw instrumental magnitudes transformed to standard Rc magnitudes.

Table 3. Average reported errors for 48 AAVSO M-67 stars.

| *Filter Band* | *B* | *V* | *Rc* | *Ic* |
|---|---|---|---|---|
| Average of Reported Errors Appendix C | 0.020 | 0.017 | 0.019 | 0.023 |

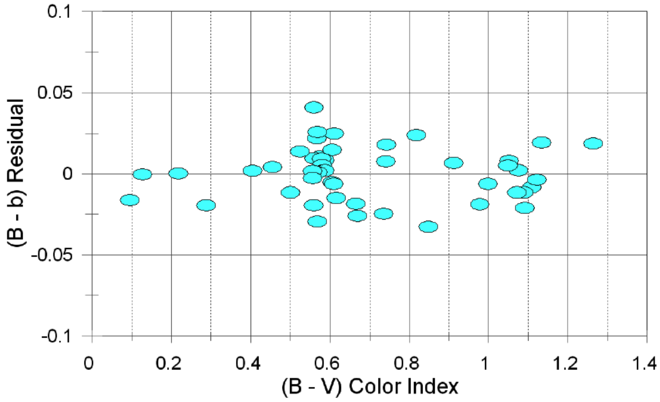

Figure 6. Residuals (B–b) plotted against (B–V) color index; Residual Std Dev = 0.016.

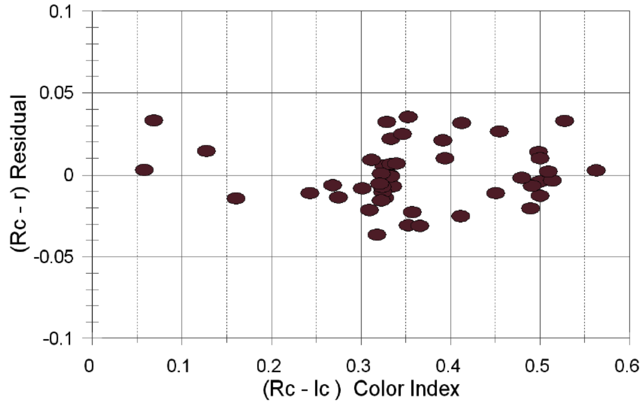

Figure 7. Residuals (Rc–r) plotted against (Rc–Ic) color index; Residual Std Dev = 0.018.

are similar to making transformations from the Rc passband to the B, V, and Ic passbands.

This paper deals with the B, V, Rc, Ic passbands. It is necessary, then, to recognize the limits in making transformations of unfiltered instrumental magnitudes to these passbands. This procedure works because the imaging system acts as a wide band “filter” over the B, V, Rc, Ic wavelength range. Caution is due for stars that are very blue (high UV) or very red (high IR) with spectrums that peak outside of the CCD’s nominal “filter” range. In this circumstance, the CCD imaging system will not work as a functional filter.

Figure 8 shows images of the long term variable UX Cyg (Spectral type M4–M6). The target star is not quite as bright as the close-by star in the red image (right), but it is much brighter in the image with no filter (left). This is because the response of the KAF-0402ME CCD chip in the camera peaks at about 6,500 angstroms, but its sensitivity extends well beyond 9,000 angstroms. In Figure 9 the spectrum for an M5v star (Pickles

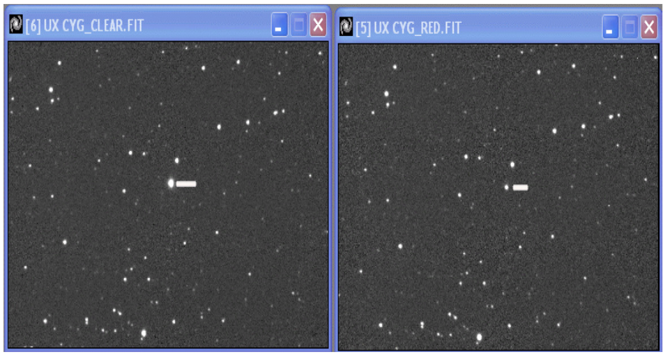

Figure 8. Images of the long term variable UX Cyg (Spectral type M4–M6). The target star is not quite as bright as the close-by star in the red image (right), but it is much brighter in the image with no filter (left). Author's data.

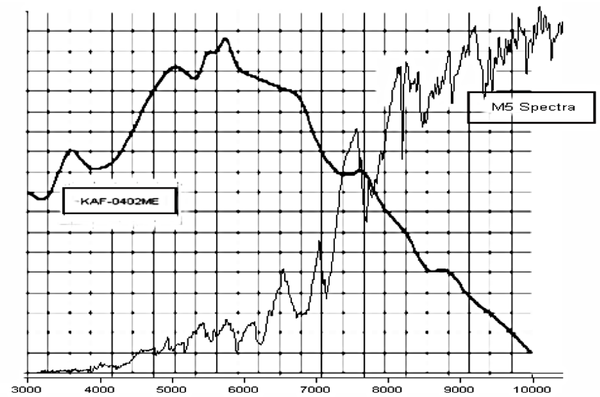

Figure 9. The spectrum for an M5 star shown together with the efficiency curve of the KAF-0402ME camera (Pickles 1998; Diffraction Limited 2015).

1998) is shown together with the efficiency curve of the camera (Diffraction Ltd. 2015). It is evident that the spectram of the star peaks well beyond the camera's IR response. Since the IR light extends beyond the nominal range of the camera's broadband "filter," this star's unfiltered image will not properly transform to the standard B, V, Rc, Ic system.

Noting the cautions for using this method of photometry, it is demonstrated that, for a star field of well-calibrated stars, it is possible to accurately derive standard magnitudes for the B, V, Rc, and Ic filter bands from a single unfiltered image.

While the color indices of the catalogued reference stars in an image field can be determined from the catalogue data, the target star may not have a proper color index. The color index for the target star must be determined in order to calculate its standard magnitudes (section 4.3, item 5).

Setting up a spreadsheet using the "solver" or "optimizer" tool provides a simple and quick method to calculate derived standard magnitudes. A sample spreadsheet can be downloaded from: http://users.eoni.com/~garlitzj/Sample_Unfiltered_1.xls.

This procedure requires that the subject star field has a number of well calibrated catalogued stars. The GSC, APASS, and CMC14 catalogues, as well as star charts prepared for measuring variable stars, are available and suitable for most star fields.

## 7. Acknowledgements

I thankfully acknowledge the AAVSO's presentation of the calibrated catalogue of M-67 stars, and the prior work of Arne Henden in presenting the M-67 unfiltered photometry referenced in this paper.

I also acknowledge the wealth of work on amateur photometry presented by Bruce Gary which has been an invaluable resource for my adventures into all sky photometry (brucegary.net/DifferentialPhotometry/dp.htm).

This research was made possible through the use of the AAVSO Photometric All-Sky Survey (APASS), funded by the Robert Martin Ayers Sciences Fund.

## References

AAVSO. 2016, Transform Generator (TG; https://www.aavso.org/tg).Henden, A. A. 2000, *J. Amer. Assoc. Var. Star Obs.*, **29**, 35.

Berry, R., and Burnell, J. 2005, AIP4WIN software and *Handbook of Astronomical Image Processing*, Willmann-Bell, Richmond, VA.

Boyd, D. 2012, *J. Amer. Assoc. Var. Star Obs.*, **40**, 990.

Copenhagen University Observatory, Institute of Astronomy. 2006, *Carlsberg Meridian Catalog 14* (CMC14), Copenhagen Univ. Obs. Inst. Astron., Cambridge.

Diffraction Limited. 2015, Data sheet for KAF-0402ME CCD sensor (http://diffractionlimited.com/product/stf-402m/).

Dunckel, N. 2014, in *The Society for Astronomical Sciences 33rd Annual Symposium on Telescope Science*, Society for Astronomical Sciences, Rancho Cucamonga, CA, 105.

Dymock, R., and Miles, R. 2009, *J. Br. Astron. Assoc.*, **119**, 149.

Gary, B. L. 2009, All sky photometry for V, R, and r' using unfiltered images—a novel approach (http://brucegary.net/DifferentialPhotometry/dp.htm#6._ALL_SKY).

Henden, A. A. 2000, Boulder swri numbers, M67 standard stars (https://www.aavso.org/files/m67-Arne.pdf).

Henden, A. A., *et al.* 2015, AAVSO Photometric All-Sky Survey, data release 9 (http://www.aavso.org/apass).

Myers, G. 2012, M67 Henden Field Comps.STAR (https://groups.yahoo.com/neo/groups/AIP4Win-Photometry/files?prop=eupdate).

Myers, G. 2016, private communication (key for AAVSO-VSP AUIDs to M-67 Boulder swri numbers).

Pickles, A. J. 1998, *Publ. Astron. Soc. Pacific*, **110**, 863.

Space Telescope Science Institute. 2001, *The Guide Star Catalog*, Version 2.2 (VizieR On–line Data Catalog: I/271), STScI, Baltimore.

Yoshida, S. 2010, Magnitude system and color conversion formulas; unfiltered CCD instrumental magnitudes (http://www.aerith.net/astro/color_conversion.html).

## Appendix A: M-67 field with original Boulder swri numbers

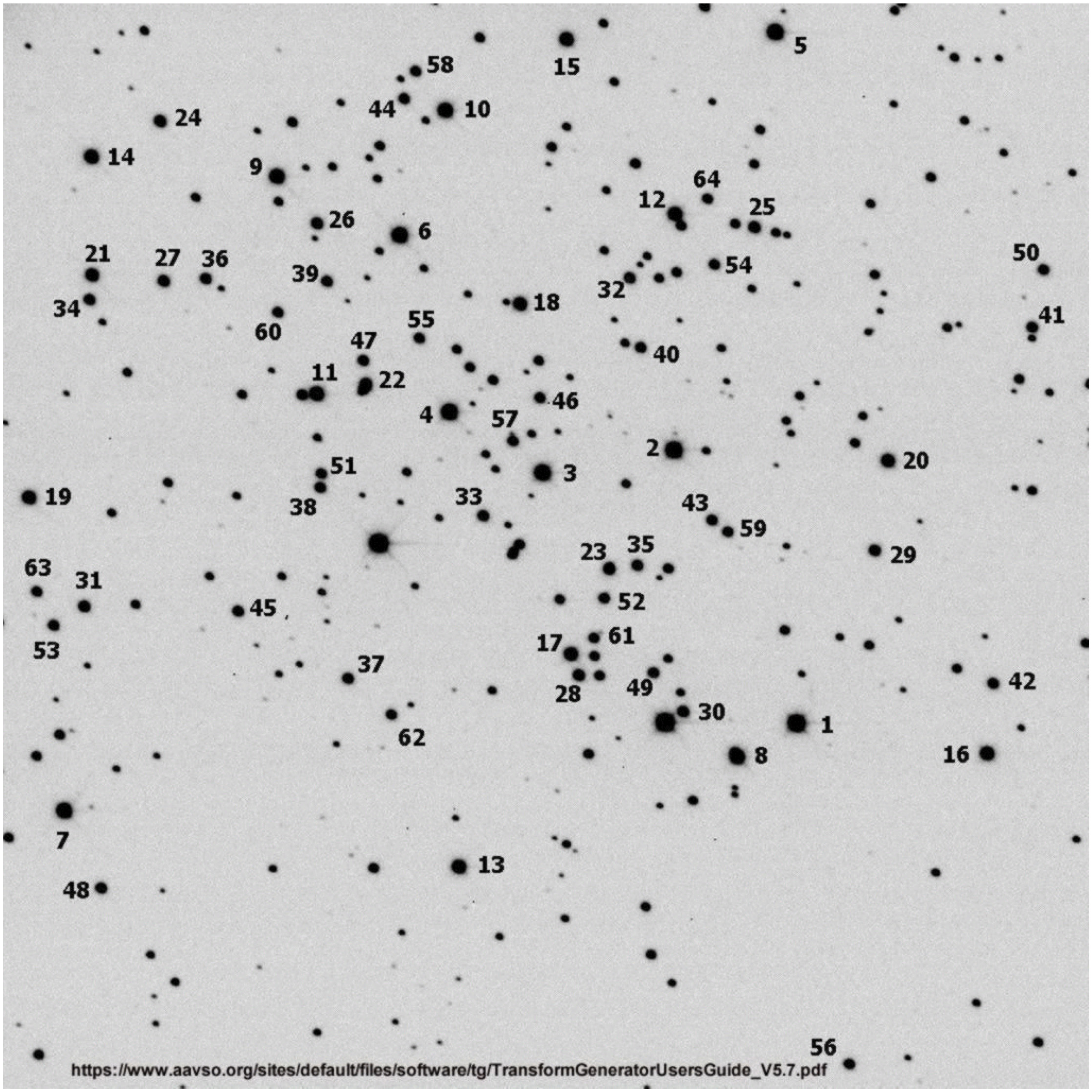

https://www.aavso.org/sites/default/files/software/tg/TransformGeneratorUsersGuide_V5.7.pdf

Figure 10. M-67 field with original Boulder swri numbers (AAVSO 2016). Fifteen Boulder swri number stars have been culled by AAVSO from the current VSP data. These are stars 1, 8, 9, 18, 22, 26, 32, 35, 45, 46, 49, 52, 55, 61, 62 (April 2016). Note: Star 56 was out of the author's image frame and was not measured.

## Appendix B: Correlation key for M-67

Correlation key for M-67 AAVSO VSP AUID to Boulder swri numbers (Myers 2016). The AAVSO VSP stars labled "000-000-000" are culled from original Henden (2000) M-67 Stars.

| *swri Number* | *AUID* | *swri Number* | *AUID* | *swri Number* | *AUID* | *swri Number* | *AUID* |
|---|---|---|---|---|---|---|---|
| 1 | 000-000-000 | 17 | 000-BLG-899 | 33 | 000-BLG-911 | 49 | 000-000-000 |
| 2 | 000-BLG-886 | 18 | 000-000-000 | 34 | 000-BLG-912 | 50 | 000-BLG-925 |
| 3 | 000-BLG-887 | 19 | 000-BLG-900 | 35 | 000-000-000 | 51 | 000-BLG-926 |
| 4 | 000-BLG-888 | 20 | 000-BLG-901 | 36 | 000-BLG-913 | 52 | 000-000-000 |
| 5 | 000-BLG-889 | 21 | 000-BLG-902 | 37 | 000-BLG-914 | 53 | 000-BLG-927 |
| 6 | 000-BLG-890 | 22 | 000-000-000 | 38 | 000-BLG-915 | 54 | 000-BLG-928 |
| 7 | 000-BLG-891 | 23 | 000-BLG-903 | 39 | 000-BLG-916 | 55 | 000-000-000 |
| 8 | 000-000-000 | 24 | 000-BLG-904 | 40 | 000-BLG-917 | 56 | 000-BLG-929 |
| 9 | 000-000-000 | 25 | 000-BLG-905 | 42 | 000-BLG-918 | 57 | 000-BLG-930 |
| 10 | 000-BLG-892 | 26 | 000-000-000 | 41 | 000-BLG-919 | 58 | 000-BLG-931 |
| 11 | 000-BLG-893 | 27 | 000-BLG-906 | 43 | 000-BLG-920 | 59 | 000-BLG-932 |
| 12 | 000-BLG-894 | 28 | 000-BLG-907 | 44 | 000-BLG-921 | 60 | 000-BLG-934 |
| 13 | 000-BLG-895 | 29 | 000-BLG-908 | 45 | 000-000-000 | 61 | 000-000-000 |
| 14 | 000-BLG-896 | 30 | 000-BLG-909 | 46 | 000-000-000 | 62 | 000-000-000 |
| 15 | 000-BLG-897 | 31 | 000-BLG-910 | 47 | 000-BLG-923 | 63 | 000-BLG-935 |
| 16 | 000-BLG-898 | 32 | 000-000-000 | 48 | 000-BLG-924 | 64 | 000-BLG-936 |

## Appendix C: Data on M-67 stars

AAVSO M-67 data (April 2016); Boulder swri number Henden (2000). Data taken from VSP Field photometry for EV Cnc; Sequence X16215DHF.

| | *Measured Instr Magnitudes (average of 6 20-sec exposures)* | | | | | *Calibrated and Culled AAVSO M-67 Stars* | | | | *Average Errors; vsp* | | | |
|---|---|---|---|---|---|---|---|---|---|---|---|---|---|
| *Bldr swri* | *Airmas 1.2* | *Airmas 1.4* | *Airmas 1.6* | *Airmas 2.0* | *VSP AUID* | *B* | *V* | *Rc* | *Ic* | *0.02 B err* | *0.017 V err* | *0.019 Rc err* | *0.023 Ic err* |
| 1 | 9.285 | 9.49 | 9.71 | 9.735 | — | star culled from swri tlist | | | | — | — | — | — |
| 2 | 9.024 | 9.2 | 9.401 | 9.412 | 000-BLG-886 | 11.553 | 10.289 | 9.626 | 9.063 | 0.023 | 0.016 | 0.021 | 0.027 |
| 3 | 9.278 | 9.458 | 9.656 | 9.673 | 000-BLG-887 | 11.562 | 10.453 | 9.886 | 9.386 | 0.018 | 0.014 | 0.016 | 0.020 |
| 4 | 9.512 | 9.696 | 9.899 | 9.912 | 000-BLG-888 | 11.064 | 10.489 | 10.149 | 9.822 | 0.016 | 0.013 | 0.015 | 0.021 |
| 5 | 9.368 | 9.536 | 9.729 | 9.748 | 000-BLG-889 | 11.617 | 10.524 | 9.961 | 9.471 | 0.023 | 0.016 | 0.020 | 0.022 |
| 6 | 9.347 | 9.526 | 9.722 | 9.742 | 000-BLG-890 | 11.656 | 10.533 | 9.952 | 9.438 | 0.018 | 0.012 | 0.014 | 0.017 |
| 7 | 9.549 | 9.732 | 9.926 | 9.927 | 000-BLG-891 | 11.898 | 10.763 | 10.185 | 9.657 | 0.019 | 0.016 | 0.020 | 0.023 |
| 8 | 9.986 | 10.183 | 10.396 | 10.408 | — | star culled from swri tlist | | | | — | — | — | — |
| 9 | 10.108 | 10.298 | 10.487 | 10.517 | — | star culled from swri tlist | | | | — | — | — | — |
| 10 | 10.19 | 10.377 | 10.59 | 10.609 | 000-BLG-892 | 11.042 | 10.946 | 10.902 | 10.844 | 0.021 | 0.019 | 0.022 | 0.024 |
| 11 | 10.241 | 10.428 | 10.635 | 10.66 | 000-BLG-893 | 11.283 | 11.064 | 10.948 | 10.82 | 0.019 | 0.017 | 0.020 | 0.024 |
| 12 | 9.968 | 10.142 | 10.339 | 10.353 | 000-BLG-894 | 12.221 | 11.132 | 10.56 | 10.059 | 0.018 | 0.014 | 0.017 | 0.021 |
| 13 | 10.478 | 10.678 | 10.894 | 10.911 | 000-BLG-895 | 11.391 | 11.263 | 11.215 | 11.146 | 0.019 | 0.016 | 0.017 | 0.023 |
| 14 | 10.093 | 10.268 | 10.463 | 10.469 | 000-BLG-896 | 12.342 | 11.266 | 10.697 | 10.187 | 0.016 | 0.012 | 0.016 | 0.020 |
| 15 | 10.31 | 10.488 | 10.692 | 10.709 | 000-BLG-897 | 11.911 | 11.305 | 10.945 | 10.609 | 0.020 | 0.013 | 0.018 | 0.020 |
| 16 | 10.482 | 10.683 | 10.903 | 10.918 | 000-BLG-898 | 11.604 | 11.314 | 11.149 | 10.988 | 0.020 | 0.017 | 0.021 | 0.025 |
| 17 | 10.269 | 10.454 | 10.652 | 10.661 | 000-BLG-899 | 12.500 | 11.427 | 10.867 | 10.376 | 0.017 | 0.014 | 0.016 | 0.020 |
| 18 | 10.396 | 10.575 | 10.773 | 10.787 | — | star culled from swri tlist | | | | — | — | — | — |
| 19 | 10.324 | 10.506 | 10.697 | 10.705 | 000-BLG-900 | 12.546 | 11.494 | 10.941 | 10.442 | 0.016 | 0.011 | 0.014 | 0.017 |
| 20 | 10.644 | 10.837 | 11.041 | 11.059 | 000-BLG-901 | 11.949 | 11.544 | 11.293 | 11.050 | 0.017 | 0.014 | 0.017 | 0.021 |
| 21 | 10.47 | 10.652 | 10.844 | 10.852 | 000-BLG-902 | 12.686 | 11.636 | 11.081 | 10.580 | 0.017 | 0.012 | 0.015 | 0.020 |
| 22 | 10.707 | 10.895 | 11.097 | 11.100 | — | star culled from swri tlist | | | | — | — | — | — |
| 23 | 11.192 | 11.384 | 11.593 | 11.601 | 000-BLG-903 | 12.572 | 12.116 | 11.835 | 11.566 | 0.016 | 0.013 | 0.015 | 0.020 |
| 24 | 11.003 | 11.174 | 11.369 | 11.375 | 000-BLG-904 | 13.138 | 12.138 | 11.602 | 11.122 | 0.016 | 0.012 | 0.018 | 0.021 |
| 25 | 11.232 | 11.409 | 11.62 | 11.627 | 000-BLG-905 | 12.883 | 12.213 | 11.83 | 11.477 | 0.016 | 0.012 | 0.014 | 0.018 |
| 26 | 11.402 | 11.604 | 11.804 | 11.822 | — | star culled from swri tlist | | | | — | — | — | — |
| 27 | 11.273 | 11.457 | 11.659 | 11.664 | 000-BLG-906 | 12.808 | 12.246 | 11.914 | 11.588 | 0.016 | 0.013 | 0.016 | 0.021 |
| 28 | 11.317 | 11.515 | 11.723 | 11.743 | 000-BLG-907 | 12.823 | 12.254 | 11.917 | 11.599 | 0.017 | 0.015 | 0.019 | 0.020 |
| 29 | 11.266 | 11.451 | 11.656 | 11.660 | 000-BLG-908 | 13.359 | 12.38 | 11.86 | 11.409 | 0.016 | 0.013 | 0.015 | 0.021 |
| 30 | 11.337 | 11.525 | 11.723 | 11.738 | 000-BLG-909 | 13.136 | 12.392 | 11.965 | 11.571 | 0.016 | 0.011 | 0.015 | 0.020 |
| 31 | 11.406 | 11.602 | 11.799 | 11.803 | 000-BLG-910 | 12.971 | 12.41 | 12.069 | 11.716 | 0.016 | 0.013 | 0.015 | 0.018 |
| 32 | 11.579 | 11.765 | 11.963 | 11.977 | — | star culled from swri tlist | | | | — | — | — | — |
| 33 | 11.557 | 11.747 | 11.947 | 11.961 | 000-BLG-911 | 13.129 | 12.54 | 12.194 | 11.860 | 0.021 | 0.018 | 0.020 | 0.026 |
| 34 | 11.58 | 11.758 | 11.969 | 11.973 | 000-BLG-912 | 13.139 | 12.56 | 12.216 | 11.876 | 0.022 | 0.019 | 0.022 | 0.024 |
| 35 | 11.516 | 11.707 | 11.911 | 11.916 | — | star culled from swri tlist | | | | — | — | — | — |
| 36 | 11.612 | 11.789 | 12.001 | 12.004 | 000-BLG-913 | 13.171 | 12.589 | 12.242 | 11.909 | 0.022 | 0.02 | 0.022 | 0.024 |
| 37 | 11.635 | 11.829 | 12.027 | 12.039 | 000-BLG-914 | 13.191 | 12.623 | 12.287 | 11.953 | 0.024 | 0.021 | 0.022 | 0.025 |
| 38 | 11.62 | 11.804 | 12.001 | 12.013 | 000-BLG-915 | 13.241 | 12.629 | 12.272 | 11.925 | 0.022 | 0.02 | 0.022 | 0.023 |
| 39 | 11.659 | 11.842 | 12.042 | 12.055 | 000-BLG-916 | 13.215 | 12.633 | 12.29 | 11.961 | 0.022 | 0.019 | 0.021 | 0.023 |
| 40 | 11.664 | 11.852 | 12.058 | 12.074 | 000-BLG-917 | 13.246 | 12.64 | 12.285 | 11.96 | 0.022 | 0.019 | 0.021 | 0.024 |
| 41 | 11.675 | 11.86 | 12.06 | 12.065 | 000-BLG-918 | 13.263 | 12.652 | 12.299 | 11.975 | 0.023 | 0.019 | 0.022 | 0.025 |
| 42 | 11.682 | 11.885 | 12.084 | 12.101 | 000-BLG-919 | 13.271 | 12.653 | 12.298 | 11.975 | 0.021 | 0.019 | 0.021 | 0.024 |
| 43 | 11.738 | 11.936 | 12.136 | 12.153 | 000-BLG-920 | 13.166 | 12.665 | 12.367 | 12.092 | 0.022 | 0.019 | 0.021 | 0.023 |
| 44 | 11.684 | 11.864 | 12.064 | 12.071 | 000-BLG-921 | 13.339 | 12.672 | 12.285 | 11.927 | 0.021 | 0.019 | 0.021 | 0.024 |
| 45 | 11.651 | 11.835 | 12.037 | 12.047 | 000-BLG-922 | star culled from swri tlist | | | | — | — | — | — |
| 46 | 11.734 | 11.921 | 12.118 | 12.134 | — | star culled from swri tlist | | | | — | — | — | — |
| 47 | 11.716 | 11.899 | 12.096 | 12.119 | 000-BLG-923 | 13.280 | 12.692 | 12.344 | 12.01 | 0.023 | 0.020 | 0.023 | 0.025 |
| 48 | 11.715 | 11.91 | 12.11 | 12.114 | 000-BLG-924 | 13.278 | 12.708 | 12.378 | 12.049 | 0.022 | 0.019 | 0.022 | 0.024 |
| 49 | 11.762 | 11.952 | 12.158 | 12.171 | — | star culled from swri tlist | | | | — | — | — | — |
| 50 | 11.721 | 11.908 | 12.096 | 12.129 | 000-BLG-925 | 13.468 | 12.731 | 12.311 | 11.945 | 0.021 | 0.019 | 0.021 | 0.024 |
| 51 | 11.661 | 11.853 | 12.048 | 12.051 | 000-BLG-926 | 13.57 | 12.752 | 12.303 | 11.89 | 0.023 | 0.021 | 0.023 | 0.025 |
| 52 | 11.796 | 11.989 | 12.189 | 12.210 | — | star culled from swri tlist | | | | — | — | — | — |
| 53 | 11.728 | 11.925 | 12.113 | 12.125 | 000-BLG-927 | 13.513 | 12.772 | 12.364 | 11.972 | 0.022 | 0.019 | 0.021 | 0.022 |
| 54 | 11.847 | 12.024 | 12.222 | 12.246 | 000-BLG-928 | 13.349 | 12.79 | 12.459 | 12.149 | 0.020 | 0.018 | 0.02 | 0.024 |
| 55 | 11.925 | 11.99 | 12.199 | 12.241 | — | star culled from swri tlist | | | | — | — | — | — |
| 56 | - | - | - | - | 000-BLG-929 | out of image not measured | | | | — | — | — | — |
| 57 | 11.847 | 12.034 | 12.243 | 12.259 | 000-BLG-930 | 13.386 | 12.815 | 12.478 | 12.155 | 0.022 | 0.019 | 0.022 | 0.024 |
| 58 | 11.856 | 12.041 | 12.236 | 12.261 | 000-BLG-931 | 13.376 | 12.819 | 12.481 | 12.160 | 0.023 | 0.019 | 0.022 | 0.025 |
| 59 | 11.862 | 12.06 | 12.264 | 12.276 | 000-BLG-932 | 13.378 | 12.821 | 12.489 | 12.187 | 0.023 | 0.021 | 0.023 | 0.025 |
| 60 | 11.891 | 12.078 | 12.274 | 12.291 | 000-BLG-934 | 13.380 | 12.854 | 12.533 | 12.221 | 0.021 | 0.019 | 0.021 | 0.025 |
| 61 | 11.971 | 12.177 | 12.38 | 12.389 | — | star culled from swri tlist | | | | — | — | — | — |
| 62 | 11.792 | 11.977 | 12.186 | 12.186 | — | star culled from swri tlist | | | | — | — | — | — |
| 63 | 11.845 | 12.031 | 12.231 | 12.244 | 000-BLG-935 | 13.871 | 12.958 | 12.470 | 12.015 | 0.024 | 0.02 | 0.023 | 0.025 |
| 64 | 11.938 | 12.102 | 12.307 | 12.317 | 000-BLG-936 | 13.835 | 12.986 | 12.521 | 12.109 | 0.022 | 0.02 | 0.022 | 0.024 |

## Appendix D: Unfiltered instrumental magnitudes transformed to “standard” B, V, Rc, Ic magnitudes

Unfiltered instrumental magnitudes for 48 Calibrated Stars transformed to “standard” B, V, Rc, Ic magnitudes (b, v, r, i) for air mass (X) of 1.2, 1.4, 1.6, and 2.0. “—” in column 2 indicates culled reference star.

| | | | | | | Magnitudes Derived from Unfiltered Image Instrumental Magnitudes (Imag) | | | | | | | | | | | | | | | | | | | |
|---|---|---|---|---|---|---|---|---|---|---|---|---|---|---|---|---|---|---|---|---|---|---|---|---|---|
| Bldr | M-67 | Reference Magnitudes | | | | X=1.2 | Derived Mags | | | | X=1.4 | Derived Mags | | | | X=1.6 | Derived Mags | | | | X=2.0 | Derived Mags | | | |
| swri | VSP AUID | B | V | Rc | Ic | Imag | b | v | r | i | Imag | b | v | r | i | Imag | b | v | r | i | Imag | b | v | r | i |
| 1 | — | | | | | | | | | | | | | | | | | | | | | | | | |
| 2 | 000-BLG-886 | 11.553 | 10.289 | 9.626 | 9.063 | 9.024 | 11.534 | 10.27 | 9.624 | 9.061 | 9.200 | 11.536 | 10.272 | 9.623 | 9.062 | 9.401 | 11.542 | 10.278 | 9.630 | 9.068 | 9.412 | 11.543 | 10.279 | 9.631 | 9.069 |
| 3 | 000-BLG-887 | 11.562 | 10.453 | 9.886 | 9.386 | 9.278 | 11.570 | 10.46 | 9.890 | 9.390 | 9.458 | 11.573 | 10.464 | 9.892 | 9.393 | 9.656 | 11.574 | 10.465 | 9.892 | 9.393 | 9.673 | 11.58 | 10.471 | 9.898 | 9.399 |
| 4 | 000-BLG-888 | 11.064 | 10.489 | 10.149 | 9.822 | 9.512 | 11.053 | 10.478 | 10.163 | 9.836 | 9.696 | 11.051 | 10.476 | 10.173 | 9.836 | 9.899 | 11.048 | 10.473 | 10.169 | 9.834 | 9.912 | 11.045 | 10.470 | 10.167 | 9.833 |
| 5 | 000-BLG-889 | 11.617 | 10.524 | 9.961 | 9.471 | 9.368 | 11.638 | 10.545 | 9.982 | 9.492 | 9.536 | 11.628 | 10.535 | 9.970 | 9.482 | 9.729 | 11.624 | 10.531 | 9.966 | 9.477 | 9.748 | 11.632 | 10.539 | 9.973 | 9.485 |
| 6 | 000-BLG-890 | 11.656 | 10.533 | 9.952 | 9.438 | 9.347 | 11.659 | 10.536 | 9.955 | 9.441 | 9.526 | 11.662 | 10.539 | 9.958 | 9.444 | 9.722 | 11.661 | 10.538 | 9.957 | 9.443 | 9.742 | 11.669 | 10.546 | 9.9650 | 9.451 |
| 7 | 000-BLG-891 | 11.898 | 10.763 | 10.185 | 9.657 | 9.549 | 11.879 | 10.744 | 10.152 | 9.624 | 9.732 | 11.885 | 10.750 | 10.159 | 9.630 | 9.926 | 11.882 | 10.747 | 10.157 | 9.628 | 9.927 | 11.872 | 10.737 | 10.147 | 9.619 |
| 8 | — | | | | | | | | | | | | | | | | | | | | | | | | |
| 9 | — | | | | | | | | | | | | | | | | | | | | | | | | |
| 10 | 000-BLG-892 | 11.042 | 10.946 | 10.902 | 10.844 | 10.19 | 11.058 | 10.962 | 10.899 | 10.841 | 10.377 | 11.050 | 10.954 | 10.886 | 10.832 | 10.590 | 11.05 | 10.954 | 10.885 | 10.830 | 10.609 | 11.050 | 10.954 | 10.885 | 10.829 |
| 11 | 000-BLG-893 | 11.283 | 11.064 | 10.948 | 10.820 | 10.241 | 11.283 | 11.064 | 10.933 | 10.805 | 10.428 | 11.276 | 11.057 | 10.925 | 10.799 | 10.635 | 11.273 | 11.054 | 10.921 | 10.794 | 10.660 | 11.279 | 11.060 | 10.927 | 10.799 |
| 12 | 000-BLG-894 | 12.221 | 11.132 | 10.560 | 10.059 | 9.968 | 12.233 | 11.144 | 10.573 | 10.072 | 10.142 | 12.229 | 11.140 | 10.567 | 10.068 | 10.339 | 12.230 | 11.141 | 10.568 | 10.068 | 10.353 | 12.233 | 11.144 | 10.571 | 10.072 |
| 13 | 000-BLG-895 | 11.391 | 11.263 | 11.215 | 11.146 | 10.478 | 11.391 | 11.263 | 11.182 | 11.113 | 10.678 | 11.397 | 11.269 | 11.180 | 11.117 | 10.894 | 11.401 | 11.273 | 11.183 | 11.119 | 10.911 | 11.399 | 11.271 | 11.181 | 11.115 |
| 14 | 000-BLG-896 | 12.342 | 11.266 | 10.697 | 10.187 | 10.093 | 12.340 | 11.264 | 10.695 | 10.185 | 10.268 | 12.337 | 11.261 | 10.692 | 10.182 | 10.463 | 12.335 | 11.259 | 10.691 | 10.181 | 10.469 | 12.331 | 11.255 | 10.687 | 10.177 |
| 15 | 000-BLG-897 | 11.911 | 11.305 | 10.945 | 10.609 | 10.310 | 11.896 | 11.290 | 10.952 | 10.616 | 10.488 | 11.887 | 11.281 | 10.950 | 10.608 | 10.692 | 11.887 | 11.281 | 10.950 | 10.609 | 10.709 | 11.889 | 11.283 | 10.952 | 10.612 |
| 16 | 000-BLG-898 | 11.604 | 11.314 | 11.149 | 10.988 | 10.482 | 11.623 | 11.333 | 11.164 | 11.003 | 10.683 | 11.632 | 11.342 | 11.170 | 11.011 | 10.903 | 11.643 | 11.353 | 11.181 | 11.021 | 10.918 | 11.641 | 11.351 | 11.178 | 11.018 |
| 17 | 000-BLG-899 | 12.500 | 11.427 | 10.867 | 10.376 | 10.269 | 12.511 | 11.438 | 10.874 | 10.383 | 10.454 | 12.518 | 11.445 | 10.876 | 10.389 | 10.652 | 12.520 | 11.447 | 10.878 | 10.390 | 10.661 | 12.520 | 11.447 | 10.877 | 10.389 |
| 10 | — | | | | | | | | | | | | | | | | | | | | | | | | |
| 19 | 000-BLG-900 | 12.546 | 11.494 | 10.941 | 10.442 | 10.324 | 12.538 | 11.486 | 10.927 | 10.428 | 10.506 | 12.541 | 11.489 | 10.930 | 10.431 | 10.697 | 12.535 | 11.483 | 10.924 | 10.425 | 10.705 | 12.532 | 11.480 | 10.921 | 10.423 |
| 20 | 000-BLG-901 | 11.949 | 11.544 | 11.293 | 11.050 | 10.644 | 11.947 | 11.542 | 11.304 | 11.061 | 10.837 | 11.950 | 11.545 | 11.312 | 11.065 | 11.041 | 11.947 | 11.542 | 11.309 | 11.062 | 11.059 | 11.949 | 11.544 | 11.311 | 11.065 |
| 21 | 000-BLG-902 | 12.686 | 11.636 | 11.081 | 10.580 | 10.470 | 12.681 | 11.631 | 11.071 | 10.570 | 10.652 | 12.684 | 11.634 | 11.073 | 10.572 | 10.844 | 12.680 | 11.630 | 11.07 | 10.569 | 10.852 | 12.677 | 11.627 | 11.067 | 10.567 |
| 22 | — | | | | | | | | | | | | | | | | | | | | | | | | |
| 23 | 000-BLG-903 | 12.572 | 12.116 | 11.835 | 11.566 | 11.192 | 12.568 | 12.112 | 11.841 | 11.572 | 11.384 | 12.571 | 12.115 | 11.847 | 11.576 | 11.593 | 12.574 | 12.118 | 11.850 | 11.580 | 11.601 | 12.567 | 12.111 | 11.843 | 11.572 |
| 24 | 000-BLG-904 | 13.138 | 12.138 | 11.602 | 11.122 | 11.003 | 13.144 | 12.144 | 11.604 | 11.124 | 11.174 | 13.135 | 12.135 | 11.592 | 11.114 | 11.369 | 13.134 | 12.134 | 11.592 | 11.114 | 11.375 | 13.130 | 12.130 | 11.588 | 11.110 |
| 25 | 000-BLG-905 | 12.883 | 12.213 | 11.830 | 11.477 | 11.232 | 12.909 | 12.239 | 11.861 | 11.508 | 11.409 | 12.901 | 12.231 | 11.853 | 11.500 | 11.620 | 12.910 | 12.24 | 11.863 | 11.509 | 11.627 | 12.904 | 12.234 | 11.857 | 11.503 |
| 26 | — | | | | | | | | | | | | | | | | | | | | | | | | |
| 27 | 000-BLG-906 | 12.808 | 12.246 | 11.914 | 11.588 | 11.273 | 12.799 | 12.237 | 11.908 | 11.582 | 11.457 | 12.794 | 12.232 | 11.909 | 11.579 | 11.659 | 12.794 | 12.232 | 11.909 | 11.579 | 11.664 | 12.785 | 12.223 | 11.900 | 11.571 |
| 28 | 000-BLG-907 | 12.823 | 12.254 | 11.917 | 11.599 | 11.317 | 12.852 | 12.283 | 11.954 | 11.636 | 11.515 | 12.862 | 12.293 | 11.965 | 11.646 | 11.723 | 12.867 | 12.298 | 11.971 | 11.651 | 11.743 | 12.874 | 12.305 | 11.977 | 11.658 |
| 29 | 000-BLG-908 | 13.359 | 12.380 | 11.860 | 11.409 | 11.266 | 13.378 | 12.399 | 11.871 | 11.420 | 11.451 | 13.383 | 12.404 | 11.867 | 11.423 | 11.656 | 13.392 | 12.413 | 11.876 | 11.431 | 11.660 | 13.385 | 12.406 | 11.87 | 11.424 |
| 30 | 000-BLG-909 | 13.136 | 12.392 | 11.965 | 11.571 | 11.337 | 13.118 | 12.374 | 11.955 | 11.561 | 11.525 | 13.121 | 12.377 | 11.960 | 11.564 | 11.723 | 13.120 | 12.376 | 11.959 | 11.564 | 11.738 | 13.123 | 12.379 | 11.961 | 11.566 |
| 31 | 000-BLG-910 | 12.971 | 12.410 | 12.069 | 11.716 | 11.406 | 12.930 | 12.369 | 12.034 | 11.681 | 11.602 | 12.938 | 12.377 | 12.052 | 11.690 | 11.799 | 12.932 | 12.371 | 12.046 | 11.686 | 11.803 | 12.922 | 12.361 | 12.037 | 11.678 |
| 32 | — | | | | | | | | | | | | | | | | | | | | | | | | |
| 33 | 000-BLG-911 | 13.129 | 12.54 | 12.194 | 11.860 | 11.557 | 13.121 | 12.532 | 12.188 | 11.854 | 11.747 | 13.123 | 12.534 | 12.192 | 11.856 | 11.947 | 13.121 | 12.532 | 12.191 | 11.855 | 11.961 | 13.122 | 12.533 | 12.192 | 11.856 |
| 34 | 000-BLG-912 | 13.139 | 12.56 | 12.216 | 11.876 | 11.580 | 13.130 | 12.551 | 12.209 | 11.869 | 11.758 | 13.120 | 12.541 | 12.204 | 11.860 | 11.969 | 13.129 | 12.550 | 12.213 | 11.870 | 11.973 | 13.119 | 12.540 | 12.204 | 11.861 |
| 35 | — | | | | | | | | | | | | | | | | | | | | | | | | |
| 36 | 000-BLG-913 | 13.171 | 12.589 | 12.242 | 11.909 | 11.612 | 13.166 | 12.584 | 12.242 | 11.909 | 11.789 | 13.155 | 12.573 | 12.235 | 11.899 | 12.001 | 13.165 | 12.583 | 12.245 | 11.91 | 12.004 | 13.155 | 12.573 | 12.235 | 11.900 |
| 37 | 000-BLG-914 | 13.191 | 12.623 | 12.287 | 11.953 | 11.635 | 13.169 | 12.601 | 12.265 | 11.931 | 11.829 | 13.175 | 12.607 | 12.275 | 11.937 | 12.027 | 13.171 | 12.603 | 12.271 | 11.934 | 12.039 | 13.169 | 12.601 | 12.269 | 11.933 |
| 38 | 000-BLG-915 | 13.241 | 12.629 | 12.272 | 11.925 | 11.62 | 13.216 | 12.604 | 12.247 | 11.900 | 11.804 | 13.213 | 12.601 | 12.247 | 11.897 | 12.001 | 13.209 | 12.597 | 12.243 | 11.894 | 12.013 | 13.208 | 12.596 | 12.242 | 11.893 |
| 39 | 000-BLG-916 | 13.215 | 12.633 | 12.29 | 11.961 | 11.659 | 13.213 | 12.631 | 12.29 | 11.961 | 11.842 | 13.209 | 12.627 | 12.287 | 11.957 | 12.042 | 13.206 | 12.624 | 12.285 | 11.954 | 12.055 | 13.206 | 12.624 | 12.285 | 11.955 |
| 40 | 000-BLG-917 | 13.246 | 12.640 | 12.285 | 11.960 | 11.664 | 13.251 | 12.645 | 12.295 | 11.970 | 11.852 | 13.252 | 12.646 | 12.294 | 11.971 | 12.058 | 13.256 | 12.65 | 12.299 | 11.975 | 12.074 | 13.260 | 12.654 | 12.303 | 11.979 |
| 41 | 000-BLG-918 | 13.263 | 12.652 | 12.299 | 11.975 | 11.675 | 13.269 | 12.658 | 12.306 | 11.982 | 11.86 | 13.267 | 12.656 | 12.301 | 11.980 | 12.06 | 13.265 | 12.654 | 12.300 | 11.978 | 12.065 | 13.258 | 12.647 | 12.293 | 11.971 |
| 42 | 000-BLG-919 | 13.271 | 12.653 | 12.298 | 11.975 | 11.682 | 13.286 | 12.668 | 12.314 | 11.991 | 11.885 | 13.302 | 12.684 | 12.325 | 12.006 | 12.084 | 13.300 | 12.682 | 12.324 | 12.003 | 12.101 | 13.304 | 12.686 | 12.328 | 12.007 |
| 43 | 000-BLG-920 | 13.166 | 12.665 | 12.367 | 12.092 | 11.738 | 13.178 | 12.677 | 12.381 | 12.106 | 11.936 | 13.186 | 12.685 | 12.386 | 12.114 | 12.136 | 13.183 | 12.682 | 12.383 | 12.110 | 12.153 | 13.186 | 12.685 | 12.386 | 12.113 |
| 44 | 000-BLG-921 | 13.339 | 12.672 | 12.285 | 11.927 | 11.684 | 13.357 | 12.690 | 12.308 | 11.950 | 11.864 | 13.351 | 12.684 | 12.300 | 11.943 | 12.064 | 13.351 | 12.684 | 12.301 | 11.943 | 12.071 | 13.345 | 12.678 | 12.296 | 11.938 |
| 45 | — | | | | | | | | | | | | | | | | | | | | | | | | |
| 46 | — | | | | | | | | | | | | | | | | | | | | | | | | |
| 47 | 000-BLG-923 | 13.28 | 12.692 | 12.344 | 12.010 | 11.716 | 13.278 | 12.690 | 12.345 | 12.011 | 11.899 | 13.274 | 12.686 | 12.342 | 12.007 | 12.096 | 13.269 | 12.681 | 12.338 | 12.002 | 12.119 | 13.278 | 12.69 | 12.347 | 12.012 |
| 48 | 000-BLG-924 | 13.278 | 12.708 | 12.378 | 12.049 | 11.715 | 13.252 | 12.682 | 12.346 | 12.017 | 11.910 | 13.259 | 12.689 | 12.354 | 12.023 | 12.11 | 13.256 | 12.686 | 12.353 | 12.022 | 12.114 | 13.248 | 12.678 | 12.344 | 12.013 |
| 49 | — | | | | | | | | | | | | | | | | | | | | | | | | |
| 50 | 000-BLG-925 | 13.468 | 12.731 | 12.311 | 11.945 | 11.721 | 13.493 | 12.756 | 12.342 | 11.976 | 11.908 | 13.495 | 12.758 | 12.338 | 11.977 | 12.096 | 13.484 | 12.747 | 12.328 | 11.966 | 12.129 | 13.505 | 12.768 | 12.349 | 11.986 |
| 51 | 000-BLG-926 | 13.570 | 12.752 | 12.303 | 11.890 | 11.661 | 13.546 | 12.728 | 12.271 | 11.858 | 11.853 | 13.555 | 12.737 | 12.277 | 11.866 | 12.048 | 13.552 | 12.734 | 12.274 | 11.863 | 12.051 | 13.545 | 12.727 | 12.267 | 11.856 |
| 52 | — | | | | | | | | | | | | | | | | | | | | | | | | |
| 53 | 000-BLG-927 | 13.513 | 12.772 | 12.364 | 11.972 | 11.728 | 13.505 | 12.764 | 12.343 | 11.951 | 11.925 | 13.518 | 12.777 | 12.355 | 11.963 | 12.113 | 13.506 | 12.765 | 12.344 | 11.952 | 12.125 | 13.507 | 12.766 | 12.344 | 11.952 |
| 54 | 000-BLG-928 | 13.349 | 12.790 | 12.459 | 12.149 | 11.847 | 13.369 | 12.810 | 12.481 | 12.171 | 12.024 | 13.358 | 12.799 | 12.468 | 12.159 | 12.222 | 13.353 | 12.794 | 12.464 | 12.155 | 12.246 | 13.364 | 12.805 | 12.475 | 12.166 |
| 55 | — | | | | | | | | | | | | | | | | | | | | | | | | |
| 56 | 000-BLG-929 | Out of Frame Not Measured | | | | | | | | | | | | | | | | | | | | | | | |
| 57 | 000-BLG-930 | 13.386 | 12.815 | 12.478 | 12.155 | 11.847 | 13.385 | 12.814 | 12.477 | 12.154 | 12.034 | 13.385 | 12.814 | 12.477 | 12.154 | 12.243 | 13.392 | 12.821 | 12.485 | 12.161 | 12.259 | 13.395 | 12.824 | 12.487 | 12.164 |
| 58 | 000-BLG-931 | 13.376 | 12.819 | 12.481 | 12.160 | 11.856 | 13.374 | 12.817 | 12.486 | 12.165 | 12.041 | 13.372 | 12.815 | 12.485 | 12.163 | 12.236 | 13.365 | 12.808 | 12.479 | 12.156 | 12.261 | 13.377 | 12.82 | 12.49 | 12.169 |
| 59 | 000-BLG-932 | 13.378 | 12.821 | 12.489 | 12.187 | 11.862 | 13.381 | 12.824 | 12.497 | 12.195 | 12.060 | 13.390 | 12.833 | 12.503 | 12.204 | 12.264 | 13.393 | 12.836 | 12.506 | 12.206 | 12.276 | 13.391 | 12.834 | 12.505 | 12.204 |
| 60 | 000-BLG-934 | 13.380 | 12.854 | 12.533 | 12.221 | 11.891 | 13.366 | 12.840 | 12.524 | 12.212 | 12.078 | 13.365 | 12.839 | 12.524 | 12.210 | 12.274 | 13.358 | 12.832 | 12.518 | 12.205 | 12.291 | 13.362 | 12.836 | 12.522 | 12.208 |
| 61 | — | | | | | | | | | | | | | | | | | | | | | | | | |
| 62 | — | | | | | | | | | | | | | | | | | | | | | | | | |
| 63 | 000-BLG-935 | 13.871 | 12.958 | 12.47 | 12.015 | 11.845 | 13.864 | 12.951 | 12.444 | 11.989 | 12.031 | 13.869 | 12.956 | 12.444 | 11.992 | 12.231 | 13.873 | 12.960 | 12.449 | 11.996 | 12.244 | 13.875 | 12.962 | 12.451 | 11.999 |
| 64 | 000-BLG-936 | 13.835 | 12.986 | 12.521 | 12.109 | 11.938 | 13.868 | 13.019 | 12.546 | 12.134 | 12.102 | 13.849 | 13.000 | 12.520 | 12.114 | 12.307 | 13.856 | 13.007 | 12.528 | 12.121 | 12.317 | 13.856 | 13.007 | 12.528 | 12.121 |

## Appendix E: Determination of target star Ci

It is possible to use two images taken with different filters and the spreadsheet process described above to determine a color index for the target star (Dunckel 2014). Making two different filtered images of the subject star field such as B and V, the color index (B–V) can be calculated. The filtered images are photometrically processed just like the unfiltered images, giving Imag_B and Imag_V. Two spreadsheets are set up using the catalogued magnitudes, one for B and the other for V. The two filtered instrumental magnitude sets are used as the data source (Imag_B) for the B spreadsheet, and (Imag_V) for the V spreadsheet. Using the spreadsheets, the two filtered data sets are each processed using the same "test" value for the color index of the target star at cells {C8}, Figure 3. In one of the spreadsheets, a cell is set to calculate the derived (b–v) value. The value (b) is from the B spreadsheet and (v) from the V spreadsheet at cells {C10}, Figure 3. The same test value (B–V) for the target is placed in each spreadsheet and repeatedly changed until the calculated (b–v) is equal to the test (B–V). Using the calculated (b–v) value as the next "test" (B–V) value, works well and is found to quickly converge to the proper (v–b) = (V– B) value thus giving a Ci = (B–V). Note: the filtered images must be made during the same session and close to the same time as the unfiltered images.

## Appendix F: Slope factor—a proposition for discussion

The slope factor, S', is an empirically determined transformation coefficient. In using the spreadsheet model, it was discovered that without a slope coefficient, a linear fit of the derived magnitudes (f) was generally "skewed" to the slope of the reference magnitudes (F). With a slope coefficient S' applied to the instrumental magnitudes (Equation 3), the linear fit of the derived magnitudes better aligns with the reference magnitudes. The standard deviation of the residuals (V–v, for example) is improved as would be expected. Experience has shown that generally the improvement to the standard deviation is from 0.001 to 0.010, depending on the quality of the instrumental magnitudes and the calibration of the reference stars.

Figures 11a and 11b show the effect on the residuals for two different star fields. Figure 11a is for the well calibrated M-67 cataloged stars using a relatively high number of stars (48). This data set is well calibrated and the improvement made by using S' is negligible.

Figure 11b is for the Rubin 152 star field using APASS magnitudes for reference. The transformation for this star field is with fewer stars and the calibration of the stars is of somewhat less quality. The application of the S' factor here is significant. As stated, this is an empirical factor and may or may not suit a given imaging system and or star field.

The "slope" factor is easily calculated. Simply place the factor (S') into Equation 2, thus:

$$f = S' \times Imag + Ci \times T' + Z'. \qquad (3)$$

The spread sheet is modified to have three unknown constants, T', Z', and S'. The calculations within the spreadsheet will then automatically provide the three constants and the derived magnitude values for the selected passband are calculated as before.

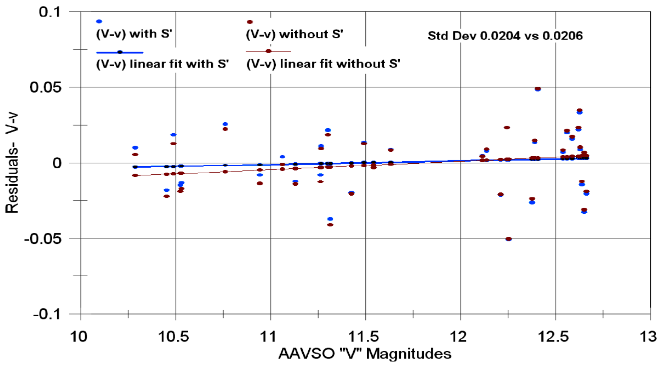

Figure 11a. M-67 catalogued stars using a relatively high number of stars.

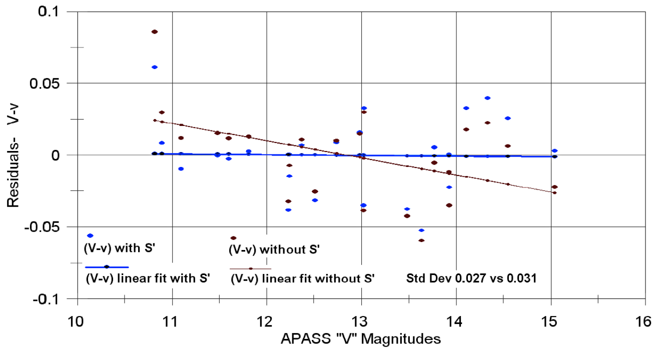

Figure 11b. Rubin 152 star field using APASS magnitudes for reference.

# Southern Clusters for Standardizing CCD Photometry

**Terry T. Moon**
*Centauri Observatory, 14 Ada St, Scottsdale, Tasmania 7260, Australia; texmoon0@gmail.com*

*Received November 7, 2016; revised November 24, 2016; accepted December 2, 2016*

**Abstract** Standardizing photometric measurements typically involves undertaking all-sky photometry. This can be laborious and time-consuming and, for CCD photometry, particularly challenging. Transforming photometry to a standard system is, however, a crucial step when routinely measuring variable stars, as it allows photoelectric measurements from different observers to be combined. For observers in the northern hemisphere, standardized UBVRI values of stars in open clusters such as M67 and NGC 7790 have been established, greatly facilitating quick and accurate transformation of CCD measurements. Recently the AAVSO added the cluster NGC 3532 for southern hemisphere observers to similarly standardize their photometry. The availability of NGC 3532 standards was announced on the AAVSO Variable Star Observing, Photometry forum on 27 October 2016. Published photometry, along with some new measurements by the author, provide a means of checking these NGC 3532 standards which were determined through the AAVSO's Bright Star Monitor (BSM) program (see: https://www.aavso.org/aavsonet-epoch-photometry-database). New measurements of selected stars in the open clusters M25 and NGC 6067 are also included.

## 1. Choice of southern clusters for establishing standard magnitudes and colors

Stars in bright open clusters are well-suited for standardizing CCD photometry undertaken with small telescopes, the brighter stars in such clusters encompassing a range in magnitude from 6 to 11. While there are many bright southern clusters with stars in this magnitude range most of these clusters are young; their brighter stars being predominantly of earlier spectral types (e.g. NGC 4755). As such, their brighter stars do not span a suitably wide range of color index.

NGC 3532 is a cluster at a southern declination of about –59° that has a suitably wide range in the color indices of its stars. NGC 6067 is a more compact southern cluster (declination about –54°) with surrounding field stars of diverse spectral type. Both open clusters are readily visible from southern latitudes through low air masses. While further north, at a declination of about –19°, M25 also has bright stars that encompass a wide range of spectral type. As there were multiple sources of published UBV measurements for these three clusters, I concentrated on measuring selected brighter stars in or around these three clusters in V and I bands only.

## 2. Choice of BVI photometric passbands

The contemporary UBVRI system (Bessell 1990, 1995, 2005) has evolved from the original UBV system introduced by Johnson and Morgan (1953). Initially the UBV system was established with reference to only ten primary standard stars from spectral type B8 to K5. Further photometric standards were added by Johnson and Harris (1954), producing a system with accuracies of 0.02 to 0.03 in V, 0.01 to 0.015 in B–V, and 0.02 to 0.03 in U–B (Johnson and Harris 1954; Harmanec *et al.* 1994).

Despite observers using different detectors, filters, observing approaches, and processing techniques, V magnitudes and B–V indices have been routinely and reliably standardized to within 0.02 magnitude (Bohm-Vitense 1981; Henden and Kaitchuck 1990; Harmanec *et al.* 1994; Henden 2004, Bessell and Murphy 2011). Since its inception the original UBV system has been able to be reproduced using many different detectors ranging from photomultiplier tubes and photographic emulsions through photodiodes to, more recently, CCDs. Usefully, V and B–V can be readily related to the earlier photographic magnitude and color index and those of many other photometric systems (Harmanec 1998; Bessell 2000; Harmanec and Božić 2001).

Kron and Smith (1951), Johnson (1966), and Cousins (1976) all extended the original UBV system with R and I bands but they used different R- and I-band filter sets, resulting in substantially different RI systems (Bessell 1979; Bessell 1983; Bessell 2005). The UBVRI system in widespread use today has been developed by combining the Johnson UBV and Cousins RI systems. Passbands for this contemporary UBVRI system are defined by Bessell (1990, 2005) and Bessell and Murphy (2011). Measurements made using appropriate filter sets can then be readily and accurately standardized using values given in the lists published by Menzies *et al.* (1989), Landolt (1983, 1992) and Kilkenny *et al.* (1998). As the Johnson, Kron, and Eggen RI systems have fallen into disuse I have chosen to drop the subscripts, with UBV referring to the Johnson bands and RI to the Cousins bands.

Measurements in five bands can be time-consuming and, for many observing programs, unnecessary. It is then prudent to consider the trade-off between numbers of bands in which measurements are made and the number of measurements of a particular star or group of stars. This can be critical when measuring short-period variations in a star or for accumulating measurements of a sufficiently large sample of long-period variables.

Challenges for standardizing measurements in the U-band are well documented (AAVSO 2011; Bessell 1990, 2005; Bessell and Murphy 2011; Bond 2005; Cousins 1966; Cousins and Jones 1976; Harmanec *et al.* 1994). The problems with accurately reducing and transforming such measurements to the standard system range from equipment vagaries such as poor response of CCDs in the ultraviolet region and the red leak of U filters, through a large correction for atmospheric extinction and adjustment of the zero-point for different temperature ranges, to astrophysical considerations associated with the Balmer jump.

In many instances an assessment of return on investment by observers undertaking CCD photometry of variable stars is likely to lead to a decision not to make U-band measurements.

Bessell (1990) also discusses the vagaries of measurement in the R band and problems that can arise in standardizing color indices constructed from it. Like Bond (2005), and in accord with a suggestion from Bessell (2003), I came to the conclusion that a good compromise is to focus on the BVI bands of the contemporary UBVRI system. I thus sought to investigate V, B–V, and V–I values for selected stars in the southern cluster NGC 3532, some of the brighter stars in M25, and stars in and around the more compact open cluster NGC 6067.

## 3. Equipment and techniques

The equipment and techniques used are described by Moon (2013) and follow methods outlined in the *AAVSO CCD Observing Manual* (AAVSO 2011). For CCD-camera measurements an observation in a particular band comprised a suitable number of stacked images. The general approach was to emulate that taken with photomultiplier tubes and photodiodes (e.g. as described by Optec 2012), where up to six consecutive measurements (each being a ten-second integration) are made for each observation, resulting in an observation spanning about a minute. The light frames taken were processed by subtracting dark frames taken at the same detector temperature and exposure time, then corrected using flat field images for the filter through which the light frames were taken.

AAVSO (2011) discusses the problems that can arise from short exposure times. Such effects were confirmed through analysis of 1-, 2-, and 4-second exposures. Where possible, CCD photometry of the clusters was standardized using standard stars (Menzies *et al.* 1989) measured using the same exposure times. Scaling factors were, however, determined for short exposure times and applied in those instances where longer exposures would have resulted in "saturation" for the stars being measured. (A similar situation arises when using photomultiplier tubes or photodiodes. Typical sensitivity settings of 1, 10, and 100 are notional and it is advisable to either measure standard, comparison, and program stars on the same sensitivity setting or determine the actual ratios of the sensitivity settings.)

## 4. NGC 3532

### 4.1. Published photometry

WEBDA (2014) gives V, B–V, and V–I values for many of the brighter stars in NGC 3532, with the cluster having been measured in UBV bands by Koelbloed (1959), Fernandez and Salgado (1980), and Claria and Lapasset (1988) and in UBVRI bands by Wizinowich and Garrison (1982). However, further examination of Wizinowich and Garrison (1982) photometry gave cause for concern as V-I values listed were inconsistent with the B–V values and spectral types. Reportedly, the I-band measurements were made on the Cousins system but the values listed are clearly discrepant.

More recently Clem *et al.* (2011) undertook a deep, wide-field CCD survey of the open cluster NGC 3532. Their new BVRI photometry covers a one square degree area reaching from the brighter stars in the cluster down to stars with V ~ 21. This catalogue thus appears to be the ideal source for choosing cluster stars to standardize BVI photometry. Importantly, Clem *et al.* (2011) compared their results with the other photometric studies of NGC 3532 listed in WEBDA. They also identified the discrepant RI values of Wizinowich and Garrison (1982) and a systematic difference in the V magnitudes, noting there were no other published measurements in RI bands that could help resolve the discrepancy. They did, however, note the excellent accord between their measured and the published values for the standard stars they observed.

Figure 1a shows the difference between the V magnitudes measured by Clem *et al.* (2011) and the average from other sources as a function of B–V; there is no appreciable color trend, with the average difference being –0.024 magnitude. Figure 1b shows the difference between B-V as measured by Clem *et al.* and the average from other sources. Again, there is good agreement, the average difference being 0.004 magnitude. Overall, there is good agreement of the measured V and B–V of Clem *et al.* with the mean values from the other sources listed in WEBDA for 41 of the brighter stars in NGC 3532.

NGC 3532 standards were recently added to the AAVSO's VSP database. The values used are measurements from the AAVSO's Bright Star Monitor (BSM) program (AAVSO 2016) and provide a homogeneous source of well-transformed values from the brighter stars (~ 7th magnitude) down to about 11th magnitude. Figure 2 shows the differences between new AAVSO standard values and those of Clem *et al.* (2011) in V, B–V, and V–I. The 32 brighter stars of NGC 3532 used in this analysis were those measured in the AAVSO BSM program, by Clem *et al.*, and by the author, thus providing three independent sources for the V and I magnitudes.

Winizowich and Garrison (1982) claimed to have used the UBVRI photometer described by Fernie (1974) and values for Cousins E-region standards given by Menzies *et al.* (1980). Fernie describes the I-band filter for this photometer as a combination of Schott BG3 and RG610 glasses. This gives a passband that cuts on at about 660 nm and extends out past 1000 nm, matching the Johnson rather than the Cousins I-band (which cuts on at about 710 nm and only extends to around 900 nm). Fernie (1974) also notes that he used stars listed by Iriarte *et al.* (1965), i.e. measured on the Johnson RI system, to standardize

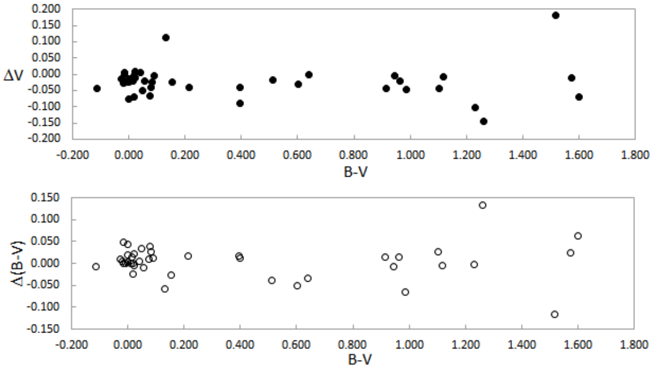

Figure 1. (a, upper plot) Difference between V magnitudes measured by Clem *et al.* (2011) and mean of other published photometry. (b, lower plot) Difference between B–V measured by Clem *et al.* and mean of other published photometry.

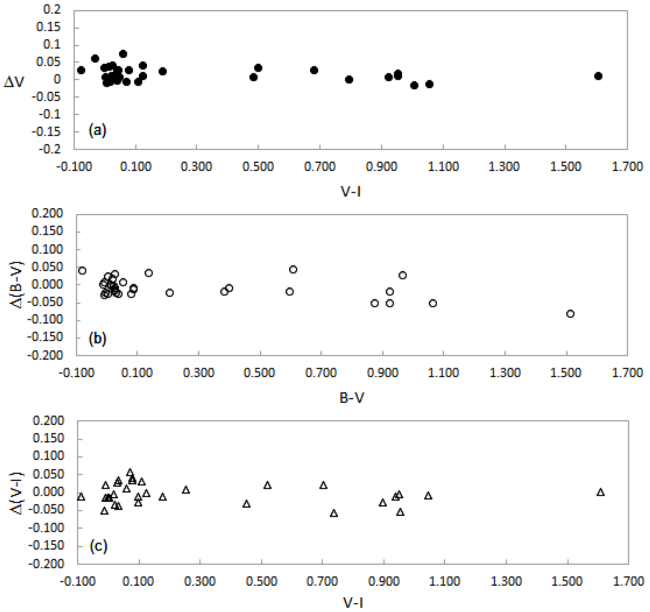

Figure 2. (a, upper plot) Difference between BSM_Berry and Clem *et al.* (2011) V magnitudes. (b, middle plot) Difference between BSM_Berry (AAVSO 2016) and Clem *et al.* B–V indices. (c, lower plot) Difference between BSM_Berry and Clem *et al.* V–I indices.

his system. The values of V–I given by Wizinowich and Garrison thus appear to have been made in the Johnson I-band but standardized against Cousins standards. Wizinowich and Garrison also noted that their V magnitudes were several hundredths of a magnitude fainter than those of Koelbloed (1959) and Fernandez and Salgado (1980). Owing to errors arising from their using a Johnson-like instrumental system and Cousins standards, Wizinowich and Garrison's measurements were not used in my analysis of BVI photometry for stars in NGC 3532.

### 4.2. New VI measurements of 41 of the brighter stars in NGC 3532

To check the I-band photometry of Clem *et al.* for the brighter stars in NGC 3532, I observed a selection of stars of different spectral types in the range of 6 < V < 11 on four nights in 2012–2013 and eight nights in 2015 in both V and I. Each night, extinction stars and Cousins E-region standards (Menzies *et al.* 1989) were also measured. The focus was on measurements of V and V–I as, discounting the photometry of Wizinowich and Garrison, the dispersions in V and B–V between the various sources were small (within acceptable transformation errors as discussed above). There was also good agreement with V and B–V from photographic UBV photometry, V from uvby and Geneva photometry, and V derived from Tycho $B_T$ and $V_T$.

Table 1 lists the mean value of my measured V and V–I for 41 of the brighter stars in NGC 3532. Column 1 gives the Fernandez and Salgado (1980) number for each star; this is the numbering system used for NGC 3532 in both the GCPD (Mermilliod *et al.* 1997) and WEBDA (2014). Column 2 gives the HD, CPD, or GSC number as a cross-reference and Column 3 lists the spectral type.

Figure 3 compares my V and V–I measurements with those of Clem *et al.* There is no color trend for the V magnitudes, the average difference being 0.019 magnitude. For the V–I index there is also good agreement, with the average difference being –0.021 magnitude.

Table 1. V and V–I measured by the author for 41 brighter stars in NGC 3532 (light variations of star number 221 are appreciable).

| *Star* | *HD/CPD/GSC* | *Sp. type* | *V* | *V–I* |
|---|---|---|---|---|
| 4 | –58 3069 | A1V | 8.959 | 0.076 |
| 19 | 96445 | G6II–III | 7.702 | 0.955 |
| 37 | 96260 | A | 9.319 | 0.021 |
| 38 | –58 3044 | A1V | 9.556 | 0.091 |
| 40 | 96227 | A2V | 8.208 | 0.031 |
| 49 | 96305 | A0/1IV–V | 8.549 | –0.023 |
| 50 | 96246 | A0V | 8.319 | 0.042 |
| 100 | –58 3092 | G9III | 7.454 | 0.999 |
| 113 | 96472 | A0IV | 8.560 | 0.043 |
| 122 | –58 3077 | G6III | 8.163 | 0.935 |
| 132 | 8627-02126 | | 11.243 | 0.445 |
| 139 | 96245 | A0 | 8.336 | –0.01 |
| 152 | 96174 | G8III | 7.765 | 0.903 |
| 160 | 96175 | G5 | 7.654 | 0.949 |
| 182 | –58 3051 | | 9.471 | 1.025 |
| 199 | 96489 | A2III–IV | 8.063 | 0.074 |
| 215 | 96564 | B9IV | 7.809 | 0.019 |
| 221 | 96544 | K2II/III | 6.069 | 1.217 |
| 236 | 96584 | K3/4 | 8.225 | 1.592 |
| 246 | 96386 | A0 | 9.815 | 0.086 |
| 273 | 96122 | F2Ib | 7.932 | 0.765 |
| 278 | 96137 | A0IV | 8.201 | –0.042 |
| 285 | –58 3004 | A5III | 10.597 | 0.189 |
| 317 | 96473 | B9.5V | 8.435 | –0.021 |
| 337 | 96668 | A0V | 8.294 | 0.023 |
| 345 | 96620 | A0IV | 7.385 | 0.062 |
| 356 | –58 3143 | | 10.307 | 0.422 |
| 361 | 96653 | A0III | 8.37 | 0.049 |
| 362 | –58 3139 | A2V | 9.585 | 0.121 |
| 363 | 96609 | B9 | 8.591 | 0.007 |
| 380 | 96652 | A2 | 9.247 | 0.05 |
| 409 | 96226 | B8 | 8.037 | –0.138 |
| 420 | 96059 | A0III | 8.008 | 0.049 |
| 447 | 96685 | B9 | 9.676 | 0.223 |
| 448 | –58 3151 | G1: | 9.951 | 0.618 |
| 473 | 95990 | G | 9.236 | 0.44 |
| 480 | 96247 | G1 Iab/b | 7.715 | 0.076 |
| 483 | 96285 | A0V | 8.998 | –0.004 |
| 495 | 96755 | A0 | 8.43 | 0.019 |
| 498 | 8628-0884 | M4 | 10.599 | 2.653 |
| 522 | 96118 | K3 III | 7.644 | 1.33 |

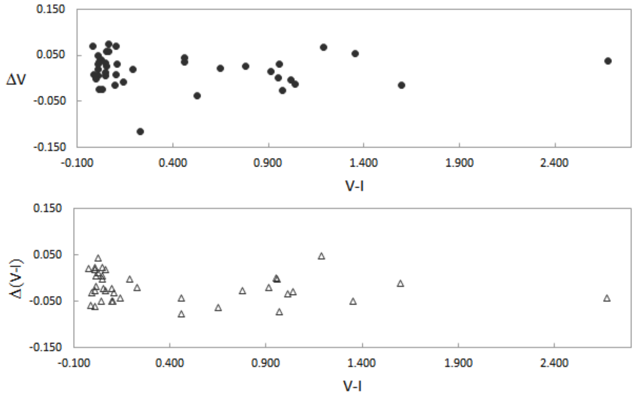

Figure 3. (a, upper plot) Difference between V magnitudes measured by the author and Clem *et al.* (2011). (b, lower plot) Difference between V–I measured by the author and that measured by Clem *et al.*

In summary, there is good agreement between the various published sources for V and B–V, and between my V–I measurements and those of Clem *et al.* (2011). Importantly, the V and I measurements by the author and by Clem *et al.* are in excellent agreement with the new AAVSO standard values while B and V values by Clem *et al.* and from other sources are also in good agreement with the new AAVSO standard values. This strongly supports use of the new AAVSO NGC 3532 standards by southern hemisphere observers for standardizing their BVI photometry.

## 5. M25

V and B-V measurements of stars in M25 (WEBDA 2014) have been made by Niconov *et al.* 1957; Johnson 1960; Sandage 1960; Wampler *et al.* 1961; Landolt 1964; Stoy 1963; Marlborough 1964; Lee 1970; Stobie 1970; Eggen 1971; Schmidt 1971; Corben *et al.* 1972; Epps 1972; Cousins 1973; Klare and Neckel 1977; Gieren 1981; Schild *et al.* 1983; Pedreros 1984; Shobbrook 1992; and An *et al.* 2007. Unfortunately, there remains a paucity of I-band measurements for what are relatively bright stars. Twelve of the brighter stars in M25 were thus measured in V and I-band on five nights in 2015. On each night extinction stars and Cousins E-region standard stars (Menzies *et al.* 1989) were also measured.

Table 2 lists the V, B–V, and V–I values for twelve of the brighter stars in M25. Column 1 gives the cluster number for each star as used in WEBDA (2014) and GCPD (Mermilliod *et al.* 1997). Column 2 gives the HD or Tycho number as a cross-reference and Column 3 lists the spectral type from SIMBAD. The V magnitudes, and B–V and V–I color indices listed were determined as follows:

- V magnitudes given in Column 4 are the average of measurements from all available sources including measurements made by the author. No weightings were applied.
- B–V colors given in Column 5 were determined by averaging published measurements from all available sources. Again, no weightings were applied.
- V–I color indices listed in Column 7 are mostly the author's measurements. There are three sources for I-band measurements of HD 170657: Eggen (1971), Mermilliod *et al.* (1997), and Koen *et al.* (2010). There are also I-band measurements of HD 170886 by Eggen (1971) and listed in Mermilliod *et al.* (1997), and for HD 170820 listed in Mermilliod *et al.* (1997). All published values are in close agreement with my measurements. For these three stars, V–I values given in Table 2 are the averages of my measurements and published values; no weightings were applied.

Column 6 lists the number of sources used to determine B–V (for V, my measurements were combined with published values from the number of sources listed). There were no photoelectric measurements of B–V listed for stars 233 and 268; B–V for star 233 was thus determined using Tycho photometry but for star 268, the listed photographic measurement of B–V has been used. These B–V values are italicized to indicate that they were not derived from direct BV photoelectric measurements.

There are published V magnitudes derived from uvby photometry for six of these stars. On average, they differed from the V given in Table 2 by 0.011 magnitude. Geneva photometry was available for only three of the stars; again, agreement was good.

Table 2. V, B–V, and V–I for selected stars in M25.

| *Star* | *HD/Tyc* | *Sp. Type* | *V* | *B–V* | *s* | *V–I* |
|---|---|---|---|---|---|---|
| 26 | 170657 | K2V | 6.818 | 0.850 | 11 | 0.918 |
| 49 | 6274-1625-1 | M2 | 9.071 | 1.927 | 4 | 2.543 |
| 70 | 6274-1131-1 | F0V | 8.980 | 0.427 | 3 | 0.541 |
| 91 | 170719 | B5/7III | 8.086 | 0.302 | 5 | 0.438 |
| 111 | 6274-1331-1 | A1V | 9.004 | 0.393 | 5 | 0.445 |
| 150 | 170820 | K0III | 7.385 | 1.567 | 7 | 1.638 |
| 163 | 170835 | B2Ve | 8.827 | 0.237 | 6 | 0.286 |
| 167 | 170836 | B8II | 8.956 | 0.307 | 3 | 0.418 |
| 153 | 170860 | B9IV/V | 9.404 | 0.318 | 4 | 0.475 |
| 174 | 6275-0720-1 | M3III | 8.961 | 2.028 | 2 | 2.621 |
| 233 | 170763 | B8/9II/IIIe | 8.935 | *0.25* | 1* | 0.432 |
| 251 | 170886 | G3/5Ib | 6.949 | 1.385 | 3 | 1.436 |
| 268 | 170887 | G8/K0III | 7.966 | *1.45* | 1* | 1.488 |

Table 3. V, B–V, and V–I for selected stars in NGC 6067.

| *Star* | *HD/Tyc* | *Sp. Type* | *V* | *B–V* | *s* | *V–I* |
|---|---|---|---|---|---|---|
|  | 145039 | K7 | 8.883 | *1.602* | 1* | 1.822 |
|  | 145040 | B8 IV | 9.252 | *0.061* | 1* | 0.038 |
|  | 145041 | K1 III | 8.803 | 1.290 | 1 | 1.345 |
|  | 145109 | A2 e | 8.724 | 0.260 | 1 | 0.179 |
|  | 145110 | B9 IV | 6.528 | 0.020 | 1 | 0.049 |
| 229 | 145175 | K3 III | 8.640 | 1.280 | 1 | 1.337 |
|  | 145304 | B1/B2 III/IVe | 8.820 | 0.127 | 2 | 0.422 |
|  | 145324 | A5 Ib/II | 7.295 | 0.360 | 3 | 0.518 |
|  | 145523 | G2 V | 7.808 | 0.580 | 2 | 0.618 |
|  | 8710-2212-1 | G8 | 9.644 | *1.637* | 1* | 1.592 |
|  | 8711-0788-1 |  | 9.656 | *1.321* | 1* | 1.496 |
|  | 8711-1458-1 | G7 | 9.796 | *1.203* | 1* | 1.081 |
| 261 | 8710-0033-1 | K2 Ib | 8.764 | 1.743 | 4 | 1.650 |
| 267 | 8710-0209-1 | B2 III | 9.031 | 0.181 | 5 | 0.314 |
| 271 | 8710-0125-1 | B5 III | 10.534 | 0.220 | 3 | 0.390 |
| 275 | 8710-0049-1 | K3 (II) | 9.141 | 1.793 | 7 | 1.900 |
| 276 | 8710-0126-1 | K3 II+K3Ib | 9.495 | 1.915 | 3 | 2.030 |
| 298 | 8710-0170-2 | A7 II | 8.995 | 0.500 | 5 | 0.748 |
| 303 | 8711-0530-1 | K2 II-Ib | 10.004 | 1.520 | 3 | 1.403 |
| 306 | 8711-1312-1 | K3 II | 10.051 | 1.663 | 6 | 1.792 |

V, B–V, and V–I listed here may prove useful to southern hemisphere observers for:

- Setting up suitable comparison stars for variables in M25 (such as V3508 Sgr) as the values currently listed for comparison stars have been largely derived from Tycho photometry.
- Occasional checking of the transformation coefficients used to standardize their photometry.

As M25 may be visible to some northern hemisphere observers, it could also provide a means for those collaborating with southern hemisphere observers to check that they have similarly standardized systems.

## 6. NGC 6067

WEBDA (2014) gives V, B–V for stars in NGC 6067 and the GCPD (Mermilliod *et al.* 1997) lists V and B–V for a number of brighter, field stars immediately surrounding the cluster. Piatti *et al.* (1998) and An *et al.* (2007) have measured V–I for a few of these cluster stars but there are no V–I values listed in the GCPD for the surrounding field stars. Eleven field stars and one cluster star were measured on nine nights in 2015 with the focus being on measuring their V–I indices. Measurements of several cluster stars from the 2011-12 season were also included.

Table 3 lists the V, B–V, and V–I values for nine stars in NGC 6067 and eleven fields surrounding it. Column 1 gives the cluster number as used in WEBDA (2014). Column 2 gives the HD or Tycho number as a cross-reference and Column 3 lists the spectral type from SIMBAD or WEBDA. The V magnitudes, and B–V and V–I color indices listed were determined as follows:

- V magnitudes given in Column 4 are the average of measurements from all available sources including measurements made by the author. No weightings were applied.
- B–V colors given in Column 5 were determined by averaging published measurements from all available sources. Again, no weightings were applied. For five of the stars (values shown in italics), the B–V was determined from the Tycho photometry.
- V–I color indices listed in Column 7 are mostly the author's measurements. For stars 267 and 275 the author's measurements were combined with published values. For stars 271, 276, 298, and 306 the published values are listed.

Column 6 lists the number of measurements from published sources used.

## 7. Concluding remarks and recommendations

New VI measurements of 41 brighter stars in NGC 3532, published BV measurements as listed in WEBDA, and the BVRI measurements published by Clem *et al.* (2011) confirm the veracity of the new NGC 3532 standard stars added to the AAVSO's VSP database. The only published photometry not in agreement, that of Winizowich and Garrison (1982), is shown to be discrepant owing to use of Cousins standards with a Johnson I-band filter.

The newly added NGC 3532 standards are well supported by published and new measurements and can be used with confidence by southern hemisphere observers for determining BVI transformation coefficients. As R-band measurements are of interest to those doing DSLR photometry, it would be useful for some southern hemisphere observers to check the values of the NGC 3532 standards in R-band.

For variables in M25, such as V3508 Sgr, there are currently no I-band measurements for the comparison stars. Also, their assigned V and B–V values have been largely derived from Tycho photometry. The BVI photometry listed in Table 2 thus provides a resource for determining BVI magnitudes and colors for M25 variable and comparison stars. Additionally, this BVI photometry may be used to check transformation coefficients. Where northern and southern hemisphere observers are collaborating, M25 may also provide an additional means to check if their systems are similarly standardized, as it is at a southern declination of only –19°.

BVI photometry for stars in and around NGC 6067 (Table 3) can be used to establish comparison stars with well-determined magnitudes for variables near NGC 6067. An example is QZ Nor, for which AAVSO comparison stars are yet to be chosen. Again, the BVI photometry listed may be used to check transformation coefficients.

## References

AAVSO. 2011, *AAVSO CCD Observing Manual* (https://www.aavso.org/ccd-observing-manual).

AAVSO. 2016, BSM_Berry (https://www.aavso.org/bsm-berrys-enclosure-setup).

An, D., Terndrup, D. M., and Pinsonneault, M. H. 2007, *Astrophys. J.*, **671**, 1640.

Bessell, M. S. 1979, *Publ. Astron. Soc. Pacific*, **91**, 589.

Bessell, M. S. 1983, *Publ. Astron. Soc. Pacific*, **95**, 480.

Bessell, M. S. 1990, *Publ. Astron. Soc. Pacific*, **102**, 1181.

Bessell, M. S. 1995, in *New Developments in Array Technology and Applications*, eds. A. G. D. Philip, K. A. Janes, A. R. Upgren, IAU Symp. 167, Kluwer Academic Publishers, Dordrecht, 175.

Bessell, M. S. 2000, *Publ. Astron. Soc. Pacific*, **112**, 961.

Bessell, M. S. 2003, personal communication, Mt. Stromlo Observatory, February.

Bessell, M. S. 2005, *Ann. Rev. Astron. Astrophys.*, **43**, 293.

Bessell, M. S., and Murphy, S. J. 2011, arXiv:1112.2698 [astro-ph.SR].

Bohm-Vitense, E. 1981, *Ann. Rev. Astron. Astrophys.*, **19**, 295.

Bond, H. E. 2005, *Astron. J.*, **129**, 2914.

Claria, J. J., and Lapasset, E. 1988, *Mon. Not. Roy. Astron. Soc.*, **235**, 1129.

Clem, J. L., Landolt, A. U., Hoard, D. W., and Wachter, S. 2011, *Astron. J.*, **141**, 115.

Corben, P. M., Carter, B. S., Banfield, R. M., and Harvey, G. M. 1972, *Mon. Not. Astr. Soc. S. Afr.*, **31**, 8.

Cousins, A. W. J. 1966, *Observatory*, **86**, 69.

Cousins, A. W. J. 1973, *Mon. Not. Astr. Soc. S. Afr.*, **32**, 11.

Cousins, A. W. J. 1976, *Mem. Roy. Astron. Soc.*, **81**, 25.

Cousins, A. W. J., and Jones, D. H. P. 1976, *Mem. Roy. Astron. Soc.*, **81**, 1.

Eggen, O. J. 1971, *Astrophys. J., Suppl. Ser.*, **22**, 389.

Epps, E. A. 1972, *Roy. Obs. Bull.*, No. 176, 127.

Fernandez, J. A., and Salgado, C. W. 1980, *Astron. Astrophys., Suppl. Ser.*, **39**, 11.

Fernie, J. D. 1974, *Publ. Astron. Soc. Pacific*, **86**, 838.

Gieren, W. 1981, *Astrophys. J., Suppl. Ser.*, **47**, 315.

Harmanec, P. 1998, *Astron. Astrophys.*, **335**, 173.

Harmanec, P., and Božić, H. 2001, *Astron. Astrophys.*, **369**, 1140.

Harmanec, P., Horn, J., and Juza, K. 1994, *Astron. Astrophys., Suppl. Ser.*, **104**, 121.

Henden, A. A. 2004, "Tricks for High-Precision CCD Photometry" (www.phys.vt.edu/~jhs/phys3154/photometryhighpre.pdf).

Henden, A. A., and Kaitchuck, R. H. 1990, *Astronomical Photometry*, Willmann-Bell, Richmond, VA.

Henden, A. A., *et al.* 2014, *AAVSO Guide to CCD Photometry*, (http://www.aavso.org/sites/default/files/publications_files/ccd_photometry_guide/CCDPhotometryGuide.pdf).

Iriarte, B., Johnson, H. L., Mitchell, R. I., and Wisniewski, W. K. 1965, *Sky & Telescope*, **30**, 21.

Johnson, H. L. 1960, *Astrophys. J.*, **131**, 620.

Johnson, H. L. 1966, *Ann. Rev. Astron. Astrophys.*, **4**, 193.

Johnson, H. L., and Harris III, W. W. 1954, *Astrophys. J.*, **120**, 196.

Johnson, H. L., and Morgan, W. W. 1953, *Astrophys. J.*, **117**, 313.

Kilkenny, D., van Wyk, F., Roberts, G., Marang, F., and Cooper, D. 1998, *Mon. Not. Roy. Astron. Soc.*, **294**, 93.

Klare, G., and Neckel, T. 1977, *Astron. Astrophys., Suppl. Ser.*, **27**, 215.

Koelbloed, D. 1959, *Bull. Astron. Inst. Netherlands*, **14**, 265.

Koen, C., Kilkenny, D., van Wyk, F., and Marang, F. 2010, *Mon. Not. Roy. Astron. Soc.*, **403**, 1949.

Kron, G. E., and Smith, J. L. 1951, *Astrophys. J.*, **113**, 324.

Landolt, A. U. 1964, *Astrophys. J., Suppl. Ser.*, **8**, 352.

Landolt, A. U. 1983, *Astron. J.*, **88**, 439.

Landolt, A. U. 1992, *Astron. J.*, **104**, 340, 436.

Lee, T. A. 1970, *Astrophys. J.*, **162**, 217.

Marlborough, J. M. 1964, *Astron. J.*, **69**, 215.

Menzies, J. W., Banfield, R. M., and Laing, J. D. 1980, *S. Afr. Astron. Obs. Circ.*, No. 1, 149.

Menzies, J. W., Cousins, A. W. J., Banfield, R. M., and Laing J. D. 1989, *S. Afr. Astron. Obs. Circ.*, No. 13, 1.

Mermilliod, J.-C., Mermilliod, M., and Hauck, B. 1997, "General Catalogue of Photometric Data (GCPD). II," *Astron. Astrophys., Suppl. Ser.*, **124**, 349 (http://obswww.unige.ch/gcpd/gcpd.html).

Moon, T. T. 2013, *J. Amer. Assoc. Var. Star Obs.*, **41**, 360.

Niconov, V. B., Nekrasova, S.V., Polosuina, N. S., Rachkouvsky, N. D., and Chuvajev, W. K. 1957, *Izv. Krym. Astrofiz. Obs.*, **17**, 42.

Optec Inc. 2012, Model SSP-3 Solid-State Stellar Photometer, Lowell, MI (http://www.optecinc.com/).

Pedreros, M. H. 1984, Ph.D. thesis, University of Toronto.

Piatti, A. E., Clariá, J. J., and Bica, E. 1998, *Astrophys. J., Suppl. Ser.*, **116**, 263.

Sandage, A. R. 1960, *Astrophys. J.*, **131**, 610.

Schild, R. E., Garrison, R. F., and Hiltner, W. A. 1983, *Astrophys. J., Suppl. Ser.*, **51**, 321.

Schmidt, E. G. 1971, *Astrophys. J.*, **165**, 335.

Shobbrook, R. R. 1992, *Mon. Not. Roy. Astron. Soc.*, **255**, 486.

Stobie, R. S. 1970, *Mon. Not. Roy. Astron. Soc.*, **148**, 1.

Stoy, R. H. 1963, *Mon. Not. Astron. Soc. S. Afr.*, **22**, 157.

Wampler, J., Pesch, P., Hiltner, W. A., and Kraft, R. P. 1961, *Astrophys. J.*, **133**, 895.

WEBDA. 2014, database (http://www.univie.ac.at/webda/webda.html).

Wizinowich, P., and Garrison, R. F. 1982, *Astron. J.*, **87**, 1390.

# Digital Single Lens Reflex Photometry in White Light: a New Concept Tested on Data from the High Amplitude δ Scuti Star V703 Scorpii

**Roy Andrew Axelsen**
*P.O. Box 706, Kenmore, Queensland 4069, Australia; reaxelsen@gmail.com*

*Received November 21, 2016; revised March 19, 2017; accepted March 22, 2017*

**Abstract** A novel method of digital single lens reflex (DSLR) photometry is described. It derives non-transformed instrumental magnitudes from white light (green, blue, and red channels of the DSLR sensor combined), and is assessed by comparing the results with non-transformed instrumental magnitudes from the green channel alone, and with green channel magnitudes transformed to the Johnson V standard. The white light data and the non-transformed green channel data allow differential photometry only; true magnitude values cannot be calculated. The same time series images of the high amplitude δ Scuti star V703 Scorpii were processed by all three methods. The light curves from the white light data were almost identical to those from the non-transformed green channel data and to those in V magnitude, but with a slightly greater amplitude for the variable star (from highest peak to lowest trough of the light curve on each night) in the white light curves. There was also an impression, in some areas, of slightly smoother curves from the white light data, implying improved precision. The check star data in white light showed slightly smaller ranges and standard deviations for most nights, and for all nights averaged, than those for the non-transformed green channel data, and for the transformed V magnitude data, implying that the best precision was achieved by using the data in white light. For most of the peaks in the light curve, the times of maximum in white light differed little from those in V magnitude. Fourier analysis using the Lomb-Scargle method revealed identical power spectra and identical discovered frequencies in white light and in V magnitude. DSLR photometry in white light is a valid procedure, at least in those cases where the color indices of the variable and comparison stars differ by only small values. It is considered promising for the timing of maxima and minima of light curves and for Fourier analysis of those stars with more than one period.

## 1. Introduction

Following the ground breaking work of Hoot (2007) and Loughney (2010), amateur astronomers have used DSLR cameras to make significant contributions to variable star photometry (Kloppenborg *et al.* 2012; Richards 2012; Axelsen 2014a–2014d, 2015; Axelsen and Napier Munn 2015, 2016; Deshmukh 2015; Walker *et al.* 2015). The AAVSO provides detailed methods for observers who wish to avail themselves of this technique, which is capable of yielding results with high precision using modest equipment (AAVSO 2016).

Aperture photometry on images from a DSLR camera must take account of the fact that the camera sensor is composed of a color filter array (Bayer matrix) of green, blue, and red elements. The processing of images from one of the three color channels, usually the green channel, provides the opportunity for simple differential photometry to study events such as the timing of maxima of light curves of pulsating variable stars, and the timing of eclipses in binary stellar systems. In such cases, it is not necessary to transform the magnitude data to a standard system. For more stringent work, photometry of images from two channels (green and blue, for example) or all three channels does allow transformation of the results to a standard system (AAVSO 2016).

One of the disadvantages of photometry with a DSLR camera in comparison with CCD photometry is that not all of the pixels of the DSLR sensor are used, as the green-, blue-, and red-filtered pixels comprise 50%, 25%, and 25%, respectively, of the surface of the sensor. For photometry based on the green channel, 50% of the light reaching the sensor therefore cannot be used, and for each of the blue and red channels, the proportion of unused pixels increases to 75%.

In view of these disadvantages, it was decided to trial differential photometry with a DSLR camera using all of the light reaching the sensor, by processing images containing data from all three color channels simultaneously (i.e., images in white light). To the author's knowledge, this strategy has not previously been used. The high amplitude δ Scuti star V703 Scorpii was chosen as a test case for the procedure. It is accepted by most authors to have two periods, 0.11521803 d and 0.14996 d (Plaut 1948 quoted in Ponsen 1963; Ponsen 1961, 1963; Oosterhoff 1966; Koen 2001). Two different sets of measures were used to compare the performance of white light DSLR photometry with differential photometry using non-transformed magnitudes from the green channel, and photometric data transformed to the Johnson V standard; the amplitude of the light curve of V703 Sco in magnitude units, measured from the lowest trough to the highest peak each night; and the standard deviation of the check star magnitudes from each night's time series data. A further two sets of measures applied to the variable star data were used to compare the performance of white light DSLR with photometric data transformed to the Johnson V system; Fourier analysis to identify pulsation frequencies; and the determination of the times of maximum of the peaks of the light curve.

## 2. Data and analysis

### 2.1. Observations

V703 Sco was observed by DSLR photometry over 12 nights in 2016 from 11 May to 1 July. A total of 1,254 magnitude determinations were obtained from a total observing time of 62.78 hours. The minimum number of observations on one night was 88, over 4.41 hours, and the maximum number was

123, over 6.19 hours. The target field was imaged mostly to the east of the meridian, and for a short time after transit. No meridian flips were performed because incremental shifts in magnitude values were seen after meridian flips when V703 Sco was studied in the 2014 season.

RAW images were taken with a Canon EOS 500D DSLR camera through an 80-mm refracting telescope with a focal length of 600 mm on a Losmandy GM8 German equatorial mount. Exposures of 170 seconds were made at ISO 400, at intervals of 180 seconds (i.e., one image was taken every 180 seconds). Dark frames were taken after the completion of light frames. Flat fields were captured near sunrise the following morning through a white acrylic sheet placed over the front of the telescope, which was aimed at the zenith.

### 2.2. Data reduction

Aperture photometry was performed with the software AIP4WIN version 2.4.0 (Berry and Burnell 2011). Measurements from the green channel enabled the calculation of non-transformed differential magnitudes from the formulae:

$$\text{Var g} - \text{Comp g} \tag{1}$$

$$\text{Chk g} - \text{Comp g} \tag{2}$$

where g is the instrumental magnitude and Var, Comp, and Chk refer to the variable, comparison, and check stars, respectively. Measurements from the green and blue channels were used to calculate magnitudes transformed to the Johnson V system, employing transformation coefficients determined from standard stars in the E regions (Menzies *et al.* 1989). For white light differential photometry, the settings in AIP4WIN were as follows. In *Preferences > DSLR Conversion Settings > DeBayer, Convert Color to Grayscale*, the red, green, and blue scales were all set to 1.0 simultaneously. Differential magnitudes for white light photometry were calculated from the formulae:

$$\text{Var wl - Comp wl} \tag{3}$$

$$\text{Chk wl - Comp wl} \tag{4}$$

where wl is the white light instrumental magnitude and Var, Comp, and Chk refer to the variable, comparison, and check stars respectively.

The comparison and check stars were HD 160927 and HD 160432, respectively. The V magnitude and B–V color index for the comparison star were taken to be 8.727 and 0.533, respectively, and the corresponding values for the check star were taken to be 9.159 and 0.457. These two stars were chosen because their B–V color indices are close to that of V703 Sco, which from the author's photometry varies from 0.2 to 0.5 approximately.

The time in JD of each magnitude calculation was taken to be the mid point of each DSLR exposure. The heliocentric correction for each night's data was calculated for the mid point in time of the observing run for the night, and the correction applied to all data points for that night. Fourier analyses and the determination of the times of maximum of the light curve used the heliocentric data.

### 2.3. Time series analysis and determination of the times of maximum of the variable star light curve

The software PERANSO (Vanmuster 2014) was used. Fourier analysis employed the Lomb-Scargle routine. The times of maximum of the light curve were taken as the maximum values of fifth order polynomial functions fitted to the magnitude values around each peak in the light curve.

## 3. Results

### 3.1. Metrics of the light curves of V703 Sco and the check star

Light curves from two representative nights are shown in Figures 1 and 2, respectively. In each figure, the top panel shows transformed V magnitudes (hereafter referred to simply as "V magnitudes"), the middle panel shows non-transformed differential magnitudes from the green channel (hereafter referred to simply as "green magnitudes"), and the bottom panel shows differential magnitudes in white light (hereafter referred to simply as "white light magnitudes"). Each light curve shows data both for the variable star and the check star, with the check star magnitudes represented as the calculated magnitudes minus 1.3 so that variable and check star data can both be seen optimally. The variation in the amplitude between adjacent peaks in the light curves of V703 Sco is typical of a variable star with more than one period.

The variable star light curves in Figure 1, from 11 May 2016, show peaks 1 and 2 (labelled in the top panel of the figure), corresponding to the numbers of the peaks in the first column of Tables 3 and 4. Figure 2, from 13 May 2016, shows peak 4 (labelled in the top panel of the figure), with the latter

Table 1. Photometric data for V703 Sco, listing transformed V magnitudes, non-transformed differential magnitudes from the green channel, and differential magnitudes in white light.

| *Date (2016)* | *Var V Range* | *Var g Range* | *Var wl Range* | *Var g, Var V Δ Range* | *Var wl, Var V Δ Range* |
|---|---|---|---|---|---|
| May–11 | 0.479 | 0.496 | 0.506 | 0.017 | 0.027 |
| May–12 | 0.469 | 0.486 | 0.491 | 0.017 | 0.022 |
| May–13 | 0.483 | 0.500 | 0.516 | 0.017 | 0.033 |
| May–14 | 0.482 | 0.498 | 0.509 | 0.016 | 0.027 |
| Jun–08 | 0.461 | 0.469 | 0.474 | 0.008 | 0.013 |
| Jun–09 | 0.471 | 0.489 | 0.503 | 0.018 | 0.032 |
| Jun–10 | 0.488 | 0.503 | 0.516 | 0.015 | 0.028 |
| Jun–25 | 0.414 | 0.428 | 0.440 | 0.014 | 0.026 |
| Jun–27 | 0.475 | 0.489 | 0.490 | 0.014 | 0.015 |
| Jun–28 | 0.390 | 0.402 | 0.407 | 0.012 | 0.017 |
| Jun–29 | 0.454 | 0.469 | 0.476 | 0.015 | 0.022 |
| Jul–01 | 0.353 | 0.366 | 0.374 | 0.013 | 0.021 |
| | | | | | |
| Mean | 0.452 | 0.466 | 0.475 | 0.015 | 0.024 |
| SD | 0.043 | 0.044 | 0.046 | 0.003 | 0.006 |

*Notes. Abbreviations in the above table: Var = Variable star; V = Transformed V magnitude photometric data; Range = Difference between the maximum and minimum magnitudes for each night; g = Non–transformed differential magnitudes from the green channel; wl = White light non–transformed differential magnitudes from all three channels; Δ Range = Difference between the two ranges as indicated at the head of each column; SD = Standard deviation.*

Table 2. Photometric data for the check star, listing transformed V magnitudes, non-transformed differential magnitudes from the green channel, and differential magnitudes in white light.

| *Date (2016)* | *Chk V Range* | *Chk g Range* | *Chk wl Range* | *Chk g, Chk V Δ Range* | *Chk wl, Chk V Δ Range* | *Chk V SD* | *Chk g SD* | *Chk wl SD* |
|---|---|---|---|---|---|---|---|---|
| May-11 | 0.082 | 0.067 | 0.060 | -0.015 | -0.022 | 0.014 | 0.012 | 0.010 |
| May-12 | 0.068 | 0.064 | 0.053 | -0.004 | -0.015 | 0.013 | 0.011 | 0.009 |
| May-13 | 0.105 | 0.079 | 0.056 | -0.026 | -0.049 | 0.016 | 0.012 | 0.010 |
| May-14 | 0.054 | 0.061 | 0.047 | 0.007 | -0.007 | 0.011 | 0.009 | 0.007 |
| Jun-08 | 0.092 | 0.065 | 0.048 | -0.027 | -0.044 | 0.011 | 0.009 | 0.007 |
| Jun-09 | 0.088 | 0.075 | 0.078 | -0.013 | -0.010 | 0.015 | 0.013 | 0.012 |
| Jun-10 | 0.183 | 0.151 | 0.129 | -0.032 | -0.054 | 0.018 | 0.016 | 0.014 |
| Jun-25 | 0.043 | 0.033 | 0.042 | -0.010 | -0.001 | 0.009 | 0.007 | 0.007 |
| Jun-27 | 0.058 | 0.052 | 0.048 | -0.006 | -0.010 | 0.011 | 0.010 | 0.009 |
| Jun-28 | 0.039 | 0.031 | 0.031 | -0.008 | -0.008 | 0.008 | 0.006 | 0.006 |
| Jun-29 | 0.046 | 0.040 | 0.037 | -0.006 | -0.009 | 0.010 | 0.008 | 0.007 |
| Jul-01 | 0.036 | 0.035 | 0.033 | -0.001 | -0.003 | 0.008 | 0.007 | 0.006 |
| Mean | 0.075 | 0.063 | 0.055 | -0.012 | -0.019 | 0.012 | 0.010 | 0.009 |
| SD | 0.041 | 0.032 | 0.027 | 0.012 | 0.019 | 0.003 | 0.003 | 0.002 |

*Notes. Abbreviations in the above table: Chk = Check star; V, Range, g, wl, Δ Range and SD are as for the Notes to Table 1.*

being one of the two peaks for which the time of maximum light differed by an unacceptably large value between V magnitude data and white light magnitude data (see below).

The light curves showing magnitudes in white light are similar to those showing green magnitudes and V magnitudes, but there is an impression of slightly smoother areas in the curves for the variable star in the white light panels. Columns 2, 3, and 4 of Table 1 show the data for the amplitudes of the V703 Sco light curves for each night and averaged over all nights. The amplitudes of the variable star light curves from the three different photometric methods show very little difference, with the greatest being on average only 0.024 magnitude units, between the light curves in white light and the light curves in V magnitude.

The check star light curves show poor precision during the early part of each night, when the airmass was 4.2 on 11 May 2016 (Figure 1) and 3.8 on 13 May 2016 (Figure 2). The precision improves later in the night, as the altitude of the star increases and the air mass decreases. There is an impression that the variance is better for the green magnitude data than for the V-magnitude data, and better again for the white light data. These impressions are confirmed by the analysis of the numerical values shown in Table 2, which are considered in detail in the following paragraph.

Columns 2, 3, and 4 list the ranges in magnitude units of the observations for the check star for each night, and at the bottom of the table, the means and standard deviations for all nights. For each observing night, the range is slightly less for the green magnitude data than for the data in V magnitude. For most observing nights, the range for the white light magnitude is less again. The means and standard deviations of the magnitude ranges for the check star show that the most precise data are those for white light magnitudes, and the least precise the V magnitudes, although the differences are small. Columns 7, 8, and 9 analyze the standard deviation of the magnitude values for each night, and their averages. The differences are again small, but once more the white light data are more precise than those for the other two methods of magnitude calculation.

The times of maximum (TOM) of all peaks with long ascending and long descending limbs are shown in Table 3. Peaks associated with a short ascending or descending limb were not measured. The times were determined in PERANSO as the maximum values of fifth-order polynomial expressions fitted to the peaks of the light curve. After this was done for the white light data and the V magnitude data, the difference between the TOM for white light and V magnitude was calculated for each peak, using the formula: TOM in white light minus TOM in V magnitude. All but two of the differences lay within a range of 2.30 min. (from –1.44 min. to 0.86 min.), whereas the other two differences were –6.38 min. and 8.80 min. Those results which lay within a range of 2.30 min. were considered acceptable, because they compared favourably with results in the author's previous DSLR photometric study of ZZ Mic (Axelsen 2015) in which the O–C values for 14 TOM obtained over a span of 9.3 days lay within a range of 2.62 min. The other two results (–6.38 min. and 8.80 min.) were therefore considered to be unacceptable. Figure 3 shows part of the light curve of V703 Sco, representing the region around peak 4 (as listed in Tables 3 and 4) plotted in PERANSO, with a fitted fifth-order polynomial expression. The upper panel is the light curve in V magnitude, and the lower panel the light curve from white light magnitude data. The white light plot is smoother than the V magnitude plot.

In view of the two unacceptable results, the TOM for all of the peaks were recalculated from the light curve data, but using center moving averages across three data points instead of the individual magnitude determinations. The results are shown in Table 4. Again, peaks 4 and 10 show unacceptably large differences between the white light and V magnitude data.

The TOM of the two peaks giving the discrepant results were remeasured using the Podgson method (Percy 2007), which involved printing the parts of the light curve containing the peaks to be measured and drawing by hand a smooth curve through the data. Several equally spaced horizontal chords are then drawn between the ascending and descending limbs of the light curve, and the mid points of the chords marked. A smooth

Table 3. Times of maximum (TOM) of V703 Sco in heliocentric Julian days (HJD) in white light (wl) and V magnitude.

| *Peak* | *HJD TOM wl* | *Error* | *HJD TOM V Mag* | *Error* | *wl TOM – V Mag TOM (d)* | *wl TOM – V Mag TOM (min)* |
|---|---|---|---|---|---|---|
| 1 | 2457520.0102 | 0.0010 | 2457520.0102 | 0.0012 | 0.0 | –0.01 |
| 2 | 2457520.1309 | 0.0007 | 2457520.1310 | 0.0007 | –0.0001 | –0.14 |
| 3 | 2457521.0485 | 0.0009 | 2457521.0489 | 0.0013 | –0.0004 | –0.58 |
| 4 | 2457522.0822 | 0.0007 | 2457522.0866 | 0.0091 | –0.0044 | –6.34 |
| 5 | 2457523.0059 | 0.0008 | 2457523.0069 | 0.0008 | –0.0010 | –1.44 |
| 6 | 2457523.1278 | 0.0005 | 2457523.1278 | 0.0009 | 0.0 | 0.0 |
| 7 | 2457548.0171 | 0.0008 | 2457548.0169 | 0.0010 | 0.0002 | 0.29 |
| 8 | 2457548.9330 | 0.0010 | 2457548.9331 | 0.0013 | –0.0001 | –0.14 |
| 9 | 2457549.0592 | 0.0010 | 2457549.0590 | 0.0012 | 0.0002 | 0.29 |
| 10 | 2457549.9725 | 0.0007 | 2457549.9664 | 0.0009 | 0.0061 | 8.78 |
| 11 | 2457564.9573 | 0.0008 | 2457564.9569 | 0.0008 | 0.0004 | 0.58 |
| 12 | 2457566.9124 | 0.0011 | 2457566.9127 | 0.0010 | –0.0003 | –0.43 |
| 13 | 2457567.9544 | 0.0011 | 2457567.9538 | 0.0011 | 0.0006 | 0.86 |
| 14 | 2457568.9956 | 0.0009 | 2457568.9959 | 0.0014 | –0.0003 | –0.43 |
| 15 | 2457570.9520 | 0.0012 | 2457570.9516 | 0.0013 | 0.0004 | 0.58 |

*Notes: The TOM were determined in* PERANSO *using a 5th order polynomial expression fitted to the peaks of the light curve. The last two columns on the right show the differences in days (d) and minutes (min) between the TOM in wl and the TOM in V magnitude. Unacceptably large differences are seen for peak 4 and peak 10.*

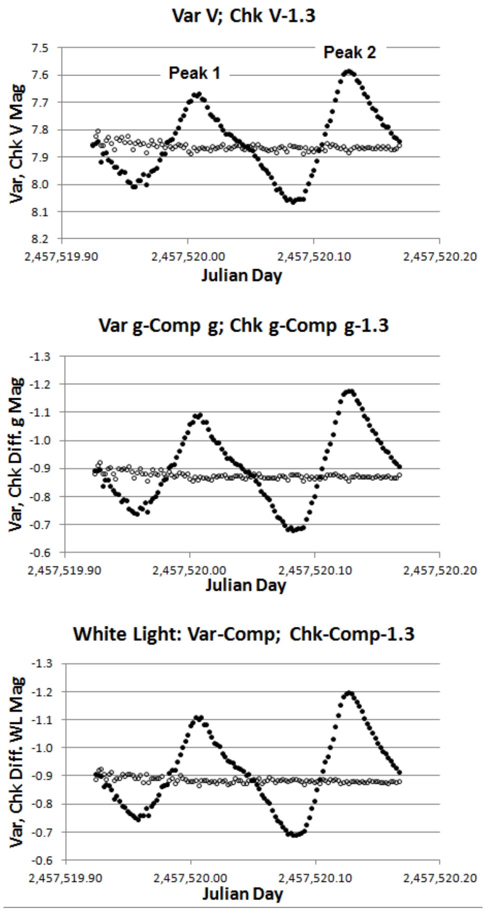

Figure 1. Light curves of V703 Sco and the check star from observations taken on one night and showing Peaks 1 and 2 (as listed in Tables 3 and 4). The check star magnitudes shown are the actual calculated magnitudes minus 1.3. The upper panel shows magnitudes transformed to the Johnson V system. The middle panel shows non-transformed magnitudes from the green channel data. The bottom panel shows non-transformed magnitudes from white light images.

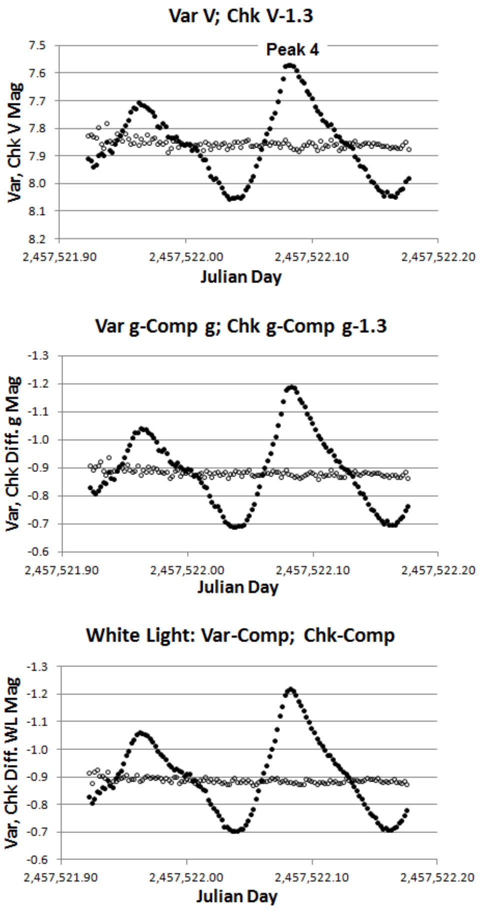

Figure 2. Light curves of V703 Sco and the check star from observations taken on one night and including Peak 4 (as listed in Tables 3 and 4).

Table 4. Times of maximum (TOM) of V703 Sco from center moving averages (over 3 magnitude determinations), in heliocentric Julian days (HJD) in white light (wl) and V magnitude.

| *Peak* | *HJD TOM wl* | *Error* | *HJD TOM V Mag* | *Error* | *wl TOM – V Mag TOM (d)* | *wl TOM – V Mag TOM (min)* |
|---|---|---|---|---|---|---|
| 1 | 2457520.0105 | 0.0006 | 2457520.0112 | 0.0007 | -0.0007 | -1.01 |
| 2 | 2457520.1310 | 0.0004 | 2457520.1312 | 0.0004 | -0.0002 | -0.29 |
| 3 | 2457521.0486 | 0.0005 | 2457521.0487 | 0.0006 | -0.0001 | -0.14 |
| 4 | 2457522.0824 | 0.0004 | 2457522.0868 | 0.0005 | -0.0044 | -6.34 |
| 5 | 2457523.0061 | 0.0005 | 2457523.0067 | 0.0004 | -0.0006 | -0.86 |
| 6 | 2457523.1279 | 0.0003 | 2457523.1279 | 0.0006 | 0.0 | 0.00 |
| 7 | 2457548.0173 | 0.0005 | 2457548.0172 | 0.0006 | 0.0001 | 0.14 |
| 8 | 2457548.9325 | 0.0006 | 2457548.9323 | 0.0006 | 0.0002 | 0.29 |
| 9 | 2457549.0590 | 0.0005 | 2457549.0591 | 0.0007 | -0.0001 | -0.14 |
| 10 | 2457549.9728 | 0.0006 | 2457549.9669 | 0.0007 | 0.0059 | 8.50 |
| 11 | 2457564.9574 | 0.0006 | 2457564.9573 | 0.0006 | 0.0001 | 0.14 |
| 12 | 2457566.9123 | 0.0006 | 2457566.9127 | 0.0006 | -0.0004 | -0.58 |
| 13 | 2457567.9544 | 0.0007 | 2457567.9538 | 0.0006 | 0.0006 | 0.86 |
| 14 | 2457568.9954 | 0.0005 | 2457568.9954 | 0.0006 | 0.0 | 0.00 |
| 15 | 2457570.9520 | 0.0005 | 2457570.9519 | 0.0008 | 0.0001 | 0.14 |

*Notes: The TOM were determined in* PERANSO *using a 5th order polynomial expression fitted to the peaks of the light curve. The last two columns on the right show the differences in days (d) and minutes (min) between the TOM in wl and the TOM in V magnitude. Unacceptably large differences are seen for peak 4 and peak 10.*

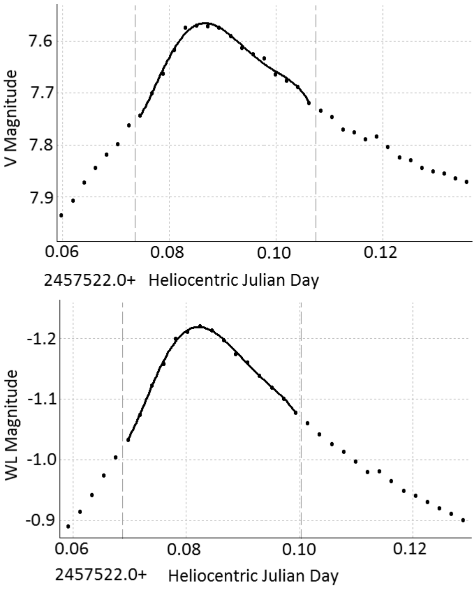

Figure 3. Part of the light curve of V703 Sco, comprising the region around Peak 4 (as listed in Tables 3 and 4). This is one of the peaks where the TOM differed markedly between the V magnitude data (top panel) and white light magnitude data (bottom panel). The curves were fitted in PERANSO as 5th order polynomial expressions. The Peak and the descending limb of the light curve in white light are smoother than those in the V magnitude light curve.

line is then drawn by hand through the mid points of the chords, and the point at which that line intersects the light curve is taken to be the TOM of the peak. The results for this procedure are shown in Table 5, which reveals that the large discrepancies between the white light TOM and the V magnitude TOM, as seen in Tables 1 and 2, did not persist.

### 3.2. Fourier analysis of the light curve of V703 Sco in V magnitude and in white light

The Lomb-Scargle routine in the software PERANSO was employed for this analysis which was applied to the V-magnitude data and the data in white light, with identical results. Each frequency search requires the input of the start and end frequencies and the resolution, i.e., the number of steps between those frequencies. For f1 (the first frequency sought), start and end frequencies initially selected were 0 and 20 c d$^{-1}$ with a resolution of 800, yielding a dominant frequency of 8.67783 c d$^{-1}$. This frequency was refined by a second search between 8.5 and 8.8 c d$^{-1}$ with a resolution of 1,000, the new frequency being 8.67760 c d$^{-1}$. In each case, the corresponding period to four decimal places was 0.1152 d. The data were then prewhitened for the refined frequency, and f2 (the second frequency sought) was found between start and end frequencies of 0 and 20 c d$^{-1}$ with a resolution of 750, yielding a frequency of 6.67333 c d$^{-1}$. This frequency was refined by a second search between 6 and 7 c d$^{-1}$ with a resolution of 1,000, yielding a frequency of 6.66900 c d$^{-1}$. In each case the corresponding period to four decimal places was 0.1499 d. The power spectra from these analyses for the light curve in white light are shown in Figure 4. As the power spectra for the V-magnitude light curve were identical, they are not shown. The two periods, 0.1152 d and 0.1499 d, are identical (to four decimal places) to those reported in the previous literature.

## 4. Discussion

The purpose of this study was to determine whether or not DSLR photometry in white light yielded valid data by comparing the results with photometry based on non-transformed data from the green channel of the DSLR sensor, and with photometry based on data from the green channel transformed to the Johnson V standard. Because only simple differential photometry could be achieved from the non-transformed data from the green channel and from white light data, no useful information about the color of the variable star could be gained. Therefore, analyses of the results were confined to parameters involving time, namely, the times of maximum of the light curve and period analysis using Fourier

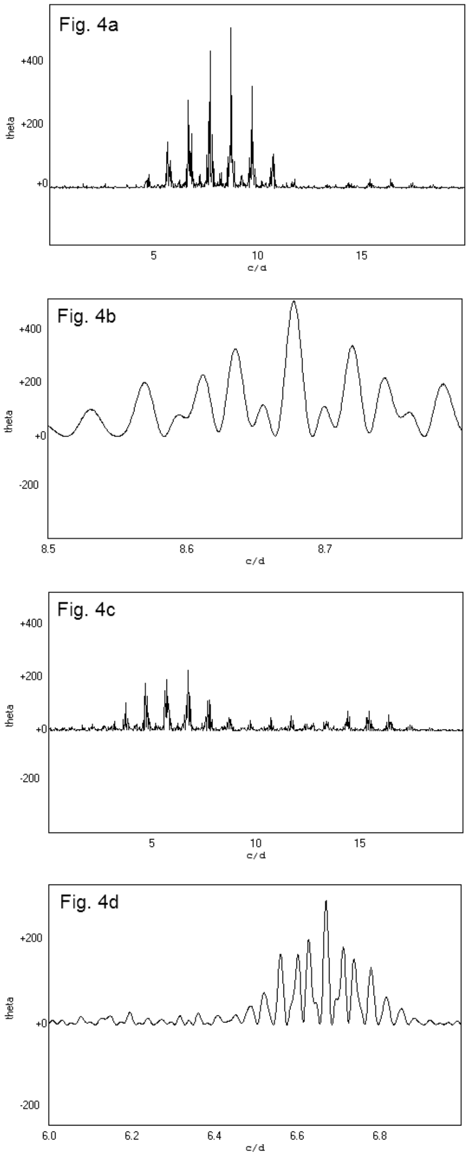

Figure 4. PERANSO Lomb-Scargle power spectra of V703 Sco from white light images. The power spectra of V magnitude data were identical, and are not shown. In the following, f1 is the first discovered frequency and P1 its corresponding period; f2 is the second discovered frequency and P2 its corresponding period. 4a: f1=8.67783 c d-1, P1=0.1152 d, from 0-20 c d-1 at a resolution of 800. 4b: refined frequency for f1=8.6770 c d-1, P1=0.1152, from 8.5-8.8 c d-1 at a resolution of 1000. 4c: after prewhitening for 8.6770 c d-1, f2=6.67333 c d-1, P2=0.1499 d, from 0-20 c d-1 at a resolution of 750. 4d: refined frequency for f2=6.66900 c d-1, P2=0.1499 d, from 6-7 c d-1 at a resolution of 1000.

Table 5. Times of maximum (TOM) of peaks 4 and 10 (from Tables 3 and 4 above) of the light curve of V703 Sco, remeasured by the Podgson method (see text of paper).

| *Peak* | *HJD TOM wl* | *HJD TOM V Mag* | *wl TOM – V Mag TOM (d)* | *wl TOM – V Mag TOM (min)* |
|---|---|---|---|---|
| 4 | 2457522.082 | 2457522.081 | 0.001 | 1.44 |
| 10 | 2457549.966 | 2457549.966 | 0.0 | 0.0 |

*Note: Abbreviations are as for Table 4.*

decomposition. The amplitudes of the light curves for each night, and the ranges and standard deviations of the check star magnitude data for each night were also compared between transformed V magnitude data, non-transformed data from the green channel, and white light data.

When the TOM of the light curve were determined by fitting fifth-order polynomial expressions to the peaks, 13 of the 15 measured peaks gave similar results in white light and V magnitude, with the largest difference being 2.30 min. However, peaks 4 and 10 (from Table 1) had discrepancies of –6.34 min and 8.78 min, respectively, between the white light and V magnitude times, which are too large to be acceptable. In view of these results, the TOM were recalculated from light curve data plotted as center moving averages over three consecutive magnitude values. As in the case of the non-averaged magnitude data large discrepancies between white light and V magnitude TOM were still present for peaks 4 and 10, whereas all of the other peaks had acceptable results (Table 3).

It was considered likely that the large discrepancies between TOM were based upon imprecision in the magnitude determinations near the peaks of the light curve, resulting in spurious assignment of the TOM based on the fitting of the fifth-order polynomial expressions in PERANSO. Therefore, the TOM of the peaks with the discrepant results for the raw magnitude data (not the moving average data) were recalculated using the Podgson method of bisected chords, a manual method requiring the use of curve fitting by hand. With the latter, the discrepancies between white light and V magnitude TOM became much less, the largest now being 1.44 min.

In order to set these results in the context of other studies which have published the TOM of light curves for the construction of O–C (observed minus computed) diagrams of variable stars, the author's previously published work on the δ Scuti star ZZ Mic is considered. The range of O–C values calculated from observations taken over a time of 9.3 d was 2.62 min. (Axelsen and Napier-Munn 2015). It is therefore concluded that the precision of the determination of TOM of light curve peaks from white light photometry would be sufficient for successful application to the study of variable stars using O–C diagrams. However, in view of the unacceptably large differences between the TOM of white light and V magnitude data for 2 of 15 light curve peaks for V703 Sco, caution is required in the use of white light DSLR photometry. If this method is used for O–C diagrams, it would be necessary to gather TOM data from several peaks over relatively short periods of time to ensure that the variance of the data is acceptable.

The final test was to compare results of Fourier analysis of V703 Sco white light data with the results of a similar analysis of data in V magnitude. The comparison clearly showed that the analyses were identical in all respects: the appearances of the power spectra, the dominant frequencies revealed before and after refining the frequency searches, and the outcome of a second frequency search after prewhitening for the first frequency. It is concluded that it is valid to carry out Fourier analysis of DSLR photometric data taken in white light.

Finally, it is necessary to consider the colors of the variable, comparison, and check stars used in this study. The B–V for

V703 Sco varies from 0.2 to 0.5 from the author's DSLR photometry in B and V. The B–V color indices of the comparison and check stars (HD 160927 and HD 160432) were 0.533 and 0.457, respectively. The latter two values are relatively close to the range of B–V values displayed by V703 Sco as it cycles through a period. Therefore, if DSLR photometry in white light is to be attempted with variable and comparison stars having markedly differing colors and thus markedly differing B–V color indices, caution should be observed in the interpretation of the results, as it should not be assumed that the precision of the measurements would be similar to the precision described in the present paper.

## 5. Conclusions

A novel technique of DSLR photometry, involving analyzing images in white light, has been investigated using data obtained from a study of the high amplitude δ Scuti star V703 Sco. Images in white light can be used only to analyze variable star parameters involving time. Aperture photometry was performed on images taken in white light, and repeated on the same set of images to obtain non-transformed differential magnitudes from the green channel, and magnitudes transformed to the Johnson V system. Analysis indicates that the precision of white light photometry is slightly greater than the precision of photometry with non-transformed green channel data, and slightly greater than the precision of measurements in V magnitude. For the majority of peaks, the TOM of the light curves in white light and V magnitude differed by only small time intervals. Fourier analysis by the Lomb-Scargle method showed identical results for white light data and data in V magnitude. It is concluded that DSLR photometry of variable stars in white light is a valid technique for timing the peaks (and by inference the troughs) of light curves, and for Fourier analysis of pulsating variable stars, at least for variable and comparison stars having similar color indices.

## References

AAVSO. 2016, *The AAVSO DSLR Observing Manual, Version 1.4*, AAVSO, Cambridge, MA (https://www.aavso.org/dslr-observing-manual).

Axelsen, R. A. 2014a, *J. Amer. Assoc. Var. Star Obs.*, **42**, 37.

Axelsen, R. A. 2014b, *J. Amer. Assoc. Var. Star Obs.*, **42**, 44.

Axelsen, R. A. 2014c, *J. Amer. Assoc. Var. Star Obs.*, **42**, 287.

Axelsen, R. A. 4014d, *J. Amer. Assoc. Var. Star Obs.*, **42**, 292.

Axelsen, R. A. 2015, *J. Amer. Assoc. Var. Star Obs.*, **43**, 182.

Axelsen, R. A., and Napier-Munn, T. 2015, *J. Amer. Assoc. Var. Star Obs.*, **43**, 50.

Axelsen, R. A., and Napier-Munn, T. 2016, *J. Amer. Assoc. Var. Star Obs.*, **44**, 119.

Berry, R., and Burnell, J. 2011, "Astronomical Image Processing for Windows," version 2.4.0, provided with *The Handbook of Astronomical Image Processing*, Willmann-Bell, Richmond, VA.

Deshmukh, S. 2015, *J. Amer. Assoc. Var. Star Obs.*, **43**, 172.

Hoot, J. E. 2007, in *The Society for Astronomical Sciences 26th Annual Symposium on Telescope Science*, Society for Astronomical Sciences, Rancho Cucamonga, CA., 67.

Kloppenborg, B. K., Pieri, R., Eggenstein, H.-B., Maravelias, G., and Pearson, T. 2012. *J. Amer. Assoc. Var. Star Obs.*, **40**, 815.

Koen, C. 2001, *Mon. Not. Roy. Aston. Soc.*, **321**, 44.

Loughney, D. 2010, *J. Br. Astron. Assoc.*, **120**, 157.

Menzies, J. W., Cousins, A. W. J., Banfield, R.M., and Laing, J. D. 1989, *S. Afr. Astron. Obs. Circ.*, **13**, 1.

Oosterhoff, P. Th. 1966, *Bull. Astron. Inst. Netherlands*, **18**, 140.

Percy, J. R. 2007, *Understanding Variable Stars*, Cambridge Univ. Press, New York, 62.

Ponsen, J. 1961, *Bull. Astron. Inst. Netherlands*, **15**, 325.

Ponsen, J. 1963, *Bull. Astron. Inst. Netherlands*, **17**, 29.

Richards, T. 2012, *J. Amer. Assoc. Var. Star Obs.*, **40**, 983.

Vanmuster, T. 2014, Light curve and period analysis software, PERANSO V.2.51 (http://www.peranso.com/).

Walker, S., Butterworth, N., and Pearce, A. 2015, *J. Amer. Assoc. Var. Star Obs.*, **43**, 227.

# Inter-observer Photometric Consistency Using Optec Photometers

**Tom Calderwood**
*1184 NW Mt. Washington Drive, Bend, OR 97703; tjc@cantordust.net*

**Jim Kay**
*26 Steeplebush Road, Shelburne, VT 05482; jimjanekay@msn.com*

**Scott Burgess**
*4 Rob Clark Street, Winterport, ME 04496; ScottAstroNut@aol.com*

**Erwin van Ballegoij**
*De Rogge 6, Heesch, 5384 XD, Netherlands; AAVSO.ID.BVE@HOME.NL*

*Received February 8, 2017; revised March 29, 2017; accepted March 30, 2017*

**Abstract** Four observers, over a wide geographic range, observe slowly-varying stars in Johnson B and V bands using Optec SSP-3 and SSP-5 photometers on telescopes of modest size. Significant corrections for transformation and extinction were applied to their data, and we find very close agreement among them. In paired same-night observations, the median absolute difference between observers was 7 mmag. For the two observers with the most measurements in common, we estimate a systematic difference of 3.2 mmag or less.

## 1. Background

According to Henden (2017), published evaluations of consistency among photoelectric photometry (PEP) observers practicing differential photometry are difficult to find. Landis *et al.* (1985) describe a two-observer project to determine time-of-maximum of V396 Per. Based upon fitted data, they claim about ± 3 mmag rms deviation from the fit for each observer, and a systematic difference of about ± 1 mmag between observers. However, no documentation for the fit is provided, and the authors note that the exact period (which would affect the fit) is not known. All the authors are now deceased, so no further details are available. This study was conducted in V band only, with transformation adjustments of approximately 1 mmag, and it is not clear if measured or assumed extinction coefficients were employed. In the authors' words, "Differential photometry of this accuracy was possible because every pertinent factor was nearly ideal." Key factors were the small color difference between variable and comparison, minor differential extinction, and small transformation coefficients. It appears that Landis owned a DC photomultiplier photometer at the time of the study (Landis 1984), while Louth had a pulse-counting photometer (Skillman 1980), but it is not certain if these were the instruments used.

Cortesi and Poretti (1993) describe PEP observations of 44 Tau from two sites. They estimate a difference of 8.5 mmag between the observers, again V band only, based upon a fit. Transformations, if applied, would have been very small, on account of Δ(B–V) on the order of –0.007 (Tycho). It is not clear if extinction corrections were applied, and the authors note an ambiguity in the fit.

In Calderwood *et al.* (2015), two photoelectric observers operating simultaneously at the same location with closely-matched equipment achieved V-band measurements of common target stars with a median difference of 0.006 magnitude. Optec SSP-3 photometers were used at a fairly dark mountain location, and transformation corrections greater than those found in the Landis study were employed.

In this study, we step beyond the 1985, 1993, and 2015 projects. Data were taken in both B and V bands, with transformation effected largely using measured color contrast, and extinction corrected largely using measured extinction coefficients. Data are compared on a same-night basis rather than a fit. The participants used a variety of instrumentation as shown in Table 1 (the SSP-3 device has a photodiode sensor, while the SSP-5 uses a photomultiplier tube (Optec 2016)). CTOA was at an altitude of approximately 1,000 m, while the other observers were within 100 m of sea level. All locations had significant light pollution.

Table 1. Observers and equipment.

| *Observer* | *Location* | *Photometer* | *Filters* | *Optics* |
|---|---|---|---|---|
| CTOA | Oregon | SSP-5 | B,V | 9.25" Schmidt-cassegrain |
| KJMB | Vermont | SSP-3 | B,V | 14" Schmidt-cassegrain |
| BSO | Maine | SSP-3 | V | 8.3" cassegrain |
| BVE | Netherlands | SSP-3 | B,V | 10" Schmidt-cassegrain |

## 2. Observations

Stars already of interest in the AAVSO Photoelectric Photometry (PEP) program (AAVSO 2016a) were selected for this study. Since simultaneous observations would not generally be possible, targets of modest short-term variability were chosen: α Com, P Cyg, W Boo, ρ Cas, and R Lyr. These were bright enough that observers with small apertures could participate. Data were taken between May and September 2016. Difficulties with weather and equipment limited the number of same-night pairs to 31, which are summarized in Table 2.

Table 2. Observation summary.

| *Star* | *B pairs* | *V pairs* |
|---|---|---|
| α Com | 1 | 1 |
| W Boo | 2 | 2 |
| P Cyg | 0 | 3 |
| ρ Cas | 8 | 13 |
| R Lyr | 0 | 1 |

Table 3. Example adjustments to ρ Cas instrumental magnitudes, in mmag.

| *Obs* | *RJD* | *1st ext*$_B$ | *1st ext*$_V$ | *2nd ext*$_B$ | *xform*$_B$ | *xform*$_V$ | *net*$_B$ | *net*$_V$ |
|---|---|---|---|---|---|---|---|---|
| CTOA | 57645 | –4 | –2 | –16 | –4 | 24 | –24 | 22 |
| KJMB | 57634 | –3 | –2 | –16 | –42 | 16 | –61 | 14 |
| BSO | 57643 | — | –3 | — | — | 9 | — | 6 |
| BVE | 57693 | –2 | –1 | –14 | –57 | 12 | –73 | 11 |

Magnitudes were measured differentially using the PEP program comparison stars (AAVSO 2016b). The PEP protocol uses an alternating sequence of multiple comparison/variable samples (AAVSO 2016c), with the variable usually sampled three times, and sky samples accompanying each star sample. Individual differential magnitudes are computed for each variable sample, and the mean is taken as the reduced magnitude. The 1σ error is computed as the standard deviation of that mean. Two-color data were gathered by interleaving B and V samples in a single sequence.

## 3. Reductions

All data were reduced using a PYTHON program written by one of us. Instrumental magnitudes were adjusted for transformation, first-order differential extinction between the variable and comparison, and, likewise, for second-order extinction in B band. Assumed first-order extinction coefficients were used for BSO and BVE reductions, while CTOA and KJMB reductions almost always used measured extinctions. A priori, it was decided to establish an upper limit for acceptable errors. Any observation with a 1σ error greater than 0.015 was discarded (for the bright stars in this study, 0.015 is a large uncertainty). If either band's measurement in a two-band sequence failed this test, both bands were discarded. Whenever available, the measured Δ(b–v) was used to calculate Δ(B–V) to effect transforms, otherwise a catalog Δ(B–V) was used (Δ(b–v) was always available for second-order extinction calculations).

## 4. Problems and limitations

CTOA's system showed systematically bright B magnitudes, on the order of 40–60 mmag for R Lyr and P Cyg when compared to other observers. These excesses, as will be seen, are far greater than other inter-observer discrepancies. The B pairs involving CTOA for these two stars have been dropped, which partially accounts for the relative shortfall of B band data in this study.

While the target/comparison pairs collectively exhibited a considerable range of color contrast, no Δ(B–V) was extreme. W Boo and ρ Cas, with contrasts of approximately 0.64 and –0.40, were the most challenging in this respect. The stars were generally measured at low airmass (X < 1.2), which minimized the effects of first- and second-order extinction. Table 3 illustrates typical extinction and transformation adjustments for ρ Cas.

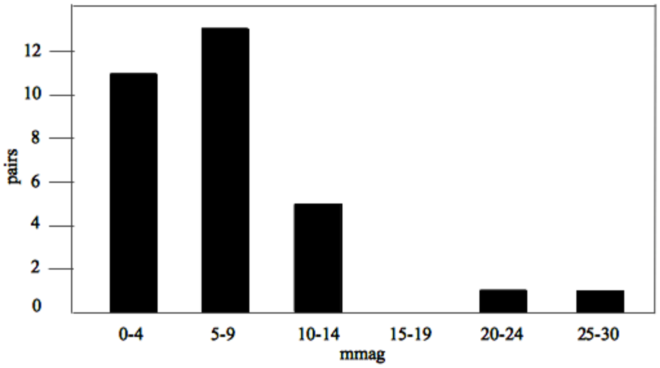

Figure 1. |ΔM| histogram, all observers.

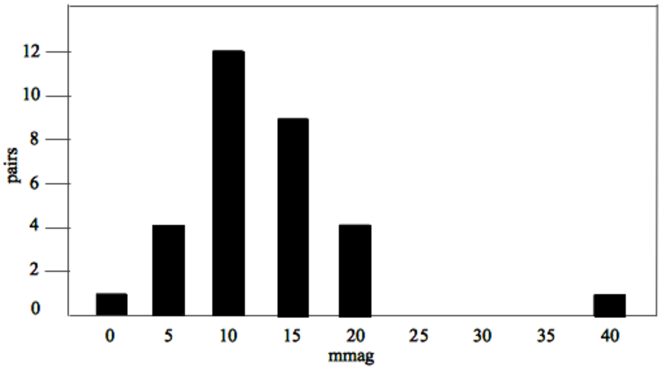

Figure 2. 2σ error budget histogram, all observers.

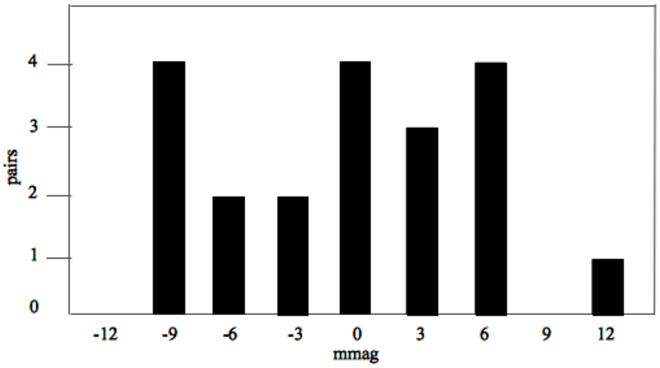

Figure 3. CTOA/KJMB ΔM histogram.

## 5. Evaluation

For comparison with the 2015 study, we first applied a 2σ overlap as a criterion for inter-observer consistency.

If the difference between a pair of magnitudes was less than or equal to the sum of their 2σ errors, we deemed them to be in agreement. The data are summarized in Table 4 and Figures 1 and 2 (both figures include the pairs that failed to agree). Twenty-nine of the thirty-one pairs achieved agreement, with the median absolute delta being 7 millimags. Note that on 57636 and 57641, all three of CTOA, KJMB, and BSO had V measurements of ρ Cas, and each pairwise comparison is included.

Table 4. Pairwise observation data.

| *RJD* | *Star* | *Band* | *Obs$_1$* | *JD Frac$_1$* | *M$_1$* | *err$_1$* | *Obs$_2$* | *JD Frac$_2$* | *M$_2$* | *err$_2$* | *ΔM* | *2•err$_{1+2}$* | *agree* |
|---|---|---|---|---|---|---|---|---|---|---|---|---|---|
| 57519 | α Com | B | CTOA | 0.739 | 4.783 | 0.003 | KJMB | 0.623 | 4.778 | 0.007 | 0.005 | 0.020 | Y |
| 57519 | α Com | V | CTOA | 0.740 | 4.332 | 0.004 | KJMB | 0.621 | 4.337 | 0.002 | –0.005 | 0.012 | Y |
| 57573 | W Boo | B | CTOA | 0.761 | 6.429 | 0.006 | KJMB | 0.631 | 6.438 | 0.003 | –0.009 | 0.018 | Y |
| 57573 | W Boo | V | CTOA | 0.762 | 4.744 | 0.002 | KJMB | 0.630 | 4.742 | 0.003 | 0.002 | 0.010 | Y |
| 57575 | W Boo | B | CTOA | 0.756 | 6.432 | 0.006 | KJMB | 0.652 | 6.429 | 0.003 | 0.003 | 0.018 | Y |
| 57575 | W Boo | V | CTOA | 0.756 | 4.739 | 0.001 | KJMB | 0.651 | 4.726 | 0.006 | 0.013 | 0.014 | Y |
| 57607 | ρ Cas | B | CTOA | 0.866 | 5.754 | 0.005 | KJMB | 0.676 | 5.747 | 0.003 | 0.007 | 0.016 | Y |
| 57607 | ρ Cas | V | CTOA | 0.866 | 4.475 | 0.002 | KJMB | 0.674 | 4.475 | 0.003 | 0.000 | 0.010 | Y |
| 57608 | ρ Cas | B | CTOA | 0.804 | 5.744 | 0.004 | KJMB | 0.825 | 5.744 | 0.004 | 0.000 | 0.016 | Y |
| 57608 | ρ Cas | V | CTOA | 0.804 | 4.469 | 0.004 | KJMB | 0.824 | 4.479 | 0.003 | –0.010 | 0.014 | Y |
| 57634 | ρ Cas | B | CTOA | 0.825 | 5.692 | 0.002 | KJMB | 0.664 | 5.695 | 0.004 | –0.003 | 0.012 | Y |
| 57634 | ρ Cas | V | CTOA | 0.825 | 4.446 | 0.002 | KJMB | 0.665 | 4.448 | 0.002 | –0.002 | 0.008 | Y |
| 57636 | ρ Cas | B | CTOA | 0.749 | 5.688 | 0.001 | KJMB | 0.737 | 5.697 | 0.007 | –0.009 | 0.016 | Y |
| 57636 | ρ Cas | V | CTOA | 0.749 | 4.451 | 0.001 | KJMB | 0.735 | 4.459 | 0.005 | –0.008 | 0.012 | Y |
| 57636 | ρ Cas | V | CTOA | 0.749 | 4.451 | 0.001 | BSO | 0.618 | 4.451 | 0.002 | 0.000 | 0.006 | Y |
| 57636 | ρ Cas | V | BSO | 0.618 | 4.451 | 0.002 | KJMB | 0.735 | 4.459 | 0.005 | –0.008 | 0.012 | Y |
| 57639 | ρ Cas | B | CTOA | 0.769 | 5.685 | 0.003 | BVE | 0.455 | 5.710 | 0.007 | –0.025 | 0.020 | N |
| 57639 | ρ Cas | V | CTOA | 0.770 | 4.451 | 0.001 | BVE | 0.454 | 4.441 | 0.011 | 0.010 | 0.024 | Y |
| 57641 | ρ Cas | B | CTOA | 0.772 | 5.689 | 0.001 | KJMB | 0.592 | 5.682 | 0.002 | 0.007 | 0.006 | N |
| 57641 | ρ Cas | V | CTOA | 0.772 | 4.446 | 0.002 | BSO | 0.638 | 4.439 | 0.006 | 0.007 | 0.016 | Y |
| 57641 | ρ Cas | V | CTOA | 0.772 | 4.446 | 0.002 | KJMB | 0.594 | 4.446 | 0.003 | 0.000 | 0.010 | Y |
| 57641 | ρ Cas | V | KJMB | 0.594 | 4.446 | 0.003 | BSO | 0.638 | 4.439 | 0.006 | 0.007 | 0.016 | Y |
| 57643 | ρ Cas | V | CTOA | 0.798 | 4.447 | 0.003 | BSO | 0.569 | 4.446 | 0.007 | 0.001 | 0.020 | Y |
| 57644 | ρ Cas | B | CTOA | 0.780 | 5.691 | 0.001 | KJMB | 0.744 | 5.696 | 0.003 | –0.005 | 0.008 | Y |
| 57644 | ρ Cas | V | CTOA | 0.781 | 4.446 | 0.004 | KJMB | 0.744 | 4.446 | 0.001 | 0.000 | 0.010 | Y |
| 57645 | ρ Cas | B | CTOA | 0.695 | 5.697 | 0.006 | BVE | 0.422 | 5.721 | 0.015 | –0.024 | 0.042 | Y |
| 57645 | ρ Cas | V | CTOA | 0.696 | 4.452 | 0.002 | BVE | 0.421 | 4.463 | 0.004 | 0.011 | 0.012 | Y |
| 57643 | R Lyr | V | CTOA | 0.696 | 3.959 | 0.001 | KJMB | 0.585 | 3.957 | 0.001 | 0.002 | 0.004 | Y |
| 57608 | P Cyg | V | CTOA | 0.763 | 4.770 | 0.004 | KJMB | 0.751 | 4.765 | 0.001 | 0.005 | 0.010 | Y |
| 57641 | P Cyg | V | CTOA | 0.794 | 4.788 | 0.002 | BSO | 0.602 | 4.781 | 0.006 | 0.007 | 0.016 | Y |
| 57643 | P Cyg | V | CTOA | 0.717 | 4.802 | 0.008 | BSO | 0.535 | 4.788 | 0.001 | 0.014 | 0.018 | Y |

## 6. Statistical evaluation

CTOA and KJMB had 20 observations in common, which provided an opportunity for statistical analysis through a paired t test. The null hypothesis, $H_0$, is that the means of the difference of the pairs of observations is zero, or equivalently that the systematic error between the observations is not significant compared to the random error. The variances of the underlying distributions for each observer were not assumed to be the same, so we used the Welch t-test method of determining the t statistic, and degrees of freedom. The resulting p value is 0.80, so we cannot reject the null hypothesis at our chosen significance level of 0.05.

The actual sample mean of the differences between these observation pairs is 0.000 magnitude, with a median value of 0.000 and a standard deviation of 0.006 magnitude. The 95% confidence interval of the mean of the difference between two readings is –0.0032 mag to 0.0025 mag. Our interpretation of the confidence interval is that with 95% confidence the systematic difference between these two observers is less than 3.2 mmag for the stars observed.

We interpret the sample mean value as our best estimate of the systematic error between observations, with the standard deviation as our estimate of the random error. These estimates are with respect to internal consistency between the two observers. We make no estimates of systematic or random errors with respect to magnitudes in the UBV standard system.

Figure 3 summarizes the magnitude deltas for the 20 pairs, the median of which was 0 mmag.

## 7. Conclusion

It is clearly possible for well-calibrated observers using good technique to achieve highly consistent results using the Optec photometers. We do not wish to attach great importance to the specific value of the estimate of offset between CTOA and KJMB—individual millimags are significant in the calculations and rounding effects come into play. The point is that the number is quite small.

## 8. Future work

We wish to track down the cause of B band excess in CTOA measurements of the above-noted stars, which we believe are due to a systematic effect in the CTOA instrument. Since the conclusion of the study, weather conditions at the site have not permitted significant investigation of this problem.

## 9. Acknowledgements

The authors would like to thank Philip Kaaret for helpful suggestions in the preparation of this paper. The authors would also like to thank the referee for helpful feedback.

## References

AAVSO. 2016a, Photoelectric Photometry Program (https://www.aavso.org/content/aavso-photoelectricphotometry-pep-program).

AAVSO. 2016b, List of Target, Comparison, and Check Stars for PEP-V Observations (https://www.aavso.org/pep-starparm).

AAVSO. 2016c, The Photoelectric Photometry (PEP) Observing Program of the AAVSO: An Introduction (https://www.aavso.org/photoelectric-photometry-pep-observing-program-aavso-introduction).

Calderwood, T., Getz, E., McBratney, T., and Holcomb, E. 2015, *J. Amer. Assoc. Var. Star Obs.*, **43**, 241.

Cortesi, S., and Poretti, E. 1993, *I.A.P.P.P. Commun.*, **50**, 19.

Henden, A. 2017, private communication.

Landis, H. 1984, *AAVSO Photoelectric Photometry Newsletter*, March 1984.

Landis, H., Louth, H., and Hall, D. S. 1985, *Inf. Bull. Var. Stars*, No. 2662, 1.

Optec. 2016, SSP Photometer Series (http://optecinc.com/astronomy/catalog/ssp/index.htm).

Skillman, B. 1980, *AAVSO Photoelectric Photometry Newsletter*, May 1980, 2.

# Digitizing Olin Eggen's Card Database

**Jack Crast**
*1784 Lisle Rd, Owego, NY 13827; jackcrast@gmail.com*

**George Silvis**
*194 Clipper Rd, Bourne, MA 02532; SGEO@GASilvis.net*

*Received October 31, 2016; revised December 20, 2016; accepted February 10, 2017*

**Abstract** The goal of the Eggen Card Database Project is to recover as many of the photometric observations from Olin Eggen's Card Database as possible and preserve these observations, in digital forms that are accessible by anyone. Any observations of interest to the AAVSO will be added to the AAVSO International Database (AID). Given to the AAVSO on long-term loan by the Cerro Tololo Inter-American Observatory, the database is a collection of over 78,000 index cards holding all Eggen's observations made between 1960 and 1990. The cards were electronically scanned and the resulting 108,000 card images have been published as a series of 2,216 PDF files, which are available from the AAVSO web site. The same images are also stored in an AAVSO online database where they are indexed by star name and card content. These images can be viewed using the EGGEN CARD PORTAL online tool. Eggen made observations using filter bands from five different photometric systems. He documented these observations using 15 different data recording formats. Each format represents a combination of filter magnitudes and color indexes. These observations are being transcribed onto spreadsheets, from which observations of value to the AAVSO are added to the AID. A total of 506 U, B, V, R, and I observations were added to the AID for the variable stars S Car and l Car. We would like the reader to search through the card database using the EGGEN CARD PORTAL for stars of particular interest. If such stars are found and retrieval of the observations is desired, e-mail the authors, and we will be happy to help retrieve those data for the reader.

## 1. Introduction

Olin Jeuck Eggen was born on July 9, 1919, in Rock County, Wisconsin. He earned a B.A. from the University of Wisconsin in 1940. After serving in World War II as a civilian with the U.S. Air Force, U.S. Navy, and as a courier for the Office of Strategic Services (OSS), he returned to the University of Wisconsin and earned a Ph.D. in astronomy in 1948. He held staff positions at Lick Observatory, Royal Greenwich Observatory, California Institute of Technology, Mt. Wilson Observatory, Mt. Stromlo Observatory (as Director), Australian National University, and Cerro Tololo Inter-American Observatory (Freeman *et al.* 2000). Eggen was well known as a proponent of small-telescope science.

Eggen was an extremely prolific researcher, publishing some 400 papers during his fifty-year career, with articles being written up until his death in 1998 from a heart attack. However, Eggen published only a small part of the enormous amount of data he collected over his lifetime.

The Eggen Archive is held in the Steenbock Library at University of Wisconsin, Madison. The AAVSO is most interested in this untapped data resource. All his observations were handwritten onto index cards that he kept in his office. Often, when a visitor would ask a question about a star, he would look up the coordinates, go to his card file, and retrieve observations that he had made of that target.

In early 2007, the AAVSO contacted Cerro Tololo Inter-American Observatory (CTIO) to find out what had happened to that card catalog, mainly because they were interested in some observations that Eggen had made on a variable star but had never published. CTIO had taken the cards out of Eggen's office upon his passing, and had placed them in storage at La Serena. Since they were not serving any useful purpose in storage, CTIO Director Alistair Walker gave the AAVSO the entire collection of 78,000 cards on long-term loan.

The American Astronomical Society (AAS) helped with a Small Research Grant in 2007 to pay for the equipment to scan the cards. John Menke gave a grant for the publishing of the scans (Henden 2009).

## 2. Tools and methods

The Eggen cards are presently stored at AAVSO Headquarters (Figure 1). One of several cards for the variable star S Car is shown in Figure 2. On the left side of the card are UBV observations and on the right side are RI observations. This card contains a portion of a sequence of observations spanning multiple cards. Note that Eggen didn't record the observation times on this card. This was a common practice when observing stars not considered to be variable and for some long period variables.

This card will serve as an example throughout section 2 to show how cards in Eggen's database progress from card box to AID observations.

Figure 1. The Eggen Card Database as it arrived from CTIO (Henden 2009).

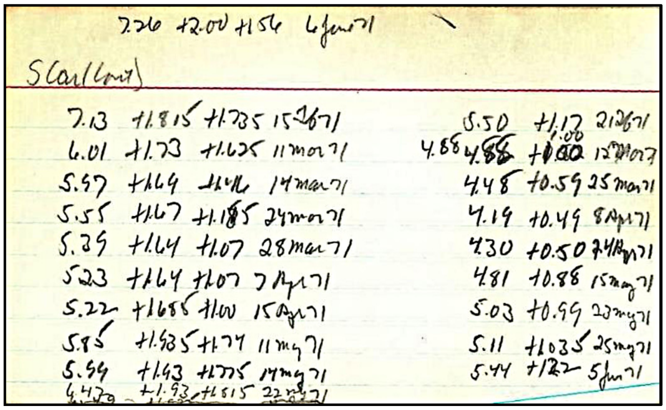

7.26 +2.00 +1.56 6Jun71

S Car (Cont)

7.13 +1.815 +1.735 15Feb71 5.50 +1.12 21Feb71
6.01 +1.73 +1.625 11Mar71 4.88 4.88 +1.00 12Mar71
5.97 +1.69 +1.6 14Mar71 4.48 +0.59 25Mar71
5.55 +1.67 +1.185 24Mar71 4.19 +0.49 8Apr71
5.39 +1.64 +1.07 28Mar71 4.30 +0.50 24Apr71
5.23 +1.64 +1.07 7Apr71 4.81 +0.88 15May71
5.22 +1.685 +1.00 15Apr71 5.03 +0.99 23May71
5.85 +1.935 +1.77 11May71 5.11 +1.035 25May71
5.94 +1.43 +1.775 14May71 5.44 +1.22 5Jun71
6.420 +1.93 +1.515 22May71

Figure 2. One of Eggen's cards documenting observations of the variable star S Car during 1971.

Table 1. Arrangement of bundles and PDF files in box 8B. The card shown in Figure 2 is addressed as page 5 of PDF file 7, in bundle C, in box 8B.

| *Box* | *Bundle* | *PDF Files* |
|---|---|---|
| 8B | A | 1,2,3,4,5,6,7,8,9,10 |
| | B | 1,2,3,4,5,6,7,8,9,10,11,12,13 |
| | C | 1,2,3,4,5,6,7,8,9,10<br>└──▶ Page 5 |
| | D | 1,2,3,4,5,6,7,8,9,10 |

## 2.1. Card scanning and publishing the card images

During the summers of 2007 and 2009, assistants scanned the 78,000 cards, creating over 108,000 images. The organization of the card images was based upon the organization of the physical cards in their 64 boxes. Each box was assigned an alphanumeric identification code. Some boxes contained groups of bundled cards, 258 in total. These bundles were assigned alphabetical identifiers.

The images were saved into 2,216 PDF files, grouped into 258 bundles which in turn were grouped into 64 boxes (Table 1). Individual cards images are found by their Box/Bundle/PDF file/Page address (Silvis 2013). This is not a one-to-one mapping between physical card and card image since many cards have data written on both sides, requiring two card images to be generated. The card in Figure 2 has the address "8B/C/7/5". Loose cards within a box are documented in separate PDF files under the bundle identifier of null. These card images are addressed as Box//PDF file/Page.

## 2.2. Indexing and classifying the cards

George Silvis, the project leader, copied the card images from the 2,216 PDF files into a MYSQL database residing on an AAVSO server. Indexing and categorizing the card images were performed using the EGGEN CARD PORTAL also developed by Silvis.

The card images are addressed using the same Box/Bundle/PDF file/Page system used for the original PDF files. Figure 3 shows the portal displaying card 8B/C/7/5, the card in Figure 2. The address has been entered in the input boxes in the line "Select Batch" line. This is a card search function which can be performed without needing special edit authorization. The "76" following the Request button shows the number of cards remaining in this PDF file after the card shown. The fields in the two "Edit Card:" lines cannot be altered without edit authority.

Card 8B/C/7/5 was retrieved from the database by entering "8B", "C", "7", and "5" into the "Box", "Bundle", "PDF", and "Page" boxes found on the "Select Batch" line. In the two "Edit Card" lines the card's color, orientation, and classification are displayed. Here the card's color is the default value of white, its orientation is "0" since the card did not need any rotation to properly view it, and its classification of "P" as a card with usable photometric observations. The "Note" box holds any comments concerning the card. To the right under the "Star" label is the star name assigned to this card. Next to it are buttons to display the SIMBAD entry for this star and a button to remove the name. Below the buttons is an input box for additional names, if more than one star is identified on the card (Silvis 2016a).

When indexing card images, the user must sign onto the portal by entering their AAVSO observer identification code and an edit authority password assigned by Silvis. The user enters the box and bundle codes (also assigned by Silvis) into the boxes labeled "Box" and "Bundle" on the second line. Next, "N", standing for not indexed, is entered into the "Classification" box, and finally the user presses the Request button. The first unindexed card image is then displayed.

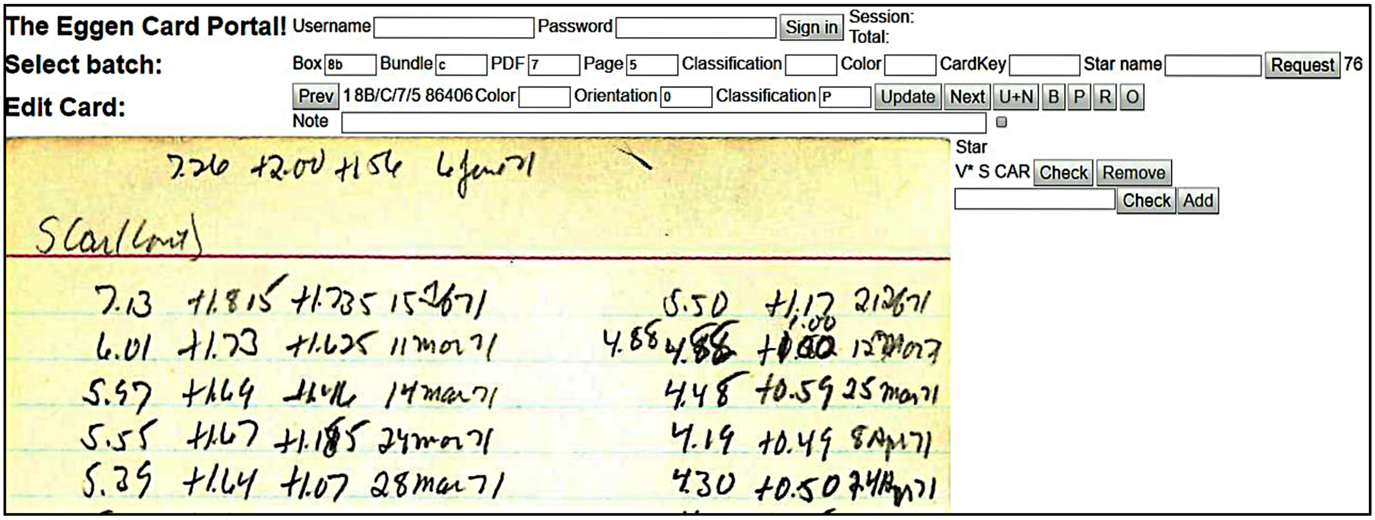

**The Eggen Card Portal!** Username Password Sign in Session: Total:

**Select batch:** Box 8b Bundle c PDF 7 Page 5 Classification Color CardKey Star name Request 76

**Edit Card:** Prev 1 8B/C/7/5 86406 Color Orientation 0 Classification P Update Next U+N B P R O

Note

Star

V* S CAR Check Remove

Check Add

7.26 +2.00 +1.56 6Jun71

S Car (Cont)

7.13 +1.815 +1.735 15Feb71 5.50 +1.12 21Feb71
6.01 +1.73 +1.625 11Mar71 4.88 4.88 +1.00 12Mar71
5.97 +1.69 +1.6 14Mar71 4.48 +0.59 25Mar71
5.55 +1.67 +1.185 24Mar71 4.19 +0.49 8Apr71
5.39 +1.64 +1.07 28Mar71 4.30 +0.50 24Apr71

Figure 3. Card 8B/C/7/5 (Figure 2) as displayed on the EGGEN CARD PORTAL. Only a portion of the card is shown (Silvis 2016a).

Each card may have multiple star designations written upon it. These designations may all be synonyms referring to the same star, a list of unrelated star names each referring to an individual star, or a mixture of the two. The user enters one of these names into the box next to the Check button, found to the right of the card image. Pressing the Check button starts a search by SIMBAD, the results of which will appear in a new browser tab.

The SIMBAD entry, if one is found for the name being checked, is verified to be Eggen's intended star by cross checking the star's coordinates, cross checking additional names on the card against the list of alternative names provided by SIMBAD, V band magnitude, spectral type, or other clues provided by the card. If the name represents the intended star, then pressing the "Add" button will assign the star name to the card.

If the card holds multiple star designations, then these names also need to be verified. Unrelated designations are added to the list of names assigned to the card while synonymous names are not.

Initially each card image is assigned the default classification "N" . When the card is indexed, the classification is reassigned to one of the following:

B Blank card.

S Special (not a star card, but some other document).

R To be reviewed (Let the supervisor look at this one).

P A card which identifies a single star or a list of unrelated stars. At least one star is found either by name or by coordinates in SIMBAD, and has usable photometric observations.

O A card for which none of the star references found on the card are found in SIMBAD.

D A card which identifies a single star or a list of unrelated stars. For each star found either by name or by coordinates in SIMBAD there are no usable observational data on the card.

Several properties of the card such as the color of the card, the card's orientation, and its new classification are entered on the first of two "Edit Card:" lines. Comments are typed into the "Note" box, above the card image. The card's classification is updated, by pressing the Update button, which replaces the existing "N" class with the new classification. The next card is displayed by pressing the "Next" button and the process is repeated.

The portal also provides a search function to find all cards indexed under a particular star identifier or one of the star's alternative names. No special authorization is needed to use the search feature. Enter the star identifier into the "Star name" box and press the "Request" button.

The reader may wish to use the EGGEN CARD PORTAL for the following example and gain a little hands-on experience with this database tool.

As an example, let's look for all the card images indexed under the name of "S Car". Enter "S Car" into the "Star name" box and click the "Request" button. The portal will display the first card in the sequence of cards indexed under "S Car" or one of its alternative star names. The star name displayed on each card in the sequence may differ from the search name.

To the right of the "Prev" button is displayed the text string "1 12B/E/1/37 77914" Displaying respectively the place of the card in the stack, the card's address in the database, and the cardkey which is discussed later. Continuing to press the Next button will increment through each card in the sequence, eventually arriving at the card addressed as 8B/C/7/5, the card shown in Figures 2 and 3.

The number of cards found in the search is displayed to the right of the "Request" button. The "Prev" and "Next" buttons, found above the displayed card, allow the viewer to move through the card sequence.

The number "86406" shows this card was the 86,406th image to be produced from the scanning of the original cards. This number is the cardkey number.

Both the cardkey and card address can be used to find an individual card image. The line labeled "Select batch" contains input boxes for entering the address of a specific card.

Finding the correct star from the designation(s) written on the card can be a problem. These Identifiers were written by Eggen for his own use and in his own handwriting. While the identification may have been clear to him it often is not clear to the person indexing the card. Often Eggen recorded more than one designation for the same star on the same card. This can be of great help if the handwriting is legible. Often when indexing a card with multiple designations we select the most legible and search upon that identifier.

Many cards have only a partial identifier such as "509", which could stand for HR 509, HD 509, LTT 509, and so on. The person indexing must query all of the possible names in SIMBAD. By comparing the star's coordinates, U, B, V, R, and I band magnitudes, and other star related data provided by SIMBAD against the data recorded on the card one hopes to determine which name is the correct one. If no coordinates were specified on the card, then the person indexing must choose between stars using whatever clues remain on the card. The magnitudes within the observations, a note on the spectral type, or a finder chart on the card may be the key to correct identification.

More information on star name conventions used by Eggen and how they relate to the catalogues used by SIMBAD can be found on the AAVSO web page https://www.aavso.org/content/eggen-card-instructions.

### 2.3. Identifying patterns in observational data and the corresponding photometric systems

While indexing these cards, we are always looking for new patterns in the recording of observational data. Fourteen different patterns used to record observational data have been found. The associated photometric systems have been identified for eleven of these patterns.

The photometric systems used by Eggen and recorded on his cards are as follows:

*Eggen's UBV system,* an equivalent version of the 1953 Johnson and Morgan system (Eggen and Sandage 1960; Bessell 2005).

*Eggen's 102,65,62 narrowband system,* which was used alongside his UBV system to make measurements of stars of type K5 and later. This system was used before Eggen's adoption of the RI system (Kron *et al.* 1953; Eggen 1967).

*Eggen's RI system,* based upon standard stars defined by Kron with additional standard stars of later spectral type added by Eggen (Eggen 1965; Bessell 2005).

*Eggen's uvbyβ system,* which while originally based upon

Table 2. The observational data formats found on Eggen's cards (Crast 2016).

| *Format Name* | *Associated Photometric(s) System* | *Map of Observational Data (on Card)[1]* | *Corresponding Magnitude, Color Index, or Other Value* | *Remarks* | *Example Card[2]* |
|---|---|---|---|---|---|
| UBV | Eggen UBV | Md <±d> <±d> | V (B–V) (U–B) | note 4 | 5B/A/4/14 |
| RI | Eggen RI | Md <±d> | R (R–I) | | 5B/A/4/14 |
| VRIphase | Eggen UBV & RI | Md Md ±d d | V R (R–I) phase | | 19A/B/5/12 |
| phaseVRI | Eggen UBV & RI | d Md Md ±d | phase V R (R–I) | | D1/C/5/28 |
| 102,65,62 | Eggen 102,65,62 | ±d ±d Md | (65–62) (102–65) (102) | (102) ≡ m$_{102}$ | B6//1/16 |
| 102,65 | Eggen 102,65,62 | “[“ Md ±d “]” | (102) (102-65) | (102) ≡ m$_{102}$ | 6A/A/15/9 |
| uvbyβ | Eggen uvbyβ$^6$ | Md ±i ±i ±i <Md> | V' (b–y)$_1$' m$_1$' c$_1$' Hβ' | not cc$^{4, 6}$ | D1/C/1/1 |
| uvbyβ(cc) | Eggen uvbyβ$^7$ | Md ±i ±i ±i <Md> | V (b–y)$_1$ M$_1$ C$_1$ Hβ | cc$^{4, 7}$ | B6//34/16 |
| DDO | note 3 | Md ±i ±i ±i | (48) na na na | (48) ≡ m$_{48}^{5}$ | B3//27/10 |
| Hβ | Eggen uvbyβ | Md | Hβ | | B6//1/29 |
| [.2.]$^n$ | unknown | “[“ Md ±d “]”$^n$ | na na ]$^n$ | note 9 | B6//32/26 |
| [.4.] | unknown | “[“ Md ±i ±I ±I “]” | na na na na | | B6//34/15 |
| [.4.]$^n$ | unknown | “[“ Md ±i ±i ±i “]”$^n$ | na na na na ]$^n$ | note 9 | B6//34/16 |
| M±±±M± | note 8 | Md ±i ±i ±i Md ±i | (48) na na na na na | | B5//8/42 |
| [1/2 D T] | uvbyβ | [Md ±i ±i ±i <Md> date <time><br>Md ±i ±i ±i <Md>] | [V' (b–y)$_1$' m$_1$' c$_1$' Hβ' date <time><br>V' (b–y)$_1$' m$_1$' c$_1$' Hβ’] | note 10 | C4/C/3/61 |

*Notes:*

1. *Some records may vary with respect to color index format, such as ±i instead of ±d.*
2. *Example cards can be viewed by entering the card address into the* EGGEN CARD PORTAL.
3. *David Dunlap Observatory (DDO) The identity of the three indexes in the DDO data and what processing is still required to convert these values to those in Eggen’s published tables are not fully understood. Therefore, labels have not been assigned yet.*
4. *Value of first Md is close to or equal to SIMBAD’s V magnitude.*
5. *Value of first Md is greater than SIMBAD’s V magnitude by 0.1 magnitude or more.*
6. *Color indexes and Hβ are those computed using Strömgren’s uvby system. Eggen’s transformation equations need to be applied. The observational data are not computationally complete (cc).*
7. *Color indexes and Hβ have been transformed using Eggen’s equations prior to recording on card. Denoted “cc” for computationally complete observational data.*
8. *The M±±± portion is a DDO observation. The remaining M± has not been resolved. The identity of the three indexes in the DDO data and what processing is still needed to convert these values to those in Eggen’s published tables are not fully understood. Therefore, labels have not been assigned yet.*
9. *“]$^n$” represents the value of the exponent n.*
10. *Two observations within a single set of square brackets, sharing a single date and optional time. Both observations use either the Eggen uvbyβ or uvbyβ(cc) system. The top observation is for the star named on the card. The bottom observation is for a nearby star.*

the uvbyβ system introduced by Bengt Strömgren and extended by David Crawford, was later adopted as an independent system due to a defective v filter (Strömgren 1966; Crawford and Perry 1966; Eggen 1976).

*The David Dunlap Observatory (DDO) system,* developed by Robert D. McClure and Sidney van den Bergh. Eggen also added his own standard stars to the original list to extend this system for later spectral type stars (McClure and van den Bergh 1968; Eggen 1990).

Table 2 summarizes the data recording patterns (data formats) found on the cards. Except for the [1/2 D T] format, the date and time of the observation are not shown as part of the data formats. The map of each format shows the ordering of the data values and the expected data type of each value. The key word here is “expected,” as some observations will have data values of a type not matching what is specified below. The most common data type variation is the use of decimal numbers when integers are expected and vice-versa. Some measurements are not always included within the observation and are defined as optional. Some observations use literal characters such as “[]” to distinguish between data records with similar mappings.

The last column of Table 2 contains the addresses of sample cards which contain observations in the data format named in column 1. These cards may be viewed using the EGGEN CARD PORTAL discussed in section 2.1.

Table 3 defines the terms used in Table 2.

### 2.4. Recording and organizing the observations using spreadsheets

Spreadsheets allow us to enter the observational data in an orderly manner using the mappings defined in Table 2 as guides for photometric system identification and correct data input. The spreadsheet also allows us to manipulate the data to make it suitable for WEBOBS input, and document the observations for future reference.

The “Eggen Photometry” workbook served as a proof of concept to demonstrate that we could transcribe UBV and RI observations from the cards of a few variable stars and add those observations into the AID. The workbook was developed using GOOGLE SHEETS software. The workbook is stored in the Google cloud which allows shared access to the sheet by multiple users. Anyone with a link to the workbook may view it on a read-only basis. Users must log into a Google account to gain edit access. Access authority and resource contention, when multiple users are accessing the workbook at the same time, is handled by the Google cloud. S Car and l Car were the first stars to be entered into AID. A total of 300 U, B, V, R, and I observations were entered for S Car and 206 for l Car (Silvis 2015).

“Eggen Card Database: Photometric Observations Ver 3.0” is our current workbook. It too was written using GOOGLE SHEETS and is stored in the Google cloud. Its goal is to capture as many photometric observations as possible as they are recorded on the cards, regardless of photometric system.

Table 3. Terms used in Tables 2, 4, and 5 (Crast 2016).

| *Term* | *Description* |
|---|---|
| d | a decimal number |
| i | an integer |
| Md | relative magnitude in the form of a decimal number |
| ±d | a signed decimal number representing a color index |
| ±i | a signed integer representing a color index |
| U,V,B,R,I | Johnson U-,V-,B-,R-, and I-band magnitudes, respectively |
| $m_1'$ | Metal abundance parameter derived using Strömgren's uvby system calculations but using Eggen's v filter. Value still requires the application of Eggen's uvbyβ transformation. |
| $M_1$ | Transformed value of $m_1'$ |
| tag | date tag—Epoch of star coordinates found on some cards, especially cards with DDO obs |
| Hβ or β | hydrogen beta absorption line magnitude |
| (A–B) | Color index Magnitude A – Magnitude B |
| $V_E$,$V_J$,$V_K$ | V band magnitude derived from the UBV system defined by Eggen, Johnson, and Kron, respectively |
| cc | Computationally complete. The uvbyβ observation does not need Eggen's transformation applied by spreadsheet |
| n | a number in decimal or integer form |
| t | a text string |
| < > | an optional term (optional in the sense that the recorded observation may not contain the corresponding value) |
| \| | A\|B (the value can be A or B) |
| na | not available or not yet defined |
| $c_1'$ | Continuum parameter derived using Strömgren's uvby system calculations but using Eggen's v filter. This value still requires Eggen's uvbyβ transformation. |
| $C_1$ | Transformed value of $c_1'$ |
| $(b–y)_1'$ | (b–y) index derived using Strömgren's uvby system calculations. Still requires the application of Eggen's uvbyβ transformation. |
| $(b–y)_1$ | Transformed value of $(b–y)_1'$ |
| V' | $V_E$ included with Eggen's uvbyβ records |
| u,v,b,y | Eggen's four-color system u, v, b, and y filters, respectively |
| — | unassigned spreadsheet cell |
| “ ” | Text string literal contained within the data record |

Problems such as observations having illegible date or data, or difficulty figuring out the correct data format are frequently encountered. Our spreadsheet allows entry of observations with data, date, or time problems. These problem observations are marked with a generic format of “.?.” so that they can still be recorded and flagged for later review and resolution.

In addition, all card images which do not contain usable observational data are recorded on the spreadsheet under a generic “NoObs” format.

Each sheet of the database workbook is assigned to one star and each row of that sheet documents an observation. The photometric system(s) used for each observation are identified by the data format, other comments, or labels on the cards. Each row holds:

*The address of the image,* within the card image database, that has the observation.

*The card's color;* white is the default if no value is assigned.

*The date and time* of the observation in both Gregorian calendar and Julian date formats. All dates and times are displayed in GMT.

*The format* in which the observational data were written on the card.

*Input observational data* which are entered onto the input area using the chosen format.

*The results* of any numerical calculation, or reordering of the input data.

*The AAVSO observer code* of the person entering the observation.

*Comments* concerning the observational data.

*Status* on whether the observation(s) has been entered into the AID.

*The input record generated* for WEBOBS for entry of the observation(s) into the AID.

The data type for each input and output cell within a row is defined by assigning each row a data format chosen using Table 2 as a guide. The chosen format is assigned to the row by selecting it from a menu showing valid format entries (see the Card Data Format column in Figure 4). By selecting the same format in the heading menu the correct data mapping will be displayed in the headings. The column headings show the data type terms and corresponding magnitude, index, or other value.

Table 4 lists the data formats and the heading for each cell in the “Data From Cards” section of a star's spreadsheet. Note that the uvbyβ format has two variations. The difference between the two is the application of Eggen's transformation equations to the observational data. The uvbyβ observations still require the application of Eggen's transformation equations to produce the values shown in Eggen's papers. For the uvbyβ(cc) observations Eggen's transformations were applied before Eggen recorded the observations on the card. The uvbyβ(cc) observations are termed computationally complete (cc).

Table 5 displays the layout of the output section of a row for each data format. The output section is shown in Figure 4 under the heading “Data for WebObs”.

Figures 4 and 5 display portions of the S Car sheet showing observations transcribed from the card in Figure 2. Figure 5 shows the dates and times of observation in Gregorian and Julian formats. When no time of observation is recorded on the card then only the date is entered in to the “Date Time (UTC)” cell and the time of observation defaults to midnight. This default is also reflected in the Julian Date (JD) cell. Observational dates can be entered on the spreadsheet in either Gregorian or JD format to match the format recorded on the card. A spreadsheet routine fills in the blank “Date Time” or “JD” cell and processes the “Data from Cards” observation records into the proper form for storage in the corresponding “Data for WebObs” section shown in Figure 4.

Since any star recorded on an Eggen card may be referenced by more than one identifier we needed to choose one identifier for the spreadsheet which is in common use and is compatible with the conventions for star name use in astronomical papers. The source we chose was the main star identifier returned from an identifier query of the SIMBAD Astronomical Database. This identifier also becomes the sheet name. The brief description and V band magnitude from the identifier query are also entered on the sheet.

Table 4. Mapping of observational data values onto spreadsheet input data columns (Crast 2016).

| *Format Name* | *Map of Spreadsheet Input Data* | | | | | | | *Corresponding Magnitude, Color Index, or Value* | | | | | | |
|---|---|---|---|---|---|---|---|---|---|---|---|---|---|---|
| UBV | Md | <±d> | <±d> | — | — | — | — | V | (B–V) | (U–B) | — | — | — | — |
| RI | Md | <±d> | — | — | — | — | — | R | (R–I) | — | — | — | — | — |
| VRIphase | Md | Md | ±d | d | — | — | — | V | R | (R–I) | phase | — | — | — |
| phaseVRI[8] | d | Md | Md | ±d | — | — | — | phase | V | R | (R–I) | — | — | — |
| 102,65,62 | ±d | ±d | Md | — | — | — | — | (65–62) | (102–65) | (102) | — | — | — | — |
| 102,65 | Md | ±d | — | — | — | — | — | (102) | (65–62) | — | — | — | — | — |
| uvbyβ[1, 7] | Md | ±i | ±i | ±i | <Md> | — | <t> | V' | $(b–y)_1'$ | $m_1'$ | $c_1'$ | Hβ' | — | tag[3] |
| uvbyβ(cc)[1, 7] | Md | ±i | ±i | ±i | <Md> | — | <t> | V | $(b–y)_1$ | $M_1$ | $C_1$ | Hβ | — | tag[3] |
| DDO | Md | ±i | ±i | ±i | — | — | <t> | (48) | na | na | na | — | — | tag[3] |
| Hβ | Md | — | — | — | — | — | — | Hβ | — | — | — | — | — | — |
| [.note 2.]$^{n}$ | Md | ±d | — | — | d | — | <t> | na | na | na | na | ]$^{n2}$ | na | tag[3] |
| [.note 4.] | Md | ±i | ±i | ±i | — | — | <t> | na | na | na | na | na | na | tag[3] |
| [.note 4.]$^{n}$ | Md | ±i | ±i | ±i | d | — | <t> | na | na | na | na | ]$^{n2}$ | na | tag[3] |
| M±±±M± | Md | ±i | ±i | ±i | Md | ±d | <t> | (48) | na | na | na | na | na | tag[3] |
| .?.[5] | t | t | t | t | t | t | t | text | text | text | text | text | text | text[4] |
| NoObs[6] | — | — | — | — | — | — | — | — | — | — | — | — | — | — |

*Notes:*

1. *uvbyβ—Eggen's transformation calculations must be applied to observation values V', (b-y)', $m_1'$, and $c_1'$; uvbyβ (cc)—Eggen's transformation calculations were applied to observation values before observation was recorded on the card.*
2. *The value of the numerical exponent n.*
3. *Enter a date tag if one exists.*
4. *Write values into cells in corresponding order as they appear on card.*
5. *The .?. format is a generic format for identifying and recording problem observations requiring more investigation.*
6. *NoObs is a generic description for a card which has no usable photometric observations. This is used to record cards indexed under the star name which would otherwise be undocumented due to a lack of observations. Such cards would include those with attached paper tapes and cards with comparisons between Eggen's observations and observations made by other astronomers.*
7. *Each observation from a [1/2 D T] observation pair (see Table 2) is recorded on its respective star sheet using the uvbyβ or uvbyβ(cc) format. The same date and time (if the time exists) are recorded for each star. The comment section of each record is updated to record the bundling of the two observations.*
8. *A variation of the VRIphase format requiring spreadsheet headings and processing changes.*

Table 5. Mapping of processed values onto the spreadsheet output data columns (Crast 2016).

| *Format Name* | *Map of Spreadsheet Output Data* | | | | | | | *Corresponding Magnitude, Color Index, or Other Value* | | | | | | |
|---|---|---|---|---|---|---|---|---|---|---|---|---|---|---|
| UBV | Md | Md | Md | — | — | — | — | U | B | V | — | — | — | — |
| RI | — | — | — | Md | Md | — | — | — | — | — | R | I | — | — |
| VRIphase & phaseVRI | — | — | Md | Md | Md | d | — | — | — | V | R | I | note2 | — |
| 102,65,62 | Md | ±d | ±d | — | Md | — | — | (102) | (65–62) | (102–65) | — | $I_J$[1] | — | — |
| 102,65 | Md | ±d | — | — | — | — | — | (102) | (65–62) | — | — | $I_J$[1] | — | — |
| uvbyβ & uvbyβ(cc)[3] | — | — | Md | ±i | ±i | ±i | Md | — | — | V | (b–y) | $M_1$ | $C_1$ | Hβ |
| DDO | Md | ±d | ±d | ±d | — | — | — | (48) | (45–48) | (42–45) | (41–42) | — | — | — |
| [.note 2.]$^{n}$ | na | na | na | na | na | na | na | na | na | na | na | na | na | na |
| [.note 4.] | na | na | na | na | na | na | na | na | na | na | na | na | na | na |
| [.note 4.]$^{n}$ | na | na | na | na | na | na | na | na | na | na | na | na | na | — |
| Hβ | Md | — | — | — | — | — | — | Hβ | — | — | — | — | — | — |
| M±±±M± | Md | ±d | ±d | ±d | Md | Md | — | (48) | (45–48) | (42–45) | (38–42) | na | na | — |
| .?. | — | — | — | — | — | — | — | — | — | — | — | — | — | — |

*Notes:*

1. $I_J = 0.15 \times m_{102}$ *(Eggen 1976)*
2. *phase*
3. *The uvbyβ(cc) format signals to the spreadsheet processing routine that Eggen's transformation calculations have been applied to this observation prior to its recording. No further calculations need to be performed for this datum.*

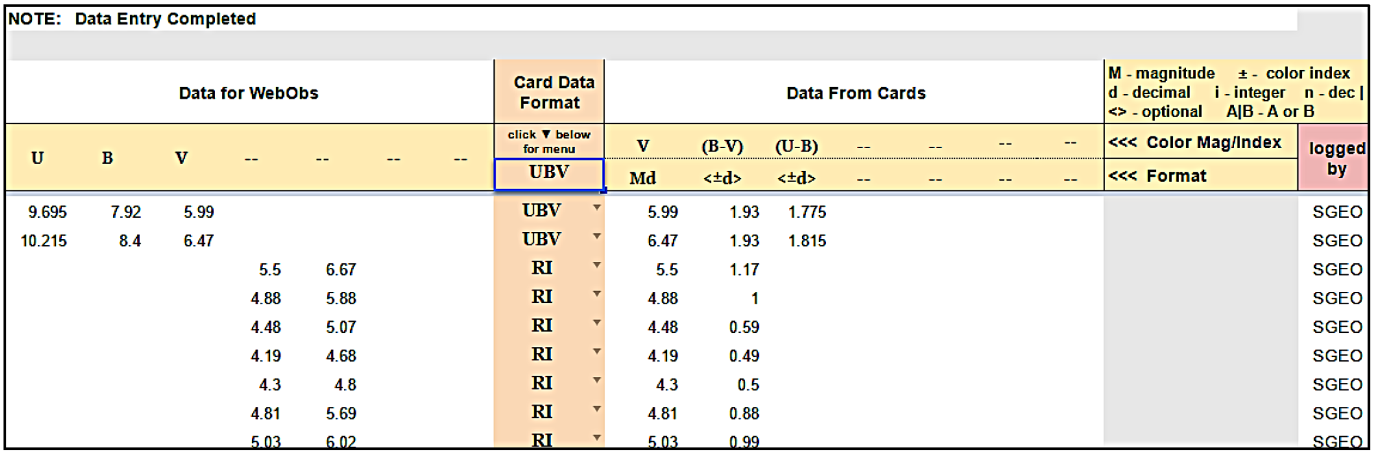

NOTE: Data Entry Completed

M - magnitude ± - color index
d - decimal i - integer n - dec |
<> - optional A|B - A or B

| Data for WebObs | | | | | | | Card Data Format | Data From Cards | | | | | | | | |
|---|---|---|---|---|---|---|---|---|---|---|---|---|---|---|---|---|
| U | B | V | -- | -- | -- | -- | click ▼ below for menu | V | (B-V) | (U-B) | -- | -- | -- | -- | <<< Color Mag/Index | logged by |
| | | | | | | | UBV | Md | <±d> | <±d> | -- | -- | -- | -- | <<< Format | |
| 9.695 | 7.92 | 5.99 | | | | | UBV | 5.99 | 1.93 | 1.775 | | | | | | SGEO |
| 10.215 | 8.4 | 6.47 | | | | | UBV | 6.47 | 1.93 | 1.815 | | | | | | SGEO |
| | | | 5.5 | 6.67 | | | RI | 5.5 | 1.17 | | | | | | | SGEO |
| | | | 4.88 | 5.88 | | | RI | 4.88 | 1 | | | | | | | SGEO |
| | | | 4.48 | 5.07 | | | RI | 4.48 | 0.59 | | | | | | | SGEO |
| | | | 4.19 | 4.68 | | | RI | 4.19 | 0.49 | | | | | | | SGEO |
| | | | 4.3 | 4.8 | | | RI | 4.3 | 0.5 | | | | | | | SGEO |
| | | | 4.81 | 5.69 | | | RI | 4.81 | 0.88 | | | | | | | SGEO |
| | | | 5.03 | 6.02 | | | RI | 5.03 | 0.99 | | | | | | | SGEO |

Figure 4. Observations transcribed from Eggen card 8B/C/7/5 (Figure 2) to the S Car spreadsheet in Eggen Card Database: Photometric Observations. The UBV column headings for the "Data for WebObs" and "Data from Cards" columns were set by choosing "UBV" from the menu displayed by clicking on the "▼" symbol in the highlighted cell. The uppermost yellow block on the right side of the spreadsheet is a short summary of the data type terms documented in Table 3 (Crast and Silvis 2016).

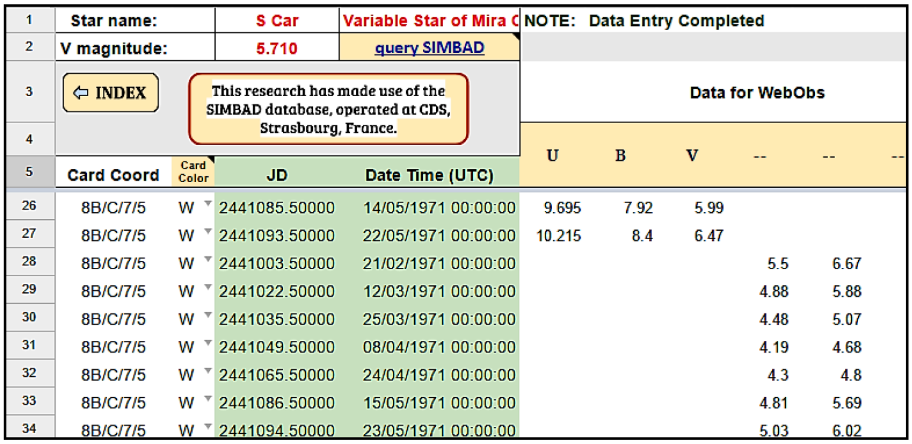

| | | | | | | | | | | |
|---|---|---|---|---|---|---|---|---|---|---|
| 1 | Star name: | | S Car | Variable Star of Mira C | NOTE: Data Entry Completed | | | | | |
| 2 | V magnitude: | | 5.710 | query SIMBAD | | | | | | |
| 3 | ⇦ INDEX | | This research has made use of the SIMBAD database, operated at CDS, Strasbourg, France. | | Data for WebObs | | | | | |
| 4 | | | | | | | | | | |
| 5 | Card Coord | Card Color | JD | Date Time (UTC) | U | B | V | -- | -- | -- |
| 26 | 8B/C/7/5 | W | 2441085.50000 | 14/05/1971 00:00:00 | 9.695 | 7.92 | 5.99 | | | |
| 27 | 8B/C/7/5 | W | 2441093.50000 | 22/05/1971 00:00:00 | 10.215 | 8.4 | 6.47 | | | |
| 28 | 8B/C/7/5 | W | 2441003.50000 | 21/02/1971 00:00:00 | | | | 5.5 | 6.67 | |
| 29 | 8B/C/7/5 | W | 2441022.50000 | 12/03/1971 00:00:00 | | | | 4.88 | 5.88 | |
| 30 | 8B/C/7/5 | W | 2441035.50000 | 25/03/1971 00:00:00 | | | | 4.48 | 5.07 | |
| 31 | 8B/C/7/5 | W | 2441049.50000 | 08/04/1971 00:00:00 | | | | 4.19 | 4.68 | |
| 32 | 8B/C/7/5 | W | 2441065.50000 | 24/04/1971 00:00:00 | | | | 4.3 | 4.8 | |
| 33 | 8B/C/7/5 | W | 2441086.50000 | 15/05/1971 00:00:00 | | | | 4.81 | 5.69 | |
| 34 | 8B/C/7/5 | W | 2441094.50000 | 23/05/1971 00:00:00 | | | | 5.03 | 6.02 | |

Figure 5. The time and date section for the same observations of S Car shown in Figure 4. The card color is specified as "W" for white. The "query SIMBAD" cell holds a hyperlink to the SIMBAD identifier query result for the "Star name:" entry. The headings in rows 1–5 are frozen in position, allowing the viewer to scroll through the data rows and still view or change the column headings above the "Data from Cards" and "Data for WebObs" sections (Crast and Silvis 2016).

## 3. Results

The indexing phase of the project is nearing completion. As this paper was being written another box holding another 500 cards was discovered. These cards have yet to be scanned and organized into PDF files.

A minimum of 15,503 cards have been classified as "P". This number will increase as the cards classified "D", "R", and "O" are re-examined later.

The PDF files discussed in section 2.1 can be viewed and downloaded from the AAVSO at the Olin Eggen Observation Cards web page.

*AAVSO Bulletin* stars also found in the card database are listed in Table 6. No search for AAVSO comparison and check stars has been performed yet.

Six data formats—UBV, RI, uvbyβ, uvbyβ(cc), VRIphase, and phaseVRI—hold observations in the U, B, V, R, and I bands that can be added to the AID. The remaining unmapped formats may also hold useful observational data for AID as well.

The Eggen Card Database workbook contains 53 star sheets in various stages of completion. Most of the sheets document observations of standard stars for Eggen's customized photometric systems. Data from these sheets are used for computing the transformation constants for Eggen's uvbyβ system and the transformation coefficients for standardizing his DDO observations. See Appendices 1–3 in the "Eggen Card Database: Photometric Observations" workbook for documentation. The uvbyβ system transformation constants have been computed and are used when processing uvbyβ formatted observational data

## 4. Future work

In the next phase of this project we will:

1. Begin the extraction of the photometric observations from the cards and entering them into AID. Priority will go to AAVSO-related stars and special requests from the astronomical community.

2. Continue to identify new data formats and variations of currently identified formats.

3. Create expanded documentation concerning what types of stars are recorded within Eggen's database.

4. Start to identify variable, comparison, and check stars in AID that have usable data in Eggen's card database.

Table 6. *AAVSO Bulletin* stars found in Eggen's card database (Silvis 2016b).

R And
T And
SV And
R Aql
R Aqr
T Aqr
W Aql
S Aql
R Ari
S Ari
R Aur
W Aur
X Aur
R Boo
S Boo
S Cam
X Cam
R Cnc
V Cnc
W Cnc
R CVn
T CVn
R CMi
S CMi
R Car
S Car
R Cas
V Cas
T Cen
W Cen
X Cen
T Cep
R Cet
U Cet
V Cet
W Cet
Z Cet
o Cet
S Col
T Col
R Com
S CrB
V CrB
R Cyg
S Cyg
U Cyg
RS Cyg
RT Cyg
RU Cyg
$\chi$ Cyg
S Del
R Dra
T Eri
R Gem
S Gem
V Gem
T Gru
S Her
T Her
U Her
W Her
RS Her
RU Her
SS Her
R Hor
T Hor
R Hya
S Hya
T Hya
X Hya
RU Hya
R Leo
R LMi
R Lep
S Lib
U Lib
RS Lib
S Lup
R Lyn
W Lyr
S Mic
V Mon
X Mon
Y Mon
RR Mon
T Nor
R Oct
R Oph
V Oph
X Oph
Z Oph
RU Oph
R Ori
S Ori
U Ori
S Pav
R Peg
T Phe
V Phe
S Pic
T Pic
R Psc
W Pup
S Pyx
R Ret
R Sgr
RR Sgr
RU Sgr
S Sco
RR Sco
RS Sco
RZ Sco
S Scl
T Scl
U Scl
V Scl
X Scl
R Ser
U Ser
R Tri
S Tuc
T Tuc
R UMa
S UMa
T UMa
Y Vel
R Vir
RU Vir
S Vir
SS Vir
SU Vir
R Vul

5. Continue to investigate and implement a plan for organizing the many stars named in Eggen's card database. Multiple database workbooks will be needed at some point in time.

6. Develop a more secure storage system for our data and processing software. The cloud is not the most secure means of storing critical data. We need to bring these data back under the control and security of the AAVSO.

7. Begin education of a small team to transcribe observations from the portal to the spreadsheet-based database.

8. Improve the quality control process over observational data transcription and with any data processing being performed by the spreadsheet programs.

9. Continue our investigative work on the unresolved observational data formats and make the necessary changes to the spreadsheet database.

10. Improve the performance of our spreadsheet's processing and organizing tasks. Our implementation of reading from and writing to the spreadsheet significantly degrades performance. The necessity of working within the Google cloud and not locally on the user's home system can degrade performance greatly when network traffic or cloud usage is heavy.

11. Begin work to modify the workbook to make the data more accessible to the AAVSO Variable Star Index (VSX).

## 5. Summary

Our intentions for now are to leave the transcription of data to the spreadsheet to a few volunteers familiar with the use of the Eggen Portal, the identification of the various data formats on the cards, and the data entry procedures for the spreadsheets. A small team can more easily deal with the ongoing changes being made to the spreadsheet code and The Eggen Card Database Reference and still ensure that we are producing a quality product.

What we would like the reader to do is search through the card database using the EGGEN CARD PORTAL for stars of interest to them. If such stars are found and retrieval of the observations is desired, please e-mail George Silvis, the team leader, and we will be happy to help retrieve those data. Questions concerning the data formats and use of the spreadsheet should be directed to Jack Crast.

If you would like to become part of the Eggen team, send an e-mail to George Silvis.

## 6. Acknowledgements

This research has made use of:

- The SIMBAD database, operated at CDS, Strasbourg, France
- The Asiago Database on Photometric Systems (ADPS)
- The WEBDA database, operated at the Department of Theoretical Physics and Astrophysics of Masaryk University.

Without the generosity of the American Astronomical Society (AAS) and John Menke we could not have scanned the cards or published the PDF files.

Table 7. Volunteers who have indexed the Eggen cards.

| *Volunteer* | *Cards* |
|---|---|
| Carlos Adib | 40 |
| Wendy Bauer | 783 |
| Michael Cook | 1 |
| Jack Crast | 18,960 |
| Duane Dedrickson | 6,754 |
| Mark de Jong | 1,183 |
| Michael Geldorp | 319 |
| Richard Glassner | 48 |
| David Jackson | 99 |
| James Kay | 90 |
| Kris Larsen | 2 |
| Ranald McIntosh | 260 |
| Bob Neuman | 96 |
| John Ritzel | 37,013 |
| Jeff Robertson | 327 |
| Michael Saladyga | 5,275 |
| Ed Schmidt | 3,436 |
| George Silvis | 22,852 |
| Elizabeth Waagen | 1,679 |
| Glen Ward | 1,337 |
| Doug Welch | 606 |
| Paul York | 782 |

Arne Henden and Matt Templeton of the AAVSO have been very generous with their ongoing technical help.

We of course wish to thank those who volunteered to tackle the difficult job of indexing cards; they are listed in Table 7.

## References

Bessell, M. S. 2005, *Annu. Rev. Astron. Astrophys.*, **43**, 293.

Crast, J. 2016, "The Eggen Card Database Reference" (http://www.crastjh.com/aavso/).

Crast, J., and Silvis, G. 2016,"Eggen Card Database: Photometric Observations" (http://www.crastjh.com/aavso/).

Crawford, D. L., and Perry, C. L. 1966, *Astron. J.*, **71**, 206.

Eggen, O. J. 1965, *Astron. J.*, **70**, 19.

Eggen, O. J. 1967, *Astrophys. J., Suppl. Ser.*, **14**, 307.

Eggen, O. J. 1976, *Publ. Astron. Soc. Pacific*, **88**, 732.

Eggen, O. J. 1990, *Publ. Astron. Soc. Pacific*, **102**, 242.

Eggen, O. J., and Sandage, A. R. 1960, *Mon. Not. Roy. Astron. Soc.*, **120**, 79.

Freeman, K. C., Whitford, A., Greenstein, J., Kron, K., Kron, G., and Trimble, V. 2000, *Bull. Amer. Astron. Soc.*, **32**, 1661.

Henden, A. 2009, "Digitizing Olin Eggen's Legacy" (https://www.aavso.org/olin-eggen-observation-cards).

Kron, G. E., White, H. S., and Gascoigne, S. C. B. 1953, *Astrophys. J.*, **118**, 502.

McClure, R., and van den Bergh, S. 1968, *Astron. J.*, **73**, 313.

Silvis, G. 2013, "Eggen Card Project" (https://www.aavso.org/content/eggen-card-project).

Silvis, G. 2015, "Eggen Photometry" (http://www.crastjh.com/aavso/).

Silvis, G. 2016a, THE EGGEN CARD PORTAL (http://www.gasilvis.com/EggenCard2/).

Silvis, G. 2016b, "*Bulletin* stars that have Eggen cards" (http://www.crastjh.com/aavso/).

Strömgren, B. 1966, *Annu. Rev. Astron. Astrophys.*, **4**, 433.

# Recent Maxima of 82 Short Period Pulsating Stars

**Gerard Samolyk**
*P.O. Box 20677, Greenfield, WI 53220; gsamolyk@wi.rr.com*

*Received January 24, 2017; accepted January 24, 2017*

**Abstract** This paper contains times of maxima for 82 short period pulsating stars (primarily RR Lyrae and δ Scuti stars). This represents the CCD observations received by the AAVSO Short Period Pulsator (SPP) section in 2016.

## 1. Recent observations

Table 1 contains times of maxima calculated from CCD observations made by participants in the AAVSO's Short Period Pulsator (SPP) section. This list will be web-archived and made available through the AAVSO ftp site at ftp:ftp.aavso.org/public/datasets/gsamoj451.txt. The error estimate is included. RR Lyr stars in this list, along with data from earlier AAVSO publications, are included in the GEOS database at: http://rr-lyr.irap.omp.eu/dbrr/. This database does not include δ Scuti stars. These observations were reduced by the writer using the PERANSO program (Vanmunster 2007). Column F indicates the filter used; a "C" indicates a clear filter.

The linear elements in the *General Catalogue of Variable Stars* (Kholopov *et al.* 1985) were used to compute the O–C values for most stars. For a few exceptions where the GCVS elements are missing or are in significant error, light elements from another source are used: RZ Cap and DG Hya (Samolyk 2010), and VY LMi (Henden and Vidal-Sainz 1997).

## 2. Errata

The following times of maxima published in Samolyk (2016) contain a one-day error.

| | | |
|---|---|---|
| SW And | 57347.3755 | T. Arranz |
| SW And | 57351.3525 | T. Arranz |

Corrected times of maxima are included in this paper.

### References

Henden, A. A., and Vidal-Sainz, J. 1997, *Inf. Bull. Var. Stars*, No. 4535, 1.

Kholopov, P. N., *et al.* 1985, *General Catalogue of Variable Stars*, 4th ed., Moscow.

Samolyk, G. 2010, *J. Amer. Assoc. Var. Stars*, **38**, 12.

Samolyk, G. 2016, *J. Amer. Assoc. Var. Stars*, **44**, 66.

Vanmunster, T. 2007, PERANSO period analysis software (http://www.peranso.com).

Table 1. Recent times of maxima of stars in the AAVSO Short Period Pulsator program.

| *Star* | *JD (max) Hel. 2400000 +* | *Cycle* | *O–C* | *F* | *Observer* | *Error* |
|---|---|---|---|---|---|---|
| SW And | 57348.3755 | 88668 | -0.4506 | V | T. Arranz | 0.0005 |
| SW And | 57352.3525 | 88677 | -0.4541 | V | T. Arranz | 0.0005 |
| SW And | 57601.7894 | 89241 | -0.4628 | V | G. Samolyk | 0.0011 |
| SW And | 57620.8020 | 89284 | -0.4682 | V | K. Menzies | 0.0015 |
| SW And | 57674.7611 | 89406 | -0.4672 | V | R. Sabo | 0.0009 |
| SW And | 57698.6417 | 89460 | -0.4697 | V | G. Samolyk | 0.0009 |
| XX And | 57595.8210 | 25608 | 0.2750 | V | G. Samolyk | 0.0017 |
| XX And | 57642.7985 | 25673 | 0.2739 | V | N. Simmons | 0.0019 |
| XX And | 57650.7482 | 25684 | 0.2734 | V | G. Samolyk | 0.0015 |
| XX And | 57660.8668 | 25698 | 0.2735 | V | R. Sabo | 0.0014 |
| XX And | 57697.7299 | 25749 | 0.2765 | V | R. Sabo | 0.0011 |
| ZZ And | 57621.8029 | 59137 | 0.0295 | V | K. Menzies | 0.0013 |
| ZZ And | 57706.6468 | 59290 | 0.0300 | V | K. Menzies | 0.0015 |
| AC And | 57606.5840 | 47873 | -0.1829 | V | T. Arranz | 0.0014 |
| AT And | 57602.7960 | 24735 | -0.0108 | V | G. Samolyk | 0.0011 |
| AT And | 57610.8241 | 24748 | -0.0026 | V | G. Samolyk | 0.0022 |
| AT And | 57634.8807 | 24787 | -0.0057 | V | G. Samolyk | 0.0025 |
| AT And | 57673.7494 | 24850 | -0.0026 | V | R. Sabo | 0.0013 |
| AT And | 57699.6599 | 24892 | -0.0026 | V | G. Samolyk | 0.0017 |
| DY And | 57630.8420 | 35747 | -0.1750 | V | K. Menzies | 0.0011 |
| DY And | 57711.6522 | 35881 | -0.1785 | V | K. Menzies | 0.0012 |
| DY And | 57728.5380 | 35909 | -0.1791 | V | K. Menzies | 0.0018 |
| SW Aqr | 57595.8294 | 70756 | -0.0035 | V | G. Samolyk | 0.0008 |
| SW Aqr | 57635.7903 | 70843 | -0.0020 | V | G. Samolyk | 0.0007 |
| SW Aqr | 57699.6329 | 70982 | -0.0025 | V | G. Samolyk | 0.0008 |
| TZ Aqr | 57640.6720 | 35175 | 0.0125 | V | G. Samolyk | 0.0006 |
| TZ Aqr | 57660.6652 | 35210 | 0.0139 | V | R. Sabo | 0.0016 |
| YZ Aqr | 57601.8444 | 40290 | 0.0791 | V | G. Samolyk | 0.0015 |
| YZ Aqr | 57601.8458 | 40290 | 0.0805 | V | R. Sabo | 0.0021 |
| YZ Aqr | 57658.6915 | 40393 | 0.0773 | V | G. Samolyk | 0.0009 |
| AA Aqr | 57633.7663 | 60578 | -0.1632 | V | G. Samolyk | 0.0011 |
| AA Aqr | 57669.6907 | 60637 | -0.1633 | V | G. Samolyk | 0.0011 |
| BO Aqr | 57679.6674 | 23138 | 0.2130 | V | G. Samolyk | 0.0018 |
| BR Aqr | 57623.8476 | 41479 | -0.2097 | V | G. Samolyk | 0.0008 |
| CY Aqr | 57633.7543 | 382142 | 0.0141 | V | G. Samolyk | 0.0004 |
| CY Aqr | 57633.8158 | 382143 | 0.0146 | V | G. Samolyk | 0.0004 |
| CY Aqr | 57633.8769 | 382144 | 0.0147 | V | G. Samolyk | 0.0003 |
| CY Aqr | 57633.9376 | 382145 | 0.0143 | V | G. Samolyk | 0.0005 |
| CY Aqr | 57642.7272 | 382289 | 0.0145 | V | G. Samolyk | 0.0003 |
| CY Aqr | 57642.7884 | 382290 | 0.0146 | V | G. Samolyk | 0.0004 |
| CY Aqr | 57642.8498 | 382291 | 0.0150 | V | G. Samolyk | 0.0007 |
| CY Aqr | 57671.5986 | 382762 | 0.0147 | V | G. Samolyk | 0.0006 |
| CY Aqr | 57671.6592 | 382763 | 0.0142 | V | G. Samolyk | 0.0005 |
| CY Aqr | 57671.7205 | 382764 | 0.0145 | V | G. Samolyk | 0.0005 |
| CY Aqr | 57671.7815 | 382765 | 0.0144 | V | G. Samolyk | 0.0005 |
| DN Aqr | 57668.6328 | 46143 | 0.0420 | V | G. Samolyk | 0.0011 |
| TZ Aur | 57398.6340 | 95733 | 0.0157 | V | N. Simmons | 0.0008 |
| TZ Aur | 57679.8567 | 96451 | 0.0160 | V | G. Samolyk | 0.0008 |
| TZ Aur | 57686.9057 | 96469 | 0.0149 | V | K. Menzies | 0.0008 |
| TZ Aur | 57724.8984 | 96566 | 0.0151 | V | K. Menzies | 0.0006 |
| BH Aur | 57643.8917 | 32652 | 0.0056 | V | G. Samolyk | 0.0011 |
| BH Aur | 57679.9240 | 32731 | 0.0068 | V | G. Samolyk | 0.0012 |
| BH Aur | 57700.9040 | 32777 | 0.0066 | V | R. Sabo | 0.0008 |
| RS Boo | 57433.8306 | 41510 | 0.0004 | V | K. Menzies | 0.0006 |

*Table continued on following pages*

Table 1. Recent times of maxima of stars in the AAVSO Short Period Pulsator program, cont.

| *Star* | *JD (max) Hel. 2400000 +* | *Cycle* | *O–C* | *F* | *Observer* | *Error* |
|---|---|---|---|---|---|---|
| RS Boo | 57460.6184 | 41581 | -0.0029 | V | T. Arranz | 0.0006 |
| RS Boo | 57462.5033 | 41586 | -0.0047 | V | T. Arranz | 0.0005 |
| RS Boo | 57463.6357 | 41589 | -0.0043 | V | T. Arranz | 0.0005 |
| RS Boo | 57465.5239 | 41594 | -0.0028 | V | T. Arranz | 0.0005 |
| RS Boo | 57472.6894 | 41613 | -0.0067 | V | T. Arranz | 0.0007 |
| RS Boo | 57484.7659 | 41645 | -0.0051 | V | K. Menzies | 0.0006 |
| RS Boo | 57485.5211 | 41647 | -0.0046 | V | T. Arranz | 0.0006 |
| RS Boo | 57495.7098 | 41674 | -0.0040 | V | G. Samolyk | 0.0008 |
| RS Boo | 57496.8465 | 41677 | 0.0007 | V | K. Menzies | 0.0008 |
| RS Boo | 57528.5409 | 41761 | -0.0014 | V | T. Arranz | 0.0006 |
| RS Boo | 57547.4041 | 41811 | -0.0052 | V | T. Arranz | 0.0005 |
| RS Boo | 57553.4427 | 41827 | -0.0040 | V | T. Arranz | 0.0006 |
| RS Boo | 57559.4834 | 41843 | -0.0007 | V | T. Arranz | 0.0005 |
| RS Boo | 57567.4055 | 41864 | -0.0027 | V | T. Arranz | 0.0005 |
| RS Boo | 57587.3959 | 41917 | -0.0113 | V | T. Arranz | 0.0006 |
| RS Boo | 57590.4191 | 41925 | -0.0068 | V | T. Arranz | 0.0007 |
| RS Boo | 57593.4350 | 41933 | -0.0096 | V | T. Arranz | 0.0006 |
| ST Boo | 57502.8565 | 61581 | 0.0877 | V | K. Menzies | 0.0009 |
| ST Boo | 57511.5651 | 61595 | 0.0842 | V | T. Arranz | 0.0007 |
| ST Boo | 57518.4095 | 61606 | 0.0834 | V | T. Arranz | 0.0007 |
| ST Boo | 57602.4189 | 61741 | 0.0836 | V | T. Arranz | 0.0009 |
| ST Boo | 57607.3988 | 61749 | 0.0852 | V | T. Arranz | 0.0012 |
| SW Boo | 57494.8611 | 29061 | 0.4610 | V | G. Samolyk | 0.0009 |
| SW Boo | 57566.7600 | 29201 | 0.4660 | V | R. Sabo | 0.0012 |
| SW Boo | 57572.4073 | 29212 | 0.4644 | V | T. Arranz | 0.0011 |
| SW Boo | 57573.4348 | 29214 | 0.4649 | V | T. Arranz | 0.0009 |
| SW Boo | 57591.4126 | 29249 | 0.4692 | V | T. Arranz | 0.0007 |
| SW Boo | 57592.4389 | 29251 | 0.4684 | V | T. Arranz | 0.0009 |
| SW Boo | 57610.4125 | 29286 | 0.4686 | V | T. Arranz | 0.0007 |
| SZ Boo | 57494.8201 | 57103 | 0.0101 | V | G. Samolyk | 0.0009 |
| SZ Boo | 57588.4056 | 57282 | 0.0108 | V | T. Arranz | 0.0006 |
| TV Boo | 57409.8945 | 104941 | 0.0877 | V | K. Menzies | 0.0009 |
| TV Boo | 57450.8726 | 105072 | 0.1205 | V | K. Menzies | 0.0017 |
| TV Boo | 57464.6057 | 105116 | 0.1010 | V | T. Arranz | 0.0011 |
| TV Boo | 57481.5074 | 105170 | 0.1245 | V | T. Arranz | 0.0015 |
| TV Boo | 57510.5747 | 105263 | 0.1238 | V | T. Arranz | 0.0015 |
| TV Boo | 57552.4287 | 105397 | 0.0948 | V | T. Arranz | 0.0009 |
| TV Boo | 57559.6425 | 105420 | 0.1198 | V | K. Menzies | 0.0015 |
| TV Boo | 57603.3766 | 105560 | 0.0956 | V | T. Arranz | 0.0019 |
| TW Boo | 57447.9166 | 57408 | -0.0884 | V | K. Menzies | 0.0007 |
| TW Boo | 57476.6593 | 57462 | -0.0884 | V | N. Simmons | 0.0009 |
| UU Boo | 57486.8679 | 46840 | 0.3017 | V | R. Sabo | 0.0009 |
| UU Boo | 57539.4140 | 46955 | 0.3019 | V | T. Arranz | 0.0006 |
| UU Boo | 57560.4334 | 47001 | 0.3030 | V | T. Arranz | 0.0007 |
| UY Boo | 57489.8507 | 24051 | 0.8880 | V | R. Sabo | 0.0015 |
| UY Boo | 57495.7147 | 24060 | 0.8945 | V | N. Simmons | 0.0011 |
| UY Boo | 57527.6123 | 24109 | 0.9011 | V | G. Samolyk | 0.0011 |
| UY Cam | 57398.5283 | 81760 | -0.0924 | V | G. Samolyk | 0.0019 |
| UY Cam | 57398.7928 | 81761 | -0.0950 | V | G. Samolyk | 0.0016 |
| UY Cam | 57684.7939 | 82832 | -0.0962 | V | G. Samolyk | 0.0028 |
| RW Cnc | 57436.8045 | 32676 | 0.2160 | V | G. Samolyk | 0.0009 |
| RW Cnc | 57733.9379 | 33219 | 0.2203 | V | K. Menzies | 0.0009 |
| TT Cnc | 57390.0167 | 30962 | 0.1294 | V | R. Sabo | 0.0015 |
| TT Cnc | 57428.8665 | 31031 | 0.1012 | V | R. Sabo | 0.0018 |
| VZ Cnc | 57436.6569 | 98334 | 0.0158 | V | G. Samolyk | 0.0008 |
| VZ Cnc | 57436.8428 | 98335 | 0.0234 | V | G. Samolyk | 0.0007 |
| VZ Cnc | 57446.6422 | 98390 | 0.0128 | V | G. Samolyk | 0.0011 |
| KV Cnc | 57450.5988 | 9341 | -0.0764 | V | T. Arranz | 0.0004 |
| KV Cnc | 57453.6144 | 9347 | -0.0728 | V | T. Arranz | 0.0004 |
| KV Cnc | 57457.6356 | 9355 | -0.0676 | V | T. Arranz | 0.0005 |
| KV Cnc | 57474.7541 | 9389 | -0.0171 | V | R. Sabo | 0.0027 |
| KV Cnc | 57487.7680 | 9415 | -0.0552 | V | R. Sabo | 0.0018 |
| KV Cnc | 57507.3788 | 9454 | -0.0224 | V | T. Arranz | 0.0016 |
| KV Cnc | 57509.3829 | 9458 | -0.0263 | V | T. Arranz | 0.0012 |
| KV Cnc | 57510.3853 | 9460 | -0.0279 | V | T. Arranz | 0.0013 |
| KV Cnc | 57511.3878 | 9462 | -0.0294 | V | T. Arranz | 0.0011 |
| KV Cnc | 57512.3903 | 9464 | -0.0309 | V | T. Arranz | 0.0009 |
| KV Cnc | 57513.3931 | 9466 | -0.0321 | V | T. Arranz | 0.0011 |
| KV Cnc | 57525.4129 | 9490 | -0.0603 | V | T. Arranz | 0.0008 |
| KV Cnc | 57526.4130 | 9492 | -0.0642 | V | T. Arranz | 0.0006 |
| KV Cnc | 57527.4136 | 9494 | -0.0676 | V | T. Arranz | 0.0005 |
| KV Cnc | 57528.4161 | 9496 | -0.0691 | V | T. Arranz | 0.0004 |
| KV Cnc | 57529.4201 | 9498 | -0.0691 | V | T. Arranz | 0.0005 |
| KV Cnc | 57531.4276 | 9502 | -0.0696 | V | T. Arranz | 0.0005 |
| SS CVn | 57409.8932 | 37172 | -0.3944 | V | K. Menzies | 0.0011 |
| SS CVn | 57477.8739 | 37314 | -0.3637 | V | K. Menzies | 0.0008 |
| RV Cap | 57607.7855 | 52987 | -0.0884 | V | G. Samolyk | 0.0021 |
| RZ Cap | 57598.8368 | 15496 | 0.0015 | V | R. Sabo | 0.0011 |
| VW Cap | 57604.8207 | 102447 | 0.2265 | V | G. Samolyk | 0.0035 |
| YZ Cap | 57602.7733 | 50732 | 0.0473 | V | G. Samolyk | 0.0012 |
| AN Cap | 57579.8145 | 6627 | -0.0065 | V | G. Samolyk | 0.0012 |
| AN Cap | 57659.6913 | 6739 | 0.0020 | V | G. Samolyk | 0.0015 |
| RR Cet | 57631.8981 | 44212 | 0.0140 | V | R. Sabo | 0.0022 |
| RU Cet | 57658.8273 | 30416 | 0.1238 | V | G. Samolyk | 0.0011 |
| RU Cet | 57668.7950 | 30433 | 0.1248 | V | G. Samolyk | 0.0010 |
| RV Cet | 57390.5542 | 29318 | 0.2620 | V | G. Samolyk | 0.0021 |
| RV Cet | 57649.8885 | 29734 | 0.2607 | V | G. Samolyk | 0.0017 |
| RV Cet | 57659.8480 | 29750 | 0.2458 | V | R. Sabo | 0.0012 |
| RV Cet | 57669.8201 | 29766 | 0.2434 | V | G. Samolyk | 0.0012 |
| RX Cet | 57659.8705 | 30563 | 0.3290 | V | G. Samolyk | 0.0011 |
| RZ Cet | 57406.5196 | 46023 | -0.2105 | V | G. Samolyk | 0.0014 |
| RZ Cet | 57663.8664 | 46527 | -0.2115 | V | G. Samolyk | 0.0017 |
| TY Cet | 52314.5591 | 2742 | -0.0115 | V | G. Samolyk | 0.0048 |
| TY Cet | 52581.6121 | 3567 | 0.0056 | V | G. Samolyk | 0.0039 |
| TY Cet | 52602.6511 | 3632 | 0.0054 | V | G. Samolyk | 0.0032 |
| TY Cet | 53672.7431 | 6938 | 0.0112 | V | G. Samolyk | 0.0027 |
| XX Cyg | 57531.6511 | 96958 | 0.0050 | V | G. Samolyk | 0.0008 |
| XX Cyg | 57531.7855 | 96959 | 0.0045 | V | G. Samolyk | 0.0008 |
| XX Cyg | 57557.6792 | 97151 | 0.0041 | V | G. Samolyk | 0.0005 |
| XX Cyg | 57557.8143 | 97152 | 0.0043 | V | G. Samolyk | 0.0009 |
| XX Cyg | 57564.6924 | 97203 | 0.0043 | V | G. Samolyk | 0.0007 |
| XX Cyg | 57564.8265 | 97204 | 0.0036 | V | G. Samolyk | 0.0008 |
| XX Cyg | 57579.6616 | 97314 | 0.0035 | V | G. Samolyk | 0.0007 |
| XX Cyg | 57595.7105 | 97433 | 0.0034 | V | G. Samolyk | 0.0009 |
| XX Cyg | 57595.8458 | 97434 | 0.0039 | V | G. Samolyk | 0.0006 |
| XZ Cyg | 57501.7529 | 28669 | -2.5094 | V | G. Samolyk | 0.0008 |
| XZ Cyg | 57528.8000 | 28727 | -2.5309 | V | G. Samolyk | 0.0009 |
| XZ Cyg | 57528.8022 | 28727 | -2.5287 | V | H. Smith | 0.0009 |
| XZ Cyg | 57542.8101 | 28757 | -2.5218 | V | G. Samolyk | 0.0009 |
| XZ Cyg | 57549.8093 | 28772 | -2.5231 | V | R. Sabo | 0.0016 |
| XZ Cyg | 57556.8129 | 28787 | -2.5200 | V | G. Samolyk | 0.0008 |
| XZ Cyg | 57559.6117 | 28793 | -2.5214 | V | T. Arranz | 0.0004 |
| XZ Cyg | 57561.4804 | 28797 | -2.5195 | V | T. Arranz | 0.0007 |
| XZ Cyg | 57564.7420 | 28804 | -2.5248 | V | G. Samolyk | 0.0009 |
| XZ Cyg | 57566.6056 | 28808 | -2.5280 | V | T. Arranz | 0.0005 |
| XZ Cyg | 57567.5399 | 28810 | -2.5271 | V | T. Arranz | 0.0006 |
| XZ Cyg | 57568.4710 | 28812 | -2.5294 | V | T. Arranz | 0.0005 |
| XZ Cyg | 57579.6641 | 28836 | -2.5371 | V | G. Samolyk | 0.0011 |
| XZ Cyg | 57581.5248 | 28840 | -2.5432 | V | T. Arranz | 0.0005 |
| XZ Cyg | 57583.3925 | 28844 | -2.5423 | V | T. Arranz | 0.0006 |
| XZ Cyg | 57595.5302 | 28870 | -2.5388 | V | T. Arranz | 0.0006 |
| XZ Cyg | 57602.5389 | 28885 | -2.5306 | V | T. Arranz | 0.0006 |
| XZ Cyg | 57603.4724 | 28887 | -2.5305 | V | T. Arranz | 0.0006 |
| XZ Cyg | 57609.5359 | 28900 | -2.5341 | V | T. Arranz | 0.0005 |
| XZ Cyg | 57610.4683 | 28902 | -2.5351 | V | T. Arranz | 0.0006 |
| XZ Cyg | 57611.4004 | 28904 | -2.5364 | V | T. Arranz | 0.0006 |
| XZ Cyg | 57614.6672 | 28911 | -2.5365 | V | G. Samolyk | 0.0011 |
| XZ Cyg | 57616.5275 | 28915 | -2.5430 | V | T. Arranz | 0.0006 |
| XZ Cyg | 57676.7229 | 29044 | -2.5519 | V | H. Smith | 0.0007 |
| DM Cyg | 57559.7339 | 35672 | 0.0820 | V | K. Menzies | 0.0009 |
| DM Cyg | 57566.8734 | 35689 | 0.0839 | V | R. Sabo | 0.0009 |
| DM Cyg | 57586.6070 | 35736 | 0.0840 | V | T. Arranz | 0.0006 |

*Table continued on next page*

Table 1. Recent times of maxima of stars in the AAVSO Short Period Pulsator program, cont.

| *Star* | *JD (max) Hel. 2400000 +* | *Cycle* | *O–C* | *F* | *Observer* | *Error* |
|---|---|---|---|---|---|---|
| DM Cyg | 57590.8040 | 35746 | 0.0824 | V | R. Sabo | 0.0009 |
| DM Cyg | 57592.4844 | 35750 | 0.0834 | V | T. Arranz | 0.0007 |
| DM Cyg | 57594.5857 | 35755 | 0.0854 | V | T. Arranz | 0.0007 |
| DM Cyg | 57597.5266 | 35762 | 0.0873 | V | T. Arranz | 0.0007 |
| DM Cyg | 57600.4624 | 35769 | 0.0841 | V | T. Arranz | 0.0006 |
| DM Cyg | 57601.7212 | 35772 | 0.0833 | V | R. Sabo | 0.001 |
| DM Cyg | 57605.5027 | 35781 | 0.0860 | V | T. Arranz | 0.0007 |
| DM Cyg | 57607.6009 | 35786 | 0.0849 | V | T. Arranz | 0.0006 |
| DM Cyg | 57611.7979 | 35796 | 0.0833 | V | R. Sabo | 0.0009 |
| DM Cyg | 57613.4780 | 35800 | 0.0840 | V | T. Arranz | 0.0007 |
| DM Cyg | 57622.7142 | 35822 | 0.0833 | V | R. Sabo | 0.0011 |
| DM Cyg | 57624.8146 | 35827 | 0.0844 | V | K. Menzies | 0.001 |
| DM Cyg | 57627.7551 | 35834 | 0.0859 | V | R. Sabo | 0.0013 |
| DM Cyg | 57659.6655 | 35910 | 0.0869 | V | R. Sabo | 0.0008 |
| RW Dra | 57524.8155 | 40972 | 0.2292 | V | G. Samolyk | 0.0009 |
| RW Dra | 57541.6648 | 41010 | 0.2476 | V | G. Samolyk | 0.0011 |
| RW Dra | 57594.3896 | 41129 | 0.2653 | V | T. Arranz | 0.0006 |
| RW Dra | 57601.4631 | 41145 | 0.2521 | V | T. Arranz | 0.0008 |
| RW Dra | 57609.4070 | 41163 | 0.2235 | V | T. Arranz | 0.0009 |
| RW Dra | 57629.3723 | 41208 | 0.2576 | V | T. Arranz | 0.0008 |
| XZ Dra | 57526.8457 | 32736 | -0.1341 | V | G. Samolyk | 0.0009 |
| XZ Dra | 57569.7358 | 32826 | -0.1287 | V | G. Samolyk | 0.0008 |
| XZ Dra | 57622.6210 | 32937 | -0.1347 | V | G. Samolyk | 0.0008 |
| SV Eri | 57680.8343 | 31000 | 1.0369 | V | G. Samolyk | 0.0018 |
| SV Eri | 57743.6412 | 31088 | 1.0297 | V | G. Samolyk | 0.0021 |
| BB Eri | 57423.6097 | 31346 | 0.2960 | V | G. Samolyk | 0.0011 |
| BB Eri | 57750.7407 | 31920 | 0.3055 | V | G. Samolyk | 0.0012 |
| RX For | 57424.6287 | 29454 | -0.0449 | V | G. Samolyk | 0.0009 |
| RX For | 57668.9246 | 29863 | -0.0504 | V | G. Samolyk | 0.0016 |
| RR Gem | 57423.4842 | 40439 | -0.5642 | V | T. Arranz | 0.0007 |
| RR Gem | 57686.8844 | 41102 | -0.5809 | V | K. Menzies | 0.0009 |
| RR Gem | 57719.8522 | 41185 | -0.5899 | V | G. Samolyk | 0.0006 |
| TW Her | 57482.8540 | 89934 | -0.0158 | V | R. Sabo | 0.0010 |
| TW Her | 57494.8410 | 89964 | -0.0168 | V | N. Simmons | 0.0007 |
| TW Her | 57496.8383 | 89969 | -0.0175 | V | K. Menzies | 0.0006 |
| TW Her | 57528.8080 | 90049 | -0.0158 | V | G. Samolyk | 0.0007 |
| TW Her | 57577.5576 | 90171 | -0.0174 | V | T. Arranz | 0.0004 |
| TW Her | 57583.5520 | 90186 | -0.0170 | V | T. Arranz | 0.0005 |
| TW Her | 57585.5504 | 90191 | -0.0166 | V | T. Arranz | 0.0007 |
| TW Her | 57587.5479 | 90196 | -0.0171 | V | T. Arranz | 0.0006 |
| TW Her | 57591.5440 | 90206 | -0.0170 | V | T. Arranz | 0.0006 |
| TW Her | 57593.5416 | 90211 | -0.0174 | V | T. Arranz | 0.0005 |
| TW Her | 57599.5360 | 90226 | -0.0170 | V | T. Arranz | 0.0006 |
| TW Her | 57615.5193 | 90266 | -0.0177 | V | T. Arranz | 0.0006 |
| VX Her | 57499.9284 | 78506 | -0.0529 | V | R. Sabo | 0.0013 |
| VX Her | 57586.4455 | 78696 | -0.0566 | V | T. Arranz | 0.0008 |
| VX Her | 57606.4829 | 78740 | -0.0556 | V | T. Arranz | 0.0008 |
| VZ Her | 57495.8373 | 47026 | 0.0799 | V | K. Menzies | 0.0007 |
| VZ Her | 57603.7198 | 47271 | 0.0821 | V | R. Sabo | 0.0009 |
| VZ Her | 57630.5793 | 47332 | 0.0816 | V | K. Menzies | 0.0006 |
| AR Her | 57487.9249 | 34114 | -0.9573 | V | R. Sabo | 0.0014 |
| AR Her | 57511.8481 | 34165 | -1.0055 | V | G. Samolyk | 0.0012 |
| AR Her | 57520.8182 | 34184 | -0.9660 | V | R. Sabo | 0.0016 |
| AR Her | 57527.8685 | 34199 | -0.9661 | V | G. Samolyk | 0.0011 |
| AR Her | 57538.6339 | 34222 | -1.0113 | V | G. Samolyk | 0.0011 |
| AR Her | 57547.5932 | 34241 | -0.9825 | V | T. Arranz | 0.0012 |
| AR Her | 57548.5490 | 34243 | -0.9668 | V | T. Arranz | 0.0012 |
| AR Her | 57550.8942 | 34248 | -0.9717 | V | R. Sabo | 0.0019 |
| AR Her | 57558.4233 | 34264 | -0.9631 | V | T. Arranz | 0.0008 |
| AR Her | 57560.7616 | 34269 | -0.9749 | V | G. Samolyk | 0.0009 |
| AR Her | 57563.5769 | 34275 | -0.9798 | V | T. Arranz | 0.0006 |
| AR Her | 57564.5101 | 34277 | -0.9867 | V | T. Arranz | 0.0006 |
| AR Her | 57565.4507 | 34279 | -0.9861 | V | T. Arranz | 0.0008 |
| AR Her | 57568.7283 | 34286 | -0.9987 | V | G. Samolyk | 0.0015 |
| AR Her | 57581.4531 | 34313 | -0.9647 | V | T. Arranz | 0.0011 |
| AR Her | 57582.4063 | 34315 | -0.9515 | V | T. Arranz | 0.0019 |
| AR Her | 57605.3755 | 34364 | -1.0137 | V | T. Arranz | 0.0007 |
| AR Her | 57611.5013 | 34377 | -0.9983 | V | T. Arranz | 0.0014 |
| AR Her | 57613.3987 | 34381 | -0.9810 | V | T. Arranz | 0.0008 |
| DL Her | 57541.6928 | 32678 | 0.0494 | V | G. Samolyk | 0.0012 |
| DL Her | 57557.6641 | 32705 | 0.0467 | V | G. Samolyk | 0.0012 |
| DY Her | 57437.9194 | 161463 | -0.0312 | V | K. Menzies | 0.0005 |
| DY Her | 57484.8862 | 161779 | -0.0320 | V | K. Menzies | 0.0005 |
| DY Her | 57495.8847 | 161853 | -0.0322 | V | R. Sabo | 0.0008 |
| DY Her | 57541.6643 | 162161 | -0.0310 | V | G. Samolyk | 0.0006 |
| DY Her | 57541.8123 | 162162 | -0.0317 | V | G. Samolyk | 0.0006 |
| DY Her | 57543.7446 | 162175 | -0.0316 | V | R. Sabo | 0.0007 |
| LS Her | 57484.8612 | 127725 | -0.0006 | V | K. Menzies | 0.0012 |
| LS Her | 57542.7835 | 127976 | -0.0110 | V | N. Simmons | 0.0025 |
| SZ Hya | 57423.8188 | 31168 | -0.2964 | V | G. Samolyk | 0.0012 |
| SZ Hya | 57429.7640 | 31179 | -0.2608 | V | G. Samolyk | 0.0013 |
| UU Hya | 57421.9633 | 34251 | 0.0037 | V | G. Samolyk | 0.0011 |
| DG Hya | 57406.8903 | 6672 | 0.0180 | V | G. Samolyk | 0.0016 |
| DH Hya | 57422.8337 | 53674 | 0.1003 | V | G. Samolyk | 0.0009 |
| DH Hya | 57473.6917 | 53778 | 0.1025 | V | N. Simmons | 0.0011 |
| RR Leo | 57451.8456 | 31292 | 0.1525 | V | G. Samolyk | 0.0008 |
| SS Leo | 57473.7307 | 25054 | -0.1034 | V | G. Samolyk | 0.0009 |
| ST Leo | 57490.7291 | 61859 | -0.0197 | V | R. Sabo | 0.0008 |
| TV Leo | 57451.8300 | 30334 | 0.1292 | V | G. Samolyk | 0.0012 |
| TV Leo | 57455.8658 | 30340 | 0.1279 | V | R. Sabo | 0.0015 |
| WW Leo | 57445.7345 | 37428 | 0.0477 | V | G. Samolyk | 0.0012 |
| AA Leo | 57498.7483 | 29904 | -0.1068 | V | R. Sabo | 0.0015 |
| VY LMi | 57502.6292 | 13333 | 0.0176 | V | K. Menzies | 0.0015 |
| U Lep | 57698.8493 | 28112 | 0.0444 | V | G. Samolyk | 0.0011 |
| SZ Lyn | 57411.7092 | 160014 | 0.0363 | V | G. Samolyk | 0.0008 |
| SZ Lyn | 57411.8287 | 160015 | 0.0352 | V | G. Samolyk | 0.0008 |
| SZ Lyn | 57433.5245 | 160195 | 0.0348 | V | K. Menzies | 0.0008 |
| SZ Lyn | 57436.5389 | 160220 | 0.0358 | V | G. Samolyk | 0.0006 |
| SZ Lyn | 57436.6602 | 160221 | 0.0365 | V | G. Samolyk | 0.0005 |
| SZ Lyn | 57436.7804 | 160222 | 0.0362 | V | G. Samolyk | 0.0006 |
| SZ Lyn | 57436.9019 | 160223 | 0.0372 | V | G. Samolyk | 0.0008 |
| SZ Lyn | 57442.6868 | 160271 | 0.0364 | V | R. Sabo | 0.0013 |
| SZ Lyn | 57494.6387 | 160702 | 0.0377 | V | G. Samolyk | 0.0007 |
| SZ Lyn | 57524.6530 | 160951 | 0.0389 | V | G. Samolyk | 0.0007 |
| SZ Lyn | 57676.8892 | 162214 | 0.0394 | V | G. Samolyk | 0.0008 |
| SZ Lyn | 57686.7710 | 162296 | 0.0374 | V | G. Samolyk | 0.0008 |
| SZ Lyn | 57686.8914 | 162297 | 0.0372 | V | G. Samolyk | 0.0007 |
| SZ Lyn | 57696.8959 | 162380 | 0.0374 | V | G. Samolyk | 0.0006 |
| SZ Lyn | 57701.7170 | 162420 | 0.0371 | V | G. Samolyk | 0.0007 |
| SZ Lyn | 57701.8375 | 162421 | 0.0370 | V | G. Samolyk | 0.0005 |
| SZ Lyn | 57701.9581 | 162422 | 0.0371 | V | G. Samolyk | 0.0006 |
| SZ Lyn | 57736.6715 | 162710 | 0.0364 | V | G. Samolyk | 0.0006 |
| SZ Lyn | 57736.7916 | 162711 | 0.0360 | V | G. Samolyk | 0.0007 |
| RR Lyr | 57494.9216 | 25706 | -0.4003 | V | G. Samolyk | 0.0009 |
| RR Lyr | 57556.7029 | 25815 | -0.4076 | V | G. Samolyk | 0.0012 |
| RZ Lyr | 57506.8174 | 31929 | -0.0640 | V | K. Menzies | 0.0009 |
| RZ Lyr | 57552.8500 | 32019 | -0.0432 | V | R. Sabo | 0.0021 |
| RZ Lyr | 57569.7117 | 32052 | -0.0525 | V | G. Samolyk | 0.0017 |
| CX Lyr | 57706.4744 | 39951 | 1.5270 | V | K. Menzies | 0.0016 |
| KM Lyr | 57477.8725 | 42297 | -0.1998 | V | K. Menzies | 0.0012 |
| V340 Lyr | 57624.6998 | 47426 | -0.0355 | V | K. Menzies | 0.0021 |
| ST Oph | 57524.8286 | 64612 | -0.0259 | V | G. Samolyk | 0.0009 |
| AV Peg | 57594.9204 | 35362 | 0.1743 | V | R. Sabo | 0.0009 |
| AV Peg | 57614.8316 | 35413 | 0.1763 | V | G. Samolyk | 0.0009 |
| BH Peg | 57614.7991 | 28471 | -0.1926 | V | G. Samolyk | 0.0008 |
| BH Peg | 57675.7430 | 28566 | -0.1430 | V | G. Samolyk | 0.0015 |
| DY Peg | 57646.5819 | 180244 | -0.0160 | V | G. Samolyk | 0.0005 |
| DY Peg | 57646.6546 | 180245 | -0.0163 | V | G. Samolyk | 0.0005 |
| DY Peg | 57646.7265 | 180246 | -0.0173 | V | G. Samolyk | 0.0006 |
| DY Peg | 57646.8009 | 180247 | -0.0158 | V | G. Samolyk | 0.0008 |
| DY Peg | 57646.8722 | 180248 | -0.0174 | V | G. Samolyk | 0.0006 |
| DY Peg | 57671.5217 | 180586 | -0.0170 | V | G. Samolyk | 0.0004 |

*Table continued on next page*

Table 1. Recent times of maxima of stars in the AAVSO Short Period Pulsator program, cont.

| *Star* | *JD (max) Hel. 2400000 +* | *Cycle* | *O–C* | *F* | *Observer* | *Error* |
|---|---|---|---|---|---|---|
| DY Peg | 57671.5951 | 180587 | -0.0166 | V | G. Samolyk | 0.0005 |
| DY Peg | 57671.6685 | 180588 | -0.0160 | V | G. Samolyk | 0.0004 |
| DY Peg | 57671.7391 | 180589 | -0.0184 | V | G. Samolyk | 0.0007 |
| DF Ser | 57447.9172 | 63367 | 0.0998 | V | K. Menzies | 0.0013 |
| DF Ser | 57501.7681 | 63490 | 0.1019 | V | G. Samolyk | 0.0009 |
| DF Ser | 57604.6483 | 63725 | 0.1003 | V | G. Samolyk | 0.0012 |
| RV UMa | 57411.8305 | 26356 | 0.1301 | V | G. Samolyk | 0.0012 |
| RV UMa | 57563.4802 | 26680 | 0.1284 | V | T. Arranz | 0.0006 |
| RV UMa | 57564.4170 | 26682 | 0.1291 | V | T. Arranz | 0.0005 |
| RV UMa | 57571.4362 | 26697 | 0.1274 | V | T. Arranz | 0.0005 |
| RV UMa | 57586.4105 | 26729 | 0.1238 | V | T. Arranz | 0.0007 |
| AE UMa | 57158.4059 | 250579 | 0.0003 | V | T. Arranz | 0.0003 |
| AE UMa | 57390.7357 | 253280 | -0.0020 | V | G. Samolyk | 0.0001 |
| AE UMa | 57392.6348 | 253302 | 0.0047 | V | G. Samolyk | 0.0008 |
| AE UMa | 57392.7175 | 253303 | 0.0014 | V | G. Samolyk | 0.0005 |
| AE UMa | 57392.7996 | 253304 | -0.0025 | V | G. Samolyk | 0.0006 |
| AE UMa | 57392.8903 | 253305 | 0.0022 | V | G. Samolyk | 0.0007 |
| AE UMa | 57392.9780 | 253306 | 0.0039 | V | G. Samolyk | 0.0004 |
| AE UMa | 57405.5347 | 253452 | 0.0021 | V | G. Samolyk | 0.0009 |
| AE UMa | 57405.6240 | 253453 | 0.0054 | V | G. Samolyk | 0.0012 |
| AE UMa | 57405.7061 | 253454 | 0.0014 | V | G. Samolyk | 0.0007 |
| AE UMa | 57405.7963 | 253455 | 0.0056 | V | G. Samolyk | 0.0013 |
| AE UMa | 57406.5606 | 253464 | -0.0042 | V | G. Samolyk | 0.0006 |
| AE UMa | 57406.6491 | 253465 | -0.0017 | V | G. Samolyk | 0.0007 |
| AE UMa | 57406.7402 | 253466 | 0.0033 | V | G. Samolyk | 0.0009 |
| AE UMa | 57406.8232 | 253467 | 0.0003 | V | G. Samolyk | 0.0006 |
| AE UMa | 57406.9077 | 253468 | -0.0012 | V | G. Samolyk | 0.0009 |
| AE UMa | 57712.7860 | 257024 | 0.0005 | V | G. Samolyk | 0.0006 |
| AE UMa | 57712.8698 | 257025 | -0.0018 | V | G. Samolyk | 0.0008 |
| AE UMa | 57712.9608 | 257026 | 0.0032 | V | G. Samolyk | 0.0009 |
| AE UMa | 57736.6984 | 257302 | 0.0001 | V | G. Samolyk | 0.0009 |
| AE UMa | 57736.7884 | 257303 | 0.0041 | V | G. Samolyk | 0.0009 |
| AE UMa | 57737.7311 | 257314 | 0.0006 | V | G. Samolyk | 0.0006 |
| AE UMa | 57737.8141 | 257315 | -0.0024 | V | G. Samolyk | 0.0006 |
| AE UMa | 57750.7168 | 257465 | -0.0023 | V | G. Samolyk | 0.0005 |

# Visual Times of Maxima for Short Period Pulsating Stars I

**Gerard Samolyk**
*P.O. Box 20677, Greenfield, WI 53220; gsamolyk@wi.rr.com*

*Received March 3, 2017; accepted March 3, 2017*

**Abstract** This compilation contains 463 times of maxima of 6 short period pulsating stars (primarily RR Lyrae). These were reduced from a portion of the visual observations made from 1966 to 2014 that are included in the AAVSO International Database.

## 1. Observations

This is the first in a series of papers to publish of times of maxima derived from visual observations reported to the AAVSO International Database as part of the RR Lyr committee legacy program. The goal of this project is to fill some historical gaps in the O–C history for these stars. This list contains times of maxima for RR Lyr stars located in the constellations Andromeda, Aqrarius, and Auriga. This list will be web-archived and made available through the AAVSO ftp site at ftp://ftp.aavso.org/public/datasets/gsamo-451-rrlyr-1.txt.

These observations were reduced by the writer using the PERANSO program (Vanmunster 2007). The linear elements in the *General Catalogue of Variable Stars* (GCVS; Kholopov *et al.* 1985) were used to compute the O–C values for all stars.

Figures 1 and 2 are O–C plots for two of the stars listed.

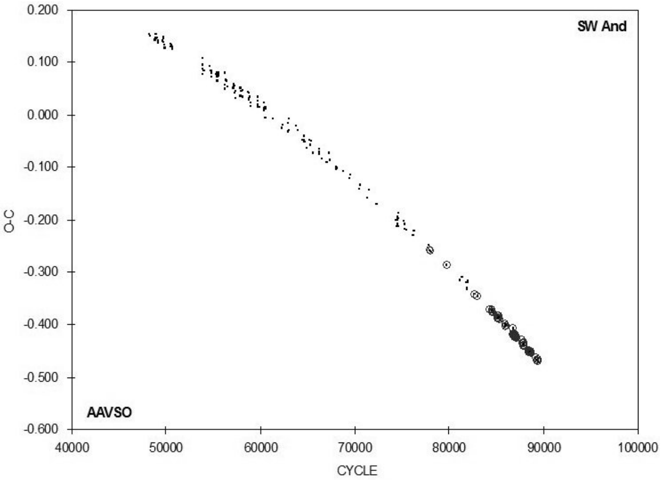

Figure 1. O–C plot for SW And. The circled times of maxima are from CCD papers published in *JAAVSO* (Samolyk 2010–2016).

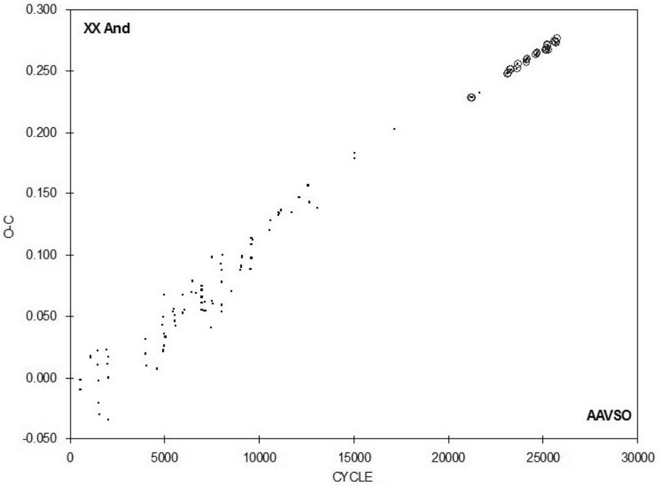

Figure 2. O–C plot for XX And. The circled times of maxima are from CCD papers published in *JAAVSO* (Samolyk 2010–2016).

## References

Kholopov, P. N., et al. 1985, *General Catalogue of Variable Stars*, 4th ed., Moscow.

Samolyk, G. 2010, *J. Amer. Assoc. Var. Star Obs.,* **38**, 1.

Samolyk, G. 2011, *J. Amer. Assoc. Var. Star Obs.,* **39**, 1.

Samolyk, G. 2012, *J. Amer. Assoc. Var. Star Obs.,* **40**, 2.

Samolyk, G. 2013, *J. Amer. Assoc. Var. Star Obs.,* **41**, 1.

Samolyk, G. 2014, *J. Amer. Assoc. Var. Star Obs.,* **42**, 1.

Samolyk, G. 2015, *J. Amer. Assoc. Var. Star Obs.,* **43**, 1.

Samolyk, G. 2016, *J. Amer. Assoc. Var. Star Obs.,* **44**, 1.

Vanmunster, T. 2007, PERANSO period analysis software (http://www.peranso.com).

Table 1. Recent times of minima of stars in the AAVSO short period pulsator program.

| Star | JD (max) Hel. 2400000 + | Cycle | O–C (day) | Observer | Error (day) |
|---|---|---|---|---|---|
| SW And | 39471.603 | 48247 | 0.155 | M. Baldwin | 0.003 |
| SW And | 39505.655 | 48324 | 0.151 | M. Baldwin | 0.002 |
| SW And | 39757.746 | 48894 | 0.143 | M. Baldwin | 0.003 |
| SW And | 39761.731 | 48903 | 0.147 | M. Baldwin | 0.003 |
| SW And | 39772.794 | 48928 | 0.153 | M. Baldwin | 0.004 |
| SW And | 39800.648 | 48991 | 0.144 | M. Baldwin | 0.002 |
| SW And | 39823.650 | 49043 | 0.147 | M. Baldwin | 0.003 |
| SW And | 39826.745 | 49050 | 0.146 | M. Baldwin | 0.003 |
| SW And | 39884.675 | 49181 | 0.138 | M. Baldwin | 0.002 |
| SW And | 39892.639 | 49199 | 0.141 | M. Baldwin | 0.002 |
| SW And | 40098.742 | 49665 | 0.142 | M. Baldwin | 0.003 |
| SW And | 40125.728 | 49726 | 0.148 | M. Baldwin | 0.004 |
| SW And | 40128.815 | 49733 | 0.140 | M. Baldwin | 0.003 |
| SW And | 40156.684 | 49796 | 0.145 | M. Baldwin | 0.002 |
| SW And | 40178.781 | 49846 | 0.128 | M. Baldwin | 0.003 |
| SW And | 40186.748 | 49864 | 0.134 | M. Baldwin | 0.003 |
| SW And | 40225.663 | 49952 | 0.128 | T. Cragg | 0.003 |
| SW And | 40455.650 | 50472 | 0.130 | L. Hazel | 0.004 |
| SW And | 40478.653 | 50524 | 0.134 | L. Hazel | 0.004 |
| SW And | 40482.629 | 50533 | 0.130 | L. Hazel | 0.002 |
| SW And | 40512.707 | 50601 | 0.133 | M. Baldwin | 0.003 |
| SW And | 40562.677 | 50714 | 0.125 | M. Baldwin | 0.004 |
| SW And | 40566.662 | 50723 | 0.130 | M. Baldwin | 0.005 |
| SW And | 41972.647 | 53902 | 0.108 | M. Baldwin | 0.003 |
| SW And | 41982.789 | 53925 | 0.078 | M. Baldwin | 0.003 |
| SW And | 41983.682 | 53927 | 0.086 | M. Baldwin | 0.002 |
| SW And | 41988.556 | 53938 | 0.095 | M. Baldwin | 0.003 |
| SW And | 42018.620 | 54006 | 0.084 | M. Baldwin | 0.002 |
| SW And | 42305.669 | 54655 | 0.094 | M. Baldwin | 0.004 |
| SW And | 42342.810 | 54739 | 0.084 | M. Baldwin | 0.004 |
| SW And | 42371.555 | 54804 | 0.080 | B. Small | 0.006 |
| SW And | 42374.643 | 54811 | 0.072 | M. Baldwin | 0.004 |
| SW And | 42386.595 | 54838 | 0.083 | M. Baldwin | 0.003 |
| SW And | 42637.804 | 55406 | 0.077 | M. Baldwin | 0.004 |
| SW And | 42660.789 | 55458 | 0.064 | M. Baldwin | 0.003 |
| SW And | 42665.670 | 55469 | 0.080 | M. Baldwin | 0.003 |
| SW And | 42668.759 | 55476 | 0.073 | M. Baldwin | 0.002 |
| SW And | 42669.645 | 55478 | 0.074 | M. Baldwin | 0.002 |
| SW And | 42688.665 | 55521 | 0.076 | M. Baldwin | 0.003 |
| SW And | 42692.643 | 55530 | 0.074 | M. Baldwin | 0.003 |
| SW And | 42715.648 | 55582 | 0.080 | M. Baldwin | 0.005 |
| SW And | 43021.675 | 56274 | 0.050 | M. Baldwin | 0.004 |
| SW And | 43028.758 | 56290 | 0.056 | M. Baldwin | 0.004 |
| SW And | 43033.647 | 56301 | 0.080 | M. Baldwin | 0.003 |
| SW And | 43044.691 | 56326 | 0.067 | M. Baldwin | 0.002 |
| SW And | 43098.646 | 56448 | 0.064 | M. Baldwin | 0.003 |
| SW And | 43144.632 | 56552 | 0.053 | M. Baldwin | 0.003 |
| SW And | 43397.614 | 57124 | 0.051 | M. Baldwin | 0.004 |
| SW And | 43404.698 | 57140 | 0.059 | M. Baldwin | 0.004 |
| SW And | 43416.634 | 57167 | 0.053 | M. Baldwin | 0.003 |
| SW And | 43423.708 | 57183 | 0.051 | M. Baldwin | 0.002 |
| SW And | 43447.596 | 57237 | 0.055 | M. Baldwin | 0.003 |
| SW And | 43466.613 | 57280 | 0.054 | M. Baldwin | 0.004 |
| SW And | 43489.598 | 57332 | 0.041 | M. Baldwin | 0.003 |
| SW And | 43493.583 | 57341 | 0.045 | M. Baldwin | 0.003 |
| SW And | 43505.525 | 57368 | 0.046 | M. Baldwin | 0.004 |
| SW And | 43512.601 | 57384 | 0.045 | M. Baldwin | 0.003 |
| SW And | 43520.548 | 57402 | 0.031 | M. Baldwin | 0.004 |
| SW And | 43756.729 | 57936 | 0.035 | M. Baldwin | 0.003 |
| SW And | 43760.725 | 57945 | 0.051 | M. Baldwin | 0.005 |
| SW And | 43776.641 | 57981 | 0.045 | M. Baldwin | 0.004 |
| SW And | 43822.627 | 58085 | 0.033 | M. Baldwin | 0.004 |
| SW And | 43841.659 | 58128 | 0.047 | M. Baldwin | 0.004 |
| SW And | 44101.716 | 58716 | 0.044 | M. Baldwin | 0.003 |
| SW And | 44128.683 | 58777 | 0.032 | M. Baldwin | 0.003 |
| SW And | 44132.673 | 58786 | 0.042 | M. Baldwin | 0.002 |
| SW And | 44136.653 | 58795 | 0.041 | M. Baldwin | 0.004 |
| SW And | 44140.620 | 58804 | 0.028 | M. Baldwin | 0.003 |
| SW And | 44194.584 | 58926 | 0.033 | M. Baldwin | 0.002 |
| SW And | 44216.682 | 58976 | 0.018 | M. Baldwin | 0.004 |
| SW And | 44217.572 | 58978 | 0.023 | M. Baldwin | 0.003 |
| SW And | 44539.562 | 59706 | 0.034 | G. Hanson | 0.005 |
| SW And | 44542.651 | 59713 | 0.027 | G. Hanson | 0.003 |
| SW And | 44550.604 | 59731 | 0.019 | M. Baldwin | 0.003 |
| SW And | 44554.584 | 59740 | 0.018 | G. Hanson | 0.003 |
| SW And | 44554.593 | 59740 | 0.027 | M. Baldwin | 0.002 |
| SW And | 44562.542 | 59758 | 0.015 | G. Hanson | 0.003 |
| SW And | 44623.577 | 59896 | 0.015 | G. Hanson | 0.003 |
| SW And | 44872.577 | 60459 | 0.012 | M. Baldwin | 0.003 |
| SW And | 44874.787 | 60464 | 0.011 | L. Cook | 0.004 |
| SW And | 44875.669 | 60466 | 0.008 | M. Baldwin | 0.003 |
| SW And | 44876.567 | 60468 | 0.022 | M. Baldwin | 0.005 |
| SW And | 44898.653 | 60518 | -0.006 | M. Baldwin | 0.003 |
| SW And | 44907.520 | 60538 | 0.015 | M. Baldwin | 0.002 |
| SW And | 44926.534 | 60581 | 0.011 | M. Baldwin | 0.002 |
| SW And | 45266.627 | 61350 | -0.009 | G. Chaple | 0.004 |
| SW And | 45672.623 | 62268 | -0.025 | G. Chaple | 0.003 |
| SW And | 45699.607 | 62329 | -0.021 | G. Chaple | 0.004 |
| SW And | 45989.729 | 62985 | -0.034 | M. Baldwin | 0.005 |
| SW And | 45993.727 | 62994 | -0.016 | M. Baldwin | 0.003 |
| SW And | 46005.654 | 63021 | -0.031 | M. Baldwin | 0.004 |
| SW And | 46020.693 | 63055 | -0.029 | M. Baldwin | 0.004 |
| SW And | 46021.598 | 63057 | -0.009 | M. Baldwin | 0.004 |
| SW And | 46354.621 | 63810 | -0.022 | M. Baldwin | 0.004 |
| SW And | 46442.627 | 64009 | -0.030 | M. Baldwin | 0.003 |
| SW And | 46679.670 | 64545 | -0.049 | M. Baldwin | 0.003 |
| SW And | 46702.676 | 64597 | -0.041 | M. Baldwin | 0.003 |
| SW And | 46710.626 | 64615 | -0.052 | M. Baldwin | 0.004 |
| SW And | 46714.611 | 64624 | -0.048 | M. Baldwin | 0.002 |
| SW And | 46722.579 | 64642 | -0.041 | M. Baldwin | 0.003 |
| SW And | 46744.682 | 64692 | -0.052 | M. Baldwin | 0.003 |
| SW And | 46833.569 | 64893 | -0.063 | M. Baldwin | 0.005 |
| SW And | 46973.786 | 65210 | -0.049 | M. Baldwin | 0.003 |
| SW And | 47023.754 | 65323 | -0.058 | M. Baldwin | 0.002 |
| SW And | 47082.585 | 65456 | -0.050 | M. Baldwin | 0.004 |
| SW And | 47139.617 | 65585 | -0.072 | M. Baldwin | 0.005 |
| SW And | 47410.735 | 66198 | -0.072 | M. Baldwin | 0.002 |
| SW And | 47422.674 | 66225 | -0.074 | M. Baldwin | 0.003 |
| SW And | 47449.662 | 66286 | -0.065 | M. Baldwin | 0.004 |
| SW And | 47557.559 | 66530 | -0.085 | M. Baldwin | 0.004 |
| SW And | 47807.884 | 67096 | -0.090 | G. Samolyk | 0.003 |
| SW And | 47894.588 | 67292 | -0.072 | G. Samolyk | 0.004 |
| SW And | 47940.571 | 67396 | -0.087 | M. Baldwin | 0.002 |
| SW And | 48219.637 | 68027 | -0.099 | M. Baldwin | 0.002 |
| SW And | 48235.555 | 68063 | -0.103 | M. Baldwin | 0.003 |
| SW And | 48296.591 | 68201 | -0.101 | M. Baldwin | 0.002 |
| SW And | 48545.589 | 68764 | -0.107 | M. Baldwin | 0.003 |
| SW And | 48866.669 | 69490 | -0.122 | M. Baldwin | 0.002 |
| SW And | 48893.654 | 69551 | -0.116 | M. Baldwin | 0.004 |
| SW And | 49338.561 | 70557 | -0.142 | M. Baldwin | 0.003 |
| SW And | 49361.567 | 70609 | -0.134 | M. Baldwin | 0.003 |
| SW And | 49662.734 | 71290 | -0.160 | L. Hazel | 0.004 |
| SW And | 49744.571 | 71475 | -0.144 | M. Baldwin | 0.004 |
| SW And | 50104.560 | 72289 | -0.171 | M. Baldwin | 0.004 |
| SW And | 51045.701 | 74417 | -0.201 | R. Berg | 0.003 |
| SW And | 51088.591 | 74514 | -0.212 | R. Berg | 0.005 |
| SW And | 51100.547 | 74541 | -0.197 | R. Berg | 0.003 |
| SW And | 51106.735 | 74555 | -0.201 | R. Berg | 0.003 |
| SW And | 51111.592 | 74566 | -0.209 | R. Berg | 0.005 |
| SW And | 51115.572 | 74575 | -0.210 | R. Berg | 0.004 |

Table continued on following pages

Table 1. Recent times of minima of stars in the AAVSO short period pulsator program, cont.

| *Star* | *JD (max) Hel. 2400000 +* | *Cycle* | *O–C (day)* | *Observer* | *Error (day)* |
|---|---|---|---|---|---|
| SW And | 51133.720 | 74616 | -0.195 | L. Hazel | 0.004 |
| SW And | 51142.563 | 74636 | -0.198 | R. Berg | 0.004 |
| SW And | 51149.650 | 74652 | -0.187 | R. Berg | 0.004 |
| SW And | 51161.566 | 74679 | -0.213 | M. Baldwin | 0.004 |
| SW And | 51397.754 | 75213 | -0.202 | M. Baldwin | 0.004 |
| SW And | 51421.631 | 75267 | -0.208 | M. Baldwin | 0.003 |
| SW And | 51424.717 | 75274 | -0.218 | M. Baldwin | 0.004 |
| SW And | 51436.658 | 75301 | -0.219 | M. Baldwin | 0.004 |
| SW And | 51501.671 | 75448 | -0.221 | R. Berg | 0.004 |
| SW And | 51853.716 | 76244 | -0.230 | R. Berg | 0.003 |
| SW And | 51881.588 | 76307 | -0.222 | R. Berg | 0.004 |
| SW And | 52539.673 | 77795 | -0.249 | R. Berg | 0.003 |
| SW And | 54049.548 | 81209 | -0.316 | R. Harvan | 0.007 |
| SW And | 54118.549 | 81365 | -0.310 | R. Harvan | 0.004 |
| SW And | 54324.642 | 81831 | -0.319 | R. Harvan | 0.004 |
| SW And | 54347.630 | 81883 | -0.330 | R. Harvan | 0.008 |
| SW And | 54350.724 | 81890 | -0.332 | R. Harvan | 0.004 |
| SW And | 54405.581 | 82014 | -0.318 | R. Harvan | 0.005 |
| SW And | 54412.655 | 82030 | -0.320 | R. Harvan | 0.004 |
| XX And | 39472.659 | 533 | -0.002 | M. Baldwin | 0.007 |
| XX And | 39477.710 | 540 | -0.010 | M. Baldwin | 0.005 |
| XX And | 39884.642 | 1103 | 0.016 | M. Baldwin | 0.002 |
| XX And | 39897.653 | 1121 | 0.018 | M. Baldwin | 0.012 |
| XX And | 40129.659 | 1442 | 0.022 | M. Baldwin | 0.007 |
| XX And | 40147.716 | 1467 | 0.010 | M. Baldwin | 0.009 |
| XX And | 40178.782 | 1510 | -0.003 | M. Baldwin | 0.005 |
| XX And | 40186.714 | 1521 | -0.021 | M. Baldwin | 0.005 |
| XX And | 40207.664 | 1550 | -0.030 | M. Baldwin | 0.006 |
| XX And | 40457.787 | 1896 | 0.022 | M. Baldwin | 0.009 |
| XX And | 40512.704 | 1972 | 0.011 | M. Baldwin | 0.009 |
| XX And | 40554.629 | 2030 | 0.017 | M. Baldwin | 0.007 |
| XX And | 40556.780 | 2033 | -0.001 | M. Baldwin | 0.006 |
| XX And | 40559.638 | 2037 | -0.034 | M. Baldwin | 0.006 |
| XX And | 41982.780 | 4006 | 0.019 | M. Baldwin | 0.005 |
| XX And | 41988.575 | 4014 | 0.032 | M. Baldwin | 0.009 |
| XX And | 41990.721 | 4017 | 0.009 | M. Baldwin | 0.006 |
| XX And | 42392.566 | 4573 | 0.007 | M. Baldwin | 0.006 |
| XX And | 42631.831 | 4904 | 0.043 | M. Baldwin | 0.010 |
| XX And | 42660.747 | 4944 | 0.049 | M. Baldwin | 0.007 |
| XX And | 42665.778 | 4951 | 0.021 | M. Baldwin | 0.002 |
| XX And | 42668.671 | 4955 | 0.023 | M. Baldwin | 0.004 |
| XX And | 42688.920 | 4983 | 0.035 | M. Baldwin | 0.003 |
| XX And | 42689.675 | 4984 | 0.067 | M. Baldwin | 0.009 |
| XX And | 42715.653 | 5020 | 0.026 | M. Baldwin | 0.010 |
| XX And | 42728.669 | 5038 | 0.033 | M. Baldwin | 0.001 |
| XX And | 43033.689 | 5460 | 0.054 | M. Baldwin | 0.009 |
| XX And | 43080.670 | 5525 | 0.056 | M. Baldwin | 0.005 |
| XX And | 43098.734 | 5550 | 0.051 | M. Baldwin | 0.001 |
| XX And | 43101.620 | 5554 | 0.046 | M. Baldwin | 0.008 |
| XX And | 43127.635 | 5590 | 0.042 | M. Baldwin | 0.009 |
| XX And | 43398.675 | 5965 | 0.052 | M. Baldwin | 0.007 |
| XX And | 43403.749 | 5972 | 0.067 | M. Baldwin | 0.009 |
| XX And | 43466.616 | 6059 | 0.055 | M. Baldwin | 0.006 |
| XX And | 43721.761 | 6412 | 0.070 | M. Baldwin | 0.007 |
| XX And | 43776.699 | 6488 | 0.079 | M. Baldwin | 0.010 |
| XX And | 43891.605 | 6647 | 0.069 | M. Baldwin | 0.003 |
| XX And | 44128.663 | 6975 | 0.066 | M. Baldwin | 0.007 |
| XX And | 44133.712 | 6982 | 0.055 | M. Baldwin | 0.005 |
| XX And | 44133.728 | 6982 | 0.072 | M. Heifner | 0.009 |
| XX And | 44141.667 | 6993 | 0.060 | M. Heifner | 0.012 |
| XX And | 44141.681 | 6993 | 0.074 | M. Baldwin | 0.013 |
| XX And | 44193.699 | 7065 | 0.055 | M. Heifner | 0.005 |
| XX And | 44222.617 | 7105 | 0.062 | M. Baldwin | 0.009 |
| XX And | 44274.647 | 7177 | 0.055 | M. Heifner | 0.006 |
| XX And | 44506.635 | 7498 | 0.041 | M. Heifner | 0.005 |
| XX And | 44514.607 | 7509 | 0.062 | M. Baldwin | 0.011 |
| XX And | 44522.593 | 7520 | 0.098 | M. Baldwin | 0.019 |
| XX And | 44553.633 | 7563 | 0.060 | M. Baldwin | 0.006 |
| XX And | 44871.674 | 8003 | 0.092 | M. Baldwin | 0.007 |
| XX And | 44876.694 | 8010 | 0.053 | M. Heifner | 0.005 |
| XX And | 44876.719 | 8010 | 0.078 | M. Baldwin | 0.008 |
| XX And | 44884.678 | 8021 | 0.087 | M. Baldwin | 0.007 |
| XX And | 44897.659 | 8039 | 0.059 | M. Heifner | 0.005 |
| XX And | 44926.610 | 8079 | 0.100 | M. Baldwin | 0.011 |
| XX And | 45249.649 | 8526 | 0.071 | M. Heifner | 0.009 |
| XX And | 45593.694 | 9002 | 0.088 | M. Heifner | 0.006 |
| XX And | 45614.656 | 9031 | 0.090 | M. Heifner | 0.004 |
| XX And | 45635.616 | 9060 | 0.091 | M. Heifner | 0.006 |
| XX And | 45653.692 | 9085 | 0.098 | M. Heifner | 0.008 |
| XX And | 45666.702 | 9103 | 0.099 | L. Cook | 0.006 |
| XX And | 45989.760 | 9550 | 0.088 | M. Baldwin | 0.001 |
| XX And | 46005.669 | 9572 | 0.097 | M. Baldwin | 0.012 |
| XX And | 46021.581 | 9594 | 0.109 | M. Baldwin | 0.005 |
| XX And | 46026.645 | 9601 | 0.113 | M. Baldwin | 0.009 |
| XX And | 46057.722 | 9644 | 0.112 | M. Baldwin | 0.003 |
| XX And | 46725.548 | 10568 | 0.120 | M. Baldwin | 0.006 |
| XX And | 46735.675 | 10582 | 0.128 | M. Baldwin | 0.004 |
| XX And | 47037.788 | 11000 | 0.133 | M. Baldwin | 0.011 |
| XX And | 47040.681 | 11004 | 0.135 | M. Baldwin | 0.004 |
| XX And | 47087.658 | 11069 | 0.134 | M. Baldwin | 0.009 |
| XX And | 47152.708 | 11159 | 0.137 | M. Baldwin | 0.008 |
| XX And | 47543.713 | 11700 | 0.135 | R. Hill | 0.005 |
| XX And | 47859.566 | 12137 | 0.147 | G. Samolyk | 0.002 |
| XX And | 48177.584 | 12577 | 0.157 | M. Baldwin | 0.006 |
| XX And | 48211.553 | 12624 | 0.157 | M. Baldwin | 0.006 |
| XX And | 48237.558 | 12660 | 0.143 | M. Baldwin | 0.007 |
| XX And | 48547.612 | 13089 | 0.138 | M. Baldwin | 0.006 |
| XX And | 49962.795 | 15047 | 0.183 | M. Baldwin | 0.005 |
| XX And | 49965.683 | 15051 | 0.179 | M. Baldwin | 0.009 |
| XX And | 51493.594 | 17165 | 0.202 | M. Baldwin | 0.001 |
| AT And | 39505.618 | -4600 | 0.005 | M. Baldwin | 0.007 |
| AT And | 39851.703 | -4039 | 0.001 | M. Baldwin | 0.003 |
| AT And | 39859.711 | -4026 | -0.011 | M. Baldwin | 0.009 |
| AT And | 39893.656 | -3971 | 0.004 | M. Baldwin | 0.005 |
| AT And | 40184.849 | -3499 | 0.013 | M. Baldwin | 0.011 |
| AT And | 40207.665 | -3462 | 0.003 | M. Baldwin | 0.003 |
| AT And | 40566.718 | -2880 | 0.012 | M. Baldwin | 0.011 |
| AT And | 41683.325 | -1070 | 0.003 | M. Baldwin | 0.005 |
| AT And | 42270.612 | -118 | -0.013 | H. Smith | 0.011 |
| AT And | 42598.835 | 414 | 0.012 | M. Baldwin | 0.009 |
| AT And | 43130.596 | 1276 | -0.008 | M. Baldwin | 0.007 |
| AT And | 43397.723 | 1709 | -0.005 | M. Baldwin | 0.005 |
| AT And | 43753.681 | 2286 | -0.007 | M. Baldwin | 0.007 |
| AT And | 44217.616 | 3038 | 0.008 | M. Baldwin | 0.009 |
| AT And | 45993.715 | 5917 | 0.010 | M. Baldwin | 0.009 |
| AT And | 46027.629 | 5972 | -0.006 | M. Baldwin | 0.007 |
| AT And | 46679.714 | 7029 | 0.000 | M. Baldwin | 0.003 |
| AT And | 46996.805 | 7543 | -0.003 | M. Baldwin | 0.005 |
| AT And | 47001.737 | 7551 | -0.007 | M. Baldwin | 0.007 |
| AT And | 47027.660 | 7593 | 0.006 | M. Baldwin | 0.007 |
| AT And | 47064.667 | 7653 | -0.002 | M. Baldwin | 0.003 |
| AT And | 47331.803 | 8086 | 0.010 | M. Baldwin | 0.009 |
| AT And | 51512.636 | 14863 | 0.012 | M. Baldwin | 0.011 |
| AT And | 55429.400 | 21212 | -0.016 | J. Starzomski | 0.014 |
| SW Aqr | 40549.709 | 33643 | -0.005 | T. Cragg | 0.001 |
| SW Aqr | 49635.650 | 53425 | 0.001 | G. Samolyk | 0.004 |
| SW Aqr | 50003.556 | 54226 | 0.005 | G. Samolyk | 0.005 |
| SW Aqr | 50257.549 | 54779 | 0.003 | I. Fernandez | 0.002 |
| SW Aqr | 50257.549 | 54779 | 0.003 | M. Tejera | 0.003 |
| SW Aqr | 50257.555 | 54779 | 0.009 | F. Turi | 0.008 |

*Table continued on next page*

Table 1. Recent times of minima of stars in the AAVSO short period pulsator program, cont.

| *Star* | *JD (max) Hel. 2400000 +* | *Cycle* | *O–C (day)* | *Observer* | *Error (day)* |
|---|---|---|---|---|---|
| SW Aqr | 50347.565 | 54975 | -0.004 | G. Chaple | 0.002 |
| SW Aqr | 51045.706 | 56495 | -0.004 | R. Berg | 0.004 |
| SW Aqr | 51051.678 | 56508 | -0.003 | R. Berg | 0.004 |
| SW Aqr | 51056.727 | 56519 | -0.007 | R. Berg | 0.003 |
| SW Aqr | 51109.551 | 56634 | -0.002 | R. Berg | 0.003 |
| SW Aqr | 51429.686 | 57331 | -0.002 | R. Berg | 0.003 |
| SW Aqr | 51435.650 | 57344 | -0.009 | R. Berg | 0.008 |
| SW Aqr | 51785.642 | 58106 | -0.006 | R. Berg | 0.008 |
| SW Aqr | 51812.743 | 58165 | -0.004 | R. Hill | 0.004 |
| SW Aqr | 51837.554 | 58219 | 0.005 | G. Samolyk | 0.004 |
| TZ Aur | 39892.738 | 51038 | 0.017 | M. Baldwin | 0.007 |
| TZ Aur | 39894.681 | 51043 | 0.001 | M. Baldwin | 0.004 |
| TZ Aur | 39912.700 | 51089 | 0.003 | M. Baldwin | 0.004 |
| TZ Aur | 39915.830 | 51097 | 0.000 | M. Baldwin | 0.003 |
| TZ Aur | 39917.796 | 51102 | 0.007 | M. Baldwin | 0.008 |
| TZ Aur | 40203.716 | 51832 | 0.005 | M. Baldwin | 0.005 |
| TZ Aur | 40207.637 | 51842 | 0.009 | M. Baldwin | 0.002 |
| TZ Aur | 40270.697 | 52003 | 0.010 | M. Baldwin | 0.007 |
| TZ Aur | 40293.799 | 52062 | 0.003 | M. Baldwin | 0.002 |
| TZ Aur | 40566.798 | 52759 | 0.005 | M. Baldwin | 0.003 |
| TZ Aur | 41683.472 | 55610 | 0.014 | M. Baldwin | 0.004 |
| TZ Aur | 41705.405 | 55666 | 0.013 | M. Baldwin | 0.003 |
| TZ Aur | 41752.402 | 55786 | 0.010 | M. Baldwin | 0.003 |
| TZ Aur | 41765.327 | 55819 | 0.009 | M. Baldwin | 0.009 |
| TZ Aur | 41766.488 | 55822 | -0.005 | M. Baldwin | 0.008 |
| TZ Aur | 42429.609 | 57515 | 0.011 | M. Baldwin | 0.005 |
| TZ Aur | 42843.605 | 58572 | 0.007 | M. Baldwin | 0.003 |
| TZ Aur | 42861.618 | 58618 | 0.003 | M. Baldwin | 0.002 |
| TZ Aur | 43130.704 | 59305 | 0.009 | M. Baldwin | 0.005 |
| TZ Aur | 43219.614 | 59532 | 0.008 | M. Baldwin | 0.004 |
| TZ Aur | 43246.638 | 59601 | 0.007 | M. Baldwin | 0.004 |
| TZ Aur | 43505.534 | 60262 | 0.006 | M. Baldwin | 0.002 |
| TZ Aur | 43512.585 | 60280 | 0.007 | M. Baldwin | 0.002 |
| TZ Aur | 43519.634 | 60298 | 0.006 | M. Baldwin | 0.003 |
| TZ Aur | 43548.620 | 60372 | 0.008 | M. Baldwin | 0.004 |
| TZ Aur | 43550.583 | 60377 | 0.012 | M. Baldwin | 0.004 |
| TZ Aur | 43566.651 | 60418 | 0.022 | M. Baldwin | 0.007 |
| TZ Aur | 43606.584 | 60520 | 0.004 | M. Baldwin | 0.004 |
| TZ Aur | 43935.605 | 61360 | 0.018 | M. Baldwin | 0.008 |
| TZ Aur | 44340.588 | 62394 | 0.010 | M. Baldwin | 0.007 |
| TZ Aur | 44553.660 | 62938 | 0.011 | M. Baldwin | 0.002 |
| TZ Aur | 44629.650 | 63132 | 0.016 | G. Hanson | 0.001 |
| TZ Aur | 44696.619 | 63303 | 0.008 | M. Baldwin | 0.004 |
| TZ Aur | 44907.743 | 63842 | 0.020 | M. Baldwin | 0.007 |
| TZ Aur | 44979.794 | 64026 | 0.003 | L. Cook | 0.004 |
| TZ Aur | 44985.671 | 64041 | 0.005 | G. Chaple | 0.005 |
| TZ Aur | 45993.842 | 66615 | 0.005 | M. Baldwin | 0.002 |
| TZ Aur | 46024.785 | 66694 | 0.006 | M. Baldwin | 0.004 |
| TZ Aur | 46028.711 | 66704 | 0.015 | M. Baldwin | 0.006 |
| TZ Aur | 46057.687 | 66778 | 0.007 | M. Baldwin | 0.003 |
| TZ Aur | 46117.627 | 66931 | 0.021 | M. Baldwin | 0.013 |
| TZ Aur | 46437.609 | 67748 | 0.005 | G. Samolyk | 0.001 |
| TZ Aur | 46475.605 | 67845 | 0.008 | G. Chaple | 0.002 |
| TZ Aur | 46511.644 | 67937 | 0.013 | M. Baldwin | 0.004 |
| TZ Aur | 46518.703 | 67955 | 0.022 | M. Baldwin | 0.006 |
| TZ Aur | 46520.655 | 67960 | 0.016 | M. Baldwin | 0.003 |
| TZ Aur | 46527.697 | 67978 | 0.008 | M. Baldwin | 0.004 |
| TZ Aur | 46529.663 | 67983 | 0.015 | M. Baldwin | 0.004 |
| TZ Aur | 46531.624 | 67988 | 0.018 | M. Baldwin | 0.007 |
| TZ Aur | 46744.686 | 68532 | 0.009 | M. Baldwin | 0.009 |
| TZ Aur | 46829.682 | 68749 | 0.011 | M. Baldwin | 0.005 |
| TZ Aur | 46831.635 | 68754 | 0.006 | M. Baldwin | 0.004 |
| TZ Aur | 46833.590 | 68759 | 0.003 | M. Baldwin | 0.005 |
| TZ Aur | 46916.639 | 68971 | 0.017 | M. Baldwin | 0.004 |
| TZ Aur | 47171.620 | 69622 | 0.018 | M. Baldwin | 0.006 |
| TZ Aur | 47227.622 | 69765 | 0.010 | M. Baldwin | 0.005 |
| TZ Aur | 47236.630 | 69788 | 0.010 | M. Baldwin | 0.002 |
| TZ Aur | 47425.799 | 70271 | 0.000 | M. Baldwin | 0.003 |
| TZ Aur | 47445.788 | 70322 | 0.013 | M. Baldwin | 0.006 |
| TZ Aur | 47543.710 | 70572 | 0.017 | R. Hill | 0.004 |
| TZ Aur | 47558.593 | 70610 | 0.016 | M. Baldwin | 0.003 |
| TZ Aur | 47914.624 | 71519 | 0.015 | M. Baldwin | 0.008 |
| TZ Aur | 47915.796 | 71522 | 0.012 | M. Baldwin | 0.003 |
| TZ Aur | 47921.671 | 71537 | 0.012 | M. Baldwin | 0.003 |
| TZ Aur | 47923.633 | 71542 | 0.015 | M. Baldwin | 0.002 |
| TZ Aur | 47943.613 | 71593 | 0.020 | M. Baldwin | 0.003 |
| TZ Aur | 47948.697 | 71606 | 0.012 | M. Baldwin | 0.003 |
| TZ Aur | 48362.697 | 72663 | 0.012 | M. Baldwin | 0.003 |
| TZ Aur | 48648.619 | 73393 | 0.012 | M. Baldwin | 0.004 |
| TZ Aur | 48655.667 | 73411 | 0.009 | M. Baldwin | 0.003 |
| TZ Aur | 49416.700 | 75354 | 0.019 | M. Baldwin | 0.003 |
| TZ Aur | 49720.631 | 76130 | 0.010 | M. Baldwin | 0.002 |
| TZ Aur | 49832.651 | 76416 | 0.011 | M. Baldwin | 0.005 |
| TZ Aur | 50130.721 | 77177 | 0.017 | R. Hill | 0.009 |
| TZ Aur | 50190.642 | 77330 | 0.012 | M. Baldwin | 0.004 |
| TZ Aur | 50546.676 | 78239 | 0.013 | M. Baldwin | 0.003 |
| TZ Aur | 50575.656 | 78313 | 0.009 | M. Baldwin | 0.002 |
| TZ Aur | 50902.703 | 79148 | 0.008 | M. Baldwin | 0.003 |
| TZ Aur | 51157.684 | 79799 | 0.009 | M. Baldwin | 0.002 |
| TZ Aur | 51161.605 | 79809 | 0.013 | M. Baldwin | 0.002 |
| TZ Aur | 51253.654 | 80044 | 0.019 | R. Berg | 0.005 |
| TZ Aur | 51262.661 | 80067 | 0.017 | R. Berg | 0.003 |
| TZ Aur | 51489.822 | 80647 | 0.007 | R. Berg | 0.003 |
| TZ Aur | 51609.678 | 80953 | 0.010 | R. Berg | 0.007 |
| TZ Aur | 51627.693 | 80999 | 0.008 | R. Berg | 0.001 |
| TZ Aur | 51989.608 | 81923 | 0.016 | G. Samolyk | 0.003 |
| BH Aur | 39152.620 | -7891 | -0.017 | M. Baldwin | 0.005 |
| BH Aur | 39168.590 | -7856 | -0.011 | M. Baldwin | 0.006 |
| BH Aur | 39173.626 | -7845 | 0.008 | M. Baldwin | 0.014 |
| BH Aur | 39178.623 | -7834 | -0.012 | M. Baldwin | 0.007 |
| BH Aur | 39443.635 | -7253 | 0.012 | M. Baldwin | 0.006 |
| BH Aur | 39473.721 | -7187 | -0.004 | M. Baldwin | 0.006 |
| BH Aur | 39474.632 | -7185 | -0.005 | M. Baldwin | 0.006 |
| BH Aur | 39495.613 | -7139 | -0.004 | M. Baldwin | 0.004 |
| BH Aur | 39500.635 | -7128 | 0.001 | M. Baldwin | 0.005 |
| BH Aur | 39505.661 | -7117 | 0.010 | M. Baldwin | 0.006 |
| BH Aur | 39506.553 | -7115 | -0.010 | M. Baldwin | 0.004 |
| BH Aur | 39530.742 | -7062 | 0.006 | M. Baldwin | 0.004 |
| BH Aur | 39537.573 | -7047 | -0.004 | M. Baldwin | 0.004 |
| BH Aur | 39556.715 | -7005 | -0.018 | M. Baldwin | 0.005 |
| BH Aur | 39567.689 | -6981 | 0.010 | M. Baldwin | 0.003 |
| BH Aur | 39884.660 | -6286 | -0.002 | M. Baldwin | 0.005 |
| BH Aur | 39894.701 | -6264 | 0.006 | M. Baldwin | 0.007 |
| BH Aur | 39920.686 | -6207 | -0.007 | M. Baldwin | 0.006 |
| BH Aur | 40184.761 | -5628 | -0.008 | M. Baldwin | 0.005 |
| BH Aur | 40186.599 | -5624 | 0.006 | M. Baldwin | 0.005 |
| BH Aur | 40211.679 | -5569 | 0.001 | M. Baldwin | 0.006 |
| BH Aur | 40293.776 | -5389 | 0.002 | M. Baldwin | 0.009 |
| BH Aur | 40294.684 | -5387 | -0.002 | M. Baldwin | 0.007 |
| BH Aur | 40565.606 | -4793 | 0.002 | L. Hazel | 0.007 |
| BH Aur | 41374.714 | -3019 | 0.007 | T. Cragg | 0.008 |
| BH Aur | 41683.484 | -2342 | 0.004 | M. Baldwin | 0.006 |
| BH Aur | 41705.364 | -2294 | -0.008 | M. Baldwin | 0.010 |
| BH Aur | 41751.434 | -2193 | -0.003 | M. Baldwin | 0.005 |
| BH Aur | 41752.349 | -2191 | 0.000 | M. Baldwin | 0.008 |
| BH Aur | 41982.675 | -1686 | 0.000 | M. Baldwin | 0.008 |
| BH Aur | 42003.655 | -1640 | 0.000 | M. Baldwin | 0.003 |
| BH Aur | 42387.685 | -798 | 0.003 | M. Baldwin | 0.007 |
| BH Aur | 42429.630 | -706 | -0.013 | M. Baldwin | 0.009 |
| BH Aur | 42506.712 | -537 | -0.010 | T. Cragg | 0.003 |

*Table continued on next page*

Table 1. Recent times of minima of stars in the AAVSO short period pulsator program, cont.

| *Star* | *JD (max) Hel. 2400000 +* | *Cycle* | *O–C (day)* | *Observer* | *Error (day)* |
|---|---|---|---|---|---|
| BH Aur | 42660.886 | -199 | 0.006 | M. Baldwin | 0.007 |
| BH Aur | 42665.878 | -188 | -0.019 | M. Baldwin | 0.007 |
| BH Aur | 42751.648 | 0 | 0.006 | M. Baldwin | 0.007 |
| BH Aur | 42845.597 | 206 | 0.001 | M. Baldwin | 0.004 |
| BH Aur | 42871.599 | 263 | 0.005 | M. Baldwin | 0.004 |
| BH Aur | 43055.842 | 667 | -0.012 | M. Baldwin | 0.005 |
| BH Aur | 43130.652 | 831 | -0.001 | M. Baldwin | 0.005 |
| BH Aur | 43131.573 | 833 | 0.008 | M. Baldwin | 0.007 |
| BH Aur | 43136.584 | 844 | 0.002 | M. Baldwin | 0.007 |
| BH Aur | 43219.595 | 1026 | 0.005 | M. Baldwin | 0.009 |
| BH Aur | 43489.607 | 1618 | 0.012 | M. Baldwin | 0.005 |
| BH Aur | 43493.690 | 1627 | -0.010 | M. Baldwin | 0.004 |
| BH Aur | 43494.614 | 1629 | 0.002 | M. Baldwin | 0.008 |
| BH Aur | 43505.558 | 1653 | 0.000 | M. Baldwin | 0.006 |
| BH Aur | 43520.594 | 1686 | -0.015 | M. Baldwin | 0.005 |
| BH Aur | 44216.602 | 3212 | 0.000 | M. Heifner | 0.006 |
| BH Aur | 44221.606 | 3223 | -0.013 | M. Baldwin | 0.005 |
| BH Aur | 44226.627 | 3234 | -0.009 | M. Baldwin | 0.008 |
| BH Aur | 44227.542 | 3236 | -0.007 | M. Baldwin | 0.009 |
| BH Aur | 44319.665 | 3438 | -0.014 | M. Heifner | 0.003 |
| BH Aur | 44598.809 | 4050 | 0.003 | G. Hanson | 0.004 |
| BH Aur | 44614.758 | 4085 | -0.011 | G. Samolyk | 0.004 |
| BH Aur | 44616.589 | 4089 | -0.004 | G. Hanson | 0.003 |
| BH Aur | 44938.596 | 4795 | 0.003 | M. Baldwin | 0.007 |
| BH Aur | 44957.746 | 4837 | -0.002 | G. Samolyk | 0.003 |
| BH Aur | 44994.685 | 4918 | -0.007 | G. Chaple | 0.005 |
| BH Aur | 44995.608 | 4920 | 0.004 | G. Samolyk | 0.004 |
| BH Aur | 45348.615 | 5694 | -0.002 | G. Chaple | 0.004 |
| BH Aur | 46028.656 | 7185 | 0.009 | M. Baldwin | 0.007 |
| BH Aur | 46033.649 | 7196 | -0.015 | M. Baldwin | 0.006 |
| BH Aur | 46038.678 | 7207 | -0.003 | M. Baldwin | 0.006 |
| BH Aur | 46058.743 | 7251 | -0.006 | M. Baldwin | 0.004 |
| BH Aur | 46112.573 | 7369 | 0.005 | M. Baldwin | 0.006 |
| BH Aur | 46117.588 | 7380 | 0.003 | M. Baldwin | 0.006 |
| BH Aur | 46475.607 | 8165 | -0.008 | G. Chaple | 0.003 |
| BH Aur | 46490.653 | 8198 | -0.013 | M. Heifner | 0.001 |
| BH Aur | 46490.673 | 8198 | 0.007 | M. Baldwin | 0.005 |
| BH Aur | 46511.642 | 8244 | -0.004 | M. Baldwin | 0.003 |
| BH Aur | 46521.673 | 8266 | -0.007 | M. Baldwin | 0.003 |
| BH Aur | 46532.623 | 8290 | -0.003 | M. Baldwin | 0.005 |
| BH Aur | 46734.681 | 8733 | 0.007 | M. Baldwin | 0.007 |
| BH Aur | 46744.694 | 8755 | -0.014 | M. Baldwin | 0.004 |
| BH Aur | 46787.581 | 8849 | 0.000 | M. Baldwin | 0.007 |
| BH Aur | 46790.775 | 8856 | 0.002 | R. Hill | 0.007 |
| BH Aur | 46875.612 | 9042 | 0.006 | G. Samolyk | 0.005 |
| BH Aur | 46911.635 | 9121 | -0.002 | M. Baldwin | 0.002 |
| BH Aur | 47114.599 | 9566 | 0.002 | M. Baldwin | 0.006 |
| BH Aur | 47140.596 | 9623 | 0.002 | M. Baldwin | 0.007 |
| BH Aur | 47151.550 | 9647 | 0.010 | M. Baldwin | 0.007 |
| BH Aur | 47835.659 | 11147 | -0.016 | M. Baldwin | 0.007 |
| BH Aur | 47940.583 | 11377 | 0.007 | M. Baldwin | 0.003 |
| BH Aur | 47950.607 | 11399 | -0.003 | G. Samolyk | 0.002 |
| BH Aur | 48236.561 | 12026 | -0.017 | M. Baldwin | 0.002 |
| BH Aur | 48328.693 | 12228 | -0.015 | R. Hill | 0.004 |
| BH Aur | 48682.633 | 13004 | -0.001 | M. Baldwin | 0.004 |
| BH Aur | 49010.550 | 13723 | -0.012 | M. Baldwin | 0.007 |
| BH Aur | 49397.782 | 14572 | -0.001 | M. Baldwin | 0.003 |
| BH Aur | 50490.566 | 16968 | -0.008 | G. Chaple | 0.006 |
| BH Aur | 50541.654 | 17080 | -0.002 | M. Baldwin | 0.002 |
| BH Aur | 51149.625 | 18413 | 0.002 | R. Berg | 0.007 |
| BH Aur | 51212.558 | 18551 | -0.006 | R. Berg | 0.004 |
| BH Aur | 51438.787 | 19047 | 0.003 | M. Baldwin | 0.006 |
| BH Aur | 51491.683 | 19163 | -0.008 | R. Berg | 0.005 |
| BH Aur | 51512.670 | 19209 | -0.001 | M. Baldwin | 0.004 |
| BH Aur | 51513.593 | 19211 | 0.010 | M. Baldwin | 0.003 |
| BH Aur | 51621.674 | 19448 | -0.002 | R. Berg | 0.005 |
| BH Aur | 51627.605 | 19461 | -0.001 | R. Berg | 0.005 |
| BH Aur | 52354.603 | 21055 | -0.010 | R. Berg | 0.007 |

# Recent Minima of 298 Eclipsing Binary Stars

**Gerard Samolyk**
*P.O. Box 20677, Greenfield, WI 53220; gsamolyk@wi.rr.com*

*Received February 17, 2017; accepted February 17, 2017*

**Abstract** This paper continues the publication of times of minima for eclipsing binary stars from observations reported to the AAVSO EB section. Times of minima from observations received from August 2016 thru January 2017 are presented.

## 1. Recent observations

The accompanying list contains times of minima calculated from recent CCD observations made by participants in the AAVSO's eclipsing binary program. This list will be web-archived and made available through the AAVSO ftp site at ftp://ftp.aavso.org/public/datasets/gsamoj451eb.txt. This list, along with the eclipsing binary data from earlier AAVSO publications, is also included in the Lichtenknecker database administrated by the Bundesdeutsche Arbeitsgemeinschaft für Veränderliche Sterne e. V. (BAV) at: http://www.bav-astro.eu/index.php/veroeffentlichungen/service-for-scientists/lkdb-engl. These observations were reduced by the observers or the writer using the method of Kwee and Van Woerden (1956). The standard error is included when available. Column F indicates the filter used. A "C" indicates a clear filter.

The linear elements in the *General Catalogue of Variable Stars* (GCVS; Kholopov *et al.* 1985) were used to compute the O–C values for most stars. For a few exceptions where the GCVS elements are missing or are in significant error, light elements from another source are used: CD Cam (Baldwin and Samolyk 2007), AC CMi (Samolyk 2008), CW Cas (Samolyk 1992a), DV Cep (Frank and Lichtenknecker 1987), DF Hya (Samolyk 1992b), and GU Ori (Samolyk 1985) .

The light elements used for QX And, V404 And, V463 And, EF Aqr, FS Aqr, IU Cnc, AP CMi, CZ CMi, LS Del, BC Her, V728 Her, V899 Her, V1033 Her, V1034 Her, WZ Leo, V423 Oph, V1363 Ori, V351 Peg, AQ Psc, CP Psc, DS Psc, DV Psc, DZ Psc, GR Psc, V1121 Tau, V1128 Tau, V1223 Tau, HT Vir, and MS Vir are from Kreiner (2004).

The light elements used for DD Aqr, GK Aqr, V1542 Aql, XY Boo, DN Boo, GH Boo, GM Boo, GP Boo, IK Boo, CW CMi, CX CMi, V2477 Cyg, V2643 Cyg, MZ Del, KK Gem, V1092 Her, V1097 Her, V470 Hya, V474 Hya, XX Leo, CE Leo, GV Leo, HI Leo, V1853 Ori, V2790 Ori, V740 Per, VZ Psc, ET Psc, V1332 Tau, GR Vir, IR Vir, and NN Vir are from Paschke (2014).

The light elements used for MW And, V459 Aur, V348 Cyg, V382 Cyg, V2247 Cyg, V337 Gem, V390 Hya, V613 Peg, BB Per, V881 Per, HO Psc, and V495 Vul are from Nelson (2016).

The light elements used for V1470 Aql, V380 Gem, V383 Gem, V388 Gem, EU Hya, V534 Peg, V737 Per, V996 Per, and V391 Vir are from the AAVSO VSX site (Watson *et al.* 2014). O–C values listed in this paper can be directly compared with values published in the AAVSO EB monographs.

## References

Baldwin, M. E., and Samolyk, G. 2007, *Observed Minima Timings of Eclipsing Binaries No. 12*, AAVSO, Cambridge, MA.

Frank, P., and Lichtenknecker, D. 1987, *BAV Mitt.*, No. 47, 1.

Kholopov, P. N., *et al.* 1985, *General Catalogue of Variable Stars*, 4th ed., Moscow.

Kreiner, J. M. 2004, "Up-to-date linear elements of eclipsing binaries," *Acta Astron.*, **54**, 207 (http://www.as.up.krakow.pl/ephem/).

Kwee, K. K., and van Woerden, H. 1956, *Bull. Astron. Inst. Netherlands*, **12**, 327.

Nelson, R. 2016, Eclipsing Binary O–C Files (https://www.aavso.org/bob-nelsons-o-c-files).

Paschke, A. 2014, "O–C Gateway" ( http://var.astro.cz/ocgate/).

Samolyk, G. 1985, *J. Amer. Assoc. Var. Star Obs.*, **14**, 12.

Samolyk, G. 1992a, *J. Amer. Assoc. Var. Star Obs.*, **21**, 34.

Samolyk, G. 1992b, *J. Amer. Assoc. Var. Star Obs.*, **21**, 111.

Samolyk, G. 2008, *J. Amer. Assoc. Var. Star Obs.*, **36**, 171.

Watson, C., Henden, A. A., and Price, C. A. 2014, AAVSO International Variable Star Index VSX (Watson+, 2006–2016; https://www.aavso.org/vsx).

Table 1. Recent times of minima of stars in the AAVSO eclipsing binary program.

| *Star* | *JD (min) Hel. 2400000 +* | *Cycle* | *O–C (day)* | *F* | *Observer* | *Error (day)* |
|---|---|---|---|---|---|---|
| RT And | 57607.8799 | 26181 | –0.0127 | V | G. Samolyk | 0.0001 |
| RT And | 57684.6107 | 26303 | –0.0113 | V | G. Samolyk | 0.0001 |
| TW And | 57634.6771 | 4515 | –0.0579 | V | G. Samolyk | 0.0003 |
| UU And | 57608.7866 | 10737 | 0.0864 | V | G. Samolyk | 0.0001 |
| UU And | 57684.5883 | 10788 | 0.0871 | V | G. Samolyk | 0.0001 |
| WZ And | 57623.7991 | 24080 | 0.0741 | V | G. Samolyk | 0.0001 |
| WZ And | 57630.7561 | 24090 | 0.0745 | V | K. Menzies | 0.0001 |
| WZ And | 57676.6706 | 24156 | 0.0756 | V | G. Samolyk | 0.0001 |
| XZ And | 57633.7960 | 24797 | 0.1819 | V | G. Samolyk | 0.0001 |
| XZ And | 57754.5949 | 24886 | 0.1831 | V | G. Samolyk | 0.0001 |
| AB And | 57603.8708 | 64763 | –0.0398 | V | R. Sabo | 0.0001 |
| AB And | 57609.8443 | 64781 | –0.0403 | V | K. Menzies | 0.0001 |

*Table continued on following pages*

Table 1. Recent times of minima of stars in the AAVSO eclipsing binary program, cont.

| *Star* | *JD (min) Hel. 2400000 +* | *Cycle* | *O–C (day)* | *F* | *Observer* | *Error (day)* |
|---|---|---|---|---|---|---|
| AB And | 57646.6842 | 64892 | –0.0405 | V | G. Samolyk | 0.0003 |
| AB And | 57690.3268 | 65023.5 | –0.0417 | V | L. Corp | 0.0001 |
| AB And | 57690.4935 | 65024 | –0.0409 | V | L. Corp | 0.0001 |
| AB And | 57698.6245 | 65048.5 | –0.0413 | V | G. Samolyk | 0.0001 |
| AD And | 57623.7660 | 18882 | –0.0347 | V | K. Menzies | 0.0001 |
| AD And | 57649.9016 | 18908.5 | –0.0333 | V | G. Samolyk | 0.0001 |
| AD And | 57711.5364 | 18971 | –0.0357 | V | K. Menzies | 0.0001 |
| BD And | 57642.7817 | 48996 | 0.0206 | V | G. Samolyk | 0.0003 |
| BD And | 57699.7154 | 49119 | 0.0173 | V | G. Samolyk | 0.0001 |
| BX And | 57622.8179 | 34574 | –0.0876 | V | G. Samolyk | 0.0001 |
| BX And | 57649.6626 | 34618 | –0.0879 | V | N. Simmons | 0.0001 |
| CN And | 57699.5678 | 34837 | –0.1500 | V | G. Persha | 0.0002 |
| DS And | 57606.8394 | 21241 | 0.0043 | V | G. Samolyk | 0.0002 |
| DS And | 57680.6066 | 21314 | 0.0036 | V | G. Samolyk | 0.0001 |
| DS And | 57693.7430 | 21327 | 0.0033 | V | K. Menzies | 0.0001 |
| MW And | 57667.7432 | 12188.5 | –0.0075 | V | K. Menzies | 0.0002 |
| QX And | 57606.8365 | 12390 | 0.0014 | V | G. Samolyk | 0.0002 |
| QX And | 57627.8546 | 12441 | –0.0013 | V | K. Menzies | 0.0003 |
| QX And | 57680.6184 | 12569 | 0.0045 | V | G. Samolyk | 0.0002 |
| QX And | 57680.8213 | 12569.5 | 0.0013 | V | G. Samolyk | 0.0002 |
| QX And | 57711.5277 | 12644 | 0.0009 | V | K. Menzies | 0.0001 |
| V404 And | 57680.7620 | 7663 | 0.0007 | C | G. Frey | 0.0001 |
| V463 And | 57685.7127 | 12769 | –0.0025 | C | G. Frey | 0.0001 |
| RY Aqr | 57634.7256 | 8548 | –0.1339 | V | G. Samolyk | 0.0001 |
| SU Aqr | 57688.6788 | 21393 | –0.0206 | C | G. Frey | 0.0001 |
| CX Aqr | 57608.8452 | 38050 | 0.0153 | V | G. Samolyk | 0.0001 |
| CX Aqr | 57666.6675 | 38154 | 0.0150 | C | G. Frey | 0.0001 |
| CX Aqr | 57686.6835 | 38190 | 0.0155 | V | G. Samolyk | 0.0001 |
| CZ Aqr | 57606.8496 | 16500 | –0.0604 | V | G. Samolyk | 0.0001 |
| CZ Aqr | 57664.6536 | 16567 | –0.0609 | V | G. Samolyk | 0.0001 |
| DD Aqr | 57656.6598 | 13634 | 0.0026 | C | G. Frey | 0.0002 |
| EF Aqr | 57698.7061 | 1821 | 0.0014 | C | G. Frey | 0.0001 |
| EX Aqr | 57668.6978 | 5811 | 0.0162 | C | G. Frey | 0.0008 |
| FS Aqr | 57663.6904 | 19704 | –0.0009 | C | G. Frey | 0.0001 |
| GK Aqr | 57661.6977 | 33649 | 0.0154 | C | G. Frey | 0.0001 |
| XZ Aql | 57643.7342 | 7358 | 0.1794 | V | G. Samolyk | 0.0001 |
| KO Aql | 57622.6925 | 5494 | 0.1019 | V | G. Samolyk | 0.0001 |
| OO Aql | 57634.5794 | 37533 | 0.0652 | V | G. Samolyk | 0.0001 |
| OO Aql | 57637.6190 | 37539 | 0.0640 | V | N. Simmons | 0.0001 |
| OO Aql | 57647.7535 | 37559 | 0.0628 | V | S. Cook | 0.0004 |
| OO Aql | 57657.6375 | 37578.5 | 0.0644 | V | G. Samolyk | 0.0001 |
| V343 Aql | 57604.7087 | 15809 | –0.0371 | V | G. Samolyk | 0.0001 |
| V346 Aql | 57648.6397 | 14218 | –0.0134 | V | S. Cook | 0.0004 |
| V609 Aql | 57643.7130 | 35500 | –0.0695 | C | G. Frey | 0.0002 |
| V724 Aql | 57657.7126 | 5110 | –0.0146 | C | G. Frey | 0.0001 |
| V1470 Aql | 57632.3620 | 10937 | –0.1050 | V | L. Corp | 0.0005 |
| V1542 Aql | 57630.7437 | 13217 | 0.0161 | C | G. Frey | 0.0001 |
| RX Ari | 57753.5447 | 18798 | 0.0654 | V | G. Silvis | 0.0001 |
| RX Ari | 57754.5725 | 18799 | 0.0636 | V | G. Samolyk | 0.0002 |
| SS Ari | 57643.8535 | 45852.5 | –0.3630 | V | G. Samolyk | 0.0001 |
| SS Ari | 57755.4970 | 46127.5 | –0.3678 | V | G. Silvis | 0.0001 |
| SX Aur | 57698.8370 | 14492 | 0.0192 | V | G. Samolyk | 0.0001 |
| WW Aur | 57719.7670 | 9811.5 | 0.0016 | V | G. Samolyk | 0.0001 |
| AP Aur | 57680.8776 | 26761.5 | 1.6121 | V | G. Samolyk | 0.0002 |
| AP Aur | 57702.7957 | 26800 | 1.6117 | V | G. Samolyk | 0.0001 |
| AP Aur | 57733.8279 | 26854.5 | 1.6164 | V | K. Menzies | 0.0001 |
| AR Aur | 57702.8133 | 4668 | –0.1262 | V | G. Samolyk | 0.0001 |
| CL Aur | 57696.6955 | 19873 | 0.1778 | V | G. Samolyk | 0.0001 |
| EM Aur | 57677.8640 | 14647 | –1.1094 | V | K. Menzies | 0.0003 |
| EP Aur | 57642.8721 | 53017 | 0.0190 | V | G. Samolyk | 0.0001 |
| EP Aur | 57719.7027 | 53147 | 0.0185 | V | G. Samolyk | 0.0001 |
| EP Aur | 57754.5707 | 53206 | 0.0171 | V | G. Samolyk | 0.0001 |
| HP Aur | 57743.6184 | 10533.5 | 0.0681 | V | G. Samolyk | 0.0002 |
| IM Aur | 57696.9191 | 13775 | –0.1298 | V | G. Samolyk | 0.0002 |
| V459 Aur | 57719.7361 | 637.5 | –0.0005 | V | G. Samolyk | 0.0002 |
| TZ Boo | 57608.6805 | 60491.5 | 0.0636 | V | R. Sabo | 0.0004 |
| XY Boo | 57531.7259 | 47435 | 0.0106 | C | G. Frey | 0.0001 |
| DN Boo | 57512.7338 | 5838 | 0.0014 | C | G. Frey | 0.0002 |
| GH Boo | 57510.6921 | 9478 | –0.0070 | C | G. Frey | 0.0002 |
| GM Boo | 57524.7314 | 15295 | 0.0163 | C | G. Frey | 0.0002 |
| GP Boo | 57525.7179 | 7654 | –0.0081 | C | G. Frey | 0.0002 |
| IK Boo | 57521.6857 | 13655 | –0.0166 | C | G. Frey | 0.0001 |
| SV Cam | 57684.7449 | 25444 | 0.0579 | V | G. Samolyk | 0.0002 |
| CD Cam | 57684.7998 | 6441 | –0.0096 | V | G. Samolyk | 0.0004 |
| IU Cnc | 57769.8131 | 12498 | 0.0113 | V | K. Menzies | 0.0001 |
| R CMa | 57712.8909 | 11817 | 0.1210 | V | G. Samolyk | 0.0001 |
| UU CMa | 57696.8943 | 6046 | –0.0812 | V | G. Samolyk | 0.0001 |
| XZ CMi | 57669.9872 | 26305 | 0.0016 | V | G. Samolyk | 0.0001 |
| YY CMi | 57433.6938 | 26883 | 0.0152 | C | G. Frey | 0.0001 |
| AC CMi | 57432.6799 | 6289 | 0.0037 | C | G. Frey | 0.0001 |
| AC CMi | 57698.9155 | 6596 | 0.0038 | V | G. Samolyk | 0.0001 |
| AC CMi | 57745.7449 | 6650 | 0.0035 | V | G. Silvis | 0.0001 |
| AP CMi | 57417.6932 | 2273 | –0.0214 | C | G. Frey | 0.0001 |
| CW CMi | 57431.7048 | 16619.5 | –0.0249 | C | G. Frey | 0.0002 |
| CX CMi | 57445.6668 | 4897 | 0.0192 | C | G. Frey | 0.0001 |
| CZ CMi | 57423.7355 | 11547 | –0.0088 | C | G. Frey | 0.0001 |
| TY Cap | 57611.7084 | 9005 | 0.0910 | V | G. Samolyk | 0.0001 |
| RZ Cas | 57673.6293 | 12109 | 0.0771 | V | G. Samolyk | 0.0001 |
| RZ Cas | 57673.6315 | 12109 | 0.0793 | V | S. Cook | 0.0003 |
| TV Cas | 57676.6760 | 7213 | –0.0295 | V | G. Samolyk | 0.0001 |
| TW Cas | 57622.8332 | 10932 | 0.0079 | V | N. Simmons | 0.0001 |
| ZZ Cas | 57611.6796 | 19440 | 0.0197 | V | G. Samolyk | 0.0002 |
| AB Cas | 57640.8584 | 10920 | 0.1338 | V | G. Samolyk | 0.0002 |
| AB Cas | 57673.6637 | 10944 | 0.1341 | V | G. Samolyk | 0.0001 |
| AB Cas | 57736.5410 | 10990 | 0.1352 | V | G. Samolyk | 0.0001 |
| CW Cas | 57607.6551 | 50101.5 | –0.0996 | V | G. Samolyk | 0.0001 |
| CW Cas | 57642.7298 | 50211.5 | –0.1000 | V | G. Samolyk | 0.0001 |
| DZ Cas | 57604.8500 | 37165 | –0.2023 | V | G. Samolyk | 0.0002 |
| IR Cas | 57606.6543 | 22393 | 0.0121 | V | G. Samolyk | 0.0001 |
| IS Cas | 57610.7344 | 15658 | 0.0702 | V | G. Samolyk | 0.0001 |
| IS Cas | 57728.5912 | 15722 | 0.0702 | V | K. Menzies | 0.0001 |
| IT Cas | 57671.6601 | 7419 | 0.0688 | V | G. Samolyk | 0.0001 |
| IV Cas | 57623.6960 | 16794 | –0.1215 | V | N. Simmons | 0.0001 |
| IV Cas | 57649.6581 | 16820 | –0.1210 | V | G. Samolyk | 0.0001 |
| IV Cas | 57684.6057 | 16855 | –0.1217 | V | G. Samolyk | 0.0001 |
| IV Cas | 57702.5796 | 16873 | –0.1213 | V | G. Samolyk | 0.0001 |
| MM Cas | 57604.8310 | 19166 | 0.1120 | V | G. Samolyk | 0.0003 |
| MM Cas | 57676.6588 | 19228 | 0.1146 | V | G. Samolyk | 0.0001 |
| OR Cas | 57646.6041 | 10786 | –0.0302 | V | G. Samolyk | 0.0003 |
| OX Cas | 57635.8405 | 6574.5 | 0.0214 | V | G. Samolyk | 0.0002 |
| PV Cas | 57600.7830 | 9925 | –0.0348 | V | S. Cook | 0.0002 |
| PV Cas | 57686.5559 | 9974 | –0.0349 | V | G. Samolyk | 0.0001 |
| V364 Cas | 57633.6008 | 15100 | –0.0240 | V | G. Samolyk | 0.0001 |
| V364 Cas | 57697.6376 | 15141.5 | –0.0245 | V | K. Menzies | 0.0001 |
| V375 Cas | 57606.6633 | 15586 | 0.2404 | V | N. Simmons | 0.0001 |
| V375 Cas | 57634.6586 | 15605 | 0.2414 | V | G. Samolyk | 0.0001 |
| V380 Cas | 57686.5768 | 23607 | –0.0719 | V | G. Samolyk | 0.0002 |
| V523 Cas | 57573.8554 | 69979 | 0.1117 | V | B. Harris | 0.0001 |
| U Cep | 57622.8289 | 5247 | 0.2056 | V | G. Samolyk | 0.0001 |
| U Cep | 57647.7644 | 5257 | 0.2106 | V | S. Cook | 0.0007 |
| U Cep | 57702.6056 | 5279 | 0.2047 | V | G. Samolyk | 0.0001 |
| SU Cep | 57635.6374 | 34735 | 0.0052 | V | G. Samolyk | 0.0002 |
| WW Cep | 57635.7111 | 21261 | 0.3465 | V | G. Samolyk | 0.0001 |
| WZ Cep | 57642.6077 | 70912.5 | –0.1658 | V | G. Samolyk | 0.0001 |
| XX Cep | 57608.6315 | 5463 | 0.0141 | V | G. Samolyk | 0.0001 |
| XX Cep | 57622.6564 | 5469 | 0.0150 | V | N. Simmons | 0.0001 |
| DL Cep | 57601.6895 | 14508 | 0.0632 | V | G. Samolyk | 0.0002 |
| DL Cep | 57650.6030 | 14538 | 0.0622 | V | G. Samolyk | 0.0002 |
| DV Cep | 57633.6217 | 9355 | –0.0056 | V | G. Samolyk | 0.0001 |
| EG Cep | 57616.6986 | 27583 | 0.0122 | V | S. Cook | 0.0004 |

*Table continued on following pages*

Table 1. Recent times of minima of stars in the AAVSO eclipsing binary program, cont.

| *Star* | *JD (min) Hel. 2400000 +* | *Cycle* | *O–C (day)* | *F* | *Observer* | *Error (day)* |
|---|---|---|---|---|---|---|
| EK Cep | 57581.7515 | 4196 | 0.0098 | V | S. Cook | 0.0007 |
| SS Cet | 57719.7862 | 5134 | 0.0644 | V | G. Samolyk | 0.0001 |
| TT Cet | 57684.7692 | 51731 | –0.0765 | V | G. Samolyk | 0.0001 |
| TT Cet | 57687.6844 | 51737 | –0.0770 | C | G. Frey | 0.0002 |
| TW Cet | 57640.8540 | 48185 | –0.0328 | V | G. Samolyk | 0.0003 |
| TW Cet | 57697.7305 | 48364.5 | –0.0312 | V | G. Samolyk | 0.0002 |
| TW Cet | 57768.5457 | 48588 | –0.0324 | V | G. Samolyk | 0.0002 |
| TX Cet | 57643.8625 | 19655 | 0.0131 | V | G. Samolyk | 0.0001 |
| TX Cet | 57675.7177 | 19698 | 0.0122 | C | G. Frey | 0.0001 |
| VV Cet | 57706.7024 | 50495 | 0.1364 | C | G. Frey | 0.0002 |
| RW Com | 57769.9632 | 74775 | 0.0072 | V | K. Menzies | 0.0001 |
| RZ Com | 57748.9158 | 67684 | 0.0532 | V | K. Menzies | 0.0001 |
| SS Com | 57748.9577 | 79327 | 0.9046 | V | K. Menzies | 0.0003 |
| SS Com | 57767.9471 | 79373 | 0.9056 | V | K. Menzies | 0.0001 |
| CC Com | 57728.9196 | 82449 | –0.0265 | V | K. Menzies | 0.0001 |
| U CrB | 57580.7408 | 11828 | 0.1317 | V | S. Cook | 0.0005 |
| RW CrB | 57606.6567 | 23203 | 0.0028 | V | G. Samolyk | 0.0001 |
| SW Cyg | 57635.6256 | 3448 | –0.3581 | V | G. Samolyk | 0.0002 |
| WW Cyg | 57623.7880 | 5198 | 0.1387 | V | G. Samolyk | 0.0001 |
| ZZ Cyg | 57602.7903 | 20048 | –0.0691 | V | G. Samolyk | 0.0001 |
| AE Cyg | 57623.7301 | 13452 | –0.0048 | V | K. Menzies | 0.0001 |
| AE Cyg | 57693.5122 | 13524 | –0.0042 | V | K. Menzies | 0.0001 |
| CG Cyg | 57583.7539 | 28771 | 0.0741 | V | S. Cook | 0.0002 |
| CG Cyg | 57607.7380 | 28809 | 0.0748 | V | K. Menzies | 0.0001 |
| DK Cyg | 57649.6155 | 41747 | 0.1133 | V | G. Samolyk | 0.0001 |
| DK Cyg | 57715.5138 | 41887 | 0.1149 | V | G. Silvis | 0.0001 |
| DK Cyg | 57715.5140 | 41887 | 0.1151 | I | G. Silvis | 0.0002 |
| DK Cyg | 57715.5141 | 41887 | 0.1152 | B | G. Silvis | 0.0001 |
| DO Cyg | 57575.7546 | 7654 | –0.0321 | V | B. Harris | 0.0001 |
| GO Cyg | 57634.6225 | 33025 | 0.0668 | B | G. Persha | 0.0001 |
| GO Cyg | 57634.6225 | 33025 | 0.0668 | V | G. Persha | 0.0001 |
| KV Cyg | 57642.6235 | 9924 | 0.0620 | V | G. Samolyk | 0.0002 |
| MY Cyg | 57710.5141 | 5958 | 0.0012 | V | K. Menzies | 0.0002 |
| V346 Cyg | 57649.6547 | 8006 | 0.1890 | V | G. Samolyk | 0.0002 |
| V348 Cyg | 57607.8391 | 7811.5 | 0.0743 | V | K. Menzies | 0.0001 |
| V348 Cyg | 57668.6668 | 8025.5 | 0.0762 | V | K. Menzies | 0.0001 |
| V382 Cyg | 57636.6227 | 410 | –0.0118 | V | G. Persha | 0.0002 |
| V382 Cyg | 57636.6228 | 410 | –0.0118 | B | G. Persha | 0.0003 |
| V387 Cyg | 57624.5966 | 46268 | 0.0214 | V | K. Menzies | 0.0002 |
| V387 Cyg | 57699.5458 | 46385 | 0.0208 | V | G. Samolyk | 0.0002 |
| V388 Cyg | 57611.7523 | 18228 | –0.1151 | V | G. Samolyk | 0.0001 |
| V388 Cyg | 57673.5988 | 18300 | –0.1193 | V | G. Samolyk | 0.0001 |
| V401 Cyg | 57675.5724 | 23751 | 0.0832 | V | G. Samolyk | 0.0001 |
| V456 Cyg | 57637.6282 | 14280 | 0.0506 | V | G. Samolyk | 0.0001 |
| V466 Cyg | 57609.7370 | 20721.5 | 0.0071 | V | K. Menzies | 0.0001 |
| V477 Cyg | 57604.6265 | 5716 | –0.0357 | V | G. Samolyk | 0.0002 |
| V704 Cyg | 57623.5975 | 34491 | 0.0368 | V | G. Samolyk | 0.0002 |
| V1034 Cyg | 57621.7429 | 15030 | 0.0110 | V | R. Sabo | 0.0001 |
| V1073 Cyg | 57638.3537 | 24134 | –0.1659 | V | G. Persha | 0.0005 |
| V2247 Cyg | 57680.5592 | 640 | –0.0116 | V | K. Menzies | 0.0001 |
| V2477 Cyg | 57621.6623 | 19691 | 0.0035 | V | K. Menzies | 0.0001 |
| V2643 Cyg | 57666.5592 | 10354 | –0.0078 | V | K. Menzies | 0.0002 |
| W Del | 57650.7615 | 2980 | 0.0340 | V | G. Samolyk | 0.0002 |
| TT Del | 57606.8296 | 4310 | –0.1123 | V | G. Samolyk | 0.0002 |
| TY Del | 57649.6824 | 12333 | 0.0695 | V | S. Cook | 0.0002 |
| YY Del | 57631.7268 | 18500 | 0.0091 | C | G. Frey | 0.0001 |
| YY Del | 57643.6244 | 18515 | 0.0103 | V | G. Samolyk | 0.0001 |
| YY Del | 57697.5546 | 18583 | 0.0102 | V | G. Samolyk | 0.0001 |
| FZ Del | 57634.7674 | 33593 | –0.0225 | V | S. Cook | 0.0006 |
| FZ Del | 57642.5971 | 33603 | –0.0249 | V | G. Samolyk | 0.0001 |
| FZ Del | 57671.5769 | 33640 | –0.0240 | V | N. Simmons | 0.0001 |
| LS Del | 57613.4178 | 14053 | –0.0038 | V | L. Corp | 0.0002 |
| LS Del | 57636.7060 | 14117 | –0.0016 | C | G. Frey | 0.0004 |
| MZ Del | 57627.4107 | 12450 | –0.0242 | V | L. Corp | 0.0002 |
| MZ Del | 57634.3831 | 12459.5 | –0.0164 | V | L. Corp | 0.0006 |
| TW Dra | 57586.6840 | 4792 | –0.0218 | V | S. Cook | 0.0009 |
| UZ Dra | 57576.7549 | 4908 | –0.0003 | V | S. Cook | 0.0004 |
| UZ Dra | 57607.7415 | 4917.5 | 0.0039 | V | G. Samolyk | 0.0001 |
| AI Dra | 57582.7287 | 11921 | 0.0329 | V | S. Cook | 0.0008 |
| BH Dra | 57610.6642 | 9680 | –0.0034 | V | G. Samolyk | 0.0002 |
| S Equ | 57629.7350 | 4375 | 0.0676 | V | S. Cook | 0.0004 |
| TZ Eri | 57701.7763 | 5866 | 0.3343 | V | G. Samolyk | 0.0001 |
| TZ Eri | 57761.7170 | 5889 | 0.3354 | V | G. Samolyk | 0.0001 |
| YY Eri | 57684.9425 | 50088.5 | 0.1588 | V | G. Samolyk | 0.0001 |
| YY Eri | 57760.6547 | 50324 | 0.1591 | V | G. Samolyk | 0.0001 |
| RW Gem | 57754.8235 | 13768 | 0.0031 | V | G. Samolyk | 0.0001 |
| SX Gem | 57728.8668 | 28311 | –0.0579 | V | K. Menzies | 0.0001 |
| SX Gem | 57750.7374 | 28327 | –0.0574 | V | G. Samolyk | 0.0002 |
| TX Gem | 57698.9625 | 13518 | –0.0388 | V | R. Sabo | 0.0001 |
| WW Gem | 57701.9589 | 25624 | 0.0328 | V | G. Samolyk | 0.0001 |
| AF Gem | 57698.9572 | 24557 | –0.0673 | V | G. Samolyk | 0.0001 |
| EG Gem | 57446.6574 | 23639 | 0.3089 | C | G. Frey | 0.0001 |
| KK Gem | 57437.6822 | 7574 | 0.0100 | V | K. Menzies | 0.0003 |
| V337 Gem | 57424.7116 | 1766.5 | 0.1082 | C | G. Frey | 0.0002 |
| V380 Gem | 57711.7790 | 18116 | 0.0220 | V | K. Menzies | 0.0001 |
| V383 Gem | 57769.7523 | 5842 | –0.0047 | V | K. Menzies | 0.0001 |
| V388 Gem | 57399.7296 | 9656 | 0.0064 | C | G. Frey | 0.0001 |
| RX Her | 57634.6609 | 13755 | –0.0005 | V | S. Cook | 0.0007 |
| TT Her | 57539.7260 | 19235 | 0.0465 | V | G. Persha | 0.0002 |
| TT Her | 57539.7278 | 19235 | 0.0483 | B | G. Persha | 0.0004 |
| TT Her | 57612.6906 | 19315 | 0.0451 | V | S. Cook | 0.0005 |
| TT Her | 57615.4284 | 19318 | 0.0467 | V | L. Corp | 0.0003 |
| UX Her | 57609.7114 | 11581 | 0.1253 | V | S. Cook | 0.0003 |
| BC Her | 57646.7517 | 1667 | 0.0126 | C | G. Frey | 0.0002 |
| CC Her | 57575.7113 | 10327 | 0.2914 | V | S. Cook | 0.0008 |
| V728 Her | 57607.6309 | 10837 | 0.0131 | V | K. Menzies | 0.0002 |
| V899 Her | 57544.7532 | 11977 | –0.0004 | C | G. Frey | 0.0003 |
| V1033 Her | 57564.6960 | 16992 | –0.0049 | C | G. Frey | 0.0001 |
| V1034 Her | 57562.7508 | 6209 | –0.0034 | C | G. Frey | 0.0001 |
| V1092 Her | 57547.7223 | 13337 | –0.0127 | C | G. Frey | 0.0002 |
| V1097 Her | 57551.7259 | 14101 | 0.0013 | C | G. Frey | 0.0001 |
| WY Hya | 57725.8128 | 23959 | 0.0376 | V | B. Harris | 0.0001 |
| DF Hya | 57754.9414 | 45272 | 0.0053 | V | G. Samolyk | 0.0001 |
| EU Hya | 57450.7670 | 29972 | –0.0332 | C | G. Frey | 0.0002 |
| V390 Hya | 57434.6403 | 3060 | –0.0777 | C | G. Frey | 0.0001 |
| V470 Hya | 57448.7317 | 12006 | 0.0074 | C | G. Frey | 0.0003 |
| V474 Hya | 57435.6820 | 9939 | –0.0114 | C | G. Frey | 0.0001 |
| SW Lac | 57610.6711 | 38461.5 | –0.0835 | V | G. Samolyk | 0.0001 |
| SW Lac | 57610.8321 | 38462 | –0.0829 | V | G. Samolyk | 0.0001 |
| SW Lac | 57615.4817 | 38476.5 | –0.0837 | V | L. Corp | 0.0002 |
| SW Lac | 57637.6108 | 38545.5 | –0.0844 | V | G. Samolyk | 0.0002 |
| SW Lac | 57640.6621 | 38555 | –0.0799 | V | S. Cook | 0.0005 |
| SW Lac | 57671.6139 | 38651.5 | –0.0777 | V | G. Persha | 0.0001 |
| SW Lac | 57732.5482 | 38841.5 | –0.0803 | V | G. Silvis | 0.0001 |
| VX Lac | 57606.6364 | 11492 | 0.0831 | V | G. Samolyk | 0.0001 |
| VX Lac | 57622.7549 | 11507 | 0.0841 | V | S. Cook | 0.0004 |
| VX Lac | 57623.8290 | 11508 | 0.0837 | V | K. Menzies | 0.0001 |
| AR Lac | 57643.6348 | 8093 | –0.0507 | V | G. Samolyk | 0.0001 |
| CM Lac | 57640.6180 | 19078 | –0.0043 | V | G. Samolyk | 0.0001 |
| CO Lac | 57601.7090 | 19496.5 | –0.0123 | V | G. Samolyk | 0.0001 |
| CO Lac | 57604.7940 | 19498.5 | –0.0117 | V | K. Menzies | 0.0001 |
| CO Lac | 57608.6684 | 19501 | 0.0071 | V | G. Samolyk | 0.0001 |
| DG Lac | 57633.6249 | 5948 | –0.2263 | V | G. Samolyk | 0.0001 |
| DG Lac | 57633.6249 | 5948 | –0.2263 | V | N. Simmons | 0.0001 |
| DG Lac | 57666.7234 | 5963 | –0.2258 | V | K. Menzies | 0.0001 |
| UV Leo | 57458.6546 | 31692 | 0.0414 | C | G. Frey | 0.0004 |
| VZ Leo | 57463.6902 | 24130 | –0.0576 | C | G. Frey | 0.0002 |
| WZ Leo | 57444.6775 | 3511 | 0.0004 | C | G. Frey | 0.0001 |
| XX Leo | 57502.6881 | 9074 | –0.0116 | C | G. Frey | 0.0001 |
| XZ Leo | 57753.8513 | 26097 | 0.0704 | V | K. Menzies | 0.0001 |

*Table continued on following pages*

Table 1. Recent times of minima of stars in the AAVSO eclipsing binary program, cont.

| *Star* | *JD (min) Hel. 2400000 +* | *Cycle* | *O–C (day)* | *F* | *Observer* | *Error (day)* |
|---|---|---|---|---|---|---|
| CE Leo | 57473.7462 | 32278 | –0.0080 | C | G. Frey | 0.0001 |
| GV Leo | 57457.7023 | 17633 | –0.0314 | C | G. Frey | 0.0001 |
| HI Leo | 57492.7329 | 15251 | 0.0091 | C | G. Frey | 0.0001 |
| Z Lep | 57657.8969 | 30425 | –0.1930 | V | G. Samolyk | 0.0001 |
| RR Lep | 57699.8977 | 29847 | –0.0438 | V | G. Samolyk | 0.0002 |
| δ Lib | 57585.7528 | 6284 | –0.0410 | V | S. Cook | 0.0006 |
| RY Lyn | 57753.8968 | 10360 | –0.0219 | V | K. Menzies | 0.0001 |
| UZ Lyr | 57609.6679 | 7360 | –0.0407 | V | G. Samolyk | 0.0001 |
| EW Lyr | 57556.7701 | 15937 | 0.2746 | V | G. Samolyk | 0.0001 |
| FL Lyr | 57637.6182 | 8914 | –0.0026 | V | G. Samolyk | 0.0001 |
| FL Lyr | 57650.6883 | 8920 | –0.0014 | V | S. Cook | 0.0008 |
| β Lyr | 57576.89 | 663.5 | 2.09 | V | G. Samolyk | 0.05 |
| β Lyr | 57576.94 | 663.5 | 2.15 | B | G. Samolyk | 0.03 |
| β Lyr | 57576.99 | 663.5 | 2.20 | R | G. Samolyk | 0.03 |
| β Lyr | 57583.34 | 664 | 2.08 | V | G. Samolyk | 0.03 |
| β Lyr | 57583.35 | 664 | 2.08 | R | G. Samolyk | 0.01 |
| β Lyr | 57583.41 | 664 | 2.14 | B | G. Samolyk | 0.01 |
| U Oph | 57608.7043 | 7865 | –0.0097 | V | S. Cook | 0.0006 |
| V423 Oph | 57635.6839 | 4266 | –0.0334 | C | G. Frey | 0.0002 |
| V501 Oph | 57629.7192 | 27603 | –0.0107 | C | G. Frey | 0.0001 |
| V508 Oph | 57523.6519 | 36083 | –0.0255 | V | B. Harris | 0.0001 |
| V508 Oph | 57625.3650 | 36378 | –0.0261 | R | L. Corp | 0.0001 |
| V508 Oph | 57642.6042 | 36428 | –0.0265 | V | G. Samolyk | 0.0001 |
| V839 Oph | 57614.6597 | 41971 | 0.3042 | V | G. Samolyk | 0.0001 |
| CQ Ori | 57474.6546 | 6941 | –0.0060 | C | G. Frey | 0.0003 |
| ER Ori | 57664.8881 | 37880 | 0.1303 | V | G. Samolyk | 0.0002 |
| ER Ori | 57696.8557 | 37955.5 | 0.1313 | V | R. Sabo | 0.0001 |
| ER Ori | 57755.7090 | 38094.5 | 0.1322 | V | G. Silvis | 0.0001 |
| ET Ori | 57701.8975 | 32618 | –0.0029 | V | G. Samolyk | 0.0001 |
| FR Ori | 57768.7205 | 33863 | 0.0409 | V | G. Samolyk | 0.0001 |
| FT Ori | 57768.6666 | 5212 | 0.0205 | V | G. Samolyk | 0.0001 |
| FZ Ori | 57684.9696 | 34152.5 | –0.0311 | V | G. Samolyk | 0.0002 |
| FZ Ori | 57754.7637 | 34327 | –0.0346 | V | G. Samolyk | 0.0003 |
| FZ Ori | 57769.5628 | 34364 | –0.0350 | V | G. Silvis | 0.0015 |
| GU Ori | 57686.8386 | 31055 | –0.0629 | V | G. Samolyk | 0.0002 |
| GU Ori | 57748.7338 | 31186.5 | –0.0622 | V | K. Menzies | 0.0001 |
| GU Ori | 57750.6165 | 31190.5 | –0.0622 | V | G. Silvis | 0.0001 |
| V343 Ori | 57422.7512 | 29443 | 0.2754 | C | G. Frey | 0.0001 |
| V1363 Ori | 57425.7344 | 11404 | 0.0273 | C | G. Frey | 0.0002 |
| V1853 Ori | 57416.6789 | 8747 | 0.0001 | C | G. Frey | 0.0001 |
| V2790 Ori | 57755.7640 | 21658 | –0.0022 | V | K. Menzies | 0.0001 |
| U Peg | 57606.8290 | 56287 | –0.1621 | V | N. Simmons | 0.0001 |
| U Peg | 57606.8294 | 56287 | –0.1617 | V | G. Samolyk | 0.0001 |
| U Peg | 57638.8730 | 56372.5 | –0.1619 | V | B. Harris | 0.0001 |
| U Peg | 57683.4724 | 56491.5 | –0.1615 | V | L. Corp | 0.0001 |
| TY Peg | 57634.8264 | 5557 | –0.4241 | V | G. Samolyk | 0.0002 |
| UX Peg | 57607.7926 | 11124 | –0.0059 | V | G. Samolyk | 0.0001 |
| AQ Peg | 57435.9899 | 2922 | 0.5599 | V | G. Samolyk | 0.0001 |
| AQ Peg | 57635.7494 | 2958 | 0.5733 | V | G. Samolyk | 0.0002 |
| AT Peg | 57677.7280 | 10870 | 0.0213 | C | G. Frey | 0.0001 |
| BB Peg | 57622.8551 | 38336 | –0.0228 | V | R. Sabo | 0.0001 |
| BB Peg | 57657.7413 | 38432.5 | –0.0216 | V | G. Samolyk | 0.0001 |
| BB Peg | 57670.5730 | 38468 | –0.0232 | V | N. Simmons | 0.0001 |
| BG Peg | 57607.8184 | 6185 | –2.2728 | V | R. Sabo | 0.0003 |
| BN Peg | 57667.7330 | 33326 | –0.0021 | C | G. Frey | 0.0001 |
| BO Peg | 57641.6874 | 20725 | –0.0494 | C | G. Frey | 0.0002 |
| BX Peg | 57622.7867 | 47883.5 | –0.1198 | V | G. Samolyk | 0.0001 |
| BX Peg | 57697.5162 | 48150 | –0.1224 | V | K. Menzies | 0.0001 |
| BX Peg | 57698.6379 | 48154 | –0.1224 | V | G. Samolyk | 0.0001 |
| DF Peg | 57655.7010 | 1643 | 0.1169 | C | G. Frey | 0.0005 |
| DI Peg | 57649.7293 | 17495 | 0.0064 | V | G. Samolyk | 0.0001 |
| DI Peg | 57684.6082 | 17544 | 0.0063 | V | G. Samolyk | 0.0001 |
| DI Peg | 57736.5709 | 17617 | 0.0063 | V | G. Samolyk | 0.0001 |
| DK Peg | 57700.6724 | 7458 | 0.1547 | C | G. Frey | 0.0001 |
| KW Peg | 57698.6328 | 11685.5 | 0.2101 | V | G. Samolyk | 0.0002 |
| V351 Peg | 57684.7322 | 15481 | 0.0316 | C | G. Frey | 0.0002 |
| V534 Peg | 57700.5856 | 4682 | 0.0141 | V | K. Menzies | 0.0003 |
| V613 Peg | 57748.5327 | 2434 | 0.0012 | V | K. Menzies | 0.0002 |
| Z Per | 57697.7321 | 3939 | –0.3046 | V | G. Samolyk | 0.0001 |
| RT Per | 57675.8076 | 28608 | 0.1049 | V | G. Samolyk | 0.0001 |
| RT Per | 57693.6451 | 28629 | 0.1050 | V | K. Menzies | 0.0001 |
| RV Per | 57684.8722 | 7924 | 0.0038 | V | G. Samolyk | 0.0001 |
| ST Per | 57701.7103 | 5764 | 0.3146 | V | G. Samolyk | 0.0002 |
| XZ Per | 57696.6878 | 12321 | –0.0736 | V | G. Samolyk | 0.0001 |
| BB Per | 57681.8405 | 3858.5 | 0.1099 | V | K. Menzies | 0.0002 |
| IQ Per | 57612.9622 | 7641 | –0.0030 | V | S. Cook | 0.0009 |
| IT Per | 57667.8768 | 18442 | –0.0401 | V | K. Menzies | 0.0003 |
| IU Per | 57675.7878 | 14077 | 0.0095 | V | G. Samolyk | 0.0002 |
| KW Per | 57707.7255 | 16433 | 0.0170 | V | G. Samolyk | 0.0001 |
| V432 Per | 57642.8887 | 67705.5 | 0.0435 | V | G. Samolyk | 0.0003 |
| V432 Per | 57693.8678 | 67864 | 0.0621 | V | K. Menzies | 0.0001 |
| V432 Per | 57737.5644 | 68000 | 0.0324 | V | G. Samolyk | 0.0002 |
| V737 Per | 57769.6378 | 17005 | –0.0649 | V | K. Menzies | 0.0001 |
| V740 Per | 57724.7910 | 16960 | 0.0037 | V | K. Menzies | 0.0001 |
| V881 Per | 57755.6725 | 2007 | –0.0096 | V | K. Menzies | 0.0001 |
| V996 Per | 57755.6421 | 4990 | –0.0305 | V | K. Menzies | 0.0003 |
| β Per | 57675.7178 | 4197 | 0.1282 | V | G. Samolyk | 0.0001 |
| β Per | 57698.6591 | 4205 | 0.1310 | V | G. Samolyk | 0.0006 |
| Y Psc | 57719.5663 | 3209 | –0.0210 | V | G. Samolyk | 0.0001 |
| RV Psc | 57671.8732 | 60092 | –0.0610 | V | G. Samolyk | 0.0002 |
| UV Psc | 57682.6812 | 16580 | –0.0205 | C | G. Frey | 0.0001 |
| VZ Psc | 57634.5067 | 52830 | 0.0021 | V | L. Corp | 0.0002 |
| VZ Psc | 57665.7279 | 52949.5 | 0.0029 | C | G. Frey | 0.0001 |
| VZ Psc | 57692.3753 | 53051.5 | 0.0018 | V | L. Corp | 0.0002 |
| VZ Psc | 57723.3341 | 53170 | 0.0014 | V | L. Corp | 0.0002 |
| AQ Psc | 57741.2984 | 11019.5 | 0.0016 | V | L. Corp | 0.0001 |
| CP Psc | 57673.7036 | 7563 | 0.0019 | C | G. Frey | 0.0001 |
| DS Psc | 57726.6456 | 15260 | –0.0035 | C | G. Frey | 0.0001 |
| DV Psc | 57727.6480 | 16943 | 0.0057 | C | G. Frey | 0.0001 |
| DZ Psc | 57678.7019 | 14144 | 0.0126 | C | G. Frey | 0.0001 |
| ET Psc | 57707.6454 | 11564 | –0.0067 | C | G. Frey | 0.0001 |
| ET Psc | 57753.3318 | 11668 | –0.0072 | V | L. Corp | 0.0002 |
| ET Psc | 57757.2886 | 11677 | –0.0041 | V | L. Corp | 0.0004 |
| GR Psc | 57703.6649 | 12615 | –0.0005 | C | G. Frey | 0.0001 |
| HO Psc | 57695.6654 | 1155 | 0.0010 | C | G. Frey | 0.0001 |
| AO Ser | 57607.6326 | 26695 | –0.0116 | V | G. Samolyk | 0.0001 |
| CC Ser | 57614.6384 | 39015 | 1.0865 | V | G. Samolyk | 0.0002 |
| CC Ser | 57620.5743 | 39026.5 | 1.0883 | V | K. Menzies | 0.0004 |
| RW Tau | 57686.8355 | 4335 | –0.2708 | V | G. Samolyk | 0.0001 |
| RW Tau | 57761.5917 | 4362 | –0.2732 | V | G. Samolyk | 0.0001 |
| RZ Tau | 57664.7827 | 48086 | 0.0821 | V | G. Samolyk | 0.0002 |
| RZ Tau | 57666.8619 | 48091 | 0.0829 | V | K. Menzies | 0.0001 |
| RZ Tau | 57698.8694 | 48168 | 0.0835 | V | R. Sabo | 0.0001 |
| RZ Tau | 57706.7673 | 48187 | 0.0835 | V | K. Menzies | 0.0001 |
| RZ Tau | 57726.7195 | 48235 | 0.0833 | V | K. Menzies | 0.0001 |
| RZ Tau | 57742.7242 | 48273.5 | 0.0846 | C | G. Frey | 0.0001 |
| RZ Tau | 57760.3901 | 48316 | 0.0843 | V | L. Corp | 0.0003 |
| TY Tau | 57696.7004 | 33883 | 0.2690 | V | G. Samolyk | 0.0001 |
| WY Tau | 57675.8962 | 29265 | 0.0636 | V | G. Samolyk | 0.0001 |
| WY Tau | 57698.7568 | 29298 | 0.0632 | V | G. Samolyk | 0.0001 |
| AM Tau | 57698.8116 | 6089 | –0.0708 | V | G. Samolyk | 0.0001 |
| CT Tau | 57750.6561 | 18515 | –0.0659 | V | G. Samolyk | 0.0002 |
| EQ Tau | 57634.8643 | 51037.5 | –0.0337 | V | G. Samolyk | 0.0001 |
| EQ Tau | 57670.8753 | 51143 | –0.0350 | V | R. Sabo | 0.0001 |
| EQ Tau | 57676.8497 | 51160.5 | –0.0342 | V | K. Menzies | 0.0001 |
| EQ Tau | 57702.7923 | 51236.5 | –0.0341 | V | G. Samolyk | 0.0001 |
| EQ Tau | 57728.7346 | 51312.5 | –0.0343 | V | K. Menzies | 0.0001 |
| EQ Tau | 57731.6340 | 51321 | –0.0363 | C | G. Frey | 0.0002 |
| EQ Tau | 57731.6362 | 51321 | –0.0342 | V | G. Silvis | 0.0001 |
| GQ Tau | 57443.6963 | 13677 | 0.1989 | C | G. Frey | 0.0001 |

*Table continued on next page*

Table 1. Recent times of minima of stars in the AAVSO eclipsing binary program, cont.

| *Star* | *JD (min) Hel. 2400000 +* | *Cycle* | *O–C (day)* | *F* | *Observer* | *Error (day)* |
|---|---|---|---|---|---|---|
| HU Tau | 57760.7090 | 8017 | 0.0324 | V | G. Samolyk | 0.0001 |
| V781 Tau | 57724.7641 | 40155 | –0.0509 | V | G. Silvis | 0.0001 |
| V1121 Tau | 57750.6304 | 11223 | –0.0119 | C | G. Frey | 0.0002 |
| V1128 Tau | 57692.5295 | 17003.5 | 0.0001 | V | L. Corp | 0.0001 |
| V1128 Tau | 57725.5092 | 17111.5 | –0.0004 | V | L. Corp | 0.0001 |
| V1128 Tau | 57773.2988 | 17268 | –0.0013 | R | L. Corp | 0.0001 |
| V1223 Tau | 57752.6897 | 12279 | 0.0016 | C | G. Frey | 0.0002 |
| V1332 Tau | 57749.6602 | 14947 | 0.0122 | C | G. Frey | 0.0003 |
| V Tri | 57633.8085 | 56663 | –0.0071 | V | N. Simmons | 0.0001 |
| V Tri | 57640.8298 | 56675 | –0.0082 | V | G. Samolyk | 0.0003 |
| X Tri | 57614.8615 | 15555 | –0.0895 | V | G. Samolyk | 0.0001 |
| RS Tri | 57680.6109 | 10341 | –0.0560 | V | G. Samolyk | 0.0001 |
| RS Tri | 57745.5146 | 10375 | –0.0557 | V | K. Menzies | 0.0002 |
| RV Tri | 57642.7453 | 15404 | –0.0412 | V | G. Samolyk | 0.0001 |
| W UMa | 57760.7401 | 35952.5 | –0.1003 | V | G. Samolyk | 0.0001 |
| W UMa | 57760.9062 | 35953 | –0.1010 | V | G. Samolyk | 0.0001 |
| TX UMa | 57720.0013 | 4153 | 0.2256 | V | G. Samolyk | 0.0004 |
| TY UMa | 57712.9126 | 51278 | 0.3858 | V | G. Samolyk | 0.0002 |
| ZZ UMa | 57697.8829 | 9458 | –0.0022 | V | G. Samolyk | 0.0001 |
| BM UMa | 57747.8946 | 75213 | 0.0141 | V | B. Harris | 0.0001 |
| AG Vir | 57491.7436 | 18765 | –0.0123 | C | G. Frey | 0.0001 |
| AW Vir | 57505.6676 | 35263 | 0.0282 | C | G. Frey | 0.0001 |
| AZ Vir | 57518.6936 | 38729 | –0.0264 | C | G. Frey | 0.0001 |
| AZ Vir | 57579.7118 | 38903.5 | –0.0248 | V | S. Cook | 0.0005 |
| BF Vir | 57535.7248 | 17898 | 0.1189 | C | G. Frey | 0.0001 |
| BH Vir | 57783.9818 | 17816 | –0.0118 | V | G. Samolyk | 0.0001 |
| GR Vir | 57543.7320 | 35816.5 | 0.0075 | C | G. Frey | 0.0002 |
| HT Vir | 57542.7585 | 12369 | 0.0037 | C | G. Frey | 0.0002 |
| IR Vir | 57519.6899 | 20829.5 | –0.0048 | C | G. Frey | 0.0001 |
| MS Vir | 57538.7102 | 16127 | 0.0033 | C | G. Frey | 0.0001 |
| NN Vir | 57517.7231 | 18759 | 0.0074 | C | G. Frey | 0.0002 |
| V391 Vir | 57520.7296 | 17671 | 0.0036 | C | G. Frey | 0.0002 |
| AW Vul | 57609.6305 | 14042 | –0.0252 | V | K. Menzies | 0.0001 |
| AW Vul | 57697.5328 | 14151 | –0.0261 | V | G. Samolyk | 0.0001 |
| AW Vul | 57697.5329 | 14151 | –0.0260 | V | K. Menzies | 0.0001 |
| BE Vul | 57680.6217 | 11320 | 0.1026 | V | G. Samolyk | 0.0001 |
| BO Vul | 57697.5274 | 11156 | –0.0182 | V | G. Samolyk | 0.0001 |
| BS Vul | 57640.6474 | 30189 | –0.0333 | V | G. Samolyk | 0.0001 |
| BS Vul | 57702.5248 | 30319 | –0.0322 | V | G. Samolyk | 0.0001 |
| BT Vul | 57607.6557 | 19458 | 0.0061 | V | G. Samolyk | 0.0002 |
| BT Vul | 57623.6327 | 19472 | 0.0063 | V | G. Samolyk | 0.0001 |
| BU Vul | 57606.6531 | 42308 | 0.0143 | V | G. Samolyk | 0.0001 |
| CD Vul | 57623.7158 | 16563.5 | 0.0005 | V | G. Samolyk | 0.0002 |
| CD Vul | 57646.6209 | 16597 | 0.0001 | V | N. Simmons | 0.0002 |
| V495 Vul | 57667.5354 | 732.5 | 0.0722 | V | K. Menzies | 0.0001 |

# Abstracts of Papers and Posters presented at the 105th Annual Meeting of the AAVSO, Held in Burlington, Massachusetts, November 10–12, 2016

## The Crucial Role of Amateur-Professional Networks in the Golden Age of Large Surveys

**Joseph E. Rodriguez**
*Vanderbilt Astronomy Group, Physics and Astronomy Department, Vanderbilt University, 6301 Stevenson Center, Nashville, TN 37235; rodriguez.jr.joey@gmail.com*

**Abstract** With ongoing projects such as HATNet, SuperWASP, KELT, MEarth, and the CoRoT and Kepler/K2 missions, we are in a golden era of large photometric surveys. In addition, LSST and TESS will be coming online in the next three to five years. The combination of all these projects will increase the number of photometrically monitored stars by orders of magnitude. It is expected that these surveys will enhance our knowledge of circumstellar architecture and the early stages of stellar and planetary formation, while providing a better understanding of exoplanet demographics. However, the success of these surveys will be dependent on simultaneous and continued follow-up by large networks. With federal scientific funding reduced over the past few years, the availability of astronomical observations has been directly affected. Fortunately, ground based amateur-professional networks like the AAVSO and the KELT Follow-up Network (KELT-FUN) are already providing access to an international, independent resource for professional grade astronomical observations. These networks have both multi-band photometric and spectroscopic capabilities. I provide an overview of the ongoing and future surveys, highlight past and current contributions by amateur-professional networks to scientific discovery, and discuss the role of these networks in upcoming projects.

## The Transiting Exoplanet Survey Satellite

**Ryan J. Oelkers**
*Department of Physics and Astronomy, Vanderbilt University, 6301 Stevenson Center, Nashville, TN 37235; ryan.j.oelkers@vanderbilt.edu*

**Abstract** The Transiting Exoplanet Survey Satellite (TESS) will be conducting a nearly all-sky, photometric survey over the course of two years, with a core mission goal to discover small transiting exoplanets orbiting nearby, bright stars. The satellite will obtain 30-minute cadence observations for more than 1 billion objects in the 26 TESS fields of view and 2-minute cadence observations of 200,000 to 400,000 selected stars. The TESS mission is expected to detect 1,500 transiting planet candidates, including 500 Earth-sized objects, over the course of its two-year mission. The choice of which stars to observe at the 2-minute cadence is driven by the need to detect small, transiting planets, leading to the selection of primarily bright, cool dwarfs. These stars will be 10 to 100 times brighter than the stars observed by Kepler, providing a unique opportunity for an amateur-professional collaboration to heavily contribute to candidate follow-up. I describe the TESS science mission, its current status and the mission's photometric and spectroscopic follow-up needs.

## Photometric Surveys (and Variability Studies) at the Observatorio Astrofísico de Javalambre

**Alessandro Ederoclite**
*Centro de Estudio de Física del Cosmos de Aragón, Plaza San Juan 1, Planta 2, Teruel 44001, Spain; aederocl@cefca.es*

**Abstract** The Observatorio Astrofísico de Javalambre (OAJ) is a new astronomical facility located in mainland Spain. This observatory is equipped with telescopes with large field of view and a unique filter system. The first two surveys to be carried out at the OAJ are the Javalambre Photometry of the Local Universe Survey (J-PLUS) and the Javalambre Physics of the accelerating universe Astrophysical Survey (J-PAS), devoted to the study of the star formation in the local universe and the expansion of the universe through baryonic acoustic oscillations. I introduce the OAJ and its instrumentation but also the potential for the study of variable sources (both within the J-PLUS and J-PAS projects and through "open time" projects). Finally, I stress the use of APASS for the calibration of our instruments.

## The Role of Small Telescopes in the Upcoming Era of the Giant Magellan Telescope and Other Extremely Large Telescopes

**Charles Alcock**
*Harvard-Smithsonian Center for Astrophysics, 60 Garden Street, MS-45, Cambridge, MA 02138; calcock@cfa.harvard.edu*

**Abstract** The Giant Magellan Telescope will be a 25-meter telescope located close to the twin Magellan Telescopes at the Las Campanas Observatory. I describe this telescope and some of the science goals we have developed, and also discuss the evolving balance between astronomy conducted with telescopes of a range of sizes, from 10 cm to 25 meters.

## Big Software for Big Data: Scaling Up Photometry for LSST

**Meredith Rawls**
*Department of Astronomy, University of Washington, Seattle, WA 98195; meredith.rawls@gmail.com*

**Abstract** The Large Synoptic Survey Telescope (LSST) will capture mosaics of the sky every few nights, each containing more data than your computer's hard drive can store. As a result, the software to process these images is as critical to the science as the telescope and the camera. I discuss the algorithms and software being developed by the LSST Data Management team to handle such a large volume of data. All of our work is open source and available to the community. Once LSST comes online, our software will produce catalogs of objects and a stream of alerts. These will bring exciting new opportunities for follow-up observations and collaborations with LSST scientists.

## The Galactic Plane Exoplanet Survey (GPX)—an Amateur Designed Transiting Exoplanet Wide-Field Search

**Paul Benni**
*3 Concetta Circle, Acton, MA 01720; pbenni@verizon.net*

**Abstract** GPX is designed to search high density star fields that other surveys such as WASP, HATNet, XO, and KELT would find challenging due to blending of transit-like events. Using readily available amateur equipment, a survey telescope (Celestron RASA, 279 mm f/2.2, based in Acton, Massachusetts) was configured first with a SBIG ST-8300M camera then later upgraded to an FLI ML16200 camera and tested under different sampling scenarios with multiple image fields to obtain a 9- to 11-minute cadence per field. The resultant image resolution of GPX is about 2 arcsec/pixel compared to 13.7–23 arcsec/pixel of the aforementioned surveys and the future TESS space telescope exoplanet survey.

GPX is based on the Kourovka Planet Search (KPS) prototype survey and uses the K-pipe data reduction pipeline. K-pipe performs all steps of the data handling from basic photometric reduction of the FITS files to the search of the transit-like events in the photometric time-series. K-pipe consists of several sequential scripts for astrometry (Astrometry.net), photometry (IRAF), and Box-fitting Least Squares transit search, and runs on a LINUX based laptop computer potentially operable by advanced amateurs.

One Hot Jupiter was discovered with the RASA telescope and validated by RV measurements from the SOPHIE spectrograph in the frames of KPS prototype survey (publication pending). Several more GPX exoplanet candidate stars of magnitude 11–13 have been identified, with some showing achromatic transit events, a sign of a possible Hot Jupiter, and are now awaiting RV follow-up. This survey demonstrates that advanced amateurs can operate star survey equipment, and with professional help with follow-up and validation, expanded ground-based surveys can be conducted in star fields that are challenging for other surveys.

## The AAVSO Photometric All-Sky Survey (APASS) at Data Release 10

**Stephen Levine**
*900 E. Hilltop Avenue, Flagstaff, AZ 86001; selevi@gmail.com*

**Abstract** The AAVSO Photometric All-Sky Survey (APASS) was designed to provide precise calibrated photometry in Johnson B and V and Sloan g', r', and i' passbands for stars over all the sky within the magnitude range from 7 to 17. Data Release 10 of APASS represents an improved and full re-reduction of all of the data collected since the survey started in 2009. We provide an overview of the project aims, methods, and instrumentation. We look at some of the ways APASS is already being fruitfully used by both the variable star and the broader astronomical communities.

## *Kepler* and K2: Spawning a Revolution in Astrophysics from Exoplanets to Supernovae

**David Ciardi**
*Chief Scientist, NASA Exoplanet Science Institute, Caltech/IPAC-NExScI, 1200 East California Avenue, Mail Code: 100-22, Pasadena, CA 91125; ciardi@ipac.caltech.edu*

**Abstract** Launched in 2009, the *Kepler* Mission helped to redefine our understanding of the extra-solar planets and began a revolution in how we view our own Solar System. But *Kepler* was more than an exoplanet finding mission, Kepler helped to redefine how we looked at stars and greatly improved upon our knowledge of how stars work and evolve. After *Kepler* suffered a mechanical failure which nearly ended the mission, Kepler was reborn at K2. Unlike *Kepler* which just stared at spot on the sky, K2 has pointed at 11 different areas of the galaxy and has enabled studies not previously possible with *Kepler,* including supernovae studies and searches for planets with microlensing events. I present an overview of the results of *Kepler* and K2 and how this is leading us to the future with TESS.

## Exploration of the Time Domain

**George Djorgovski**
*California Institute of Technology, 1200 E. California Boulevard, Pasadena, CA 91125; george@astro.caltech.edu*

**Abstract** Time-domain astronomy is one of the most active and growing areas of astronomical research today, thanks to the new generation of synoptic sky surveys, and leading to LSST. Catalina Real-Time Transient Survey (CRTS; http://crts.caltech.edu) is systematically exploring and characterizing the variable sky since 2008, with the archival data going back to 2005. The survey covers the total area of ~33,000 deg2, down to ~19–21 mag per exposure, with time baselines from 10 min to ~10 years, and growing; there are now typically ~200–400 exposures per pointing, and coadded images reach deeper than ~23 magnitude. The survey has so far detected over 13,000 unique, high-amplitude transients, including ~4,000 confirmed or likely supernovae, nearly 2,000 CVs (the great majority of them previously uncatalogued), about 4,000 blazars and other flaring AGN, and a broad variety of other types of objects. Many of these objects can benefit from a follow-up by the amateur community. CRTS is intended to be a data resource for the entire astronomical community. We have a completely open data policy: all discovered transient events are published in real time with no proprietary delay period, and all data are made public, in order to better serve the entire community, and maximize the scientific returns. This includes an archive of ~500 million light curves, which are being updated continuously. This is an unprecedented data set for the exploration of the time domain, in terms of the area, depth, and temporal coverage. Numerous scientific projects have been enabled by this data stream, including: discoveries of ultraluminous and otherwise peculiar SNe; unusual CVs and dwarf novae; mapping of the structure in the Galactic halo using RR Lyrae; variability-based discovery of AGN and probes of their physics; and so on.

## Clear-sky Forecasting for Variable Star Observers

**Frank Dempsey**
*RR #1, 3285 Sideline 20, Locust Hill, ON L0H 1J0, Canada; cosmicfrank99@gmail.com*

**Abstract** Many amateur astronomers seem to rely on computer model-generated weather forecasts for clear sky predictions and get frustrated by imperfect forecasts. It is worthwhile to consider the shortcomings of computer model forecasts and look at some resources to help the variable star observer plan for clear skies, whether for visual observers wanting to get an observation of a particular target star in long-term light curve programs, multi-hour observations of short-period pulsating variables or eclipsing binaries, or photometry. I discuss difficult-to-forecast factors including low clouds caused by local terrain and topographic effects, persistent low-level stratocumulus during the cold season, fog, post-cold front dry intrusions, pre-warm front waves of clouds, gradual sinking and clearing of cloud layers, jetstream-level cirrus, debris clouds persisting from upwind thunderstorms and distant thunderstorm complexes, large-scale blocking patterns, and other situations to hopefully help the variable star observer to make optimum use of limited time under clear skies.

## Cepheids and Miras: Recent Results and Prospects for the Era of Large Surveys

**Lucas Macri**
*Texas A&M University, 5313 Riviera Court, College Station, TX 77845; macri.lucas@gmail.com*

**Abstract** I present results from two recently-completed projects: (1) the determination of the Hubble constant with a total uncertainty of only 2.4%, using the Hubble Space Telescope to discover more than 2,000 Cepheids and calibrate the luminosity of white-dwarf supernovae; (2) the discovery and classification of over 1,800 Miras in M33 using a new technique that outperforms traditional methods when dealing with noisy and sparsely-sampled light curves. I discuss prospects for the Extragalactic Distance Scale in the era of large surveys, focusing on Gaia and LSST.

## Gravitational Radiation in ES Ceti

**Joseph Patterson**
*25 Claremont Avenue, Apt. 7C, New York, NY 10027; jop@astro.columbia.edu*

**Abstract** We present time-series photometry of ES Ceti, a close binary with an orbital period of 10.3 minutes. The star is a member of the "AM CVn" class of cataclysmic variable, in which the two components are both white dwarfs, and the transferred matter is pure helium. Photometry during 2001–2016 shows that the orbital period is rapidly increasing, with P/(dP/dt) = 10 million years. This is consistent with the hypothesis that the mass transfer and binary evolution are driven by gravitational radiation, and appears to be the first such demonstration in any cataclysmic variable.

## Observing the Low States of VY Scl Stars

**Linda Schmidtobreick**
*Eurpean Southern Observatory, ESO Vitacura, Alonso de Córdova 3107, Vitacura, Casilla 19001, Santiago de Chile, Chile; lschmidt@eso.org*

**Abstract** Novalikes just above the period gap play an important role in our understanding of the evolution of cataclysmic variables. Most of them belong to the group of SW Sextantis stars and experience very high mass transfer rates. This results in extremely hot, bright and dense accretion discs which do not allow to observe the stellar components in these binaries. To therefore get information about the physical parameters of these objects, i.e. the masses of the two components, the stars need to be observed in a low state when the accretion is at least partly suppressed. Many of the novalike stars are known to experience such low states that are also called VY Scl low states.

Within a large campaign, we have monitored these stars photometrically and triggered time resolved spectroscopic ToO observations when they went into a low state. I present some results of this campaign and would like to discuss the possibility of restarting it with the help of the AAVSO.

## Advances in Exoplanet Observing by Amateur Astronomers

**Dennis M. Conti**
*141 E. Bay View Drive, Annapolis, MD 21403; dennis_conti@hotmail.com*

**Abstract** This past year has seen a marked increase in amateur astronomer participation in exoplanet research. This has ranged from amateur astronomers helping professional astronomers confirm candidate exoplanets, to helping refine the ephemeris of known exoplanets. In addition, amateur astronomers have been involved in characterizing such exotic objects as disintegrating planetesimals. However, the involvement in such pro/am collaborations has also required that amateur astronomers follow a more disciplined approach to exoplanet observing.

This talk will discuss the results of some of these pro/am collaborations, as well as the evolution of best practices and software tools that have resulted. In addition, it will present recent advances in speckle interferometry, shaped aperture masks, and charge injection devices that may help overcome

the seeing, diffraction, and differential magnitude limitations that amateur astronomers face in direct exoplanet imaging. Finally, the status of an AAVSO database for storing exoplanet observations will be presented.

## The Impact of Large Optical Surveys on Stellar Astronomy and Variable Star Research

**Zeljko Ivezic**
*University of Washington, 2555 NE 85th Street, Seattle, WA 98115; ivezic@astro.washington.edu*

**Abstract** The advent of large optical surveys, such as SDSS, ongoing Pan-STARRS and Gaia, and soon to start LSST, has delivered unprecedentedly large and precise datasets. These new data have already enabled major new research areas and the impact of surveys is expected to grow further over the next few decades. I discuss how to use public data, such as from SDSS SkyServer, to select most interesting stars for followup, and show a few specific examples of my collaboration with amateur variable star observers.

## Engaging AAVSO members in Stellar Astrophysics Follow-up from The Evryscope Data

**Octavi Fors**
**Nicholas M. Law**
**Jeffrey Ratzloff**
**Henry Corbett**
*Department of Physics and Astronomy, University of North Carolina at Chapel Hill, Chapel Hill, NC 27599; octavi@live.unc.edu*

**Daniel del Ser**
*Department of Physics and Astronomy, University of North Carolina at Chapel Hill, Chapel Hill, NC 27599 and Departament de Física Quàntica i Astrofísica, Institut de Ciències del Cosmos (ICCUB), Universitat de Barcelona, Martí Franquès 1, E08028 Barcelona, Spain*

**Ward Howard**
*Department of Physics and Astronomy, University of North Carolina at Chapel Hill, Chapel Hill, NC 27599; octavi@live.unc.edu*

**Stephen Cox**
*Renaissance Computing Institute, 100 Europa Drive, Suite 540, Chapel Hill, NC 27517*

**Abstract** The Evryscope is a gigapixel-scale array of 24 telescopes which covers an instantaneous 8,640-square-degree field-of-view at two-minute cadence. This telescope opens a new parameter space in time-domain astronomy, trading instantaneous depth (g ~16mag) and sky sampling (~13") for continuous coverage (97% survey time efficiency) of the largest sky area of any active survey.

The system is obtaining 25,000 photometric measurements per target and per year, with a per-exposure 100-degree declination range. The Evryscope photometric precision is one percent-level at two-minute cadences on bright (g < 12) stars, and ~5 mmags ~12-minute binning.

The first science case The Evryscope is undertaking is the first large-scale survey of transiting planetesimals around the 4,500+ brightest white dwarfs (WDs). As byproducts of this survey long-term measurements of WDs pulsations, eclipsing WD binaries and periodically variable WDs will be obtained. Other science cases already recorded in The Evryscope dataset and to be started analyzed in the next weeks are: transiting habitable-zone rocky planets around the ~5,000 nearby M-dwarfs, nearby microlensing events, increasing TESS long-period giant planets return, the discovery and characterization of a wide range of stellar variability, including the measure of the mass-radius relation by using a complete inventory of eclipsing binary systems, detecting young stars by their flare behavior, detecting stellar merger events, accreting compact objects, and exotic pulsators.

The Evryscope was deployed at CTIO in May 2015. The telescope is fully operational, streaming raw imaging data per night at 109MB/sec. All data are stored and analyzed on-site by a high-speed server. Two more Evryscopes are planned to be deployed in near future: at Mount Laguna Observatory (collaboration with SDSU) and in the High Arctic (collaboration with NARIT and University of Toronto).

The Evryscopes are capable of monitoring almost every star brighter than 16th magnitude. After the discovery of variability of any type, the next step is follow-up, whether to confirm a transiting planet, obtain multi-color light curves of a microlensing events, or cover any of the host of stellar variability phenomena. I discuss the vital role AAVSO members could have in obtaining these observations. I show some characteristic examples of the kind of variable stars light curves which are in The Evryscope dataset.

## Using AAVSO Tools to Calibrate Secondary Standard Stars

**Michael D. Joner**
*Brigham Young University, Department of Physics and Astronomy, N488 ESC, Provo, UT 84602; xxcygni@gmail.com*

**Abstract** New discoveries often make it necessary to work in fields without adequate standard comparison sequences for coverage of faint magnitudes or atypical color ranges. Using available tools provided by the AAVSO such as VPHOT, Transform Generator, Transform Applier, and APASS, a method is outlined to add additional stars to standard comparison star sequences within a science field. Results are presented for BVRI secondary standards in the field of the active galaxy NGC 4151 and the recent supernova SN 2016coj in NGC 4125.

## Solar Data in the J and H Bands

**Rodney Howe**
*3343 Riva Ridge Drive, Fort Collins, CO 80526; ahowe@frii.com*

**Abstract** Early work of stellar astronomers established the

nomenclature for the infrared wavelength bands in the 1,000 to 5,000 nm range known as J, H, K, L, and M. This study is using the AAVSO SSP-4 photometer to collect solar data in the J and H bands, where the central wavelengths of these bands are roughly 1,300 nm for the J, and 1,600 nm for the H band. The continuum radiation from the sun is formed at the deepest level in the sun around 40 km from the surface at 1,600 nm (H band), and then the spectral continuum begins as the height increases with increasing wavelength in the infrared spectrum. From data collected here the H band has slightly larger values than the J band, however, there are distinct cross-overs on different days of observing. The telescope being used is a 60-mm LUNT, a blocking factor of 12 with a tilt-etalon filter (https://luntsolarsystems.com/product/ls60tds/) which can be adjusted to look at "white light"; in that configuration the SSP-4 photometer captures the sun's disc centered in the SSP-4 eyepiece (1 inch focal length ~ 25.4 mm). The Orion equatorial mount has an Astro-view Right Accession motor, which tracks the sun, and for an average data capture session of about 10 minutes, it is quite stable. Capturing data in the early morning is best as the weight of the SSP-4 helps the little RA motor, rather than in the afternoon when the balance would be against the direction of the earth's rotation.

## Variations in the Orbital Light Curve of the Magnetic Cataclysmic Variable Star QQ Vulpeculae

**Sanaea Cooper Rose**
*Wellesley College, 106 Central Street, Wellesley, MA 02481 and Maria Mitchell Observatory, 3 Vestal St, Nantucket, MA 02554; srose2@wellesley.edu*

**Abstract** Magnetic cataclysmic variable stars have brightness variations that repeat with each revolution of the two stars about the center of mass of the system. However, in the case of QQ Vulpeculae, this brightness variation pattern changes in the long term. This study makes use of two decades worth of data from the Roboscope Telescope as well as data from the American Association of Variable Star Observers' (AAVSO) database to examine the long-term evolution of QQ Vul's phase curves. Nightly observations using the Maria Mitchell Association Vestal and Loines Observatory supplemented this analysis by clarifying short-term brightness variation. The long-term data were divided into four commonly observed behavioral types ranging from a double-peaked curve of ~15.5 magnitude to a ~15.0 magnitude curve that had a primary minimum and a slow, linear rise in brightness in place of the secondary minimum. The nightly data kept within the confines of these categories, though the secondary minimum in the nightly data never vanished. No periodicity was found in the long-term variations. The model often invoked to explain the double-peaked curve consists of single-pole accretion in which a partial self-eclipse causes the secondary minimum and cyclotron beaming causes the primary minimum. However, the long-term variation may indicate a changing accretion rate, which may manifest itself in changes to the shape, size, or location of the accretion spot on the white dwarf such that it lessens or removes the secondary minimum. This project was supported by the NSF REU grant AST-1358980, the Massachusetts Space Grant, and the Nantucket Maria Mitchell Association.

## Coast-to-Coast Photometry: A Study in Consistency

**Tom Calderwood**
*1184 NW Mt. Washington Drive, Bend, OR 97703; tjc@cantordust.net*

**Abstract** Two photometric telescopes on opposite sides of North America are used to collect same-night data in Johnson B and V for selected stars. We find close agreement between the instruments, with a median difference of 4 millimagnitudes in twenty-two paired measurements. Data were gathered with Optec SSP3 and SSP5 photometers, and corrected for transformation and principal extinction in both bands, and for second-order extinction in B.